Sustainable Structures & Materials
An International Journal

THE WORLD UNIVERSITY RANKINGS 601 - 800 (2023)

THE WORLD UNIVERSITY RANKINGS TOP RANKED

2nd International Conference on Advances in Civil and Environmental Engineering (ICACEE - 2023)

2nd International Conference on Advances in

Civil and Environmental Engineering

22nd & 23rd Feb, 2023

Sustainable Structures & Materials

An International Journal

Conference Proceedings

ICACEE-2023

ISBN: 978-969-23675-1-6

Organized by:
Department of Civil and Environmental Engineering
University of Engineering and Technology Taxila, Pakistan

Suggested citation:

AUTHOR, A. (2023), Title of the Paper. In: International Conference on Advances in Civil and Environmental Engineering 2023. University of Engineering & Technology, Taxila Pakistan, pp. xx-xx. ISBN: 978-969-23675-1-6

ISBN: 978-969-23675-1-6

Media Partners: MDPI Sustainability
Sustainable Structures and Materials: An International Journal
Email: icacee@uettaxila.edu.pk
https://web.uettaxila.edu.pk/icacee2023

Foreword

Civil and Environmental Engineering Department, University of Engineering and Technology Taxila organized two days International Conference on Advances in Civil and Environmental Engineering (ICACEE-2023) which was held on 22nd and 23rd February 2023 at UET Taxila.

The aim of this conference was to bring together renowned researchers from academia and industry to share their expert knowledge on the latest theoretical, experimental, and practical domains of Civil and Environmental engineering. The event included 1.5 CPD points to all the authors and 0.5 CPD point to all the participants. Theme of the conference was;

- Sustainable Structures and materials
- Innovative Methods and Techniques in Civil Engineering
- Advance materials for Construction
- Traffic and Pavement
- Soil and Geoscience
- Water and Wastewater Treatment
- Waste Management and Resource Recovery
- Climate Change Mitigation and Adoption
- Sustainable Water Resources
- Renewable, Smart and Green Energy Development

We would like to thank all the members of the organizing committee, the session chairs and all the people who helped with the reviewing procedure of the contributed papers. Our special thanks to the Vice Chancellor UET Taxila, Director Advanced Studies & Research and Chairman Civil and Environmental Engineering departments for their support and guidance. The financial and technical support of different institutions and industries are also gratefully acknowledged.

Dr. Ghufran Ahmed Pasha
Conference Vice-Chair

Dr. Naveed Ahmad
Conference Chair

Engr. Sadia Fida
Conference Vice-Chair

Engr. Hammad Raza
Member

Engr. Aamar Danish
Member

Chief Guest

Prof. Dr. Jameel-Un Nabi
Vice Chancellor
University of Wah

Members of Advisory Board

Prof. Dr. Muhammad Inayatullah Khan
Patron

Prof. Dr. Qaiser-uz-Zaman Khan
Vice-Patron

Members of Advisory Board

Prof. Dr. Muhammad Yaqub
Principle Advisor

Prof. Dr. Ayub Elahi
Chief Advisor

Mr. Khalid Mahmood
General Advisor

Mr. Muhammad Nawaz
Finance Advisor

Technical Advisors

Prof. Dr. Imran Hafeez

Prof. Dr. Usman Ghani

Prof. Dr. Naeem Ejaz

Prof. Dr. Naveed Ahmad

Prof. Dr. Faisal Shabbir

Prof. Dr. Fiaz Tahir

Organizing Committee

Dr. Naveed Ahmad
Conference Chair

Dr. Ghufran Ahmed Pasha
Conference Vice-Chair

Engr. Sadia Fida
Conference Vice-Chair

Engr. Hammad Raza
Member

Engr. Aamar Danish
Member

Keynote Speakers

- Prof. Dr. Togay Ozbakkaloglu (Texas State University, USA)
- Dr. Mohammad Ali Mosaberpanah (Cyprus International University, Cyprus)
- Dr. Ikuo Towhata (Kanto Gakuin University, Yokohama, Japan)
- Dr. George Wardeh (IUT of Cergy, Pontoise, France)
- Dr. Manousos Valyrakis (University of Glasgow, UK)
- Dr. Marcos Quintela Baluja (University of Santiago de Compostela, Spain)
- Dr. Ashraf Aly Hassan (United Arab Emirates University, Al Ain, UAE)
- Dr. Mohsin Usman Qureshi (Sohar University, Oman)
- Dr. Ghulam Mustafa Shah (COMSATS University Islamabad, Vehari Campus)

Conference Co-Chairs

- Prof Dr. Imran Hafeez (UET Taxila)
- Prof Dr. Usman Ghani (UET Taxila)
- Prof. Dr. Naeem Ejaz (UET Taxila)
- Prof. Dr. Naveed Ahmad (UET Taxila)
- Prof. Dr. Faisal Shabbir (UET Taxila)
- Prof. Dr. Fiaz Tahir (UET Taxila)
- Dr. Sadia Nasreen (UET Taxila)

Schedule of Activities

	Conference Dates	**22nd & 23rd Feb 2023**	
	Mode of Conference	**Physical and Online**	
	PLAN OF ACTIVITIES		
	1st Day of Conference *(22nd Feb 2023)*		
1.	Registration and Reception of Guests	08:30 to 09:00	**Details of Inaugural Session** Venue: MPH, UET TAXILA 09:00= Ribbon Cutting Ceremony 09:05= National Anthem on the Arrival of Chief Guest 09:10= Recitation of Holy Quran 09:15= Naat 09:20=Introduction of Departments 09:25=Introduction of Conference 09:30=Welcome Speech of worth VC 09:45=Address of Chief Guest
2.	**Inauguration Ceremony & Chief Guest Speech**	**09:00 to 10:00**	
3.	Keynote Speakers Talk	10:00 to 11:30	
4.	**Tea Break & Poster Presentation**	**11:30 to 12:00**	
5.	Technical Sessions in Parallel	12:00 to 13:30	At MPH, CED & Env.ED
6.	**Lunch/Prayer Break**	**13:30 to 14:15**	MP Hall & Jamia Masjid
7.	Technical Sessions in Parallel	14:15 to 15:30	At MPH, CED & Env.ED
8.	**Tea Break & Poster Presentation**	**15:30 to 16:00**	At MPH
9.	Site Seeing tour of UNESCO World Heritage Sites (optional)	16:00 to 18:00	Through University Transport
	2nd Day of Conference *(23rd Feb 2023)*		
1.	Keynote Speakers Talk	9:00 to 10:30	At MPH
2.	**Tea Break & Poster Presentation**	**10:30 to 11:00**	At MPH
3.	Technical Sessions in Parallel	11:00 to 12:30	At MPH, CED & Env.ED
4.	**Chief Guest Speech**	**12:30 to 13:00**	At MPH
5.	Signing of MOUs & Closing Ceremony	13:00 to 13:30	
6.	**Lunch**	**13:30**	

Articles included in Sustainable Structures and Materials: An International Journal (SSMIJ)

Vol. 6 No. 1 (2023)

https://www.ssmij.org/index.php/ssm/issue/view/10

Vol. 6 No. 2 (2023)

https://www.ssmij.org/index.php/ssm/issue/view/11

Vol. 6 No. 3 (2023)

https://www.ssmij.org/index.php/ssm/issue/view/12

Paper ID	Title of Paper	Vol No., Issue No. & Page No.
102	A simulation and experimental study investigating 2D magnetic flux leakage (MFL) for defects in reinforcing steel	6 (02), 1-5
103	Recycling of Steel Scraps as a Strength Enhancement Material in Concrete	6(01), 39-43
104	Review of Sustainable Concrete: Building a Waste-Free and Sustainable Future	6(02), 23-31
105	Probabilistic Analysis of Strength of Structural Concrete for Post-Code Buildings in Developing Countries	6(03), 1-9
106	Consideration of simple approaches for structural health monitoring of structures in developing countries - An overview	6(01),139-143
107	Fresh properties of concrete having banana leaf ash and banana fibers	6(01), 88-95
108	Enhancing the Mechanical Properties of Concrete and Self-Healing Phenomena by adding Bacteria, Silica fume and Fibres	6(01), 32-38
115	Performance of Partially Bonded Engineered Cementitious Composites (Ecc) in Concrete Block Masonry	6(01), 74-77
116	A Review on Properties of Concrete Having Crumb Rubber as Partial Replacement of Fine Aggregate	6(02), 42-48
122	Comparative Analysis of Flexural Capacity of Bamboo Reinforced and Conventional Steel Reinforced Concrete Beams Through Numerical Evaluation	6(01),101-105
123	Mortarless Structures with Hollow Interlocking Blocks – A Comprehensive Review	6(01), 96-100
125	Influence of Waste PET Bottle Particles and Steel Fibers on Fresh Properties of Concrete	6(02), 49-57
127	Non-Destructive Testing of Fully Recycled Aggregate Concrete Bricks Prepared by Compression Casting Technique	6(01),106-110

128	Effect of Casting Pressure on the Properties of 100% Recycled Aggregate Concrete Pavers	6(01),127-131
130	Comparative analysis of fly ash based geopolymer concrete and Ordinary Portland Cement Concrete	6 (2), 6-11
131	An experimental study on axial behaviour of recycled plastic aggregate concrete columns	6(03), 10-16
133	Numerical evaluation of dry-stacked masonry walls against blast loading	6(02), 77-81
135	Seismic Performance Assessment of Deteriorating Reinforced Concrete Box Culverts	6(01), 44-48
138	IoT Based Real Time Early Age Concrete Compressive Strength Monitoring	6(01), 26-31
139	Numerical Study on The Out-of-Plane Behaviour of Brick Masonry Walls Strengthened with Cement Sand Mortar.	6(01),116-120
149	Effect of Casting Technique on the Compressive Behaviour of Fully Recycled Aggregate Concrete	6(01),111-115
150	Experimental Study on Seismic Response Characteristics of Soil on Building Models Using 1-D Shake Table	6(03), 27-35
152	Fly Ash an Alternative of Clay in Bricks: A Sustainable Solution for Future Constructions	6(02), 65-68
154	Model Updating of a Full-Scale Building Structure Under Train Induced Vibration	6(01), 68-73
203	Effect of Passenger Car Unit on Highway Capacity under Different Traffic Spectrum	6(02), 82-87
204	Development of Lane Utilization and Speed-Density Model for multilane highway: a case study in Islamabad Pakistan	6(02), 88-95
213	An Activity-Based Tour Generation Model with Peshawar as Case Study	6(2), 12-16
215	Intermolecular Bonding Study of Bituminous Materials Using Compositional Analysis	6(01),132-138
301	Regression Model for Predicting Soaked CBR from UCC	6(01), 54-58
302	Rock Quality Analysis using Empirical Techniques (RMR & Q-System) along The Headrace Of Hydropower Project In Kalam, Swat, Pakistan	6(01),144-148
304	Experiment Evaluation of the Infiltration Capacity of Urban Soils Using a Lab-Scale Model	6(01), 78-83
307	An overview on use of waste plastic for soil stabilization.	6(01),64-67
313	Numerical investigation of the slope stability under the rainfall infiltration of different intensities and duration using finite element code	6(2), 17-22
314	Experimental Study of Physio Mechanical Behaviour of Clayey Soil Incorporating Hydraulic Lime and Nano-Silica	6(02), 58-64
404	Study of Debris Flow Impact on Bridge Pier	6(03), 17-26
501	An overview of construction waste management	6(01),121-126
511	Optimal design of box composting plant; a case study of Pakistan	6(01), 84-87

517	Recent Progress in the Use of Flow Capacitive Deionization and Microbial Desalination Cell for Water Treatment - A Critical Review	6(02), 69-76
601	A Review of Sustainability Indicators for Small-scale Construction Projects by Private Contractors	6(02), 32-41
604	Development of a framework for Automating Material Supply in Construction Projects using Programming and Primavera P6 Schedule	6(01), 49-53
605	To study the procurement process and develop a conceptual framework model in the Pakistani construction industry	6(01), 59-63

Table of Contents

Articles included in conference proceedings of 2nd ICACEE-2023

2nd International Conference on Advances in Civil and Environmental Engineering (ICACEE-2023)

University of Engineering & Technology Taxila, Pakistan

Conference date: 22nd and 23rd February, 2023

Optimizing Energy Consumption of Building by Implementing Energy-Efficient Materials and EUI Influencing Parameters using BIM

Muhammad Osama Sajjad[1], Muhammad Noman[2], Muhammad Salman[3]

[1] Comsats University Islamabad, Wah Campus. Pakistan, osamasajjad20@gmail.com

[2] University of Engineering & Technology Taxila, Pakistan, 2016n5608@gmail.com

[3] University of Engineering & Technology Taxila, Pakistan, MMSalman02@gmail.com

ABSTRACT

Buildings consume a large amount of energy and spoil the environment in various ways. Optimizing building's energy consumption is a significant issue. This study aims to analyze the effect on the energy usage of a building when different choices regarding construction materials are made. An architectural design of a seven-story building is modelled using Revit – a leading platform for Building Information Modelling (BIM). Upon successful completion of the architectural model, energy analysis employing Insight 360 was undertaken. The effect of material choice on the energy utilization of a building was examined such that one material dyad acted as an 'experimental' component of the analysis. At the same time, the rest was considered a 'control' component. Such as, in the masonry domain, the analysis of brick-block dyads shows that lightweight blocks are far superior in reducing the energy consumption of buildings compared to bricks. Similar analyses were performed using other material dyads and parameters affecting the energy efficiency of the buildings. The analysis shows that material choices can significantly impact energy consumption on a building's complete lifespan. Therefore, considering the results of this exploratory study, it would assist the construction industry members to reduce energy consumption and pave the way to develop energy-efficient and sustainable buildings.

KEYWORDS: Building Information Modelling, Energy analysis, Energy Optimization

INTRODUCTION

The construction sector is one of the most energy-utilizing sections of a country's economy [1-3], especially in developing countries like Pakistan. Different studies have been done regarding measuring energy utilization in buildings According to the present study, the building sector utilizes over 40% of the total energy, over 30% of the natural reserves, over 70% of the generated electricity, and over 30% of the greenhouse gasses emissions [4-6]. One of the key causes of global environmental instability is energy usage. The general public's health is impacted by this environmental instability [7-8]. The energy a building uses over the course of its lifetime is responsible for around 90% of a building's environmental impact [9]. Pakistan has a population of 207 million; the residential houses and buildings utilize 49% of the electricity and natural gas with an estimated rate of 15.7 $MtCo_2$. These releases of harmful gases increase the temperature by about 0.8 ^{o}C in total temperature [10-11]. In this study, we aim to select energy-efficient materials and Energy Use Intensity (EUI) influencing parameters that can help in decreasing the energy utilization of the building. Buildings' façades play an important part in energy saving, as almost

20–60% of the building's energy utilization is due to these factors. Therefore, the use of innovative materials in the buildings' façades is among the most effective tactics to achieve Sustainability.

RESEARCH OBJECTIVE AND METHODOLOGY

The overall objective of the research program is to promote the optimization of energy patterns in buildings and to achieve Sustainability in the performance assessment of the building sector by introducing BIM-based energy solutions. BIM-enabled energy optimization of the commercial building supported by its BIM modelling energy analysis can help reduce energy usage and provide guidance for resolving building energy analysis and optimization issues. [12-14]. It has the potential to naturally put together energy-efficient techniques into building models and enhance performance, simulation speed, and the accuracy of energy simulation [15]
A seven-story building was selected as a case study to perform an energy optimization analysis. The building is located in the northern region of Pakistan, Muree. This was a seven-story building with a covered area of 168,000 sft and a height of 92 ft. The ground and first-floor plans were unique whereas the above floor followed the same typical plan. There are six apartments on each floor. A 3D parametric architectural model was created in Revit Architecture which was later subjected to insight to make an energy model (figure 1).

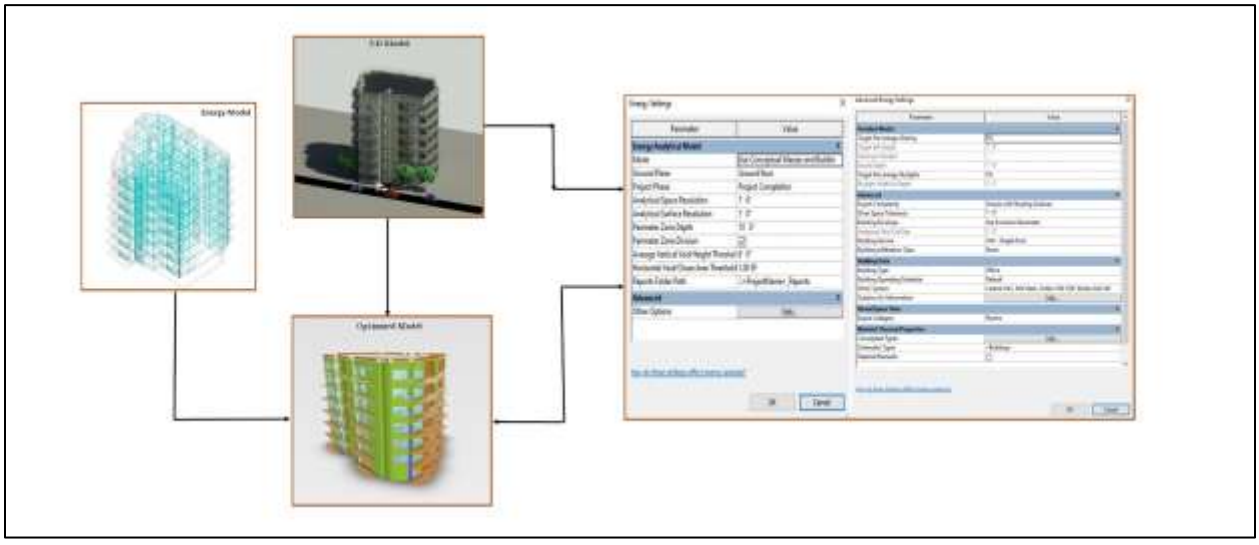

Figure 1: 3D Model of Building

RESULT AND DISCUSSION

After performing an energy optimization for our building to create an energy model and perform energy analysis, we have used Autodesk insight to understand, assess and design operational factor for improving performance

Results of the study are presented in form of comparisons between different conditions of the factors from obtained data which are explained below in details (all EUI (Energy Use Intensity) values are taken in kWh/m^2/year units).

Comparisons

Standard Brick Wall Vs Lightweight Concrete Wall

First of all we modified the energy settings in Revit to obtain results for more optimized material between standard brick walls and lightweight concrete block walls. Energy setting and analysed data from insight 360 are shown below:

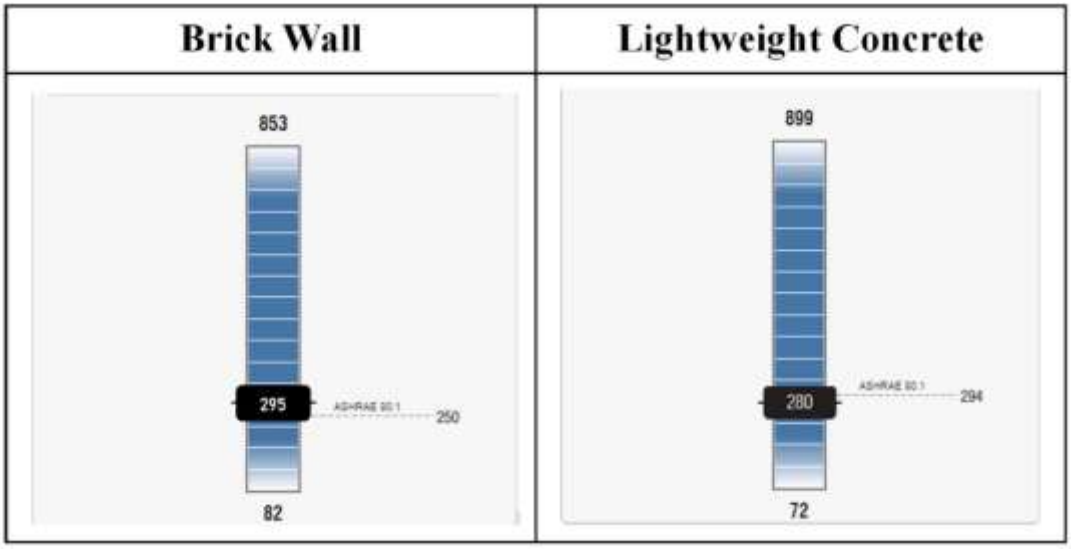

Figure 2: Standard Brick Wall VS Lightweight Concrete Wall Optimized Model

According to insight analysis, the EUI of a Lightweight concrete wall is more efficient, so we picked our model with lightweight concrete for further optimization. Afterward, we made different comparisons for EUI implementing parameters and materials under three categories:

i) The phase where the building consumed the maximum amount of energy.
ii) The phase where the building is already consuming a certain amount of energy is based on our model and energy setting in Revit.
iii) The phase where the building consumed a minimum amount of energy

Building Orientation (from True North)

The first comparison is for building orientation. It consumes the maximum energy when the façade (i.e., the front face of the building) is facing the **East direction**. Similarly, it consumes the least amount of energy when facing in the **South direction**. **EUI Difference (Max-Min) = 7 kWh/m^2/yr.**

Window Wall Ratio

The second comparison is for Window-Wall Ratio (WWR). The Window-to-Wall Ratio (WWR), which is computed as the ratio of the wall fenestration area to the gross above grade wall area, is the percentage of the above grade wall area that is covered by fenestration. It turned out that consumption of energy is maximum when WWR was 95%. And least amount of energy was consumed when WWR was 0% (i.e., no windows).

Table 1: Energy Comparison for Window Wall Ratio

Southern walls			**Northern Walls**			**Western Walls**			**Eastern Walls**		
Max	Model	Min	Max	Model	Min	Max	Model	Min	Max	Model	Min
95%	21%	0%	95%	13%	0%	95%	14%	0%	95%	2%	0%
EUI Difference (Max - Min) = 29 kWh/m2/yr			EUI Difference (Max - Min) = 33 kWh/m2/yr			EUI Difference (Max - Min) = 37 kWh/m2/yr			EUI Difference (Max - Min) = 17 kWh/m2/yr		

Window Glass

The third comparison is for window glass material used. It was concluded that the maximum amount of energy was consumed when windows were made of single clear glass. On the other hand, it consumes the least amount of energy when windows are made up of triple low-energy glass.

Table 2: Energy Comparison for Window Glass

Southern Glass			**Northern Glass**			**Western Glass**			**Eastern Glass**		
Max	Model	Min	Max	Model	Min	Max	Model	Min	Max	Model	Min
Single Clear	Double Glazed	Triple Low-E	Single Clear	Double Glazed	Triple Low-E	Single Clear	Double Glazed	Triple Low-E	Single Clear	Double Glazed	Triple Low-E
EUI Difference (Max - Min) = 26 kWh/m2/yr			EUI Difference (Max - Min) = 29 kWh/m2/yr			EUI Difference (Max - Min) = 22 kWh/m2/yr			EUI Difference (Max - Min) = 14 kWh/m2/yr		

Wall Insulation

Here we have compared the results against different types of wall insulation material. It was observed that maximum amount of energy was consumed when walls were left uninsulated. But consumption of energy was least when walls are provided with 14-inch Insulated Concrete Forms (ICF). **EUI Difference (Max - Min) = 63 kWh/m^2/yr.**

Roof Insulation

When roof insulation is considered the consumption of energy is maximum when the roof was left uninsulated. And the least amount of energy consumed when the roof is provided with R-60 type insulation**. EUI Difference (Max - Min) = 19 kWh/m^2/yr.**

Infiltration

If we check the EUI against the amount of infiltration it is concluded that the building consumes maximum amount of energy when infiltration is as high as 2.0 ACH (Air Changes per Hour). And the consumption of energy is least when infiltration is as low as 0.17ACH. **EUI Difference (Max - Min) = 30 kWh/m^2/yr.**

Day lighting and Occupancy Controls

When we studied the effect of day lighting and occupancy controls on EUI of building It was observed that maximum amount of energy amount of energy is consumed when there was no day lighting and occupancy control system installed and the consumption is least when both day lighting and occupancy control systems are installed**. EUI Difference (Max - Min) = 7 kWh/m^2/yr.**

HVAC (Heating, Ventilation, and Air conditioning)

The final comparison is for the (HVAC) system type installed in the building. It turned out that the building consumes maximum amount of energy when ASHRAE VAV (Variable Air Volume) system was installed. Similarly, least consumption was observed when the ASHRAE PACKAGE TERMINAL HEAT PUMP system was installed. **EUI Difference (Max - Min) = 125 kWh/m^2/yr.** After complete analysis of the building against different conditions of the factors that are affecting the EUI, the results are divided into three scenarios: When the energy consumption is maximum in a building that is set to be **Worst-Case Sce**nario. On the other hand, there is an **Ideal Case Scenario**, in which the consumption of energy is minimum but becomes impractical to provide all the parameters which tend towards minimum energy consumption, e.g., giving no windows in the whole building is very impractical and not possible. So, then there is a final scenario, i.e., the **Most Likely Scenario**, in this we have reduced the energy consumption considering the practicality of the parameters as well.

Worst Case Scenario	Ideal Case Scenario	Most Likely Scenario
In this case, all parameters and materials are set to maximum EUI values.	In this case, all parameters and materials are set to minimum EUI values.	In this case, all parameters and materials are set to minimum EUI values, which can be practically achieved.
EUI (805 kWh/m²//yr)	**EUI (43 kWh/m²//yr)**	**EUI (159 kWh/m²/yr)**
Cost (63.1 USD/m²//yr)	**Cost (4.07 USD/m²//yr)**	**Cost (15.6 USD/m²//yr)**

Figure 3: showing comparisons between different scenarios

After achieving the most likely scenario we can save **EUI up to 646 kWh/m²/yr** and cost up to **47.5 USD/m²/yr.**

CONCLUSIONS

Energy generation depends on various factors such as the orientation of the building, sun path setting, energy setting, location, and weather data. During analysis, a complete building was selected. However, in reality, such results might be hard to achieve therefore to achieve practically feasible results a number of different combinations would be required for analysis by selecting different combinations of faces of building feasible to Photovoltaic panel areas and comparing the results for the most feasible one.

The results obtained in this research can also help any other building but the pre-defined energy setting differs from region to region and building to building. From the above results, it is

concluded that the following five parameters are most important while considering the EUI of a building which are HVAC, Wall insulation, plug load efficiency, lighting efficiency and window to wall ratio.

REFRENCES

1. Köhler, M., 2008. Green facades—a view back and some visions. *Urban Ecosystems*, *11*(4), pp.423-436.
2. Tomaszewska, J., 2020. Polish transition towards circular economy: Materials management and implications for the construction sector. *Materials*, *13*(22), p.5228.
3. Chaichaloempreecha, A., Winyuchakrit, P. and Limmeechokchai, B., 2017. Long-term energy savings and GHG mitigations in Thailand's building sector: impacts of energy efficiency plan. *Energy procedia*, *138*, pp.847-852.
4. Yang, L., Yan, H. and Lam, J.C., 2014. Thermal comfort and building energy consumption implications–a review. *Applied energy*, *115*, pp.164-173.
5. Dixit, M.K., Fernández-Solís, J.L., Lavy, S. and Culp, C.H., 2012. Need for an embodied energy measurement protocol for buildings: A review paper. *Renewable and sustainable energy reviews*, *16*(6), pp.3730-3743..
6. Muto, A., 2020. Human Security Norms in East Asia: Towards Conceptual and Operational Innovation. *Journal of Conflict Transformation & Security*, *8*, pp.68-84.
7. Hernández, D., 2013. Energy insecurity: a framework for understanding energy, the built environment, and health among vulnerable populations in the context of climate change. *American Journal of Public Health*, *103*(4), pp.e32-e34.
8. Ding, G.K., 2008. Sustainable construction—The role of environmental assessment tools. *Journal of environmental management*, *86*(3), pp.451-464.
9. D. Castro-Lacouture, J.A. Sefair, L. Flórez, A.L. Medaglia, Optimization model for the selection of materials using a LEED-based green building rating system in Colombia, Build. Environ. 44 (6) (2009) 1162–1170.
10. Abbasi, K.R., Abbas, J. and Tufail, M., 2021. Revisiting electricity consumption, price, and real GDP: A modified sectoral level analysis from Pakistan. Energy Policy, 149, p.112087.
11. Abbasi, K.R., Hussain, K., Abbas, J., Adedoyin, F.F., Shaikh, P.A., Yousaf, H. and Muhammad, F., 2021. Analyzing the role of industrial sector's electricity consumption, prices, and GDP: A modified empirical evidence from Pakistan. Aims Energy, 9(1), pp.29-49.
12. Tushar, Q., Bhuiyan, M.A., Zhang, G. and Maqsood, T., 2021. An integrated approach of BIM-enabled LCA and energy simulation: The optimized solution towards sustainable development. *Journal of Cleaner Production*, *289*, p.125622.
13. Gao, X. and Pishdad-Bozorgi, P., 2019. BIM-enabled facilities operation and maintenance: A review. *Advanced engineering informatics*, *39*, pp.227-247.
14. Al-Shalabi, F. and Turkan, Y., 2015, June. A novel framework for BIM enabled facility energy management: A concept paper. In *Proceedings of the International Construction Specialty Conference (ICSC 15)*.
15. Chi, H.L., Wang, X. and Jiao, Y., 2015. BIM-enabled structural design: impacts and future developments in structural modelling, analysis and optimisation processes. *Archives of computational methods in engineering*, *22*(1), pp.135-151.

2nd International Conference on Advances in Civil and Environmental Engineering (ICACEE-2023)

University of Engineering & Technology Taxila, Pakistan

Conference date: 22nd and 23rd February, 2023

A Review Study on the Behaviour of Hollow Core Reinforced Concrete Slab System

Rana Shahmir[1], Naseer Ahmed[1], Sohail Rahman[1], Akhtar Gul[1]

[1]Department of Civil Engineering University of Engineering and Technology Peshawar Bannu Campus

Abstract;

Keeping in view the versatile benefits, the hollow core slab system is now getting popularity and trigger the attention of researchers to make this technology easy and implementable in local and rural construction industry. This paper explains and categorize the efforts and results of the previous research studies on different aspects of hollow core slabs. Mainly the studies on structural behavior have been focused, and conclusions of all the studies have been summarized. The hollow core slab system can be locally implemented in the rural areas by the simple embedment of pipes with suitable diameter. The flexure strength of hollow core slab can be archived easily as equal to solid reinforced concrete slab. This review study reveals that further research efforts are needed with different sizes of pipes and steel reinforcement.

KEYWORDS; Hollow core slabs, reinforced concrete members, hollow structural members.

Introduction;

Raw materials that are used in concrete are mostly excavated from earth. These raw materials are not unlimited and are decreasing as time passes, one of the ways to reduce the consumption of raw materials is such making structures that use less concrete. Hollow core slabs are an example of structural members that reduce the quantity of raw materials needed for concrete. A hollow core (HC) slab is a concrete component having holes that spread along the span of the slab. Voids in HC slabs reduce the structure's dead load, making it light weight, provide sound insulation; saves considerable amount of energy by providing thermal insulation[1], [2]. These slabs are mostly used as surface or roof deck system and also used as partition walls and bridge deck elements. HC slabs provide economical and effective floor and roof systems. By properly coordinating and aligning, holes in these slabs can be used as ducts for mechanical and electrical systems.

Figure 1 Hollow Core Slabs

Al-Fakher et al., performed an experimental and numerical study on the behavior precast HC slabs after adding a composite reinforcing system (CRS) [3]. The hollow CRS was made of glass fiber reinforcement and vinyl-ester resin using process of pultrusion. Six slab specimens were tested under 4-point bending test, out of six one was solid slab, one was simple hollow cores, one with epoxy coated CRS and others with different amount of CRS. Their study concluded that the HC slabs acts almost in the similar way as the solid RC slabs with same amount of reinforcement. The use of CRS significantly improved the load carrying capacity of slabs by minimizing the crack's propagation and contributing to the flexural capacity of slabs. It was reported that the number of CRS was not proportional to the increase in the load carying capacity of slabs so number of CRS to be used should be considered carefully. This study also discovered that using epoxy coated CRS provided better bond between the CRS tubes and concrete which resulted in higher load carrying capacity.

Al-Rubaye et al., [9] tested 4 full scale slabs and studied the effect of CRS and Glass Fiber Reinforced Polymer (GFRP) reinforcement bars on structural behavior of HC slabs. Out of 4 slabs, 1 was solid concrete slab reinforced with GFRP bars, 1 was HC slab with GFRP bars reinforcement, 1 contained CRS and had GFRP reinforcement, and 1 slab was reinforced with steel rebars and CRS. Effect of CRS was similar on the HC slabs as found by [3] in terms of propagation of cracks and contribution of flexural capacity of slabs. CRS increased the strength and stiffness of slabs without significantly increasing the self-weight of slabs. It was interesting to see that CRS and GFRP bars simultaneously resisted the load until it reached ultimate load while slab with steel reinforcement and CRS all the load was taken by CRS after yielding of steel. This showed that CRS was more compatible with GFRP than the steel reinforcement because of similar elastic modulus. A simple fiber analysis model was created to validated the results which verified the results with 13.8% difference in failure load.

Qureshi et al., [10] added glass fiber reinforced concrete topping of different depths, on precast prestressed HC slabs, to study its effect on the flexural capacity of slabs. Four slabs having width 990mm and five holes of diameter 155 mm running along their 2.4m length were tested. There were two control slabs having 265 mm and 200 mm depth respectively. Among the other two 200 mm depth original slabs, 32 mm topping was added on one slab and the other was added with 65 mm thick topping. It was found that 32mm topping increased the flexural capacity by 6% while a huge increase of 50% was seen in the flexural strength of the slab with 65mm topping. It was also observed that the flexural strength of the slabs with concrete topping was same as the slab with same depth and without topping.

Prakashan et al., [11] investigated the validation of conventional flexure capacity equations for prediction of flexural capacity of HC slabs. 5 slab specimens with different reinforcement and different number of hollow cores were tested and it was found that conventional flexural capacity equations can predict the flexural capacity of HC slabs with accuracy about ±19% and the serviceability and load-defection behaviour of HC slabs was better than the conventional RC slabs.

An experimental study was done by **Sreejith, n.d.,** [12] to observe the flexural behavior of partially prestressed HC slabs. Two slabs having dimensions of 4000 mm × 600 mm × 120 mm were casted, one prestressed HC slab and one sloid RC slab as control specimen. Weight of HC slabs was less 21% less the solid RC slab. Depth requirement of HC slab was found to be less than solid RC slab, for same load this may be because the weight of HC slab was less the solid RC slab.

Wariyatno et al., [13] used Styrofoam and PVC pipes to create hollow cores in slabs with different amount of reinforcement and studied their flexural behavior experimentally. Test specimens consisted of a solid slab as reference specimen, a HC slab in which PVC pipes were used to create hollow cores and a slab having hollow cores made using Styrofoam. Experimental results concluded that the flexural capacity of solid slab was more than the HC slabs with for all amounts of reinforcements. Cracks that developed in solid slab were flexural cracks while shear cracks developed in HC slabs upon loading.

Gul et al., [14] performed a research on the structural behavior of HC slabs with varying cross section shape and different used different materials for creating hollow cores. 14 slab samples were tested four specimens were prepared as solid slabs and were used as a control specimen while 10 samples were constructed as HC slab units in five sets, two samples for each type of pipes. It was concluded that the one-way HC slabs can be cast in situ with conventional methods. It was interesting to see that 7-8% reduction occurred in flexural capacity of HC slabs having concrete pipes while the flexural capacity of slabs with PVC and plaster of Paris (POP) pipes was comparable with that of solid slab specimens. HC slabs with triangular POP pipes showed higher flexural strength than all other slab specimens.

Table 1 Slab Specimens Designations [14]

Specimen	Mark
Solid Slab	HCS
Hollow core with concrete Pipes with 152.40 mm on centers (two pipes in 457.20 mm width of slab)	HCC1
Hollow core with concrete Pipes with 114.30mm on centers (three pipes in 457.20 mm width of slab)	HCC2
Hollow core with rectangular plaster of Paris Pipes	HCRP
Hollow core with PVC Pipes	HCP
Hollow core with triangular plaster of Paris Pipes	HCTP

Figure 2 Force vs Deformation Curves [14]

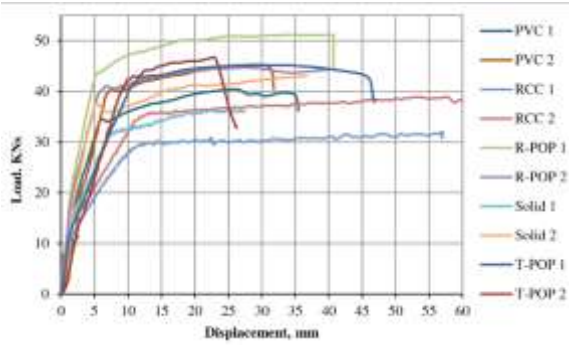

Hosny et al., [5] performed an experimental study on the capacity of HC slabs to resist the negative moments. Carbon fiber reinforced polymer (CFRP) tubes were added to the top side of HC slabs to increase the resistance to negative moments. 9 full-scale precast prestressed HC slabs were tested to perform this research. Thickness of all the slabs was 150 mm, with 1.20 m width, and 5.00 m length. Specimens were tested monotonically under negative and positive moments till failure. Results showed that the proposed technique improved the strength of HC slabs significantly. An increase of 277% to 574% and 183% to 225%, respectively in the negative moment and the cracking moment resistance of the CFRP-bonded hollow core slabs was recorded. Authors used S806–02 (CSA 20020 and CSA A23.3-94 (R2000) (CSA 2000) specifications to predict the moments and failure loads in slabs and suggested that while predicting the behavior of CFRP bonded HC slabs crack-induced debonding failure mode should be taken into account.

Rahman et al., [15] tested 15 HC slab samples, 5000mm and 2500mm in span and having three different depths, 200mm, 250mm and 300 mm to failure using 4-point loading test, in order to study the shear and flexural strength of precast prestressed HC slabs with different a/d ratios. Experimental results varied from the results predicted by ACI code equations. Flexure-shear failure was predicted by equations of ACI code for slabs with a/d ratio > 8 but flexural failure was observed as result of full-scale testing. ACI code equations underestimated the shear flexural capacity of precast prestress HC slabs with a/d ratio $3.5 < a/d < 8$. Results predicted by ACI code equations were good only for slabs with a/d ratio < 3.5.

Table 2 Comparison between the experimental results and ACI code equations [15]

Slab code	a/d	Experimental failure load (kN)	Flexural capacity ACI (kN)	Flexure/web shear ACI		Shear capacity ACI (kN)	ACI predicted/ observed failure mode	Diff. %
				V_{ci}(kN)	V_{cw}(kN)			
S1-5-200-1	11.4	160	167.4	74.6	226.3	149	FS/F	6.8
S2-5-200-2	11.4	158	167.4	74.6	226.3	149	FS/F	5.6
S3-5-250-1	8.7	226.8	226.4	96.5	224.6	193	FS/FS	14.9
S4-5-250-2	8.7	233.9	226.4	96.5	224.6	193	FS/FS	17.5
S5-5-300-1	7.1	381	354.6	148	302.5	296	FS/FS	22.3
S6-5-300-2	7.1	383	354.6	148	302.5	296	FS/FS	22.7
S8-2.5-200-1	3.7	287	361.2	143.2	191.9	286.4	FS/FS	0.2
S9-2.5-200-2	3.7	301	361.2	143.2	191.9	286.4	FS/FS	4.9
S10-2.5-200-3	3.7	259	361.2	143.2	191.9	286.4	FS/FS	−10.5
S11-2.5-250-1	2.8	433	698	253.5	224.6	449.3	WS/WS	3.6
S12-2.5-250-2	2.8	397	698	253.5	224.6	449.3	WS/WS	−13.2
S13-2.5-300-1	2.3	529	1093.4	400.3	302.5	605	WS/WS	−14.4
S14-2.5-300-2	2.3	597.7	1093.4	400.3	302.5	605	WS/WS	1.2
S15-2.5-300-3	2.3	508	1093.4	400.3	302.5	605	WS/WS	−19.1

F flexure, *FS* flexural-shear, *WS* web-shear

Conforti et al., [7]**.** performed a study to improve the shear capacity of HC slabs, they used polypropylene fibers reinforced concrete (PFRC) in HC slabs to study its effect on shear strength of HC slabs. Five full-scale HC slabs of dimension (420 mm deep, 1200 mm in width and 6000 mm in length) were tested under shear loading (one in RC and four in PFRC). Two tests were done on each slab specimen changing the a/d ratio (a/d equal to 2.8 according to EN 1168 and a/d equal to 3.5). Authors concluded that PFRC can add to the end zone shear strength up to 25 % and provide good post cracking resistance. Increase in end zone shear strength of HC slabs was mainly because PFRC provided better connection between tendons and concrete. Comparison between test results with different a/d ratio showed that samples with a/d equal to 2.8 (suggested by EN1168) showed a greater influence of arch action as compared to the slabs with a/d equal to 3.5, a/d ratio of 3.5 provided a good compromise between need of carrying end zone test and avoiding arch effects. Therefore, author suggested that, suggested test setup by EN1168 should be revised. Comparison between actual and theoretical shear capacity of HC slabs predicted by ACI318, Eurocode 2 and EN1168 level I, showed that these codes were too much unconservative and are needed to be revised.

Girhammer and Pajari., [6] observed the effects of adding concrete topping on the shear strength of prestressed HC slabs, both theoretically and experimentally. Two types of toppings were used plane concrete (PC) topping and steel fiber reinforced concrete (FRC) topping, for evaluating the bond formed between the slab's surface and concrete topping no special treatment was given to the slab top surfaces. Authors compared the results with one of their own studies in which they performed quality control tests on non-composite 200 mm deep HC slabs [16] and concluded that concrete topping can increase the shear capacity of HC slabs by 35 % which was also predicted analytically this match in theoretical and experimental results proved that adequate bond was formed between concrete topping and slabs. According to theoretical calculations concrete's tensile strength in web of HC slabs governed the shear capacity of slabs, not the interface shear

strength between concrete topping and slab, same results were observed experimentally. Effect of PC topping and FRC topping on shear strength of slabs was same.

Two studies were done by **Nguyen et al.,** in 2018 and 2019 [17] [18] performed an experimental study on shear behavior of deep precast prestressed HC slabs and compared the results to those predicted by equations of EN 1168 and ACI 318-14. Experimental studies revealed that EN 1168 and ACI 318-14 overestimated the capacity of HC slabs in some instances as some slabs failed at less loads then predicted by these codes. Two different modes of failure were observed during testing web-shear and flexural-shear. Arch action was not considered by EN 1168 and ACI 318 in the calculation of web-shear capacity of slabs. Finite element modeling was also done to understand the web-shear mechanism in deep HC slabs. Numerical studies predicted that web-shear capacity is related to the dilation angle and the strength of concrete used. Shear capacity of a slab in FE model designed increased by two times when dilation angle was increased from 20° to 40° and an increase of 2.4 times was recorded in web-shear capacity when strength of concrete escalated from 40 to 70 MPa and increase in tensile strength was from 3.51 to 4.61 MPa.

Cuenca and serna., [19] tested 26 HC slab specimens made of fiber reinforced concrete (FRC) using extrusion method and studied the shear capacity by variying the steel fibers amount = 0 kg/m3, 50 kg/m3 and 70 kg/m3 and a/d ratio varying from 2.3–4.4 and 8.6. No technical problems were faced in creating HC slabs with FRC. It was obsereved that fiber increased the shear strenth of slabs significantly and adequate ductility was achieved. Brittle failure ws obsereved in slabs with low a/d ratio but a/d ratio was increased failure mode converted toward ductile. It was suggested by author after extensive testing that FRC is a possible solution for overcoming the shear failure without disturbing the construction process of HC slabs.

J. M. Mhalhal., [8] performed an experimental on HC slabs with different a/d ratio and obsereved the behavior of slabs as a/d ratio changed. 4 full scale prestreesed precast HC slab specimens were tested by applying 4-point loading with different a/d values = 1.5, 2, 3.5 and 5. The slabs were of dimensions 2000 mm, 1200 mm and 150 mm. It was observed that the mode of failure of slabs dependended on the a/d ratio. Specimens with lower a/d ratio were stffer as compared to the elements with higher a/d ratio and failure loads increased as a/d ratio decreased. Variation in failure mode with different a/d ratio is given in following table

Table 3 Variation in failure mode with different a/d ratio [8]

Slab ID	a/d	Cracking load (Pcr) kN	Load at (Pu) Failure kN	% (Pcr) / Pu	Failure mode
HCS 1.5	1.5	110	143	77.92	tension shear and anchora failure
HCS 2	2	70	135	51.85	Shear compression Failure
HCS 3.5	3.5	55	120	45.84	Flexural shear Failure
HCS 5	5	42	115	36.52	Flexural failure

Conclusions;

We can conclude on the basis of above studies that;

- CRS tubes prevent the propagation of cracks increase the flexural capacity of HC slabs, without significantly increasing the self-weight of the structure.
- Glass fiber reinforced concrete topping and concrete topping can add to the flexural capacity of HC slabs. FRC topping and concrete topping can also increase the shear capacity of HC slabs, shear capacity increases with increase in depth of slabs. Effect of fiber reinforced topping and plain concrete topping is
- Flexural behavior of HC slabs can be predicted using conventional flexural capacity equations with around 19% accuracy.
- Depth requirement of HC slabs is less than the normal reinforced concrete slabs, for same amount of loading.
- Conventional methods can be used to construct cast in situ HC slabs.
- Plaster of Paris pipes can be used to create the voids in HC slabs without significantly effecting the strength of slabs.
- Out of different cross-section shapes (circular, rectangular and Triangular) slabs with triangular shaped voids showed highest flexural capacity.
- CFRP tubes can be added on top side of HC slabs to resist the negative bending moment.
- Web shear failure occurs in slabs with low a/d ratio as a/d ratio increases failure mode converts towards flexural failure.
- Failure loads decrease as a/d ratio increases and vice versa.
- Using polypropylene fibers in concrete in HC slabs can add to the end zone shear capacity of slabs up to 25 %.
- ACI 318 and EN1168 are unconservative in prediction of shear strength of HC slabs.
- FRC can be used for controlling shear failure in HC slabs without having any technical issues.

References;

[1] K. M. Monisha and G. Srinivasan, "EXPERIMENTAL BEHAVIOUR OF PRESTRESS HOLLOW CORE SLAB, RC HOLLOW CORE SLAB AND NORMAL RC SOLID SLAB," vol. 04, no. 04, p. 4.

[2] X. Xu, J. Yu, S. Wang, and J. Wang, "Research and application of active hollow core slabs in building systems for utilizing low energy sources," *Applied Energy*, vol. 116, pp. 424–435, Mar. 2014, doi: 10.1016/j.apenergy.2013.09.064.

[3] U. Al-Fakher *et al.*, "Bending behaviour of precast concrete slab with externally flanged hollow FRP tubes," *Engineering Structures*, vol. 241, p. 112433, Aug. 2021, doi: 10.1016/j.engstruct.2021.112433.

[4] K. S. Elliott, C. H. Peaston, and K. A. Paine, "Experimental and theoretical investigation of the shear resistance of steel fibre reinforced prestressed concrete X-beams—Part II: Theoretical analysis and comparison with experiments," *Mat. Struct.*, vol. 35, no. 9, pp. 528–535, Nov. 2002, doi: 10.1007/BF02483120.

[5] A. Hosny, E. Y. Sayed-Ahmed, A. A. Abdelrahman, and N. A. Alhlaby, "Strengthening precast-prestressed hollow core slabs to resist negative moments using carbon fibre reinforced polymer strips: an experimental investigation and a critical review of Canadian Standards Association S806-02," *Can. J. Civ. Eng.*, vol. 33, no. 8, pp. 955–967, Aug. 2006, doi: 10.1139/l06-040.

[6] U. A. Girhammar and M. Pajari, "Tests and analysis on shear strength of composite slabs of hollow core units and concrete topping," *Construction and Building Materials*, vol. 22, no. 8, pp. 1708–1722, Aug. 2008, doi: 10.1016/j.conbuildmat.2007.05.013.

[7] A. Conforti, F. Ortiz-Navas, A. Piemonti, and G. A. Plizzari, "Enhancing the shear strength of hollow-core slabs by using polypropylene fibres," *Engineering Structures*, vol. 207, p. 110172, Mar. 2020, doi: 10.1016/j.engstruct.2020.110172.

[8] J. M. Mhalhal, "Prestressed Precast Hollow-Core Slabs with Different Shear Span to Effective Depth Ratio: Precast," *ejuow*, vol. 5, no. 2, pp. 1–11, Oct. 2017, doi: 10.31185/ejuow.Vol5.Iss2.53.

[9] M. Al-Rubaye *et al.*, "Flexural behaviour of concrete slabs reinforced with GFRP bars and hollow composite reinforcing systems," *Composite Structures*, vol. 236, p. 111836, Mar. 2020, doi: 10.1016/j.compstruct.2019.111836.

[10] University of Engineering & Technology, Taxila, Pakistan and L. A. Qureshi, "Effect of Adding Glass Fibre Reinforced Concrete Topping on Flexural Behaviour of Hollow Core Slab Units," *ETJ*, vol. 03, no. 07, Jul. 2018, doi: 10.31142/etj/v3i7.02.

[11] L. V. Prakashan, J. George, J. B. Edayadiyil, and J. M. George, "Experimental Study on the Flexural Behavior of Hollow Core Concrete Slabs," *AMM*, vol. 857, pp. 107–112, Nov. 2016, doi: 10.4028/www.scientific.net/AMM.857.107.

[12] V. S. Sreejith, "FLEXURAL BEHAVIOUR OF PRESTRESSED HOLLOW SLAB," p. 10.

[13] N. G. Wariyatno, Y. Haryanto, and G. H. Sudibyo, "Flexural Behavior of Precast Hollow Core Slab Using PVC Pipe and Styrofoam with different Reinforcement," *Procedia Engineering*, vol. 171, pp. 909–916, 2017, doi: 10.1016/j.proeng.2017.01.388.

[14] A. Gul *et al.*, "Experimental Study on the Structural Behavior of Cast in-situ Hollow Core Concrete Slabs," *Civ Eng J*, vol. 6, no. 10, pp. 1983–1991, Oct. 2020, doi: 10.28991/cej-2020-03091597.

[15] M. K. Rahman, M. H. Baluch, M. K. Said, and M. A. Shazali, "Flexural and Shear Strength of Prestressed Precast Hollow-Core Slabs," *Arab J Sci Eng*, vol. 37, no. 2, pp. 443–455, Mar. 2012, doi: 10.1007/s13369-012-0175-8.

[16] M. Pajari, "Resistance of prestressed hollow core slabs against web shear failure".

[17] H. T. N. Nguyen, K. H. Tan, and T. Kanda, "Experimental and Numerical Studies on Shear Behavior of Deep Prestressed Concrete Hollow Core Slabs," in *High Tech Concrete: Where Technology and Engineering Meet*, D. A. Hordijk and M. Luković, Eds. Cham: Springer International Publishing, 2018, pp. 1110–1118. doi: 10.1007/978-3-319-59471-2_129.

[18] T. N. H. Nguyen, K.-H. Tan, and T. Kanda, "Investigations on web-shear behavior of deep precast, prestressed concrete hollow core slabs," *Engineering Structures*, vol. 183, pp. 579–593, Mar. 2019, doi: 10.1016/j.engstruct.2018.12.052.

[19] E. Cuenca and P. Serna, "Failure modes and shear design of prestressed hollow core slabs made of fiber-reinforced concrete," *Composites Part B: Engineering*, vol. 45, no. 1, pp. 952–964, Feb. 2013, doi: 10.1016/j.compositesb.2012.06.005.

2nd International Conference on Advances in Civil and Environmental Engineering (ICACEE-2023)

University of Engineering & Technology Taxila, Pakistan

Conference date: 22nd and 23rd February, 2023

Mechanical and Physical Properties Assessment of Coarse and Fine Aggregates of Local Quarries; A Review

Muhammad Asim[1], Farhat Ullah[1], Faisal Khan[1], Azmat Ullah[2], Akhtar Gul[1]

[1]*Department of Civil Engineering University of Engineering and Technology Peshawar Bannu Campus*

[2]*Communication and Works Department Khyber Pakhtunkhwa*

ABSTRACT

In order to search for suitable aggregates in the locally available quarries, a vast research study is needed. As aggregate is the central part of concrete and is extensively used around the globe in construction industry. As per the survey of the authors and the field experience of the local parent department of construction Communication and Works Department Khyber Pakhtunkhwa, most of the local aggregates do not satisfy the minimum requirements of ASTM standards. In this paper, a review study has been presented for various experimental and numerical research studies made on mechanical and physical properties of aggregates. Subsequently, the conclusions of research carried out to study the characteristics of aggregate behaviour have been presented. In the end, recommendations have been made for future research on the assessment of the locally available materials and quarries.

KEYWORDS: Physical Properties, Mechanical Properties, local available materials

1 INTRODUCTION

This study mainly focuses on the assessment of physical and mechanical properties of aggregates extracted from natural quarries. For each government project, a campaign is started for searching a good quality of aggregates from the locally available resources, which imposes a financial burden on each individual project. Therefore, it is needed to assess the local available aggregates for physical and mechanics properties. The local government construction departments and builders are facing problems in selection of building materials in nearby quarries. The percentage of aggregate in concrete is approximately 80% (Oluwasola et al., 2020)., [1].The high percentage of aggregates is not only make the concrete economical but also make the concrete more stable and durable (Oluwasola et al., 2020). The compressive strength of concrete is greatly affected by the water cement ratio, ratio of cement and aggregate, bond between mortar and aggregate, strength, size, and type of aggregate (Abdullahi, 2012)., [2]. Hundreds of aggregate quarries are available in the local areas of Khyber Pakhtunkhwa, which are abundantly used for the construction materials but research work has not been done on these quarries till now. There is no research-based data or guidelines to be followed by the builders in the selection of buildings materials;

hence, the local aggregates need proper assessments. In case, the local aggregates are not fulfilling the ASTM standards requirements then guidelines for mix design of concrete or in other use of civil engineering can be finalized with help of suitable experimental scheme. To know about different parameters and aspects for the assessment of local available aggregates, an effort is made in this paper by reviewing the already research articles and their conclusive recommendations. The conclusion of this study will define a research gap for a vast experimental campaign for the scrutinization of local available coarse and fine aggregates.

2 EXPERIMENTAL INVESTIGATION

2.1 General Behaviour

In the study they were set the geological setting, which includes the muzaffarabad dolomite, Margalla Hill Limestone etc. Nanga Parbat and Hazara Kashmir syntaxes were developed because of regional change in strike(Fig. 1)., [3]. In another study, according to this geological setting Kohat Hills Range is situated in the north-western apex of the southern fold and thrust belt that borders the entire Himalayan foothills in India and Pakistan (Ahmad et al. 2006). The area for study has been divided into 9 formations consist of rock ranging in the period from central Jurassic to Miocene (Fig.02)., [4]. In the study of Peshawar aggregate assessment, they examine river Bara and river Kabul. The Bazid Khel (Dara Adam Khel) and Khyber rivers were found the sources of limestone., [5]. In another study they assess the Margalla Hill., [6].

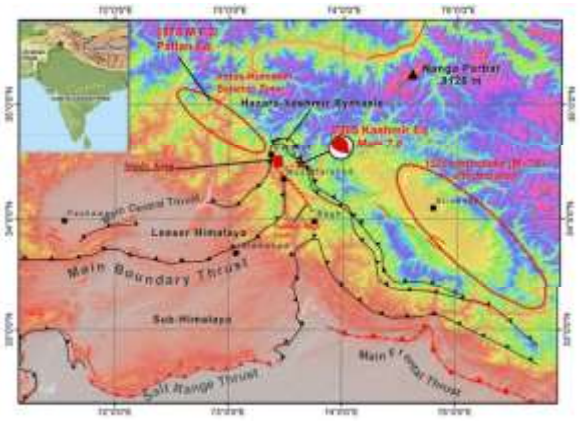

Figure 1 Frontal Himalayans tectonic map (Riaz et al. 2018).

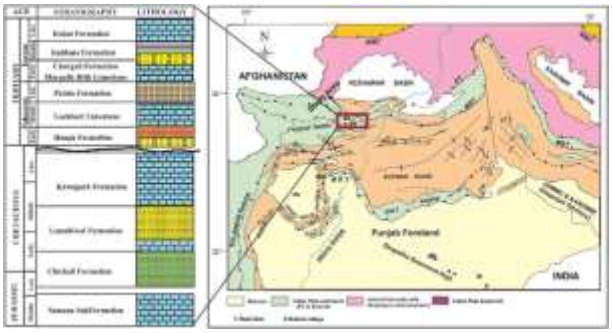

Figure 2 Northwest Himalayan foreland fold and thrust belt Geologic map.

2.2 Material and Method

In the research study, properties of local aggregates from different quarries have been reviewed. Quarries of Muzaffarabad region were studied for characterisation of CRA having different mineralogical and petrographic properties. The results obtained in the experiment study are analyse to differentiate the different characteristics of CRA and to emphasise the petrographic/mineralogical as well as the mechanical influencing factors affecting the crushed

aggregate characteristics. The method in the research is comprising with literature review on studies (for example Ahsan et al., 2009) and basic principle are interrelated to the present research. In the Yadgar area field visit are carried out of main sites to collect samples of CRA of 19 to 4,75mm size for laboratory testing. 30 samples of dolomite and limestone were collected from 6 active different quarries. The results obtained from laboratory and field work are analysed and discussed comprehensively. Finally, results are compared with standard of ASTM and BS standard and reported.

2.2.1 Testing Methodology

Different researchers conducted various tests according to BS and ASTM standards to find out the Abrasion value (ASTM C131/C131M)., [7], Crushing value (BS 812:110, 812-11)., [8], Impact value (BS 812, 112, 1990; 2000)., [9], Soundness (ASTM C88/C88M-18)., [10], Particle size distribution (ASTM C136 – 06)., [11], Relative density and Absorption (ASTM C 127–7)., [12]. Mineralogical and Petrographic evaluations of carbonate aggregates were conducted to get the constituent mineral's relative percentages. Semi-quantitative and qualitative Powder X-Ray Diffraction (PXRD) mineralogical examinations were performed on 1 samples of the Margalla hill and 2 of Muzaffarabad dolomite Limestone. The steps for methodology adopted for the current study is illustrated in Fig 03.

In another study, the basic engineering evaluations, the Kohat hills Range Mesozoic carbonates were chosen. 12 bulk samples from Kawagarh and Samana Suk formation were collected. Six were examined for petrographic study and six for aggregate analysis, which are performed at China University of Geosciences Wuhan. Another two study were performed one is for Peshawar and other is for Mardan regions.

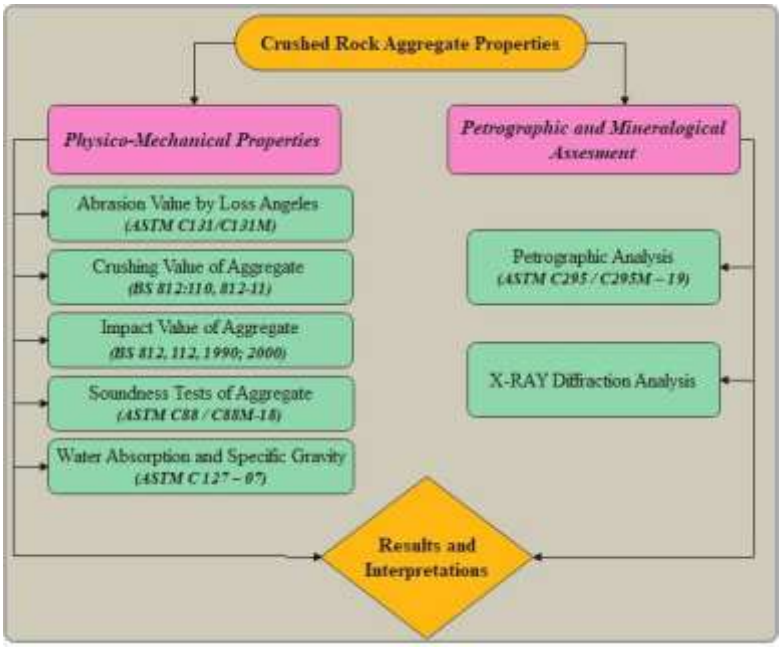

Fig 03 Methodology

3 Result and Discussion

To evaluate the mechanical and physical properties of aggregates the tests were checked with the suitable BS and ASTM standards for each kind of test in several studies.

3.1 Abrasion Value of Aggregate (AVA)

The durability and toughness tests of crushed rough aggregate were conducted on the samples for Los Angles Abrasion value (LAAV). Allowable value according to ASTM is 0% to 50%. The abrasion value of muzaffarabad, Margalla hill, Samana Suk and Kawagarh are 20.33% to 32.12%, 15.27% to 19.8%, 27.10% and 20.86% respectively. In another study, the abrasion values of Bara River, Basai, Loye Khawar and Zangali sites are 21.20, 18.50, 20.00 and 24.00 % respectively.

3.2 Aggregate Crushing Value (ACV)

The strength is basic property of aggregate against crushing. The Muzaffarabad dolomite and dolomite limestone formation show significant deviancy in the strength against crushing. The values are in between 17.30 % and 22.76 %, fall between 0 to 30 % (BS 812:110, 812-11). The Margalla Hill Limestone crushing values ranges from 17.93 % to 24.9 %. In another study, the values got for Samana Suk, crushing value and Kawagarh formations are 12.84%, 15% to 30% and 13.26% respectively.

3.3 Aggregate Impact Value (AIV)

The toughness and resistance of aggregate to sudden shocks is termed as impact value of aggregate. The Muzaffarabad Formation and Margalla Hill Dolomite and Dolomitic limestone aggregate are 14.86 % - 25.76 % and 15.54 % - 25.72 % respectively fall in range from 0-30% (BS 812, 112, 1990; 2000). In another study, the range of impact value from Kawagarh and Samana Suk formations are 14.89% and 14.09% respectively fall in range from 20-30 % (BS 812-112:1990 2013). According to BS 882 criteria the District Mardan aggregates of Jamal Garhi and Palodheri are not good for heavy constructions.

3.4 Aggregate Soundness tests (AST)

The soundness is the stability of the rock aggregates to chemical weathering. Muzaffarabad Formation dolomite and limestone ranges from 1.09 to 1.96% and 0.47 to 1.14%. In another study, values for Samana Suk and Kawagarh formations the average Soundness value are noted as 1.88% and 2.14% respectively. In the assessment of aggregate in Peshawar study shows that River, Basai and Zangali are 13.05, 6.61, and 8.94% respectively, which are within the range. But, the Soundness value for Loye Khawar aggregate sample is 17.69%, which is somewhat greater than the upper limit range (0 to 15). This aggregate are suitable for low freeze and thaw regions.

3.5 Specific Gravity and Water Absorption

The Margalla Hill and Muzaffarabad Formation rang aggregates have the specific gravity recorded from 2.520 to 2.730 and 2.620 to 2.890 respectively are shown in figure 04, whereas the value for water absorption are in between from 0.43% to 0.98% an 0.53% to 0.83% respectively. These values correspond to the ASTM specification limits. In another study, For Kawagarh and Samana Suk formations the average specific gravity values are noted from 2.68 to 2.73, whereas average water absorption is 0.81% and 0.89% respectively. In the study of district Mardan on aggregates the bulk specific gravity 2.4-3.0 (ASTM C 125 -03), which falls on normal weight aggregates queries.

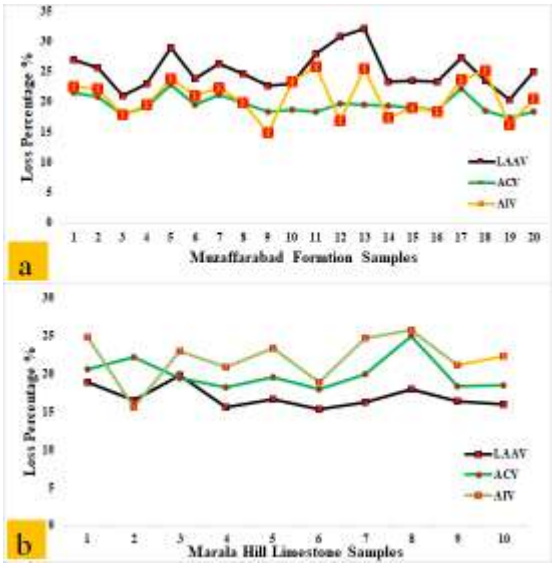

Figure 04 comparison of samples

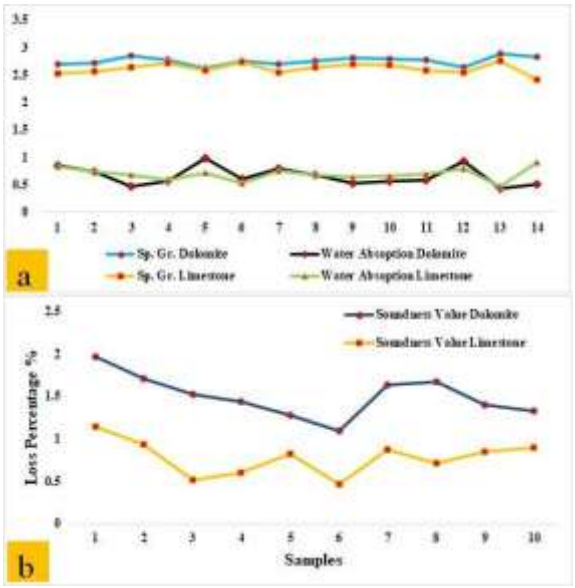

Figure 05 Comparisons of samples

3.5 Shape Test (Flakiness and Elongation)

The Kawagarh formations and Samana Suk aggregates are known to have a flakiness index respectively from 9.970% to 11.560%, while the elongation index 12.56% and 12.07% respectively. The standard limit is 25% (BSI 1990) so all values fall under the standard.

3.7 Petrographic Characteristics of the Aggregates

This study was performed on Muzaffarabad formation and Margalla hill limestone to classify the aggregate under study of their chemical proportion. Petrographic, Margalla Hill Limestone contains a modular composition of 20-30% micrite, 10-15% bioclasts, 50-65 calcite with some dolomite and debris Quartz followed by pyrite and hematite. In another study, the limestone units were categorized into different microfacies according to ASTM C-125 in 1993.

3.8 X-Ray Diffraction Analysis

X-ray diffraction the investigations made it possible to establish the crystalline nature, percentage of mineral constituents and stage composition as well. A Three rock samples selected, one from Margalla hill Limestone and two from Muzaffarabad formation was chosen, ground into powder and under-inspected an x-ray. The following results were obtained;

- Muzaffarabad Formation are composed of dolomite 0-36%, mineral calcite ranging from 38-79% and followed by quartz 12-26% are shown in figure 05.

- Likewise, the Margalla hill limestone is 7% quartz and 93% calcite.

4 Discussion on results

From the Petrological analysis of Margalla hill limestone shows that it dominantly comprised of bioclasts, calcite and micrite with traces of dolomite, pyrite, detrital quartz and hematite. Generally, due to minor calcite presence does not affect Los Angeles properties of aggregates.
Due to presence of micrite and bioclasts it effects the mechanical properties of aggregates. Due to micrite (20 to 35%) and bioclasts (10 to 15%) highly percentage it greatly affects the mechanical properties of Margalla hill limestone. In addition, with the carbonate minerals the dolomite contains much amount of quartz. Clay and silt particles are also found in samples. Moreover, the iron sulphide i.e., oxide and pyrite rapidly reduce the strength and cause staining of concrete shown in Fig 06.

In another study, Late Cretaceous and middle Jurassic carbonates were studied for fundamental engineering properties. The limestone is significant and dolomite are sub ordinate facies. The middle Jurassic samana Suk formation has dominantly the grain stone facies while mud and wacke stone are also present. No deformation is observed however some diagenetic features like calcite, dolomitization and stylolite.

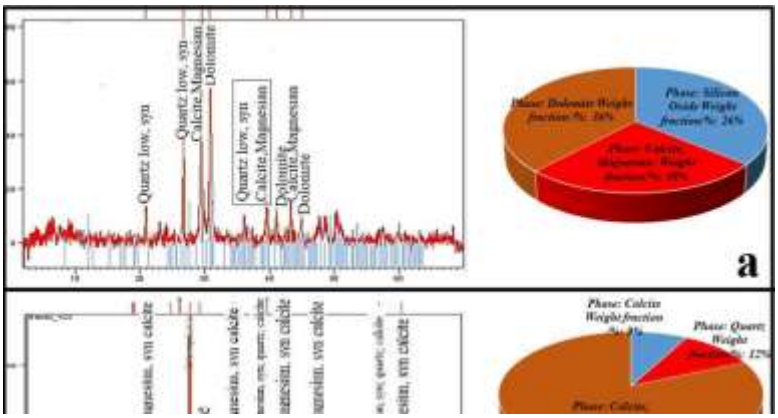

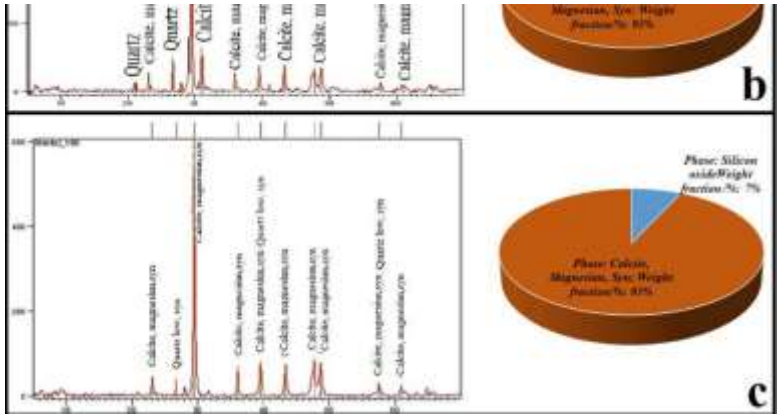

Fig. 06. Graphical and quantitative distribution of X-Ray Diffraction analysis. a,b) Muzaffarabad Formation, c) Margalla Hill Limestone.

5 Conclusion

Following results have been taken from different studies.

Case study of sub-Himalaya Pakistan

- Dolomitic and dolomite limestone of muzaffarabad formation (MF) fulfil all requirement of BS and ASTM standard of texture, mechanical and physical properties.
- It has enough percentage of cherty, i.e. 3 to 6% which enough in cement concrete to initiate ASR.
- The results from MF shows high ACV (20 to 22%), high LAV (25 to 32%), high AIV (20 to 25%) and high absorption of water values (0.74 to 0.98%), shows that the quarries which are placed near to MF zone shows high micro fractures percentage observed in petrography.
- The lower percentage of ACV (17 to 20%), LAV (20 to 25%), AIV (14 to 20%) and absorption of water values (0.43 to 0.7%) shows that the quarries which are placed away from MF zone shows fewer micro fractures percentage observed in petrography.
- Also, the XRD shows that the MF has a significant amount of quartz and dolomite.
- However, the CRA values from the study shows that it are suitable for road, pavement, concrete etc only the Margalla hill limestone is suitable.

Other study

- The Jurassic Samana-Suk Formation and the late Cretaceous Kawagarh Formation are well according to the different international standard are strongly recommended for any civil engineering works from the test results of physical, chemical and mechanical properties shown in Fig 8 and 9.
- According to the petrographic examination, the aggregate does not have structural flaws due to the result of alkali-silica reaction (ASR) or the alkali-carbonate reaction (ACR).

- The detail mapping based on remote sensing are much needed for the area to easily differentiate various lithological variations, i.e., marls, limestone and dolomites.
- In Pakistan, the blasting are done to obtain the aggregate, mostly 50% loss the aggregate material. Therefore, detailed work needed on accurate processing of aggregate.
- Due to quarrying vegetation are disturbed, therefore, quick re vegetation process are needed.

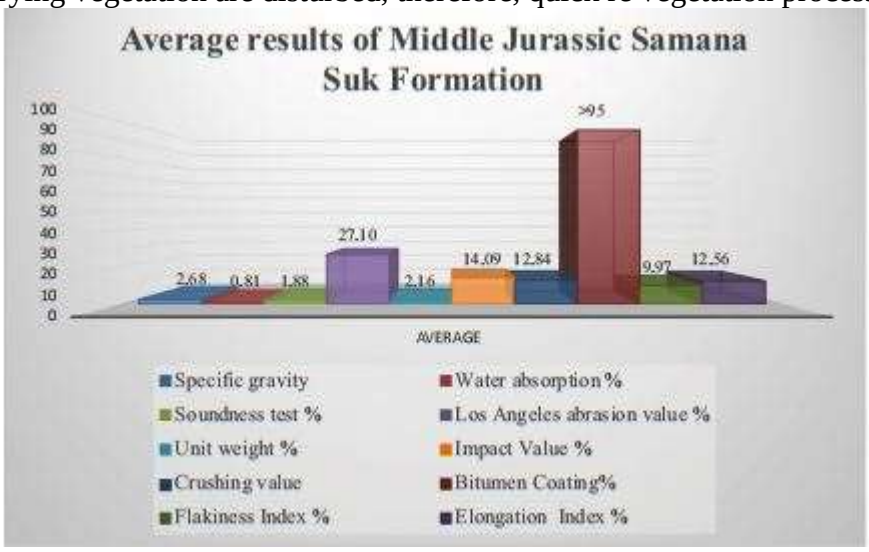

Fig 8 Average results of JSSF

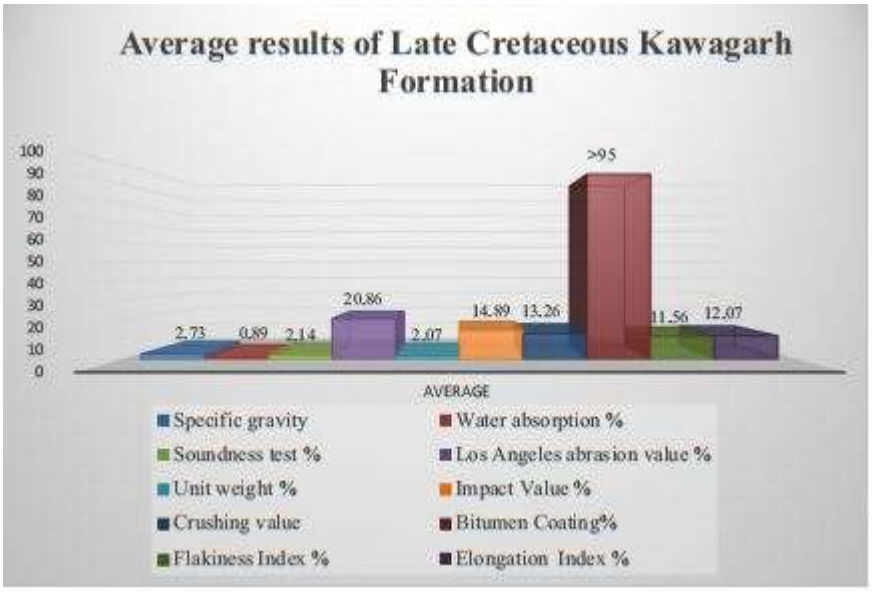

Fig 09 Average results of LCKF

Aggregate in Peshawar study shows the following conclusions;

Based on experimental data they recommended the following results

- The physical properties like bulk density and Specific gravity are upto standard.

- Loye khawar aggregate have some weak properties against soundness and other sites aggregates are within standard.
- According to test result the Los Angeles abrasion value ranges from 10-45, which fall in between standard.
- Alkali silica test results are also within range.
  - After 28 days no expansion occurred in Alkali carbonate Rock reaction.

Study of aggregates in District Mardan

- The recommendations of this research were that the Palai quarries aggregate are suitable for any construction work, but the Margalla quarries aggregate have little bit poor properties than the Palai quarries. That is why they recommended Margalla quarries aggregate for ordinary construction work.
- Despite the fact that the Maneri combination didn't be suitable for the chemical evaluation but it confirmed very decent consequences in physical and mechanical checks. Additionally, if a significant amount of water comes into contact with the concrete made from this material after construction, it may degrade.

REFERENCES

1. Chen, M., et al., *Evaluation of particle size distribution and mechanical properties of mineral waste slag as filling material.* Construction and Building Materials, 2020. **253**: p. 119183.
2. Abdullahi, M., *Effect of aggregate type on compressive strength of concrete.* International Journal of Civil and structural engineering, 2012. **2**(3): p. 782.
3. Mouhamed, B.B. and Y. Qiu, *Evaluation of physical and mechanical properties of quarry stones in the southern Republic of Benin.* Journal of Sustainable Development of Transport and Logistics, 2017. **2**(1 (2)): p. 61-66.
4. Rehman, G., et al., *The engineering assessments and potential aggregate analysis of mesozoic carbonates of Kohat Hills Range, KP, Pakistan.* Acta Geodaetica et Geophysica, 2020. **55**(3): p. 477-493.
5. Ayub, M., et al., *Engineering assessment of coarse aggregates used in Peshawar.* International Journal of Advanced Structures and Geotechnical Engineering, 2012. **1**(2): p. 61-64.
6. Malahat, F., A. Naseer, and R. Bilqees, *Engineering and Mineralogical Assessment of Coarse Aggregates used in District Mardan.* Journal of Himalayan Earth Science, 2018. **51**(1).
7. Gautam, P.K., et al., *Sustainable use of waste in flexible pavement: A review.* Construction and Building Materials, 2018. **180**: p. 239-253.
8. Sarfraz, Y., et al., *Evaluation of Physico-Mechanical Properties of Crushed Rock Aggregates: A Case Study from the Sub-Himalaya, Pakistan.* Acta Montanistica Slovaca, 2021. **26**(3).
9. Pedersen, P.J., M. Pytlikova, and N. Smith, *Selection and network effects—Migration flows into OECD countries 1990–2000.* European Economic Review, 2008. **52**(7): p. 1160-1186.

10. Muhmood, A.A.L. *Using Geotextile to Reduce the Required Thickness of Sub Base Layer of the Road and Improvement in CBR Value*. in *Journal of Physics: Conference Series*. 2021. IOP Publishing.
11. Arman, A., *Kajian Kuat Tekan Beton Normal Menggunakan Standar SNI 7656-2012 Dan ASTM C 136-06.* Rang Teknik Journal, 2018. **1**(2): p. 271221.
12. Pourtahmasb, M.S., M.R. Karim, and S. Shamshirband, *Resilient modulus prediction of asphalt mixtures containing recycled concrete aggregate using an adaptive neuro-fuzzy methodology*. Construction and Building Materials, 2015. **82**: p. 257-263.

2nd International Conference on Advances in Civil and Environmental Engineering (ICACEE-2023)

University of Engineering & Technology Taxila, Pakistan

Conference date: 22nd and 23rd February, 2023

Effects of Jute Fiber on the Mechanical Properties of Concrete

Muhammad Sudais Khan[1], Shaheed Ullah[2]

[1] [1]Capital University of Science and Technology, Sudaisbtk2@gmail.com

[2] [2]Capital University of Science and Technology, Shaheed.ullah@cust.edu.pk

ABSTRACT

Natural fibres are a great substitute since they are readily available in fibrous form and reasonably priced. Jute fibre (JTF) can be used in concrete to improve its durability and longevity. The characteristics and possible applications of various jute fibres in concrete are discussed in this paper. The fixed ratio of jute fiber is important to improve the strength of concrete. This review's major focus is on summarizing JTF's impact on concrete's fresh qualities, strength metrics. Jute fibres enhanced concrete's strength and durability but reduced its fluidity similarly to synthetic fibres. Shorter length of jute fiber has positive effect on the properties of concrete. On the endurance of fibre concrete with JTF, Jute fibre is excellent. The compressive, split tensile, and flexural characteristics of concrete reinforced with jute fibres were assessed in this study. Furthermore, The optimum JTF level in concrete is crucial since, due to a lack of fluidity, a higher dose may have a negative impact on strength and durability. Depending on the length and thickness of the jute fibres, the appropriate dose of JTF is often between 0.5% and 1%. The evaluation also focuses on the crucial data that prospective researchers would require in order to improve the characteristics of fibre concrete using JTF.

KEYWORDS: Effects of jute fibre ; Concrete Durability ; Concrete strength ; Improve Quality.

INTRODUCTION

Jute fibres are produced from annual plants, have low cost and easily availability might be thought to be a suitable component for concrete composites. The chopped jute fibre reinforcement increases the cement matrix's ability to absorb energy, converting brittle material into ductile material. Jute fibres are said to operate as crack arrestors, halt fracture propagation, and finally cause non-catastrophic failure when utilized as reinforcement material in cement or cement cementitious products. A new class of construction materials with enhanced tensile strength and flexibility has been created thanks to the use of continuous jute fibre reinforcing. The most crucial element in the enhancement of ductility and strength is the insertion of fibre reinforcement into matrices. Jute fibres have been discovered to work as reinforcing agents as a result. The kind and quantity of the fibres employed may both affect the characteristics of natural fibres as reinforcement concrete (NFRC), among other factors. The fibre content and filler used in the composite, in addition to the fibre's hydrophilic properties, can change the characteristics of NFRC. As was noted, the impact of fibre content on NFRC properties is crucial. Instead of steel fibres, several researches focus on jute fibre (JTF).[3]

Figure 3 Jute Fiber in Raw Form

PHYSICAL AND CHEMICAL PROPERTIES OF JUTE FIBERS

To enhance the mechanical and physical characteristics of cement mortar, jute fibers are used as a reinforcement component. The fibre content of the mix design was raised from 0.0 to 4.0 weight percentages (relative to cement) to make the concrete. Jute fibers were chopped into length varying from 5 to 20 mm for use as cement mortar support[1]. The composite will exhibit great strength if the jute fibre's strength is strong. The elongation a fibre displays just at highest breaking stress is referred to as break elongation. As the fibre content rises, the void content decreases the increased

compressive strength of cured jute composite may be due to the smaller void percentage and higher volume fractions[2].The highest compressive strength (measured after 28 days) was found at 2% addition of JTF, which is 20% higher than the control concrete[3]. Raw jute threads from the middle area was cut into varying lengths. The sliced reeds were carefully cleaned so eliminate the dust, loose sticks, and dirt. [13]

Table 4Physical Properties of jute fibers

Physical Properties Of Jute Fibres	**Ratios**
Specific gravity [kg/m3]	1460
Specific modulus (GPa-cm3 /g)	20.4
Specific strength (MPa-cm3 /g)	306–592
Young's modulus (GPA)	26.5
Density (g/cm3)	1.3
Elongation at breaking point (%)	7–8
Water Absorption (%)	13
Tensile strength (MPa)	393–773

Table 5 Chemical Properties of Jute Fibre

Chemical Properties Of Jute Fibres			
Name of fibre	Cellulose (wt %)	Hemi cellulose (wt %)	Lignin (wt %)
Jute Fibre	59-71.5	13.6-20.4	11.8-13

The findings of the experiments show that the raw fibre does have very low levels of Copper, Nickel, Chromium, and magnesium. This may be due to these salt solutions absorbing impurities from underground sources.[12]

FACTORS AFFECTING CHARACTERISTICS OF JUTE FIBER

Some are the factors discussed below, which effect the properties.
Fiber Geometry : The length, Cross section, Rings and Hook ends will effect the result.
Fibre form : strands, crimped, single-knotted
Surface of fiber: Either it is coating or smoothness

RESULTS AND DISCUSSION

EFFECTS OF JUTE FIBER ON CONCRETE'S PROPERTIES

Jute fibre has an effect both on natural sources and chemically modified jute fibres concrete's apparent porosity, wet and dry bulk densities, and water absorption. The experiment leads to the conclusion that UJP has relatively lower densities than normal concrete without jute fibre, whether wet and dry (RP). [9] Considering the fibre content, fibre length, and fibre type, the maximal crack width and length do not demonstrate a significant variation.[15]

WORKABILITY TEST

The workability of concrete was assessed using a slump test in accordance with IS1199-1959 to determine whether the addition of jute fibres to concrete affected its workability in any way. The control mix was able to accomplish the design slump even though the mix was supposed to slump between 50 and 75 mm. Compared to the control mix, the inclusion of fibres reduces workability, although the values are still well below the design slump limit.[10]

FLEXURAL STRENGTH

Flexural strength test was performed on specimens and illustrates the impact of the jute fiber's volume and length on the concrete rupture modulus. As can be shown, apart from the 10 mm fibre at a dosage of 0.50%, the addition of jute fibre did not improve the concrete modulus of rupture; instead, it increased by almost 6.0%.
The fracture modulus reduced for the three investigated fiber contents of 0.25, 0.5,1.00% for the fiber length of 20mm. The result also tell us regardless of the fiber ratio of 100 and 200, addition of jute fiber at a greater level of 1.00% had a negative impact on the rupture modulus.[8]

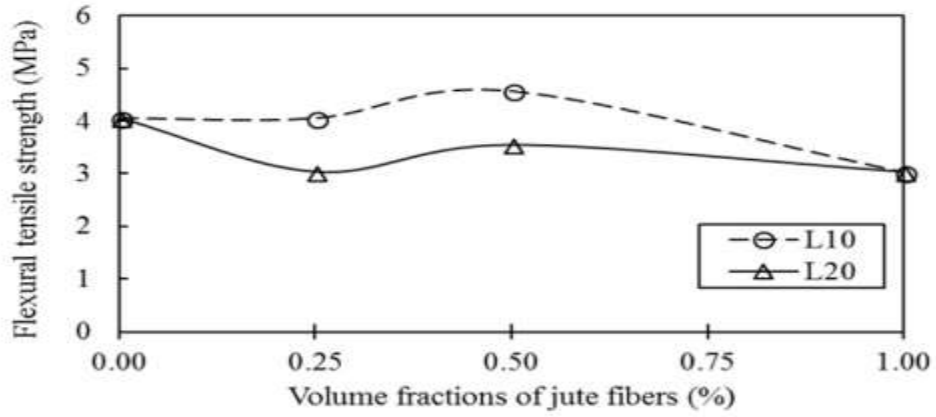

Graphs : Effect of jute fiber length and fiber content on flexural strength of concrete

TENSILE STRENGTH OF JUTE FIBER

It should be noted that the concrete composites is made up of different mix ratios of 1:2:4 and 1:1.5:3 and some various volumetric dosage of jute. The cylinders failure against tensile load for JFC was determined to have the maximum strength increment. In this instance as well, shorter fibres with less solid reinforcement develop more promisingly than longer fibres. The maximum value of improvement, 38% was attained for 10 mm jute fiber with volumetric dozing in comparison to concrete in the case of a 1:1.5:3 mix ratio, which is only 35% for 15 mm fibre and

0.10% dozing. It implies that it is also clear that jute fiber contributed a greater impact to the rise in tensile strength.

COMPRESSIVE STRENGTH

Concrete's ability to resist static loads with the potential to crush it is used to determine its compressive strength. The graphs below illustrates that jute fibre concrete's compressive strength varies according to the environment. In general, when w/c rises, so does concrete's compressive strength. Ratios of 0.35 to 0.55, fibre lengths of 6 to 18, and a range of 0.2% to 1.2% again for volume of the fibres in the concrete as a percentage of the total volume. However, as can be seen, the compressive strength reduces at 0.55 w/c ratio and used 1.2% of fibre with a length of 12 mm.[6] Using a pneumatic control press and a loading rate of 0.8 to 1.0 MPa/s, 2000 kN of force was delivered to the cubic test specimens during the compression test. [5]

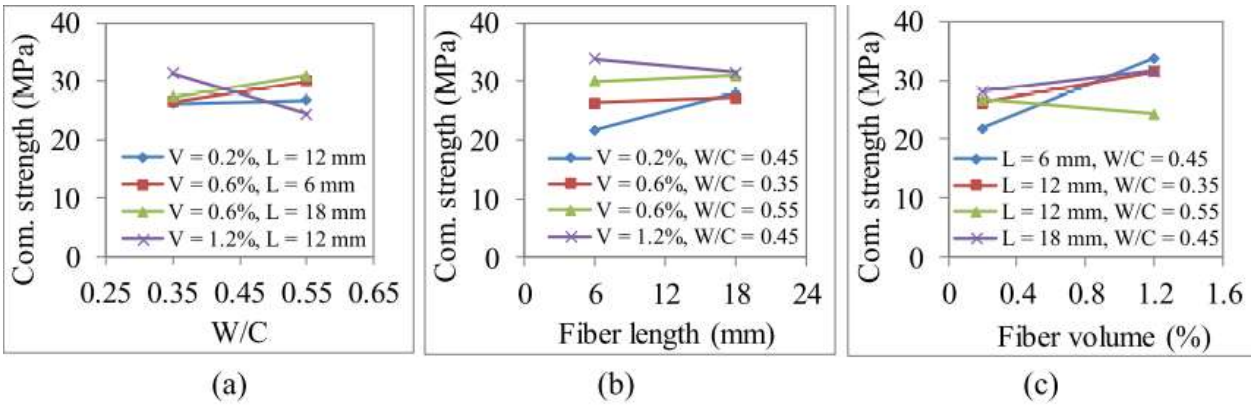

Graphs: Variation observed in Compressive Strength

CONCLUSION

- By adding Jute fibers up to 0.5% the strength of concrete was increased. But on 0.6% the strength of concrete start losses its strength.
- Workability of our designed concrete was decreases, although the values of slump are still less than the design slump limit.
- Increasing amount of 1.00% jute fibre had a detrimental effect on the rupture modulus. Jute fibre concrete have positive impact on strength and have some increments on the tensile ratio of strength.
- Compressive strength is somewhat higher for direct addition. Short fibres at high volumetric dosages result in decreased strength, but long fibres at high volumetric dosages nearly always produce balls of fibre. As the amount of jute fibre in the mix increased, the droop of freshly poured concrete reduced.

REFERENCES

[1] Hasan, R., Sobuz, M. H. R., Akid, A. S. M., Awall, M. R., Houda, M., Saha, A., ... & Sutan, N. M. (2022). Eco-friendly self-consolidating concrete production with reinforcing jute fiber. Journal of Building Engineering, 105519.

[2] Wang, H., Memon, H., AM Hassan, E., Miah, M. S., & Ali, M. A. (2019). Effect of jute fiber modification on mechanical properties of jute fiber composite. Materials, 12(8), 1226.

[3] Ahmad, J., Arbili, M. M., Majdi, A., Althoey, F., Farouk Deifalla, A., & Rahmawati, C. (2022). Performance of concrete reinforced with jute fibers (natural fibers): A review. Journal of Engineered Fibers and Fabrics, 17, 15589250221121871.

[4] Srinivas, K., Naidu, A. L., & Bahubalendruni, M. R. (2017). A review on chemical and mechanical properties of natural fiber reinforced polymer composites. International Journal of Performability Engineering, 13(2), 189.

[5] Zhang, T., Yin, Y., Gong, Y., & Wang, L. (2020). Mechanical properties of jute fiber-reinforced high-strength concrete. Structural Concrete, 21(2), 703-712.

[6] Sultana, N., Hossain, S. Z., Alam, M. S., Islam, M. S., & Al Abtah, M. A. (2020). Soft computing approaches for comparative prediction of the mechanical properties of jute fiber reinforced concrete. Advances in Engineering Software, 149, 102887.

[7] Zakaria M, Ahmed M, Hoque MM, Hannan A. Effect of jute yarn on the mechanical behavior of concrete composites. Springerplus 2015;4:1–8 https://doi.org/10.1186/s40064-015-1504-7.

[8] Islam, Mohammad S.; Ahmed, Syed Ju (2018). Influence of jute fiber on concrete properties. Construction and Building Materials, 189(), 768–776. doi:10.1016/j.conbuildmat.2018.09.048

[9] Kundu, Sarada Prasad; Chakraborty, Sumit; Chakraborty, Subrata (2018). Effectiveness of the surface modified jute fibre as fibre reinforcement in controlling the physical and mechanical properties of concrete paver blocks. Construction and Building Materials, 191(), 554–563. doi:10.1016/j.conbuildmat.2018.10.045

[10] urugan R B, Gayke A, C N, M.K H G M. K P.. Influence of treated natural jute fiber on flexural properties of reinforced concrete beams. Int. J. Eng. Technol. 2018;7:148 https://doi.org/10.14419/ijet.v7i3.12.15906

[11] Zakaria, Mohammad; Ahmed, Mashud; Hoque, Mozammel; Shaid, Abu (2018). A Comparative Study of the Mechanical Properties of Jute Fiber and Yarn Reinforced Concrete Composites. Journal of Natural Fibers, (), 1–12. doi:10.1080/15440478.2018.1525465

[12] Alamgir, M., H. Monimul, I. Rabiul, and S. B. Quraishi. 2008. Studies on metal complex of various substituted benzenediazonium salts treated jute fiber. Journal of Natural Fibers 5 (2):148–53. AS 1012. 2002. Compressive test of concrete specimen, Standards Australia.

[13] Ashis Kumar, S., B. Gautam, and G. Premamoy. 2008. Structural features of glycol and acrylamide treated jute fiber. Journal of Natural Fibers 5 (4):444–60.

[14] B. Adhikari, S.B. Majumder, R. Sen, R.K. Basak, S.P. Kundu, S. Chakraborty, A.Roy, Development of jute fiber reinforced cement concrete composites.Technical Project, Project No: JMDC/JTM/MM-IV/7.1/2008, 2011, Materials Science Centre, Indian Institute of Technology, Kharagpur, India. www.jute.com/documents/10437/0/.../971388b6-640a-44db-8465-bea71f9244a4

[15] G. Ramakrishna; T. Sundararajan (2005). Impact strength of a few natural fibre reinforced cement mortar slabs: a comparative study. , 27(5), 547–553. doi:10.1016/j.cemconcomp.2004.09.006

2nd International Conference on Advances in Civil and Environmental Engineering (ICACEE-2023)

University of Engineering & Technology Taxila, Pakistan

Conference date: 22nd and 23rd February, 2023

Numerical Investigation of Fibre Reinforced Compressed Earth Blocks

Salman Javed[1], Dr. Muhammad Ali[2], Dr. Afaq Ahmad[3]
[1]Civil Engineering Department, UET Taxila, Salmanwaraich@yahoo.com
[2] School of Civil Engineering and Surveying, University of Portsmouth UK
Muhammad.Ali@port.ac.uk
[3] Civil Engineering Department, UET Taxila, afaq.ahmad@uettaxila.edu.pk

ABSTRACT

Compressed earthen blocks (CEBs) are sustainable building material that is made up of soil and fibers that is compressed mechanically in a machine. These are cost-effective and environmentally friendly alternatives to traditional burnt bricks. CEBs are a basic need of today's era because they can help to reduce the environmental impact of construction and also provide a durable and affordable building material that can be used in a variety of applications. In this study, numerical analysis of the experimental observations of CEBs is performed. Numerical validation of experimental work is necessary to ensure that results obtained from the experiments can be accurately modelled and predicted using mathematical equations. This helps to confirm that the experimental setup and procedures were conducted accurately and results are valid. This work examines the stress vs. strain properties of compressive-loaded CEBs. The three-dimensional macro modelling approach and concrete damage plasticity model are used to calibrate parameters based on the homogenous material for the CEBs. In this numerical approach, the Monte-Carlo simulation is carried out using Simulia-Isight, the data matching component in the optimization module used to reduce the computational cost, and the analysis is performed on ABAQUS. In terms of stress vs. strain response, the numerical analysis results were accurately matched with experimental results. Parametric analysis for CEBs is performed for the parameters like dilation angle, and mesh sensitivity, it was found that viscosity and the dilation angle have a much greater influence on the outcomes than the other parameters. The displacement analysis approach is used and the value obtained at the peak displacement of 3.15mm was 6.85Mpa for compression loading of CEBs which is same as the experimental result, while the variation of the parameters is also included in the paper. A numerical equation is developed for potential future modelling.

KEYWORDS: Compressed Earthen Blocks (CEBs), Finite Element Analyses, Abaqus, Simulia-Isight.

INTRODUCTION

Masonry is a composite material that consists of bricks and mortar. The cost increases with each unit of brick used in the masonry structure; nowadays, masonry has become very costly, and there is a need to introduce alternative economical materials [1][2]. Moulding of standard burnt bricks has a lot of devastating effects on the environment because of the manufacturing process and carbon dioxide emission. [3]. For commercial utilization of the CEBs properties of the basic

compressed earth blocks units and their effect on the whole structure need to be analysed. By using the results of CEBs from experimental observations, and then the addition of the geometric details in the finite element analysis, it is possible to check the performance of the brick masonry structures [1][4]. Various studies have been performed in the brick masonry structures, such as the study by Pandey, in which the equivalent elastic module block masonry was studied, assuming that no slippage occurred between the mortar layer in the brick unit [5].

Using CEBs not only reduces the cost of the structure but also has a good impact on the energy consumption in the manufacturing process, and building consumes more than 30% of primary energy to maintain the inside temperature, which varies due to heating and cooling losses [5][6]. This energy consumption has increased dramatically over the last few years due to the population spending more time indoors, drastic climate changes, and no use of energy-efficient building materials [7].

This current study was performed with the conversion of the clay into compressed blocks [8]. The enhancement of the strength and characteristics must be checked due to the addition of hybrid fibers. So, this enhancement is studied in this research work with the fiber-reinforced compressed earthen blocks the composition of blocks has some effects on the compression strength as well as improves the flexible performance of the bricks, research has been performed in this era due to the increase of material's flexibility [9]. This research investigates the finite element analysis of fiber-reinforced compressed earthen blocks their experimental work has already been performed, and its results are used in this study, and parametric sensitivity analysis of dilation angle, meshing is performed to validate the numerical results with experimental outcomes by using the traditional finite element analyses software ABAQUS.

NUMERICAL ANALYSES

The numerical analysis was carried out using eight-node brick elements for CEBs and steel plates which are discretized into various numbers of elements, mentioned in the mesh sensitivity analysis. CEBs and steel plates are represented as a macro model, so each model is represented as a solid compression model for the solid element. Concrete Damage Plasticity (CDP) is used for the materials and the initial stiffness is adjusted after the completion of the Monte Carlo simulation using the Simulia-Isight tool and numerical analysis executed by using commercially available software ABAQUS. In this paper, compressive load simulation is shown only but this behavior is enough for validation of both compression and tensile strength of compressed earthen blocks as material defined in Abaqus has shown an excellent response in both cases. The material initial stiffness adjustment is shown in figure 1.

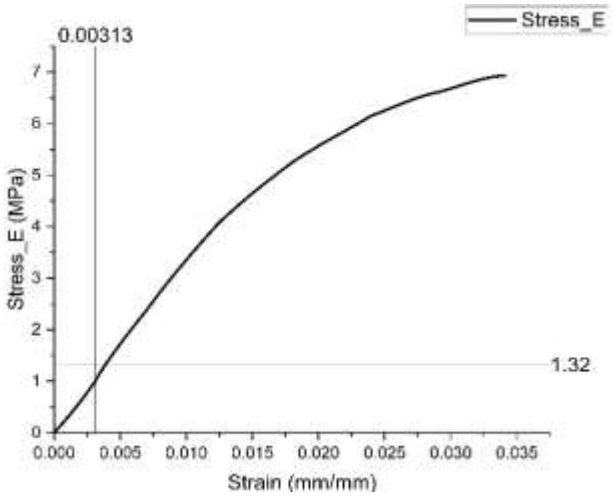

Figure 1: Consideration of Modulus of Elasticity using Origin-Pro for Input Material in ABAQUS

The earthen block is placed between the two steel bearing plates having 20mm thickness, and an interface was defined with tangential and normal behavior, the coefficient of fraction was 0.3. The concrete damage plasticity approach is adapted after calibrating the parameter using Monte-Carlo simulation, for which the mapping is shown in **Error! Reference source not found.**. T he fixity was assigned at the bottom plate in which all six degrees of freedom are restrained, displacement boundary condition was defined at the top plate and rotation is not restrained. Displacement-based analysis was performed so that the load applied in the shape of displacement which was 3.15mm. Reference points at the top and bottom were included in the sets for getting the stress-strain curves. Finally, results were obtained. The whole assembly with the loading and boundary conditions is shown in Figure 2.

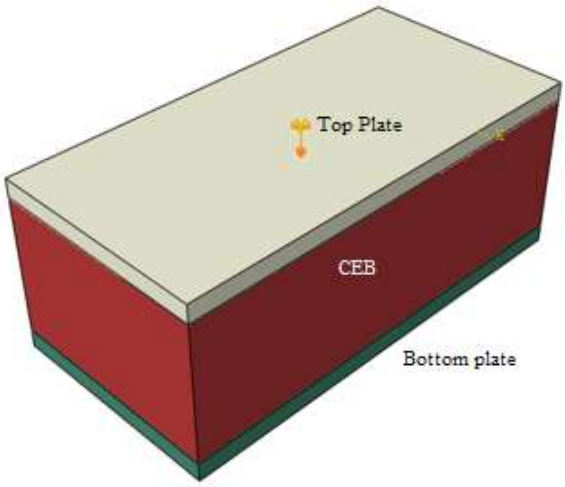

Figure 2: Assembly of Compressed Earth Block with Steel plate on top and bottom

The mesh sensitivity analysis is a key process for the authenticity of the finite element study. So mesh sensitive analysis was performed for 10, 15, 20, 30, 40, and 50-mm seed ratios. The results are checked by looking at this seed ratio from 50 to 40, 40 to 30, 30 to 20, 20 to 15, and finally from 15 to 10 mm seed ratio, the effect of variation of stresses reducing from larger size to smaller size.

This is a dominant phenomenon by reducing the seed ratio, the stress variations are reduced and then further reduction in mesh size doesn't affect stress variations. By increasing the number of elements, forces resulted in smooth behavior and tend to close. Mesh sensitivity analysis is performed, as shown in 3.

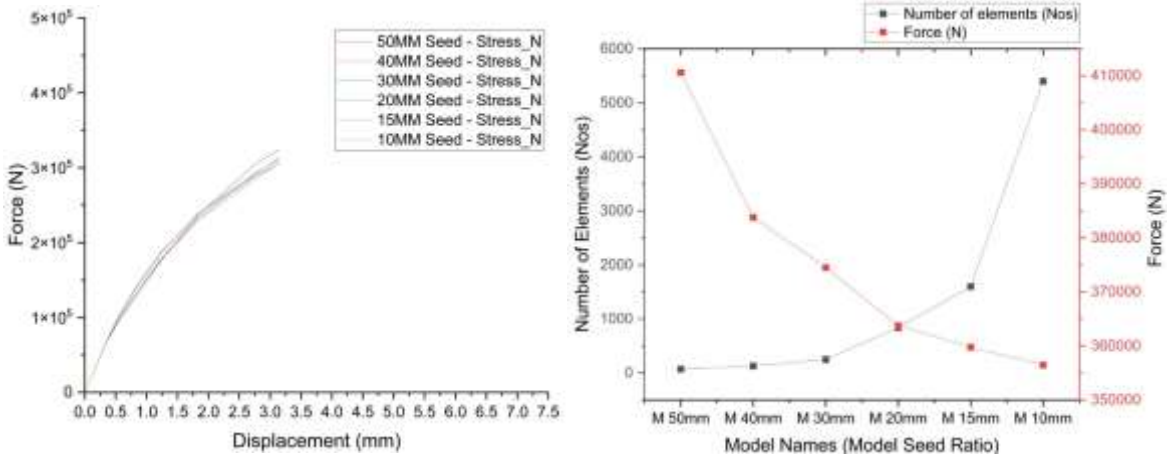

Figure 3: Mesh Sensitivity Analyses for the Solid Block

A dilation angle study was performed in which values are used from 55 to 30 degrees, it is concluded that reduction in dilation angle, the curves show smooth behavior and tend to close as shown in figure 4.

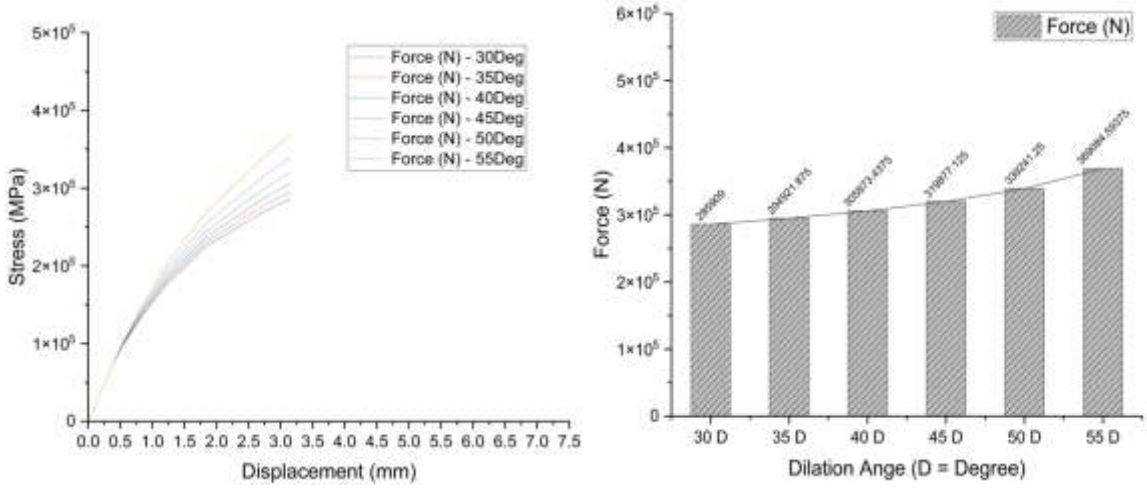

Figure 4: Effect of Dilation angle

RESULTS

After completing the simulation, various parameters were obtained. The stress vs. displacement curve is included in this study. This simulation includes an equivalent plastic strain, failure, and stress versus strain calibration. Variation exists in the numerical study in comparison to the experimental study after the initial stiffness reduction in the model, which is obvious in the comparison curve of stress versus strain as shown in figure 5.

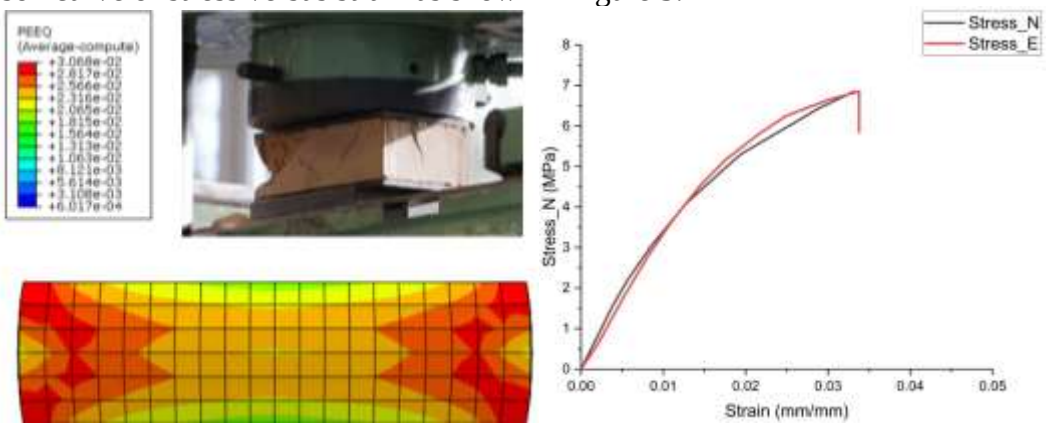

Figure 5: Deformation obtained after simulation in ABAQUS

As compressed earthen block is brittle material, Post peak behavior is not considered in this research because it is not found in the past studies due to high computational cost. It is observed that the stresses have been consistently matching close to the experimental results. A numerical equation is also predicted with the performance of the stress vs strain behavior by using the statistical approach of curve fitting in Origin-pro software as shown in figure 6.

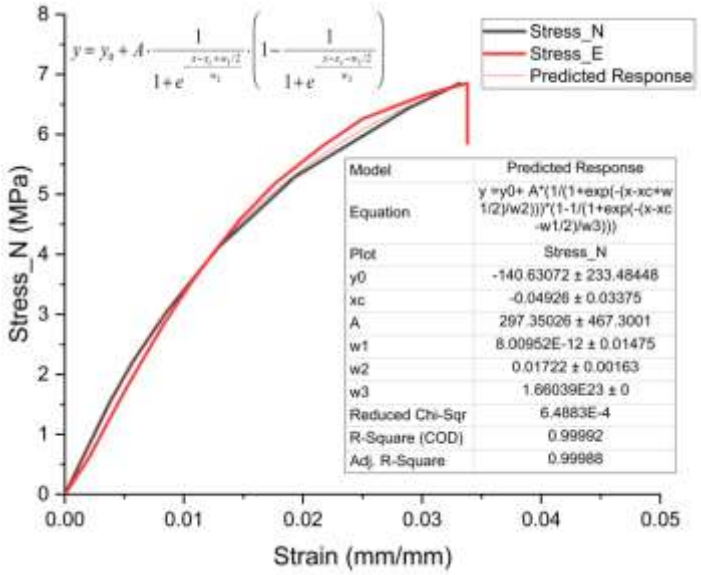

Figure 6: Prediction of Numerical Equation

CONCLUSION AND RECOMMENDATIONS

This study performed a simulation to overcome validation issues and made several conclusions. The experimental and numerical result for the peak stress of 6.58Mpa is almost similar hence a good result is obtained. The equivalent plastic strain was used to show the performance of damage in the model, Damage in compression and tension was neglected due to numerical instability. Stiffness was reduced and deviation occurred between experimental and numerical work with increased loading. The dilation angle was found to have a larger magnitude for larger stiffness and vice versa. The parametric study of the dilation angle mesh sensitivity analysis showed that the change in the result is obvious by reducing the dilation angle and mesh size from 55 to 30 degrees and 50 to 10mm respectively, the stress variations are reduced and then further reduction doesn't affect stress variations, hence It is recommended to use a smaller dilation angle and smaller mesh size for accurate displacement-based approach and to first use Monte-Carlo simulation for reduction of stiffness and computational cost.

ACKNOWLEDGEMENTS

This research work is done in collaboration with Professor Dr. MUHAMMAD ALI and Professor Dr. Afaq Ahmad. I am sincerely thankful to my supervisor, Dr. Afaq Ahmad for his assistance and supervision, which makes this research possible. All the data presented in this research work is original and accurate.

REFERENCES

[1] P. Foraboschi, "Masonry does not limit itself to only one structural material: Interlocked masonry versus cohesive masonry," *J. Build. Eng.*, vol. 26, p. 100831, Nov. 2019, doi: 10.1016/J.JOBE.2019.100831.

[2] A. Almssad, A. Almusaed, and R. Z. Homod, "Masonry in the Context of Sustainable Buildings: A Review of the Brick Role in Architecture," *Sustain. 2022, Vol. 14, Page 14734*, vol. 14, no. 22, p. 14734, Nov. 2022, doi: 10.3390/SU142214734.

[3] M. W. Khan, Y. Ali, F. De Felice, A. Salman, and A. Petrillo, "Impact of brick kilns industry on the environment and human health in Pakistan," *Sci. Total Environ.*, vol. 678, pp. 383–389, Aug. 2019, doi: 10.1016/J.SCITOTENV.2019.04.369.

[4] C. Chisari, L. Macorini, C. Amadio, and B. A. Izzuddin, "Identification of mesoscale model parameters for brick-masonry," *Int. J. Solids Struct.*, vol. 146, pp. 224–240, Aug. 2018, doi: 10.1016/J.IJSOLSTR.2018.04.003.

[5] S. Mollaei, R. Babaei Ghazijahani, E. Noroozinejad Farsangi, and D. Jahani, "Investigation of Behavior of Masonry Walls Constructed with Autoclaved Aerated Concrete Blocks under Blast Loading," *Appl. Sci. 2022, Vol. 12, Page 8725*, vol. 12, no. 17, p. 8725, Aug. 2022, doi: 10.3390/APP12178725.

[6] M. Ridwan, I. Yoshitake, and A. Y. Nassif, "Proposal of Design Formulae for Equivalent Elasticity of Masonry Structures Made with Bricks of Low Modulus," *Adv. Civ. Eng.*, vol. 2017, 2017, doi: 10.1155/2017/6456070.

[7] M. Santamouris and K. Vasilakopoulou, "Present and future energy consumption of buildings: Challenges and opportunities towards decarbonisation," *e-Prime - Adv. Electr. Eng. Electron. Energy*, vol. 1, p. 100002, Jan. 2021, doi: 10.1016/J.PRIME.2021.100002.

[8] F. V. Riza and I. A. Rahman, "The properties of compressed earth-based (CEB) masonry blocks," *Eco-efficient Mason. Bricks Blocks Des. Prop. Durab.*, pp. 379–392, 2015, doi: 10.1016/B978-1-78242-305-8.00017-6.

[9] M. El-Emam and A. Al-Tamimi, "Strength and Deformation Characteristics of Dune Sand Earth Blocks Reinforced with Natural and Polymeric Fibers," *Sustain. 2022, Vol. 14, Page 4850*, vol. 14, no. 8, p. 4850, Apr. 2022, doi: 10.3390/SU14084850.

[10] A. Al-fakih and M. A. Al-osta, "Finite Element Analysis of Rubberized Concrete Interlocking Masonry under Vertical Loading," *Materials (Basel).*, vol. 15, no. 8, Apr. 2022, doi: 10.3390/MA15082858.

[11] K. M. Mathisen, "Finite element modelling of structural mechanics problems," pp. 1–42, 2012.

2nd International Conference on Advances in Civil and Environmental Engineering (ICACEE-2023)

University of Engineering & Technology Taxila, Pakistan

Conference date: 22nd and 23rd February, 2023

Investigation of Shear Strength of RC Beams using Combination of Industrial Waste Steel Chips and Wire Mesh

Hasnain Kazam[1], Saqib Mehboob[2]

[1]University of Engineering and Technology Taxila, hasnainkazam828@gmail.com

[2] University of Engineering and Technology Taxila, syed.saqib@uettaxila.edu.pk

ABSTRACT

This work deals with the shear behaviour of reinforced concrete beams using steel chips and varying wire mesh width. The shear test was carried out on 6"×6"×36" beam samples to investigate the shear strength, cracks pattern and failure mode. The steel chips were selected as 0.9% weight of concrete mix, and the eight sets of specimens containing one sample with no mesh and others with 0.5", 1", 1.5", 2", 2.5", 3", 3.5" wide strips of wire mesh were used in this study. The addition of steel chips increases the shear behaviour of concrete beams, which is common in all the samples. Steel chips increased the shear strength to some extent due to better interlocking of concrete constituents. Using wire mesh as shear reinforcement distributes the stresses to the entire cross-section. With the addition of wire mesh, Diagonal cracks were observed on the beam's surface differently than in conventional concrete. The number of cracks increased by increasing the wire mesh width, whereas the crack width decreased by increasing the mesh width.

KEYWORDS: Steel Chips, Wire Mesh, Shear Strength, Crack Pattern

INTRODUCTION

Recent developments in materials and production methods in the field of construction have increased. One of these developments is the introduction of steel fibres into the concrete mix for various applications. Although the use of Steel fibres/Chips has been around for quite a while, e.g., the Romans used straw fibres in clay to improve the properties of bricks, in the early 1960s, steel fibre-reinforced concrete was developed [1]. After that, numerous studies were conducted to assess and identify further applications for steel fibre-reinforced concrete.

Using steel fibers into the concrete mix may be effective in increasing the shear properties of concrete beams. As the shear failure is catastrophic and fails without warning, so it is desirable that the beam should fails in flexure than in shear [1]. Many existing reinforced concrete beams need to be repaired because they lack shear strength. The deficiencies in shear occur due to several reasons, i.e. lack of shear reinforcement, insufficient steel area due to corrosion, increased loading and construction defects. Using steel fibres in concrete may be effective in enhancing the shear properties of concrete beams.

Waste steel scrap collected from the Hitech Manufacturing and Machine Building Industry, which specialises in producing spare parts and machines utilised by the military, was used. The waste steel chips/scrap collected from the industry was brought to the laboratory. Large strands were cut into short pieces before mixing. The corrosion effect after mixing was not taken into consideration but used steel chips were not corroded during the storage period.

Werkina [2] published a paper on waste metal steel scrap in increasing the strength of concrete. Author uses different percentages of steel scrap (i.e. 0%, 0.5%, 0.75%, and 1.5%) by the weight of the concrete mix. After testing, it was concluded that an increment of 26.8% was observed at 0.5%, 30.7% at 0.75% and a decrease of 5.3% was observed at 1.5%. Similarly, Gabule [1] used steel Chips (waste metal) to increase the shear strength of concrete beams and identify at what specific percentages the steel chips make a significant increase in the shear strength of concrete beams. Athor uses five different percentages (0%, 0.5%,1%, 1.5% and 2%) of steel chips to check the behaviour of steel chips. The test results show a decrease of -14.19% at 0.5%, -8.99% at 1.5%, and -13.15% at 2% and an increase of 9.83% was observed at 1% steel chips. Author further concluded that the growth of one large crack was divided into multiple short cracks by implying the redistribution of stresses within the core zone of the beam. Furthermore, author concluded in his research that using 0.9% steel chips by weight of concrete mix will yield optimum shear strength. Atlaoui et al. [3] conducted a study on the mechanical behaviour by shear test in which the elements of concrete beams reinforced with fibres were added. The chip material was collected from the machine waste. Three fibre contents 0%, 0.6% and 0.8% were selected for this study. The comparison of these outcomes reveals that the chip fibres significantly increase the material's ductility after the concrete cracks. Additionally, the fibres employed reduce diagonal shear cracks and increase strength and rigidity.

Noor [4] used wire mesh and steel stirrups of the same weight on different beams, and after testing, the author concluded that wire mesh shear reinforcement gives better results than stirrups alone. Author explains that the crack distribution in beams was significantly affected by beam samples. Moreover, wire mesh provides a more bonded area in concrete samples than stirrups. So the cracks formed were large in number and more closely spaced. Shehu [5] used wire mesh as core zone reinforcement in his studies and presented that the welded wire mesh was placed at 160mm (designed to be failed in shear) spacing. The beam designed in flexure also failed in shear first and then in flexure. Authors concluded in his research that only a 3% increase in shear strength was observed. The increased resistance to diagonal tension cracks offered by the core zone transverse reinforcement in the form of welded wire mesh is responsible for the increase in the shear. Elavarasi et al. [6] used wire mesh and stirrups in different combinations. The wire mesh used was equivalent to the weight of stirrups. Authors concluded in research that using wire mesh enhances the shear performance and bearing capacity. Moreover, beams with wire mesh and combination of both give more cracks than the stirrups. Raiyani et al. [7] used wire mesh on the cross-section of T shape beam. Based on the test result, authors recommended using steel mesh as a shear improvement of concrete beams. Authors concluded that using stainless steel effectively enhances the shear strength by an ultimate load of 50.54% compared with the control specimen. Yuan et al. [8] discuss the shear capacity of eco-friendly high-strength concrete (HSC) beams

reinforced with 0.75% (by volume) hooked steel fibres or shear stirrups of varying spacing. The shear capacity, failure mode, and crack patterns of five large-scale HSC beams with steel fibres or stirrups were tested and investigated. When 0.75% volume steel fibres were used in place of minimum shear reinforcement for the HSC beam, the shear strength increased by approximately 13.2%. Al-Rousan [9] worked on the heat damaged shear deficient RC beams to improve their shear behaviour. Author used wire mesh wrapping on both sides at the 1/3rd potions as to increase the shear performance of concrete beams. It was concluded that the shear cracks developed in the web show a different behaviour, and the load-carrying capacity significantly increases on increasing the layers of wire mesh. The use of welded wire mesh reinforced internally, effectively increases the shear performance and stiffness of concrete beams. Al-Bazoon et al. [10] used wire mesh (used as vertical strip, inclined strip, U-jacketing) and stirrups in two different types of beams. The U-jacketing mesh has a higher effect, increasing the shear capacity between 33.4 and 95.9% and the shear ductility index by 23% relative to the reference specimens.

The Objectives of this research were to check the behaviour of Steel Chips and wire mesh as a shear strength enhancement of concrete beams and also the contribution of mesh strip width on increasing the shear strength of beams.

METHODOLOGY OF RESEARCH

Eight Sets of specimens, namely sets A, B, C, D, E, F, G and H, were cast, containing three samples per set. Set A was treated as a controlled specimen having no wire mesh, while Set B, C, D, E, F, G and H contain 0.5",1",1.5",2",2.5",3" and 3.5" respectively wide strips of wire mesh. Three stirrups in each beam were used for holding and placing the longitudinal bars in the exact position. All the twenty-four beams and 3 cylinder samples were cast with the same steel chips with a ratio of 0.9% and varying mesh width. For the uniform distribution of steel chips throughout the beam, the concrete mix of three samples was separated and then mixed with the ratio of the respective chip. The beam dimensions are 6"×6"×36". All the reinforced concrete beams are cast with Class A mix 1:2:4 [1].

After 24 hours, the beams are removed from the moulds and left in the curing tank for 28 days. On completion of the curing period, beam samples were removed from the tank and shifted to the laboratory. The cylinder samples undergo compression test, and the beam samples for point load test in the Universal Testing Machine.

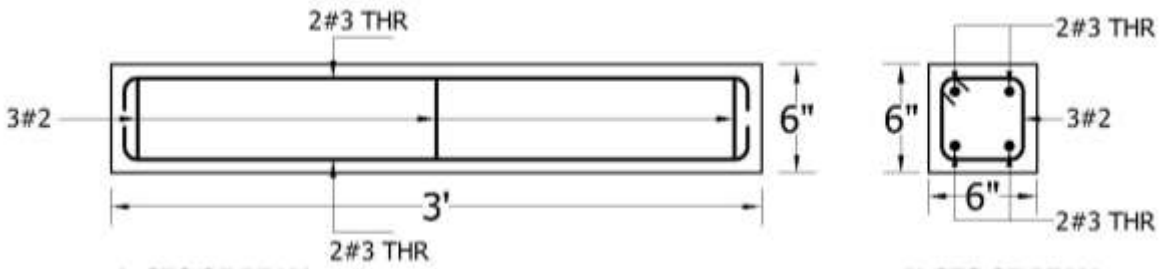

Figure 4: Typical Cross Section of Beam

(a) ***(b)***

Figure 5: ***(a)****1.5"Wide Mesh Strip* ***(b)****Actual Laboratory Test Setup*

RESULTS AND DISCUSSION

Table 6: Shear Strength of Concrete Beams

Sr. No.	Description	Shear Force (KN)				Difference with Set A	% Age Difference
		Trial 01	Trial 02	Trial 03	Mean		
1	Set A	46.0	44.0	45.5	45.17	0.00	0.00
2	Set B	50.0	51.5	52.0	51.17	6.00	13.28
3	Set C	53.0	56.5	56.5	55.33	4.17	22.51
4	Set D	59.0	58.5	60.2	59.23	3.90	31.14
5	Set E	65.5	68.5	64.5	66.17	6.93	46.49
6	Set F	69.0	72.5	69.0	70.33	4.17	55.72
7	Set G	76.5	74.0	75.5	75.33	5.00	66.79
8	Set H	79.5	81.0	81.5	80.67	5.33	78.60

As shown in table mean of set A is 45.17 KN which is the result of 0.9% of steel shavings as per the results concluded by Gabule 2020. Set B gives 51.17 KN which is the increased shear strength than that of Set A, and the percentage difference shows 13.28% higher results. Set C contains 55.33 KN, which increases the shear strength by 22.51 % more than that of Set A. Similarly, the Shear strength of Set D is 59.23 KN, which is 31.14% higher than that of the control Specimen. Shear results of Set E give 66.17 KN, which gives 46.49% good results compared with that of Set A. Similarly, Set F, G and H contain 70.33, 75.33 and 80.67 KN, which gives percentage difference in the strength as 55.72%, 66.79% and 78.60% respectively. The beams tested in the laboratory failed in both shear and flexure.

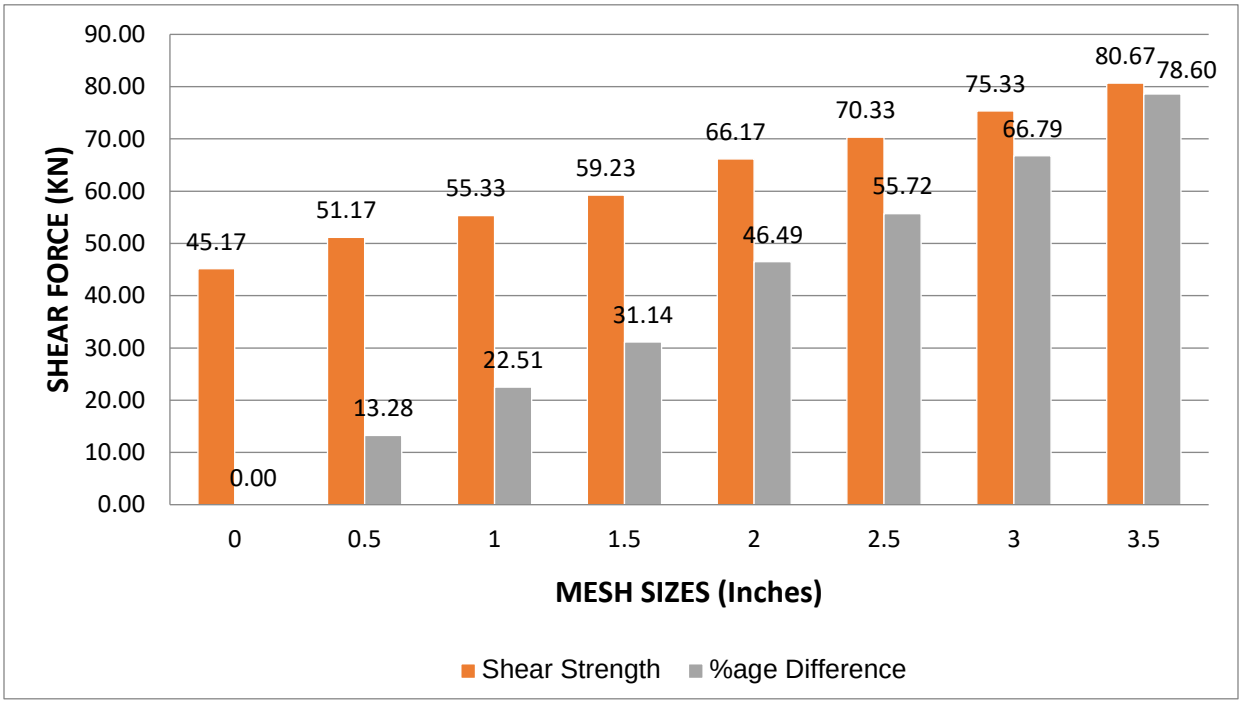

Figure 6: Comparison of Shear Strengtsh and Percentage Difference

Figure 3 compares the actual shear strength and the percentage difference. By increasing the size of the mesh width, the shear strength increases gradually and the percentage difference increases. The wire mesh provides a more bonded area than conventional stirrups. As a result of this, significant stresses are divided throughout the section. The shear strength percentage difference of Set E with the initial set is 15.35, which is more significant among all other sets.

CONCLUSION

- The test results show a percentage increase of 13.28, 22.51, 31.14, 46.49, 55.72, 66.79 and 78.60, respectively, indicating that using wire mesh is effective for increment in shear strength.
- The greater width of mesh used results in greater shear strength. These are the results of a single wrap of wire mesh which are very efficient. If we increase the number of wraps, the shear strength may increase with the higher percentages.
- The increase in shear strength will be due to the increase in shear reinforcement. One wrap of 3.5" wide-strip results in an increment of 78.60% of shear strength, almost double that of the control specimen.
- On increasing the width of the wire mesh strip, the number of cracks increases. At the same time, the width of cracks decreases by increasing the wire mesh strip width.
- The wire mesh is readily available and easily cut into desired shapes and sizes. In short, using the wire mesh provides better results than conventional stirrups.

This discussion concluded that using wire mesh effectively enhances the shear performance and may give better results using U-shaped wrapping throughout the shear zone.

FUTURE RECOMMENDATION

Based on the conclusion of the research, the following recommendations are made;

- Further studies should also be made by increasing the strip width and number of mesh layers instead of single wrap.
- Further studies should also be conducted to compare the results of wrapping of wire mesh and the conventional steel shear reinforcement.
- A study should also be made by the introduction of wire mesh and steel chips at percentages other than those used in this study and into the fresh concrete mix at proportions other than Class A mix 1:2:4.
- Cost comparison of the wire mesh and steel chips with the conventional steel should also be investigated.

ACKNOWLEDGEMENTS

The authors are thankful to the Civil Engineering Department UET Taxila for providing Laboratory support and technical assistance during the lab testing phase of this research work.

REFERENCES

1. Genevieve Gabule, *Steel Chips as Shear Capacity Enhancer of Reinforced-Concrete Beams.* MINDAyawan Journal of Culture and Society, 2009. **3**.
2. Yohannes Werkina, *Experimental study of the effect of waste steel scrap as reinforcing material on the mechanical properties of concrete.* Case Studies in Construction Materials, 2021. **14**.
3. Djamal Atlaoui and Youcef Bouafia, *Experimental Characterization of the Shear Behavior of Fiber Reinforced Concrete Beam Elements in Chips.* International Scholarly and Scientific Research & Innovation 2020. **14**: p. 296-299.
4. K. K. Ghosh and M. Mukhopadhyay, *Wire mesh as shear reinforcement in concrete.* Proc. Ins & Civ. Engrs, Part 2, 1978, Discussion 8003: p. 455-461.
5. D. Rama Seshu, et al., *A novel means of improving the performance of reinforced concrete beams using the welded wire mesh as core zone reinforcement.* Asian Journal of Civil Engineering, 2020. **21**(6): p. 959-965.
6. Elavarasi D and Sumathi A, *Behaviour of Reinforced Concrete Beams with Wire Mesh As Shear Reinforcement.* International Journal of Innovative Technology and Exploring Engineering (IJITEE), 2019. **8**(12): p. 781-784.
7. Sunil D. Raiyani and Paresh V. Patel, *Effectiveness of stainless steel wire mesh in shear strengthening of reinforced concrete flanged beam.* Int. J. Structural Engineering, 2020. **10**: p. 195-216.

8. Tian-Feng Yuan, et al., *Shear Capacity Contribution of Steel Fiber Reinforced High-Strength Concrete Compared with and without Stirrup.* International Journal of Concrete Structures and Materials, 2020. **14**.
9. Al-Rousan, R.Z., *The behavior of heated damaged shear-deficient RC beams reinforced internally with welded wire mesh.* Case Studies in Construction Materials, 2021.
10. Mustafa Al-Bazoon, et al., *Shear Strengthening of Reinforced Concrete Beam Using Wire Mesh–Epoxy Composite.* Civil Engineering Journal, 2022. **8**.

2nd International Conference on Advances in Civil and Environmental Engineering (ICACEE-2023)

University of Engineering & Technology Taxila, Pakistan

Conference date: 22nd and 23rd February, 2023

Impact of Artificial and Natural Fibre Hybridization on Properties of Fresh Concrete

Arsalan Amjid[1], Majid Ali[2]

[1] Capital University of Science and Technology, Islamabad, Pakistan.
Email: arsalan.amjid@cust.edu.pk

[2] Capital University of Science and Technology, Islamabad, Pakistan.
Email: majid.ali@cust.edu.pk

ABSTRACT

The investigation of the fresh properties of concrete under the presence of jute and nylon as hybrid fibres is the main subject of this paper. In this investigation, jute and nylon fibres were used in equal proportions for the preparation of fresh concrete. To obtain a strength of 30 MPa, a single concrete mix ratio was established, and tests on the properties of fresh concrete, including slump, compacting factor, and fresh density, were carried out. The findings showed that adding nylon and jute fibres changed the characteristics of fresh concrete. Incorporating 2.5% nylon fibre and 2.5% jute fibre led to a slump reduction of 11% in comparison to plain concrete with the same design mix ratio. Jute and nylon fibers are selected based on the easy availability and for the sustainable approach. These fibers are selected on the basis of their property to resist the formation and propagation of cracks with the enhancement of tensile strength. These fibers may help for bridging micro as well as macro-cracks and they may provide good physical properties as investigated by previous researchers. This study will provide a wide-ranging assessment of the properties of plain concrete (PC) and concrete having jute and nylon as hybrid fiber, which can be helpful in production of high performance and eco-friendly concrete for pavement construction applications.

KEYWORDS: Jute Fibre, Nylon Fibre, Compaction Factor, Slump Test

INTRODUCTION

Structures made of concrete deteriorate under freeze-thaw conditions. Day and night temperature variations in cold regions can harm solid materials like concrete. Water expands when freezing, increasing volume by up to 9% of the total volume. Although roads are used as a means of transportation, they can suffer damage in cold climates owing to temperature changes. The average life span, functionality, and strength of pavement are compromised as a result of damages and cracks induced by temperature variations. Water seeps into the pavements through leak joints and pavement fractures as the pavements thaw. Water that had penetrated the rigid pavement at the freezing stage froze, which led to expansion. This causes cracks to emerge in rigid pavement and degrades the pavement strength. Mass loss and changes in mechanical and dynamic properties are brought on by freeze-thaw cycles. Because of temperature variations, freeze-thaw is one of the main factors that reduces the durability of concrete pavement [1].

When concrete pavements are subjected to freeze-thaw cycles, loss in mass increases and relative dynamic modulus of elasticity decreases [2]. Adkins et al. [3] investigated the effects of water during freeze-thaw conditions on concrete pavements. It was determined after carrying out the experimental procedures that water was the main cause of cracks and other problems in concrete under freeze-thaw conditions. The lifespan, serviceability, durability, and strength of pavements under freeze-thaw conditions were also found to be significantly reduced by water.

Concrete is a brittle material with low strain capacity and low toughness. Owing to the fact of having low tensile strength, it becomes vulnerable towards amalgamation in micro-cracking. In an experimental study it was revealed that the resistance against impact loading significantly improved by the addition of agricultural waste natural fibers in concrete. The mechanical properties of concrete were observed to be improved by introducing short discrete fibers in concrete. Previous studies indicated that properties of concrete can be enhanced by addition of natural fibers. In this way, performance of structures can also be enhanced. This work may contribute for understanding the hybridization of agricultural wastes. The use of these agricultural wastes as sustainable construction materials to minimize the ecological effects of concrete and the harmful impacts of these agricultural wastes if not disposed properly. This study may also contribute to counter the flaws of concrete by using these agricultural wastes after hybridization process.

EXPERIMENTAL PROCEDURE

Raw Materials

Fine aggregate, Ordinary Portland cement, and 3/4" down coarse aggregate are used to prepare plain cement concrete (PCC). The same materials are mixed with 50 mm long jute and nylon fibers to produce hybrid fibre reinforced concrete (HFRC). Whereas, subject of discussion is the length of fibre. Fibers shouldn't be so short that one side of the broken surface completely pulls away from them. Additionally, fibre length should be kept to a minimum to prevent balling effect during mixing. A lot of researchers have also used concrete with 50 mm-long fibres.

Concrete Preparation

For the manufacturing of plain concrete (PC), the water cement ratio (w/c) of 0.6 is utilized along with cement, fine aggregate, and coarse aggregate in the ratios of 1:1.5:2.5. For hybrid fibre reinforced concrete, the same mix design ratio is utilized with the addition of 50 mm long jute and nylon fibres, which are added at a ratio of 5% by mass of cement. Mass is used to measure all materials. Using a non-tilting pivoting type drum concrete mixer, PC and HFRC are produced. Cement, sand, and aggregate are all put into the mixer drum with water for three minutes in order to manufacture plain concrete (PC). Using ASTM standard C143/C143M-15, the workability of HFRC and PC specimens is evaluated before to the filling of moulds at the fresh stage.

a) *b)*

Figure 1: Fresh Concrete: a) HFRC b) PC

A separate method is utilized to manufacture HFRC. To absorb the required amount of water, jute and nylon fibres are submerged into water for 24 hours. Fibers are then exposed to fresh air for 30 minutes. Materials are then added to the mixer in layer forms to avoid the balling effect. The blender drum is filled with one-third each of aggregate, sand, cement, nylon and jute fibres. Until all of the components are loaded into the blender drum, the same procedure is repeated. A third of the total water is spread over the components once they have been fully inserted into the blender drum. The remaining water is progressively poured into the mixer after it has been turned on. To get homogenous concrete, the mixer is turned for six minutes. Both ready concrete batches are shown in the figure1, where "a" shows the concrete having hybrid fibers, where "b" shows the concrete having plain concrete. Before pouring HFRC into moulds, a slump test is conducted.

Tests performed

Slump Test

The ASTM C-143 procedure is used to test the slump values. The mould was filled with three layers of concrete, with each layer being roughly one third of the mould's overall capacity. Using the rod's rounded end, each layer was temped 25 times uniformly throughout the cross section. Determine the vertical height difference between the top of the mould and the displaced original centre of the top surface of the specimen as soon as the moulds are fully filled.

Compaction Factor Test

The IS: 1199-1959, BS 1881:103/5057 procedure has been used in the compaction factor test of plain concrete and hybrid fibre reinforced concrete. The concrete sample to be tested was placed

smoothly in the first hopper of the apparatus with the help of hand scoop. The hopper was filled to the level of its edges. After that open the trap door so that the concrete falls into the lower hopper and then subsequently open the trap door again to allow the concrete to fall into the cylinder. Right after this, weigh the concrete in cylinder.

Fresh Density Test

Fresh density of the concrete was determined by filling the mould in three layers by temping 25 times with the rod (each layer). After the moulds are filled properly, the concrete in the mould was weighed and the volume of the cylinder was measured. Fresh density of concrete was determined by dividing both the values.

RESULTS AND ANALYSIS

Slump Behaviour of fresh Concretes

Table 1 shows how the slump and density of different concrete compositions vary. The use of nylon and jute fibres decreased the slump of freshly laid concrete. For PC, the largest slump recorded was 88mm. Conversely, the slump value for fibre-infused concrete, that is HFRC, was 76mm. The interlocking effect of the fibres that lower the slump of the concrete causes a significant variation in the slump value of plain concrete. However, jute fibres alone reduce the slump value of concrete to virtually nil [8]. On the other hand, adding nylon fibres alone causes the combinations' viscosities to decrease and the slump value of the concrete to increase. The smooth texture, angular particle form, and fineness of the nylon fibre all contribute to the material's better workability.

Table 7: Fresh Properties of PC and HFRC

Concrete sample	Slump (mm)	Compaction Factor		Fresh Density (kg/m^3)
		Value	Workability	
(1)	(2)	(3)	(4)	(5)
PC	88	0.89	Plastic	2310
HFRC	76	0.80	Stiff Plastic	2262

Compaction Factor

Typically, the compaction factor test is performed to assess the workability of the concrete. On the PC and HFRC, a test for the compaction factor was conducted. It was observed that the HFRC compaction factor was 0.81 whereas the PC compaction factor was 0.89. As it can be observed in

table 1 that compaction factor value of plain concrete is 0.89 which is much higher than the compaction factor value of hybrid fiber reinforced concrete that is 0.80, whereas this trend can be noted in the table 1. Plastic and stiff-Plastic workability of PC and HFRC can also be observed from the above table. It is important to mention here that stiff plastic workability of HFRC is in accordance with the slump required for the construction of concrete pavement.

Fresh Density of Hybrid Fiber Reinforced Concrete

With the addition of fibers, it was observed that the fresh density of the concrete was reduced to notable percentage as weight of concrete was reduced significantly whereas the volume was fixed. Referring to the table 1, observed densities of Plain concrete and hybrid fiber reinforced concrete were 2310 kg/m^3 and 2262 kg/m^3, respectively. Hence, a reduction of upto 2.1% was observed as compared to the reference concrete i.e., plain concrete. As a conclusion it was noted that addition of fibers significantly reduced the density of fresh concrete.

CONCLUSION

Fresh properties of concrete were assessed by casting PC and HFRC samples having ratios of 1:1.5:2.5 with water cement ratio to be 0.6. After casting of concrete different test including slump, compaction factor and fresh density of concrete were conducted. Following conclusion are drawn from the above experimentation.

- Addition of fibers in concrete reduced the slump of concrete. With the addition of 5% hybrid fibers, a reduction of 11% in slump was observed compared to PC.
- Reduction in compaction factor was observed with the addition of hybrid fibres. A reduction of 10.11% was observed in the value of compaction factor with reference to PC.
- With the addition of nylon and jute fibers, both having low densities, reduced the density of fresh concrete. This reduction was upto 2.1%, as it reduced the weight of concrete over a fix volume of concrete.

It can be concluded that properties of fresh concrete have changed considerably after the incorporation of hybrid fibers in concrete. Further investigations need to be addressed at a later stage to assess the mechanical and dynamic properties concrete prepared with hybrid fibers.

ACKNOWLEDGEMENTS

The authors would like to acknowledge the efforts of all who helped in the completion of this research, particularly Engr. Shaheer A. Janjua and Engr. Minhas Shah for helping hand in lab work.

REFERENCES

[1] Al Rikabi, F. T., Sargand, S. M., Khoury, I., & Hussein, H. H. (2018). Material Properties of Synthetic Fiber–Reinforced Concrete under Freeze-Thaw Conditions. Journal of Materials in Civil Engineering, 30(6), 04018090.

[2] Adkins, D. F., & Christiansen, V. T. (1989). Freeze-thaw deterioration of concrete pavements. Journal of Materials in Civil Engineering, 1(2), 97-104.

[3] Affan, M., & Ali, M. (2022). Experimental investigation on mechanical properties of jute fiber reinforced concrete under freeze-thaw conditions for pavement applications. Construction and Building Materials, 323, 126599.

[4] Affan, M. (2019). Effect of Freeze-Thaw Cycles on Mechanical Properties of Jute Fiber Reinforced Concrete for Pavement. Capital University of Science and Technology.

[5] Amini, B., & Tehrani, S. S. (2014). Simultaneous effects of salted water and water flow on asphalt concrete pavement deterioration under freeze–thaw cycles. International Journal of Pavement Engineering, 15(5), 383-391.

[6] Nigam, M., & Verma, M. (2023). Effect of Nano-Silica on the fresh and Mechanical Properties of Conventional Concrete. Forces in Mechanics, 100165.

[7] Chakraborty, S., Kundu, S. P., Roy, A., Basak, R. K., Adhikari, B., & Majumder, S. B. (2013). Improvement of the mechanical properties of jute fibre reinforced cement mortar: a statistical approach. Construction and Building Materials, 38, 776-784.

[8] Gupta, S., Rao, V. K., & Sengupta, J. (2008). Evaluation of polyester fiber reinforced concrete for use in cement concrete pavement works. Road Materials and Pavement Design, 9(3), 441-461.

[9] Zhao, C., Wang, Z., Zhu, Z., Guo, Q., Wu, X., & Zhao, R. (2023). Research on different types of fiber reinforced concrete in recent years: An overview. Construction and Building Materials, 365, 130075.

[10] Hasan, R., Sobuz, M. H. R., Akid, A. S. M., Awall, M. R., Houda, M., Saha, A., ... & Sutan, N. M. (2023). Eco-friendly self-consolidating concrete production with reinforcing jute fiber. Journal of Building Engineering, 63, 105519.

[11] Shen, L., Yao, X., Di Luzio, G., Jiang, M., & Han, Y. (2023). Mix optimization of hybrid steel and polypropylene fiber-reinforced concrete for anti-thermal spalling. Journal of Building Engineering, 63, 105409.

[12] Delatte, N., & Storey, C. (2005). Effects of density and mixture proportions on freeze-thaw durability of roller-compacted concrete pavement. Transportation Research Record: Journal of the Transportation Research Board, (1914), 45-52.

[13] Xia, D., Yu, S., Yu, J., Feng, C., Li, B., Zheng, Z., & Wu, H. (2023). Damage characteristics of hybrid fiber reinforced concrete under the freeze-thaw cycles and compound-salt attack. Case Studies in Construction Materials, e01814.

2nd International Conference on Advances in Civil and Environmental Engineering (ICACEE-2023)

University of Engineering & Technology Taxila, Pakistan

Conference date: 22nd and 23rd February, 2023

Mechanical Behavior of Geopolymer Paste with Micro-Carbon Fibers and Nano-$CaCO_3$

Ali Raza[1*], Mohamed Hechmi El Ouni[2,3], Muhammad Sohail Jameel[4], Muhammad Hamza[1]

[1]Department of Civil Engineering, University of Engineering and Technology Taxila, 47050, Pakistan; [*]Correspond ace: E-mail: ali.raza@uettaxila.edu.pk

[2]Department of Civil Engineering, College of Engineering, King Khalid University, PO Box 394, Abha, 61411, KSA. E-mail: melouni@kku.edu.sa

[3]Department of Mechanical Engineering, Higher Institute of Applied Sciences and Technologies of Sousse, University of Sousse, 4003, Sousse Ibn Khaldoun, Tunisia.

[4]Department of Transportation Engineering and Management, University of Engineering and Technology Lahore, 54890, Pakistan; E-mail: sohail.jameel@uet.edu.pk

ABSTRACT

The goal of the current study is to incorporate various amounts of nano-$CaCO_3$ (NCC) to increase the microstructural and mechanical effectiveness of micro carbon (MC) fiber-reinforced (FR) fly ash (FA)-based geopolymers (GP) mixtures. To produce GP mixes containing a given proportion of MC fibres (i.e., 0.5% wt.%), four different NCC proportions (1%, 2%, 3%, and 4% wt.%) were used. For comparison, a control mix without any NCC was fabricated containing 0.5% MC fibres. According to the findings of the study, the greatest results for compressive strength were obtained when using 3% NCC, while the peak outcomes for fracture toughness and paste flexural strength were obtained when using 2% NCC in a carbon-FR-GP mix.

KEYWORDS: Geopolymer; carbon fibers; nano calcium carbonate; compression stress; flexural strength.

INTRODUCTION

Geopolymer (GP) is a highly effective alternative to ordinary Portland cement (OPC) for the binder used in concrete construction projects. When combined, these composite materials demonstrate their effectiveness as binders by activating aluminosilicate compounds like fly ash (FA) in an alkaline solution [1-5]. These materials offer good structural efficacy on par with or better than traditional concrete, according to the evolution of GP over time [6-8]. However, the effectiveness of GP must be greatly boosted by adopting cutting-edge techniques to increase the practical uses of GP mixes in the manufacture of concrete. Higher flexural strength (FLS) is necessary in the building industry, the uses of this composite material as a binder are limited because the GP also shows lower early strength and displays brittle efficacy [9]. Therefore, it is crucial to develop operative and sophisticated processes to increase the structural effectiveness of GP mixtures.

Numerous research on the application of nanoparticles (NP) in the field of construction to improve the efficacy of composite materials as binder have been carried out [10-13]. The findings of these investigations indicate that the uses of nanomaterials in modest quantities are effective and functional to boost the durability and structural effectiveness of GP mixtures. Some investigations looked at the efficiency of adding nano-titanium oxide to GP mixes in order to use nano-particles [14, 15] or nano-silica [16, 17] but only a little amount of research has been done on the application of nano-$CaCO_3$ (NCC) in GP mix. To improve the mechanical and microstructural efficacy of the GP mix, however, the most current research studied the usage of NCC up to a proportion of 3 weight percent and found that 2% NCC is the most successful and operative [13].

The combined usage of NCC and micro carbon (MC) fibres in the GP mix has not been investigated in previous work. The present investigation assesses the different quantities of NCC and 0.5% MC fibres (0%, 1%, 2%, 3%, and 4% wt.%) to form the GP mixtures. The mechanical properties of GP including compressive strength (CS), stress-strain efficacy under compression, and FLS of NCC were examined.

MATERIALS AND METHODS

Materials

The current investigation has used Class F FA as an aluminosilicate precursor. The properties of FA are detailed in Table 1. Binary activators made from sodium hydroxide and sodium silicate are used to make the GP mixes. Table 2 shows several NCC parameters. The elastic modulus and tensile strength of the micro carbo-fibers are 242 GPa and 4100 MPa, respectively. The length of the nominal MC fibres is 2 millimetres. Five different GP are made and tested for CS and FLS with varying amounts of NCC by FA mass. Alkaline solution to FA has been combined at a ratio of 0.45, whereas for all GP mixes, sodium silicate and sodium hydroxide have been blended at a ratio of 2.5 [18]. A 10 M alkaline solution was made by dissolving the sodium hydroxide pallets in water and mixing them with the sodium silicate solution 24 hours before making GP mixes. All GP mix mixes included 0.5% fibre reinforcement as this quantity provided the better results [9, 19-22]. The mix design for each GP mix is shown in Table 3.

Table 1. Configuration of FA

Component	Configuration (%)	Component	Configuration (%)
SiO_2	62.3	Na_2O	1.7
Al_2O_3	26.7	MgO	0.62
CaO	2.31	K_2O	1.87
Fe_2O_3	2.67	LOI	1.44

Table 2. Properties of NCC

Feature	Quantity	Feature	Quantity
Color	White	NCC dry proportion (%)	97.5
Average size	15 – 40 nm	pH	8-9
Bulk density	0.67 g/m^3	Moisture proportion (%)	0.55

Table 3. Test matrix

GP Mix	CGP-0%NCC	CGP-1%NCC	CGP-2%NCC	CGP-3%NCC	CGP-4%NCC
NaOH (kg)	0.22	0.22	0.22	0.22	0.22
FA (kg)	1.8	1.8	1.8	1.8	1.8
MC fiber (wt.%)	0.5	0.5	0.5	0.5	0.5
Na_2SiO_4 (kg)	0.58	0.58	0.58	0.58	0.58
NCC (kg)	0	0.01	0.02	0.03	0.04
NCC (wt. %)	0	1.0	2.0	3.0	4.0

Manufacturing of Mixes

A 0.15 m^3 mechanical mixer was used to mix GP mixes. FA and carbon fibres were dry mixed for 5 minutes at a low speed in addition to the GP mix mixing method. After the two more components have been thoroughly dry mixed: an alkali solution containing various NCC quantities was mixed at 20 revs per minute at a rapid speed. Until a homogeneous GP mix was achieved, this form of mixing was used. The moulds were filled with brand-new mixes, which were then allowed to cure for 24 hours at 80°C. The subsequent 28 days of conventional temperature curing were employed to boost the mechanical effectiveness once they had finished the temperature curing.

Testing Methods

According to ASTM D 695, thirty (30) cubical testing members with dimensions of $20\ mm\ x\ 20\ mm\ x\ 20\ mm$ for five GP mixtures are produced and tested till damage under pure compression.[23]. To determine the CS of mixes containing 0%, 1%, 2%, and 3% NCC, successively, six members are evaluated for each GP mix. The average CS values for each of the five groups, which included six members, are determined and demonstrated in the present study. Compression stress is calculated by dividing the greatest load carrying capacity by the gross area of the members. Similar to the CS tests, the FLS of each GP mix containing 0%, 1%, 2%, and 3% NCC is ascertained by analysing six members, each measuring $60\ mm\ x\ 20\ mm\ x\ 20\ mm$. Three-point flexure testing is carried out on manufactured members that include 0%, 1%, 2%, 3%, and 4% NCC, in accordance with ASTM C-293 [24]. The average FLS values from the six members used in the current study's five groups are calculated and described.

RESULTS AND DISCUSSION

Compression Stress

Figure 2 demonstrates the effect on the CS by adding different amounts of NCC (0%, 1%, 2%, 3%, and 4%) to the GP mix containing 0.5% carbon fibres. It has been found that adding NCC reduces the CS when used in proportions up to 2% but adding NCC in proportions of up to 3% significantly increases the CS of the GP mix. The CS was decreased when the proportion of NCC was further increased. NCC characterised the decreases in CS of 3.3% and 13.1% in GP with proportions of 1% and 2%, respectively, compared to the mix without NCC. This could be explained by the fact that the little amounts of NCC are ineffective as a filling material to cover spaces between the GP mix and carbon fibres. While the CS of GP with 0.5% carbon fibres improved by 17.2% with the addition of 3% NCC. It is highly likely that the increase in NCC material from 1% to 2% lowers the CS of GP mix due to the effectiveness of dilution producing less hydration by-products[18]. The ability of the 3% NCC to fill the gaps left by the competency of the NCC, which in turn increased the pace of polymerization for the GP mix, may be responsible for the improvement of the CS with the addition of the NCC. The amount of hydration products is reduced by 8.4% by increasing the proportion of NCC due to the particles capacity to agglomerate [18]. The presence of NCC may speed up the polymerization for the GP mixing phase because they can provide as crystallites for the secondary products produced by the GP mix process [12, 25, 26].

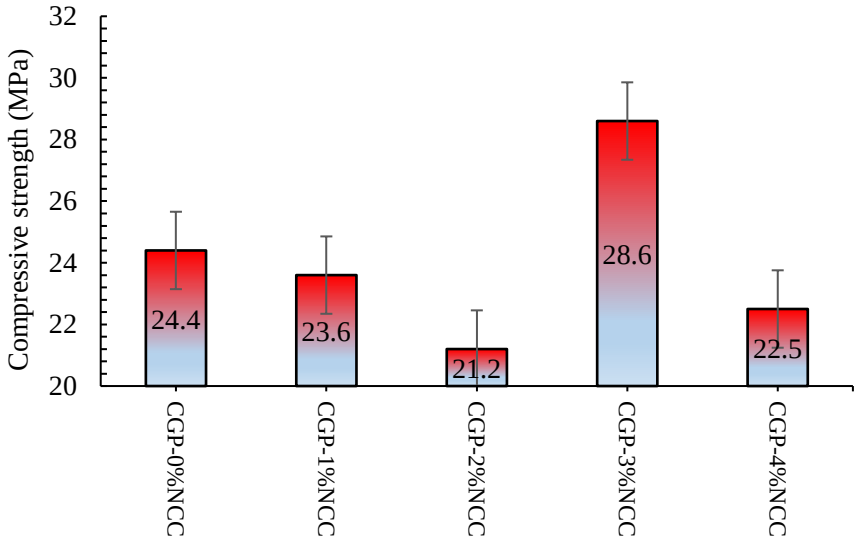

Figure 2. CS of FR-GP mix for different proportions of NCC

The CS results for the different GP mixes containing NCC (0%, 1%, 2%, 3%, and 4%, sequentially) are, for the most part, worse than the results of the current investigation with carbon fibres [13]. This adamantly supports the effectiveness of including 0.5% carbon fibres in GP

mixtures along with different concentrations of NCC. A denser microstructure of the mix at this concentration of NP may be the cause of the enhancement in the CS of GP mixes with the introduction of 3% NCC (illustrated in Figure 2). The CS of GP may therefore be improved by simultaneously incorporating a higher fraction of NCC and carbon fibres, it is found. The comparable CS of the control mix with 0.5% carbon fibres and not being satisfied with NCC was 96.7%, 86.9%, 117.2%, and 91.5% of the GP mix with 1%, 2%, 3%, and 4% levels of NCC and 0.5% carbon fibres, respectively.

Stress-Strain Behaviour

Figure 3 demonstrates the compression stress-strain performance of GP mixes containing 0%, 1%, 2%, 3%, and 4% NCC and 0.5% carbon fibres. Due to the addition of NCC, there is an increase in compressive-stress, increasing the stiffness of the GP mix to withstand greater compressive compression forces at lower compressive strains. For instance, the mix with 3% NCC presented stiffer response in elastic as well as inelastic behaviour of stress-strain diagram. The value of strain increased for increasing the content of MC fibers as can be observed from Figure 3. This may be ascribed to the densified matrix and improved internal structure of the mix due to increased quantity of micro fibers [12, 25, 26].

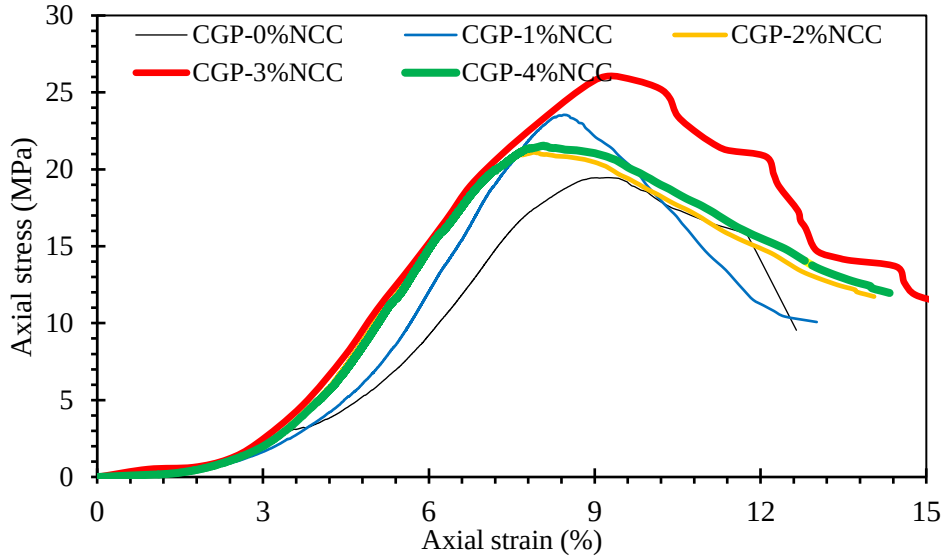

Figure 3. Stress-strain efficacy of FR-GP mixes

The control member had less compressive stiffness than the member made up of various quantities of NCC. The stress-strain curves under compression show how the values of compressive stress are enhanced at lower levels of compressive strain due to an increase in the proportion of NCC. A denser GP mix and a speedier polymerization process for the more products that NCC can serve as crystallites for within the GP mix might explain this process [12, 25, 26]. Additionally, a greater

CS reduction at lower compressive stresses was seen in the members with different NCC concentrations. This could be explained by the members' higher compressive stiffness prior to post-collapsing, which caused damage to the GP mixes in the post-peak region of stress-strain curves due to the higher fracture efficacy of the NCC-containing blends.

Flexural Behaviour

Figure 5 shows how the FLS of GP is impacted by the addition of 0.5% carbon fibres and various NCC concentrations (0%, 1%, 2%, 3%, and 4%) to the GP mix. A composite material's ability to endure loading during flexure is determined by its FLS. The average of 6 members from every GP mix were utilized in experimental measurements to find the FLS of the mixtures, which climbed up to 2% NCC percentage before beginning to decline. On the other hand, when 3% and 4% NCC particles were added, the FLS was decreased, though not below the level of the control mix. The agglomeration of NP and MC fibres may be responsible for this [27]. The higher bending stresses of these mixes, as shown in Figure 5, However, compared to the control mix, resulted in a greater FLS. (CGP-0%NCC). The improvement in microstructure caused by the NCC particles and the densification of the GP mix because of the GP mix's speedier polymerization process may be the root causes of the increase in FLS in manufactured mixes.

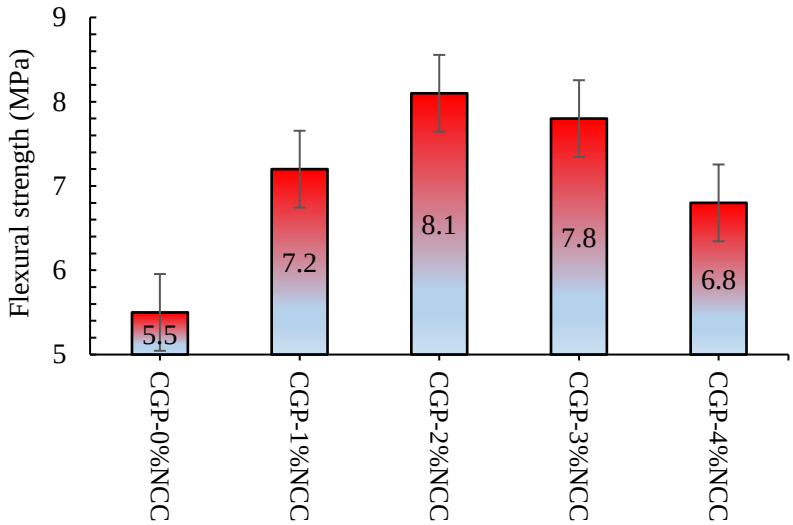

Figure 5. FLS of FR-GP mixes

The build-up of NP may be the cause of the FLS of GP decreases caused by NCC increases above 2%. However, the CS measurements (shown in Figure 2) showed that the 1% and 2% NCC had differing efficacies. It is essential that a detailed investigation be carried out to look at how different mixtures perform when compressed. The literature has noticed similar results [13] with plain GP mixes involving up to 3% NCC. A reduced FLS without carbon fibres was also disclosed in the NCC amounts of 1% and 2% [13]. The GP with 0.5% carbon fibres described an improved

FLS for all quantities of 1%, 2%, 3%, and 4% NCC, in contrast to CGP-0%NCC. The usage of 2% NCC demonstrated the highest FLS among GP mixes. The analysis carried out by an earlier investigation [28] showed that increasing NCC in the GP mix by 1% and 2%, respectively, the tensile strengths were enhanced by 5.6% and 44.5%. However, in the present study, the use of NCC at 1% and 2% resulted to an improvement in FLS of 30.9% and 47.3%, respectively. As a result, the FLS associated with using solely NCC is improved by using NCC coupled with carbon fibre reinforcement. The FLS of the GP mix, which contained 0.5% carbon fibres and the corresponding amounts of 1%, 2%, 3%, and 4% NCC, was 130.9%, 147.3%, 141.8%, and 123.6% of the FLS of the control mix, containing 0.5% carbon fibres but was not NCC-satisfied.

BENEFIT TO INDUSTRY

Sustainability is the main benefit of the present study for the construction industry due to the minimization of carbon resulted from the production of OPC. Moreover, the improved microstructural behaviour will be beneficial to the concrete structures in aggressive environments to minimize the chloride penetration and sulphate attacks resulting in the durability and serviceability loss of the structures.

CONCLUSIONS

This paper examined the mechanical features of a MC-FR-GP blend with various NCC proportions. The following are the main conclusions:

1. By using 3% NCC, the carbon-FR-GP mix's optimal CS was attained, which was 17.2% greater than the CS of the control mix without NCC. This might be explained by the NCC's capacity to speed up the polymerization of the GP mix while still containing enough NP (3% NCC) to prevent cracks.
2. By using 2% NCC, the greatest FLS was achieved. The inclusion of NCC, which enhanced the microstructure, and the GP mix's hastened polymerization process, which made the GP mix denser, may be responsible for this increase in FLS of GP.

Conclusively, the fabricated fly ash-based geopolymers mix with nano $CaCO_3$ and micro fibers will lead to improved microstructure and densified matrix to provide enhanced mechanical behaviour and durability performance of concrete structures.

Acknowledgments

None.

Conflicts of Interest

There are no conflicts of interest from authors.

REFERENCES

1. Provis, J.L. and S.A. Bernal, *Geopolymers and related alkali-activated materials*. Annual Review of Materials Research, 2014. **44**: p. 299-327.
2. Bai, Y., et al., *Utilization of municipal solid waste incineration fly ash with red mud-carbide slag for eco-friendly geopolymer preparation*. Journal of Cleaner Production, 2022. **340**: p. 130820.
3. Chen, X., et al., *Study on the effect of calcium and sulfur content on the properties of fly ash based geopolymer*. Construction and Building Materials, 2022. **314**: p. 125650.
4. Han, Q., et al., *Comprehensive review of the properties of fly ash-based geopolymer with additive of nano-SiO2*. Nanotechnology Reviews, 2022. **11**(1): p. 1478-1498.
5. Luna-Galiano, Y., et al., *Development of fly ash-based geopolymers using powder sodium silicate activator*. Materials Letters, 2022: p. 132346.
6. Adesina, A., *Performance and sustainability overview of alkali-activated self-compacting concrete*. Waste Disposal & Sustainable Energy, 2020: p. 1-11.
7. Duxson, P., et al., *Geopolymer technology: the current state of the art.* Journal of materials science, 2007. **42**(9): p. 2917-2933.
8. Zhuang, X.Y., et al., *Fly ash-based geopolymer: clean production, properties and applications.* Journal of Cleaner Production, 2016. **125**: p. 253-267.
9. Alomayri, T., A. Raza, and F. Shaikh, *Effect of nano SiO2 on mechanical properties of micro-steel fibers reinforced geopolymer composites*. Ceramics International, 2021.
10. Adesina, A. *Durability enhancement of concrete using nanomaterials: an overview.* in Materials Science Forum. 2019. Trans Tech Publ.
11. Adesina, A., *Nanomaterials in cementitious composites: review of durability performance.* Journal of Building Pathology and Rehabilitation, 2020. **5**(1): p. 1-9.
12. Gülşan, M.E., et al., *Development of fly ash/slag based self-compacting geopolymer concrete using nano-silica and steel fiber*. Construction and Building Materials, 2019. **211**: p. 271-283.
13. Assaedi, H., et al., *Characterization and properties of geopolymer nanocomposites with different contents of nano-CaCO3*. Construction and Building Materials, 2020. **252**: p. 119137.
14. Tuntachon, S., et al., *Resistance to algae and fungi formation of high calcium fly ash geopolymer paste containing TiO2*. Journal of Building Engineering, 2019. **25**: p. 100817.
15. Sastry, K.G.K., P. Sahitya, and A. Ravitheja, *Influence of nano TiO2 on strength and durability properties of geopolymer concrete.* Materials Today: Proceedings, 2020.
16. Mustakim, S.M., et al., *Improvement in fresh, mechanical and microstructural properties of fly ash-blast furnace slag based geopolymer concrete by addition of nano and micro silica.* Silicon, 2020: p. 1-14.

17. Al Bakri, A., et al. *Nano geopolymer for sustainable concrete using fly ash synthesized by high energy ball milling*. in Applied Mechanics and Materials. 2013. Trans Tech Publ.
18. Alomayri, T., *Performance evaluation of basalt fiber-reinforced geopolymer composites with various contents of nano CaCO3.* Ceramics International, 2021.
19. El Ouni, M.H., et al., *Enhancement of mechanical and toughness properties of carbon fiber-reinforced geopolymer pastes comprising nano calcium oxide.* Journal of the Australian Ceramic Society, 2022: p. 1-13.
20. Rashedi, A., et al., *Mechanical, fracture, and microstructural assessment of carbon-fiber-reinforced geopolymer composites containing Na2O*. Polymers, 2021. **13**(21): p. 3852.
21. Raza, A., et al., *Experimental study on mechanical, toughness and microstructural characteristics of micro-carbon fibre-reinforced geopolymer having nano TiO2*. Alexandria Engineering Journal, 2022.
22. Raza, A., et al., *Mechanical Performance of Geopolymer Composites Containing Nano-Silica and Micro-Carbon Fibers*. Arabian Journal for Science and Engineering, 2022: p. 1-12.
23. ASTM D695-15, *Standard Test Method for Compressive Properties of Rigid Plastics*, ASTM International, West Conshohocken, PA. 2015.
24. ASTM C78M-21, *Standard Test Method for Flexural Strength of Concrete (Using Simple Beam with Third-Point Loading)*, ASTM International, West Conshohocken, PA. 2021.
25. Saini, G. and U. Vattipalli, *Assessing properties of alkali activated GGBS based self-compacting geopolymer concrete using nano-silica*. Case Studies in Construction Materials, 2020. **12**: p. e00352.
26. Nuaklong, P., et al., *Influence of rice husk ash on mechanical properties and fire resistance of recycled aggregate high-calcium fly ash geopolymer concrete*. Journal of Cleaner Production, 2020. **252**: p. 119797.
27. Nuaklong, P., et al., *Enhancement of mechanical properties of fly ash geopolymer containing fine recycled concrete aggregate with micro carbon fiber.* Journal of Building Engineering, 2021. **41**: p. 102403.
28. Alomayri, T., *Experimental study of the microstructural and mechanical properties of geopolymer paste with nano material (Al2O3).* Journal of Building Engineering, 2019. **25**: p. 100788.

2nd International Conference on Advances in Civil and Environmental Engineering (ICACEE-2023)

University of Engineering & Technology Taxila, Pakistan

Conference date: 22nd and 23rd February, 2023

Durability of High-Strength Self Compacting Concrete (HSSCC) modified with Supplementary Cementitious Materials (SCMs)

Irfan Munir[1], Ayub Elahi[2], Saqib Zubair[3], Jawad Hussain[4]

[1]MSc Student, Department of Civil Engineering, University of Engineering and Technology Taxila, eng.irfanmunir@gmail.com
[2]Professor at Department of Civil Engineering, University of Engineering and Technology Taxila, ayub.elahi@uettaxila.edu.pk
[3]Department of Civil Engineering, University of Engineering and Technology Taxila, saqibzubair100@gmail.com
[4]Department of Civil Engineering, University of Wah, Wah Cantt, jawadbajwa767@gmail.com

ABSTRACT

High-strength self-compacting concrete (HSSCC) modified with supplementary cementitious materials (SCMs) can be highly durable if it is properly designed and constructed. In this study, a fixed percentage of silica fume (5%), and a varying percentage of fly ash (0%–50%), have been incorporated into HSSCC to evaluate the durability properties at different ages of HSSCC. A compressive strength test was performed on the cylinder samples to assess the compressive strength behaviour of HSSCC at 7, 28, and 91 days of age. Sulphate attack and chloride attack were performed to assess the weight loss at 28, 56, and 91 days of age. SEM analysis was performed on the samples cast to assess the microstructure behaviour of HSSCC. 5% SF and 20% FA replacement was found to be the optimum mix design that improves the durability properties of HSSCC due to the pozzolanic reaction and better packing of materials. These materials can reduce deterioration such as corrosion, cracking, weathering and permeability of the concrete, which can help to prevent the ingress of harmful substances such as water and chloride ions that can cause corrosion of the reinforcing steel. However, the higher percentage of fly ash than optimum has led to a decrease in the compressive strength, chloride content, and sulphate attack resistance due to the voids in the composite. This can be clearly seen in the SEM analysis.

KEYWORDS: *High-strength Self-compacting concrete (HSSCC), Fly Ash, Silica Fume, Supplementary cementitious materials*

INTRODUCTION

The biggest challenge faced by the reinforced concrete industry is the appropriate placement and compaction of freshly mixed concrete through small openings, deep, and narrow portions, such as congested areas of reinforcement. Deterioration and damage to structures are major issues in the field of civil engineering that need to be resolved with reliable, economical, and innovative materials to increase the lifespan of structures. Self-compacting concrete has gained a lot of

popularity since the 90s because of its benefits i.e., can compact itself under its own weight, and can easily fill up the spacing between narrow reinforcing bars [1]. Due to its high fluidity and resistance to segregation, self-compacting concrete is unaffected by the size, shape, or placement of reinforcement bars or the layout of the buildings. It can also be pumped to a greater distance [2]. Consideration of SCC's durability is essential to ensuring a longer lifespan for the structures built with it. The ability of SCC to maintain its original shape, dimension, and quality for its anticipated service life while being exposed to the worst weathering conditions, abrasion, and various chemical attacks is related to this characteristic. When evaluating the HSSCC's durability, tests such as those for chloride attack/acid attack, sulphate resistance, water absorption, and porosity are carried out. Self-compacting mortars including fly ash, limestone powder, and mixtures of fly ash with silica fume ash have already been investigated [3]. Fly ash replaces ordinary Portland cement (OPC) in SCC systems, reducing the amount of high-range water-reduction admixture (HRWRA) by reducing the water demand [4]. Fly ash is typically utilized in concrete, with amounts ranging from 15% to 25% of the total binder mass [5]. High fly ash content can improve some SCC properties such as viscosity, yield stress, flow rate, and spread [6]. Using ultra-fine fly ash can reduce the amount of water needed to make concrete by 3% for every 10% addition. Fly ash as fine aggregates significantly lower workability, unit weight, and compressive strength in the SCC system. Similarly, silica fume (SF) is also known to be effective in enhancing pozzolanic activity due to its small size (0.15µm) which improves the bonding between aggregates and matrix, thus improving the mechanical performance of concrete [7]. The rheological, mechanical, and chemical properties of steel-reinforced concrete are improved by silica fume as reducing corrosion. It improves the concrete's capacity to last. The cementitious composite durability can be increased using various amounts of different mineral additives [8]. The use of eco-friendly materials has drawn significant interest in scientific research because of difficulties in global warming. Nowadays, supplementary cementitious materials (SCM) are being blended into the cement manufacturing process to reduce carbon emissions [9]. Supplementary cementitious materials (SCMs) are categorized as pozzolanic materials, and some of them, like fly ash, perlite, zeolite, etc., are naturally occurring pozzolans from volcanoes while others, such as slags, silica fume, etc., are man-made. This study was performed to evaluate the durability properties of HSSC with a partial replacement of SCMs i.e. fly ash and silica fume.

EXPERIMENTAL PROGRAMM

Materials

In this study, the HSSCC mixes were developed using OPC-Type I, a locally available fine aggregate of specific gravity 2.7, and classified according to ASTM C 778-02 [10]. In this study, as per ASTM C 136-06 [11], well-graded natural coarse aggregates with a 12mm maximum size were employed. Polycarboxylic acid is used as the superplasticizer to maintain the workability of concrete. Superplasticizer contains no accelerating or retarding substances.

Mix Proportions

HSSCC mixes were developed as per the guidelines given by EFNARC [12]. A constant w/c ratio of 0.34 was applied during the batching process. Seven mixed designs were batched with one control mix (CM) and six mixes with constant 5% silica fume (SF) and increasing replacement percentage of fly ash up to 50% with an interval of 10%. Superplasticizers were added at a maximum of up to 1.10% and a lowest of 0.8% depending on the workability of the mix.

Table 1: Composition of mix design (Mix design ratio = 1:1.4:1.6, W/C ratio = 0.34)

Mixes	OPC (kg/m^3)	Silica Fume (kg/m^3)	Fly Ash (kg/m^3)	Water (kg/m^3)	Superplasticizer (kg/m^3)	FA (kg/m^3)	CA (kg/m^3)
Control mix	550	0	0	187	7.70	539	616
5%SF+0%FA	522.5	27.5	0	187	7.15	539	616
5%SF+10%FA	467.5	27.5	55	187	6.05	539	616
5%SF+20%FA	412.5	27.5	110	187	5.5	539	616
5%SF+30%FA	357.5	27.5	165	187	4.95	539	616
5%SF+40%FA	302.5	27.5	220	187	4.68	539	616
5%SF+50%FA	247.5	27.5	275	187	4.40	539	616

Methodology

Cylinders of standard size($150\,mm \times 300\,mm$) were cast to check the compressive strength at 7 days, 28 days, and 91 days. For the durability of HSSCC, the sulphate and chloride attack test was performed. SEM analysis was also conducted to assess the microstructure properties of HSSCC with partial replacement of cement with silica fume and fly ash.

RESULTS AND DISCUSSION

Compressive Strength

The results of the compressive strength test carried out at 7 days, 28 days, and 91 days are shown below.

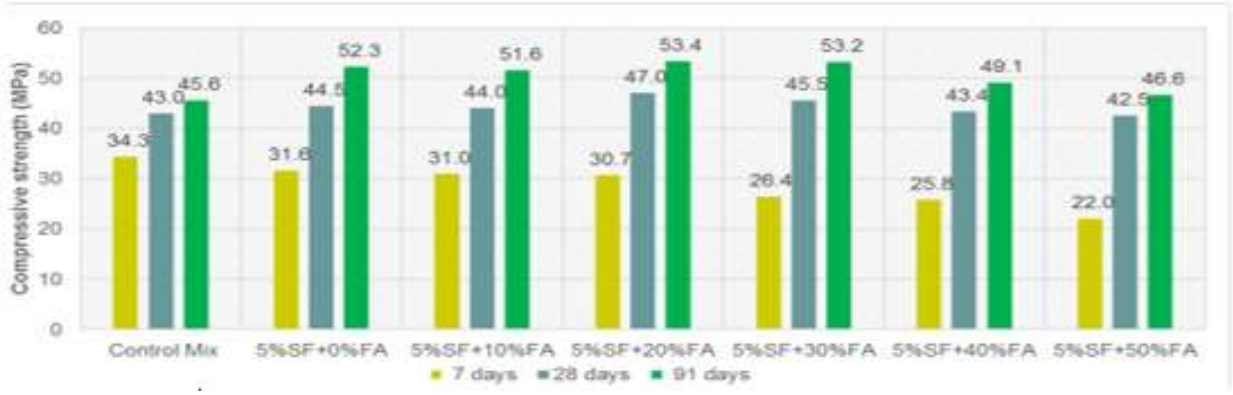

Figure 7: Compressive strength of HSSCC at different age.

Experimental data shows that at the age of 7 days, the 5%SF+0%FA slightly reduces the compressive strength with 7.8%, whereas the 5%SF+10-50%FA more significantly reduces the compressive strength with 9.6%, 10.5%, 23.03%, 24.78%, and 35.86%, respectively than control mix. Results show that at the age of 28 days, the 5%SF+0-40%FA slightly increased compressive strength, and the 5%SF+50%FA decreased compressive strength as compared to the control mix. Similarly, at the age of 91 days, the 5%SF+0-50%FA more significantly increased compressive strength as compared to the control mix. The enhancement in strength is because FA has a slow and continuous pozzolanic reaction in concrete, which only starts significantly after several weeks. However, if the FA content is added above the optimum value, the chemical reaction process is not fully impacted. From the experimental data, it is evident that the replacement of 5% SF and 20% FA with an optimum mix increased the compressive strength at 28 and 91 days of age by 8.5% & 14.6%, respectively, as compared to the control mix. In addition, higher dosages of fly ash and silica fume lead to a reduction in compressive strength.

Sulphate attack (Weight Loss) Test

This study was specific to 5% Na2SO4 in 50 litters of distilled water after mature concrete at 28, 56, and 91 days [13]. Results shows that SF and FA have improved the pore structure in hardened concrete due to better particle packing and the pozzolanic reaction. The presence of low dosages of silica fume and fly ash showed a small contribution towards sulphate resistance due to the presence of pores as evident in SEM images however the addition of high dosages of fly ash and silica fume provided sufficient resistance towards sulphate attack. Finally, it was concluded that the replacement of 5% SF and 20% FA with an optimum mix decreased the weight loss as compared to the control mix at 28, 56, and 90 days of age, with 62.5%, 63.8%, and 64.7%, respectively as shown in Figure 3.

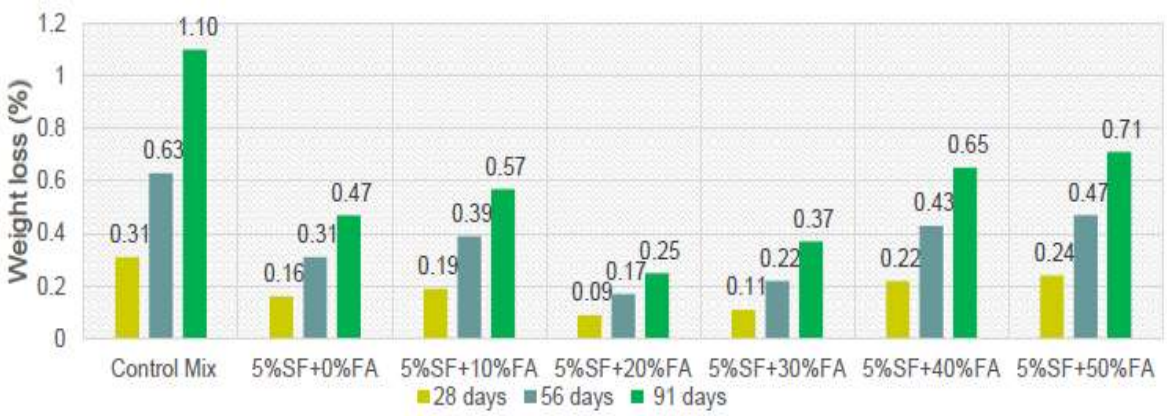

Figure 8: Sulphate Attack Weight Loss Test

Chloride attack (Weight Loss) Test

This study was specific to 3.5% sodium chloride salt in 50 litters of distilled water after maturing concrete at 28, 56, and 91 days [13]. According to the study, SF reduces weight loss due

to very fine particles and pore structure, whereas FA increases weight loss after the optimum stage due to high porosity and sodium chloride salt ion penetration into HSSCC. The optimum dosage of fly ash showed filling action which showed some resistance to chloride attack, however, the overall behaviour of concrete to chloride attack shows that the samples lost their weight. Finally, it was concluded that the replacement of 5% SF and 20% FA with an optimum mix decreased the weight loss as compared to the control mix at 28, 56, and 90 days with 42.9%, 51.8%, and 52.4%, respectively as shown in Figure 4.

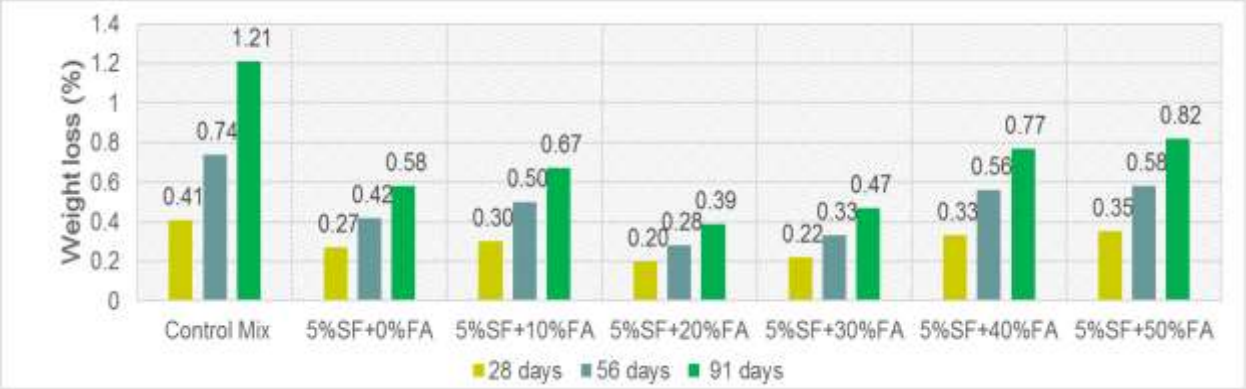

Figure 9: Chloride Attack test results.

SEM Analysis

The SEM results of each mix are shown in Figures 5 & 6. From the SEM images, it was observed that the addition of constant 5%SF and varying (0%~50%) FA formed a good interfacial transition zone (ITZ) and dense compacted structure as compared to the control mix. Study shows that SF decreases the voids due to very fine particles and FA increase the voids with increases in FA after an optimum level of 5%SF+20%FA. Study shows that C-S-H gel distribution was decreased and produced a higher percentage of C-S-H during the hydration reaction due to the combined effect of silica fume and fly ash as compared to the control mix.

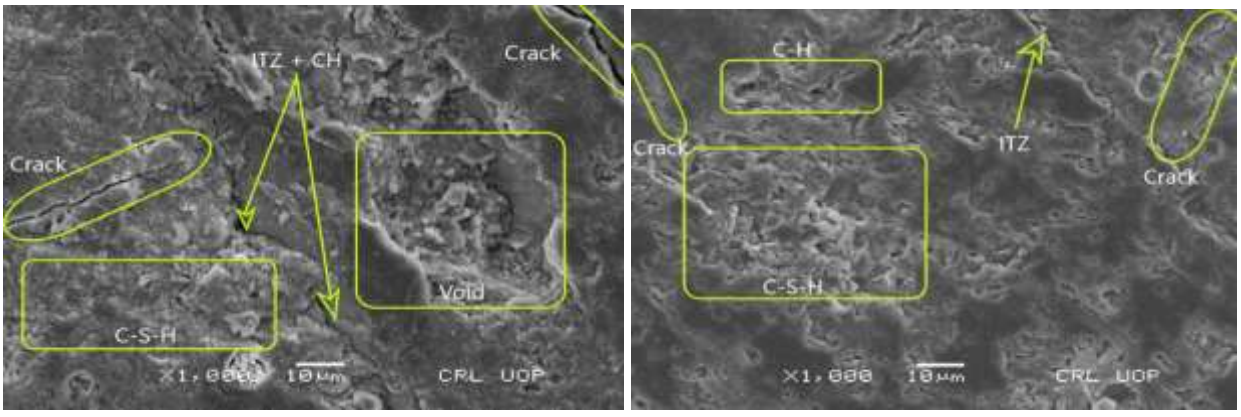

Figure 10: SEM Analysis (a) control mix (b) 5% SF & 20%FA

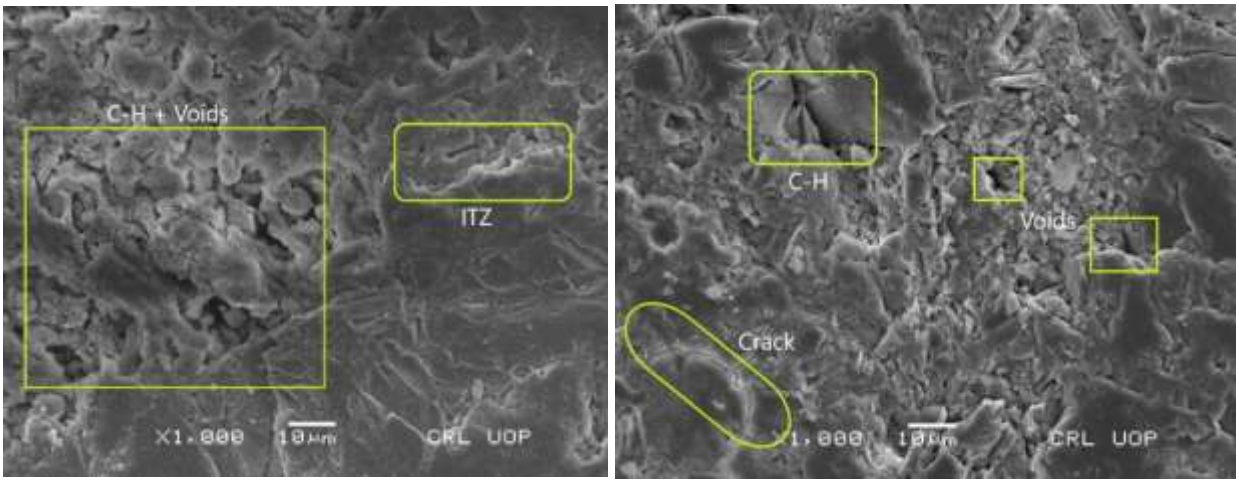

Figure 11: SEM Analysis (a) 5% SF & 40%FA (b) 5% SF & 50%FA

CONCLUSION

From the experimental results, it was concluded that:

1. The addition of less dosages of silica fume and fly ash imparted a positive effect on the mechanical and microstructural properties of concrete. It was found that the replacement of 5% SF and 20% FA with an optimum mix increased the compressive strength at 28 and 91 days of age by 8.5% & 14.6%, respectively, as compared to the control mix.
2. Results show that at the age of 7 days, the 5%SF+0%FA slightly reduces the compressive strength with 7.8%, whereas the 5%SF+10-50%FA more significantly reduces the compressive strength with 9.6%, 10.5%, 23.03%, 24.78%, and 35.86%.
3. With 5% SF and 20% FA, the mix has a better resistance against sulfate and chloride attacks. Because SF and FA have improved the pore structure in hardened concrete due to better particle packing and the pozzolanic reaction.
4. SEM images show that the mixes of concrete containing 5%SF+20% FA created denser microstructure and refined pores which resulted in significant improvement of concrete strength. The presence of silica fume and fly ash improved the bond quality between aggregate and matrix due to the formation of CSH gel in the presence of micro-particles of reactive silica.

REFERENCES

[1] H. J. H. Brouwers and H. J. Radix, "Self-compacting concrete: theoretical and experimental study," *Cem Concr Res*, vol. 35, no. 11, pp. 2116–2136, 2005.

[2] M. Ouchi, "Self-compacting concrete-development, applications and investigations," *NORDIC CONCRETE RESEARCH-PUBLICATIONS-*, vol. 23, pp. 29–34, 2000.

[3] S. A. Rizwan and T. A. Bier, "Self-consolidating mortars using various secondary raw materials," *ACI Mater J*, vol. 106, no. 1, p. 25, 2009.

[4] G. Sua-Iam and N. Makul, "Utilization of coal-and biomass-fired ash in the production of self-consolidating concrete: a literature review," *J Clean Prod*, vol. 100, pp. 59–76, 2015.

[5] M. D. A. Thomas, *Optimizing the use of fly ash in concrete*, vol. 5420. Portland Cement Association Skokie, IL, USA, 2007.

[6] A. K. H. Kwan and Y. Li, "Effects of fly ash microsphere on rheology, adhesiveness and strength of mortar," *Constr Build Mater*, vol. 42, pp. 137–145, 2013.

[7] A. M. Boddy, R. D. Hooton, and M. D. A. Thomas, "The effect of the silica content of silica fume on its ability to control alkali–silica reaction," *Cem Concr Res*, vol. 33, no. 8, pp. 1263–1268, 2003.

[8] S. Türkel and Y. Altuntaş, "The effect of limestone powder, fly ash and silica fume on the properties of self-compacting repair mortars," *Sadhana*, vol. 34, no. 2, pp. 331–343, 2009.

[9] H. Mikulčić, J. J. Klemeš, M. Vujanović, K. Urbaniec, and N. Duić, "Reducing greenhouse gasses emissions by fostering the deployment of alternative raw materials and energy sources in the cleaner cement manufacturing process," *J Clean Prod*, vol. 136, pp. 119–132, 2016.

[10] A. Standard, "C778," *Standard Specification for Standard Sand*, 2017.

[11] D. ASTM, "422/C 136-06, 1998," *Standard Test Method for Analysis of Fine and Coarse Aggregates*.

[12] S. EFNARC, "EFNARC Guidelines for self-compacting concrete," *EFNARC, UK (www. Efnarc. org)*, pp. 1–32, 2002.

[13] A. F. Bingöl and İ. Tohumcu, "Effects of different curing regimes on the compressive strength properties of self-compacting concrete incorporating fly ash and silica fume," *Mater Des*, vol. 51, pp. 12–18, 2013.

2nd International Conference on Advances in Civil and Environmental Engineering (ICACEE-2023)

University of Engineering & Technology Taxila, Pakistan

Conference date: 22nd and 23rd February, 2023

Experimental investigation on Steel Fibre Reinforced Geopolymer Concrete Circular Columns

Muhammad Haseeb[1], Dr Rana Muhammad Waqas[2], Saqib Zubair[3]
[1]Department of Civil engineering, UET Taxila, mha_47@yahoo.com
[2]Department of Civil engineering, UET Taxila, rana.waqas@uettaxila.edu.pk
[3]Department of Civil engineering, UET Taxila, saqibzubair100@gmail.com

ABSTRACT

This study investigates of the structural behaviour of fibre-reinforced GPC columns under eccentric and concentric loads. 12 columns with a total length of 1000 mm and a circular cross section of 200 mm were tested in this investigation. To create GPC mixes, fly ash and slag were employed as precursor ingredients. Ordinary Portland cement (OPC) concrete columns were prepared as reference specimens. The influence of incorporating steel fibres and loading setups (concentric and eccentric loading) on the structural behaviour of GPC columns was investigated. The test findings showed that GPC is a suitable material that may be used to develop structural concrete elements with an acceptable performance. When there were no fibres present in the GPC specimens, a lower peak load values were observed as compared to corresponding OPC group specimens. It is observed that the overall behaviour of GPC specimens is comparable to that of traditional OPC concrete specimens. It was further observed that incorporation of steel fibres results in improving the peak axial loads and displacement responses of the specimens. The ultimate load values of fibre reinforced GC specimens were roughly 5-7% higher as compared to the corresponding OPC specimens.

KEYWORDS: geopolymer concrete, columns, eccentricity, loading capacity

INTRODUCTION

The climate of our planet is changing vigorously due to increased pollution and excessive emissions of CO_2 into the environment. All researchers are focusing on sustainable approaches to save the environment by promoting the practices of sustainable living and the development of environment-friendly technologies. The construction industry is also looking for green materials which are environmentally friendly and generate less CO_2 emissions. Ordinary Portland Cement (OPC) is the most widely used binding material (4 billion tons/year approximately) in the construction activities worldwide [1-2]. The production of OPC is responsible for huge amount of CO_2 emissions into the atmosphere i.e., OPC adds 1 ton of CO_2 emission into the environment on every 1 ton production. Furthermore, the manufacturing process of OPC needs huge amount of raw material, for instance, every 1 ton of OPC production consumes 1.6 tons of raw material. The significant CO_2 emission and enormous consumption of raw material for OPC production are both against the mechanism of sustainable construction [1].

The production demand of OPC concrete is growing continuously to meet the ever-increasing infrastructural demand. The construction industry is under pressure to work out the alternatives of OPC based materials that must meet the sustainability and green material criteria; and must have properties like OPC [2].

The most effective way to promote sustainable construction practice is the use of geopolymer concrete (GPC), which completely eliminates the use of OPC and is entirely composed of industrial wastes/by-products that are activated with the help of an alkaline solution [3-4]. GPC, also recognized as geo-cement and environment friendly concrete appeared as a new construction material having ability to develop OPC free concrete for all kind of construction applications [5-6].

FA is strongly recommended as a suitable source material for the production of GPC due to its chemical composition and adequate presence of Si and Al [7-8]. It is also reported that heat curing of GPC results in better engineering properties. Normally, heat curing of FA based GPC is done at a temperature of 80^{o}C – 100^{o}C for activation due to the low reactivity of FA at ambient temperature that does not produce satisfactory results [9-10]

It is also reported that curing of GPC at elevated temperatures results in better engineering properties when compared to OPC concrete [11-12]. Wallah and Rangan (2006) observed that GPC cured at elevated temperature produces better mechanical properties [13]. Assi et al. (2016) used OPC in different percentages as a partial replacement of FA to prevent heat curing because it makes difficult to use GPC in field applications [14]. Such OPC bended GPC matrix provides excellent performance even without thermal curing, but it is not completely comprised of waste materials.

There are several studies available reporting the better mechanical properties of Class F FA when heat curing is done for 24-48 hours. But ambient curing of FA based GPC does not produce the promising results due to low reactivity of FA at lower temperatures. Further the geopolymerization process of FA does not start at low temperature. It has been reported that use of heat curing for GPC is not practically feasible for onsite and field applications.

A large portion of the studies reported so far examined the fundamental engineering attributes of GPC like characterization of material, influence of varying the source material mechanical, physical and the chemical properties of GPC [2]. On the other hand, a limited number of studies tested the behavior of GPC structural elements.

The behavior of ambient cured GPC columns was tested by Farhan et al. (2018) and it was found that majority of the tested specimens failed around the middle height of the specimen. It was also concluded that steel fibres might be added to improve the ductility and loading capacity of the columns [15].

Sumajouw et al. (2007) investigated the behaviour of FA-based GPC columns (175mm x 175mm x 1500mm) tested at various loading eccentricities. According to the experimental findings, FA-based GPC columns could be employed in structural applications [16]. Chang. E. H. (2009) investigated the shear response of reinforced GPC beams [17]. The test outcomes indicated that the post cracking response of GPC beams were most part like the OPC beams. Andalib et al. (2014) examined the structural performance of GPC beams prepared with binary mixes of palm oil fuel ash (POFA) and fly ash. The failure pattern of GPC beams were observed to be similar to that of

conventional concrete beams [18]. The test results revealed that the response of GPC beams resembled to that of conventional concrete beams. The cracking pattern and loading capacities of both beams were very close to each other.

In recent times, Albitar et al. (2017) conducted an investigation on FA and lead smelter slag-based GPC columns [19]. The results disclose that FA/GLSS blended GPC columns displays identical structural behavior to conventional concrete columns.

Geopolymeric concrete has several advantages for the environment, but its use in construction is very limited. This is partly because to the dearth of research that examine the structural behaviour of GPC. GPC is a construction material that is still gaining widespread acceptance despite being relatively new in terms of field application. Therefore this study is planned to give comprehensive understanding about the structural behavior of GPC columns under different loading conditions.

EXPERIMENTAL PROGRAM

Material properties and mix proportions

A total of 12 circular columns with 200 mm diameter and 1050 mm length were prepared. These columns were subjected to two different loading regimes i.e. concentric axial loading and eccentric axial loading (eccentricity e = 15, 35 and 50mm). Steel fibres at 0.75% fraction by volume were utilized for all the fibre reinforced columns in our study. All the specimens were grouped into two distinct groups on the basis of mixture proportions.

The first group is named as OPC (ordinary Portland cement concrete columns) while the second groups is named as GPC (geopolymer concrete columns). The mix proportions used in the present study shown in Table 1. All the columns were prepared with concrete having target compressive strength of 40 MPa at the age of 28 days. The detailing of reinforcement and dimensions of the columns is presented in Fig. 1.

In the first group, one specimen was tested under the concentric loading while the remaining three specimens were subjected to eccentric loading. However in the GPC group, one plain specimen and one fibre reinforced specimen was subjected to concentric loading while all the remaining specimens were tested under the eccentric loading.

The primary constituents of GPC are the source materials and AAS other than the coarse aggregates and sand as used in conventional concrete. The most commonly used AAS in the manufacturing of GPC is a mixture of either NaOH and Na_2SiO_3 or kOH and potassium silicate [20]. AAS plays an important role in the polymerization process. In this study, AAS was prepared by mixing NaOH and Na_2SiO_3 in the specific ratios. NaOH of 12M molarity was used by mixing the specific amount of NaOH pellets in water. In manufacturing of fiber reinforced GPC columns, hooked steel fibres were used having 28 mm length, 0.6 mm diameter and tensile strength of 2500 Mpa.

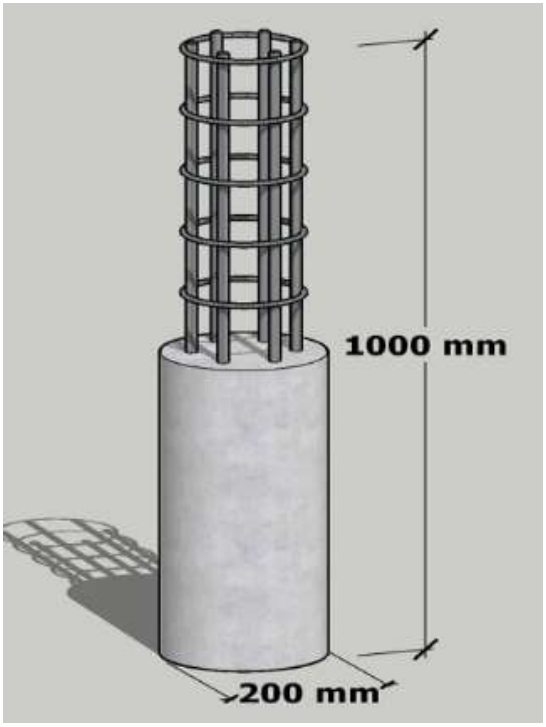

(a) Elevation

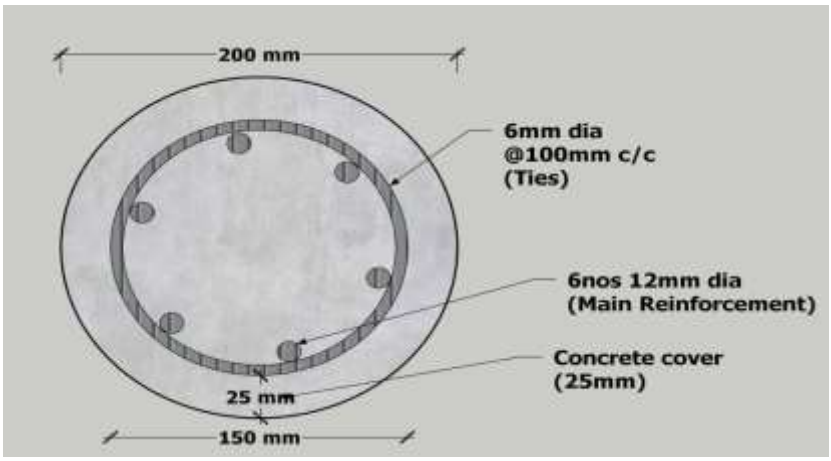

(b) Cross section

Figure 12 Detail of the test specimen

Test setup and procedure

All the columns were tested under the axial loading conditions after 28 days of curing. The load was applied gradually at the rate of 1kN/s with an electro-hydraulic testing machine having a capacity of 4800 kN. The specimens were loaded to failure with loading control criteria. The test setup employed in the present study is shown in Fig. 2. To produce the eccentric loading, steel pin having high strength were attached with the loading plate at the both ends of specimen [21]. The same loading setup was employed for the concentric loaded columns, apart from the loading pin. The axial deflections of all the specimens were measured by using two deflection gauges fixed vertically of the two opposing sides of columns.

Table 8. The detail of mix quantitites

Sr. No.	Group ID	Specimen ID	Mix quantities (kg/m^3)								
			Sand	CA	Cement	FA	SG	SH	SS	SP	water
1	OPC	OPC-0F -0E	640	1201	370	-	-	53	107	4	170
		OPC-0F -15E	643	1206	370	-	-	53	107	4	170
		OPC-0F -35E	640	1201	370	-	-	53	107	4	170
		OPC-0F -50E	643	1206	370	-	-	53	107	4	170
2	GPC	GPC-0F-0E	643	1206	-	200	200	53	107	8	-
		GPC-0F-15E	643	1206	-	200	200	53	107	8	-
		GPC-0F-35E	646	1212	-	200	200	53	107	8	-
		GPC-0F-50E	643	1206	-	200	200	53	107	8	-
		GPC-0.75F-0E	643	1206	-	200	200	53	107	12	-
		GPC-O.75F-15E	644	1208	-	200	200	53	107	12	-
		GPC-0.75F-35E	643	1206	-	200	200	53	107	12	-
		GPC-0.75F-50E	647	1214	-	200	200	53	107	12	-

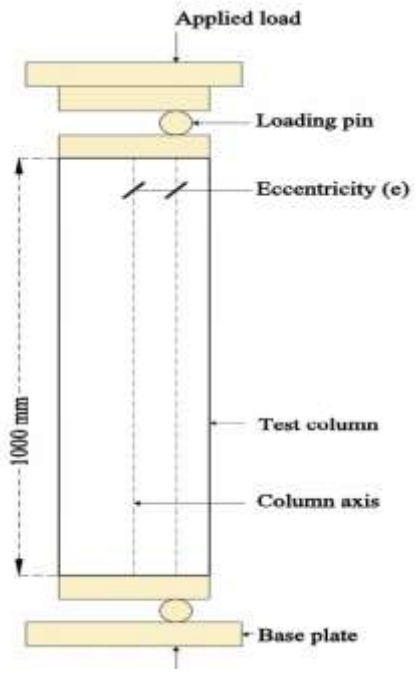

Figure 13 Test setup for eccentrically loaded specimens

RESULTS AND DISCUSSION

An electro-hydraulic testing device with a 5000 kN capability was used to apply the loading for all the axial loaded specimens at the age of 28 days. Under load control circumstances, 1kN/s intervals of load were applied to each column until it failed. The peal axial loads, failure modes, and load-displacement response of the specimens were investigated.

Ultimate loading capacity

Table 2 and Figure 3 presents the ultimate load values obtained from the experimental tests. It is depicted from the Figure 3 that failure load values of columns in GPC group are lower than the respective plain columns in OPC group (without fibres). The loading capacities of concentric loaded specimens in GPC group were 12% lower than the respective columns in OPC group. It was observed that the failure loads of GPC columns i.e. GPC-0F-0E, GPC-0F-15E, GCP-0F-35E and GPC-0F-50E were 12%, 20%, 22% and 25% lower respectively than OPC-0F-0E, OPC-0F-15E, OPC-0F-35E and OPC-0F-50E in OPC group. It was also observed that ultimate loading values of all columns were greatly affected by eccentricity values. The eccentricity of the axial load has negative effect on the loading capacities of columns. The same trend was depicted for the varying eccentricities in all the specimens of both groups. The load carrying capacities of all the columns were declined significantly as value of eccentricity was raised from the 0 to 50mm. The ultimate load values noted in eccentrically loaded specimens in GPC group i.e., GPC-0F-15E, GPC-0F-35E and GPC-0F-50E is 28%, 59% and 69% lower correspondingly than the failure load of the concentrically loaded column i.e., GPC-0F-0E.

It can be noted from the Figure 2 that fibre reinforced specimens exhibit higher ultimate load values when compared to the respective plain specimens (without fibres). All the fibre reinforced specimens were failed at 20-30% higher axial load when compared to the respective counterparts (without fibres). The peak axial loads of fibre reinforced GPC columns were approximately 6-8% more than the load carrying capacities of the respective column in OPC group. These higher ultimate load values of fibre reinforced specimens could be due to the useful role of fibres in enhancing the overall behaviour by stopping microcracks and bridging over macrocracks. This numerous cracking crack-arresting process continues until the fibres break or are pulled out that may be the possible cause of this increase in strength.

In comparison to their respective counterparts, GPC-0F-15E, GPC-0F-35E, and GCP-0F-50E, the fibre reinforced specimens of group GPC, designated as GPC-0.75F-15E, GPC-0.75F-35E, and GPC-0.75F-50E, respectively, reached maximum loads of 729kN, 460kN, and 340kN.

For the construction of reinforced concrete structures, structural engineers all around the world use several design codes as Eurocode 2, BS 8110, and ACI 318. These codes have different guiding concepts and design strategies from one another. Some codes are also more cost-effective than others.

In the present phase of study, the ultimate loading capacities of the columns were also calculated by the expressions suggested by standard codes i.e., BS 8110-97 and ACI318M-11.

According to BS 8110-97, the design ultimate axial force of a rectangular cross section column is given by the equation.

$$N = 0.4f_{cu}bh + (0.75f_y - 0.4f_{cu})A_{sc} \quad (17)$$

According to ACI Code 10.3.5, the useful design strength of an axially loaded column is given by

$$P_u = 0.85\emptyset \left[0.85f_c' \left(A_g - A_{st}\right) + A_{st}f_y\right] \quad (18)$$

The load capacity of a reinforced concrete column subjected to moment and axial loading can be estimated from the moment interaction diagram provided by design codes.

The ultimate load values predicted from the design code equations along with the test results are presented in Table 16.

The comparison between predicted and measured values showed that the test values are higher as compared to values predicted by design code models (Eq. 17 and Eq. 18). However, the values estimated by BS 8110-97 model (Eq. 17) were found to be more conservative than the predicted values of ACI 318-14. The ratio of BS 8110-97 model values to test values were found between 0.79-1.37. Whereas the ratio between ACI 318-14 model and test values were calculated as 0.74-1.24. A majority of the values estimated by BS 8110-97 model were 10-15 lower than test values. Whereas the values predicted by ACI 318-14 model were 15-25% lower than test values.

Table 9. The measured and predicted values of ultimate load

Mix ID	Ultimate load values (kN)				
	Test	ACI 318-14	BS 8110-97	Test/ ACI 318-14	Test/ BS 8110-97
OPC-0F -0E	955	790	820	0.84	0.87
OPC-0F -15E	722	592	632	0.83	0.89
OPC-0F -35E	440	355	380	0.83	0.88
OPC-0F -50E	338	250	275	0.76	0.83
GPC-0F-0E	880	727	762	0.85	0.88
GPC-0F-15E	587	505	587	0.88	1.03
GPC-0F-35E	351	290	353	0.87	1.05
GPC-0F-50E	262	208	255	0.75	1.02
GPC-0.75F-0E	1014	764	797	0.76	0.79
GPC-O.75F-15E	731	550	610	0.76	0.85
GPC-0.75F-35E	471	343	369	0.75	0.80
GPC-0.75F-50E	351	252	267	0.74	0.79

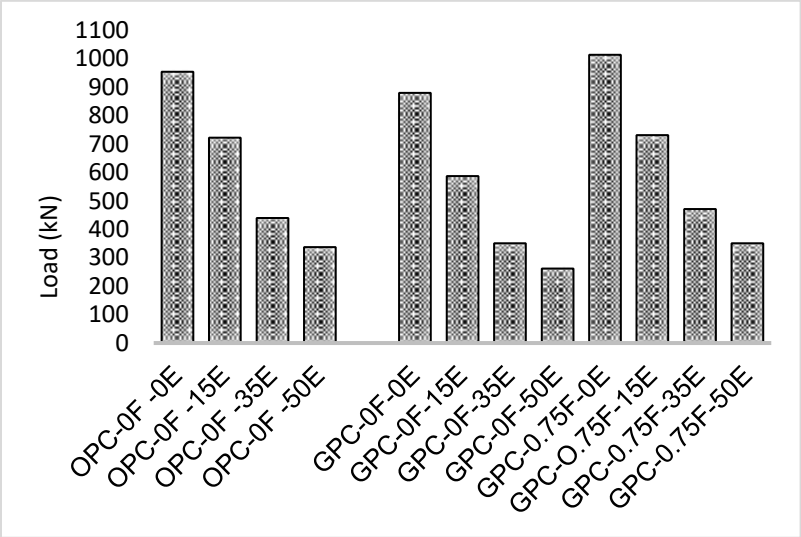

Figure 14 Ultimate loading values of columns

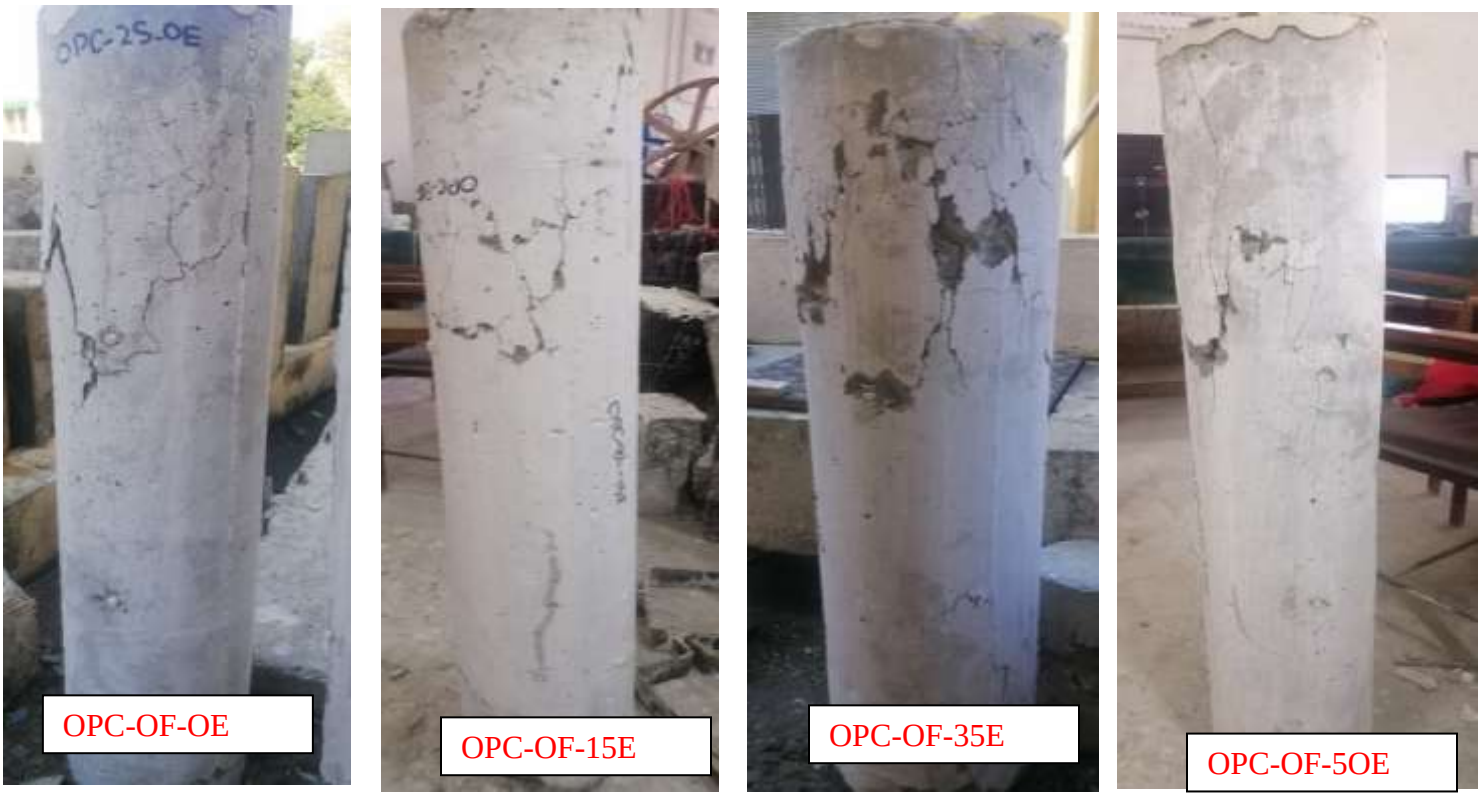

Figure 4 Failure mode of OPC specimens

Figure 5 Failure modes of GPC specimens

Axial load-displacement behavior of columns

The columns in the OPC and GPC groups were subjected to the test with axial loads that were concentric and eccentric (15, 35, and 50 mm). The columns' axial load-axial displacement characteristics are depicted in Figure 6. The failure modes of specimens are shown in Figure 4 and 5. For the columns OPC-0F-0E in the OPC group and GPC-0F-0E and GPC-0.75F-0E in the GPC group, axial loading was applied concentrically. It was observed that as soon as the tested columns reached their maximum axial stress, the concrete cover begin to spall off. However, at 90% of the maximum load, only hairline cracks were seen on the faces of columns. When the maximum load-bearing capacity was reached, the axial load in plain columns of the OPC and GPC groups decreased as a result of the removal of the concrete cover, however in the fibre-reinforced GPC columns, only the cover concrete's disintegration was seen.

In the load-displacement curve's falling phase, the columns GPC-0F-0E and GPC-0F-15E saw a sharp decline before reaching their maximum load carrying capacity. The early spalling of the concrete cover at the top and top face of the GPC-0F-0E and GPC-0F-15E specimens is to blame for this quick deterioration. The load carrying capability of the fibre reinforced columns GPC-0.75F-0E, GPC-0.75F-15E, GPC-0.75F-35E, and GPC-0.75F-50E, on the other hand, gradually decreased up until the point of failure. The addition of steel fibres caused the GPC specimens' initially brittle behaviour to gradually transition to a flexure behaviour as a result of the confinement effect the fibres supplied. These specimens, GPC-0.75F-0E, GPC-0.75F-15E, GPC-0.75F-35E, and GPC-0.75F-50E, have added fibres, which improves the ductility by 55%, 40%, 35%, and 25% greater than the corresponding specimens without fibres in the same group.

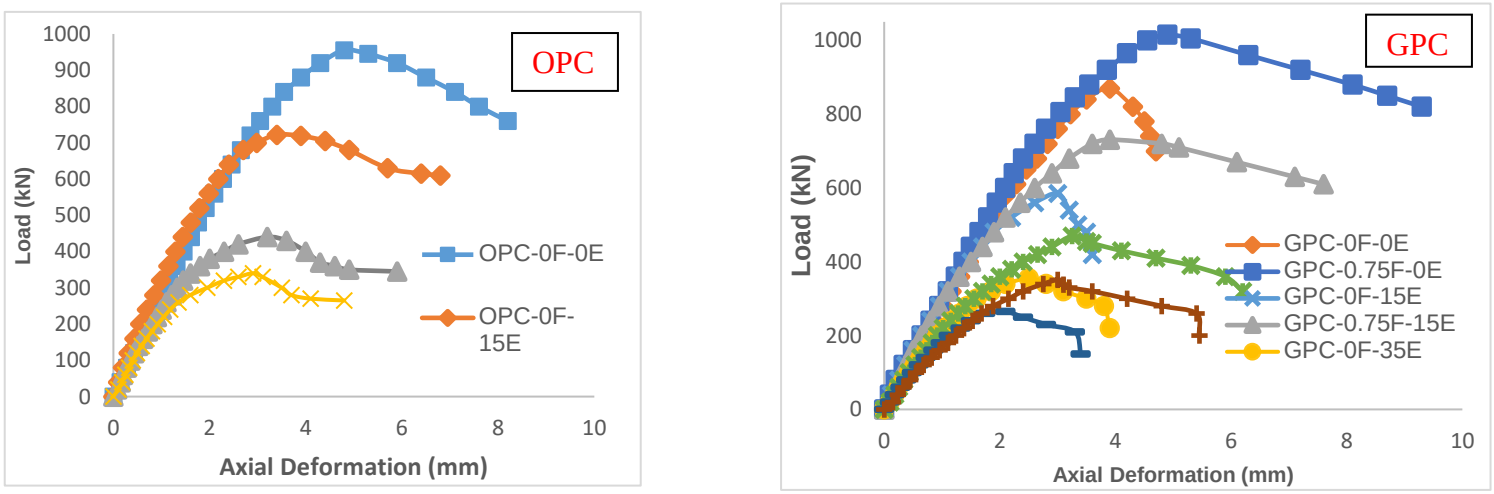

Figure 6. Axial-load displacement of columns

CONCLUSION

- When there were no fibers present in the GPC specimens, a lower peak load values was observed as compared to corresponding OPC group specimens.
- In comparison to its counterpart in the OPC group, the ultimate load values of the concentrically loaded plain specimens in the GPC group was 11% and 17% lower, respectively. The maximal axial load, however, was 20–30% higher for fibre reinforced GPC specimens than for the corresponding plain specimens in the same group. In comparison to their respective counterparts in the OPC group, the ultimate load values of fibre reinforced GC specimens were roughly 5-7% higher.
- Increase of the eccentricity of the applied load results in lowering the ultimate load values and ductility of the columns.

- Under concentric and eccentric loads, all plain OPC and GPC columns showed concrete cover spalling at the point of failure. On the other hand, there was no spalling on any of the fiber-reinforced GPC specimens.
- It has been observed that the overall behaviour of GPC specimens is comparable to that of traditional OPC concrete specimens.

REFERENCES

[1] M. Zahid, N. Shafiq, M. H. Isa, and L. Gil, "Statistical modeling and mix design optimization of fly ash based engineered geopolymer composite using response surface methodology," *Journal of cleaner production,* vol. 194, pp. 483-498, 2018.

[2] P. Duxson, A. Fernández-Jiménez, J. L. Provis, G. C. Lukey, A. Palomo, and J. S. van Deventer, "Geopolymer technology: the current state of the art," *Journal of materials science,* vol. 42, pp. 2917-2933, 2007.

[3] M. Sofi, J. Van Deventer, P. Mendis, and G. Lukey, "Bond performance of reinforcing bars in inorganic polymer concrete (IPC)," *Journal of Materials Science,* vol. 42, pp. 3107-3116, 2007.

[4] J. Aldred and J. Day, "Is geopolymer concrete a suitable alternative to traditional concrete," in *37th Conference on our world in concrete & structures,* 2012, pp. 1-14.

[5] A. Palomo, M. Grutzeck, and M. Blanco, "Alkali-activated fly ashes: A cement for the future," *Cement and concrete research,* vol. 29, pp. 1323-1329, 1999.

[6] J. Davidovits, "Geopolymers: inorganic polymeric new materials," *Journal of Thermal Analysis and calorimetry,* vol. 37, pp. 1633-1656, 1991.

[7] K. A. Komnitsas, "Potential of geopolymer technology towards green buildings and sustainable cities," *Procedia Engineering,* vol. 21, pp. 1023-1032, 2011.

[8] B. Singh, G. Ishwarya, M. Gupta, and S. Bhattacharyya, "Geopolymer concrete: A review of some recent developments," *Construction and building materials,* vol. 85, pp. 78-90, 2015.

[9] Y. Fan, S. Yin, Z. Wen, and J. Zhong, "Activation of fly ash and its effects on cement properties," *Cement and Concrete Research,* vol. 29, pp. 467-472, 1999.

[10] K. Somna, C. Jaturapitakkul, P. Kajitvichyanukul, and P. Chindaprasirt, "NaOH-activated ground fly ash geopolymer cured at ambient temperature," *Fuel,* vol. 90, pp. 2118-2124, 2011.

[11] A. S. Parveen and D. Singhal, "Mechanical properties of geopolymer concrete: A state of the art report," in *Proceedings of the 5th Asia And Pacific Young Researchers And Graduate Symposium, Jaipur, India,* 2013.

[12] A. Noushini, F. Aslani, A. Castel, R. I. Gilbert, B. Uy, and S. Foster, "Compressive stress-strain model for low-calcium fly ash-based geopolymer and heat-cured Portland cement concrete," *Cement and Concrete Composites,* vol. 73, pp. 136-146, 2016.

[13] S. Wallah and B. V. Rangan, "Low-calcium fly ash-based geopolymer concrete: long-term properties," 2006.

[14] L. Assi, S. Ghahari, E. E. Deaver, D. Leaphart, and P. Ziehl, "Improvement of the early and final compressive strength of fly ash-based geopolymer concrete at ambient conditions," *Construction and Building Materials*, vol. 123, pp. 806-813, 2016.

[15] N. A. Farhan, M. N. Sheikh, and M. N. Hadi, "Behaviour of ambient cured steel fibre reinforced geopolymer concrete columns under axial and flexural loads," in *Structures*, 2018, pp. 184-195.

[16] D. Sumajouw, D. Hardjito, S. Wallah, and B. Rangan, "Fly ash-based geopolymer concrete: study of slender reinforced columns," *Journal of materials science*, vol. 42, pp. 3124-3130, 2007.

[17] E. H. Chang, "Shear and bond behaviour of reinforced fly ash-based geopolymer concrete beams," Curtin University, 2009.

[18] R. Andalib, M. W. Hussin, M. Majid, M. Azrin, and H. H. Ismail, "Structural performance of sustainable waste palm oil fuel ash-fly ash geo-polymer concrete beams," *Journal of Environmental Treatment Techniques*, vol. 2, pp. 115-119, 2014.

[19] M. Albitar, M. M. Ali, P. Visintin, and M. Drechsler, "Effect of granulated lead smelter slag on strength of fly ash-based geopolymer concrete," *Construction and Building Materials*, vol. 83, pp. 128-135, 2015.

[20] Y. Ding, J.-G. Dai, and C.-J. Shi, "Mechanical properties of alkali-activated concrete: A state-of-the-art review," *Construction and Building Materials*, vol. 127, pp. 68-79, 2016.

[21] G. F. Huseien, J. Mirza, and M. Ismail, "Effects of high volume ceramic binders on flexural strength of self-compacting geopolymer concrete," *Advanced Science Letters*, vol. 24, pp. 4097-4101, 2018.

2nd International Conference on Advances in Civil and Environmental Engineering (ICACEE-2023)

University of Engineering & Technology Taxila, Pakistan

Conference date: 22nd and 23rd February, 2023

Comparison of UBC-1997 And IBC-2021 For Earthquake Resistant Design of High Rise RCC Building

Asad Ullah Khan, Adil Khan
University of Engineering & Technology Peshawar, Pakistan
asadullahk636@gmail.com, 18pwciv5027@uetpeshawar.edu.pk
Warda Zulhaj, Salwa Shaheen, Muhammad Ali Raza, Mohid Irfan
wardazulhaj2000@gmail.com, civilianuet222@gmail.com, tkhcollege786@gmail.com
18pwciv5184@uetpeshawar.edu.pk

ABSTRACT

This manuscript covers a study on the comparison between different aspects of reinforced concrete buildings designed according to two different codes in the specific seismic zone. The dimensions, configurations, and material properties are selected according to the usual practice in the area. For the purpose of this study, two to ten-story buildings were selected. The numerical models of selected reinforced concrete buildings were prepared in the finite element method-based software ETABS (Version 19). The seismic analysis and design of these structures were carried out for seismic zone 2B of UBC-97 and risk category III of IBC-21. After this, the design optimization study and cost comparison analysis has been done. The manuscript provides an idea about two different building codes i-e UBC-97 and IBC-21.

KEYWORDS: ETABS, UBC-97, IBC-21

INTRODUCTION

Humans started to fight against natural disasters from their first day on earth till now like earthquakes, floods, tsunamis, etc. To fulfill the needs of mankind, the development of the world started in every field of life. With the development of mankind, structures were constructed rapidly [1]. Now everyone can see hundreds of skyscrapers, bridges, and other fascinating structures across the world. To cope with the disaster of earthquakes, people started considering the earthquake-resistant structure in the design [2]. Earthquakes do not kill people but actually, people are killed by the collapse of badly designed and constructed buildings. The Kashmir earthquake of October, 2005 had devastating effects on the area with many buildings damaged or collapsed. Many people lost their lives [3]. It is almost impossible to exactly predict the occurrence of an earthquake but the histories of previous earthquakes make it possible to a great extent and with the different types of new materials available in our inventory, it is possible to construct an earthquake-resistant building [4]. Many structural typologies shall be analyzed to provide a solution to a problem that shall not only be efficient and cost-effective but also acceptable to the locality [5].

METHODOLOGY

1. Selection of Building
2. E-TABS modelling
3. Footing analysis and design in SAFE
4. Detailing in REVIT
5. Comparison on different levels

Selection of Building

Our project is about the earthquake resistant design and comparison of reinforced concrete buildings designed on UBC-97 and IBC-21 [6,7]. The hypothetical buildings of ten storeys having uniform grid of 96'x96' were selected and were designed in the software E-tabs and from there suitable sizes of structural members were selected after analysis. The dimensions of both buildings designed on UBC-97 and IBC-21 [6,7] having ten storeys, the beams are of size 15"x24", the columns provided are 30"x30" and slab thickness is 6.5".

ETABS Modelling

Two types of finite elements are used in creating the ETABS model; frame elements to model beams and columns and shell elements to model slabs and foundation.

The structure in ETABS is analysed and designed by performing the following steps.

1. First of all, we define the grid for the structure. Grid size used is of 4' x 4'. The number of bays in both directions are 4.
2. Number of stories = 10 and Height of each story = 11'.
3. The materials used in the project are: Concrete = 3000 psi (for beams and slab) Concrete = 4500 psi (for columns and foundation) Rebar = Grade 60 = 60000 psi
4. Various sections are defined for slabs, beams and columns. After much trial and error, we got the final sections as; Beams = 15" x 24", Columns = 30" x 30'', and Slabs=6.5" (thick)
5. After defining all the sections, the structure is drawn using drawing commands.
6. The load patterns and load combinations are defined as per the code.
7. The loads applied to the structure are; Dead load = Weight of the structure taken by the software itself. Live load = 40 psf (as per code) (on all floors except roof) Live load = 20 psf (as per code) (on roof only)
   Superimposed dead load = 90 psf (from floor finishes and wall loads) (on all floors except roof)
   Superimposed dead load = 40 psf (from floor finishes and wall loads) (on roof only)
8. The seismic loading parameters are defined as per the code. These values are specific to Peshawar City.
9. Mass source is defined as per code for the application of seismic forces to the model. The dead loads are used in mass source.
10. A rigid diaphragm is assigned to the model.
11. The Mat footing is modelled in SAFE.
12. The soil subgrade modulus is defined for the value of spring constant for the design of foundation.

13. The soil subgrade modulus for the design of footing is calculated as:

a) K = 12 x S.F x Bearing Capacity = 12 x 3 x 2.5 = 90 k/ft3 = 90000 lb/ft3

b) The "run" button is now pressed to run the analysis.

ANALYSIS

After carrying out the analysis the major outputs of structural analysis are the:
(1) Shear force diagrams, (2) Bending moment diagrams, and (3) Axial force diagrams

Shear Force Diagram

The SFD of the models using both the codes are given below in Figure 1 and 2. The values below are in the units of "kip**".**

UBC-97:

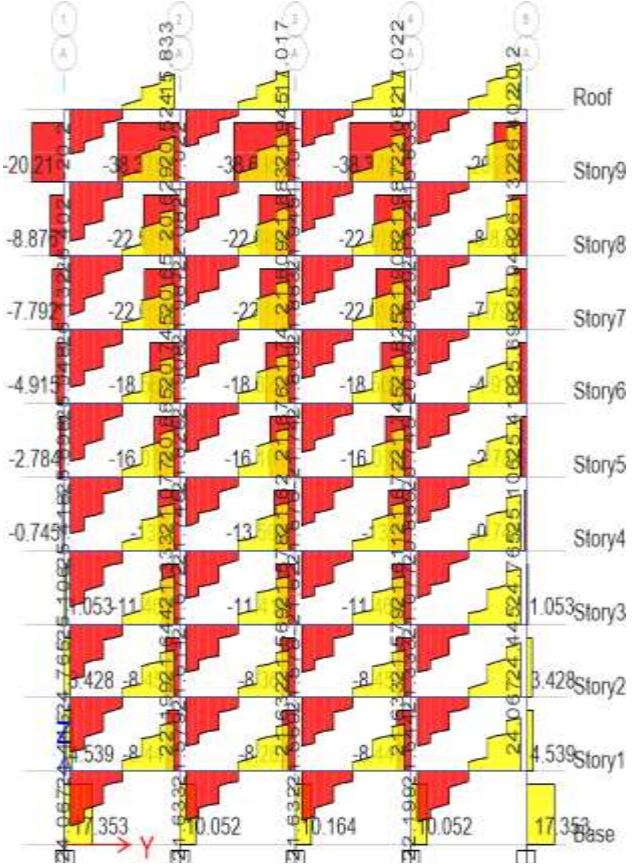

Figure 1: Shear force diagram (UBC-1997)

IBC-21

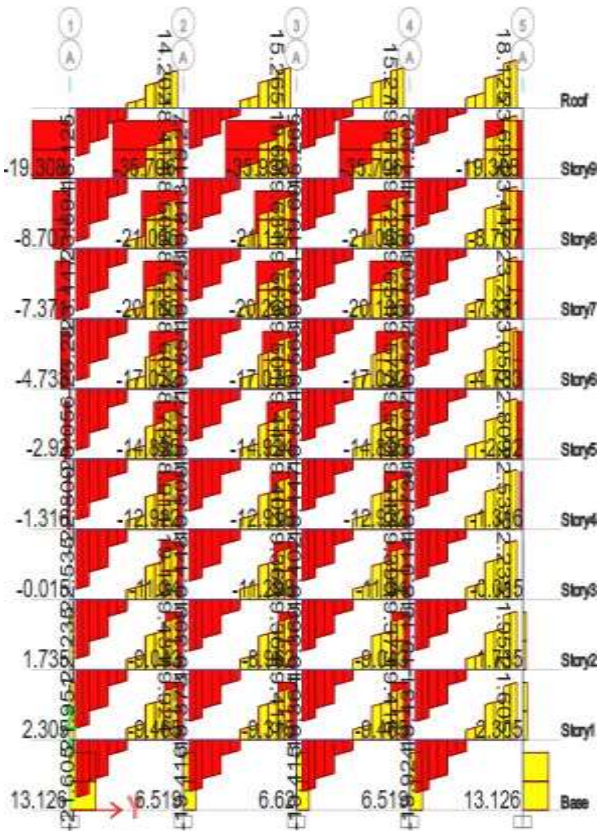

Figure 2: Shear force diagram (UBC-2021)

Bending Moment Diagram

The SFD of the models using both the codes are given below in Figure 3 and 4. The values below are in the units of "kip-in".

UBC-1997:

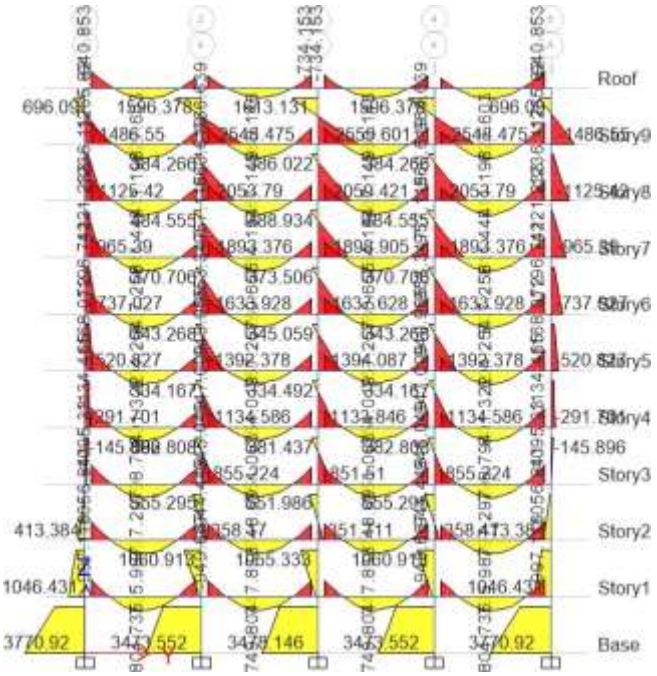

Figure 3: Bending moment diagram (UBC-97)

IBC-2021:

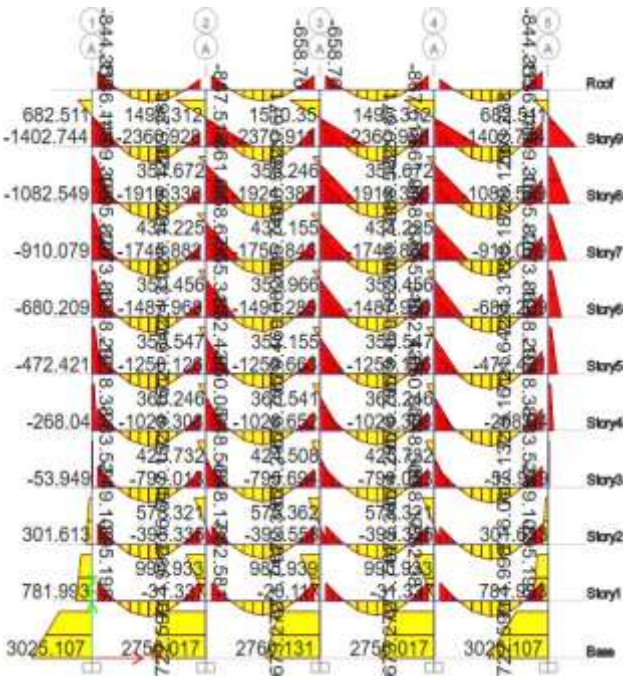

Figure 4: Bending moment diagram (UBC-21)

Axial Force Diagram

The Axial force diagrams of the models using both codes are given below in Figure 5 and 6. The values below are in the units of "kip".

UBC-97:

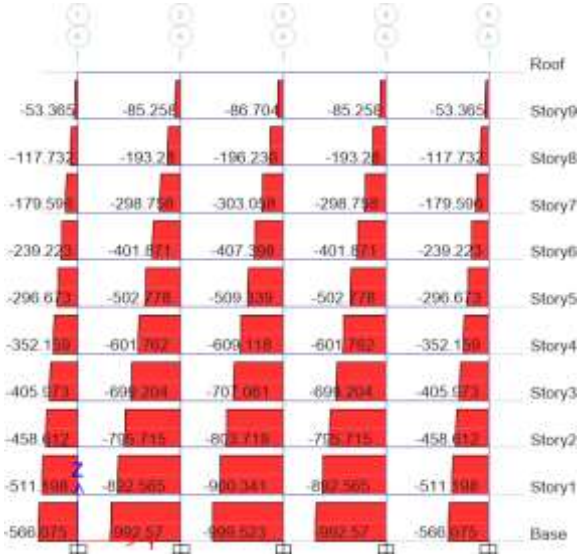

Figure 5: Axial force diagram (UBC-97)

IBC-21

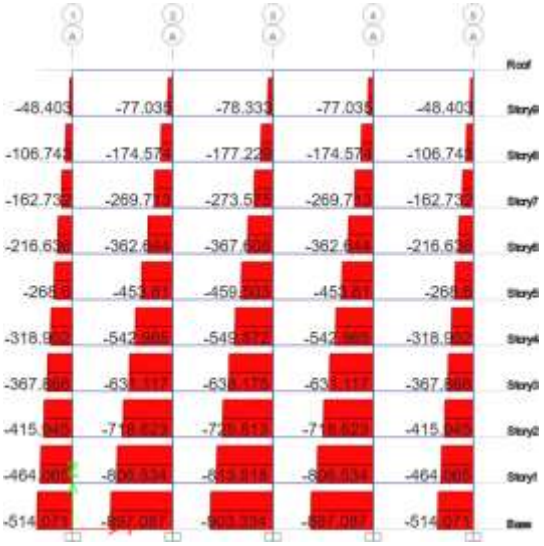

Figure 6: Axial force diagram (UBC-21)

RESULTS AND DISCUSSION

Base Shear Comparison

Base Shears are computed according to both the codes i.e. UBC-1997 and IBC-2021.

UBC-1997:

Base Shear computed from the Static lateral force procedure according to UBC-1997 is given by:

$$V = \frac{CvI}{RT}W$$

i. Cv = Coefficient of velocity I = Importance factor
ii. R = Response modification coefficient
iii. T = Time period
iv. W = Seismic weight of the structure
v. The total design base shear shall not be less than the following:

$V = 0.11CaIW$

Now: $V = \frac{2.5CaI}{R}W$ and $T = C_t(h_n)^{3/4}$

Finally, by putting all the values in these equations the Base Shear, **V = 968.66 kip**

IBC-2021:

Base Shear computed from the Static lateral force procedure according to IBC-2021 is given by:

$$V = \frac{SDSI}{R}W$$

i. SDS = Two-thirds of the maximum considered earthquake spectral response accelerations for short period (0.2s)
ii. I = Importance factor
iii. R = Response modification coefficient
iv. W = Seismic weight of the structure

$$SDS = \frac{2}{3}SMS, \text{ and } SD1 = \frac{2}{3}SM1$$

But, $S_{MS} = F_a S_S$ and $S_{M1} = F_v S_S$

For Peshawar City, Ss=0.6 to 0.8 and S1=0.25 to 0.3

i. SMS = maximum considered earthquake spectral response accelerations for short-period
ii. SM1 = maximum considered earthquake spectral response accelerations for 1 second period
iii. Fa = Site coefficient for short-period accelerations
iv. Fv = Site coefficient for 1-second period accelerations

Maximum Base Shear = $V = 0.01W$ and Maximum Base shear = $V = \frac{SD1I}{RT}W$

Finally, by putting all the values in the equations the Base Shear, **V = 954.35 kip**

Comparison

On comparing the Base Shears calculated from both codes there is not any significant difference between the two. Base Shear from IBC-2021 is slightly less than the Base Shear calculated from UBC-1997.

Shear Force and Bending Moment Comparison

The shear forces and bending moments in a particular beam designed for both codes are given below in Figure 7 and 8.

UBC-1997

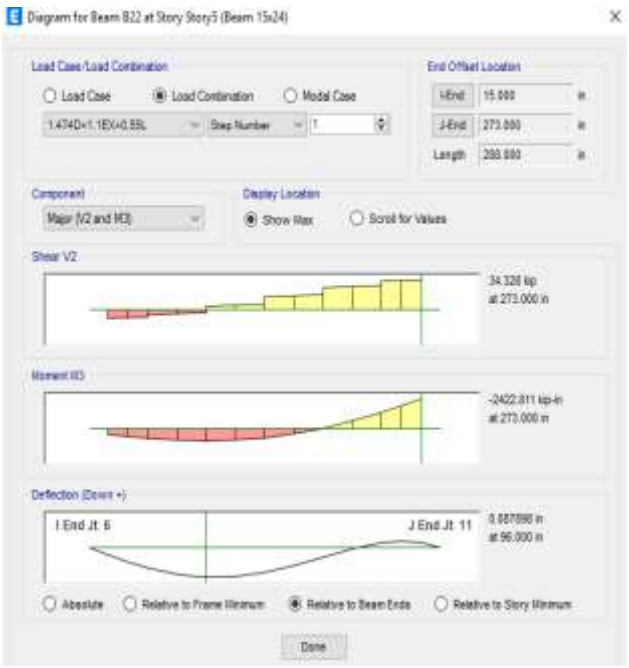

Figure 7: Shear force and bending moment diagram (UBC-1997)

Let's take a beam at level 5 of the building i.e. Beam B22 and analyzed it for the maximum load combination according to UBC-1997. Its shear force and bending moment diagram is given below:

So from the figure it is shown that the maximum shear force and bending moment in this beam are:
Maximum shear force **V = 34.328 kip**
Maximum bending moment **M=2422.81 kip-in**

IBC-2021

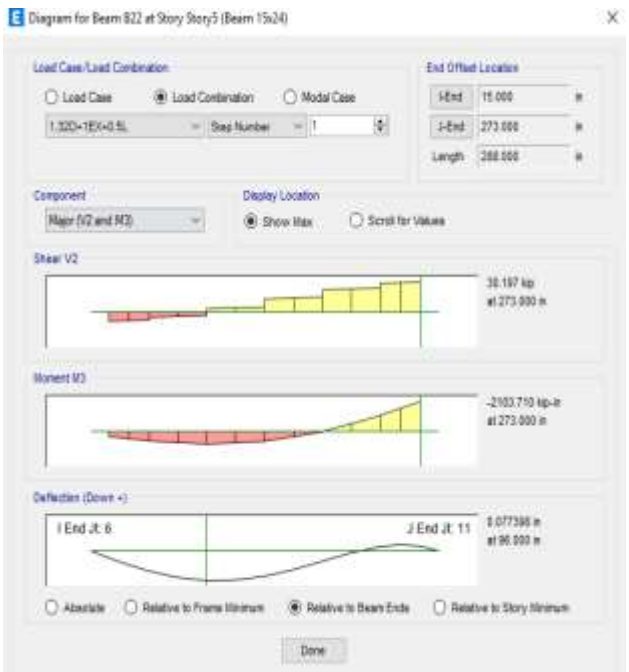

Figure 8: Shear force and bending moment diagram (IBC-2021)

Beam B22 is analyzed for the maximum load combination according to IBC-2021. Its shear force and bending moment diagram is given below:

So from the figure it is shown that the maximum shear force and bending moments in this beam are:
Maximum shear force **V = 30.197 kip**
Maximum bending moment **M=2103.71 kip-in**

Comparison

On comparing the maximum shear force and maximum bending moment developed in the beam, we can observe that the shear force and bending moment in the beam designed according to the IBC-2021 is slightly less than the shear force and bending moment in the beam designed according to the UBC-1997.

Axial Force Comparison

UBC-1997

Let's take the middle column at level 1 of the building i.e. Column C11 and analyze it for the maximum load combination according to UBC-1997. Its axial force diagram is given below in Figure 9:

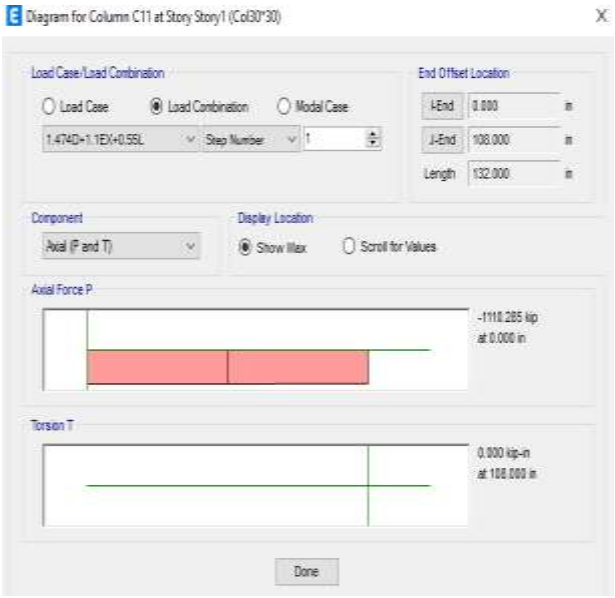

Figure 9: Axial force diagram (UBC-1997)

So from the figure it is shown that the maximum axial force **P = 1110.285 kip**

IBC-2021

Column C11 is analyzed for the maximum load combination according to IBC-2021. Its axial force diagram is given below in Figure 10:

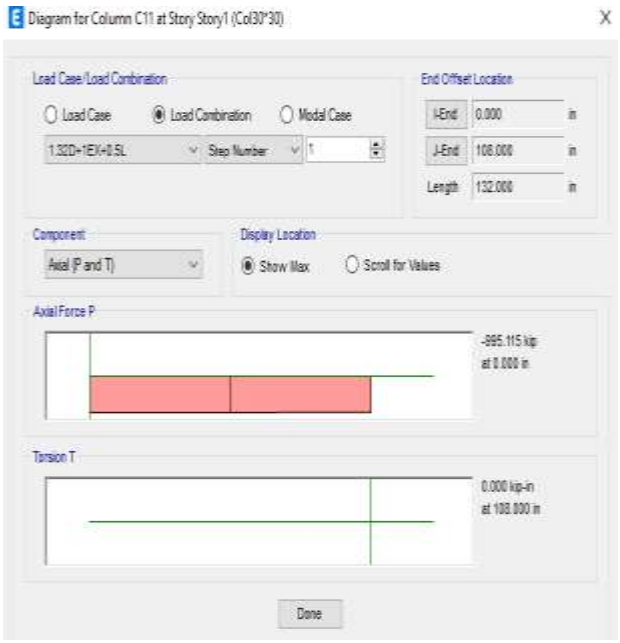

Figure 10: Axial force diagram (IBC-2021)

So from the figure it is shown that the maximum axial force **P = 995.115 kip**

Comparison

On comparing the maximum axial force developed in the column, we can observe that the axial force in the column designed according to the IBC-2021 is slightly less than the axial force in the column designed according to the UBC-1997.

CONCLUSION

1. UBC-97 estimates 1.5 % more base shear than IBC-21
2. UBC-97 estimates 13.68% more maximum shear force than IBC-21
3. UBC-97 estimates 15.16% more maximum bending moment than IBC-21
4. UBC-97 estimates 11.57% more maximum axial force than IBC-21.

REFERENCES

1 *Swenson, Alfred; Chang, Pao-Chi. History of Building (PDF). Archived from the original (PDF) on 2016-03-04.*

2 *Emerging techniques to simulate strong ground motion. Sandeep, ... A. Joshi, in Basics of Computational Geophysics, 2021*

3 *"Pakistan: A summary report on Muzaffarabad earthquake" ReliefWeb, 7 November 2005. Retrieved 23 February 2006.*

4 *O. Gunes, Turkey's grand challenge: Disaster-proof building inventory within 20 years, Case Studies in Construction Materials, Volume 2, 2015, Pages 18-34, ISSN 2214-5095, https://doi.org/10.1016/j.cscm.2014.12.003.*

5 *Wenjun Gao, Xilin Lu, Shanshan Wang, Seismic topology optimization based on spectral approaches, Journal of Building Engineering, Volume 47, 2022, 103781, ISSN 2352-7102, https://doi.org/10.1016/j.jobe.2021.103781.*

6 *UBC-1997*

7 *IBC-2021*

8 *ASCE 7-10*

9 *Design of Concrete Structures by Darwin*

2nd International Conference on Advances in Civil and Environmental Engineering (ICACEE-2023)

University of Engineering & Technology Taxila, Pakistan

Conference date: 22nd and 23rd February, 2023

Study of Old and New Building Code of Pakistan by Comparative Analysis of High-rise Building in Zone 2b and 3

Irfan Ullah[1], Muhammad Yaqub[1]

[1]Department of Structural Engineering, University of Engineering and Technology Taxila.

Engrirfan9934@gmail.com

ABSTRACT

Pakistan officially announced its building Code after the devastating Kashmir earthquake in 2005, known as Building Code of Pakistan (BCP-2007). The code was originally based on dividing the entire country into seismic Zones depending on the range of peak ground acceleration and had significant similarities with Uniform Building Code UBC-97. The building code of Pakistan was updated recently in 2021 based on seismic design category depending on short and long period spectral acceleration. This new code is derived from International Building Code IBC-21. The structural integrity and safety of buildings based on BCP-07 remains a major concern for structural engineers. This study primarily focused on the comparison of old and modified building codes of Pakistan for Seismic Zones 2b and 3. For this purpose, A 25 stories building with 3 basements, located in Rawalpindi (Seismic Zone-2B) was selected and modelled using ETABS-16. Static and dynamic Analysis were carried out by Equivalent lateral force method and Response Spectrum analysis respectively. A comparison of Story Displacement, Story Drift, Story Moments, and Base Shear between BCP-07 and BCP-21 was plotted. Static Analysis for BCP-2021 Storey displacement and Story Drift show Average increase of 48% in Zone-2b and 54% in Zone-3. The maximum Storey drift is shown in the middle floors 14th to 17 floors for all cases. Response spectrum analysis shows 19 % less value for Zone 2b and 16 % for Zone-3 for Story Drift and Story Displacement. Results indicate BCP-21 based on Ss and SI values gives the more direct information and more useful than BCP-07.

KEYWORDS: Building code of Pakistan, RSA, ELF, story shear, base shear, overturning moment.

INTRODUCTION

Pakistan is the 5th most Populus country in the entire world. In last three-years average population growth of Pakistan is about 1.83% so there is a major concern to accommodate these people [1-3]. There are several high-rise structures under construction in different Cities of Pakistan. Geologically, Pakistan is located on a seismically active Zone of Eurasian and Indian plate [4] [5]. These tectonic plates have been geologically active since the ancient times [6]. Due to the tectonic movements of these two plates the Indian subcontinent and northern south Asian region has experienced several earthquakes over the years [7] [8]. These earthquakes were primarily a result of tectonic movements and subduction Zones in the Karakoram Range, Iranian plateau, and Himalayan range [9]. The region of current Pakistan has experienced several devastating earthquakes in the past such as, Quetta in 1935, Pattan in 1974, and Kashmir in 2005 [10] [11]. These Multiple ground tremors are connected to a complex geological activity on Chaman fault

and Indo Eurasian subduction Zone [12]. All the past earthquake data revealed that Pakistan is situated in highly active Seismic region [13]. The frequency of major and minor earthquakes in the region is relatively high so the structural and design engineers need to be very careful when it comes to design Highrise buildings and structures in seismically active Zones [14].

According to researchers after the earthquake of October 8, 2005, the government of Pakistan assigned the National Engineering Services Pakistan (NESPAK) the task of developing a new seismic code for Pakistan to better safeguard structures from future damage caused by seismic activities [15]. According to reports NESPAK failed to keep up the pace with the task and the code development was delayed several times [2, 4]. Due to delay of NESPAK, the government of Pakistan assigned the task to The Earthquake Reconstruction and Rehabilitation Authority (ERRA), ERRA published the new seismic building Code for Pakistan region in 2007 and used the Uniform Building Code-97 as a reference with some modification for Pakistan region [4, 10]. UBC-97 was modified again in 2000 named as international building code IBC-2000. International council of codes used to update the code in every three years [11]. Hence in 2007 when Pakistan's building code was developed the authorities had three most recent versions of IBC code still UBC-97 was followed in Pakistan for structure designing. Now the latest version of IBC documents was updated in 2021 [16].

Wednesday, February 2, 2021, Pakistan also officially announced updated building Code which is known as (BCP-2021). following permission from the ministry of science and technology and evaluation by the International Code Council (ICC). The International Building Code (IBC-2021) is adopted in this revised version with several changes for Pakistan region [10, 15]. This Building Code include updated probabilistic seismic hazard analysis (PSHA) for Pakistan, revised design wind speeds, revised snow loads, revised rain loads, revised provisions for flood-resistant buildings, etc. Seismic design (SDC) category is included in the Building Code of Pakistan 2021 in place of the seismic Zoning idea.BCP-2021 is Based on Structure Response acceleration instead of peak ground acceleration [7] [17].

The current research is a detailed Study of comparison between BCP-2007 and BCP-2021. The significant gap between two modifications of the building code of Pakistan left a major concern among the engineering community regarding the structural integrity, safety, and design capacity of the existing buildings. It was necessary to research the differences between the two codes and how the old buildings designed under BCP-07 would perform under the modified building code BCP-21 [18].

METHODOLOGY

This research was carried out on an existing 25 stories building with 3 basements, located in Rawalpindi (Seismic Zone-2B) was selected and modelled using ETABS-16. Static and dynamic Analysis were carried out by Equivalent Lateral Force method and Response Spectrum Analysis respectively. Equivalent lateral force procedure uses a set of forces acting on a structure to Estimate future Earthquake [19]. ELF gave us minimum design base shear on which Structure must be Designed. On the other hand, response spectrum analysis was used as dynamic analysis. Response

spectrum analysis use different mode shape of a structure to define response of a structure against different load patterns [20].

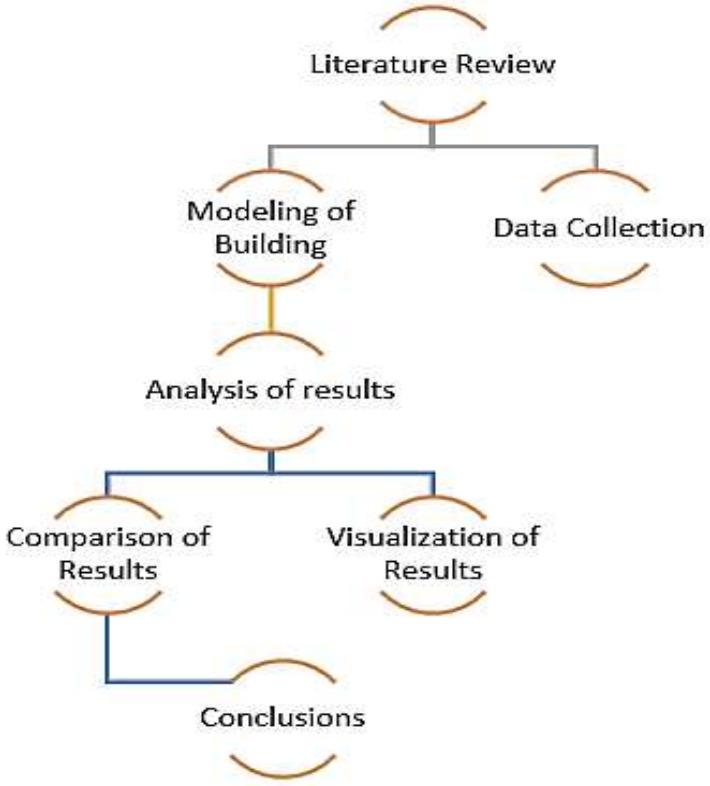

Figure 15 Flow chart of the study

Software Modeling and Analysis of Building

According to architectural plans, different story height of 10ft, 11ft, 12ft, was used for each story. Total height of building was 232ft consisting of Central lift and RCC walls in basement around four sides. The total size of the building was 148ft x 342ft. The concrete of 4500 and 6000 Psi compressive strength was used for the structural members. The sizes of members are given below in table 1.

Table 10 Size details of all structural members

Storey Heights	10-ft,11-ft,12-ft
Slab Thickness	6-in,6.5-in,7-in
Beams	12"x18",12"x21,15"x21" 15"x24",15"x30",18"x24" etc.
Columns	15"x24",24"x24",18"x30", 39"x39",42"x42",39"x48"
Shear wall	15-in

Modelling of this building was done in ETABS-2016. Following steps were followed, assigning number of stories, defining material properties, defining section properties, and further defining stiffness modifiers, Diaphragm, floor meshing, load patterns, load combinations, mass source, assigning of support to the base and finally occupancy and seismic loads were assigned to the building according to BCP-2007 and BCP-2021. After the modelling of the building the analysis was rub on the structure and ETABS generated 3D model of the building and displacements as shown in figure 1a and 1b respectively.

RESULTS AND DISCUSSIONS

The Seismic analysis results were derived from ETABS 2016 Software. Results were compared for BCP-2007 & 2021 for seismic Zone-2b and Zone-3. Story displacement, Story drift, overturning moments and base shear were compared using ELF and RSA procedure. Different Cases are shown below with the help of graphical representation.

Comparison of Story Displacement

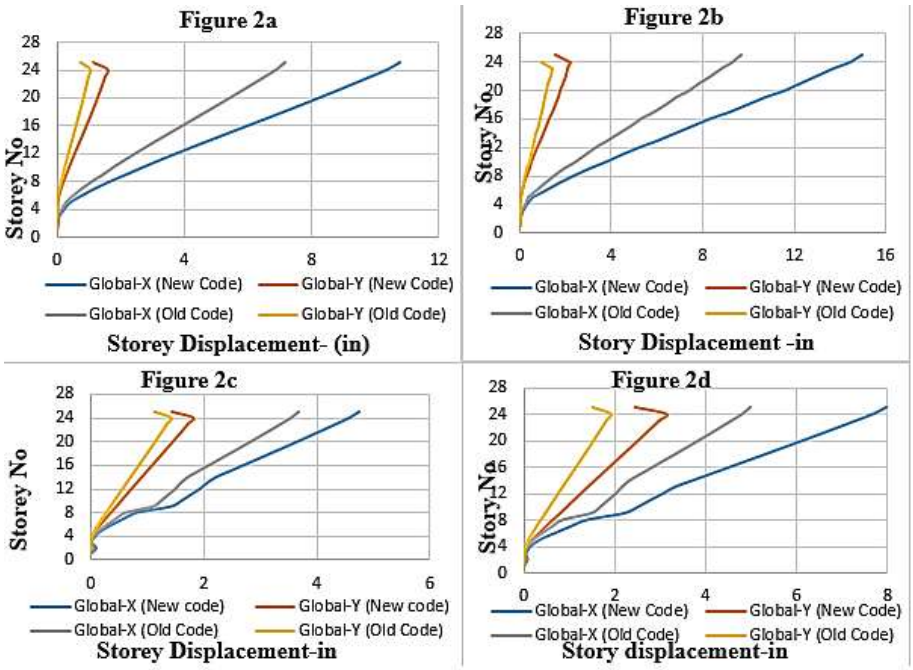

Figure 2: 16a, and 2b are Story displacement of Zone 2b and 3 for old and new codes for static analysis and figure 2c, 2d are story displacement for Zone 2b and 3 for old and new codes for dynamic analysis.

The story displacement is maximum in the case of static analysis carried under the provisions of new design BCP-21. While the maximum story displacement for response spectrum analysis was also observed for the design carried out under modified building code of Pakistan. The maximum story displacement values for modified code are because of the probabilistic seismic hazard

assessment modification in the new code. The dynamic analysis also causes the more displacement in the structure because of its high and intense impact load values [21]. The minimum story displacement values were observed for the design which was carried out under old design code. The lower values of displacement indicate an overestimated factor of safety making the design uneconomical and vulnerable to failure without any warning [22].

Comparison of Story Drift for Static and Dynamic analysis

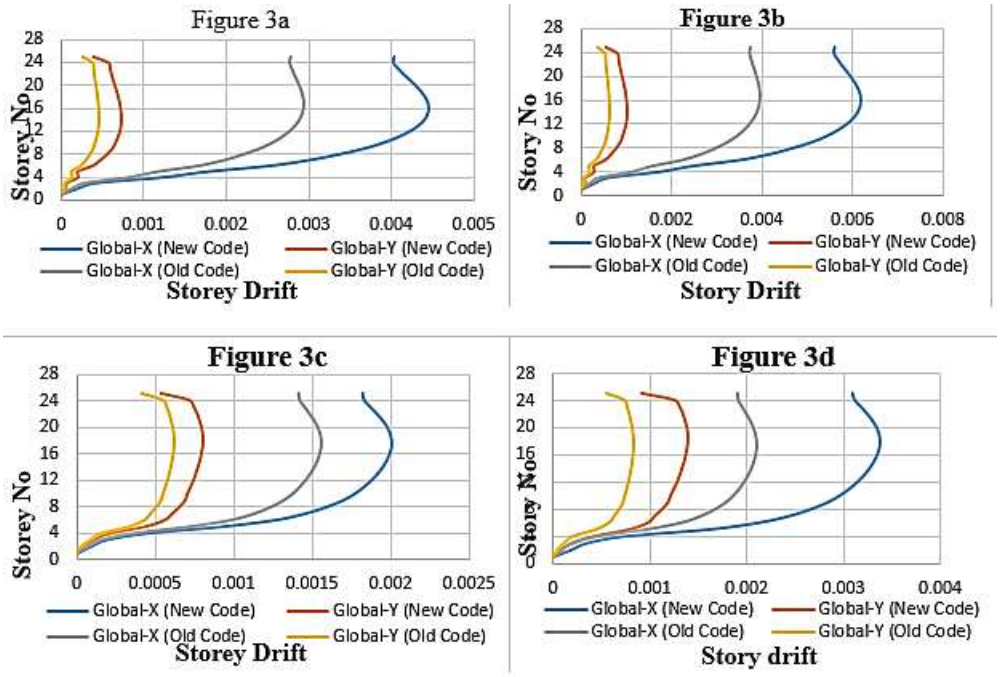

Figure 3: 17a, and 3b are story drift of Zone 2b and 3 for old and new codes for static cases and figure 3c and 3d are story drift of Zone 2b and 3 for old and new codes for dynamic cases

The maximum Storey drift is shown in the middle floors 14th to 17 floors for all cases. Response spectrum analysis show 19 % less value for Zone 2b and 16 % for Zone-3 for Story Drift.

Comparison of Base Shear and Story Shear

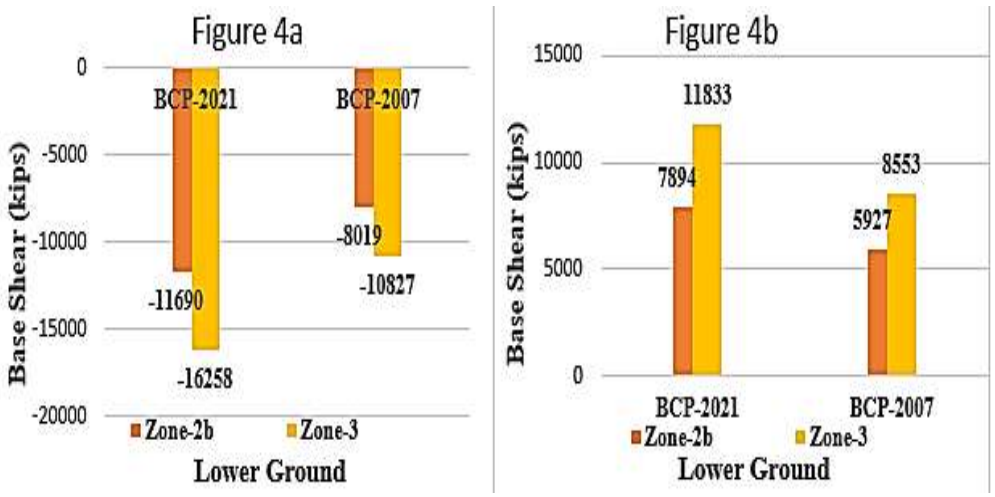

Figure 4: 18a represents base shear value and figure 4b shows the story shear value for static and dynamic cases respectively.

The base shear is maximum for new code in Zone 2b while the story shear is also maximum in Zone 2b for modified building code BCP-21. The results suggest that the BCP-21 outperformed the BCP-07.

CONCLUSIONS

- From Graphical data During Static Analysis for BCP-2021 Storey displacement and Story Drift show Average increase of 48% in Zone-2b and 54% in Zone-3.
- Storey displacement increased with the height of building. From the tables highest displacement is shown on top of the building for all cases.
- The maximum Storey drift is shown in the middle floors 14th to 17 floors for all cases.
- Response spectrum analysis show 19 % less value for Zone 2b and 16 % for Zone-3 for Story Drift and Story Displacement.
- The maximum overturning moment obtained from response spectrum method is lesser than those obtained by equivalent static lateral force method.
- The base shear from the graphical data show increase in all cases for new Code.
- Updated building Code show increase in Base shear For Zone-2b is 45% and for Zone-3 is 52% for static analysis.
- Dynamic analysis shows 16 % lesser value of base shear for Zone-2b while 12 % for Zone-3 for Updated Building Code.
- This comparison indicates that the Updated Building Code which is based on Ss and S1 value of Site giving more direct information compared to UBC Zoneing concept.

- Initial cost of the project becomes high due to advance analysis, but it is relatively less than the cost of seismic retrofitting, and human loss.
- Equivalent static lateral force method gives higher values which makes building uneconomical hence consideration of Dynamic analysis is also needed.

RECOMMENDATIONS

The research was carried out only on two seismic Zones of the country under new building code. If time allows to include all the seismic Zones in research, it could be a groundbreaking study towards the hazard and structural integrity evaluation of existing buildings under the provisions of building code of Pakistan BCP-21.

ACKNOWLEDGEMENT

The cooperation of numerous devoted and helpful persons allowed this research to be completed. It is challenging to evaluate how much they helped me with my research task. I would like to express my gratitude to my research supervisor Dr. Muhammad Yaqub, University of Engineering and Technology Taxila and Engr. Ali Abbas National University of science and technology for their capable direction in the completion of this task. they provided input both personally and professionally.

REFERENCES

1. Reddy, A.P.K. and R.M.P. Kumar, *Analysis of G+ 30 Highrise Buildings by Using Etabs for Various Frame Sections In Zone IV and Zone V.* Int J Innovative Res Sci Eng Technol, 2017. **6**(7).
2. El-Kholy, A.M., H. Sayed, and A.A. Shaheen, *Comparison of Egyptian Code 2012 with Eurocode 8-2013, IBC 2015 and UBC 1997 for seismic analysis of residential shear-walls RC buildings in Egypt.* Ain Shams Engineering Journal, 2018. **9**(4): p. 3425-3436.
3. Panchal, A. and R. Dwivedi, *Analysis and design of G+ 6 building in different seismic Zones of India.* International Journal for Innovative Research in Science, Engineering and Technology, 2017. **6**(7).
4. Siddique, A., et al., *Seismic Evaluation of high-rise RC buildings in Pakistan.*
5. Borkar, S. and G. Awchat, *Analysis and Design of G+ 6 Building in Different Seismic Zones by using Software.* 2019.
6. Hassan, W., et al. *The seismic performance evaluation of RC high-rise buildings designed to various building codes*. in *Proceedings of IABSE conference–Engineering the developing world*. 2018.
7. Kumar, C.V., et al. *Evaluation of Response Spectartrum and Equivalent Static Analysis for recognizing the safest position of Floating Columns by ETABS in Zone V*. in *2022 International Conference on Computational Intelligence and Sustainable Engineering Solutions (CISES)*. 2022. IEEE.
8. Rajeswari, P. and M.A.K. Neelakantam, *SEISMIC ANALYSIS AND DESIGN OF MULTISTOREY BUILDING IN DIFFERENT SEISMIC ZONES BY USING ETABS.* 2019.
9. Duan, H. and M.B.D. Hueste, *Seismic performance of a reinforced concrete frame building in China.* Engineering Structures, 2012. **41**: p. 77-89.
10. Karim, A.K.A., *The Seismic Analysis for a Multi-Story Building Due To UBC 1997&IBC 2006 Codes.* IWC, 2011. **5**: p. 1.
11. Ansari, T.A. and S. Jamle, *Performance Based Seismic Analysis of Regular RC Building.* International Journal of Management, Technology And Engineering, 2019: p. 342-351.
12. Zaidi, K., L. Yanhui, and A.-B. Khalil, *Dynamics History Analysis for Multi-Story Structure Building in Yemen.* Int. J. Rec. Innov. Acad. Res, 2018. **2**(1): p. 1-12.
13. Ramakrishna, B., et al. *Analysis of Multi-Storied Building in Different Seismic Zones using STAAD Pro*. in *IOP Conference Series: Earth and Environmental Science*. 2022. IOP Publishing.
14. Chittankumar, M. and B.S. Chandra, *Analysis of G+ 10 Multi-storey Building using ETABS.*
15. Ali, J., et al., *Linear Dynamic Analysis of Different Structural Systems for Medium Rise Buildings (A Case Study).*
16. Shah, A., et al. *An analysis of Seismic Provisions of Building Code of Pakistan*. in *5th World Engineering Congress (WEC 2013)*. 2013.
17. Khan, N., et al., *Effects of infills in the seismic performances of an RC factory building in Pakistan. Buildings 2021, 11, 276.* 2022, s Note: MDPI stays neutral with regard to jurisdictional claims in published ….
18. Ahmad, N., *Force-based seismic design of steel haunch retrofit for RC frames.* Earthquakes and Structures, 2021. **20**(2): p. 133-148.
19. Djibrillah, O., *SEISMIC DESIGN AND ANALYSIS OF MULTI STORY REINFORCED CONCRETE BUILDINGS IN MALAYSIA.* 2013.
20. BALARAM, M. and D.A. MURTY, *TIME HISTROY ANALYSIS OF MULTI SOREY BUILDING FOR HIGHRISE (G+ 10) STRUCTURES.* Journal of Engineering Sciences, 2018. **9**(1).
21. Dash, S.S., *Seismic Analysis of High-Rise Building by Response Spectrum Method*. 2015.
22. Babu, P.S. and K. Murali. *Comparative analysis of G+ 25 structure with and without shear walls using ETABS*. in *AIP Conference Proceedings*. 2022. AIP Publishing LLC.

2nd International Conference on Advances in Civil and Environmental Engineering (ICACEE-2023)

University of Engineering & Technology Taxila, Pakistan

Conference date: 22nd and 23rd February, 2023

Potential of waste as construction material – A Review

[1]Muhammad Afaq Khalid[1], Sohail Afzal[2]

[1]Capital University of science and technology Islamabad, Sohailafzal@cust.edu.pk
[2]Capital University of science and technology Islamabad, Afaqkhalid34@gmail.com

ABSTRACT

About 960 million tons of solid waste is being generated annually as by-products during industrial, mining, municipal, agricultural and other processes. Waste production is increasing day by day, therefore it is thrown away and has no use burning fossil fuels like gas and diesel has a significant detrimental impact on the environment on construction companies. Massive volumes of coarse pollutants, which are closely connected to heart disease, are produced by every building construction and demolition. These gas emissions from building projects, which include carbon dioxide, methane, and other waste products, pollute the air and are thought to be a factor in global warming a lot of present era studies had considerable conclusions are the no use of different wastesas construction material. Two types of wastes industrial and natural These industrial wastes, which pollute the water, air, and soil, include cafeteria waste, dirt and gravel, masonry and concrete, scrap metals, rubbish, oil, solvents, and chemicals. They also contain weed grass and trees. Organic garbage is a form of natural trash that originates from living things like plants or animals.Poor waste management directly impacts numerous habitats and species as well as air pollution and climate change.

KEYWORDS:

Use of industrial and natural waste, Cheap construction material, Sustainable construction, Save environment and Use of Walnut shell and Coconut Shell.

INTRODUCTION

The prime considerations of civil engineering are the safe and economical construction, but due to the speedy construction activities we are hurting the natural environment. To balance out the construction activities and healthy environment now civil engineers are working on sustainable development keeping the environment safe and healthy. Due to the speedy construction practices, we are running out natural resources such as stone, sand, wood, iron and lime etc. Coconut shell and Walnut shell are two waste materials which can be reused as construction material. This is a sustainable act towards construction.

We use various waste types with construction qualities in various types of construction. Debris that can be recycled and utilised as a construction material includes slag, rice husk ash, fly ash, cement dust, brick waste, coconut shell waste, sludge, glass, and other industrial and agro-wastes.For a more affordable and sustainable alternative, some wastes, such coconut shells, can be replaced with coarse aggregate. To protect concrete against sulphate attack, silica fume can also

be added. This silica fume infused concrete generated good results when compared to conventional concrete and Blast-Furnace Slag as a replacement of natural sand and cement in the concrete. To produce concrete that is both affordable and sustainable, we employ coconut shell and blast furnace slag.

It was examined how waste materials were used in concrete. Habibi,et al. (2021) concluded that the benefits and drawbacks of the waste materials utilised in concrete is the study's main goal[1].Some materials are utilised for cement, while others are used in place of coarse and fineaggregates. Fig 1 shown that the different types of wastes There is a greater use of fly ash in the cement industries. Additionally, silica fume has certain pozzolanic qualities. Glass trash has recently been used in the production of bricks, paver blocks, and other building materials. As cement and aggregates in concrete, tyres are also changed. Utilizing garbage is mostly done to reduce pollution and preserve resources for long-term growth.

(a)  (b) 

(c)  (d) 

Figure 1: Different types of waste (a) waste of plastic (b) waste of solid waste of wood (c) waste of glass (d) waste of steel

EFFECTS OF DEPICTING NATURAL RESOURCES

Industrialization is a result of economic growth, which raised the value of the natural resources that were harvested. The environment can be harmed by overuse of natural resources in mining, agriculture, and deforestation. The current study looks into how abundant natural resources affect carbon dioxide (CO2) emissions in this regard. The study makes use of annual panel data from the BRICS countries from 1990 to 2015. The augmented mean group (AMG) panel algorithm infers the heterogeneous effect of natural resources on CO2 emissions among the BRICS countries. It is robust to crosssectional dependency and heterogeneity.

Danish et al. (2021) concluded that study evaluated the EKC hypothesis and looked into how renewable energy sources and natural resources affect environmental pollution[2]. The five

BRICS countries' data, which ranges from 1990 to 2015, is used in the study. The study's recommended AMG panel estimating approach for handling CD and heterogeneity combined with efficient and consistent estimations. According to the empirical findings, Brazil, China, and India's CO2 emissions are not significantly impacted by natural resources. However, because there are so many natural resources available, their richness aids in reducing pollution in Russia. Because of the excessive resource consumption in South Africa, natural resources are not environmentally friendly. Additionally, Kulkarni et al. (2013) the use of renewable energy sources helps reduce environmental pollution using natural resources wisely to reduce reliance on fossil fuels Additionally, additional money should be set aside for R&D to investigate the nation's sources ofrenewable energy[3]. In Brazil, Russia, and India, natural resources do not contribute to environmental pollution; nonetheless, in light of the negative environmental impact of natural resources, these nations should make future plans to reduce their dependency on energy imports. Brazil, Russia, and India must act decisively to achieve this goal since economic growth, as well as increased exploitation of natural resources through mining, deforestation, and agriculture, may have an adverse impact on the environment. However, causality analysis demonstrates that renewable energy is caused by natural resources, hence the Government of India needs now we Baloch et al. (2019)concluded that the use Nonmetallic natural resources such as clay, sand, limestone, chalk, crushed stone, coarse-sand, building stone, and other nonmetallic naturalresources are considered as the prime source of material wealth for construction activities and a clear-cut focus of ecological research.[4]

POTENTIAL OF NATURAL WASTE AS CONSTRUCTION MATERIAL

One of the biggest issues facing the globe is waste, but recycling a large portion of it is incredibly challenging. The majority of waste materials, including plastic, glass, fibre, bamboo, and banana fibre, are used in the production of concrete as the globe shifts toward sustainable architecture. More than twice as much material is produced when it is rejected that could be utilised in place of cement. To produce fine and coarse aggregate for concrete, these waste materials can be partially recycled or treated. According to Rochman et al. (2012) that 280 million tonnes of plastic were produced worldwide.[5] Additionally, Kumar et al. (2012) came to the conclusion that aggregate plays a crucial role in the development of concrete strength as measured by slump value, compressive strength, dimensional stability and durability as a result, using plastic waste to replace partial aggregate in concrete mixes will give an alternative to other potential applications of plastic waste.[6] In contrast, Yin et al. (2015) conducted a study and came to the conclusion that plastic fibre (pf) can be used as a reinforcement to replace standard steel fibre and improve mechanical strength and durability.[7]

By replacing 25% of the virgin long fibre with cellulose sludge from primary effluent treatment, Wolfe and Gjinolli (1999) show the possibility of producing fibre cement blankets. Morel et al. (2001) conducted research and found that many scientists mobilise fibre wastes mechanically and chemically before mixing them with cement and the necessary amount of water.[8] According to

Benfratello et al. (2013), the decrease in strength as fibre level rises is caused by the fact that fibres are less dense than the parent material and are less likely to form voids than the parent material.[9]]According to Awal et al., various authors have found that depending on the binder material and intended usage, a few fibres may improve the strength and stiffness of the mixture, making it a desirable building material. In order to strengthen the durability of the concrete, many additional studies are being conducted in this field.[10]

POTENTIAL OF INDUSTRIAL WASTE AS CONSTRUCTION MATERIAL

The construction industry is a large industry in the globe, with around half of the people relying on it directly or indirectly. it is the backbone of all industries and makes the greatest contributionto the country's economy. however, the harmful effect of building site pollution and activity is a significant challenge for all countries, including india, pakistan, bangladesh, china, canada, ghana, turkey, taiwan, and others. construction pollution raises death rates and increases the number of patients with various major illnesses in these nations. various types of pollution, including as air, water, noise, and landfill contamination, are created throughout the building process. pollutants such as air, water, and noise interact with humans on a regular basis, affecting human health as well as the environment and ecology, Roy et al. (2019) the incertitude for evaluation index and fuzziness were explored among them, weight of each evaluation-index was optimized, thorough assessment model was constructed using a mark interval recognition model and the judgment outcome grades were compared and ranked in a comparative analysis.[11].

The requirement for processing these fibers in the context of poor nations is the fundamental reason why the economic and environmental cost for the application of these wastes is still high in general Currently, buildings account for one third of all global carbon dioxide emissions.

(a)

Figure 2 Different types of industrial waste (a) Solid waste of steel (b) Plastic waste

Table 1: Out-of-plane response of mortar-free walls by different researchers

Reference	Study	Conclusions
Afonso R. G. de Azevedo et at (2022)	Experimental study was examined to investigate the,80 percent of building trash is made up of waste concrete, waste bricks and tiles, waste	The primary cause of the high economic and environmental costs associated with the application of these wastes in poor countries is the demand

	decorating materials, dust, and other construction items.[12]	for processing these fibres. Currently
Saran et al., (2017)	Experimental study was examined to investigate the , 80 percent of building trash is made up of waste concrete, waste bricks and tiles, waste decorating materials, dust, and other construction items.[13]	Waste concrete, waste bricks and tiles, waste decorating materials, waste dust, and other construction materials made up 80% of the trash frombuildings in an experiment to find this out.
Liu et al., (2018)	Discovered that the treatment process for conventional waste ways in traditional buildings is easy, convenient, operable, and cost-effective	Discovered that resource erosion by 35.82 percent, health impact by 6.61 percent, and environmental harm areall reduced by the treatment method for conventional waste ways in traditional buildings.

CONCLUSION

Concrete is the second most commonly ingested resource on land by humans, behind water, according to Advance Construction Technology Services (ACTS). Concrete, the most commonly used building material, contributes to the general deterioration of the environment. The natural environment is running out of natural resources including sand, soil, stone, limestone, and organic soil as a result of the daily increase in construction techniques. As an example, see below. In addition to these effects, construction activities are increasing energy use, CO2 emissions by up to 33%, and global temperature rise overall. In addition, varieties of other businesses, such as building, pollute the environment.

To encounter this issue and focusing on sustainable construction practices, waste material is being used in construction activities and more precisely in concrete mixture. Waste materials are partially processed to create fine and coarse aggregate for concrete. In reinforced cement concreteplastic fibre, which is a waste material introduced as partial replacement of common steel fibre, like wise fine and coarse aggregates are partially replaced by blast furnace slag and coconut shellrespectively and found considerable improvement in durability and overall strength of concrete.

ACKNOWLEDGEMENTS

The authors would like to acknowledge CUST library for providing relevant literature which helped a lot in smooth conduct of this study. The heedful review and productive suggestions by the anonymous reviewers are gratefully acknowledged.

REFERENCES

1. Habibi, A., Ramezanianpour, A. M., & Mahdikhani, M. (2021). RSM-based optimized mix design of recycled aggregate concrete containing supplementary cementitious materials based on waste generation and global warming potential. *Resources, Conservation and Recycling*, *167*, 105420.
2. Danish, A. (2021). Potential utilization of waste material for sustainable development in construction industry. *International Journal of Recent Technology and Engineering*, *8*(3), 3435-3438.
3. *Kulkarni, V.P., Gaikwad, S., & Kumar, B. (2013). Comparative study on coconut shell aggregate with conventional concrete, J. Eng. Innov. Technol. (IJEIT)2 (12) 67–70.*
4. Baloch, M. A., Mahmood, N., & Zhang, J. W. (2019). Effect of natural resources, renewable energy and economic development on CO2 emissions in BRICS countries. *Science of the Total Environment*, *678*, 632638.
5. Rochman, C.M., et al., Policy: Classify plastic waste as hazardous. Nature, 2013. 494(7436): p. 169-171.
6. *Kumar, N. (2012). "Strength Properties of Coconut Shell as Coarse Aggregate in Concrete,"*
7. Yin, S., et al., Use of macro plastic fibers in concrete: a review. Construction and Building Materials, 2015. 93: p. 180-188.
8. Morel, J. C., Mesbah, A., Oggero, M., & Walker, P. (2001). Building houses with local materials: means to drastically reduce the environmental impact of construction. Building and Environment, 36(10), 1119-1126.
9. Benfratello, S.; Capitano, C.; Peri, G.; Rizzo, G.; Scaccianoce, G.; Sorrentino, G. Thermal and structural properties of a hemp–lime bio composite. Constr. Build. Mater. 2013, 48, 745–754.
10. Awal, A.; Mohammadhosseini, H.; Hossain, M.Z. Strength, modulus of elasticity and shrinkage behavior of concrete containing waste carpet fiber. Int. J. Geomate 2015, 9, 1441–1446
11. Roy, D., Sri, R.M.K., Mohan, C.K., 2019. Unsupervised universal attribute modelling for action recognition. IEEE Trans. Multimed. 21 (7), 1672–1680.
12. Afonso R. G. de Azevedo (2022) Possibilities for the application of agro-industrial wastes in cementitious materials: A brief review of the Brazilian perspective. *Cleaner Materials*, *3*, 100040.
13. Saran (2018) Strength, modulus of elasticity and shrinkage behavior of concrete containing

waste carpet fiber. Int. J. Geomate 2015, 9, 1441–1446

14. Liu, J., Teng, Y., Jiang, Y., et al., 2018. A cost compensation model for construction and demolition waste disposal.

2nd International Conference on Advances in Civil and Environmental Engineering (ICACEE-2023)

University of Engineering & Technology Taxila, Pakistan

Conference date: 22nd and 23rd February, 2023

Evaluation of Mechanical Properties of Available Clay Mineral Based Concrete by Varying Water to Binder Ratios

Qaisar Abbas MSc Scholar[1], Prof. Dr. Muhammad Yaqub[2]

[1]University of Engineering & Technology Taxila, Pakistan, qaisarabbasman@gmail.com

[2]University of Engineering & Technology Taxila, Pakistan, muhammad.yaqub@uettaxila.edu.pk

ABSTRACT

The purpose of this research is to study the feasibility of locally available clay mineral as partial replacement to cementitious material for production of environment friendly and low cost concrete. For the said purpose unheated and heated (500°C) bentonite was used as partial replacement (25%) along with cement content. Mechanical properties including compressive strength, tensile strength and flexural strength were better for control mix than those of bentonite. But the bentonite mix gained strength at rapid rate as the time passed. It was also observed that the heated bentonite-based concrete produced better strength concrete as compared to the one with unheated bentonite content. The workability of bentonite-based concrete was less than control concrete thus it increases its initial and final setting time. Furthermore, the effect of different water to binder ratio was also inspected. It was noticed that by reducing the water to binder ratio the gain in strength in bentonite-based concrete was less than the control mix. It was therefore concluded that the bentonite-based concrete gained strength with the time and can be used in structures where high early strength is not mandatory.

KEYWORDS**:** Mechanical Properties, Workability, Bentonite, Water to Binder Ratio

INTRODUCTION

Concrete is the most widely used material in the world and its usage is increasing day by day. Concrete being composite material consists of different types of ingredients mainly cement, water, fine and coarse aggregates. Sometimes few admixtures are also added to get specified results. Among them cement is the most expensive material. Its price has increased tremendously over the last ten years. Apart from this, it is having bad effect in climate change because its use produces a lot of carbon Dioxide which is causing the global warming.[1]

This requirement is being expressed keeping in view the above-mentioned points that there must be some material that can be used in place of cement which will also give strength to concrete and protect the environment from global warming. Many researchers used bentonite for the said purpose. Americans in the early 20th century used pozzolana as cementitious material in the concrete during the execution of public projects such as dams to control the temperature.[2] A pozzolana possesses very little cementitious property but it reacts with Calcium Hydroxide in presence of moisture to form such compounds which possess cementitious properties.[3] Its been observed that early strength of concrete while using bentonite as cement replacement was less and with the passage of time it started increasing gradually. When heated bentonite was used as partial replacement of cement the results were quite

satisfactory.[4] The most used natural pozzolana is processed to fine powder after heat treatment. By grinding this natural pozzolana to fine powder its reactivity is increased.[5] It's been studied that concrete requires more water when bentonite is added as partial replacement of cement. As the quantity of bentonite in concrete was increased, the more water content was needed to make the concrete workable.[6]

Cement is the costliest material among concrete ingredients. Its production has also bad impact on the environment. A lot of heat of hydration is generated while using it as binder. The strength of control concrete is badly affected by severe environment conditions.

The objective of the research program was to obtain low-cost and durable concrete by effective usage of locally available cheap material. Study of different water to binder ratios was observed. Mechanical and rheological properties of concrete were studied in detail.

MATERIAL

Bentonite used in this research was collected from the Swabi District in Pakhtunkhuwa province of Pakistan and the cement used was OPC conforming to ASTM Standard C150-07. Following three types of concrete mixes were prepared.

Concrete with control condition was designated as "**CM.**"

Concrete containing 25% unheated bentonite was designated as "**UBM.**"

Concrete containing 25% heated bentonite was designated as" **HBM.**"

To prepare heated bentonite mix, as received bentonite (unheated) was firstly heated to 500 Celsius and grounded to powder. It was then cooled to room temperature after heating for two hours. Then it was sieved through 325 mesh size(45mm) as per ASTM C430-17. Lawrence Pur sand with fineness modulus of 2.4 was used as fine aggregate while Margalla crush having bulk specific gravity 2.70 and maximum size of 19 mm was used as coarse aggregate.

METHODOLOGY

The workability of concrete mixes was obtained by comparing their slump values at constant W/B=0.55. The mechanical properties of concrete mixes were studied as per ASTM C39-21 by conducting the requisite tests on concrete cylinders after 28, 56 and 90 days from the date of preparation of specimens. The ratio of concrete ingredients was kept constant B:S:A=1:1.5:3 for all cases studied. The effect of varying water to binder ratio was also considered.

Table 1: Detail of various cases under different conditions.

Mechanical properties of control concrete, with 25% unheated Clay , with 25% heated Clay										
cocrete ratio	W/C	No of Samples								
		Compresive Strength			Splitting Tensile Strength			Flexural Strength		
		28 D	56 D	90 D	28 D	56D	90 D	28 D	56 D	90 D
1:1.5:3	0.55	9	9	9	9	9	9	9	9	9
1:1.5:3	0.45	9	9	9	9	9	9	9	9	9
1:1.5:3	0.35	9	9	9	9	9	9	9	9	9

RESULTS & DISCUSSION

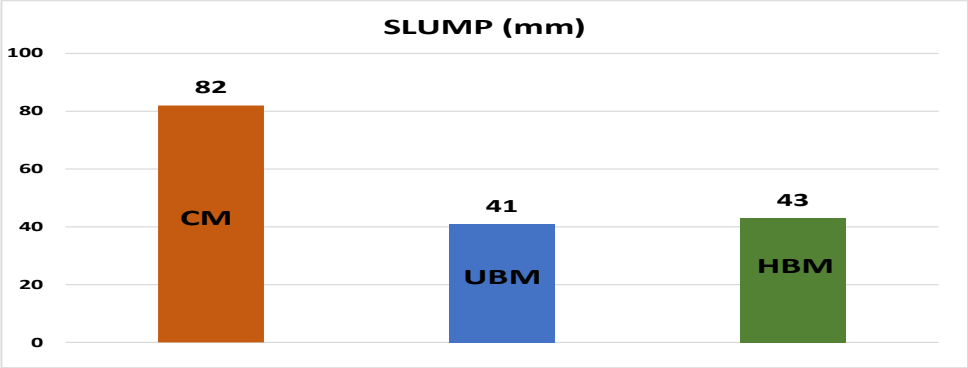

Fig. 1: Workability of concrete mixes in terms of the slump value.

The workability of unheated and heated bentonite mixes decreased as the surface area of the particles increased in case of heated and unheated bentonite.

The graphical representation of strength with time at different w/b ratios is presented below.

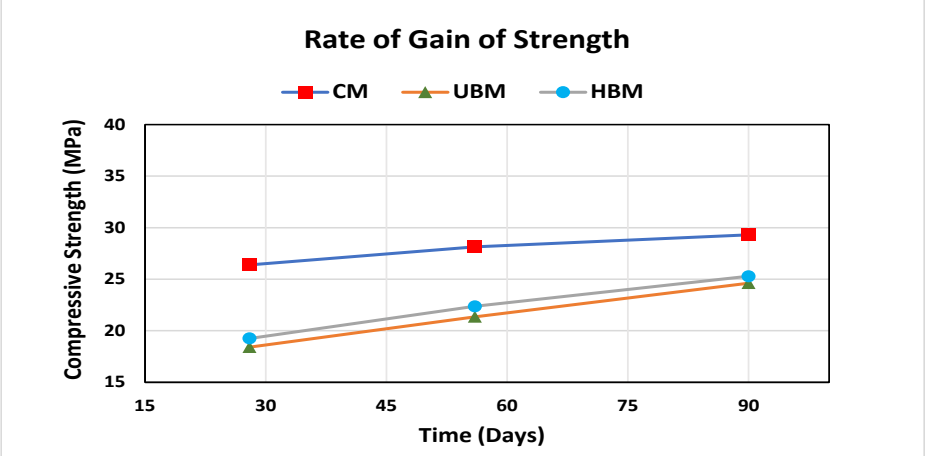

(a)

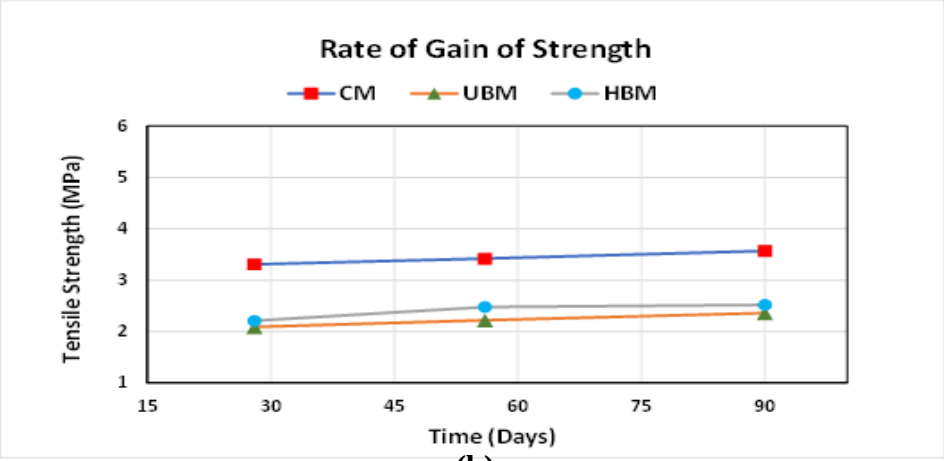

(b)

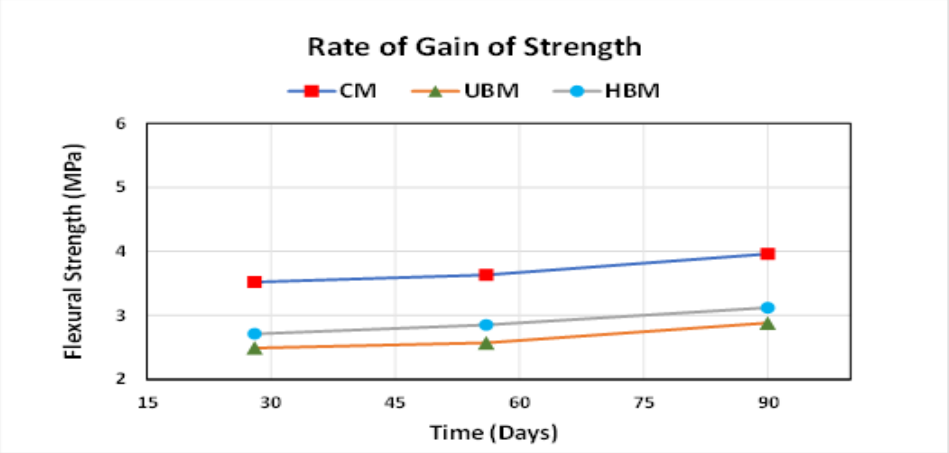

(c)

Fig. 2: a, b and c showing graphical representation of compressive, tensile, and flexural strength respectively at W/B ratio of 0.55.

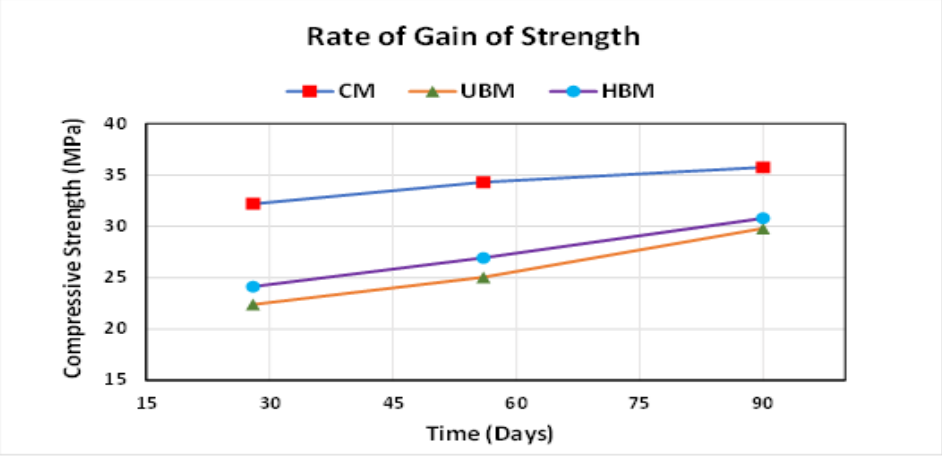

(a)

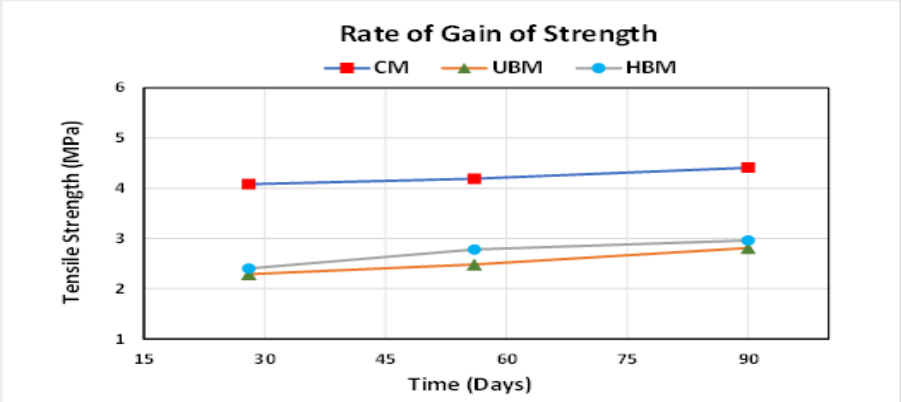

(b)

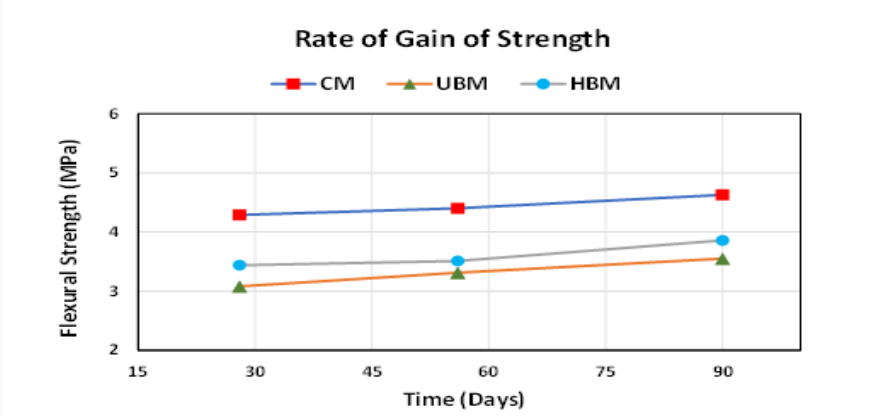

(c)

Fig. 3: a, b and c showing graphical representation of compressive, tensile, and flexural strength respectively at W/B ratio of 0.45.

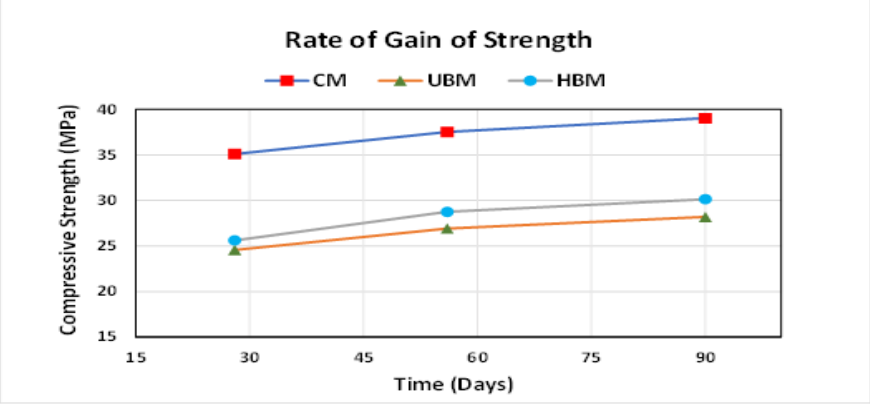

(a)

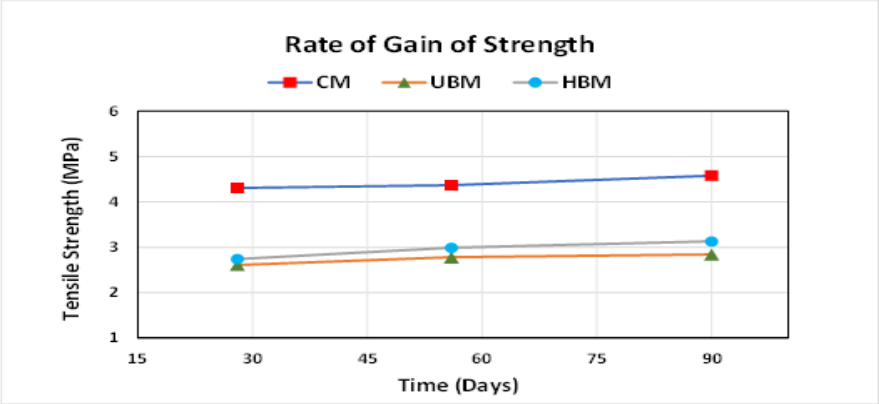

(b)

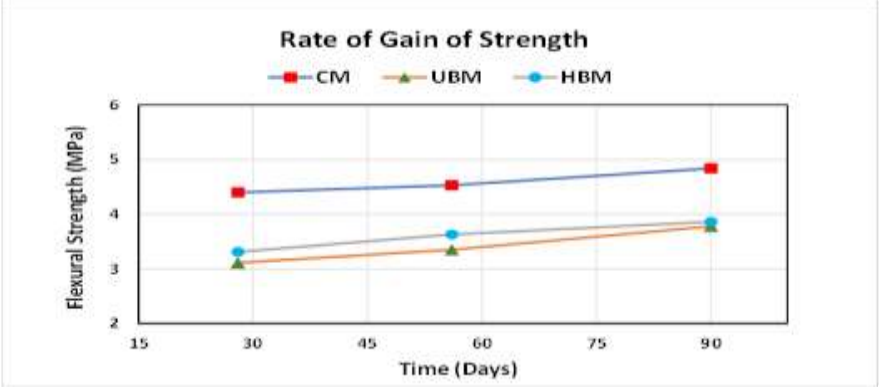

(c)

Fig. 4: a, b and c showing graphical representation of compressive, tensile, and flexural strength respectively at W/B ratio of 0.35.

From the above mentioned plots of mechanical strength, it is obvious that in case of bentonite mixes the gain in strength is less at lower w/b ratios than the one with higher w/b ratio due to the increased surface area of bentonite particles. However, the strength of control mixes increased at rapid rate with decreasing w/b ratio.

Table 2: Comparison of percentage gain in compressive, tensile and flexure strength for various W/B ratios.

Comparison in terms of Percentage (%) gain in Strength									
Mix Type	**Compressive Strength (MPa)**			**Splitting Tensile Strength (MPa)**			**Flexural Strength (MPa)**		
	28 D	**56 D**	**90 D**	**28 D**	**56 D**	**90 D**	**28 D**	**56 D**	**90 D**
W/B=0.55									
CM	100	100	100	100	100	100	100	100	100
UBM	69.76	75.87	83.99	67.93	76.16	75.86	70.73	70.79	72.72
HBM	72.98	79.49	86.28	72.88	77.90	79.31	76.98	78.51	78.78
W/B=0.45									
CM	100	100	100	100	100	100	100	100	100
UBM	69.56	73.00	83.36	71.53	72.77	75.49	71.79	75.23	76.67
HBM	74.93	78.48	86.13	73.92	78.03	77.87	80.19	79.77	83.37
W/B=0.35									
CM	100	100	100	100	100	100	100	100	100
UBM	69.99	71.72	72.23	69.11	74.50	75.41	70.68	73.95	78.10
HBM	72.98	76.63	77.20	74.22	77.61	80.53	75.23	80.13	79.75

The above said table summarized the results achieved during requisite testing. Strength development with the passing of time is quite good in case of bentonite mixes.

Cost Analysis

Table 4.22: Cost Analysis with 25 % Replacement of Cement with Bentonite

Mix Type	**Quantity (kgs)**		**Unit Rate (Rps/kg)**		**Cost (Rps)**		**Total Cost (Rps)**
	Cement	Bentonite	Cement	Bentonite	Cement	Bentonite	
CM	880	0	17	3	14960	0	14960
UBM	660	220	17	3	11220	660	11880
HBM	660	220	17	5	11220	1100	12320

Difference in Cost in Case of UBM=3080 (Rs)
Difference in Cost in Case of HBM=2640 (Rs

CONCLUSIONS

After the application of above mentioned testing procedures on specimens, following conclusions are made.

- Initial and final setting time of concrete mixes was increased from 1.5 & 4 hours (CM) to 3.5 & 6.28 hours for heated bentonite mix. It further increased to 3.6 & 6.44 hours in unheated bentonite mix.
- The slump value of control, unheated and heated bentonite mix was found to be 82, 41 and 43 mm respectively.
- Percentage gain in compressive strength at 28, 56 and 90 days found to be 69, 75 and 84 in unheated bentonite mix while 73, 79 and 86 in heated bentonite mix as compared to control mix.
- The rate of gain of strength of unheated bentonite mix and heated bentonite mix was less than control mix in case of lower water to binder ratio.
- Initially unheated bentonite mixes and heated bentonite mixes gained less strength, but with the passage of time they attained it at rapid rate than control mix.
- By using bentonite mix concrete rps 3000 per 100 cubic feet of concrete were saved.

ACKNOWLEDGMENT

I'm thankful to my supervisor Mr. Tariq Ali for his support and guidance which enabled me to do this research work in a unique and authentic way.

REFERENCES

[1] M.Aravindhraj, B.T.Sapna (2016), Influence of Bentonite in Strength and Durability of High Performance Concrete, International Research Journal of Engineering and Technology (IRJET) 2016.

[2] Kosmatka, S.H., B., Kerkhoff., Panarese, W.C., N.F., Macleod., McGrath, R. J., 2002. Design and control of concrete mixture, 7th edition, pp. 60-61.

[3] ASTM 2007a. Standard Terminology Relating to Concrete and Concrete Aggregates, C125-07, ASTM International, West Conshohocken, Pa.

[4] J. Mirza , M. Riaz , A. Naseer , F. Rehman , A.N. Khan , Q. Ali (2009), Pakistani bentonite in mortars and concrete as low cost construction material, Applied Clay Science 45 (2009) 220–226.

[5] Rodriguez Camacho R.E & Uribe Afif R. (2002). Importance of using Natural Pozzolans on Concrete Durability, Cement & Concrete Research, 32, 1851-1858.

[6] S. Ahmad , S. A. Barbhuiya , A. Elahi And J. Iqbal, 2011, Effect of Pakistani bentonite on properties of mortar and concrete, Clay Minerals, (2011) 46, 85–92.

2nd International Conference on Advances in Civil and Environmental Engineering (ICACEE-2023)

University of Engineering & Technology Taxila, Pakistan

Conference date: 22nd and 23rd February, 2023

Effect of Pre-Treated Crumb Rubber and Propylene Fibres on the Mechanical and Durability Properties of Mortar

Hamza Aamir, Kinza Aamir
COMSATS University Islamabad, Abbottabad Campus
hamzaamir9696@gmail.com; kinzamuhammadaamir@gmail.com

Dr. Muhammad Faisal Javed
COMSATS University Islamabad, Abbottabad Campus
arbabfaisal@cuiatd.edu.pk

ABSTRACT:
This paper presents the mechanical properties of mortar by the partial replacement of fine aggregates with crumb rubber in different percentages 5%,10%,15 and 20%. The crumb rubber is treated with water , NaOH and $Ca(OH)_2$. All the casting and testing is done in accordance with ASTM standards. The compressive and flexural strength tests are performed according to ASTM. In addition to replacement the propylene fibres will also be tested further for optimum content and then mix with optimum crumb rubber to find mechanical and durability properties of mortar. From the results the optimum content is 5% and the best treatment is of lime. The NaOH and $Ca(OH)_2$ treated samples show less strength loss as compare to water treated and out of all treatments lime perform best. In further study we will find out the optimum of propylene and further analyze its combination with optimum crumb rubber.
KEYWORDS: Lime, crumb rubber, mechanical properties.

INTRODUCTION

With the passage of time as the population is increasing day by day so as the automobiles are increasing day by day[1]. The automobile tyre will be effected by the friction and will their will be depreciation in its life due to use, so the waste is generated. It has been estimated that about 1.5 billion of tyres are wasted annually. The use of waste materials in mortar and concrete is increasing day by day to cope up with environmental problems[2]. The waste materials which are used widely now a days in the research is fly ash [3], paper waste from paper industry [4], electronic waste [5], crumb rubber [6] etc. The inclusion of the waste is preferred when it gives the desired result and as well as cost effectiveness. The waste which are not giving the required results will be combined with other materials for the enhancement of the concrete/ mortar property but the problem is that the with the use of crumb rubber the compressive strength reduces which is a main draw back[7]. Strength reduction in tyre reinforced concrete / mortar is due to its smooth surface , due to its smooth surface the matrix of mix becomes weak leaving the concrete porous which leads to early failure. Propylene fibres do not absorb water[8]. The use of propylene fibres have somehow increased compressive and flexural strength as compare to controlled samples[8]. It has been seen that every waste material used in concrete / mortar has its optimum content for the enhanced results so propylene fibres are showing the strength gain to 0.5%

and after that there is downfall in the mechanical properties of concrete[8]. But the point is that the fine aggregates or sand will be made available by natural resources of its partial replacement with crumb rubber can reduce the natural resource depletion and as well as reduce the environmental impacts.

METHODOLOGY

Total 150 samples are casted till now. Our study includes the treatment of crumb rubber with three different fluids i.e water, lime and caustic soda. The samples are casted according to ASTM C 39 , cement to sand ratio is 1:2.75 with the 0.48 w/c ratio according to ASTM.

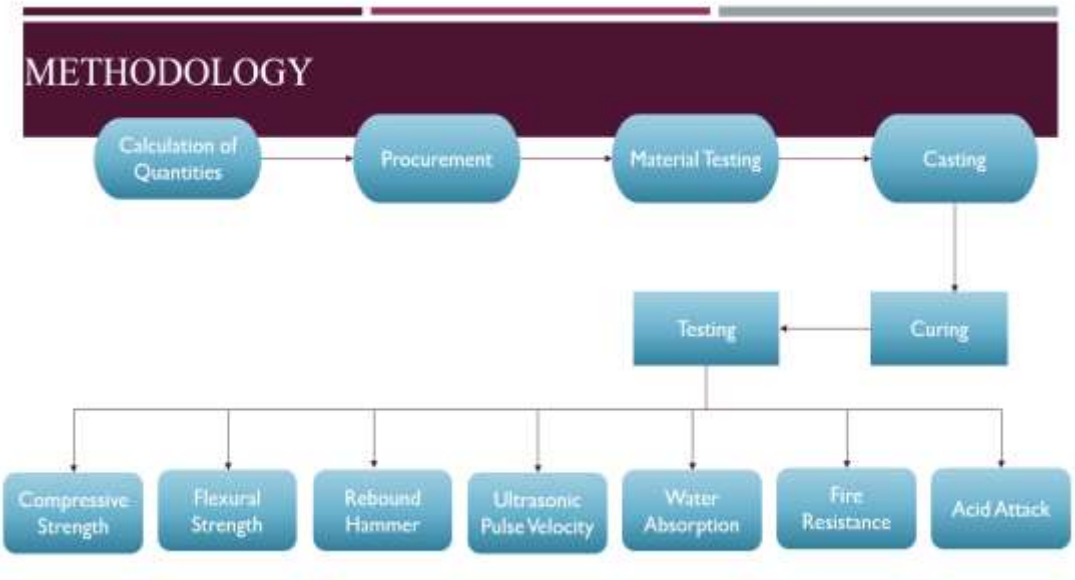

Figure 1: Summary of experimental process

MATERIALS USED AND PROPERTIES

Ordinary Portland cement is used with the initial setting time of 36 minutes and final setting time of 10 hours and 30 minutes. The crumb rubber is used with the specific gravity of 1.60 ,water absorption of 0.037% & moisture content of 0.084%, fine aggregates are used with the specific gravity of 2.62 , water absorption 1.70% & moisture content is 0.810 %. Propylene fibres with 6mm length and 0.91 specific gravity will be use.

Figure 2 : Images of Materials used

MIX PROPORTIONS

The mortar is made with the mix of 1:2.75 according to ASTM C 39 with the partial replacement of crumb rubber of 5% ,10% ,15% & 20% by weight. Controlled samples and all other sand replaced samples are made according to C 39.

TREATMENT OF CRUMB RUBBER

The crumb rubber is treated with three different fluids , water , $Ca(OH)_2$ and NaOH pellets. In water treatment the crumb rubber is treated with the mix with boiled water and after 24 hours of dipped time the sample is shifted to sunlight drying for its further use. The lime and caustic soda is mixed with water and after that the sample will be dipped for 24 hours, after 24 hours the sample is taken out from container and washed with the washing sieve , after that the sample is shifted to area with the maximum sunlight for proper drying.

SPECIMEN PREPARATION

The specimens for compressive strength test are prepared of the size of 50mm x 50mm cube and for flexural test the beams are made of the size of 160mm x 40mm x40mm. The compressive test samples are made with the material laying and compacting by rod in two layers according to ASTM and the sample will remain in mold for 24 hours after that the curing of 7/ 14 days is done. In flexural test the

same methodology is applied. The compressive testing samples are made according to ASTM C 39 and flexural samples are made with the ASTM C 348.

TESTING

Two types of testing is done in the study . The first one is compressive test and the other is flexural test. In compressive the compression testing machine is used with the pace 0f 10N/cm^2/s. The flexural test is performed in automatic universal machine with the pace of 1.25mm/min.

Figure 3: Images of Testing

RESULTS AND DISCUSSION

From the results it is clear that optimum percentage of crumb rubber is 5%. When we do comparative analysis of optimum crumb rubber with controlled samples strength the loss of 67% was observed in compression test by the water treated crumb rubber and controlled samples results. In flexural test the loss of 36% was seen by replacing 5% of water treated crumb rubber with sand than controlled samples.

Figure 4: Images of destructive testing

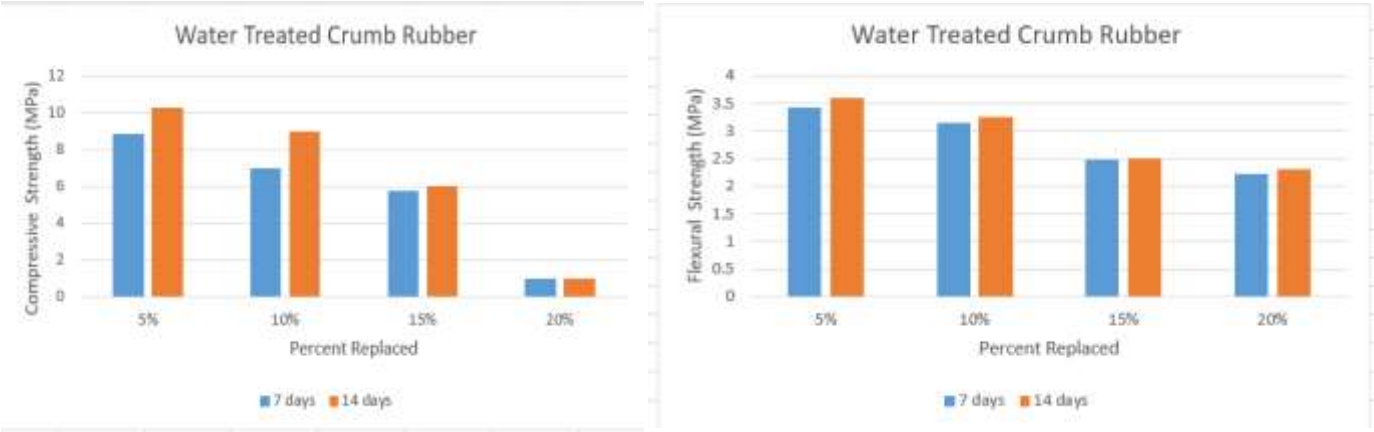

(a) (b)

Figure 5: Compressive and Flexural strength results of water treated crumb rubber

In NaOH treated crumb rubber the strength loss is 41% in case of 5% replaced NaOH treated crumb rubber. Means that the strength is enhanced by the treatment. In flexural test the strength loss is 50% as compare to controlled samples.

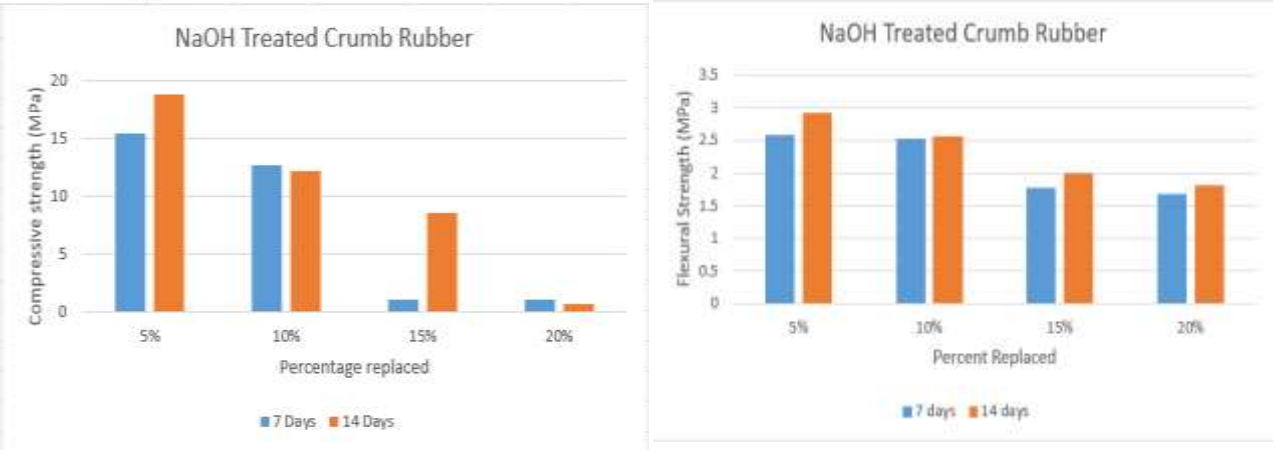

(a) (b)

Figure 6: Compressive and Flexural strength of NaOH treated crumb rubber

In Lime treated crumb rubber the strength loss is 39% in case of compressive test.In tensile test the strength loss is 30.78% which means that the matrix is improving.

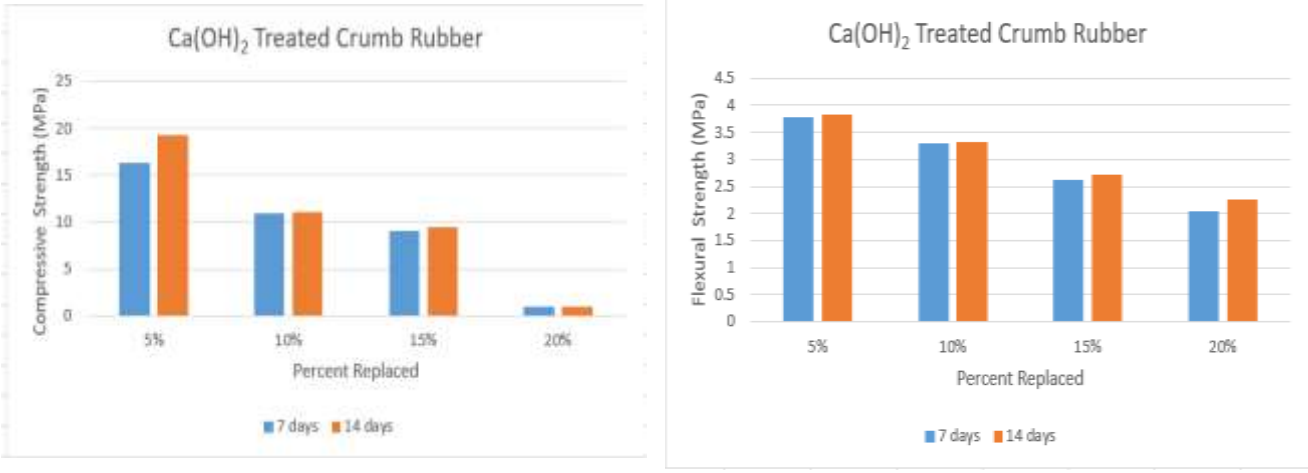

(a) (b)

Figure 7: Compressive and Flexural strength of Lime treated crumb rubber

CONCLUSION

From the above results it is concluded that the optimum percentage of crumb rubber is 5% in which the strength loss is less than the others. The improvement is seen due to the rough surface of crumb rubber after treatment , the rough surface makes the stronger matrix and ITZ in the concrete as a result the mechanical properties of mortar increases. This optimum percentage of crumb rubber is mixed with the optimum of propylene fibres and in the end we analyze about mechanical and durability properties of mortar that whether their will be more improvement or not by the inclusion of propylene fibres.

ACKNOWLEDGEMENTS

This research is done under the supervision of Dr. Muhammad Faisal Javed. We are very thankful to our supervisor Dr. Muhammad Faisal Javed for his guidance and support during this research work. All the results are authentic and unique.

REFERENCES

[1] J. XU, Z. Yao, G. Yang, and Q. Han, "Research on crumb rubber concrete: From a multi-scale review," *Construction and Building Materials*, vol. 232. Elsevier, p. 117282, Jan. 2020. doi: 10.1016/j.conbuildmat.2019.117282.

[2] R. A. Assaggaf, M. R. Ali, S. U. Al-Dulaijan, and M. Maslehuddin, "Properties of concrete with untreated and treated crumb rubber – A review," *J. Mater. Res. Technol.*, vol. 11, pp. 1753–1798, 2021, doi: 10.1016/j.jmrt.2021.02.019.

[3] K. A. Alawi Al-Sodani, M. M. Al-Zahrani, M. Maslehuddin, O. S. Baghabra Al-Amoudi, and S. U. Al-Dulaijan, "Chloride diffusion models for Type I and fly ash cement concrete exposed to field and laboratory conditions," *Mar. Struct.*, vol. 76, no. October 2020, p. 102900, 2021, doi: 10.1016/j.marstruc.2020.102900.

[4] A. R. G. de Azevedo, J. Alexandre, G. de C. Xavier, and L. G. Pedroti, "Recycling paper industry effluent sludge for use in mortars: A sustainability perspective," *J. Clean. Prod.*, vol. 192, pp. 335–346, 2018, doi: 10.1016/j.jclepro.2018.05.011.

[5] M. Masuduzzaman, S. K. S. Amit, and M. Alauddin, "Utilization of E-waste in Concrete and its Environmental Impact - A Review," *2018 Int. Conf. Smart City Emerg. Technol. ICSCET 2018*, no. January, pp. 1–4, 2018, doi: 10.1109/ICSCET.2018.8537301.

[6] S. Meherier, M. S. Alam, and N. Banthia, "Mechanical behavior of cement mortar with varying replacement level of crumb rubber," *Fifth Int. Conf. Constr. Mater.*, no. January 2016, pp. 1–11, 2015.

[7] H. H. Awan, M. F. Javed, A. Yousaf, F. Aslam, H. Alabduljabbar, and A. Mosavi, "Experimental evaluation of untreated and pretreated crumb rubber used in concrete," *Crystals*, vol. 11, no. 5, pp. 1–14, 2021, doi: 10.3390/cryst11050558.

[8] Milind V. Mohod, "Performance of Polypropylene Fibre Reinforced Concrete\n," *IOSR J. Mech. Civ. Eng.*, vol. 12, no. 1, pp. 28–36, 2015, doi: 10.9790/1684-12112836.

2nd International Conference on Advances in Civil and Environmental Engineering (ICACEE-2023)

University of Engineering & Technology Taxila, Pakistan

Conference date: 22nd and 23rd February, 2023

Experimental Investigation of Mechanical Characteristics of a Carbon Negative Sustainable Concrete by using Ferrock

Ikram ullah Khan[1], Qaiser uz Zaman Khan[2], Saqib Mehboob[3]
[1]University of Engineering and Technology Taxila, iukhan.x@gmail.com
[2] University of Engineering and Technology Taxila, dr.qaiser@uettaxila.edu.pk
[3]University of Engineering and Technology Taxila, syed.saqib@uettaxila.edu.pk

ABSTRACT

The rate at which the global population is growing is unprecedented, and projections indicate that by the beginning of the year 2050, it could have risen to as many as 9.9 billion people. The construction industry, the largest in the world, is following the trend towards sustainability and the exploration of alternative and innovative materials. These alternative building materials are both more cost-effective and environmentally friendly than the conventional materials that have been the common practice for the industry for decades. Moreover, such construction materials could reduce the environmental impact of concrete used in construction. Concrete, the second most widely used material in the world after water. Concrete accounts for 8–10% of all CO_2 emissions. The purpose of this study is to determine how better the Ferrock, as alternative, can perform as an appropriate substitute for cement in building structures. It is a binding substance based on iron that makes use of various waste products and carbon-negative building materials. This revolutionary substance is composed solely of iron powder (a steel industry waste product), trace amounts of limestone, fly ash, and metakaolin. This investigation is primarily concerned with the durability requirements associated with Ferrock ratios of 60% iron scrap, 20% fly ash, 12% metakaolin, and 8% limestone. Our goal is to identify the best optimum combination of replacement (as measured by compressive, split, and flexural tests) and sustainability by replacing cement with Ferrock at increasing percentages (3%, 7%, 11%, and 15%). Ferrock produced in Pakistan using materials that are readily available locally exhibits quite encouraging results in terms of compressive and split tensile strength of cubes and cylinders.

KEYWORDS: Ferrock, CO_2, Iron dust, Sustainable, Concrete, Alternative building materials.

1 INTRODUCTION

Pakistan is developing nation and due to which numerous construction work is going on. In this fast-developing world, people are turning their attention to infrastructure development, and development areas play an important role. Concrete is the most common substance on our planet, after water [1]. Each year, the global construction industry produces around 10 billion tons of concrete, the majority of which is composed of standard Portland cement. Concrete is the material that is used the most frequently in engineering, and the production of concrete accounts for around 6–8% of our globe total carbon dioxide discharge. This is a key part of the rise in the average temperature of the planet. This was the impetus for the publication of an article titled "Ferrock," which centred on the

reduction of by-products of fossil fuels and their utilization for the improvement of climate. This is a rundown of the several subjects that will test your knowledge. This exemplifies the most effective way to make use of the leftover powder created from iron mineral during mining operations. This is just dumped from the mines, which results in more land acquisition, increased air pollution, and potential health risks. The indirect reduction in carbon emissions using technology that provides strength superior to cement distinguishes this product from most other cement additives. Due to its carbon irony and ability to promote waste prevention, Ferrock is an excellent cohesive material from an environmental point of view [1].

The main material which is being used in construction industry is cement and on the other side cement is source of great amount of carbon dioxide and polluting the environment. The inability to produce enough regular Portland cement in regions where high-quality limestone is in scarce supply. Everything from the jobs to the income generated by the concrete sector would be negatively impacted by this. The cost of regular Portland cement will likewise increase dramatically when supply becomes scarce.

Around the world, concrete is the material of choice for construction. Every human being on Earth contributes about 1 tonne of cement to the global supply each year. The environmental impact assessment of this substance is crucial because of its many applications. To determine how harmful a material is to the environment, scientists look at how much of an effect it has on ozone-depleting gases and climate change. Considering this, the concept of "green concrete" was born [2]. It offers promising potential as an alternative to concrete and a much greener building material. Ferrock is environmentally friendly as it is made entirely from recycled elements such as metal powders, limestone, kaolin and fly- ash. Compared to traditional concrete construction methods, these new concrete construction methods are environmentally friendly, robust and durable. The main material in making of Ferrock is iron scrap, a debris which goes directly to dumping sites. Iron dust on combination with carbon di-oxide makes/forms carbonate matrix to produce Ferrock when dehydrated.

The possible reaction steps for this activity are [4]:

$$Fe + 2CO_2 + H_2O \longrightarrow Fe_2 + 2HCO_3 + H_2$$

$$Fe_2 + 2HCO_3 \longrightarrow FeCO_3 + CO_2 + H_2O$$

The end reaction then is:

$$Fe + CO_2 + H_2O \longrightarrow FeCO_3 + H_2$$

As we came to know from present literature the possible best combination of ingredients for Ferrock are iron scrap 60%, fly ash 20%, metakaolin 12% and limestone 8%. Investigation shows that a fully dried specimens of Ferrock stores between 7.5 to 11.5% of CO_2 by weight. Hence verified that Ferrock is carbon negative not like Portland Cement (PC) [4].

Ferrock

Materials and Products

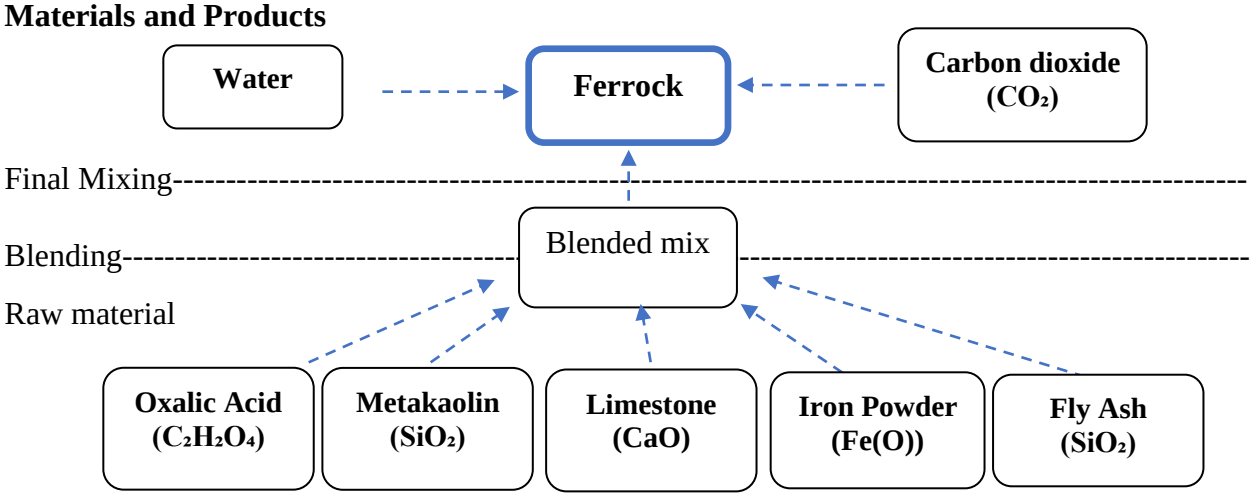

Figure 1: Material and Products of Ferrock [3]

Steel scraps with tensile properties is called Ferrock. M20 Grade Concrete is utilised in this project, and a mix design was produced using a variety of cement, Ferrock, and water compositions. After 7 days, 28 days, and 56 days of curing, the cubes are evaluated. In this investigation, the cement was substituted with Ferrock, with a percentage variation of 5%, 12%, 15%, and 25% [5]. Cement production accounts for 5% to 7% carbon emission of the total worlds. and some studies shows that the most used building material, cement, releases around 6-8% of the world's entire carbon dioxide during manufacture. Carbon dioxide is a key contributor to global warming [6].

Through the process of its hardening, it may improve the environment by absorbing CO_2 from the air. In the present study, the components of the Ferrock mortar mix were each given a different concentration of oxalic acid (Catalyst), which was used as the catalyst. Based on the findings, it was discovered that Ferrock also effectively absorbs significant amounts of CO_2 from the environment and lowers the quantity of CO_2 released by industries at the optimal molarity of oxalic acid as a catalyst, which was 10 moles [7].

The Cambridge Dictionary describes sustainability as the "concept that items and services must be created without using non-renewable resources and without harming the natural calamity." This implies that renewable materials are those that cannot deplete natural resources & have little influence on the environment when utilised. Ferrock is created from steel scrap collected from iron mills to produce a substance comparable to concrete that is even tougher than concrete [8].
Our goal is to identify the ideal ratio of substitution, which, together with sustainability, would increase desired outcome for both concrete and Ferrock, by experimenting with percentages of replacement ranging from 5% to 20% in solid. The results of the tests suggest that 10% of this ratio is more effective than the others [9].

2 METHODOLOGY OF RESEARCH

In this research study replacement of cement by Ferrock is done and cement is replaced 3%, 7%, 10% and 15% by weight to get optimum results. Ferrock concrete mixture is prepared using normal aggregate and main constituent iron powder (60%) of Ferrock is collected from raw material left in industries of metal remoulding or reshaping. The mix design ratio for Fe concrete for this research method is 1:2:4. Standard cubes of size 4inch x 4inch x 4inch used in this study. Standard size cylinders are also casted to check the tensile strength. Cubes and cylinders are de-moulded after 24 hours of concrete pouring and cured with wet covering. These cubes are crushed after 7 ,14 and 28 days and the results are compared with test specimen. The cylinder samples undergo tensile test. As shown in figure 2.

Figure 2: Compression Testing of Specimens

3 RESULTS AND DISCUSSION

Work done on Ferrock manufactured by using locally available by products provides a better understanding and material properties like fresh, hardened and durability by partial replacing of cement with Ferrock as a cohesive-adhesive material. It is verified and concluded that composition of Ferrock as iron powder 60 percent, fly-ash 20 percent, metakaolin 10 percent, limestone 8 percent, catalyst oxalic acid 2 percent are best combination. The investigational works done on Ferrock mainly centre on partial replacing of Ferrock with air and wet covering curing (in situ). Ferrock cubes and cylinders were tested for compression at 7, 14 and 28 days. Below mentioned (Table 1) are the findings of compressive strength (psi) vales that are measured after curing (wet covering) of sample cubes on 7, 14 and 28 days.

Table 1: Compressive Strength of Cubes

Sr. No.	Ferrock (%)	Compressive Strength (psi)

		7 Days	14 Days	28 Days
1	0%	1786.86	2483.04	3079.15
2	3%	1962.36	2646.937	3274.95
3	7%	2264.03	3274.8	3486.93
4	11%	2438.08	3119.83	3563.57
5	15%	2496.09	3360.60	3455.61

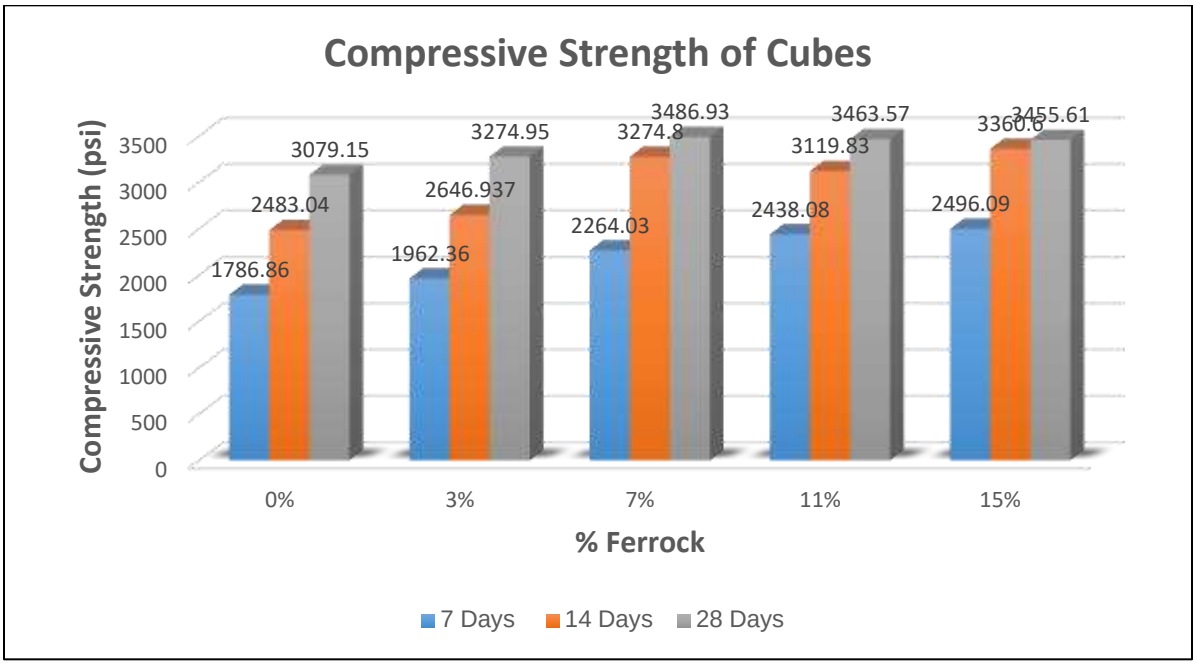

Figure 3: Compression Testing of Cubes

After getting use of waste material in Ferrock test results are very much satisfactory when compared, at 7 days, the compressive strength of the mixed cubes is 1786 psi; at 14 days, it's 2483 psi; and at 28 days, it's 3079 psi (Table 1). For all the values of 28 days of compressive strength Ferrock shows higher values as compared to controlled mix such as, 3274 psi, 3486 psi, 3463 psi, and 3455 psi. As mentioned in figure 3. Table 2 elaborate the tensile strength achieved by using locally available Ferrock as tensile strength is fundamental and important property of concrete that mainly relates to the size and stretch of cracks, above results of cylinder split tests conducted on controlled mixes and Ferrock at 7, 14, and 28 days, showing pressures of 339, 392, and 442 psi, respectively. Various Ferrock concrete percentages (3%, 7%, 11%, and 15%) were subjected to split tensile testing. All the results and as shown in graph at 28 days maximum strength was achieved. For reference, 483 psi, 529 psi, 416 psi, and 413 psi are the corresponding values as mentioned in figure 4.

Table 2: Split Tensile Strength of Cylinder

Sr. No.	Ferrock (%)	Split Tensile Strength (psi)		
		7 Days	14 Days	28 Days
1	0%	339.3	392.95	442.25
2	3%	355.25	403.1	483.575
3	7%	382.8	392.95	529.25
4	11%	381.35	358.15	416.15
5	15%	339.3	343.65	413.25

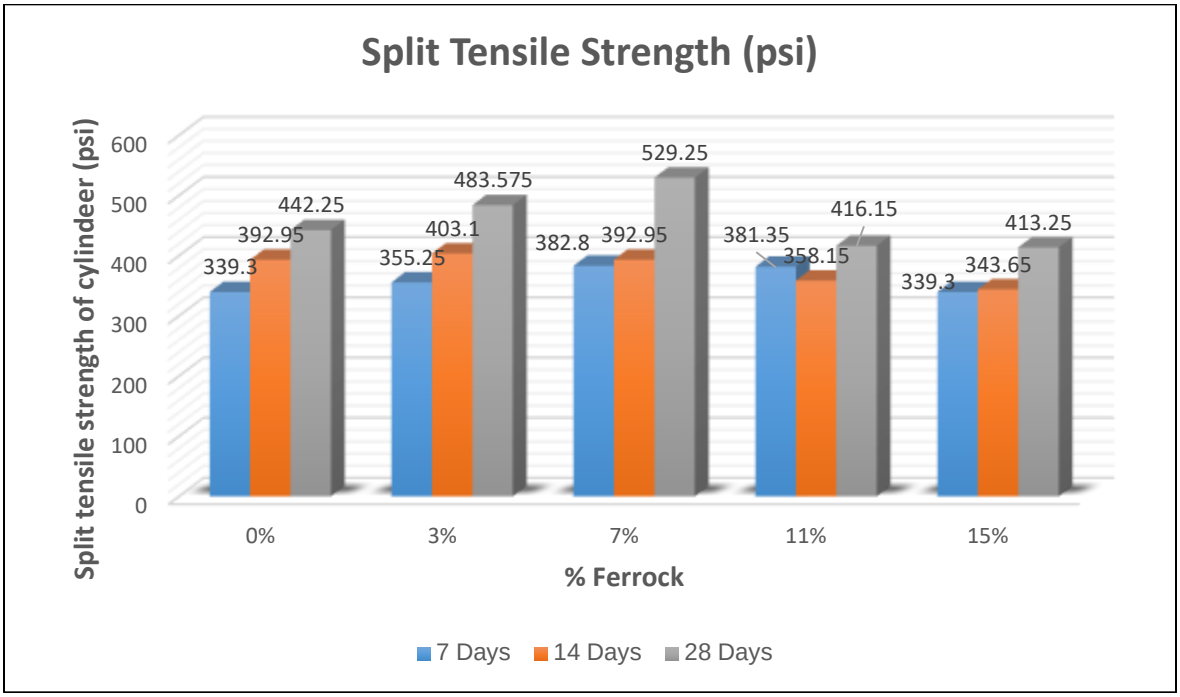

Figure 4: Split Tensile Strength of Cylinder

4 CONCLUSION

After Investigation of this study, we concluded the utilizing locally sourced, otherwise wasted raw materials to create a material with comparable strength to cement concrete: Ferrock. 7, 14, and 28 days of a destructive test were conducted to evaluate the material's compressive strength, splitting tensile test, and flexural strength, respectively. The research shows awe-inspiring compressive and tensile strength results by replacing cement with Ferrock up to 15 %.

- The resilience of Ferrock concrete was enhanced. to 3274 psi, 3406 psi, 3563 psi, and 3898 psi, respectively, with 3%, 7%, 11%, and 15%, respectively.

- The findings show that the 7% ratio is the most effective in terms of increasing the concrete's strength. There was an increase in the tensile strength of the Ferrock concrete by 483 psi, 529 psi, 416 psi, and 413 psi, respectively, with 3%, 7%, 11%, and 15%.

- As the experimental investigation is completed it is clearly seen that strength of concrete can be enhanced by adding 7% Ferrock by weight as a binding material with cement.

Hence the test results reveal that compressive strength and durability of Ferrock concrete is enhanced by adding 7% Ferrock that will be best to be used in building sector. Further increase in percentage results in reduction of strength.

Ferrock concrete is ideal and sustainable when we look after the environment, look for cost, or even when we look on the supplies of limestone that can be reduced by using byproducts such as iron dust and fly ash.

ACKNOWLEDGEMENTS

The authors are thankful to the Civil Engineering Department UET Taxila for providing Laboratory support and technical assistance during the lab testing phase of this research work. I want to express appreciation to those who have helped me in my studies, Maisam Raza, for their constant encouragement. At last, I extend my sincere gratitude to Director Lab, National Logistics Cell (NLC), for his genuine support throughout this research work.

REFERENCES

[1] M. S. Ali, S. Shukri, M. Patel, and A. Ahad, "*Alternative Building Materials for Sustainable Development in Ethiopian Construction*," International Research Journal of Engineering and Technology (IRJET) **vol. 7**, pp.2395-0056, 2020.

[2] B. Widera and D. Stone, "*Analysis of possible application of iron-based substitute for portland cement in building and its influence on carbon emissions*," International Multidisciplinary Scientific GeoConference: SGEM, **vol. 2**, pp. 455-462, 2016.

[3] B. A. Sturla BS, "*Analyzing More Sustainable Alternatives Than Using Ordinary Portland Cement in Commerical Construction*," **vol.5**, pp.2-3, 2020.

[4] Vijayan, D.S., et al., "*Evaluation of ferrock: A greener substitute to cement,".* Materials Today: Proceedings, scientific committee of the International Conference on Materials Engineering and Characterization 2019, 2019.

[5] Kavita Singh KS, "*Compressive Strength Study Of Green Concrete By Using Ferrock*," Multidisciplinary International Research Journal of Gujarat Technological University **vol. 02**, ISSN.2581-8880, 2020.

[6] Niveditha M1, Y M Manjunath, Setting H S Prasanna, "*Ferrock: A Carbon Negative Sustainable Concrete*," International Journal Of Sustainable Construction Engineering And Technology **vol. 11 no. 4**, ISSN.2180-3242, 2020.

[7] Mouli Prashanth P, Gokul V, Dr. Shanmugasundaram, "*Investigation On Ferrock Based Mortar An Environment Friendly Concrete*," International Research Journal of Engineering and Technology (IRJET) **vol. 6**, ISSN.2395-0056, 2019.

[8] Agha, A, Shibani, A, Hassan, D & Zalans, *"Modular Construction in the United Kingdom Housing Sector: Barriers and Implications," Journal of Architectural Engineering Technology,* **vol. 6 no. 2**, ISSN.2168-9717, 2021.

[9] S.Karthika, A Leema Rose, G.Priyadarshini, "*Sustainable Development On Ferrock Mortar Cubes*," Journal of Physics: Conference Series. **2040** (2021) 012020.

2nd International Conference on Advances in Civil and Environmental Engineering (ICACEE-2023)

University of Engineering & Technology Taxila, Pakistan

Conference date: 22nd and 23rd February, 2023

Improvement of Concrete Shielding to Nuclear Radiations using Magnetite

Muhammad Uzair[1], Saqib Mehboob[2]
[1]University of Engineering and Technology Taxila, enggruzair@gmail.com
[2] University of Engineering and Technology Taxila, syed.saqib@uettaxila.edu.pk

ABSTRACT

This research study presents findings on improving the shielding capabilities of concrete against Gamma-rays using magnetite as aggregate. Magnetite is a hefty mineral with a specific gravity ranging from 4.2 to 5.2. In this research, magnetite concrete's shielding capabilities and mechanical properties have been investigated for water-cement ratios from 0.40 to 0.70 to optimize the thickness of the walls and slab of radiation therapy bunkers. Experimental results showed that using magnetite minerals as aggregate improves the shielding capabilities of concrete. The maximum rise in attenuation coefficient is 41% at a water-to-cement ratio of 0.5 and varies proportionally with the variation in concrete density. Relevant ASTM standards have been used to compute concrete compressive and tensile strengths. Experimental results showed that using magnetite minerals as fine and coarse aggregate increases concrete's compressive and tensile strength.

KEYWORDS: Control samples, Treated samples, Magnetite concrete, Radiation shielding, Attenuation coefficient.

INTRODUCTION

Nuclear technology has become incredibly important in many research and technological disciples, for the betterment of humanity. The role of nuclear technology has been multidimensional, including but not restricted to electricity generation, industry, agriculture, and medicine (Alan E et al., 2004). However, this also has negative effects on living standards because it causes cell ionization, resulting in cancer. Controlling the amount of radiation from nuclear reactions that are exposed to living things is one of the fundamental requirements for employing nuclear reactions. (Y. Elmahroug et al., 2013; Maxwell et al., 2008; Gehlot Dilip et al., 2014). Many researchers have worked to introduce an efficient shield between radiation sources and the living environment. Every radiation source requires a different shield because of their nature and source of generation. Some of the radiations have charged nature due to which their penetration power is low, like Alfa particles and beta particles. These radiations can be easily stopped with the help of common construction material, whereas some of the radiation have no charge and high penetration power, like Neutron particles, X-rays and Gamma rays. These radiations require denser material to shield them. (McAlister et al. 2012). Lead (Pb) is commonly used to shield gamma rays and x-rays, but it cannot shield neutrons (Y. Elmahroug et al., 2013).

The most widely used construction material is concrete which can be used to shield this radiation but require increased thickness due to which the normal concrete is uneconomical. Normal concrete can be made denser by using heavy weight mineral as aggregate, like Magnetite, barite, Galena etc.

Magnetite is used as aggregate in this research work because of its high specific gravity and local availability. The specific gravity of magnetite reaches 5.2 at 26°C (Saidani et al., 2015). Concrete's ability to protect against gamma rays is improved by magnetite, while lighter components like hydrogen and oxygen from water mixing improve concrete's ability to shield against neutrons.

In Pakistan, normal concrete is used along with lead lining in the construction of radiation research centres and cancer treatment room (bunker) of hospitals. Regular concrete requires a larger thickness to shield Gamma radiations (for example, the primary wall thickness of the bunker is 8 feet in the IRNUM hospital, Peshawar). This study aims to increase the density of concrete to make it a more effective and affordable building material for radiation shielding.

METHODOLOGY OF RESEARCH

Materials

Natural coarse and fine aggregate, magnetite coarse and fine aggregate, cement, water, and ultra superplast-70 admixture were utilized while making the samples. Natural aggregates were obtained from the local stock of material in Margalla Rawalpindi, Pakistan as shown in Figure 1(a) & 1(b). Magnetite is an iron ore having black colour and metallic lustre as shown in Figure 1(c) & 1(d). Magnetite aggregates were obtained from local sources in Sawat, Pakistan. Ordinary Portland Cement (OPC), marketed as Bestway, was used as binding material.

Figure 1 (a)

Figure 1 (b)

Figure 1. Aggregates, (a) Natural coarse aggregate, (b) Natural fine aggregate, (c) Magnetite fine aggregate, (d) Magnetite coarse aggregate

Figure 2(c)

Figure 1(d)

According to ASTM C-33 a blend of well graded aggregate was obtained for normal concrete samples and magnetite concrete samples. Physical properties of the aggregates are given in Table 1.

Table 1: Physical Properties of Aggregates

	Max. Aggregate Size (mm)	Fineness Modulus	Bulk Density (kg/m^3)	Absorption Capacity (%)	Specific Gravity

Coarse Aggregate	25	-----	1634	1.3	2.8
Fine Aggregate	-----	2.4	-----	1.8	2.3
Magnetite Coarse Aggregate	25	-----	1870	1.1	4.7
Magnetite Fine Aggregate	-----	2.9	-----	1.4	4.4

The chemical admixture ultra superplast-70 was used to enhance the workability at lower water-cement ratios.

Mix Proportioning

Two concrete specimens were prepared, mainly named controlled and treated samples. Controlled samples consisted of natural aggregates, whereas treated samples consisted of coarse and fine aggregate magnetite. Concrete cylinders of size 300mm in height and 150mm in diameter were prepared for compression and split tensile tests and rectangular samples of sizes 15cm × 15cm having thicknesses of 4cm, 6cm, and 8cm, for Gamma Dosimetry test. The concrete mixes were prepared using a constant ratio of cement, sand, and coarse aggregate, i.e., 1:2:4, with varying water-cement ratios, i.e., 0.4, 0.45, 0.5, 0.55, 0.6, 0.65, and 0.7. Weight based proportioning was used for the mixture. The properties of the ingredients were determined through laboratory testing in order to proportion the mixes. Table 2 contains information about mix design. The admixture was added to the concrete mixture at the rate indicated in Table 2.

Table 2: Details of Mix Proportion for Normal and Magnetite Concrete

W/CM	Weight of the components for normal concrete (KG)				Admixture (%)	Weight of the components for Magnetite concrete (KG)				Admixture (%)
	CM	FA	CA	W		CM	FA	CA	W	
0.4	6.60	13.19	26.37	2.64	1	3.29	6.58	13.14	1.32	1
0.45	6.60	13.19	26.37	2.97	1	3.29	6.58	13.14	1.48	1
0.5	6.60	13.19	26.37	3.30	0.8	3.29	6.58	13.14	1.56	0.8
0.55	6.60	13.19	26.37	3.63	0.5	3.29	6.58	13.14	1.81	0.5
0.6	6.60	13.19	26.37	3.96	0	3.29	6.58	13.14	1.97	0
0.65	6.60	13.19	26.37	4.29	0	3.29	6.58	13.14	2.14	0
0.7	6.60	13.19	26.37	4.62	0	3.29	6.58	13.14	2.30	0

Note: W= Water, CM= Cement, FA= Fine aggregate, CA= Coarse aggregate

Laboratory Testing

Compressive Strength Test

This test was performed on the control and treated samples to compare their compressive strengths. For this purpose, 3 samples at each water-cement ratio, was prepared for both specimens. So total of 42 samples were tested after 28 days of curing.

Tensile Strength Test

This test was conducted on both sets of the specimens to compare their tensile strengths. For this purpose, 3 samples at each water-cement ratio, was prepared for both specimens. So total of 42 samples were tested after 28 days of curing.

Gamma Rays Dosimetry Test

This test was performed on both sets of specimens to compare their attenuation coefficients and half value layer. Attenuation coefficient determines the ability of the material to absorb or stop the radiations per unit thickness of the material whereas the half value layer is the thickness of a material at which the intensity of the incident radiation is reduced by half after passing through the material. For this purpose, 21 Nos. of normal concrete samples and 21 Nos. of magnetite concrete samples (3 samples of thickness 4cm, 6cm & 8cm at each water-cement ratio) were tested by exposing the samples to the gamma rays produced by Cobalt-60 (Co60). Equation (1) and (2) were used to calculate the linear attenuation coefficient (μ) and half value layer (HVL) respectively, for normal and magnetite concrete.

$$\mu = \frac{1}{x} . \ln\left(\frac{N_o}{N}\right) \qquad (1)$$

$$HVL = \frac{\ln(2)}{\mu} = \frac{0.693}{\mu} \qquad (2)$$

x = Thickness of the sample in cm
N_o = Radiation detected in the air
N = Radiation detected with concrete samples between detector and source.

Figure 2(a) *Figure 2(b)* *Figure 2(c)*

Figure 2. Laboratory Testing, (a) Compressive Strength Test, (b) Tensile Strength Test, (c) Gamma Dosimetry.

RESULTS AND DISCUSSION

Compressive Strength Test Results

The concrete cylinders for both specimens (Control samples & Treated samples) were tested by crushing them after 28 days of casting and curing. The results for the mentioned test are shown in Figure 2.

The compressive strength of magnetite has been found to be increased by 23.73% at water-cement ratio 0.4, as compare to normal concrete. The figure 2 shows that the compressive strength gradually decreases for both specimens, as the w/c increases from 0.4 to 0.7.

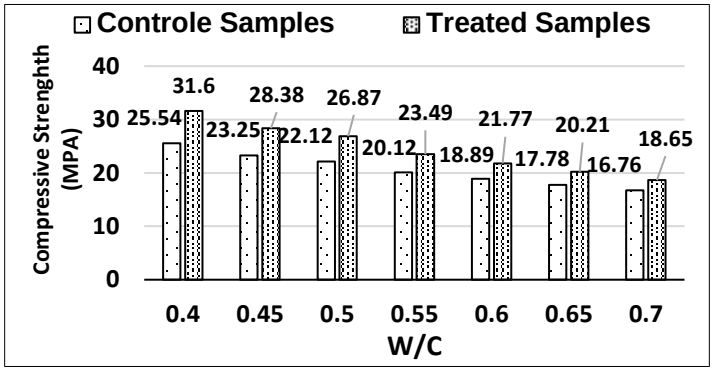

Figure 3. Compressive Strength Test Result

Tensile Strength

The concrete cylinders for both of the specimens (Control samples & Treated samples) were tested for tensile strength after 28 days of casting and curing. The results for the mentioned test are shown in Figure 3

The tensile strength of magnetite has been found to be increased by 17.26% at water-cement ratio 0.4, as compared to normal concrete. The figure 3 shows that the strength gradually decreases for both of the specimens, as the water-to-cement ratio increases from 0.4 to 0.7.

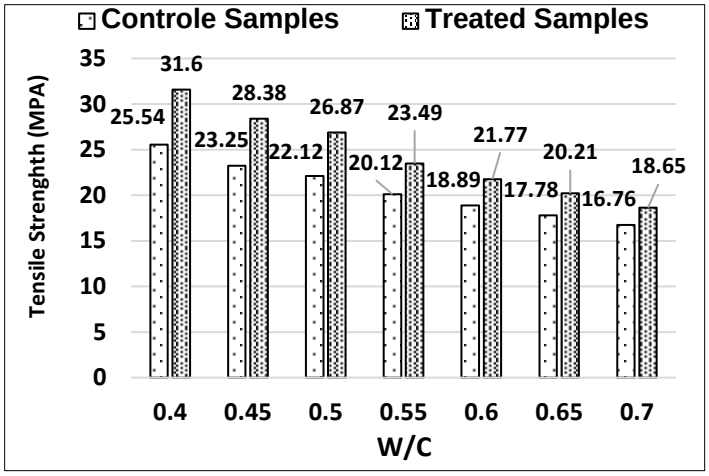

Figure 4. Tensile Strength Test Result

Gamma-Rays Dosimetry Test Results

The radiation shielding ability of a meterial is determined by the linear attinuation coefficient & half value layer. Attinuation coefficient is defined as the quantity of radiations abosrbed per unit thickness of the material whereas half value layer is defined as the thickness of a material at which the intensity of the incident radiations is reduced by half after passing through the material. Denser materials absorb more gamma-radiations. The introduction of magnetite aggregate has increased the density of the concrete and hence the gamma-rays shielding ability of the concrete. Figures 5 (a) and (b) show the linear attenuation coefficient results.

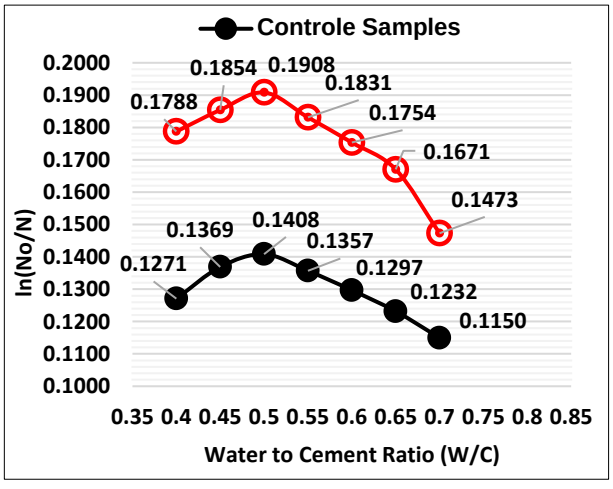

(a) Variation of Linear Attenuation Coefficient with Water-Cement Ratio

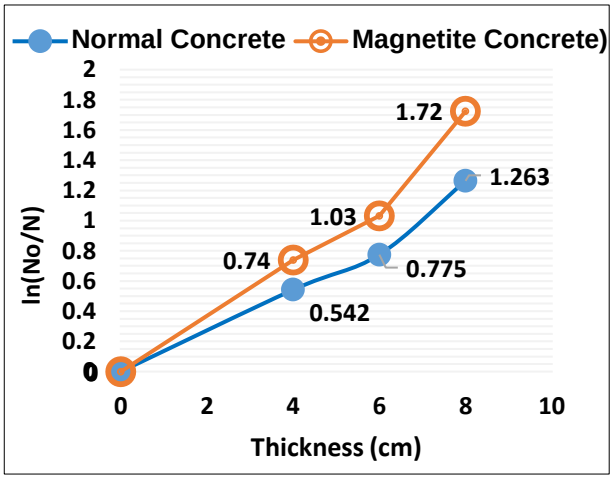

(b) Linear Attenuation Coefficient at Water-Cement Ratio of 0.5

Figure (5). Linear Attenuation Coefficient Values

The results of figure 5(a) shows that the attenuation coefficients for magnetite concrete samples are higher as compared to the samples of the normal concrete, at given water-cement ratio. Figure 5(b) illustrates that the maximum attenuation is observed for both controls and treated samples at a water-cement ratio 0.5. This is because the maximum density of normal concrete and magnetite concrete has been achieved at a water- cement ratio 0.5.

CONCLUSION

The study's findings are encapsulated as follows in light of the testing and analysis provided here:

1. Compressive and tensile strength has increased by using magnetite as aggregate in concrete.
2. Using Magnetite aggregate in treated samples increased compressive strength from 11.28% to 23.73% after 28 days of curing, with the highest compressive strength occurring at a water-cement ratio of 0.4 and the lowest at a ratio of 0.7.
3. 6.22% to 17.26% increase in 28 days tensile strength was observed by using magnetite aggregate for all mixes, with the highest tensile strength occurring at a water-cement ratio of 0.4 and the lowest at a ratio of 0.7.
4. Shielding abilities of magnetite concrete has increased as compare to normal concrete. Utilizing magnetite aggregate increased the linear attenuation coefficient by 41% and reduced the half-value layer by 40.7% compared to conventional concrete.
5. This study reveals that the ideal water-cement ratio for magnetite concrete is 0.5, which provides the most significant amount of Gamma radiation shielding, based on the evaluation of control, and treated samples with water-cement ratios ranging from 0.4 to 0.7.

Based on the above research study, the authors feel that the ratio of the ingredients of the mixes may also affects the mechanical and shielding properties of the concrete. This study can be expanded by exercising the same procedure for multiple ratios of the ingredients of concrete.

ACKNOWLEDGEMENTS

The authors are thankful to the Civil Engineering Department UET Taxila and the Institute of Radiotherapy and Nuclear Medicine (IRNUM Hospital) Peshawar, for providing Laboratory support and technical assistance during the lab testing phase of this research work.

REFERENCES

Alan E., Walter, 2004. Nuclear Technology's Numerous Uses. *Issues in Science and Technology*, 20(3): 48-54.

Ahmed S. Ouda, 2015. Development of high-performance heavy density concrete using different aggregates for gamma-ray shielding. *Progress in Nuclear Energy*, 79: 48-55.

Athira Suresh & Ranjan Abraham, 2015. Experimental Study on Heavy Weight Concrete Using Hematite and Laterite as Coarse Aggregate. *International Journal of Engineering Trends and Technology (IJETT)*, 28(4).

Berna Oto, Aycan Gür, Mustafa Recep Kaçal, Bekir Doğan & Ali Arasoğlu, 2013. Photon attenuation properties of some concrete containing magnetite and colemanite in different rates. *Annals of Nuclear Energy*, 51: 120-124.

Christopher A. Maxwell, Markus C. Fleisch, Sylvain V. Costes, Anna C. Erickson, Arnaud Boissière, Rishi Gupta, Shraddha A. Ravani, Bahram Parvin & Mary Helen Barcellos-Hoff, 2008. Targeted and nontargeted effects of ionizing radiation that impact genomic instability. Cancer research, 68(20): 8304-8311.

Davood Mostofinejad, Mohamad Reisi & Ahmad Shirani, 2012. Mix design effective parameters on γ-ray attenuation coefficient and strength of normal and heavyweight concrete. Construction and Building Materials, 28(1): 224-229.

Daniel R. McAlister, 2012. Gamma ray attenuation properties of common shielding materials. PhD thesis of University Lane Lisle, USA.

F. Demir, G. Budak, R. Sahin, A. Karabulut, M. Oltulu & A. Un. 2011. Determination of radiation attenuation coefficients of heavyweight-and normal-weight concretes containing colemanite and magnetite for 0.663 MeV γ-rays. *Annals of Nuclear Energy*, 38(6): 1274-1278.

Gehlot Dilip, Gupta Ashok Kumar & Deore Rahul. Jul- Aug. 2014. Experimental Study of Shielding Material as a Lead in a Nuclear Reactor. IOSR Journal of Mechanical and Civil Engineering, 11(4): Ver. I, 30-3.

Akkurt, H. Akyildirim, B. Mavi, S. Kilincarslan & C. Basyigit, 2010. Gamma-ray shielding properties of concrete including magnetite at different energies. *Progress in Nuclear Energy,* 52(7): 620-623.

Akkurt, H. Akyıldırım, B. Mavi, S. Kilincarslan & C. Basyigit, 2010. Photon attenuation coefficients of concrete include magnetite in different rate. *Annals of Nuclear Energy,* 37(7): 910-914.

lker Bekir Topçu, 2003. Properties of heavyweight concrete produced with magnetite. *Cement and Concrete Research,* 33(6): 815-822.

Khaled Saidani, Lasaad Ajam & Mongi Ben Ouezdou, 2015. Magnetite powder as sand substitution in concrete: Effect on some mechanical properties. *Construction and Building Materials* 95: 287-295.

2nd International Conference on Advances in Civil and Environmental Engineering (ICACEE-2023)

University of Engineering & Technology Taxila, Pakistan

Conference date: 22nd and 23rd February, 2023

An overview of study of Interfacial Transition zone of recycled aggregate concrete: A Review

Muhammad Qaisar[1], Muhammad Yaqub[2], Muhammad Nawaz Sharif [3]

[1]PhD Scholar, Department of Civil Engineering, University of Engineering and Technology, Taxila Pakistan, engr.qaisar.cvl@gmail.com

[2]Professor, Department of Civil Engineering, University of Engineering and Technology, Taxila Pakistan, muhammad.yaqub@uettaxila.edu.pk

[3]Department of Civil Engineering, University of Engineering and Technology, Taxila Pakistan, mirbrothers930@gmail.com

ABSTRACT

Sustainable development is the core principle of rapid development in all fields. Recycling is a good option to minimize unsustainable development and protect natural resources. Following water, concrete is the most common material utilised on Earth's surface. With increasing industrialization and urbanization, concrete consumes natural resources in large quantity which cause environmental problems and climate change. It is possible to make concrete more sustainable while using recycled aggregate in place of natural aggregate. The best way to reduce the environmental impact of building and demolition waste is to use recycled aggregates in place of natural materials in both partial and full replacement. Several investigators have investigated the usage of recycled aggregate in concrete and found that it has less desirable properties than traditional concrete. Previous studies have largely focused on exploring the mechanical and durability properties of RAC, and the microstructure of RAC is rarely focused on. The present study has largely focused on the microstructure properties and various techniques for its improvement. Recycled concrete turns out to have somewhat lower qualities than natural concrete, and one of the key reasons is a weak ITZ. Many suitable techniques including removal of attached mortar, incorporation of mineral admixtures, mixing techniques and carbonation method discussed in current study. It is revealed that incorporation of mineral admixtures and optimum triple mixing approach is the most suitable method for the improvement of ITZ. It was found that the combined tools (such as nanoindentation and scanning electron scope) and the latest techniques (such as nanotechnology, nanoparticles and numerical modelling) for the microstructure of recycled concrete and improvement of ITZ can be adopted for further study in the future.

KEYWORDS: Recycled Aggregate Concrete, Weakest Link, ITZ, Techniques, Improvement

INTRODUCTION

Globally, sustainable development is a big concern now a days. Sustainable development is the core principle of rapid development in all fields. It was first discussed at the Earth Summit in Brazil in 1992. Sustainable development is currently the key force of the global construction sector [1]. According to Pierrehumbert, environmental deterioration such as global warming or resource scarcity is a big problem on earth [2]. The world is acting to combat these threats. For instance, the 2015 Paris Agreement which focuses on reducing greenhouse gas emissions, was signed. The European Union has established the European Green Deal projects, which call for decoupling economic growth from resource use and achieving carbon neutrality (zero emissions) by 2050. The Chinese government likewise adopted a similar programme, stating that carbon neutrality would be attained by 2060 [3]. It is estimated that, after water, concrete is the second most widely used substance on earth's surface. With increasing industrialization and urbanization, concrete consumes natural resources in large quantity which cause environmental problems and climate change. The building industry is a major environmental polluter, accounting for up to 45% of all CO2 emissions [4]. Concrete is the most adaptable and dynamic material that is used extensively in the building and construction business. Its major components include water, aggregates (both fine and coarse), cement, and admixtures [5]. Cement is the basic element in concrete and acts as the binding material to make dense concrete. It is estimated that development will raise cement production to 4.83 billion tonnes by 2030. Since natural aggregates (NAs) normally account for between 60% and 75% of the total volume of concrete. This might allow to produce non sustainable concrete, necessitating a gradual rise in resources like natural stones. Worldwide consumption of NAs was estimated at 48.3 billion tonnes in 2015, with a growth rate of more than 5% forecasted for the prior five years. Assuming the market for NAs continues to expand at its current rate, experts expect that demand will double within the next two to three decades [3]. So, it is necessary to focus on the curtailing utilization of natural aggregate and cement in concrete production to preserve natural resources. Their use in the concrete matrix can be decreased in the future using alternative materials.

The Construction and Demolition Waste (CDW) definition provided by the United States Environmental Protection Agency (EPA) describes waste that is often created during new construction activities as well as renovation of existing structures. The complete quantity of CDW that was manufactured all around the world in 2018 is shown in Figure 1. The United States generated over 600 million tonnes, followed by India (530 million tonnes so in 2016), and China produced approximately 2360 million tonnes of CDW. The European Union (EU) produced a significant amount of CDW, with France and Germany accounting for the lion's share with 240 million tonnes and 225 million tonnes, respectively, of that production. Pakistan is a developing country and CDW can become burning issue in near future especially in big cities. A reasonable amount of CDW is generated in Pakistan from demolition of buildings and during the natural disasters such as 2005 earthquake, the 2008 Ziarat District earthquake, the 2013 Awaran Baluchistan earthquake, and the 2010 & 2022 largest Floods in Pakistan [6], [7]. Illegal dumping is a frequent and accepted technique for the disposal of CDW. This approach refers to the disposal of trash without any pre-treatment at the landfill, such as the separation of hazardous components in the waste. In the world, about 35% of CDW was landfilled, according to Kabirifar et al. [8]. In many countries, the proper disposal of CDW remains a challenge due to its

negative environmental effects and high demand for landfills. Due to the rising of CDW, sizable landfill space is required, which may even require farmland. According to Zheng et al [8], 7.5 billion m3 of CDW were disposed of in Chinese landfill sites in 2013. This quantity of CDW could cover fifty percent of Singapore's total land area if the height at which it is dumped were increased to twenty metres. This waste was normally disposed of on landfill sites which creates landfill secrecy and causes environmental problems like climate change and health hazards. This land secrecy is a burning issue globally and especially in developed countries.

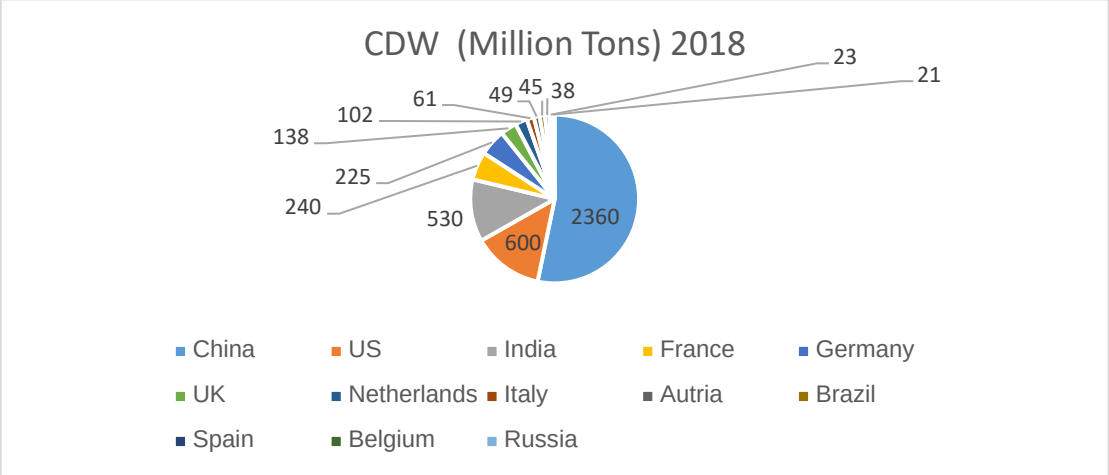

Figure 1: Construction waste generated in different countries according to United States EPA

Recycling is a good option to minimize the unsustainable development and protect natural resources. The recycling of construction waste is well expressed in Figure 2. Considering the context, governments, academic institutions, and businesses have taken substantial measures to promote CDW recycling and reuse to lessen CDW's detrimental environmental and financial effects. As an illustration, the EU set an aim in 2008 that non-hazardous CDW should make up no more than 30% of total CDW by weight by 2020. This could only be done, according to Pacheco-Torgal et al. [10], if recycling growth increased by around 2% annually, as opposed to the current growth rate of 1%.

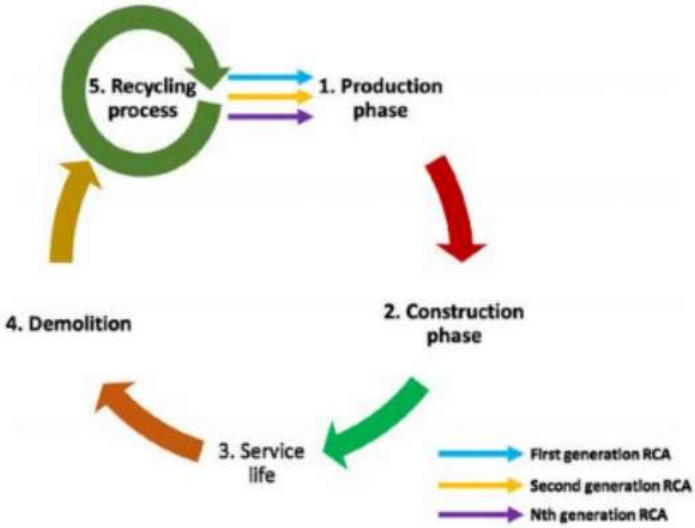

Figure 2: The aggregates' lifespan [9]

Despite this, their consumption of CDW is still quite low when measured against the total amount of CDW produced. Studies have demonstrated that using recycled aggregates (RAs) from construction and demolition waste (CDW) instead of natural aggregates (NAs) in new concrete applications can have positive benefits on the environment as well as the economy. These findings date back more than seven decades. It has been estimated that switching to RAs from NAs when working with concrete could result in a 10%–20% reduction in the amount of money spent on materials. [10]. A Hong Kong life cycle assessment of recovered aggregate indicated that recycling coarse aggregates from CDW saves 58% of non-renewable energy and 65% of greenhouse gas emissions compared to natural aggregate concrete. RAC's compression, tensile, and bending properties are usually inferior to NAC's[11].

The interface (ITZ) between the recycled natural aggregate and the matrix of cement, with any adhering mortar on top, distinguishes recycled concrete aggregate's qualities from those of natural aggregates (NA) as shown in Figure 3 and Figure 4 [12]. The literature demonstrates that RCA has an impact on concrete characteristics [13]. Because RA's characteristics differ from NA's, it behaves in a different way in concrete mixes and after it has hardened, outperforming regular concrete [14]. The characteristics of concrete formed entirely from RA are less than those of NA with the same w/c ratio. For instance, while freshly produced concrete made with NA has a density of around 2400 kg/m3, concrete made with RA has a density of about 2150 kg/m3, which is because the RA has a lower bulk-specific density and contains more air. The qualities of the new concrete that contains RCA may therefore be impacted by its implementation, which is related to the RCA's constituent parts [15].

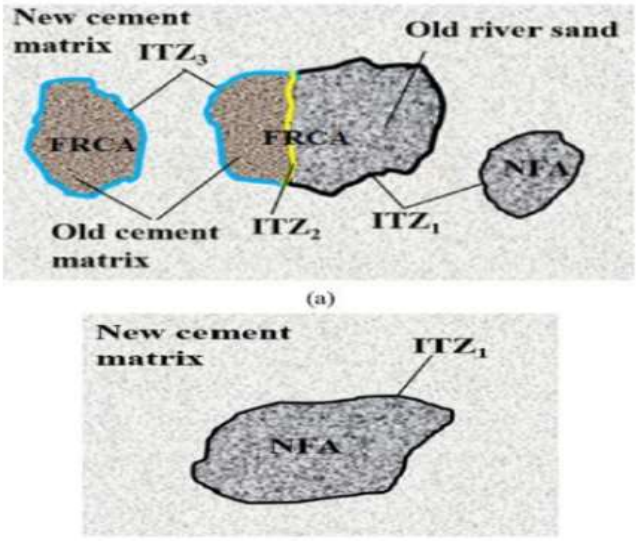

Figure 3: Three ITZ (ITZ1, ITZ2, ITZ3) in Concrete [16]

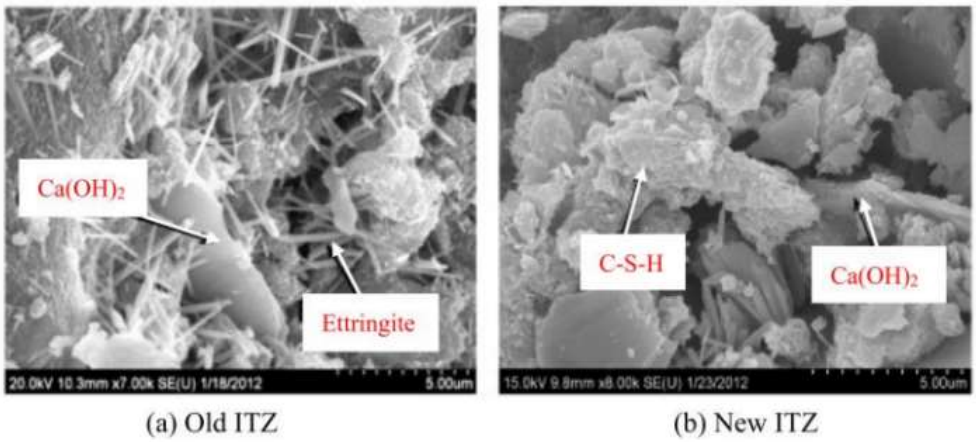

Figure 4: SEM images described the ITZ of RAC [17]

The three fundamental components of concrete are aggregate, hardened cement paste, and ITZ. The area of the hardened concrete that is most susceptible to damage is denoted by the ITZ [18]. The bulk of RCA is made up of ITZ since NA is covered by the original ITZ, adherent mortar, and the new ITZ, and the new ITZ is located between the adherent mortar and the new mortar [12]. Therefore, the improvement of ITZs is necessary to improve RCA performance. Many scholars investigated the application of various strategies and techniques to enhance the concrete properties with the addition of RCA. Their findings consist either eliminating the adhered mortar that has been bonded to surface of RCA or reinforcement of RCA using carbonation treatment [19], admixtures of industrial by

products or ashes of waste agriculture plants [20], calcium carbonate and bio deposition [21], solution of Sodium silicate [22] and polymer-treated water-repellent coat [23] are examples. There are numerous review papers available on enhancing RCA performance as illustrated in Table 1. The review article separates treatment methods for removing adhering mortar and improving its quality were studied by Shi et al. [13] and Shaban et al. [24]. It is also challenging to determine which treatment approach will improve the ITZ. In a similar way Verian et al. [25] gathered various treatment methods of enhancing RCA that are not tied to a specific area of newly fresh concrete. Wang et al[26] 's discussion of various enhancement techniques of RCA properties covered the elimination of adhered mortar from the RCA, coating of the surface of RCA and various concrete mixing techniques. The current study, however, focuses the discussion on enhancing the RCA's microstructure using suitable techniques.

Table 1: Latest Review Papers on recycled aggregate concrete

Title of Review	Focus	Future Suggestions
Wang Bo et al. 2021 [27]	Comparison of Artificial intelligence-based methods and regression analysis models	Focus on the enhancement methods for RA that are less harmful to the environment.
Bahraq et al. 2022 [28]	Cost Analysis and improvement of durability of RAC	Latest techniques for the improvement of durability of RAC
Ma et al. 2022 [29]	Cost Analysis of recycling of construction waste	To develop Optimized mix design
Andrade Salgado et al. 2022 [30]	with an emphasis on the widespread implementation of recycled aggregate concrete projects	Research to use RAC in the construction industry
Danish et al. 2022 [5]	RCA's production, properties, and enhancements were the primary areas of concentration.	Recycling of aggregate should be started in big cities.

From an environmental standpoint, the usage of RCA as an alternative for traditional aggregate has gained a lot of interest. RCA is a little bit used despite so much research on its alternative material to natural aggregate. This small use of RCA is due to the reduced properties of recycled aggregate concrete. The enhancement of properties of recycled aggregate concrete have been the subject of a great deal of study and got success with up to 30% usage of recycled aggregate. Using only recycled aggregate in concrete will help conserve our planet's natural resources. Because of its subpar quality, recycled aggregate concrete is not used as full replacement of NA in building projects. The main cause is the Interfacial transition zone, the weakest link between the aggregate and the cement matrix (ITZ). As can be seen in Table 1, while the mesostructure features of recycled aggregate concrete have received a lot of attention, the microstructure qualities have received relatively less research. Previous

reviews adequately explain physical, mechanical, and durability features; so, these aspects are omitted from the present investigation. Research and development of ITZ is the primary subject of this paper, which provides a critical description of the methods employed to achieve such development. In this study, we look at the open doors in the ITZ's development and how to fill them. As a result, there will be a significant effect on the environment and climate change if recycled aggregate is used to replace natural aggregate entirely. The construction industry's approach to green building will shift as a result.

Improvement of the Interfacial Transition Zone

Only one ITZ exists in traditional concrete, and that is between the aggregate and the cement matrix. This is not the case with recycled aggregate concrete, however, which contains two ITZs, old ITZ and New ITZ [31]. There remain pores and fissures in RA after crushing, which weakens old ITZ. According to published literature, the new ITZ, which binds RCA with the new mortar, is a weak link because the presence of areas with high water content precludes the establishment of a strong binding between RCA and the new cement paste [32]. The new ITZ contains free, hydrated particles that contribute to the RCA's high-water absorption and porosity. Yet, the overall quality of RCA can be enhanced by enhancing the aspects of ITZ [33], [34].

This procedure categorises the various approaches that can be taken to enhance the interfacial transition zone as well as other features of RAC, including: i) Removal of adhered mortar ii) Use of mineral admixtures iii) Use of mixing procedures and iv) Carbonation Technique. These methods are discussed in detail in this section.

Removal of adhered mortar

Since alkaline mortar may dissolve in acid, this technique is commonly used to thin or remove the old mortar layer. Several strong and weak acids, including nitric acid (HNO3), hydrochloric acid (HCl), sulfuric acid (H2SO4), acetic acid (CH3COOH), and others, have been employed for this treatment. Recycled concrete aggregate was soaked in HCl, H2SO4, and HNO3 solutions at room temperature for 24 hours before use [35]. Improvements in RAC microstructure and features are possible due to the correlation between RCA and ITZ porosity and RAC microstructure. There are four basic ways to enhance the microstructure of the RAC, one of which is to remove the attached mortar in the RCA. Removing the accompanying mortar improves the microstructure of RCA, enabling for the recycling of high-quality RCA. Pre-soaked RCA in HCl solution can be used in the production of structural concrete free of corrosive reinforcement; however, the concentration of HCl and the consequences of the waste liquid it generates must be considered [36]

Adhered mortar can be removed mechanically applying different techniques as used in previous studies including Mechanical impacts, microwave heating, and thermal treatment method are some other mechanical removal techniques for the attached mortar [37]–[42]. It was shown that RAC properties and ITZ were considerably impacted by the decreased amount of adhering mortar [43]. Unfortunately, these techniques unintentionally led to the creation of a new contaminant with negative environmental effects. Additionally, there are approaches to preventing RA. It was suggested to

impregnate RA with water-soluble polymers, water-repellent polymers and an agent of oil-type and a silane [37], [44]–[46], or even an oil-type polymer [47]–[52] to enhance the binding between aggregate and binder paste. It is extremely uneconomical to eradicate the adhered mortar of RCA mechanically or chemically to enrich ITZ and RAC qualities.

Incorporation of Mineral Admixtures

The inclusion of mineral admixtures is another strategy for improving the ITZ of RCA. To achieve this improvement, pozzolanic reaction is used which generates new C-S-H products and densifies ITZ by filling voids [13]. Katz proposes that admixtures act as microfillers in the ITZ between the aggregate surface and the matrix [43]. In this section, deliberates the importance of mineral admixtures for improving ITZ efficiency. One of the most used mineral admixtures that can be used to enhance ITZ, is silica fume. A denser coating is formed over the aggregate's surface by a reaction with calcium hydroxide, which also serves to enhance ITZ. The effectiveness of stone-encased pozzolanic powder (SEPP) and normal mixing method (NMA) against stone-encased portland cement (SEPC) in concrete mixes was analysed. The transition zone between the two phases was studied by scanning electron microscopy (SEM) in recycled aggregate concrete. Data from scanning electron microscopy show that the mixture of fly ash and silica fume resulted in a denser transition zone at the interface [53]. Recycled aggregate concrete had its microstructure modified by replacing Portland cement with phosphorous slag (PHS), ground granulated blast-furnace slag (GGBS), and fly ash (FA). A unique production method dubbed "W3T4" was presented to improve the performance of the interfacial transition zone (ITZ) between recycled aggregate and mortar. The smallest size of GGBS has the greatest impact on RAC performance due to its superior filling effect and substantially pozzolanic reaction. When PHS and GGBS are employed together, the delay in setting time is mitigated, and the synergistic effect aids in the development of a more compact RAC. With 25% RA replacement and 10% PHS + 10% GGBS additions, RAC compressive strength is increased by 25.4% compared to the reference concrete created with natural aggregates, while permeability is decreased by 64.3%. Micro-mechanics of these developments were studied with a scanning electron microscope (SEM). SEM photos show that the new production method, which makes use of superfine pozzolanic powders and the benefits of a super-plasticizer, results in a significantly denser ITZ in RAC. While recycled aggregate concrete (RAC) is a useful way to repurpose construction waste as a resource, it suffers from considerable mechanical and chloride ion permeability impairments because to the existence of numerous interface transition zones (ITZ), which generate complex pore defects. Fly ash (FA), silica fume (SF), and mineral powder (SL) were utilised as admixtures to enhance the RAC's pore structure. The effects of admixtures on RAC's pore structure parameters and pore size distribution were investigated using back scattering electron imaging (BSE), mercury intrusion porosimetry (MIP), and fractal dimension theory (FDT). Quantitative descriptions of the ITZ's microscopic properties, such as its porosity and pore structure, were also provided. It is clear from the results that adding an appropriate amount of admixture can reduce the porosity, average pore diameter, and maximum aperture of RAC. Macropores and capillary pores declined in quantity and were finally replaced by transition holes and gel pores. When pores are refined, RAC becomes more compact, thanks in large part to the pozzolanic effect of SF [54]**.** The mineral additives used in this experiment include varying amounts of silica fume (SF) and ground

granulated blast furnace slag (GGBFS). Compressive strength, tensile splitting strength, density, and water absorption are some of the Main characteristics tested in this experimental investigation of the effects of SF and GGBFS on hardened concrete. Compressive strength decreases by around 24% at 100% of the replacement level of RCA, and the results become more noticeable for RCA contents over 50%. Compressive strength testing has shown that increasing the amount of RCA in concrete significantly boosts that material's resistance to cracking under tension. It has been found that the ratio of tensile splitting strength to compressive strength is greater in RCA concretes containing GGBFS than in RCA concretes containing SF [55]. Three different SCMs (fy ash, ground granulated blast furnace slag, and silica fume) were used with and without TSMA. The experimental results demonstrated that the addition of SCMs and TSMA improved the RAC's workability, strength, shrinkage, and durability. The RAC that was treated with SCMs and TSMA also had a lower cost per unit strength than the untreated RAC. Using refined RAC will have positive effects on the economy, ecology, and technology [58]. Because of its high-water absorption, recycled aggregate (RA) causes changes in the microstructure of concrete, notably in the interfacial transition zone (ITZ). The purpose of this research is to determine how using recycled coarse aggregate (RCA) affects the ITZ microstructure of concrete with three distinct strengths (C25, C35, and C45) and a range of water-to-cement ratios (w/c). Scanning Electron Microscopy (SEM) analysis of the paste's porosity and anhydrous profiles was used to characterise and compare the RA in SSD condition and to search for interactions between the two. The microscopic structure of the ITZ is still highly dependent on the new paste even though the w/c ratio is lower. The purpose of this research was to analyse how using recycled coarse aggregate (RCA) altered the microstructure of the ITZ in concrete across three distinct strength ranges. A variety of concrete w/c ratios (C25, C35, and C45). Scanning Electron Microscope (SEM) analysis of the paste's porosity and anhydrous profiles was used to characterise and compare the RA in SSD condition, with the aim of identifying any interactions between the two. The ITZ of RA C25 and C35 concretes continue to show the same tendency, namely a higher porosity profile, despite the new paste's lower w/c ratio. This is because the w/c ratio of the fresh paste has a significant impact on the microscopic structure of the ITZ [56]. The high porosity of the interfacial transition zone could have a major effect on the lifespan of offshore concrete structures (ITZ). To assess the effects of aggregate surface on ITZ corrosion resistant materials that have been attacked by chloride, this work coats the ITZ microstructure with slag and silica fume. To begin, a series of chloride transport experiments was performed. Following this, an experimentally validated model was developed to help shed light on the underlying reactive-transport behaviour of chlorides in concrete in relation to different aggregate surface coating methods. According to experimental results depicted in Figure 5 [60], coating aggregate surfaces with silica fume can significantly reduce the porosity of the interfacial transition zone [57].

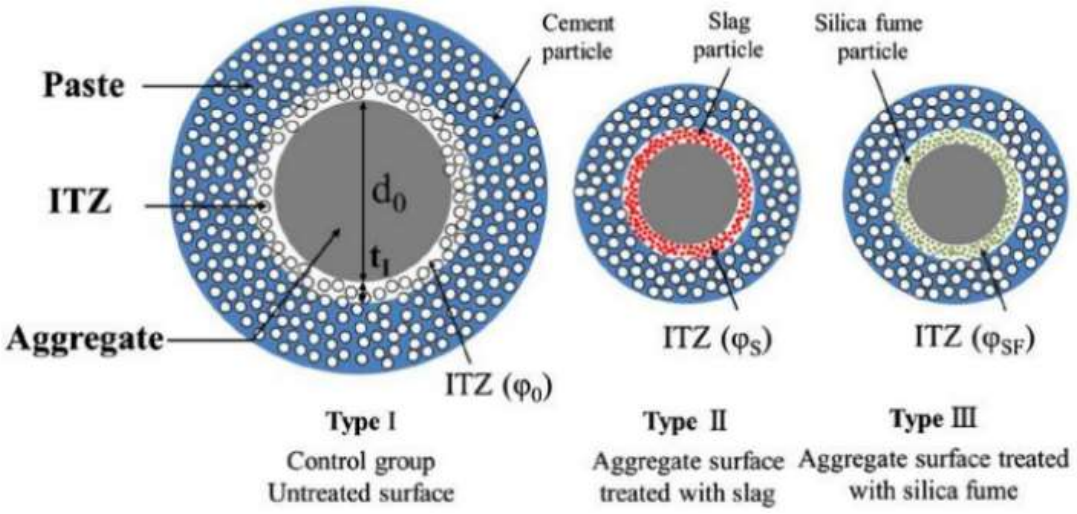

Figure 5: Study of ITZ using Numerical Modelling and pozzolanic treatment [57]

Recycled aggregate concrete's mineralogy and the effect of concrete compositions (RAC), the concept of an interfacial transition zone, and the micro - structural formation of RAC were discussed. It was suggested that the mineralogy of RAC alters because of the inclusion of cementitious materials. SEM microscopy was used to look at tiny pieces of RAC and the study also discussed the many hydration products that are commonly found in RAC [58]. The impact of the concrete compositions on the mineralogy of recycled aggregate concrete (RAC). The processes associated in the mineralogy, interfacial transition zone concept, and microstructural evolution of RAC were explained. It is also stated that additional cementitious materials have an impact on how the mineralogy of RAC changes. The study also covered the numerous hydration products often present in RAC as well as microscale examination of RAC using scanning electron microscopy [59]. It was assumed that cement, plasticizing admixtures, and pozzolanic additives would be standard fare in concrete batching facilities. Ceramic scraps from the manufacturing process used to make the aggregate and divided into two sizes (0-4 mm and 4-8 mm) to accommodate different applications. The purpose of this investigation was to develop a method of using the iterative design process of concrete mix to produce concrete that meets all the required strength criteria. Compressive and tensile strength, bulk density, water absorption, water permeability, and frost resistance were among the primary physical and mechanical properties tested for the resulting concrete. The outcomes of the analysed parameters were compared to those of reference samples generated with the identical substances. Gravel (between 0 and 4 mm in size) and basalt were from the sole building materials used (4–8 mm). The ITZ between cement paste and aggregate (ceramic and basalt) was also analysed using a scanning electron microscope (SEM). Based on these findings, hypotheses were formulated regarding how the ITZ's microstructure affects the final concrete qualities. As a result of this research, developed a proprietary model to predict how well cement paste would stick to a mixture of ceramic wastes [60]. Core findings of incorporation of mineral admixtures of latest researched are tabulated in Table 2.

Table 2: Incorporation of mineral admixtures and their core findings

Title	Mineral Admixtures	Findings
Faysal et al. 2020 [61]	Silica fume (SF), F fly ash (FA), and ground-granulated blast-furnace slag (GGBFS)	Using TSMA improved the performance of the interfaces between the old mortar and the RA's surface, while incorporating SCMs led to a densification of the microstructure with greater binding ability.
Li et al. 2009 [53]	Blast Slag, Fly Ash, and Silica Fume	Fly Ash and Silica fume gave better result in the reduction of thickness of ITZ.
Wang et al. 2013 [62]	Grinded granulated blast-furnace slag (GGBS), phosphorous slag (PHS), and fly ash (FA)	Since GGBS has a denser ITZ, it can partially replace PHS without sacrificing the hydration retardation that PHS causes. This occurs because GGBS is a more refined particle size.
Gao et al. 2022 [54]	Mineral powder, silica fume and fly ash (FA)	The use of SF has been shown to be the most effective method for enhancing RAC pores.
Çakir 2014 [55]	Silica Fume and GGBFS	Silica Fume produced denser ITZ.
Sun et al. 2020 [57]	Silica Fume and GGBFS	The coating on aggregate surface may decrease porosity in ITZ, and the effects of silica fume are still more severe (e.g., and over 40% loss of porosity micrometres from aggregate surface).
X Li et al. 2021 [58]	Bayer red mud (RM)	The RM, rather than participating in reactions that occur at the aggregate surface, enhances the interface structure of the ITZ throughout hardening.
Awoyera et al. 2022 [59]	Silica Fume, Fly Ash	The interfacial transition zone is the site of formation of several hydration products.

B Zegardło et al. 2016 [60]	Sanitary ceramic waste	the numerous hydration products often present in RAC as well as microscale examination of RAC using scanning electron microscopy

Mixing Technique

Recycled aggregate was produced using a two-stage crushing process (RA). Slump tests were performed on concrete mixes produced using three different methods: stone encased with pozzolanic powder (SEPP), the normal mixing method (NMA), and stone encased with Portland cement (SEPC). After 7 and 28 days, the curing strength was tested by applying a compressive and flexural load. The interfacial region of recycled concrete was analysed to use a scanning electron microscope (SEM). Results from scanning electron microscopy show that the new mixing technique results in a denser interfacial transition zone [53]. A unique triple mixing method (TM) was developed to surface-coat aggregate with pozzolanic materials, thereby enhancing the properties of recycled concrete and the micro - structural of the interfacial transition zone (ITZ). Several admixtures and mixing methods were tested to see how they affected RAC's compressive capacity and resistance to chloride ion penetration. Method: Using a new concrete, an old concrete, and a new concrete to create a sandwich specimen, and then using a scanning electron microscope to examine the surface of the old concrete. In addition, the effect of surface-coating the recycled aggregate (RA) in RAC with several admixtures on the ITZ microstructure was studied. The results showed that applying TM can further increase the quality of RAC compared to using the double-mixing strategy [63]. Characteristics of the new and old Interfacial Transition Zones (ITZs) in recycled aggregate concrete were analysed using atomic force microscopy (AFM), scanning electron microscopy (SEM), and nanoindentation. SEM images of both the old and new ITZ in RAC reveal obvious cavities and a significant calcium hydroxide content. The nanoindentation study found that the thickness of the original and replacement ITZs are, respectively, 40–50 micron and 55–65 micron. It is found that the average indentation modulus of the previous ITZ is between 70 and 80 percent of the previous paste matrix, whereas the average indentation modulus of the subsequent ITZ is between 80 and 90 percent of the subsequent paste matrix [64]. To investigate the features of the ITZ of RAC, a model of RAC was presented that meshes inside the aggregate itself. With this model, the ITZ's characteristics may be isolated and predicted with high accuracy. Several RAC projection mesh models were constructed to prove the model's accuracy and usefulness, and to serve as benchmark examples. To further mimic the ITZ element, which degenerates from a 3D element, a 2D element was added to the original base force element method (BFEM). The RAC models were then loaded with displacement to simulate uniaxial compression and tension testing using the BFEM. Peak/ultimate strain, crack growth, compressive strength, and tensile strength were all studied in relation to ITZ thickness. The correlation between ITZs and the relative characteristics of the corresponding mortar was also investigated. Based on the data, it's clear that the present model is a competent method for investigating the ITZ effect law. Further, this method enables researchers to isolate the effects of modifying individual factors by adjusting the many ones that contribute to the problem. An innovative approach to studying elements with extremely high aspect ratios, the

degenerate element allows for a quick and precise analysis of these objects [65]. Optimized mixing is a powerful tool for improving the microstructure of the interfacial transition zone (ITZ) in recycled aggregate concrete (RAC). The iron oxide used in this study was able to distinguish between the additional mortar (AM) and the residual mortar (RM) in RAC made with the two-stage mixing technique (TSMM), the cement paste encapsulating aggregate method (CPEAM), and the regular mixing method (NMM). RM and AM CaCO3 concentrations and pH values were studied independently. Carbonation zone and steel corrosion zone lengths of RAC were independently computed based on CaCO3 concentrations and pH values and compared. The results showed that the carbonation and steel corrosion zones were narrowed thanks to the TSMM and CPEAM, which did this by improving the microstructure of the ITZs. Results showed that carbonation and steel corrosion zone widths were reduced thanks to the TSMM and CPEAM, which did this by improving the microstructures of the ITZs and so decreasing the interfacial impact zones in the RM and AM. [66].

Water absorption, freeze-thaw resistance, and sulphate resistance of recycled aggregate concrete were examined, along with the effects of the cement-pulverized fuel ash-silica fume method (SCP), the sand envelope mixing approach (SE), and the bi-combination of SCP + SE (RAC). The microstructure of the enhanced RACs was analysed using scan electron microscopy (SEM) images to confirm the experimental results. It's worth noting that this study also included a detailed cost analysis of the various augmentation methods used. This was because of the strengthened interfacial transition zone, reinforced adhering mortar, filled-up pores and microcracks, reduced porosity, and compacted interfacial transition zone in the treated RA, among other factors. The new cement paste, reinforced adherent mortar, improved interfacial transition zone, filled-up gaps and microcracks, lowered porosity, and compacted denser microstructure all contributed to the better overall interlocking of the treated RA. Researchers, RA manufacturers, design engineers, and investors will all benefit from a deeper understanding of the durability property of RAC built with 100% treated RA according to this study's findings [67]. There are two flaws in the ITZ that cause recycled aggregate concrete (RAC) to perform poorly compared to concrete made with natural aggregates. As can be seen in Figure 6, an OTM strategy was developed in this research to enhance the ITZ in the RAC. Evidence showed that OTM considerably improved the RAC's compressive strength, freezing and thawing resistance, and water impermeability. Because OTM stuffed supplementary cementitious materials (SCMs) into the ITZ in the RAC. By covering the recycled aggregate with a thin, dense layer of SCMs, the RAC's ITZ structure was further strengthened. In addition, OTM aided in the spread of SCMs within the ITZ [68]. Different mixing techniques from latest research are tabulated in Table 3

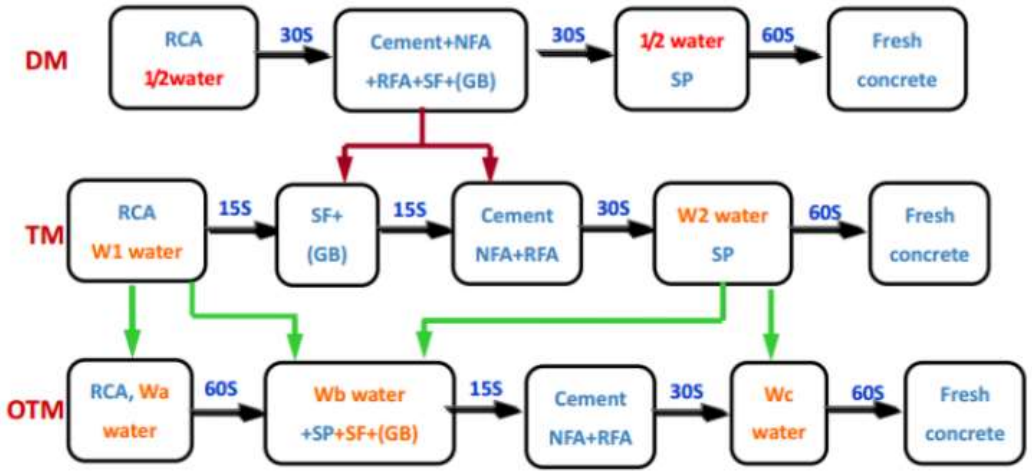

Figure 6: Double Mixing (DM), Triple Mixing (TM) and Optimum Triple Mixing (OTM)

Table 3: Mixing Techniques and their core findings

Title	Technique	Findings
Kong et al. 2010 [63]	Triple mixing method (TM)	ITZ thickness improved.
Xiao et al. 2013 [64]	Two stage Mixing Method (TSMM)	Mechanical qualities of RAC were improved due to densification of ITZ.
Wang, Yao, et al. 2020 [65]	A numerical model was created to simulate the ITZs of recycled aggregate concrete.	Numerical Modelling and experimental results have not much difference.
Mi et al. 2021 [66]	Methods include the two-stage mixing method (TSMM), the cement paste enveloping aggregate method (CPEAM), and the standard mixing method (NMM).	Better results in reducing ITZ thickness were achieved using the cement paste enveloping aggregate method (CPEAM).
Al-Waked et al. 2022 [67]	Sand envelope mixing (SE), the cement-pulverized fuel ash-silica fume method (SCP)	Using the SCP method of cement-pulverized fuel ash-silica fume, the thickness of ITZ was decreased.
Zhang et al. 2019 [68]	Optimized Triple Mixing Method (OTM)	OTM improved the thickness of ITZ.

Carbonation technique

One technique that can be utilized to improve ITZ thickness. This technique works on the penetration of CO2 into the ITZ vicinity which can then react with CH and C-S-H and densify the ITZ [69]. This treatment can be performed in controlling and changing the various parameters including carbonation pressure, starting RCA moisture concentrations and carbonation time etc.

Carbonation parameters such as carbonation pressure, initial RCA moisture concentration, and carbonation time were evaluated. It was determined that a simulation of the RACs (MIRAC) was required to accurately locate many ITZs. The impact of carbonation treatment on the RAC's micro characteristics was studied with scanning electron microscopy (SEM) and nanoindentation testing. Results showed that as carbonation pressure or time increased, ITZ modulus, old mortar composite, and new mortar matrix all improved while ITZ thickness decreased. However, after that the carbonation pressure reached 1 bar, there was no further noticeable change, and the carbonation rate began to drastically decrease after 3 hours. Higher carbonation efficiency was achieved at a moisture level of 1.81 percent. Various carbonation parameters demonstrated consistent effects on both the RAC's micro characteristics [69]. Latest research revealed that there are three main forms of ITZs in RAC: ITZ1, ITZ2 and ITZ3 as depicted in figure 5 [70]. The effects of carbonation treatment on the interface between carbonated RCA and fresh cement mortar/paste were investigated in a separate study using a variety of microstructural tests, including resistive (shear) and ultimate tensile tests, microhardness, XRD, thermal analysis (TGA), and scanning electron microscopy. Large calcite crystals were found to have precipitated out onto the exterior of RCA after being subjected to the carbonation procedure. Calcite from the new cement combined with aluminate species to form mono carbonate (Mc), which subsequently acted as nucleation sites for the formation of C-S-H on the top of RCA. As a result, the hardness value of the ITZ increased and the porosity of the interior reduced significantly due to local densification along the surface of the carbonated RCA [71] Carbonization was performed on RCAs ranging in diameter from 10-20 mm, 20-30 mm, and 30-40 mm for 0, 7, and 28 days, respectively. Scanning electron microscopy was used to examine the mean microcrack width (Wc) in the ITZ region between the aggregate and mortar in RCA, and the correlations among Wc in the ITZ zone and the mechanical characteristics of RAC were assessed. Experiments show that carbonation treatment modifies the ITZ microstructure. During curing with CO2, Wc decreases rapidly at the beginning and gradually at the end. Wc of ITZ is 14.1%-16.9% lower for 28 days of CO2 curing compared to non-curing. Using RCA during carbonation allows for increased uptake of carbon dioxide due to the aggregate's small size and high specific surface area [72] Mixing recycled coarse aggregates with nano-SiO2 and then soaking it in 3.5% NaCl for 45 and 90 days yields RAC. Ca, Si, and Cl element distribution patterns in the RAC's interstitial zones (ITZs) were characterised with great accuracy. The results show that the chloride ion first enters the interface in ITZs of RAC, and then the cement matrix through pores and cracks. Instead, ITZs treated with nano-SiO2 have a more compact internal microscopic structure and fewer fissures, providing an effective barrier and greatly reducing the depth to which chloride ions can penetrate [73]. Accelerated carbonation was used to treat recycled concrete aggregate (RCA) for 24 hours at a pressure of 0.30 MPa, with 0%, 30%, 70%, and 100%

replacement ratios. Mechanical property studies included compressive, splitting-tensile, and fracture strength evaluations after 7 and 28 days of aging. X-ray diffraction, a scanning electron microscope with an energy dispersive spectrometer, and the Vickers micro-hardness test were all used to examine the material's microscopic properties (SEM-EDS). The results showed that the properties of the CRCA were enhanced due to calcite filling the old mortar (OM) and ITZ-2 pores in the CRCA. Hence, the RAC's mechanical properties improved proportionally with the CRCA replacement ratio. When compared to earlier RAC iterations, ITZ-3 fares exceptionally well. Though it started with the fewest strengths, ITZ-3 improved the most. How the CRCA improves the ITZ-3's micro-properties can also be explained by the calcite's chemical and nucleation effects, as well as by the ITZ-3's micro-bleeding effects. To be more precise, the aluminate reacted with the calcium silicate hydrate (C-S-H) nucleation sites on the CRCA's surface to form hemicarbonate (Hc) while monocarbonate was produced in the ITZ-3 (Mc). Reduced water absorption by the CRCA also mitigated the micro-bleeding impact of the ITZ-3 [74] Several experts used carbonation techniques to improve the ITZ of recycled concrete and core findings are tabulated in table 4.

Table 4: Carbonation techniques and their core findings

Title & Year	**Carbonation Variables**	**Findings**
Wu et al. 2022 [69]	carbonation level, RCAs' starting moisture content, and how long they're left to carbonate	ITZ thickness was reduced.
Zhan et al. 2020 [71]	carbonated modeled recycled concrete aggregates	Slightly decreased the ITZ using the carbonation technique.
Li et al. 2020 [72]	CO2 Curing	The thickness of ITZ is reduced 14.1–16.9%
Gao et al. 2022 [73]	Modified recycled coarse aggregates, treated nano Sio2	Treated nano Sio2 gave better results regarding the thickness of ITZ.
Wu Jun et al. 2022 [74]	Carbonation Pressure	ITZ-3's micro-bleeding effect was lessened by a decrease in the CRCA's water absorption

It is found from the above literature that Modified recycled concrete aggregate reduce the thickness of ITZ using different carbonation techniques. This method is good to use in the reduction of ITZ thickness in future.

CONCLUSION

The results of this comprehensive examination of RAC's features are as follows:

Regarding transportation methods and distances, RAC has an advantage over NAC, but because cement and aggregate production in RAC has a greater environmental impact due to their energy-concentrated nature, it is recommended that concrete recycling be promoted, leading to the proliferation of recycling centres in major cities throughout the world. The use of RCA in the manufacturing of concrete has gained popularity in the building sector. However, RCA has distinct features than NA because due to the presence of an ITZ between the original cement and the used NA. To improve the ITZ this article compares the various treatment techniques are used by researchers.

It was determined that RCA's inferior characteristics to NA were mostly due to its porous microstructure and weak interfacial transition zone. According to studies by various experts, carbonation, mineral admixtures, mixing techniques and other processes are the main ways to improve the ITZ qualities of RCA. Several methods depending on the required qualities, each of these ITZ enhancement techniques has a range of results. Nevertheless, each treatment approach has limitations when used in real-world situations. In comparison to these techniques, the incorporation of mineral admixtures and mixing techniques offer the greatest application potential for enhancing the characteristics and functionality of ITZ. These are economical methods for the strengthening of thickness of ITZ with impregnation in the slurry of mineral admixtures and triple stage mixing approach.

However, to practically adopt RCA in the production of concrete, further study and investigation is necessary on the impacts of improvement approaches, not just on a small scale in laboratory circumstances, but in actual projects. The criteria for RCA's implementation in actual projects should also be guided by a thorough investigation of its practical use in concrete. Further thorough analysis and research are needed to apply RCA implementation to massive commercial manufacturing.

References:

[1] M. Behera, S. K. Bhattacharyya, A. K. Minocha, R. Deoliya, and S. Maiti, "Recycled aggregate from C&D waste & its use in concrete - A breakthrough towards sustainability in construction sector: A review," *Construction and Building Materials*, vol. 68. 2014. doi: 10.1016/j.conbuildmat.2014.07.003.

[2] R. Pierrehumbert, "There is no Plan B for dealing with the climate crisis," *Bulletin of the Atomic Scientists*, vol. 75, no. 5, 2019, doi: 10.1080/00963402.2019.1654255.

[3] B. Wang, L. Yan, Q. Fu, and B. Kasal, "A Comprehensive Review on Recycled Aggregate and Recycled Aggregate Concrete," *Resour Conserv Recycl*, vol. 171, p. 105565, Aug. 2021, doi: 10.1016/J.RESCONREC.2021.105565.

[4] S. A. Memon, Z. Bekzhanova, and A. Murzakarimova, "A Review of Improvement of Interfacial Transition Zone and Adherent Mortar in Recycled Concrete Aggregate," *Buildings*, vol. 12, no. 10, p. 1600, Oct. 2022, doi: 10.3390/buildings12101600.

[5] A. Danish and M. A. Mosaberpanah, "A review on recycled concrete aggregates (RCA) characteristics to promote RCA utilization in developing sustainable recycled aggregate concrete (RAC)," *European Journal of Environmental and Civil Engineering*, vol. 26, no. 13, pp. 6505–6539, Oct. 2022, doi: 10.1080/19648189.2021.1946721.

[6] J. K. Bothara and K. M. O. Hiçyilmaz, "General observations of building behaviour during the 8th October 2005 Pakistan earthquake," *Bulletin of the New Zealand Society for Earthquake Engineering*, vol. 41, no. 4, 2008, doi: 10.5459/bnzsee.41.4.209-233.

[7] Y. Zhou, J. R. Elliott, B. Parsons, and R. T. Walker, "The 2013 Balochistan earthquake: An extraordinary or completely ordinary event?," *Geophys Res Lett*, vol. 42, no. 15, pp. 6236–6243, Aug. 2015, doi: 10.1002/2015GL065096.

[8] L. Zheng *et al.*, "Characterizing the generation and flows of construction and demolition waste in China," *Constr Build Mater*, vol. 136, pp. 405–413, Apr. 2017, doi: 10.1016/J.CONBUILDMAT.2017.01.055.

[9] K. H. Yang, H. S. Chung, and A. F. Ashour, "Influence of type and replacement level of recycled aggregates on concrete properties," *ACI Mater J*, vol. 105, no. 3, 2008, doi: 10.14359/19826.

[10] Z. Zheng, S. Xie, H. Dai, X. Chen, and H. Wang, "An Overview of Blockchain Technology: Architecture, Consensus, and Future Trends," in *2017 IEEE International Congress on Big Data (BigData Congress)*, Jun. 2017, pp. 557–564. doi: 10.1109/BigDataCongress.2017.85.

[11] M. Hossain, P. Bhowmik, and K. Shaad, "Use of waste plastic aggregation in concrete as a constituent material," *Progressive Agriculture*, vol. 27, no. 3, pp. 383–391, Dec. 2016, doi: 10.3329/pa.v27i3.30835.

[12] S. C. Kou and C. S. Poon, "Enhancing the durability properties of concrete prepared with coarse recycled aggregate," *Constr Build Mater*, vol. 35, pp. 69–76, Oct. 2012, doi: 10.1016/J.CONBUILDMAT.2012.02.032.

[13] C. Shi, Y. Li, J. Zhang, W. Li, L. Chong, and Z. Xie, "Performance enhancement of recycled concrete aggregate – A review," *J Clean Prod*, vol. 112, pp. 466–472, Jan. 2016, doi: 10.1016/J.JCLEPRO.2015.08.057.

[14] K. McNeil and T. H.-K. Kang, "Recycled Concrete Aggregates: A Review," *Int J Concr Struct Mater*, vol. 7, no. 1, pp. 61–69, Mar. 2013, doi: 10.1007/s40069-013-0032-5.

[15] A. Katz, "Properties of concrete made with recycled aggregate from partially hydrated old concrete," *Cem Concr Res*, vol. 33, no. 5, pp. 703–711, May 2003, doi: 10.1016/S0008-8846(02)01033-5.

[16] H. Zhang, T. Ji, X. Zeng, Z. Yang, X. Lin, and Y. Liang, "Mechanical behavior of ultra-high performance concrete (UHPC) using recycled fine aggregate cured under different conditions and the mechanism based on integrated microstructural parameters," *Constr Build Mater*, vol. 192, pp. 489–507, Dec. 2018, doi: 10.1016/J.CONBUILDMAT.2018.10.117.

[17] M. Bravo, A. Santos Silva, J. de Brito, and L. Evangelista, "Microstructure of Concrete with Aggregates from Construction and Demolition Waste Recycling Plants," *Microscopy and Microanalysis*, vol. 22, no. 1, pp. 149–167, Feb. 2016, doi: 10.1017/S1431927615015512.

[18] Y. Li, S. Zhang, R. Wang, Y. Zhao, and C. Men, "Effects of carbonation treatment on the crushing characteristics of recycled coarse aggregates," *Constr Build Mater*, vol. 201, 2019, doi: 10.1016/j.conbuildmat.2018.12.158.

[19] A. Hosseini Zadeh, M. Mamirov, S. Kim, and J. Hu, "CO2-treatment of recycled concrete aggregates to improve mechanical and environmental properties for unbound applications," *Constr Build Mater*, vol. 275, 2021, doi: 10.1016/j.conbuildmat.2020.122180.

[20] P. Hosseini, A. Booshehrian, M. Delkash, S. Ghavami, and M. K. Zanjani, "Use of Nano-SiO2 to Improve Microstructure and Compressive Strength of Recycled Aggregate Concretes," in *Nanotechnology in Construction 3*, 2009. doi: 10.1007/978-3-642-00980-8_29.

[21] C. Feng, B. Cui, H. Ge, Y. Huang, W. Zhang, and J. Zhu, "Reinforcement of recycled aggregate by microbial-induced mineralization and deposition of calcium carbonate—influencing factors, mechanism and effect of reinforcement," *Crystals (Basel)*, vol. 11, no. 8, 2021, doi: 10.3390/cryst11080887.

[22] B. Ali, "Effect of aqueous sodium silicate on properties of recycled aggregate mortar," *SN Appl Sci*, vol. 1, no. 10, 2019, doi: 10.1007/s42452-019-1342-2.

[23] S. C. Kou and C. S. Poon, "Properties of concrete prepared with PVA-impregnated recycled concrete aggregates," *Cem Concr Compos*, vol. 32, no. 8, 2010, doi: 10.1016/j.cemconcomp.2010.05.003.

[24] W. M. Shaban, J. Yang, H. Su, K. H. Mo, L. Li, and J. Xie, "Quality improvement techniques for recycled concrete aggregate: A review," *Journal of Advanced Concrete Technology*, vol. 17, no. 4. 2019. doi: 10.3151/jact.17.4.151.

[25] K. P. Verian, W. Ashraf, and Y. Cao, "Properties of recycled concrete aggregate and their influence in new concrete production," *Resources, Conservation and Recycling*, vol. 133. 2018. doi: 10.1016/j.resconrec.2018.02.005.

[26] R. Wang, N. Yu, and Y. Li, "Methods for improving the microstructure of recycled concrete aggregate: A review," *Construction and Building Materials*, vol. 242. 2020. doi: 10.1016/j.conbuildmat.2020.118164.

[27] B. Wang, L. Yan, Q. Fu, and B. Kasal, "A Comprehensive Review on Recycled Aggregate and Recycled Aggregate Concrete," *Resour Conserv Recycl*, vol. 171, p. 105565, Aug. 2021, doi: 10.1016/J.RESCONREC.2021.105565.

[28] A. A. Bahraq, J. Jose, M. Shameem, and M. Maslehuddin, "A review on treatment techniques to improve the durability of recycled aggregate concrete: Enhancement mechanisms, performance and

cost analysis," *Journal of Building Engineering*, vol. 55, p. 104713, Sep. 2022, doi: 10.1016/j.jobe.2022.104713.

[29] M. Ma, V. WY. Tam, K. N. Le, and R. Osei-Kyei, "Factors affecting the price of recycled concrete: A critical review," *Journal of Building Engineering*, vol. 46, p. 103743, Apr. 2022, doi: 10.1016/j.jobe.2021.103743.

[30] F. de Andrade Salgado and F. de Andrade Silva, "Recycled aggregates from construction and demolition waste towards an application on structural concrete: A review," *Journal of Building Engineering*, vol. 52, p. 104452, Jul. 2022, doi: 10.1016/j.jobe.2022.104452.

[31] D. Kong, T. Lei, J. Zheng, C. Ma, J. Jiang, and J. Jiang, "Effect and mechanism of surface-coating pozzalanics materials around aggregate on properties and ITZ microstructure of recycled aggregate concrete," *Constr Build Mater*, vol. 24, no. 5, pp. 701–708, May 2010, doi: 10.1016/J.CONBUILDMAT.2009.10.038.

[32] C. Feng, B. Cui, Y. Huang, H. Guo, W. Zhang, and J. Zhu, "Enhancement technologies of recycled aggregate – Enhancement mechanism, influencing factors, improvement effects, technical difficulties, life cycle assessment," *Constr Build Mater*, vol. 317, p. 126168, Jan. 2022, doi: 10.1016/J.CONBUILDMAT.2021.126168.

[33] F. Kazemian, H. Rooholamini, and A. Hassani, "Mechanical and fracture properties of concrete containing treated and untreated recycled concrete aggregates," *Constr Build Mater*, vol. 209, pp. 690–700, Jun. 2019, doi: 10.1016/J.CONBUILDMAT.2019.03.179.

[34] B. Lu, C. Shi, J. Zheng, and T. C. Ling, "Carbon dioxide sequestration on recycled aggregates," *Carbon Dioxide Sequestration in Cementitious Construction Materials*, pp. 247–277, Jan. 2018, doi: 10.1016/B978-0-08-102444-7.00011-3.

[35] P. Saravanakumar, K. Abhiram, and B. Manoj, "Properties of treated recycled aggregates and its influence on concrete strength characteristics," *Constr Build Mater*, vol. 111, pp. 611–617, May 2016, doi: 10.1016/J.CONBUILDMAT.2016.02.064.

[36] R. Wang, N. Yu, and Y. Li, "Methods for improving the microstructure of recycled concrete aggregate: A review," *Constr Build Mater*, vol. 242, p. 118164, May 2020, doi: 10.1016/j.conbuildmat.2020.118164.

[37] H. K. A. Al-Bayati, P. K. Das, S. L. Tighe, and H. Baaj, "Evaluation of various treatment methods for enhancing the physical and morphological properties of coarse recycled concrete aggregate," *Constr Build Mater*, vol. 112, pp. 284–298, Jun. 2016, doi: 10.1016/J.CONBUILDMAT.2016.02.176.

[38] H. K. A. Al-Bayati, P. K. Das, S. L. Tighe, and H. Baaj, "Evaluation of various treatment methods for enhancing the physical and morphological properties of coarse recycled concrete aggregate," *Constr Build Mater*, vol. 112, pp. 284–298, Jun. 2016, doi: 10.1016/J.CONBUILDMAT.2016.02.176.

[39] Y. Wang, F. Liu, L. Xu, and H. Zhao, "Effect of elevated temperatures and cooling methods on strength of concrete made with coarse and fine recycled concrete aggregates," *Constr Build Mater*, vol. 210, pp. 540–547, Jun. 2019, doi: 10.1016/J.CONBUILDMAT.2019.03.215.

[40] A. Akbarnezhad, K. C. G. Ong, M. H. Zhang, C. T. Tam, and T. W. J. Foo, "Microwave-assisted beneficiation of recycled concrete aggregates," *Constr Build Mater*, vol. 25, no. 8, pp. 3469–3479, Aug. 2011, doi: 10.1016/J.CONBUILDMAT.2011.03.038.

[41] H. Choi, M. Lim, H. Choi, R. Kitagaki, and T. Noguchi, "Using Microwave Heating to Completely Recycle Concrete," *J Environ Prot (Irvine, Calif)*, vol. 05, no. 07, pp. 583–596, 2014, doi: 10.4236/jep.2014.57060.

[42] K. Bru, S. Touzé, F. Bourgeois, N. Lippiatt, and Y. Ménard, "Assessment of a microwave-assisted recycling process for the recovery of high-quality aggregates from concrete waste," *Int J Miner Process*, vol. 126, pp. 90–98, Jan. 2014, doi: 10.1016/J.MINPRO.2013.11.009.

[43] A. Katz, "Treatments for the Improvement of Recycled Aggregate," *Journal of Materials in Civil Engineering*, vol. 16, no. 6, pp. 597–603, Dec. 2004, doi: 10.1061/(ASCE)0899-1561(2004)16:6(597).

[44] R. Wang, N. Yu, and Y. Li, "Methods for improving the microstructure of recycled concrete aggregate: A review," *Constr Build Mater*, vol. 242, p. 118164, May 2020, doi: 10.1016/J.CONBUILDMAT.2020.118164.

[45] J. Vengadesh Marshall Raman and V. Ramasamy, "Various treatment techniques involved to enhance the recycled coarse aggregate in concrete: A review," *Mater Today Proc*, vol. 45, pp. 6356–6363, Jan. 2021, doi: 10.1016/J.MATPR.2020.10.935.

[46] S. F. Santos, R. S. Teixeira, and H. Savastano Junior, "Interfacial transition zone between lignocellulosic fiber and matrix in cement-based composites," *Sustainable and Nonconventional Construction Materials using Inorganic Bonded Fiber Composites*, pp. 27–68, Jan. 2017, doi: 10.1016/B978-0-08-102001-2.00003-6.

[47] S. C. Kou and C. S. Poon, "Properties of concrete prepared with PVA-impregnated recycled concrete aggregates," *Cem Concr Compos*, vol. 32, no. 8, pp. 649–654, Sep. 2010, doi: 10.1016/J.CEMCONCOMP.2010.05.003.

[48] A. A. P. Mansur, D. B. Santos, and H. S. Mansur, "A microstructural approach to adherence mechanism of poly(vinyl alcohol) modified cement systems to ceramic tiles," *Cem Concr Res*, vol. 37, no. 2, pp. 270–282, Feb. 2007, doi: 10.1016/J.CEMCONRES.2006.11.011.

[49] N. K. Bui, T. Satomi, and H. Takahashi, "Improvement of mechanical properties of recycled aggregate concrete basing on a new combination method between recycled aggregate and natural aggregate," *Constr Build Mater*, vol. 148, pp. 376–385, Sep. 2017, doi: 10.1016/J.CONBUILDMAT.2017.05.084.

[50] N. Z. Muhammad, A. Keyvanfar, M. Z. Muhd, A. Shafaghat, and J. Mirza, "Waterproof performance of concrete: A critical review on implemented approaches," *Constr Build Mater*, vol. 101, pp. 80–90, Dec. 2015, doi: 10.1016/J.CONBUILDMAT.2015.10.048.

[51] V. Spaeth and A. Djerbi Tegguer, "Improvement of recycled concrete aggregate properties by polymer treatments," *International Journal of Sustainable Built Environment*, vol. 2, no. 2, pp. 143–152, Dec. 2013, doi: 10.1016/J.IJSBE.2014.03.003.

[52] V. Spaeth and A. Djerbi Tegguer, "Improvement of recycled concrete aggregate properties by polymer treatments," *International Journal of Sustainable Built Environment*, vol. 2, no. 2, pp. 143–152, Dec. 2013, doi: 10.1016/J.IJSBE.2014.03.003.

[53] J. Li, H. Xiao, and Y. Zhou, "Influence of coating recycled aggregate surface with pozzolanic powder on properties of recycled aggregate concrete," *Constr Build Mater*, vol. 23, no. 3, pp. 1287–1291, Mar. 2009, doi: 10.1016/J.CONBUILDMAT.2008.07.019.

[54] S. Gao, Y. Ji, Z. Qin, H. Zhang, F. Xing, and A. Liu, "A comprehensive analysis of pore structures and performances of mineral admixtures modified recycled aggregate concrete based on experiment and theory," *Constr Build Mater*, vol. 358, p. 129451, Dec. 2022, doi: 10.1016/J.CONBUILDMAT.2022.129451.

[55] O. Çakir, "Experimental analysis of properties of recycled coarse aggregate (RCA) concrete with mineral additives," *Constr Build Mater*, vol. 68, pp. 17–25, Oct. 2014, doi: 10.1016/J.CONBUILDMAT.2014.06.032.

[56] A. Djerbi, "Effect of recycled coarse aggregate on the new interfacial transition zone concrete," *Constr Build Mater*, vol. 190, pp. 1023–1033, Nov. 2018, doi: 10.1016/J.CONBUILDMAT.2018.09.180.

[57] D. Sun, H. Shi, K. Wu, S. Miramini, B. Li, and L. Zhang, "Influence of aggregate surface treatment on corrosion resistance of cement composite under chloride attack," *Constr Build Mater*, vol. 248, p. 118636, Jul. 2020, doi: 10.1016/J.CONBUILDMAT.2020.118636.

[58] X. Li, Q. Zhang, and S. Mao, "Investigation of the bond strength and microstructure of the interfacial transition zone between cement paste and aggregate modified by Bayer red mud," *J Hazard Mater*, vol. 403, p. 123482, Feb. 2021, doi: 10.1016/J.JHAZMAT.2020.123482.

[59] P. O. Awoyera and M. S. Kirgiz, "Mineralogy and interfacial transition zone features of recycled aggregate concrete," *The Structural Integrity of Recycled Aggregate Concrete Produced With Fillers and Pozzolans*, pp. 243–251, Jan. 2022, doi: 10.1016/B978-0-12-824105-9.00013-5.

[60] B. Zegardło, M. Szeląg, and P. Ogrodnik, "Ultra-high strength concrete made with recycled aggregate from sanitary ceramic wastes – The method of production and the interfacial transition zone," *Constr Build Mater*, vol. 122, pp. 736–742, Sep. 2016, doi: 10.1016/J.CONBUILDMAT.2016.06.112.

[61] R. M. Faysal, M. Maslehuddin, M. Shameem, S. Ahmad, and S. K. Adekunle, "Effect of mineral additives and two-stage mixing on the performance of recycled aggregate concrete," *J Mater Cycles Waste Manag*, vol. 22, no. 5, pp. 1587–1601, Sep. 2020, doi: 10.1007/s10163-020-01048-9.

[62] H. Wang, J. Wang, X. Sun, and W. Jin, "Improving performance of recycled aggregate concrete with superfine pozzolanic powders," *J Cent South Univ*, vol. 20, no. 12, pp. 3715–3722, Dec. 2013, doi: 10.1007/s11771-013-1899-7.

[63] D. Kong, T. Lei, J. Zheng, C. Ma, J. Jiang, and J. Jiang, "Effect and mechanism of surface-coating pozzalanics materials around aggregate on properties and ITZ microstructure of recycled aggregate concrete," *Constr Build Mater*, vol. 24, no. 5, pp. 701–708, May 2010, doi: 10.1016/j.conbuildmat.2009.10.038.

[64] "Properties of interfacial transition zones in recycled aggregate concrete tested by nanoindentation," *Cem Concr Compos*, vol. 37, pp. 276–292, Mar. 2013, doi: 10.1016/J.CEMCONCOMP.2013.01.006.

[65] Y. Wang, Y. Peng, M. M. A. Kamel, and L. Gong, "Modeling interfacial transition zone of RAC based on a degenerate element of BFEM," *Constr Build Mater*, vol. 252, p. 119063, Aug. 2020, doi: 10.1016/J.CONBUILDMAT.2020.119063.

[66] R. Mi, G. Pan, and T. Kuang, "Reducing the Carbonation Zone and Steel Corrosion Zone Widths of Recycled Aggregate Concrete by Optimizing Its Mixing Process," *Journal of Materials in Civil Engineering*, vol. 33, no. 5, May 2021, doi: 10.1061/(ASCE)MT.1943-5533.0003672.

[67] Q. Al-Waked, J. Bai, J. Kinuthia, and P. Davies, "Durability and microstructural analyses of concrete produced with treated demolition waste aggregates," *Constr Build Mater*, vol. 347, p. 128597, Sep. 2022, doi: 10.1016/J.CONBUILDMAT.2022.128597.

[68] W. Zhang, S. Wang, P. Zhao, L. Lu, and X. Cheng, "Effect of the optimized triple mixing method on the ITZ microstructure and performance of recycled aggregate concrete," *Constr Build Mater*, vol. 203, pp. 601–607, Apr. 2019, doi: 10.1016/j.conbuildmat.2019.01.071.

[69] K. Wu, S. Luo, J. Zheng, J. Yan, and J. Xiao, "Influence of carbonation treatment on the properties of multiple interface transition zones and recycled aggregate concrete," *Cem Concr Compos*, vol. 127, p. 104402, Mar. 2022, doi: 10.1016/J.CEMCONCOMP.2021.104402.

[70] C. Wang, J. Xiao, G. Zhang, and L. Li, "Interfacial properties of modeled recycled aggregate concrete modified by carbonation," *Constr Build Mater*, vol. 105, pp. 307–320, Feb. 2016, doi: 10.1016/J.CONBUILDMAT.2015.12.077.

[71] B. J. Zhan, D. X. Xuan, C. S. Poon, and K. L. Scrivener, "Characterization of interfacial transition zone in concrete prepared with carbonated modeled recycled concrete aggregates," *Cem Concr Res*, vol. 136, p. 106175, Oct. 2020, doi: 10.1016/J.CEMCONRES.2020.106175.

[72] Y. Li, T. Fu, R. Wang, and Y. Li, "An assessment of microcracks in the interfacial transition zone of recycled concrete aggregates cured by CO2," *Constr Build Mater*, vol. 236, p. 117543, Mar. 2020, doi: 10.1016/J.CONBUILDMAT.2019.117543.

[73] S. Gao, J. Guo, Y. Gong, S. Ban, and A. Liu, "Study on the penetration and diffusion of chloride ions in interface transition zone of recycled concrete prepared by modified recycled coarse aggregates," *Case Studies in Construction Materials*, vol. 16, p. e01034, Jun. 2022, doi: 10.1016/J.CSCM.2022.E01034.

[74] J. Wu, "EFFECTS OF CARBONATED RECYCLED CONCRETE AGGREGATE ON MECHANICAL PROPERTIES OF CONCRETE AND MICRO-PROPERTIES OF INTERFACIAL TRANSITION ZONE," *Ceramics - Silikaty*, pp. 113–127, Feb. 2022, doi: 10.13168/cs.2022.0006.

2nd International Conference on Advances in Civil and Environmental Engineering (ICACEE-2023)

University of Engineering & Technology Taxila, Pakistan

Conference date: 22nd and 23rd February, 2023

SSI INFLUENCE ON THE SEISMIC PERFORMANCE OF VERTICALLY-IRREGULAR STRUCTURES

Moazzam Amanat[1], Zeshan Alam*[1], Muhammad Abdullah[1], Shehryar Ahmed[2]

[1]Department of Civil Engineering, International Islamic University, Islamabad, Pakistan

[2]Department of Civil Engineering, Abasyn University, Islamabad, Pakistan

ABSTRACT

The vulnerability of asymmetric and complexly configured buildings to seismic damage is higher compared to their symmetrical counterparts. The increased torsional demands during earthquakes pose a challenge to their seismic assessment, requiring advanced and stringent evaluation methods. Response history analyses have been performed on mid-rise reinforced concrete setback structures with multiple inherent irregularities to examine their seismic behavior and establish design-based conclusions for the improvement in the design-based process. The findings of this study contribute to resolving the challenges faced by the research and design community.

KEYWORDS: Planar irregularity, Soil Structure Interaction (SSI), Torsional coupling, Vertical irregularity.

INTRODUCTION

The uncertainty of seismic excitation and structural irregularities are among the numerous threats to civil infrastructure during extreme seismic events. Reinforced concrete structures are particularly susceptible to the seismic risk posed by structural irregularities, which can take the form of planar or vertical irregularity. Although building codes generally advise against irregular shapes, it is well-known that irregularity is a result of both planar and vertical irregularities. Setback, or the reduction of one side of a structure's floor plan, creates asymmetry about the vertical axis and causes the center of mass and center of rigidity to diverge. Previous research (e.g. [5-8]) has shown that interstory drifts in setback frame structures are larger compared to regular structures.

The seismic response of a structure is also influenced by the soil under and surrounding its foundation. The soil can greatly impact the dynamic properties of the structure [9]. Conventional seismic analysis of structures assumes the structure is fixed at its base and only considers the free-field motion at the ground surface. However, this disregard of the interaction between the structure, foundation, and soil during earthquakes may result in substantial differences between the fixed-base and compliant-base superstructure, particularly in the case of stiff foundation-structure systems in soft soils. Soil-Structure Interaction (SSI) modifies the dynamic response of the system through (1) elongating the fundamental period of the structure, (2) activating additional energy dissipation mechanisms, such as soil hysteretic

*Correspondence to Dr. Zeshan Alam, Department of Civil Engineering, International Islamic University, Islamabad, Pakistan, Email: zeshan.alam@iiu.edu.pk

action and radiation of seismic waves from the foundation, and (3) altering the base motion that excites the structure compared to the free-field motion at the ground surface. This is mainly due to the stiff foundation's inability to follow soil deformations with short wavelengths, leading to filtering of high-frequency components of the incident wave field within the building footprint or foundation depth for embedded foundations [10-18].

This paper aims to investigate the significance of Soil-Structure Interaction (SSI) by analyzing the impact of SSI on the response of elastic multi-degree-of-freedom (MDOF) oscillators, as well as the influence of increased natural periods and drift demands caused by SSI. The goal is to enhance the seismic resilience of infrastructure in the face of future earthquakes. Additionally, this study evaluates the rotational demands of irregular buildings. The results of this study can contribute to the improvement of code provisions and design guidelines, ensuring the seismic safety of structures.

GEOMETRIC MODELS

In the present study, two asymmetric structures have been considered comprising of different irregularity as shown in Fig 1 & 2. The models are represented as Υ_n whereas, the subscript represents group category of that model. For instance, Υ_1 in figure 1 represents the model of group category 1. Note that these notations have been associated with the considered model for better representation and for the determination of various irregularity parameters.

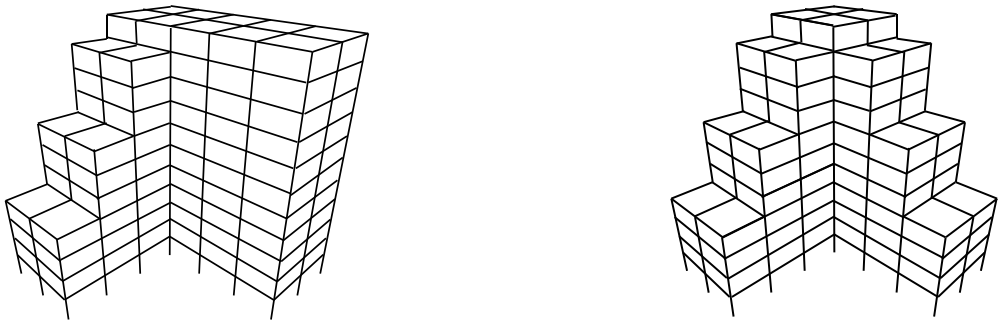

(a) *(b)*

Figure 1: (a) Category 1 - Setbacks in one wing but no setbacks in other wing (Υ_1) (b) Category 2 – Both wings with setbacks (Υ_2)

The global geometric dimensions of these models have been kept same for the purpose of comparison. Similarly, the number of floors has also been kept consistent in all numerical models. However, vertical offsets have been assigned to these structures at varying pattern in order to induce vertical irregularity in these structures.

The primary difference between the presented categories in figure 2 (d) & (e) is the intensity of irregularity. For instance, in category 1, the vertical offsets are present only in the left wing of the structures, whereas, in category 2, both the wings of the structures have inherent vertical offsets.

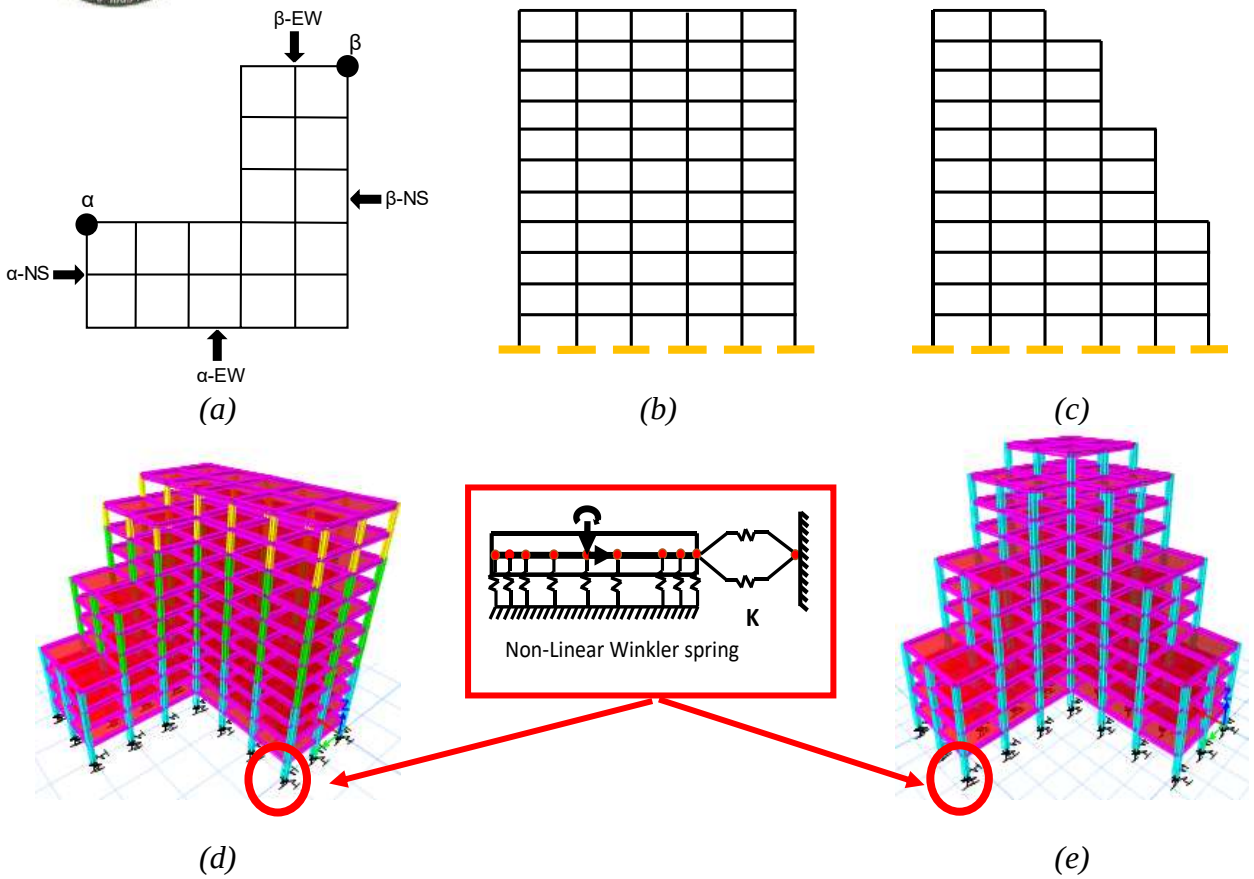

Figure 2: (a) Typical layout of asymmetric models, (b) symmetric model, (c) model with setbacks (d) numerical model Υ_1, (e) numerical model Υ_2

The selected category models with vertical irregularities (Fig. 2 (d) & (e)) have been developed by decreasing certain percentage of the areas along the height from the models. The decrease in the area of the floors represent the increase in the vertical irregularity of the models.

SELECTED GROUND MOTIONS

A period range from 0.2T1 to 2T1 is often effective for midrise buildings. The height of considered buildings fall under midrise category, therefore these buildings are sensitive to excitation at a wide range of periods. This means that it is likely useful to focus on a specific period or wide range of periods when selecting ground motions. After determining the natural periods of the asymmetric structures, ground motions were selected. Ground motions that matched the spectral shape were treated as representative ground motions for the considered buildings.

The primary period range of interest is between 0 and 3 seconds. Table 1 presents a detailed list of the ground motion records employed in this study. The moment magnitudes of the corresponding earthquakes range from 6.2 to 7.6, and the PGA ranged between 0.19 g to 0.76 g. This wide bin of ground motion set is expected to trigger a dreadful seismic response of the considered structures.

Table 1: Selected ground motion components

No	Earthquake	Year	Station	M_w[a]	Components	PGA[C] (g)	PGV[d] (cm/s)	PGD[e] (cm)
1	Chi-Chi	1999	CHY080	7.6	X	0.79	21.11	2.71
					Y	0.86	18.61	2.37
2	Crist Church	2011	Riccarton High School	6.2	X	0.28	6.66	0.69
					Y	0.24	5.03	0.27
3	Imperial Valley	1979	Bonds Corner	6.5	X	0.85	10.89	17.26
					Y	0.76	8.49	3.20
4	Kobe	1995	KJMA	6.9	X	0.83	3.56	6.04
					Y	0.60	3.84	4.67
5	Morgan	1984	Gilroy Array #3	6.2	X	0.36	1.70	0.24
					Y	0.19	2.03	1.50

RESULTS AND DISCUSSIONS

Inter Storey Drift Ratio

The seismic performance of selected asymmetric structures is assessed in terms of inter storey drift ratios. To notice the effect of different irregularities on seismic demands, linear time history analyses were performed. In Fig 5 inter-storey drift demands of the buildings with two categories i.e., Υ_1 and Υ_2 having planner and vertical irregularities have been analyzed with NSSI and SSI effect under the selected ground motions.

It is evident from Fig 5 that location and type of the irregularity contributes an important role in the seismic performance of asymmetric structures [19]. The most considerable drifts are in elevation α-NS (R), β-NS (L), β-NS (R), β-EW (R). The other drifts are relatively low along the height of the structure. The drift demands under chichi earthquake with SSI effects ranges up to 0.0065% but with NSSI effect under same earthquake gives 0.0013% for category 1 model. The inter storey drift demands for each storey with a setback, changes significantly indicating its influence on the storey above and below. This effect is greater on the intermediate floors along the height of the structure.

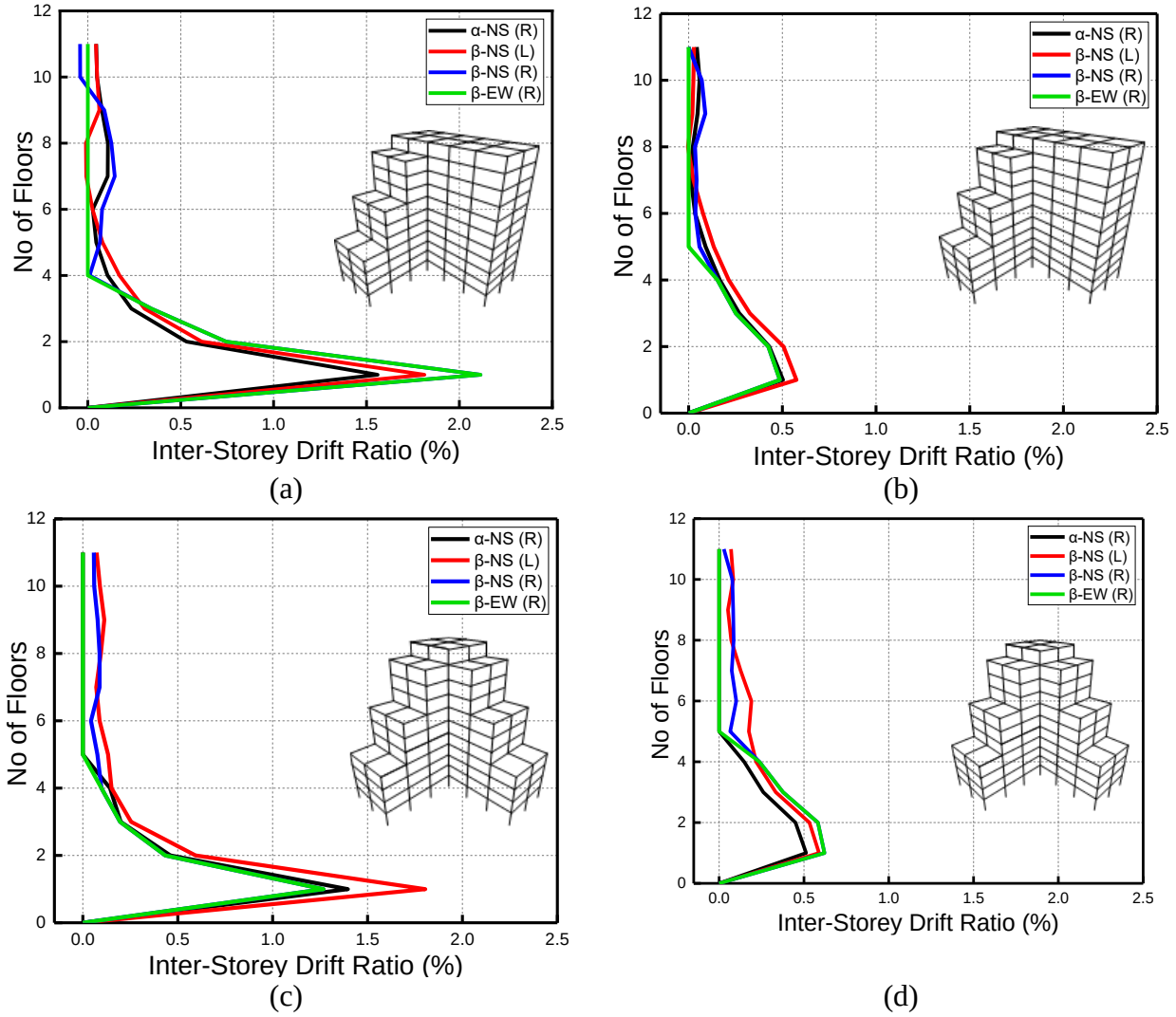

Fig 5: Inter storey drift ratios (a) Υ_1 building with NSSI (b) Υ_1 building with SSI (c) Υ_2 building with NSSI (d) Υ_2 building with SSI

Storey Shear

The seismic response of the structure in terms of the story shear is evaluated as well, internal forces over the height of the structural elements are selected as response parameters of interest as these are generally considered the most important response parameters in seismic design practice. The effect of SSI on the story shear response profile over height for considered buildings have been calculated using time history analyses and compared to those obtained from fixed base models. The effect variation of change in the storey shear due to the incorporation of soil-flexibility as compared to the same obtained at fixed-base condition is expressed as a ratio of response of SSI models to that of fixed based model

are illustrated in Figure 4. Figure 4 shows story shear response profile along the height of the structures Υ_1 and Υ_2 respectively.

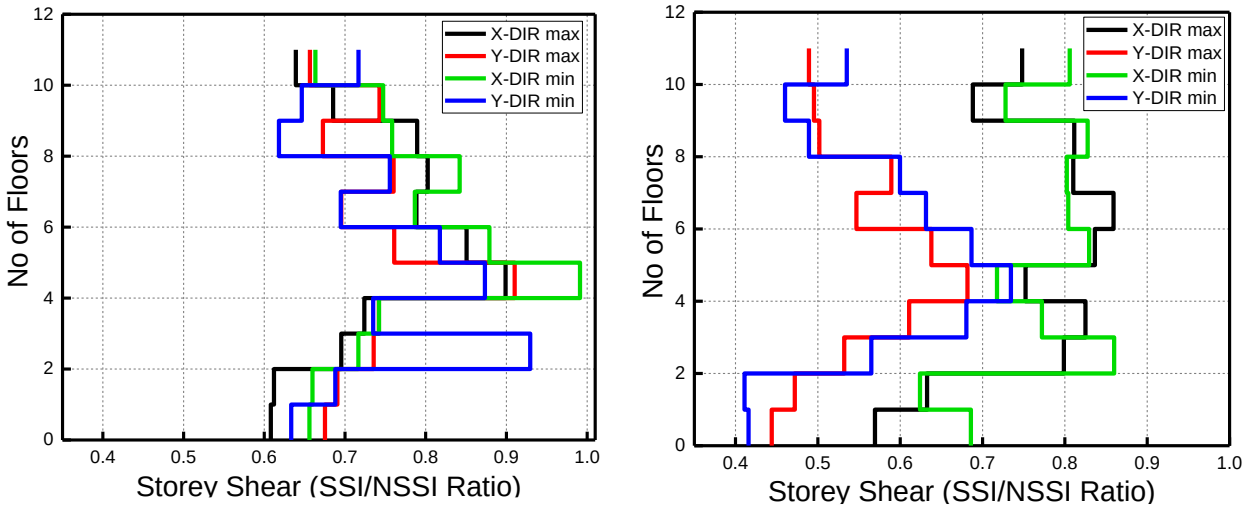

Fig 4: Storey shear profiles (a) Υ_1 building (b) Υ_2 building

CONCLUSION

In this research, the seismic response of buildings with planar and vertical irregularities was analyzed. Two irregular building shapes were selected, one with setbacks in one wing but not in the other (Υ_1) and the other with setbacks in both wings (Υ_2). Five historical ground motions were used to excite the irregular building, and various seismic features were extracted to observe the seismic responses. Results indicate that incorporating SSI effect reduces the seismic capacity and increases drift demands in setback structure. The results also indicate increased lateral shear demands in Υ_1 structures compared with Υ_2 structures. These finding will help both researchers and design practitioners in understanding the influence of SSI on the seismic response of irregular buildings and in making informed design decisions.

REFERENCES

1. Code, U.B., *International building code.* International Code Council, USA, 1997.
2. CEN, E., *8—Design of structures for earthquake resistance—Part 1: General rules, seismic actions and rules for building.* Br. Stand. Institute, London, UK, 2004.
3. Alam, Z., C. Zhang, and B. Samali, *Influence of seismic incident angle on response uncertainty and structural performance of tall asymmetric structure.* The structural design of tall and special buildings, 2020. **29**(12): p. e1750.
4. Authority, B.I., *The New Zealand Building Code Handbook.* Standards New Zealand.(NZBC), 1992.

5. Duan, X. and A. Chandler, *Seismic torsional response and design procedures for a class of setback frame buildings.* Earthquake engineering & structural dynamics, 1995. **24**(5): p. 761-777.
6. Shahrooz, B.M. and J.P. Moehle, *Seismic response and design of setback buildings.* Journal of Structural Engineering, 1990. **116**(5): p. 1423-1439.
7. Karavasilis, T.L., N. Bazeos, and D. Beskos, *Seismic response of plane steel MRF with setbacks: Estimation of inelastic deformation demands.* Journal of Constructional Steel Research, 2008. **64**(6): p. 644-654.
8. Wolf, J.P. and P. Obernhuber, *Non-linear soil-structure-interaction analysis using dynamic stiffness or flexibility of soil in the time domain.* Earthquake engineering & structural dynamics, 1985. **13**(2): p. 195-212.
9. Alam, Z., et al., *Global performance of multi-story stiffness-eccentric RC structures subjected to progressive seismic excitations: Shaking table investigations.* Journal of Building Engineering, 2023. **64**: p. 105582.
10. Veletsos, A.S. and J.W. Meek, *Dynamic behaviour of building-foundation systems.* Earthquake Engineering & Structural Dynamics, 1974. **3**(2): p. 121-138.
11. Bielak, J., *Dynamic behaviour of structures with embedded foundations.* Earthquake Engineering & Structural Dynamics, 1974. **3**(3): p. 259-274.
12. Mylonakis, G., S. Nikolaou, and G. Gazetas, *Footings under seismic loading: Analysis and design issues with emphasis on bridge foundations.* Soil Dynamics and Earthquake Engineering, 2006. **26**(9): p. 824-853.
13. Elsabee, F., J.P. Morray, and J.M. Roesset, *Dynamic behavior of embedded foundations*. 1977: Massachusetts Institute of Technology, Department of Civil Engineering ….
14. Veletsos, A., A. Prasad, and W. Wu, *Transfer functions for rigid rectangular foundations.* Earthquake engineering & structural dynamics, 1997. **26**(1): p. 5-17.
15. Stewart, J.P., *Variations between foundation-level and free-field earthquake ground motions.* Earthquake Spectra, 2000. **16**(2): p. 511-532.
16. Kim, S. and J.P. Stewart, *Kinematic soil-structure interaction from strong motion recordings.* Journal of Geotechnical and Geoenvironmental Engineering, 2003. **129**(4): p. 323-335.
17. Conti, R., M. Morigi, and G. Viggiani, *Filtering effect induced by rigid massless embedded foundations.* Bulletin of Earthquake Engineering, 2017. **15**(3): p. 1019-1035.
18. Conti, R., et al., *Filtering action of embedded massive foundations: New analytical expressions and evidence from 2 instrumented buildings.* Earthquake Engineering & Structural Dynamics, 2018. **47**(5): p. 1229-1249.
19. Alam, Z., et al., *Experimental and numerical investigation on the complex behaviour of the localised seismic response in a multi-storey plan-asymmetric structure.* Structure and infrastructure engineering, 2021. **17**(1): p. 86-102.

2nd International Conference on Advances in Civil and Environmental Engineering (ICACEE-2023)

University of Engineering & Technology Taxila, Pakistan

Conference date: 22nd and 23rd February, 2023

Performance-Based Evaluation of Tall Building by Push Over Analysis

MUHAMMAD GUL PASHA[1], MUHAMMAD YAQUB[2]

University of Engineering and Technology, Taxila
gulpasha9@gmail.com, muhammad.yaqub@uettaxila.edu.pk

ABSTRACT

The trend of the construction of tall buildings in Pakistan is becoming more popular because of the population increase and people are more interested in improving their living standards. Performance-based structure evaluation is the one which it is checked how a building will behave under the defined conditions. Design Engineers check the acceptability and serviceability of the structural building by defining all the parameters through which a building may go in its life span. By acceptability, it means that building gives the all the functionality with all the hazards. In this research, a 24-story building is designed in high seismic hazard zone in Pakistan using E-TABS. The Push over-laboratory analysis is performed to check the strength capacity of the structure and to indicate the weak region in the structure. From the results, a comprehensive comparison analysis is done to study the impact of utilizing this technique to build safer and more economical structures.

KEYWORDS: Performance Based Evaluation, Push Over Analysis, Seismic Behaviour

INTRODUCTION

Pakistan is in an earthquake-prone region[1][2]. The seismic behaviour of buildings is a serious issue nowadays[3]. An earthquake can cause damage to the infrastructure and to human life ultimately which plays a significant role in the economy of the country. It is necessary to protect buildings from earthquakes. Many techniques have been developed over the years to protect buildings. First of all, it is necessary to calculate the lateral loads induced by earthquakes to assess their effect of it. The code-based design known as linear analysis is also used to calculate the earthquake loads but it is difficult to predict the behaviour of the structure when the earthquake loads are applied[4]. Although the code-based design provides reliable safety and performance by minimum limits it cannot describe the actual performance of the building. Performance-based seismic design technique has been introduced based on non-linear computer-based analysis. The main focus of Performance-based design is on three things capacity, demand and performance.[5] The most favoured strategy to check these things is non-linear static analysis or pushover analysis. It is the procedure to check the strength capacity beyond the elastic limit up to the ultimate strength in the non-linear stage. There are two approaches in pushover analysis force controlled and

displacement controlled due to the complexity of the force method, the displacement method is used.[6] The procedure is about incrementally increasing structural loading according to a defined pattern. Hinges assigned to members and on reaching the provided displacement hinges show a

colour according to the defined performance point using FEMA 356 and ATC 40 guidelines.[7],[8]

METHODOLOGY

In this experiment, we analysed a building with 24 stories and considered it in the high seismic zone to make it economical. To perform the analysis, first we gathered accurate sectional measurements of the plan. Then, created a line diagram to ensure the joints of the beams and columns reflect thedimensions correctly. Next, we imported the plan and elevation of each floor into ETABS to view the model inboth 2D and 3D. Using available options, assigned material and section values to each element, includingslab thickness. Created static load cases for dead loads (DL), live loads (LL), floor finish (FF), earthquake(EQ), and wind loads (WL). Assign all dead loads, wind loads, live loads and floor finish loads by selecting a uniformlydistributed floor area. To create static push-over details, set the displacement magnitude to standard values andcreate a capacity curve load case. Assign the diaphragm as rigid by selecting the slab area. After locking the provided values with a general analysis, run a static non-linear analysis (PUSHOVER analysis) by selecting all beam and column elements. This will generate non-linear hinges with shear, moment, and bi-axial moment conditions, respectively. After that, we found that many members did not yield, so we kept changing the reinforcement and made sure that we were using the nonlinear properties of members.

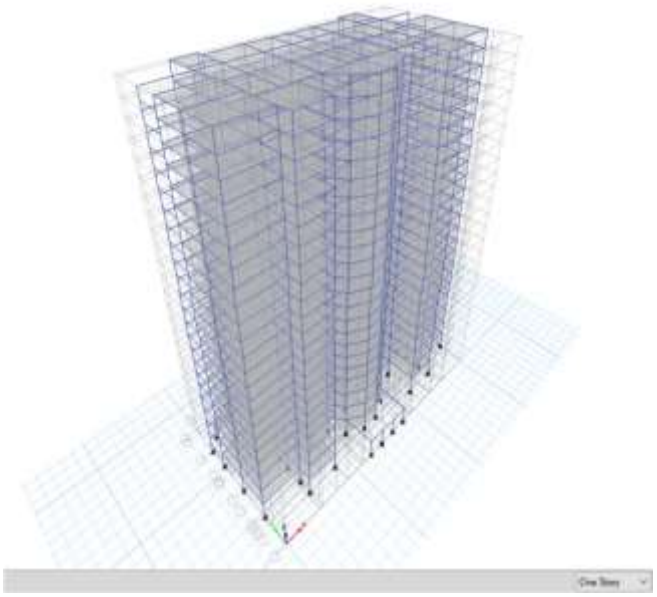

Fig. 1: 3D model

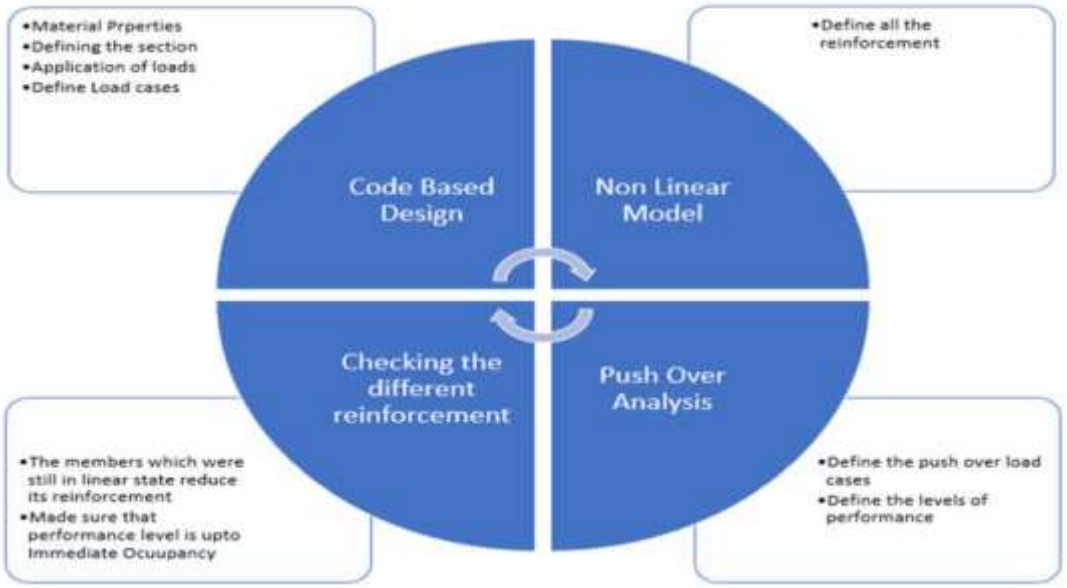

Fig.2: Flowchart of methodology

RESULTS AND DISCUSSION

It is shown in *fig.3* that when performed the nonlinear static analysis after converting our model from linear to non-linear state the hinges created in members yield and showed the level of performance by its colour. We could see that many members are in a linear state, and it showed that still we are not able to use its nonlinear properties. When we reduced the reinforcement, we can see in *fig.4* that members were in the linear state, now they are also produced, and we made sure that the performance level is up to the Immediate Occupancy. Immediate Occupancy means the structural damage is below 5%.

Fig 3: Hinges created at linear design reinforcement.

Fig 4: Hinges created after reduction of reinforcement.

Fig 3: Push-over analysis hinges formed.

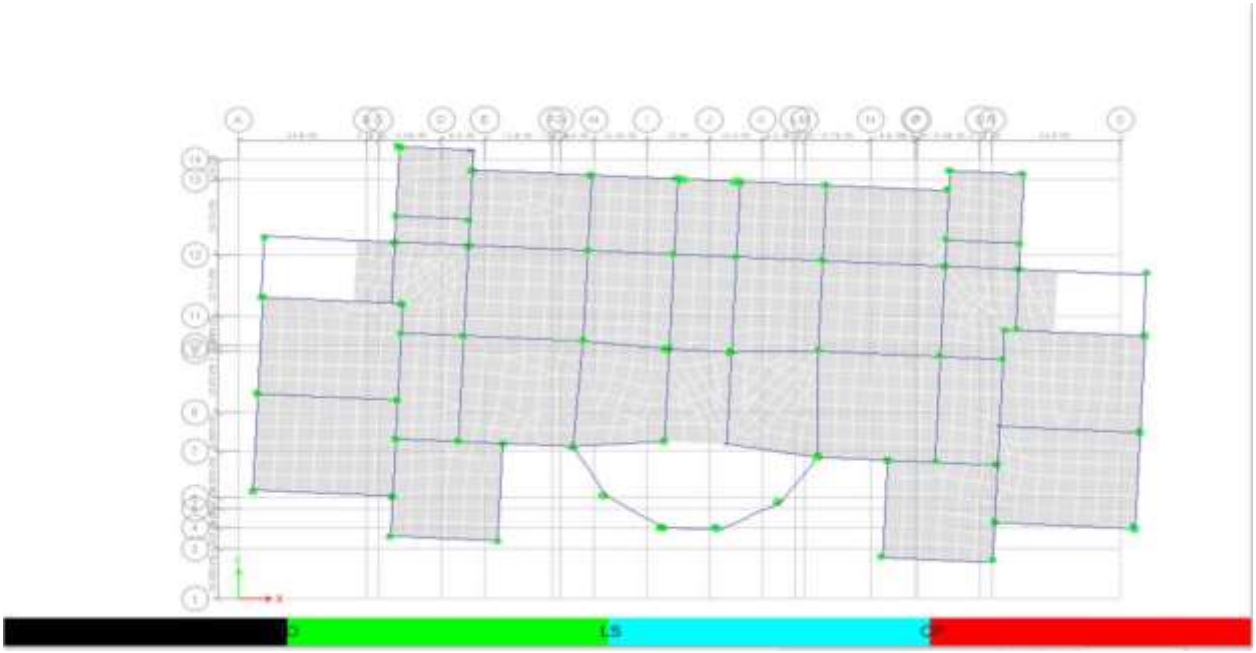

Fig 4: Push over analysis after reducing the reinforcement.

Now, if we see the table, we can analyse the difference in reinforcement before and after the reduction of reinforcement and that is how we can make our structure more economical and safer. Because we can have an idea about the performance under the loading.

Table:1 Comparison of the Reinforcement

Beams ID	**Reinforcement Before reduction As(in^2)**	**Reinforcement after reduction As(in^2)**
B92	5.671	4.5
B71	3.762	2.5

B38	3.802	2.5
B62	3.733	2.75
B38	2.497	2

B158	3.506	2.75
B161	5.119	4
B31	6.588	5
B62	8.051	6
B198	4.809	3.25
B22	3.048	2.25

CONCLUSION

This paper presents the latest seismic evaluation, known as the performance-based seismic evaluation by using pushover analysis, which is tailored to meet the specific requirements of earthquake-resistant high-rise buildings. It outlines the characteristics of such buildings and the need for new design measures. As a result of the research, the paper proposes performance-based structural seismic design countermeasures for these buildings. The study delves into the design requirements of particularly high-rise buildings. The analysis reveals that the design of these buildings should meet several requirements, including structural function usability, aesthetic performance, structural stress rationality, equipment function usability, structural construction, installation performance, and life cycle economic efficiency. As a result, the study recommends that new seismic design methods that align with the characteristics of high-rise buildings should be developed. Moreover, the study recognizes that evaluating the total cost of structural life is challenging due to the need to incorporate future costs. Using the pushover analysis, we can convert the uneconomical structure to an economical one by using the non-linear properties of members. This method is simpler for engineers to link the code to check the performance design of the structure under seismic loading.

REFERENCES

[1] M. S. Siddique, "Multi-hazard approach to assess vulnerability of the building stock in Pakistan," *15 Wcee Lisboa 2012*, no. August, pp. 1–10, [Online]. Available: http://www.iitk.ac.in/nicee/wcee/article/WCEE2012_1152.pdf

[2] M. A. Shah, "Seismic Hazard Analysis of Pakistan By Declaration of Originality," 2011.

[3] "kashmir-earthquake-october-8-2005-impacts-pakistan @ reliefweb.int." [Online]. Available: https://reliefweb.int/report/pakistan/kashmir-earthquake-october-8-2005- impacts-pakistan

[4] G. R. Martin and R. Dobry, "Earthquake site response and seismic code provisions,"
NCEER Bulletin, vol. 8, no. 4, pp. 1–6, 1994.

[5] F. Naeim, "Performance based seismic design of tall buildings," in *Earthquake engineeringin Europe*, pp. 147–169.

[6] Dimpleben P. Sonwane and Prof. Dr. Kiran B. Ladhane, "Seismic Performance based Design of Reinforced Concrete Buildings using Nonlinear Pushover Analysis," *International Journal of Engineering Research and*, vol. V4, no. 06, pp. 1110–1116, 2015,doi: 10.17577/ijertv4is061038.

[7] "Fema 356 Prestandard and Commentary for the Seismic Rehabilitation of Building,"
Rehabilitation, no. November, 2000.

[8] ATC 40, "ATC 40 Seismic Evaluation and Retrofit of Concrete Buildings Redwood City California," *Seismic safety commisionsion*, vol. 1, no. November 1996, p. 334, 1996.

2nd International Conference on Advances in Civil and Environmental Engineering (ICACEE-2023)

University of Engineering & Technology Taxila, Pakistan

Conference date: 22nd and 23rd February, 2023

DUCTILITY ENHANCEMENT BY CONFINEMENT OF LONGITUDINAL BARS IN COLUMNS

Hamza Zafar Raja [1], Chaudary Fazeel Ahmad[1*], Tahir Mehmood[1]
[1]UET Taxila, Civil Engineering Department
[1]Comsats University Islamabad, Wah Campus, Civil Engineering Department
18-CE-61@students.uettaxila.edu.pk, hamzazafar10@gmail.com,
drtahir.mehmood@ciitwah.edu.pk,

Abdul Basit[2] , **Waqas Qayyum2**
[2]Organization/Institution/Company,
abdulbasit10125@gmail.com , waqas.qayyam@students.uettaxila.edu.pk
[2]Quaid-i-Azam University, Islamabad, Department of Earth Sciences
[2]Comsats University Islamabad, Wah Campus, Civil Engineering Department

Muhammad Adeel[3]
Engr.adeel96@gmail.com
[3]Comsats University Islamabad, Wah Campus, Civil Engineering Department

ABSTRACT

Columns are a critical member of moment-resisting frames. It is essential to use a column with a more ductile deformation capacity and the tendency of energy dissipation in areas subjected to earthquakes so that the structure is not affected by the ground motion and somewhat dissipates seismic energy. Columns with enhanced ductility can be used in the Northern areas of Pakistan, which are much more prone to earthquakes. This research will discuss more sustainable methods and materials used in the column's plastic hinge region. This research presents an idea of confining longitudinal bars in potential plastic hinge regions of rectangular reinforced columns (RC) using waste materials, i.e., plastic bottles and wire gauze. Experiments were conducted on a total of 9 specimens of columns that included Control type, Bottles type, and Wire gauze type (3 of each type) of dimensions L: 24", B: 6", D: 6". A series of uniaxial compression tests are conducted on rectangular reinforced concrete columns, and the results of columns with bottles and wire gauze are compared with the control sample. Wire gauze confined sample showed the best results and reached the peak load of 656 KN, while Bottle confined, and Control samples reached the peak load of 628 KN and 548 KN, respectively. Specimens with confined longitudinal bars reached the peak load and strain, which were higher than those of the reference specimens.

KEYWORDS: Plastic hinge, Ductility, Bridge pier, Confinement, Ties

INTRODUCTION

The column is a structural member used in the structural system to safely transfer loadings from the beam to it, or it can also take load directly from the slab in the case of the flat plate slab. Bridge pier also works on the same principle. The lower portion of the pier acts as a Plastic hinge during seismic activity. The depth of seismic hinged is usually taken as 1 times the

diameter of the bridge pier. [1]. The column can have top and bottom moments and the axial load, which may be uniaxial or biaxial. The confinement of the bars and their confining principle is also important. In this research, three different confinements will be carried out, and several experiments will be conducted to plot the Force and stroke diagram. Then the graph of different experiments will be compared. Columns are the critical members among the moment-resisting structural members. Survey reports made after the earthquake show that the significant failures of structures are caused by the crushing and buckling of longitudinal bars of columns near the ends of lower stories. Those structures that did not fail have damages that cannot be repaired or rehabilitated to a functional state due to unequal settlement of upper stories. This damage is due to many factors; the lack of flexibility is one of the most critical factors [2].

LITERATURE REVIEW

The earthquake of 2005 in Pakistan was of Magnitude 7.6Mv, with its epicentre near the Muzaffarabad region of Azad Kashmir. The country suffered a great loss after that major disaster. The major reason for the destruction was the inadequacy of building capacity against seismic activity. Most buildings collapsed due to column inadequacy at the plastic hinge region or the soft story effect [3]. Seismic Evaluation and Retrofit of Concrete Buildings Volume 1 by Applied Technology Council in November 1996 [1] revealed that most of the damage to the columns occurs near the support due to the plastic hinge phenomenon, and this factor controls the structure performance during the seismic activity. Columns are relatively stronger than the beams; this is due to the stiffness which is provided during the design. Column failure can seriously affect the structure, and sudden failure of the entire structure may also occur [4]. Figure 1 shows actual pictures of column failure and how column damages occur near the support.

Figure 1: Column Failure at Various Locations

The confinement is more effective in circular columns, especially with spiral reinforcements [5]. Confinement in the columns can significantly increase the concrete's ductility [6]. California Department of Transportation (CALTRANS) in the early 1980s proposed interlocking spirals for bridges and other complex structures [7].

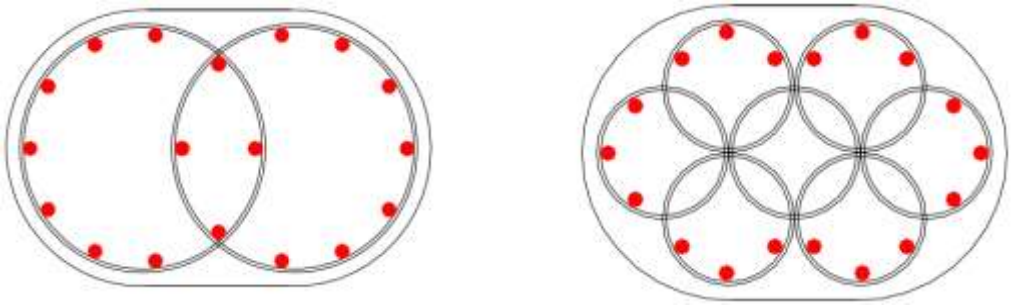

Figure 2: Bridge Column Reinforcement Spirals Both 2 and 7

The bursting phenomenon can occur more often if confinement is not provided properly [8]. In new transverse confinement, spirals are used around longitudinal bars, which significantly increase the ductility but could be uneconomical.

METHODOLOGY

The research methodology consists of 5 steps, as shown in Figure 3.

Figure 3: Adopted Methodology

EXPERIMENTATION

In total, nine column specimens were prepared, which were square in the shape which includes following:

- Control type (C)
- Bottles type (B)
- Wire gauze type (W) (3 of each type),

The specimens have cross-sections 6in x 6in and an overall height of 24in, with the middle region 12 as the test region. Cross section of each column is shown in figure 3

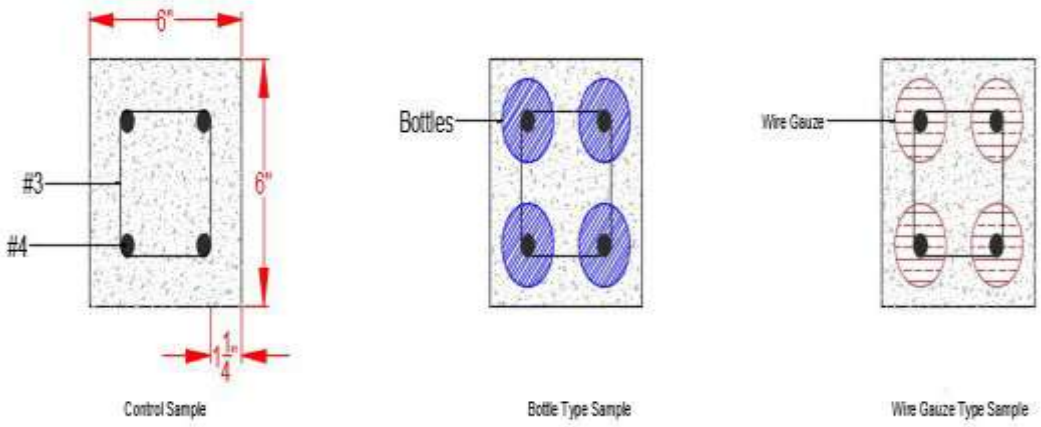

Figure 4: Cross Section of Each Column

Plastic bottles and wire gauze were used in the test region, shown in figures (b1 and w1). The two regions (each being 6in height) near the column ends were heavily reinforced to avoid unexpected failure that occurred there. A total of 10 ties were used in each specimen, including 4 ties with a spacing of 1.5in above and below portion (6in each), and 2 ties were used in the middle portion with a spacing of 4in. The configuration of ties can be seen in figure (3.1.e). Plastic bottles and wire gauze were used in the test region between the ties with a diameter of 2.5 to confine the longitudinal bars. Figure 5 shows the arrangement of bottles and wire for the confinement of longitudinal bars in the columns.

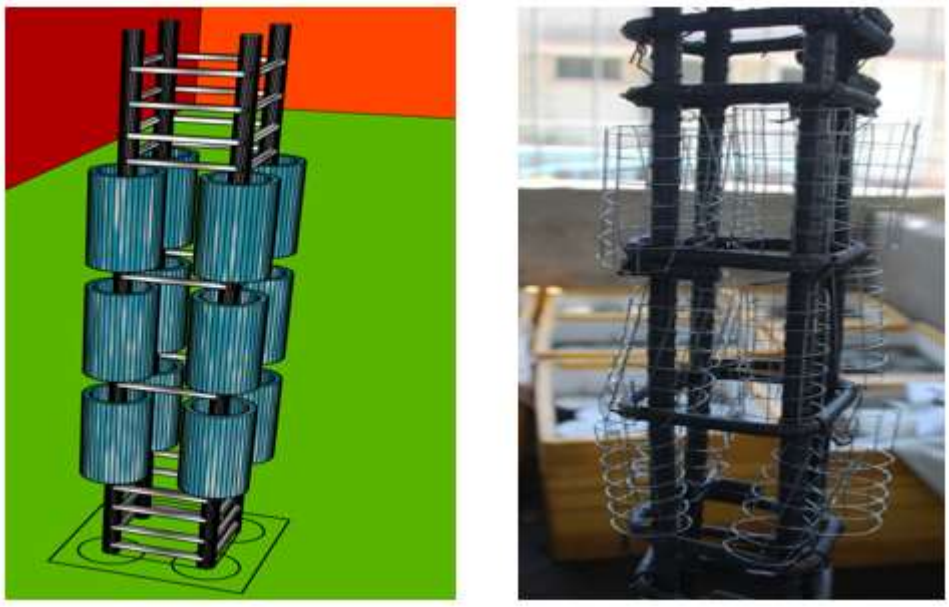

Figure 5: Plastic Bottle and Wire Gauze Region

The tests were performed using the Compression testing facility of 1000Kn capacity. All of the test data, including the stress, strains, and loads, were recorded, and the curves showing the

stress versus strain were drawn using the data from UTM, and the peak load was recorded. Figure 6 shows the general arrangement of the concrete column during the testing. The strain gauges were also installed. The load is applied using the hydraulic mechanism of the machine, and the peak load value is noted, which is critical. The casting method also greatly affects the value of the peak load which a column can take. During casting, good compaction was ensured.

Figure 6: Testing of Columns

Results

Pc denotes the peak load value, and εc is the axial strain against this peak load. C Values are given for control samples, B values for the samples with plastic bottle confinement, and W values for wire gauze samples.

Specimen	Pc (kN)	ε_c
C-1	243.1939	0.005619
C-2	465.7618	0.004649
C-3	548.2577	0.011942
B-1	_	_
B-2	326.1174	0.007372
B-3	628.1573	0.011506
W-1	456.1935	0.007751
W-2	554.3784	0.008762
W-3	656.6639	0.012215

Table 1:Maximum Load taken by the column and the strain produced

It is evident from Table 1 that the specimen with confined longitudinal bars reached the peak load and strain, which were higher than those of the reference specimens. Figure 7 shows a graph between force and stroke for C3, B3, and W3. It indicate the W3 sample have higher peak strength and area under the curve (indicating ductility).

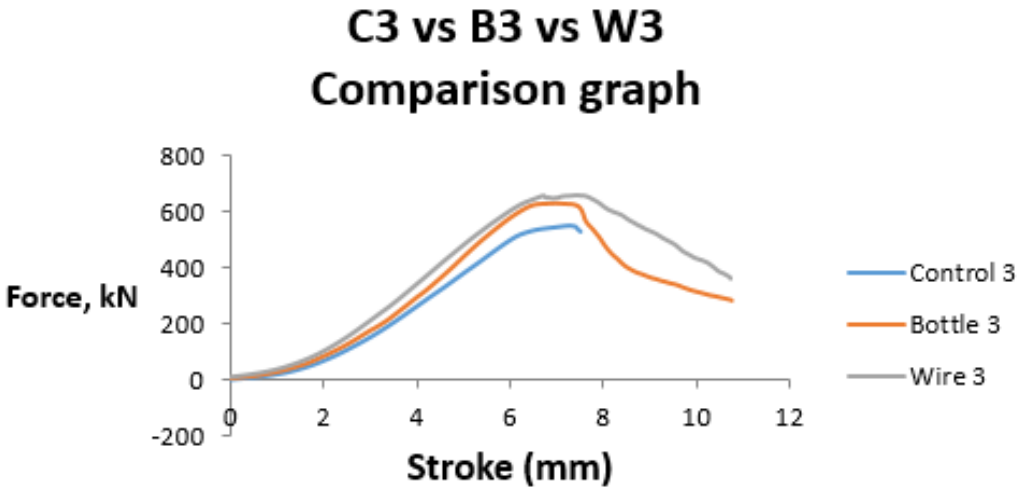

Figure 7: Force and Stoke graph comparison of different confined column

The sample with plastic bottle confinement did not increase the peak strength and ductility duc to fact that plastic bottle make weak bond with concrete. Figure 8 indicate a weak bond between concrete and bottle.

Figure 8: Pictures Showing the weak bond of Plastic Bottles with concrete

CONCLUSION

This research has presented the details of a ductility enhancement by confinement of longitudinal bars in columns for the better performance of the rectangular reinforced concrete columns. The columns consist of longitudinal bars and additional confinement provided only in the probable Plastic hinge regions of the column (in the case of the bottle and wire gauze type sample), possess more flexibility, and peak load increases. Wire gauze samples show better results than the bottles because plastic bottles make a weak bond with concrete. This problem can be better addressed if the bottle surface is rough. Confining longitudinal column bars in plastic hinge regions can significantly increase the seismic performance of the column. To make sure that Plastic bottles and circular wire gauze are filled with concrete, plasticizers have been used, which increase the workability of concrete. A vibrator should be used to remove voids in concrete during casting. In the case of Plastic bottle samples, making the bottle surface rough is recommended as it would allow the bottles to bond strongly with concrete.

REFERENCES

[1] Comartin, Seismic evaluation and retrofit of concrete buildings, Seismic Safety Commission, State of California, 1996.

[2] Faisal, "Investigation of story ductility demands of inelastic concrete frames subjected to repeated earthquakes," *Soil Dynamics and Earthquake Engineering,* pp. 42-53, 2013.

[3] M. Lisa, "Recent seismic activity in the NW Himalayan Fold and Thrust Belt, Pakistan: focal mechanism solution and its tectonic implications," *Geological Society London Special Publications 316(1):259-267,* 2009.

[4] a. M. Tahir, "Ductility of Reinforced Concrete Columns Confined with Stapled strips," *University of Engineering and Technology Taxila. Technical Journal,* p. 42, 2015.

[5] Lin-Hai, "Axial loading behavior of CFRP strengthened concrete-filled steel tubular stub columns," *Advances in Structural Engineering,* pp. 37-46, 2007.

[6] Tao, "Experimental behaviour of FRP-confined slender RC columns under eccentric loading," in *Advanced polymer composites for structural applications in construction,* Elsevier, 2004, pp. 203-212.

[7] H. Tanaka, "Seismic Design and Behavior of Reinforced," *ACI Structural Journal,* p. 192=203, 1993.

[8] Jing, "New configuration of transverse reinforcement for improved seismic resistance of rectangular RC columns: Concept and axial compressive behavior," *Engineering Structures,* pp. 383-393, 2016.

[9] Priestley, "Seismic shear strength of reinforced concrete columns," *Journal of structural engineering,* pp. 2310-2329, 1994.

2nd International Conference on Advances in Civil and Environmental Engineering (ICACEE-2023)

University of Engineering & Technology Taxila, Pakistan

Conference date: 22nd and 23rd February, 2023

Effect of Ferrocement Confinement with Silica Fumes on Different Sized Reinforced Concrete Columns

Mohammad Zulqarnain[1], Asim Shahzad[2], Muhammad Talha Amir[3], Muhammad Usman Rashid[4]

[1]University of Engineering and Technology Taxila, engr.zulqarnain884@gmail.com
[2]Communication and Works Department, asimshahzad128@gmail.com
[3]CEO HOPE Marketing, Talha.amir@uettaxila.edu.pk
[4]University of Engineering and Technology Taxila, m.usman@uettaxila.edu.pk

ABSTRACT

Ferrocement confinement of structural members can be used to enhance durability of concrete. Reinforced concrete may deteriorate by harsh weather conditions, poor mix design or by using the inappropriate methods of construction. To overcome these problems ferrocement confinement can play an important role for making concrete more durable. In this study experimental work was conducted on the ferrocement confined columns with variable sizes and a comparison was made with control specimen. The results revealed that, load carrying capacity is enhanced, reduction in deflection as well as more energy absorbed by the ferrocement confined columns as compared to the control specimens.

KEYWORDS: RC Columns, Ferrocement confinement, Selica fumes, loading capacity, stress strain behaviour.

INTRODUCTION

For construction of civil works, concrete is being used as versatile construction material around the globe. Concrete is versatile construction materials that is being used for construction of high-rise buildings, bridges and roads etc.[1]. Reinforced concrete may deteriorate by harsh weather conditions, poor mix design or by using the inappropriate methods of construction. For the betterment of concrete's durability, workability, and its strength there are different types of waste and natural materials that are being used in the concrete. By improving its strength, the service life of concrete increases. That's why to increase the service life of reinforced concrete structures, strengthening and repairing are essential and can also be done in the existing structures [2]. For the enhancement of load carrying capacity and the strength of existing buildings mostly used materials for jacketing like ferrocement with different types of fibres like glass, steel and carbon fibres can be used [3].

Ferrocement material used for rehabilitation of existing buildings and used as a confinement in reinforced concrete to strengthen the flexural behaviour of RC members. The use of ferrocement showed improvement to carry the flexural load capacity. Ferrocement has also been used for the improvement for flexural cracks [3-4]. A lot of work has been done on the structural members like RC beams or columns with or without fibre reinforced concrete. Much research has also been conducted on the fire resistance materials to investigate and repairing the fire damaged structures. By using polymer jackets and fibres into the concrete the ductility, stiffness and ultimate compressive strength have been checked [5]. Ferrocement material has been used widely to increase the strength of concrete structure due to its inherent toughness and

capacity of cracks resistance [6]. Studies have been conducted on the ferrocement jacketing on RC columns with FRP sheets. Utilization of ferrocement confinement techniques on column specimens proved much effective to cope the stress concentration problems [7]. Highly reinforced concrete with heavy ferrocement also been used in the nuclear reactor shells [8]. Experimental studies have conducted to check the strength and stiffness of heating the columns and then repairing it with ferrocement jacketing techniques with the FRP jackets. Glass fibre reinforced polymer, Steel fibre reinforced polymer, Carbon fibre reinforced polymer and ferrocement jackets used to restrengthen or repair the heated columns. the results showed that the FRP and ferrocement has improved the strength, stiffness and ductility of heated columns [9]. One of the study conducted on improving the square jacketing techniques, the concentration stress improved and successfully controlled the cracking process at corners [10]. B. Kondraivendhan et al. investigated the use of ferrocement by external confinement of concrete specimen. The Compressive strengths and failure strains was checked, the author concluded that confined specimens have more compressive strengths and can enhance the failure strains [11]. In this research experiments were conducted to compare the ultimate loads, stress strain behaviour, load vs deflection curves and energy absorptions of control and ferrocement confined specimens with varying sizes of reinforced structural memebers.

MATERIALS

Cement

According to ASTM C 150 [12] the Portland pozzolanic cement was used to make the cement mortars and reinforced concrete columns.

Silica fume

According to ASTM C 1240 [13]Silica fume having the particle size of 13 to 20 µm was used a filler.

Aggregates

According to ASTM C-33 [14] the well graded coarse aggregates were used in the concrete mix, and fine aggregates such as sand was used in the design mix.

Steel rebars

According to the ASTM A-615 [15] steel bars having 60 grades were used for main reinforcement and 40 grade bars used as a lateral reinforcement, also wire mesh having (0.45*0.45) inches square opening size for the ferrocement confinement was used.

METHODOLOGY

Total 8 specimens of different dimensions were prepared; 4 reinforced concrete columns were cast as a control specimen and 4 as a ferrocement confined columns with addition of silica fumes. Cross sectional dimensions of columns were 4×4, 5×5, 6×6 and 7×7 inches for both the sets. To prepare the ferrocement mortars the cement sand having the ratio of 1:2 was mixed. The water to cement ratio was kept 0.45 to make the mix design for ferrocement mortars.

To prepare the columns specimens reinforced concrete moulded into wooden box. Before placing the reinforcement cages into the moulds, the moulds were oiled to reduce the friction between concrete and wooden mould. the concrete was poured into the moulds in 3 layers, after each layer the concrete was compacted by an external vibrator. After 24 hours specimens were demoulded and kept into the water container for curing. Moreover, after 14 days the ferrocement confinement was applied and further curing was done for 14 days. After drying the columns specimens, the wire mesh wrapped around the specimens into two layers. To keep the uniform thickness of ferrocement jacketing, the plastering was done very carefully. It was again cured for 14 days to complete the 28 days of curing.

Table 2: Description of Samples:

Sample Designation	**Description of samples**
4-CS	Controlled Specimen having 4x4 (inches) cross-section
4-CS-SF-FC	Controlled Specimen with silica fume and ferro cement confinement having 4x4 (inches) cross-section
5-CS	Controlled Specimen having 5x5 (inches) cross-section
5-CS-SF-FC	Controlled Specimen with silica fume and ferro cement confinement having 5x5 (inches) cross-section
6-CS	Controlled Specimen having 6x6 (inches) cross-section
6-CS-SF-FC	Controlled Specimen with silica fume and ferro cement confinement having 6x6 (inches) cross-section
7-CS	Controlled Specimen having 7x7 (inches) cross-section
7-CS-SF-FC	Controlled Specimen with silica fume and ferro cement confinement having 7x7 (inches) cross-section

Compressive strength test

To check the maximum deflections, stress strain behaviour and energy absorption of the reinforced columns compressive strength test was conducted. All the specimens were tested one by one in the compression testing machine (CTM). The specimen kept into the CTM, and a dial gauge was fixed to measure the deflections in specimen as shown in figure1.

Figure 3: Specimens in compression testing machine

RESULTS AND DISCUSSION

Ultimate Loads

Figure 2 is describing the ultimate loads of all controlled and testing specimens having ferrocement confinements with silica fume. The graph is showing that the specimens with the increasing of their cross-sectional dimensions are carrying more loads. The specimens having silica fumes with ferrocement confinement carried more load as compared to control specimens because silica fume helps to gain the strength due to its extra fineness property which filled up pore spaces in concrete matrix at micro level. [16] Ferrocement confinement also enhanced the load carrying capacity due to confinement of loads within core of column specimens.

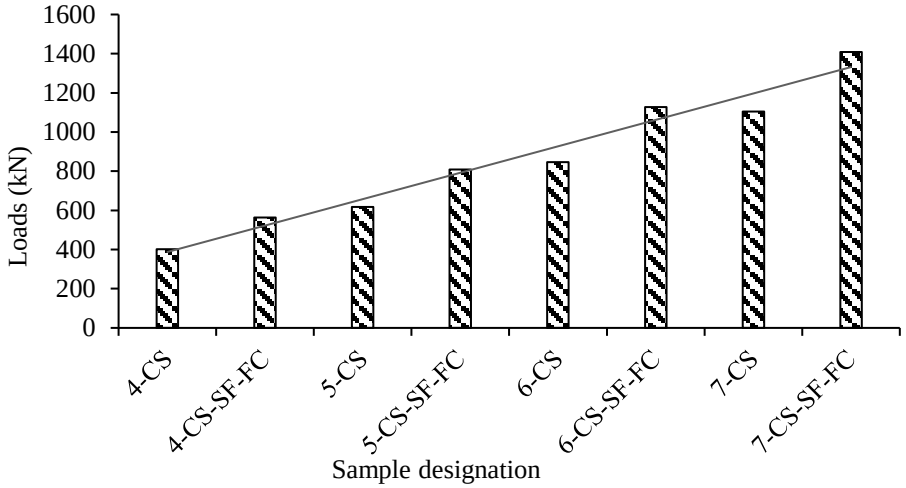

Figure 4: Ultimate loads of all column specimens

We can see that the specimen 4-CS carried about 401KN loads while column specimen 4CS-SF-FC carried up to 600kn of load. Similarly, all the specimens 5CS, 6CS and 7CS carried lower loads as compared to the specimens having silica fume.

Maximum stress- strain

The Figure 3 explains the combined stress- strain behaviour of the tested specimens. explains the maximum stress of the tested specimens. The specimen 4CS carried maximum stress of about 38 KN/m^2 while 4CS-SF-FC reached at 53.68KN/m2 due to the presence of silica fume. Similarly, the specimens 5CS, 6CS and 7CS have the maximum stress values of 36.51, 36.14 and 34.48. while the specimens with silica fume 5CS-SF-FS, 6CS-SF-FS, and 7CS-SF-FC 47.81,48.19 and 44.39 respectively. In the 4-CS-SF-FC specimen stress increment is up to 40.63% as compared to controlled specimen while the stress increment in 5-CS-SF-FC, 6CS-SF-FS, and 7CS-SF-FC The stress increment is 30.95%, 33.34% and 27.64% respectively as compared to controlled specimen. While the Strain is directly proportional to the deformation, the more the deformation more will be the strain. The specimen 4-CS-SF-FC shows the 44.4% strain as compared to 4CS. The specimen 5CS-SF-FC have 22.78% strain as to controlled specimen 5CS. Similarly, 6CS-SF-FC and 7CS-SF-FC specimens have 17.24% and 13.52% respectively.

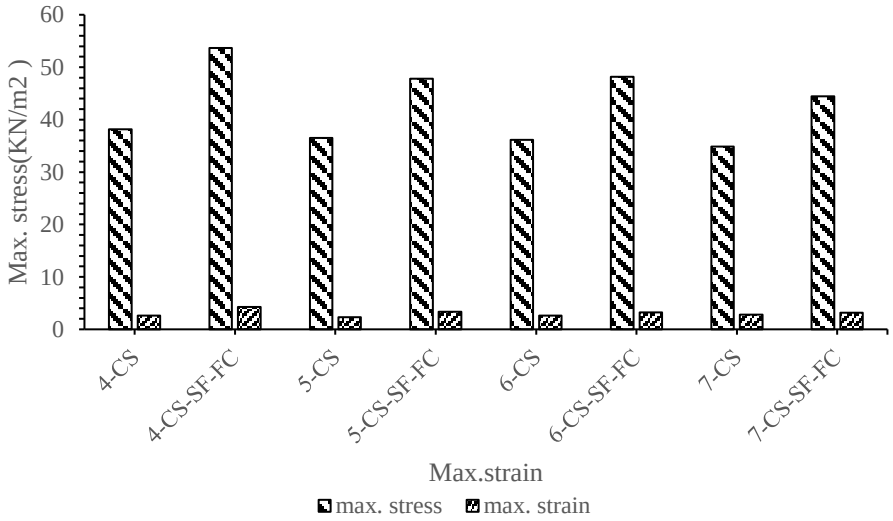

Figure 5: Maximum stress-strain of all columns

Load vs deflections

Figure 4 shows the results of maximum deflections against the loads. In the figure Specimens having different cross-sectional dimensions are showing the results against the loads. Comparison was made between controlled specimens and ferrocement confined with silica fume specimens. Results showed that the minimum deflections were noted in the ferrocement confined with silica fume as compared to controlled specimens. Also, the specimens having silica fume showed minimum deflections on dial gauge as compared to controlled. Silica fume used as a filler which made the strong bond between aggregates and proved to minimize the deflection against loads. Silica fume consists of 75% silicon contents. It prevents the cracks and better the workability of the concrete [16] and enhance the strength of concrete, that's why the specimens containing with silica fume showed less cracks during testing of specimens as compared to controlled specimens.

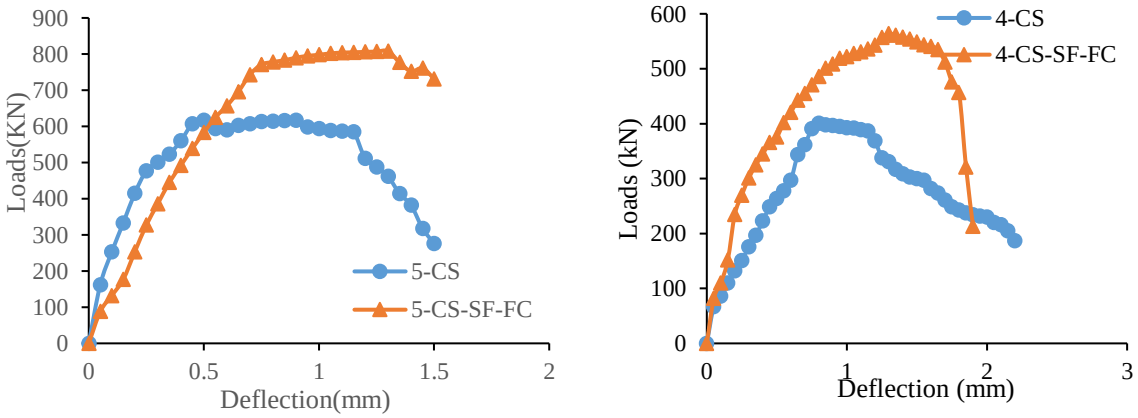

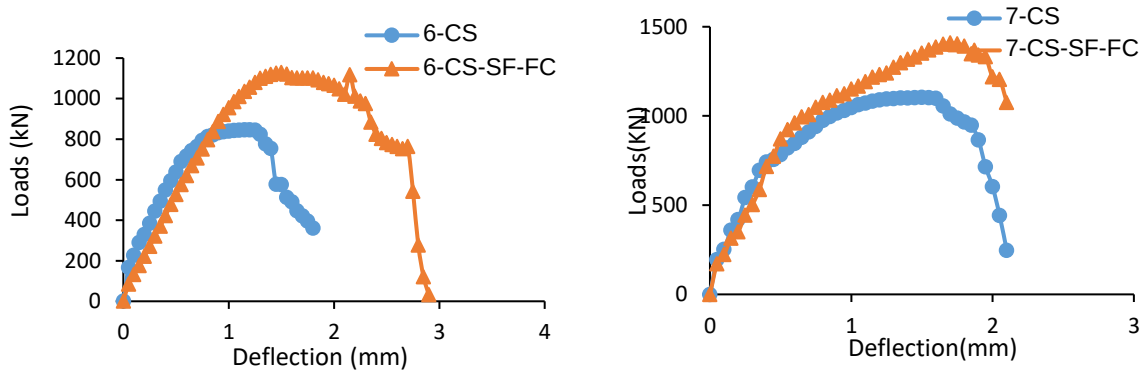

Figure 4: Load vs Deflection curves for all specimens

Stress vs strain

Figure 5 shows the stress- strain behaviour of the tested controlled and ferrocement confined columns with silica fume. Stress is directly proportion to the loads and strain is directly related to the deformations. Following the graphs shows the stress-strain behaviour of the specimens.

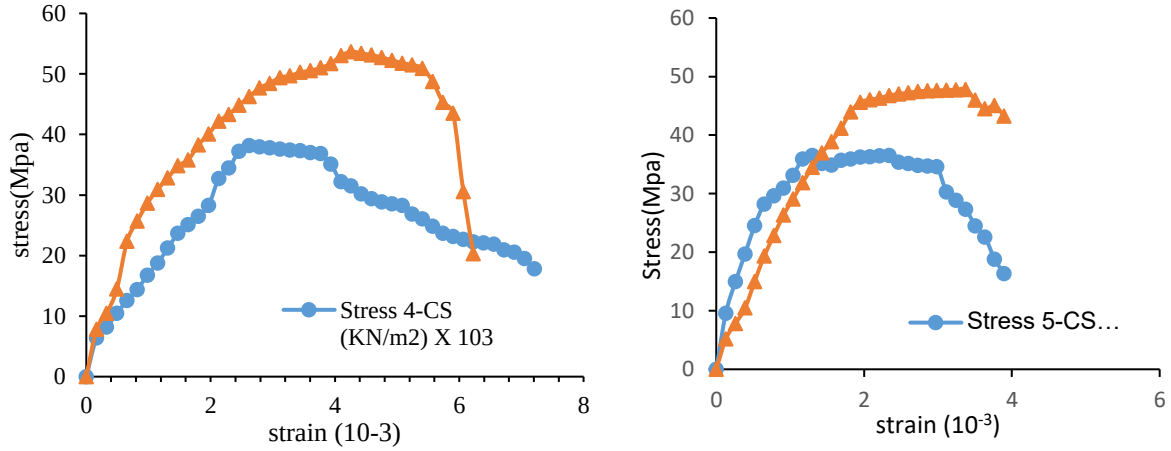

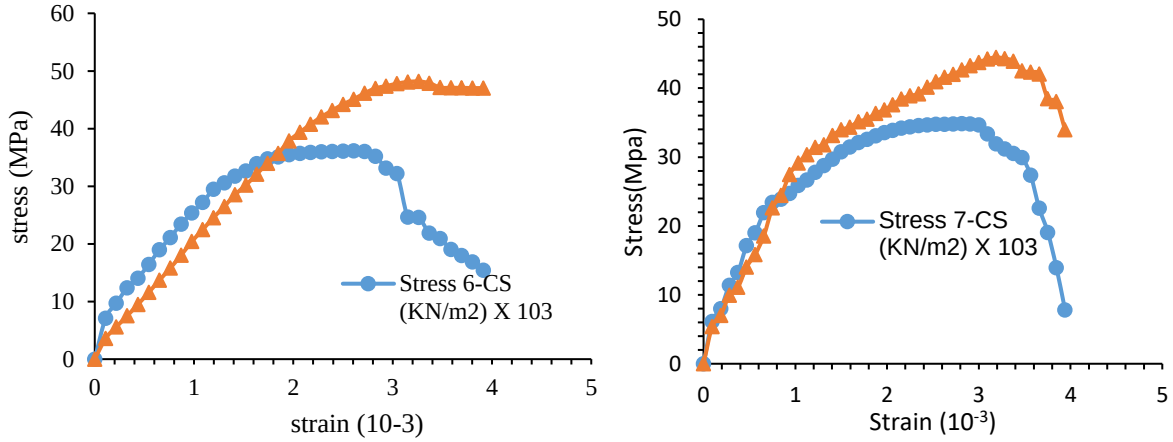

Figure 5: Load vs deflection curves of all specimens

Energy Absorption

By finding area under the stress strain curve, the energy absorption was determined. Figure 6 shows the trend of energy absorbed by testing specimens. Figure shows that energy absorption increases due to the increment of load carrying capacity. The energy absorption increases in the ferrocement confined specimens having silica fume. In the 4CS-SF-FC specimen energy absorption increases up to 35.3% with silica fume in 4-CS-SF-FC. In the case of 5CS-SF-FC, 6CS-SF-FC and 7CS-SF-FC energy absorption increases 70.19%, 107.2% and 40.39% as compared with controlled specimen. While the total energy absorption increases to 207.83% of the 7-CS-SF-FC as compared to 4-CS-SF-FC.

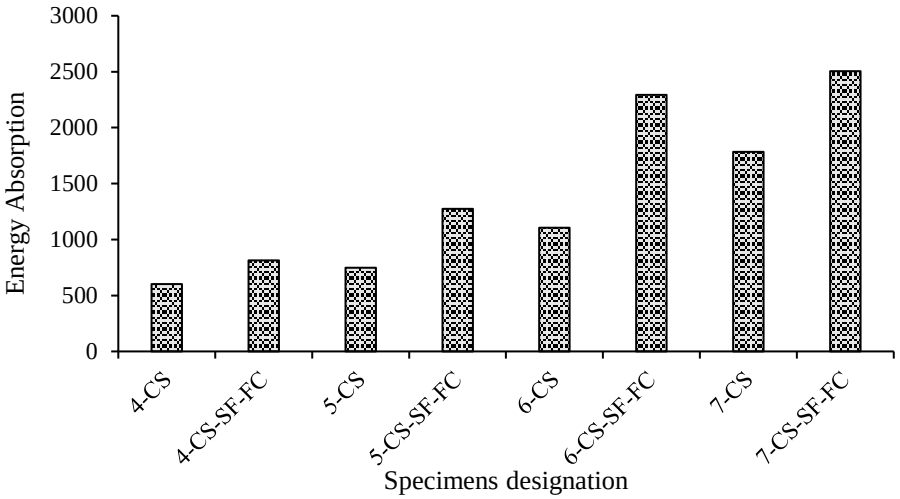

Figure 6: Energy absorption for all specimens

CONCLUSIONS

The results obtained from experimental work concluded that:

1. The specimens with ferrocement confinement having silica fume as a cementitious material enhanced the load carrying capacity as compared to the controlled specimens
2. Minimum deflections were noted in ferrocement confined columns as compared to controlled columns upon application of compressive loads with more energy absorption.
3. From the results ferrocement confinement increased the strength of the columns.
4. The failure patterns of the ferrocement confined columns proved that the jacketing of ferrocement around the specimens can be used as retrofitting and strengthening of existing columns further it also enhance the ductility of specimen with delayed cracking in inner core of columns.

REFERENCES

[1] A. S. Karzad, M. Leblouba, S. Al Toubat, and M. Maalej, "Repair and strengthening of shear-deficient reinforced concrete beams using Carbon Fiber Reinforced Polymer," *Compos. Struct.*, vol. 223, no. May, p. 110963, 2019, doi: 10.1016/j.compstruct.2019.110963.

[2] D. Baggio, K. Soudki, and M. Noël, "Strengthening of shear critical RC beams with various FRP systems," *Constr. Build. Mater.*, vol. 66, pp. 634–644, 2014, doi: 10.1016/j.conbuildmat.2014.05.097.

[3] M. Soman and J. Mohan, "Rehabilitation of RC columns using ferrocement jacketing," *Constr. Build. Mater.*, vol. 181, pp. 156–162, 2018, doi: 10.1016/j.conbuildmat.2018.05.206.

[4] M. A. Al-Kubaisy and M. Zamin Jumaat, "Flexural behaviour of reinforced concrete slabs with ferrocement tension zone cover," *Constr. Build. Mater.*, vol. 14, no. 5, pp. 245–252, 2000, doi: 10.1016/S0950-0618(00)00019-2.

[5] M. Yaqub and C. G. Bailey, "Repair of fire damaged circular reinforced concrete columns with FRP composites," *Constr. Build. Mater.*, vol. 25, no. 1, pp. 359–370, 2011, doi: 10.1016/j.conbuildmat.2010.06.017.

[6] A. B. M. A. Kaish, M. R. Alam, M. Jamil, M. F. M. Zain, and M. A. Wahed, "Improved ferrocement jacketing for restrengthening of square RC short column," *Constr. Build. Mater.*, vol. 36, pp. 228–237, 2012, doi: 10.1016/j.conbuildmat.2012.04.083.

[7] A. B. M. A. Kaish, M. Jamil, S. N. Raman, M. F. M. Zain, and L. Nahar, "Ferrocement composites for strengthening of concrete columns : A review," *Constr. Build. Mater.*, vol. 160, pp. 326–340, 2018, doi: 10.1016/j.conbuildmat.2017.11.054.

[8] V. Morozov and J. Pucharenko, "Nuclear Reactor Shells of Heavy Ferrocement," vol. 23, no. 921, pp. 31–36, 2013, doi: 10.5829/idosi.wasj.2013.23.pac.90007.

[9] M. Yaqub, C. G. Bailey, P. Nedwell, Q. U. Z. Khan, and I. Javed, "Composites : Part B Strength and stiffness of post-heated columns repaired with ferrocement and fibre reinforced polymer jackets," *Compos. Part B*, vol. 44, no. 1, pp. 200–211, 2013, doi: 10.1016/j.compositesb.2012.05.041.

[10] A. B. M. A. Kaish, M. R. Alam, M. Jamil, and M. A. Wahed, "Ferrocement Jacketing for Restrengthening of Square Reinforced Concrete Column under Concentric

Compressive Load," *Procedia Eng.*, vol. 54, pp. 720–728, 2013, doi: 10.1016/j.proeng.2013.03.066.

[11] B. Kondraivendhan and B. Pradhan, "Effect of ferrocement confinement on behavior of concrete," *Constr. Build. Mater.*, vol. 23, no. 3, pp. 1218–1222, 2009, doi: 10.1016/j.conbuildmat.2008.08.004.

[12] ASTM, "C150-Standard Specification for Portland Cement\r," pp. 1–10, 2015, doi: 10.1520/C0150.

[13] ASTM C1240, "Astm C1240," *Stand. Specif. Silica Fume Used Cem. Mix.*, vol. 15, pp. 1–7, 2005.

[14] American Society for Testing and Materials, "ASTM C33- 03 : Standard Spesification for Concrete Aggregate," *ASTM Stand. B.*, vol. 04, pp. 1–11, 2001.

[15] R. Structural, S. Bars, C. R. Wire, C. Steel, and C. R. Wire, "Standard Specification for Deformed and Plain Billet-Steel Bars for Concrete," pp. 1–5, 1999, doi: 10.1520/A0615.

[16] A. Mehta and D. K. Ashish, "Silica fume and waste glass in cement concrete production: A review," *J. Build. Eng.*, vol. 29, no. July 2019, p. 100888, 2020, doi: 10.1016/j.jobe.2019.100888.

2nd International Conference on Advances in Civil and Environmental Engineering (ICACEE-2023)

University of Engineering & Technology Taxila, Pakistan

Conference date: 22nd and 23rd February, 2023

Developing a Sustainable Eco Friendly Self-Compacting Concrete using Quarry Dust (Dolomite)

Maisam Raza[1], Qaiser uz zaman khan[2], Saqib Mehboob[3]
[1]University of Engineering and Technology Taxila, maisamraza873@gmail.com
[2]University of Engineering and Technology Taxila, dr.qaiser@uettaxil.edu.pk
[3]University of Engineering and Technology Taxila, syed.saqib@uettaxila.edu.pk

ABSTRACT

This paper deals with evolution of self compacting concrete (SCC) comprising of Dolomite and Fly Ash. An investigation on harden properties and characteristics of SCC are presented and discussed. The goal of this study is to determine if Dolomite can serve proper replacement of cement in self compacting concrete for concrete structures. This experimental study comprised of two stages. Stage I involved tests on fresh concrete properties i.e. workability. In stage II, the mechanical properties are explored. The assessment of Mechanical properties comprised of compressive strength, and splitting tensile strengths. Two design mix of SCC are prepared .In the first design mix cement is replaced with dolomite and fly ash by 10% and 5% of cement weight and In the second design mix cement is replaced with dolomite and fly ash by 20% and 10% of cement weight .compressive strength results are satisfactory as well as the tensile strength results. Cubes gain their desired strength after 7 days and compressive strength increases with time. The compressive strength results are very impressive as the strength achieved more than 4000 psi, and for tensile strength more than 2000 psi after 28 days. Crack pattern of cylinders is along the length in tensile strength test and just one crack along the length appeared during failure. Dolomite has vital role to achieve early strength as well as to reach its maximum strength and it also plays a significant role to escalate the tensile strength of concrete.

KEYWORDS: Self-compacting concrete, Dolomite, Fly Ash, Mechanical properties

INTRODUCTION

Inadequate compaction severely depresses the ultimate performance regardless of how well the concrete was made or how well the mix design was executed. Vibrators are often used to compress concrete, but they are difficult to oversee since they are generally operated by inexperienced workers. Because readily compacted, separately cast specimens are more difficult to compress, it is hard to accurately detect inferior, badly compacted concrete that has been put in situ using traditional procedures for strength testing. Both the workplace and the construction site are subject to a considerable ambient noise loading, and concrete vibrations may make employees develop the sickness known as white finger syndrome [1-4]. The use of alternate compaction techniques in lieu of vibrating concrete has so long been strongly justified [5,6]. Additionally, traditional concrete typically has inadequate compaction in layers or areas of thick reinforcing, leading to a considerable number of trapped air spaces and a reduction in the concrete's strength and durability. Self compacting concrete was eagerly employed

everywhere for together site construction [7,8]. Therefore, self-compacting concrete is not always extremely flow able concrete. The stability of concrete, on the other hand, improves together with the flow capacity of the material. Due to the new concrete's lower viscosity, this has occurred. You may add additional powder to concrete to make it more viscous, or you can use a chemical additive to change the viscosity [9–13]. However, utilising them may result in a rise in the price of raw materials due to the cost of the chemical admixtures. The essential qualities of concrete may be provided, nonetheless, by employing high-quality materials, which wouldn't increase the price. In order to achieve more cohesion, the main objective is to increase particle packing and grain size dispersion. Binders that include fly ash are regarded to be more appropriate for SCC quality control than other types of binding materials. Fly ash up to 215 kg/m3 may be used to create an inexpensive medium-strength concrete. Compressive strength of 35 megapascal at 28 days is a potential limit for SCC production [11]. Furthermore, it is doable to include significant volume of F class fly ash into SCC systems [13].

MIX DESIGN

Cement is replaced with dolomite powder and fly ash. To get the best results, cement is replaced up to 15% and 30% by weight with fly ash and powder shape dolomite, respectively. . In first mix, fly ash 5% and dolomite powder 10% of cement replacement. In second mix, fly ash 10% and dolomite make up 20% of the cement replacement.

The aggregate size for self-compacting concrete is 12 to 16 mm. Aggregate used in this study has specific gravity in oven dry condition is 2.66 ,and water absorption of this coarse aggregate is 0.3%. And for sand specific gravity is 2.6 and water absorption is 1%.For this methodology, the mix design ratio for SCC is 1:1.25:2.5. In this research, which includes slump, and V-Funnel tests, the fresh qualities of SCC are also examined. The typical cubes utilized in this investigation were 4"x 4"x4" in dimension. Additionally, standard-size cylinders are produced to test the tensile strength. After 24 hours of casting, cubes and cylinders are remolded and put in a curing tank. The effects are more pleasing when these cubes are crushed after 7, 14, and 28 days.

CHEMICAL PROPERTIES OF POWDERS

In chemical compositions of binding materials i.e. ordinary Portland cement, Fly Ash and Dolomite are given below.

Table 3: chemical composition of binding materials

Chemical Composition (%)	O.P.C	Fly Ash	Dolomite Powder
.Silicon dioxide (SiO_2)	21.00	43.58	18.61
Aluminum oxide (Al_2O_3)	5.23	22.60	4.81
Ferric oxide (Fe_2O_3)	4.10	13.38	1.05

,Calcium oxide (CaO)	63.90	14.01	53.21
.Magnesium oxide (MgO)	0.81	3.65	18.72
.Sulphur trioxide (SO_3)	1.72	1.56	1.015
Sodium oxide (Na_2O)	1.7	0.55	2.32
,Potassium oxide (K_2O)	1.54	3.48	1.02

RESULTS AND DISCUSSION

Working on Dolomite provides a better understanding and material properties like fresh, hardened, and durable by partially replacing cement with Dolomite as a cohesive, adhesive material. Compressive strength of cubes increases with time .Time taken for complete flow of fresh concrete in V-funnel test is 8.72 s. Table and Graph for Compressive strength results of cubes after 7, 14 and 28 day are given below.

Table 2: compressive strength of cubes

Compressive strength of cubes					
Sr.No	**Days**	**1st (Psi)**	**2nd (Psi)**	**3rd (Psi)**	**Mean (Psi)**
1	**7**	3616	3500	3682	3600
2	**14**	4368	4270	4410	4350
3	**28**	4536	4452	4480	4494

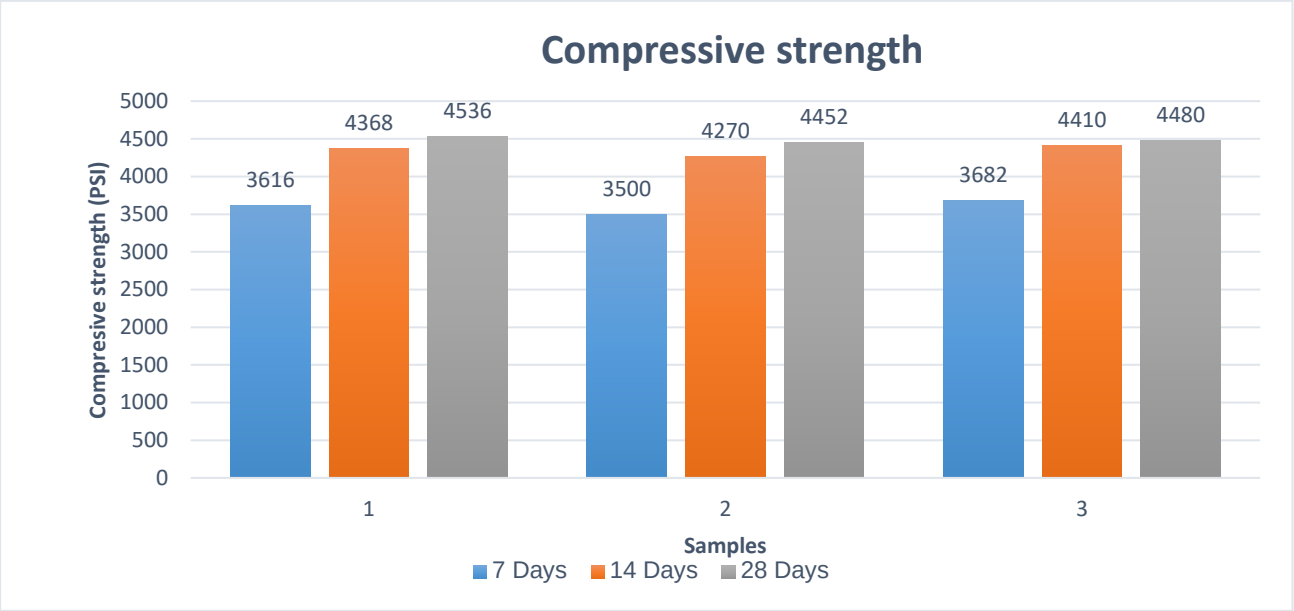

Graph 1: compressive strength of cubes after 7, 14 and 28 days

By using Dolomite, test results are very satisfactory at 7 days, the compressive strength of specimen cubes, i.e., 3600 psi; at 14 days, it is 4350 psi; and at 28 days, it is 4494 psi (see Table 2). Presence of Dolomite enhance the strength of self-compacting concrete

Tensile strength of cylinders also increases with time .Table and Graph for Tensile strength results of cubes after 7, 14 and 28 days are given below.

Table 3: Tensile strength of cylinders

Tensile strength of cylinders					
Sr.No	**Days**	**1st (Psi)**	**2nd (Psi)**	**3rd (Psi)**	**Mean (Psi)**
1	**7**	1607	1671	1710	1663
2	**14**	1909	2029	1997	1981
3	**28**	2260	2228	2283	2260

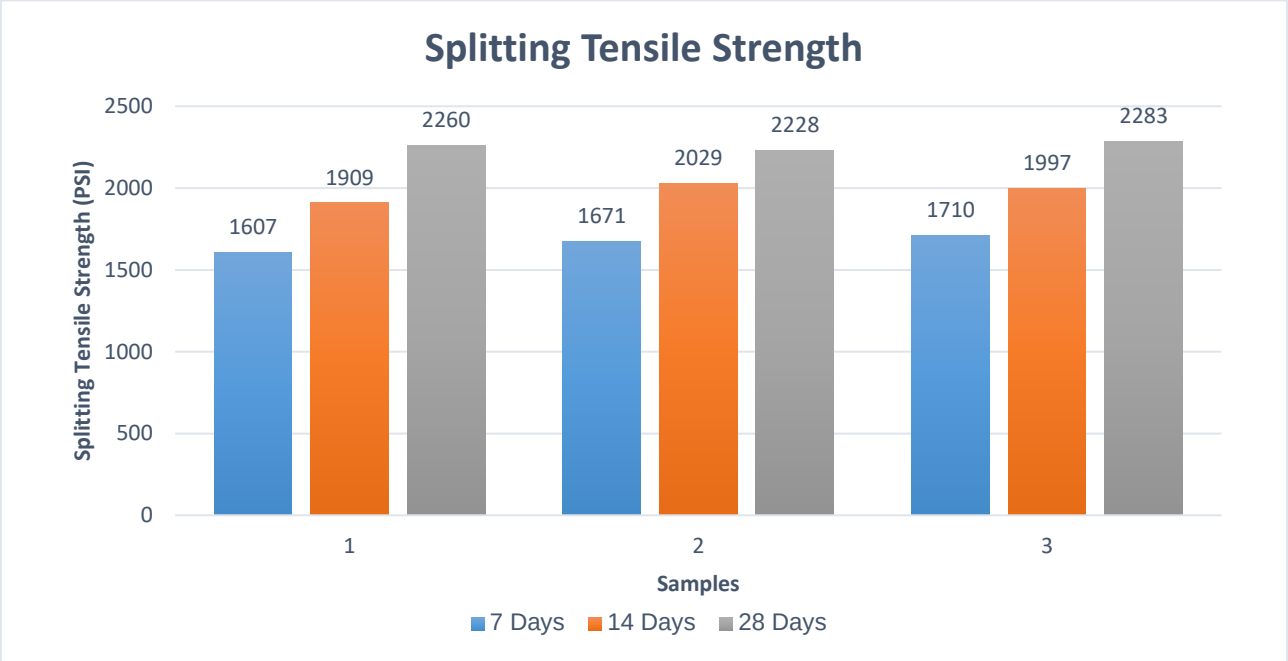

Graph 2: Tensile strength of cylinders

Table 3 elaborates on the tensile strength achieved by using locally available Dolomite, as splitting tensile strength is a fundamental and essential property of concrete that mainly relates to the size and stretch of cracks. Dolomite substantial percentages (10% and 30%) were subjected to split tensile testing. Graph 2 illustrates the results, and it is evident that Dolomite powder built concrete samples show split tensile strengths of 1663 psi, 1981 psi, and 2260 psi after 7 days, 14 days and 28 days respectively. Dolomite enhance the compressive strength and also tensile strength of self-compacting concrete

(a)

(b)

(c) (d) (e)

Figure: Images of Material/Equipment

Above figures presenting the materials and fresh and harden properties test,
(a) Material used for this research , (b) V-funnel test on fresh self-compacting concrete , (c) compression test on cube of 4"x4"x4" dimension , (d) standard dimension cylinder and cube (e) tensile strength test on standard size cylinder .

CONCLUSION

The experimental findings of our research work will guide us to select the ideal mix design parameters for the production of SCC. The following findings were made in light of the obtained results and discussion.

- The research shows very impressive compressive strength and tensile strength results by putting dolomite and fly ash in cement.
- Dolomite causes early strength and leads the concrete to gain maximum compressive strength and also enhance the tensile strength.
- Fly Ash improved the workability of concrete and increases the strength and durability of self compacting concrete.
- Cubes gain their early strength after 7 days 3600 Psi and maximum strength achieved after 28 days 4536 Psi.
- Cylinders also achieve their, maximum tensile strength after 28 days the values after 28 days 2283 Psi

Hence dolomite can be used in replacement of cement at large scale to increase the compressive strength and tensile strength of self compacting concrete.

ACKNOWLEDGEMENTS

The authors are thankful to the Civil Engineering Department UET Taxila for providing Laboratory support and technical assistance during the lab testing phase of this research work. I want to thank my friends and research colleagues, Ikram Ullah Khan, for their constant encouragement. At last, I express my special thanks to Director Lab, National Logistics Cell (NLC), for his genuine support throughout this research work.

REFERENCES

[1] De Schutter G, Bartos PJM, Domone P, Gibbs J. *Self-compacting concrete. Dunbeath, Scotland: Whittles Publishing; 2008.*

[2] Domone PL. *Self-compacting concrete: an analysis of 11 years of case studies. Cem Concr Compos 2006;***28**(2)*:197–208.*

[3] Najim KB, Hall MR. *A review of the fresh/hardened properties and applications for plain and self-compacting rubberized concrete. Construct Build Mater 2010;***24**(11)*:2043–51*.

[4] Gaimster R, Dixon N. *Self-compacting concrete. Advanced concrete technology set; 2003. p. 1–23.*

[5] Schwartzentruber D, Roy RL, Cordin J. *Rheological behaviour of fresh cement pastes formulated from a self-compacting concrete. Cem Concr Res 2006;***36**(7)*:1203–13.*

[6] Figueiras H, Nunes S, Coutinho JS, Figueiras J. *Combined effect of two sustainable technologies: self-compacting concrete and controlled permeability formwork. Construct Build Mater 2009;***23**(7)*:2518–26.*

[7] Bartos PJM, Grauers M. *Self-compacting concrete; 1999. p. 9–13.*

[8] Skarendahl A. *Market acceptance of self-compacting concrete: the Swedish experience. In: Proceedings of the 2nd international symposium on SCC. Japan; 2001. p. 1–13.*

[9] Diamantonis N, Marinos I, Katsiotis MS, Sakellariou A, Papathanasiou A, Kaloidas V, et al. *Investigations about the influence of fine additives on the viscosity of cement paste for self-compacting concrete. Construct Build Mater 2010;***24**(8)*:1518–22*

[10] L. Muhmood, S. Vitfta, D. Venkfateswaran, *Cementitious behavior of elect arc furnance steel .slags*, Cem. Concr. Res. **39** (2) (2009) 102–109.

[11] D. Adolgdfsson, R. Rodbinson, F. Engstdgröm, B. Bjögdrkman, effect *of mineralogy on the hydric properties of low slag, Cfem.* Concr. Res. **41** (8) (2011) 865– 871.

[12] Y.NN. Sgheen, H.Y. Wafdng, T.H. Sugn, *research of harden properties of cement with stainless steel slag and slag for materials*, Constr. Buhild. Mahter. **40** (2013) 239–245.

[13] L. Kriskoji, Y. Podjdikes, Ö. Cizgker, G. Mertghens, W. Veudglemans, D. Gfmeysen, et al., *impact of mechanical properties of the hydraulic properties of stainless steel slags*, Chem. Cfongcr. Res. **42** (6) (2012) 778–788

2nd International Conference on Advances in Civil and Environmental Engineering (ICACEE-2023)

University of Engineering & Technology Taxila, Pakistan

Conference date: 22nd and 23rd February, 2023

Climate Resilient Reinforced Concrete Based On Chloride Resistance

Adil Khan[1], Ayub Elahi[2]

[1]Department of Civil Engineering, University of Engineering and Technology, Taxila, Pakistan, kadil5523@gmail.com

[2] Department of Civil Engineering, University of Engineering and Technology, Taxila, Pakistan, ayub.elahi@uettaxila.edu.pk

ABSTRACT

Pakistan has a coastal length of about 1046 km and different reinforced concrete infrastructures are proposed in near future that will be more exposed to external salt attack. It would lead to made concrete with specific properties that can better resist the aggressive environment. In this study, the durability performance against chloride penetration of high performance concrete (HPC) with varying amount (30%, 45%, and 60% by weight of cement) of ground granulated blast furnace slag (GGBS) along with the use of different water-binder ratios (0.4, 0.5, and 0.6) were assessed. The samples were tested for evaluating mechanical strength (in terms of compression) and for resistance to chloride migration using Nordic standard NT Build 492. Results obtained from the testing showed that specimens prepared with optimum dosage (45%) of GGBS show more resistance to chloride migration without compromising on compressive strength.

KEYWORDS: Chloride migration; Durability; GGBS; compressive Strength

INTRODUCTION

Generally, there are two mechanisms that are involved in reinforced concrete deterioration: degradation of concrete and corrosion to embedded steel [1]. The degree and rate of deterioration in each mechanism depends on various factors: type of structure and exposure, contact with salts, materials used, workmanship, type and amount of SCM's (supplementary cementitious materials) used, type of reinforcement, depth of embedded reinforcement, use of corrosion inhibitors, degree of contamination of water used in mixing and curing etc. The most frequent causes of concrete deterioration in buildings are physical, chemical, and environmental changes combined with one another. Chemical deterioration, particularly in coastal concrete structures, is mostly caused by chloride induced corrosion of reinforcement [2]. Salinity of seawater rises as a result of climate changes, which in turn accelerates deterioration and shortens the serviceability of concrete structures [3].

As stated, Pakistan has a coastal length of about 1046 km and is one of the countries more vulnerable to climate changes; therefore, the existing and future proposed concrete structures will be more exposed to external salts attack, especially in the coastal region. This led to a rise in the demand for concrete that can better withstand the ingress of corrosive substances, such as chloride ions.

The primary effect of chloride ions is to cause corrosion of steel reinforcement, and it is only as a consequence of this corrosion that the adjacent concrete deteriorates. This special characteristic of chloride attack sets it apart from other causes of deterioration of reinforced concrete [4].

For the purpose of producing a durable concrete system, it is essential to use supplementary cementitious components, particularly slag, fly-ash, and silica fume, which have been shown to perform very well in severe environments [5].

The main purpose of the research described in this work was to develop data for producing durable concrete containing significant amount of ground granulated blast furnace slag (GGBS) and to examine their compressive strength and resistance to chloride migration.

EXPERIMENTAL METHODOLOGY

Materials

Ordinary Portland cement and GGBS made in Pakistan slag cement industry was used in this research work for casting samples of all mixes. Cement were in accordance with ASTM C150-05 standard [6]. Characteristics of cement and GGBS i.e. chemical and physical are summarized in tables 1 and 2 respectively.

Table 4: Chemical configuration of cement and GGBS (%)

	CaO	SiO_2	Al_2O_3	MgO	Fe_2O_3	Na_2O_3	K_2O_3
Cement	62.59	19	6.4	2.49	3.9	0.35	0.79
GGBS	40.39	33.56	11.42	10.53	0.52	0.68	0.62

Table 5: Physical properties of cement and GGBS

	Cement	GGBS
Bulk density (kg/m^3)	3110	2961
Specific gravity	3.1	2.8
Fineness (%)	4.1	3.5

Well graded coarse aggregates obtained from nearby crush plant and fine aggregates from nearby sand deposits were used during samples preparation. The characteristics of coarse and natural fine aggregates which were in accordance with ASTM C33 standards [7] are shown in table 3.

Table 6: Physical properties of sand and crushed coarse aggregates

Physical property	Coarse aggregates	sand
Max. aggregate size (mm)	20	
Bulk density (kg/m^3)	1326	1540
Fineness modulus (%)		2.67
Absorption capacity (%)	1.29	1.32
LA abrasion (%)	1.18	

Mix Proportions

The experimental set-up was consisting of two parts. In the first part, the water-binder ratio was held constant while the amount of GGBS was altered to evaluate how GGBS contents affect the migration coefficient of chloride ions. In the second section, the additive was fixed to examine how the water-binder ratios change the migration coefficient. In this research work BS (EB001) specifications [8] in SI units was used for designing and proportioning of concrete mixes. The details of mix proportions are shown in table 4.

Table 7: Concrete Mix Details as per BS (EB001) Specifications

Mix. reference	Water-binder ratio	Cement contents (kg/m^3)	GGBS (% by wt. of cement)	Free-water contents (Kg/m^3)	Sand (Kg/m^3)	Coarse aggregate (Kg/m^3)
R1G0	0.4	604.25	0	241.73	489.67	1040.12
R1G30		423.21	30			
R1G45		332.84	45			
R1G60		241.23	60			
R2G0	0.5	604.25	0	256.34	489.67	1040.12
R2G30		423.21	30			
R2G45		332.84	45			
R2G60		241.23	60			
R3G0	0.6	604.25	0	266.56	489.67	1040.12
R3G30		423.21	30			

R3G45		332.84	45			
R3G60		241.23	60			

Casting and Curing

Before casting, workability test was performed as shown in figure 1(a) for each mix as per ASTM C143 [9] specifications. For evaluating strength in compression, 72 cylinders with (diameter=150mm and depth=300mm) were cast (36-cylinders for 7-days strength and 36-cylinders for 28-days strength) while for evaluating durability parameter e.g. chloride migration coefficient, 24 numbers of specimens (diameter=100mm and depth=150mm) were cast as shown in figure 1(b).

a b

Figure 6: Workability test and cast cylinders

EXPERIMENTAL

The compression testing of cylinders were performed in two series: In the first series the cylinders were tested to obtain 7-days compression strength while in the second series the cylinders were tested for evaluating compression strength at 28-days as shown in figure 2.

Figure 7: Compression testing of cylinders (7-days and 28-days)

Before chloride migration testing, the cylinders (diameter=100mm and depth=150mm) were sliced and specimens with 100mm diameter and 50mm depth were obtained as shown in figure 3. The specimens in surface-dry condition were placed in vacuum saturation machine (shown in figure 3) and prepared in accordance with NT Build 492 [10] procedures. The steps involved in specimen preparation and chloride migration apparatus are shown in figure 3.

c d e

Figure 8: (c) slicing of specimens, (d) preconditioning, (e) chloride migration apparatus

RESULTS AND ANALYSIS

Effect of GGBS contents on 7-days and 28-days compressive strength of concrete

The results of compression testing are tabulated in table 5. The comparisons of 7-days and 28-days compressive strength for different mixes are shown in figure 4.

Table 8: 7-days and 28-days compressive strength of concrete cylinders

Mix reference	Water-binder ratio	GGBS (% by wt. of cement)	Slump (mm)	Strength (Mpa)	
				7-days	28-days
R1G0	0.4	0	40	10.8	20.1
R1G30		30	46	10.1	21.5
R1G45		45	51	9.6	22.1
R1G60		60	62	8.7	19.5
R2G0	0.5	0	61	8.7	18.7
R2G30		30	67	7.3	20.4
R2G45		45	74	6.3	21.3
R2G60		60	88	5.7	18.5
R3G0	0.6	0	94	7.4	17.7
R3G30		30	103	5.5	18.6
R3G45		45	112	4.9	19.2
R3G60		60	125	4.5	17.3

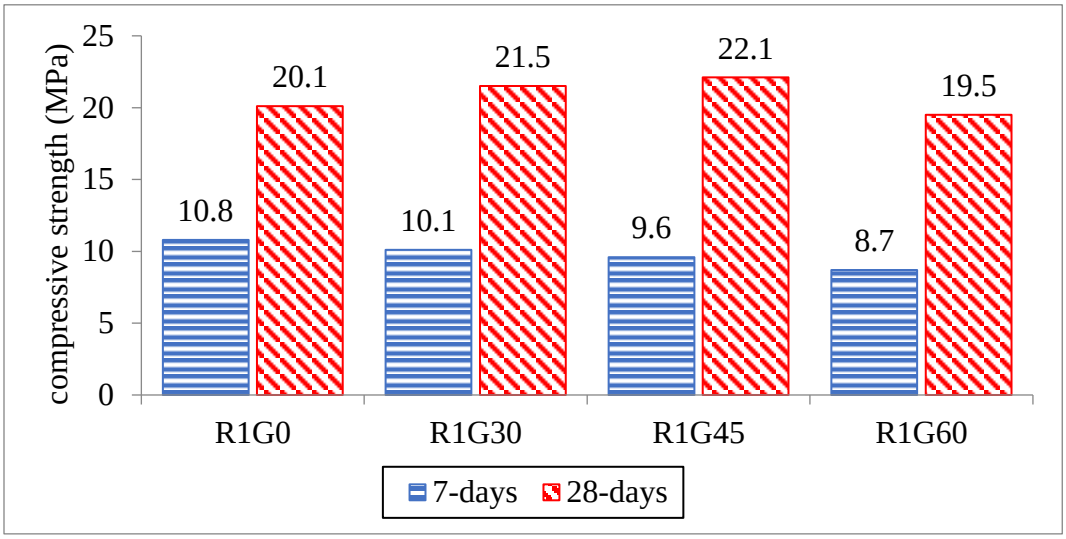

Figure 9: Comparison of 7-days and 28-days compressive strength of cylinders for same w/b =0.4

(1) From table 5 and figure 4 it is clear that at fixed water-binder ratio of 0.4, the 28-days compressive strength increased with the increase (up to 45%) in GGBS contents. In relation to control mix, about 9% increase in 28-days compressive strength was observed at 45% replacement level. This may because of the reaction of GGBS with $Ca(OH)_2$ (product of cement hydration) forming calcium silicate hydrate C-S-H gel in large amount.

(2) Figure 4 also shows that, at the replacement level of 60% the compressive strength decreased at all ages. This may come from the fact that when the replacement level of GGBS rises from 45% to 60%, due to the shortage of $Ca(OH)_2$, the degree of GGBS reaction will be reduced significantly. Mixes with replacement level of 45% were found consistently better at the age of 28-days.

(3) It was also confirmed that the early age (7-days) compressive strength decreased with the increase in GGBS contents. In comparison to mix prepared with 100%OPC, mixes with 60% GGBS showed 20% decrease in 7-days compressive strength. These findings revealed that as GGBS concentration increased, at early age, latent hydraulicity reactions by GGBS retarded the development of compressive strength.

Performance of GGBS cement concrete against chloride ions penetration

The results obtained from chloride migration testing are summarized in table 6. The results of non-steady state migration coefficient (D_{nssm}) for control mix (100% OPC) and mixes containing GGBS (30%, 45% and 60% by weight of cement) are plotted in figure 5.

Table 9: Results of chloride migration testing

Mix. reference	Water-binder ratio	GGBS (% by wt. of cement)	Applied voltage (V)	Temperature (^{0}C)	^1X_d (mm)	$^2D_{nssm}$ ($\times 10^{-12}$ m^2/s)

R1G0	0.4	0	45.23	35.25	22.5	15.3
R1G30		30	35.51	32.52	17.0	10.5
R1G45		45	32.72	30.71	15.8	8.2
R1G60		60	25.96	29.29	11.3	7.6
R2G0	0.5	0	48.17	37.16	25.3	18.6
R2G30		30	38.41	36.53	19.0	11.4
R2G45		45	34.91	34.85	16.8	8.7
R2G60		60	28.75	31.56	12.6	6.9
R3G0	0.6	0	53.42	40.12	29.0	20.1
R3G30		30	44.13	38.42	23.4	14.6
R3G45		45	41.74	35.51	21.0	13.1
R3G60		60	39.91	33.29	18.9	11.9
[1]X_d = average chloride penetration depth, [2]D_{nssm} = non-steady state migration coefficient						

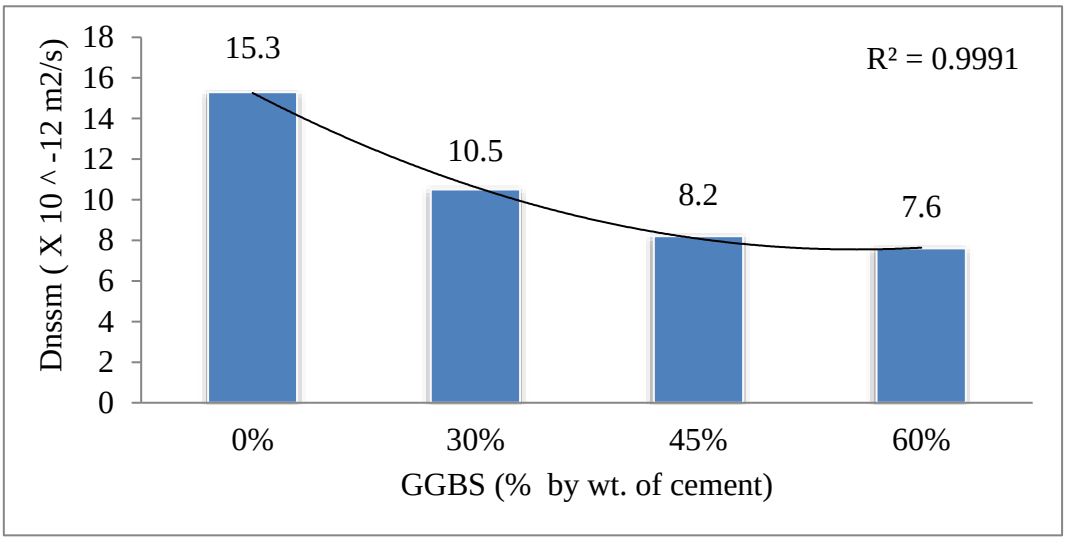

Figure 10: Relation between non-steady state migration coefficient and %GGBS used for water-binder of 0.4

It is clearly seen from figure 5 that the resistance to chloride migration improved with the rise in GGBS quantity. In comparison to control mix, 49% decrease in migration coefficient was observed at 60% replacement level.

Literature [11] indicated that Ordinary Portland cement concrete typically has pores that are 1.57 to 2 times larger than those of GGBS concrete because the latent hydraulicity reaction of GGBS not only increases the density of the cement matrix but also reduces the pore size that result in the reduction of chloride ions penetration. The formation of more C-S-H gel by adding GGBS may also enhance resistance to chloride penetration of concrete.

Influence of water-binder ratio on chloride ions penetration

Table 6 demonstrates that, for fixed replacement level, the migration of chloride ions into concrete increases as the water-binder ratio rises. An increase of about 25% to 30% in migration coefficient was observed as the water-binder ratio raised from 0.4 to 0.6. Findings imply that an increase in water-binder ratio may lead to the formation of additional pores and transporting paths, these results a decrease in the resistance to chloride ions penetration. Mixes with 45%GGBS were found to perform better (in terms of resistance to chloride ingress).

Analysis of chloride migration coefficient and compressive strength for different replacement levels of GGBS

The 28-days compressive strength and migration coefficient are presented in figure 6 for different replacement levels (30%, 45% and 60%).

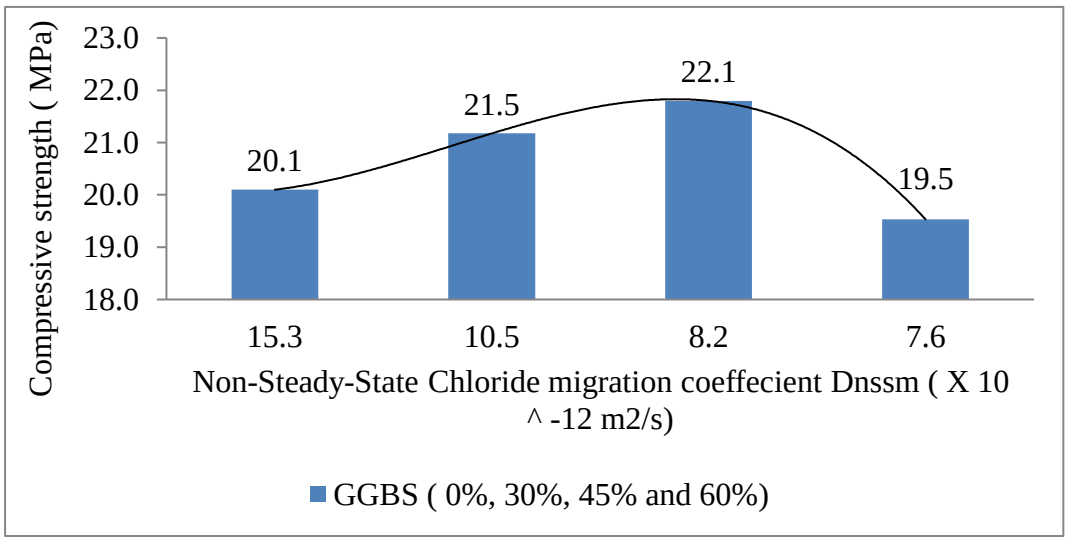

Figure 11: Relation between migration coefficient and 28-days compressive strength

Figure 6 indicate that both the later age (28-days) compressive strength and resistance to chloride migration improved with the increase in GGBS contents up to 45% replacement. Mixes with 45%GGBS were observed to perform better both in terms of 28-days compressive strength and resistance to chloride ions penetration.

CONCLUSIONS

The following conclusions have been drawn in light of the findings of this study:

(1) With the water-binder ratio held constant, the 28-days compressive strength was observed higher for mixes with 45%GGBS.
(2) The early age (7-days) compressive strength was detrimentally affected with the rise in cement replacement with GGBS.

(3) Resistance to chloride migration was enhanced by replacing cement with GGBS. Mixes with 60%GGBS were performed better in terms of chloride penetration.
(4) For the same replacement level of cement with GGBS, mixes prepared with higher water-binder ratios showed poor resistance to chloride ingress and reduction in compressive strength.

REFERENCES

[1] S. Srinivasan and I. Gibb, "Climate resilient concrete structures in marine environment of Bangladesh," no. July, 2018.
[2] S. Srinivasan and I. Gibb, "Climate resilient concrete structures in marine environment of Bangladesh," *6th Int. Conf. Durab. Concr. Struct. ICDCS 2018*, no. February, pp. 321–336, 2018.
[3] P. Vineis, Q. Chan, and A. Khan, "Climate change impacts on water salinity and health," *J. Epidemiol. Glob. Health*, vol. 1, no. 1, pp. 5–10, 2011, doi: 10.1016/j.jegh.2011.09.001.
[4] A. Neville, "Chloride attack of reinforced concrete: an overview," *Mater. Struct.*, vol. 28, no. 2, pp. 63–70, Mar. 1995, doi: 10.1007/BF02473172.
[5] M. Santhanam and M. Otieno, "Deterioration of concrete in the marine environment," in *Marine Concrete Structures*, Woodhead Publishing, 2016, pp. 137–149. doi: 10.1016/b978-0-08-100081-6.00005-2.
[6] P. W. Arbuckle, M. D. Lepech, and G. A. Keoleian, "Advances in Civil Engineering Materials The Role of Concrete Industry Standards as Institutional Barriers to More Sustainable Concrete Bridge Infrastructure," 2014, doi: 10.1520/ACEM20130109.
[7] M. Taylor, "Proposed changes to USS," no. May 2011, p. 2011.
[8] W. M. Ratio and S. Relationship, "Designing and Proportioning Normal Concrete Mixtures".
[9] "STM C143, Test method for slump of Portland cement... - Google Scholar." https://scholar.google.com/scholar?q=STM C143, Test method for slump of Portland cement concrete, Annual Book of ASTM Standards, volume 04.02, 1988, p. 85. (accessed Jan. 17, 2023).
[10] "NTBUILD-492, NORDTEST METHOD: Concrete, Mortar And... - Google Scholar." https://scholar.google.com/scholar?hl=en&as_sdt=0%2C5&q=NTBUILD-492%2C+NORDTEST+METHOD%3A+Concrete%2C+Mortar+And+Cement-Based+Repair+Materials%3A+Chloride+Migration+Coefficient+From+Non-Steady-State+Migration+Experiments.+1999.&btnG= (accessed Jan. 16, 2023).
[11] S. Hussain, *Mechanisms of high-durability performance of plain and blended cements*. 1991. Accessed: Jan. 19, 2023. [Online]. Available: https://search.proquest.com/openview/ec94e72fea92dd4906320296c9ab1007/1?pq-origsite=gscholar&cbl=18750&diss

2nd International Conference on Advances in Civil and Environmental Engineering (ICACEE-2023)

University of Engineering & Technology Taxila, Pakistan

Conference date: 22nd and 23rd February, 2023

Identifying and Assessing the Suitability of an Alternative Road Aggregates Source in Pakistan

Taimur Shah[1], Naveed Ahmad[2], Shahid Ullah[3], Salman Khan[4]

[1]MSc. Scholar, Department of Civil Engineering, University of Engineering and Technology
UET Taxila, Pakistan, Taimurshah1255@gmail.com

[2]Professor, Department of Civil Engineering, University of Engineering and Technology Taxila, Pakistan, n.ahmad@uettaxila.edu.pk

[3]MSc. Scholar, Department of Civil Engineering, University of Engineering and Technology
UET Taxila, Pakistan, engrsshahidullah@gmail.com

[4]MSc. Scholar, Department of Civil Engineering, University of Engineering and Technology
UET Taxila, Pakistan, salmankhan68t@gmail.com

ABSTRACT

Margalla aggregates are the primary aggregates source in Pakistan, but it is depleting, so new sources that can be used for road construction must be identified. A local source in Chakdara, Dir Lower KPK, is chosen as a possible aggregate source for road construction in Pakistan. The chosen aggregate source is simple to evaluate and productive. The properties of the Margalla aggregates are compared to those of the Chakdara aggregates for this purpose. The petrographic analysis of both sources is performed. Chakdara aggregate petrography reveals that it is composed of calcite to the extent of 98%, making it suitable for road construction. The Chakdara aggregate's specific gravity, water absorption, Los Angeles abrasion, soundness, shape, crushing, and impact values are compared to the Margalla aggregates. The Marshall Mix design method is employed to study the Marshall stability and flow of asphalt samples prepared with Chakdara aggregates and with Margalla aggregates sources. Asphalt samples prepared with Chakdara quarry aggregate and Margalla aggregate are subjected to the wheel tracker test to evaluate the matreial's resistance to rutting. The maximum rut depth for Chakdara aggregate samples is 4.93 mm, which is slightly greater than the samples prepared with Margalla aggregates, whose maximum rut depth is 3.66 mm but falls within the allowable range. The stripping and coating test is conducted to determine the sensitivity to the moisture of both sources. The conclusion is that the Chakdara quarry in Dir lower, Khyber Pakhtunkhwa, Pakistan, is a potential source for pavement construction, especially for local road construction projects.

KEY WORDS: Marshall Stability, Rutting, Petrographic Examination, Chakdara Quarry, Aggregates Source.

Introduction

Due to their deplorable condition, most roads in Pakistan must be upgraded. In addition to other national development initiatives, new roads, and highways are required to accelerate nation-building activities. Infrastructure initiatives are increasing aggregate demand, so it is vital to map and evaluate new resources. Due to its broad availability and extensive utilization in the cement and construction sectors, limestone is a common raw material for aggregates [1]. Aggregate is the substance that supports the weight of automotive traffic [2, 3]. The aggregate's performance determines the pavement's performance under traffic conditions [4]. As one of the major pavement components, aggregates possess numerous characteristics that greatly influence the performance of the pavement. Road construction necessitates substantial quantities of aggregates [5]. Aggregates are the primary components required for pavement construction. They must withstand stresses caused by the wheels' weight on the surface. They must also endure the wear caused by the abrasive effect of traffic on the surface course [6]. High-quality aggregates of varying types are readily available in Pakistan for constructing the base course and wearing courses. Limestone mined from the Margalla Hills is the nation's principal aggregate source. So far, the Margalla has proven to be the most reliable quarry providing top-quality aggregates for use in sub-base, base, and surface layers of roads [7]. Since Pakistan is home to many mountain ranges, the country has a great deal of untapped potential in producing concrete aggregates. In a previous study, various crushers from Margalla, Sargodha, Barnala, and Mangla were used for the experimental analysis. The aggregates from the tested quarries worked well in the concrete mixes [8]. In another study, aggregates' crushing and impact values were analyzed, and three samples were taken from Margalla, Sargodha, and Sakhi Sarwar. All aggregate samples fell within the suitable crushing range. Hence they were all chosen [9]. It has been determined that the gravel and sand deposits found along the terraces, bars, and tributaries of the Allai River are of sufficient quality to be used in the construction of the necessary engineering structures [10]. The engineering properties of these aggregates, which are used in concrete and highway construction, are mined in Punjab with good Los Angeles abrasion (24.48%), California Bearing Ratio (90.10%), soundness (4.06%), specific gravity (2.65), and water absorption (0.739%) values [11]. Engineering features determine these aggregates' in-service performance. Crushed Jutana Formation, Sakeasar Limestone, and stream gravels from Jabbi-Warchha and Katha Saghral are used in Portland cement, asphalt concrete, unbound and bound pavements, railway ballast, and riprap [12]. For the sake of conducting fundamental engineering evaluations, the Mesozoic carbonates near the Kohat Hills Range in Pakistan's Khyber Pakhtunkhwa province were investigated. In the Kohat Hills Range, the Mesozoic carbonates are well exposed [13]. Due to its superior impact and crushing strength, aggregates from Sargodha can be utilized with heavy traffic loads in road construction. [14]. Road aggregates from quarries in northern Pakistan were subjected to a comprehensive range of standard durability, form, and strength tests [15]. Based on geotechnical samples of Sakesar Limestone, its suitability for use as a Base Course, Sub Base, and Surface Course is recommended [16]. Another research study concluded that Except for Loye Khawar, which is slightly above the upper limits, the soundness of these Aggregates was observed to be resilient in the face of changes in physical conditions [17]. Mechanical properties of the concrete produced in Azad Kashmir using locally accessible aggregates were satisfactory, according to another study [18].

Materials and Methodology

Aggregate sources

The aggregates used in this research are collected from the selected quarry in Chakdara Dir Lower Khyber Pakhtunkhwa province and the Margalla aggregate quarry, which is mostly used for road construction in Pakistan. In the Chakdara quarry, the aggregate is obtained by crushing natural mountain rocks, passing it through different crushers, and screening it to different sizes. Pavement building requires robust, long-lasting aggregates that can withstand weathering and crushing. So the aggregates of Chakdara is evaluated along with the Margalla aggregates, and their properties are compared. The NHA class B gradation will be used for aggregates sources for specimen preparation. The locations of both the aggregates quarries are shown in Figure 1.

Figure 1: Location of Both aggregate quarries shown on a map of Pakistan

Methodology

A petrographic investigation of Chakdara and Margalla aggregate is performed per ASTM C-295 to determine the rock geology using a high-resolution microscope. Attock refinery restricted grade 60/70 bitumen was used to conduct this investigation. Specific gravity and water absorption (AASHTO T85-88), Los angles abrasion (AASHTO T96-87), soundness test (ASTM C88), shape test (ASTM D 4791), impact, and crushing value (BS-812 & IS-383) tests were performed on the aggregates to ensure that they meet the necessary criteria. The Marshall Mix design, according to ASTM D1559, is performed for Chakdara aggregate and Margalla aggregate to design the hot mix asphalt HMA to study aggregate affinity with bitumen in the asphalt mix. The wheel tracker test is performed for the Chakdara and Margalla aggregate to determine the rutting resistance of both aggregate sources. The moisture sensitivity of bitumen aggregate is determined by stripping and coating test according to AASHTO T182.

Figure 2: Chakdara source, Marshall Samples, Microscopic view of aggregates

RESULTS AND DISCUSSIONS

Petrographic analysis

The petrographic study of Margalla aggregates reveal that Limestone dominates Margalla aggregates quarries. The nature of aggregate is calcium-carbonate ($CaCO_3$) for about 99% and 1% quartz as shown in figure 3. A petrographic study of Chakdara aggregate revealed a coarse-grained, light-to-white rock sample. Its petrographic composition is 98% calcite. Calcite grains are usually coarse-grained but also medium-grained. Some crystals are subhedral, but most are euhedral. There is 2% silica, quartz and oxides. The petrographic examination identified the material as "Marble." Calcite rocks are strong enough for road building as shown in figure 4. The petrographic study shows that Margalla aggregate has 1% Quartzwacke, so it has less acidic properties than Chakdara aggregate, which has 2% Quartz/silica content.

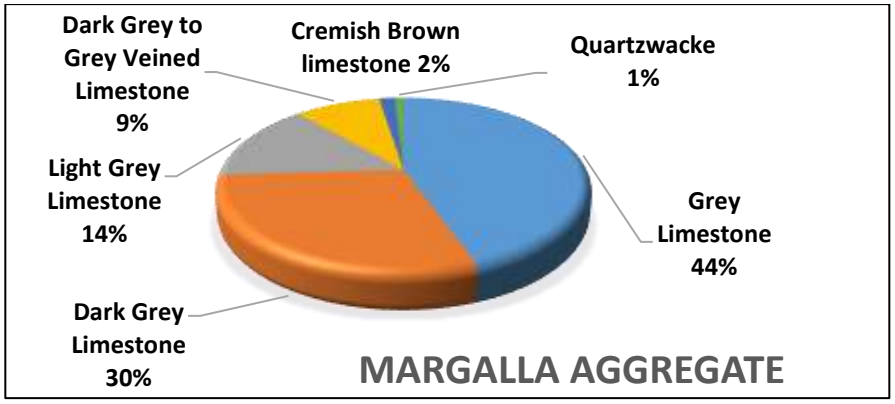

Figure 3: Mineral composition of Margalla aggregates

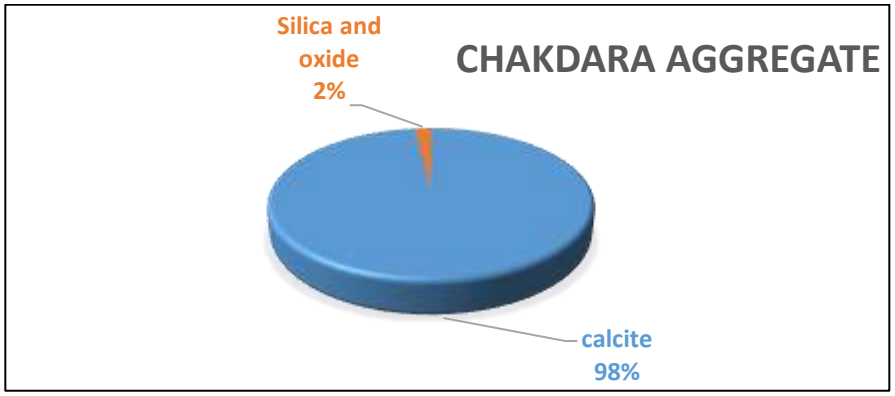

Figure 4: Mineral composition of Chakdara aggregates

Aggregate properties test

The specific gravity (ASTM C-127) range as per NHA specifications is 2.5 to 3.0, and the maximum amount of water absorption is 2%. The specific gravity and water absorption parameters for Chakdara aggregates are acceptable and equivalent to Margalla aggregates according to NHA criteria, as shown in Table 1. Thirty-five percent, 40 percent, and 50 percent of cement concrete, base course, and sub-base are allowed for aggregates in the Los Angeles abrasion resistance test (ASTM C-131). Chakdara aggregate has a little lower resistance to abrasion and degradation than Margalla aggregate (25.2 against 24), as indicated in Table 1. However, these values are within the acceptable range for usage in base, sub-base, and wearing courses. Aggregate crushing value (ACV) directly influences pavement stability. The pavement will break easily if poor aggregate is used. Strong aggregates have an ACV of about 5%, whereas weaker aggregates has 30% ACV. The

crushing values are 20% for Chakdara and 22.09% for Margalla, impact value test result is 14.28% for Margalla while it is 16.07% for Chakdara aggregates, which is a bit higher than Margalla. As per the crushing and impact load tests, the resistance of Chakdara aggregates is lower than Margalla but still falls within the country's required road construction specifications. The upper limit for both the flakiness and elongation indexes is 15%. The shape test value also confirms that Chakdara aggregate is suitable for road construction. The values given in Table 1 confirm that Chakdara aggregates are suitable for use in road bases, sub-bases, and surface courses, just like Margalla aggregates. Weathering and erosion require tough aggregate quality. The test limit is 12%. The soundness test (ASTM C 88) shows that Chakdara aggregate resists chemical attack and weathering better than Margalla.

Table 1 Aggregate Tests result

Test Title	Standard	Margalla aggregate	Chakdara aggregate	Limits
Type of Rock	----	(CaCO3)	calcite	----
Specific gravity	AASHTO T85-88	2.702	2.69	2.5-3%
Water absorption (%)	ASTM C 127	0.95	1.21	2 % (max)
Los Angeles abrasion (%)	ASTM C 131	24	25.2	30 % (max)
Impact value test (%)	BS-812 & IS-383	14.28	16.07	Strong (10-20%)
Crushing value test (%)	BS-812 & IS-383	20	22.09	30% (max)
Flakiness Index (%)	BS 812.108	5.34	6.3	11 % (max)
Elongation index (%)	BS 812.109	4.98	5.7	10 % (max)
Soundness test (% loss)	ASTM C 88	1.526	0.78	12 % (max)

Marshall Mix design (ASTM D1559)

The Marshall Mix design under ASTM D1559 is used to design Chakdara and Margalla aggregate hot mix asphalt (HMA). Extracted aggregate weighed 1200g. Mixtures were prepared using 60/70 penetration grade bitumen. The mix design uses one aggregate gradation with a maximum diameter of 19 millimeters due to excessive loads in the country. Impact loading with a hammer produces four-inch samples. Marshall Mix design determines Marshall Stability and Marshall Flow at 4.5% air voids for Chakdara and Margalla quarry aggregates to evaluate aggregate behavior in asphalt. Chakdara aggregate's Marshall Stability is slightly lower than Margalla's yet still suitable for asphalt but well high than the specified value of 6kN. Table 2 shows that asphalt mix properties

like mineral aggregates voids, asphalt-filled voids, and flow are within the prescribed range. Chakdara has a more optimum binder content than Margalla due to more voids in aggregate. This will not influence asphalt cost, and performance as lower transportation costs will save a lot of money. The Marshall Test shows that Chakdara aggregate can be used in asphalt mixtures for surface courses.

Table 2 Marshall Mix Design parameters

Property	Chakdara aggregate	Margalla aggregate
Optimum binder content [%]	4.63	4.33
Air voids [%]	4.5	4.5
Voids in mineral aggregates, VMA [%]	16.15	15.3
Voids filled with asphalt, VFA [%]	69.59	66.5
Marshall Stability [kN]	11.22	12.4
Flow [mm]	6.51	7.12

Wheel tracker test (AASHTO T324)

The wheel tracker test is performed for the Chakdara and Margalla aggregates to determine its rutting resistance. The 50mm thickness sample is prepared for aggregates sources, and the testing temperature is 55°C. Central and average Steady State Tracking Rates are 0.44 mm/1000 Passes. At 10000-wheel passes, Chakdara aggregates has a maximum rut depth of 4.93mm and Margalla aggregates of 3.6mm. Chakdara aggregate's rut depth figure shows weak rutting resistance, although it meets the country's specification, as shown in Figure 5.

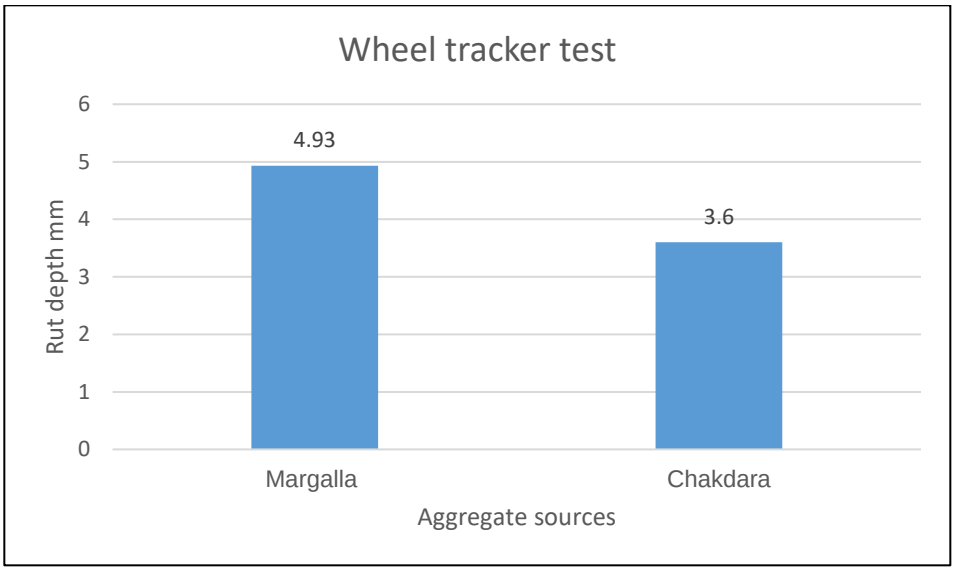

Figure 5: Comparison of rut depth of Margalla and Chakdara aggregate

Stripping and Coating test (AASHTO T182)

The Stripping and coating test is performed on the aggregate of Margalla by preparing two samples and checking them visually before and after being placed in water for 24 hours. The result of Margalla aggregate coating is about 98%. The Chakdara aggregate two samples are also prepared and checked visually before and after being placed in water for 24 hours. The coating of aggregate by bitumen is approximately 97%. The coating and stripping test result shows that the Chakdara aggregate has good moisture resistivity and bitumen coating ability. So the Chakdara aggregate is suitable for use in road construction and asphalt.

Figure 6: Stripping and Coating Samples before and after test

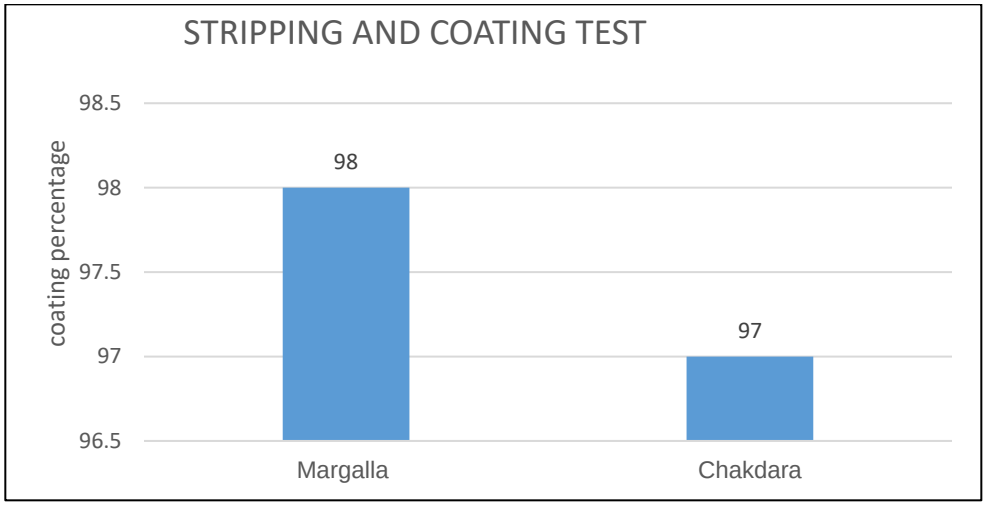

Figure 7: Stripping and Coating comparison of Margalla and Chakdara aggregate

Conclusions and recommendation

The following conclusions are drawn from this research:

- The Chakdara aggregate source is selected as a potential aggregate source and evaluated for use in pavement construction from different sources identified. The petrographic examination shows that Chakdara aggregate is limestone with 98% calcite and 2 % silica, while Margalla has 99% calcite and 1% quartz which is suitable for road construction.
- The Chakdara aggregates are tested for different physical properties, and all pass the minimum criteria in the NHA specification.

- The stability analysis found that there is only a 9.5 % difference between the stability of the asphalt mix of Margalla and Chakdara aggregates.
- From permanent deformation analysis, it was concluded that Chakdara aggregate has 36.9% less rut resistance than Margalla.
- From the striping and coating test, there is only a 1% difference between Chakdara and Margalla coating.
- Therefore, Chakdara aggregates can be used for local road construction in northern Pakistan.

References

1. Hussain, J., Zhang, J.m., Fitria, F., Shoaib, M., Hussain, H., Asghar, A. and Hussain, S. "Aggregate Suitability Assessment of Wargal Limestone for Pavement Construction in Pakistan.". *Open Journal of Civil Engineering*, 12 (2022). 56-74https://doi. org/10.4236/ojce.2022.121005.
2. Wu, Y., et al. "Aggregate toughness/abrasion resistance and durability/soundness tests related to asphalt concrete performance in Pavements." *National Center for Asphalt Technology, Auburn University, Alabama NCAT Report No. 98-4* (1998).
3. Little, D.N. Evaluation of Structural Properties of Lime Stabilized Soils and Aggregates. *National Lime Association, Arlington* (1998).
4. Kamal, M.A., Sulehri, M.A. & Hughes, D.A.B. Engineering characteristics of road aggregates from northern Pakistan and the development of a toughness index. *Geotech Geol Eng* **24**, 819–831 (2006). https://doi.org/10.1007/s10706-005-6610-9
5. Hussain, Arshad, and Yanjun Qiu. "Evaluation of Dina Aggregates for Pavement Construction in Pakistan." *Advanced Materials Research* (2012). 548 https://doi.org/10.4028/www.scientific.net/AMR.548.239.
6. Mbaezue, N., Emmanuel Ndububa, Opeyemi Kolawole, and A. Aminu. "A Comparative Study of the Quality of Various Road Aggregate Types in Abuja, Nigeria." *Global Scientific Journal*, 8 (2020).
7. Khan, M., A Laboratory Experimentation Based Ranking of Margalla Crush Aggregates. *Technical Journal, University of Engineering and Technology (UET) Taxila, Pakistan*, 2015. **20**: p. 62-67.
8. Munir, M., et al., Engineering Characteristics of widely used Coarse Aggregates in Pakistan: A Comparative Study. *Pakistan Journal of Engineering and Applied Sciences*, 2017. **20**:p. 85-93.
9. Shakeel, K. and A. Farooq, Behavior of Aggregates from different sources under uniform and impact loading. 2020.

10. Ahsan, N., et al., Allai Aggregate for rehibilitation and reconstruction of october 8, 2005 earthquake affected allai-banan area, NWFP. 43 *Geol. Bull. Punjab Univ*, 2009. **44**.
11. Ahsan Naveed, Muhammad Munawar, and Saif Rehman. "Aggregate Suitability Studies of Limestone Outcrops in Dhak Pass, Western Salt Range, Pakistan" 4 (2012).
12. Gondal, M.I.C., N. Ahsan, and A. Javid. Engineering properties of potential aggregate resources from eastern and central salt range , Pakistan. 2010.
13. Rehman, G., Zhang, G., Rahman, M.U. *et al.* The engineering assessments and potential aggregate analysis of mesozoic carbonates of Kohat Hills Range, KP, Pakistan. *Acta Geod Geophys* **55**, 477–493 (2020). https://doi.org/10.1007/s40328-020-00301-9
14. Abbas, S., et al "Engineering characteristics of widely used coarse aggregates in Pakistan: A comparative study." *Pak. J. Engg. & Appl. Sci.* (2017). *Vol.20, Jan., 2017*
15. Kamal, M.A., Sulehri, M.A. & Hughes, D.A.B. Engineering characteristics of road aggregates from northern Pakistan and the development of a toughness index. *Geotech Geol Eng* **24**, 819–831 (2006). https://doi.org/10.1007/s10706-005-6610-9.
16. Hassan EUL, Hannan A, Rashid MUR, et al. Resource assessment of sakesar limestone as aggregate from salt range Pakistan based on geotechnical properties. *Int J Hydro*. 2020;4(1):24-29. DOI: 10.15406/ijh.2020.04.00222
17. Siddiqi, Zahid, Rashid Hameed, Muhammad Saleem, Qasim Khan, and I. Ishaq. "Performance Study of Locally Available Coarse Aggregates of Azad Kashmir." *Pakistan journal of science* 65 (2013).
18. Ayub, Muhammad, Qaisar Ali, Khan Shahzada, A. Naseer, Muhammad Shoaib, and Umair Ayub. "Engineering Assessment of Coarse Aggregates Used in Peshawar." *International Journal of Advanced Structures and Geotechnical Engineering* 01 (2012).

2nd International Conference on Advances in Civil and Environmental Engineering (ICACEE-2023)

University of Engineering & Technology Taxila, Pakistan

Conference date: 22nd and 23rd February, 2023

Possible Use of Waste Cigarette Butts In Asphalt Concrete

Irfan Akbar[1], Naveed Ahmad[2]

[1]MSc. Scholar, Department of Civil Engineering, University of Engineering and Technology UET Taxila, Pakistan, irfanakbar988@gmail.com

[2]Professor, Department of Civil Engineering, University of Engineering and Technology Taxila, Pakistan, n.ahmad@uettaxila.edu.pk

ABSTRACT

Considering the widespread consumption of cigarettes around the globe, Cigarette Butts can be regarded as one of the most prevalent types of waste in the modern era. Despite the fact that various recycling techniques have been created and tried in recent years, Cigarette Butts are currently disposed of in landfills and incinerators. Cigarette Butts (CBs) make up one-third of the world's litter and are dumped in landfills in the billions every day. As a result, its use in asphalt concrete has increased significantly to decrease the cigarette waste. Cigarette Butts fibers and Encapsulated Cigarette butts are employed in asphalt concrete to enhance the stability and characteristics of asphalt. Cigarette Butt fibers are used in asphalt mixture in dosages of 0.2%, 0.4%, and 0.6% by weight of binder and different bitumen tests like penetration, softening and ductility tests are performed. Encapsulated Cigarette Butts are added to the mixture in amounts of 1%, 2%, and 3% by weight of asphalt mix. The Marshall stability is calculated at each of the six percentages. Indirect tensile tests were done to determine the resilient modulus of asphalt containing Cigarette Butt fibers and Encapsulated Cigarette butts. Wheel tracker testing determines the rutting resistance of asphalt with both CBs fibers and Encapsulated CBs. According to the tests' findings, both additives improve the mechanical performance and stability of HMA compared to the control sample. At 1% dosages, Encapsulated Cigarette Butts perform well, while cigarette butts fibers give better results at 0.6% dosage. Cigarette Butts Fibers modified asphalt mixture performed better than the one modified with Encapsulated Cigarette Butts. Addition of 0.6% CBs fiber increases the Marshall Stability value by 19.67% while addition of 1% Encapsulated Cigarette butts increases the Marshall stability by 5.73%. Addition of 0.6% CBs fiber in asphalt mixture reduced the rut depth by 30% while addition of 1% Encapsulated CBs reduced the rut depth by 10%. Also Cigarette Butts fiber in asphalt mixture enhance the stiffness better as compared to Encapsulated CBs.

KEY WORDS: Cigarette Butts, Marshal Stability, Rutting, Asphalt Concrete, Resilient Modulus

Introduction

CBs are non-biodegradable garbage that is typically improperly thrown into the environment. CBs comprise of cellulose acetate, which is recoverable by extraction and purifying methods. CBs are the most prevalent sort of garbage on the planet. Significant quantities of CBs are improperly thrown into the environment. [1]. Utilizing fibers is a standard and well-established method for producing mixes with a high bitumen concentration. The fibers act as stabilizing agents and, if appropriate, a

mechanical properties enhancer for bituminous mixes. [2]. Asphalt mixture, consisting of asphalt, aggregates, and air spaces, has been extensively utilized to produce flexible pavement due to the excellent adhesion between asphalt and aggregates, which offers improved strength and structural properties [3,4]. The feasibility of encapsulating CBs with different grades of bitumen and wax and putting them into asphalt mixture for pavements has also been explored. Encapsulation relies on restricting CBs' interface with fluids, inhibiting chemical transport [5]. CBs are similar to thermosets and thermoplastics. Therefore, they can be used to produce improved asphalt, such as crumb rubber and plastic trash. CBs can be used to improve asphalt mixture with the idea that this is an environmentally responsible resource extraction [6]. By stabilizing the entire mixture, fibers in asphalt concrete considerably lower the asphalt draining and leaking [7, 8]. Previous studies compared cellulose fibers with CBs and virgin bitumen (0% fiber). CBs can replace virgin cellulose fiber as a fiber modifier and improve bitumen's physical and rheological qualities [9]. In addition, the fibers improve certain mechanical properties of asphalt concrete, such as its static and dynamic stabilities, flexibility, susceptibility to moisture, and overall fatigue properties [10–12]. Field testing of fiber-reinforced asphalt concrete (FRAC) has also been carried out [13]. It has been found that using polypropylene, polyester, nylon, and carbon fibers in HMA increases Marshall Stability, indirect tensile strength, and toughness [14]. According to the results of thermal conductivity tests, asphalt enhanced with bitumen encapsulated cigarette butts (BECB) is more resistant to damage brought on by temperature changes [15]. The resilient modulus has been observed to decrease with a rise in the percentage of CBs enclosed in dense asphalt. Results, however, fell within the typical range of 1500-4000MPa [16, 17]. Waste cigarette butts can be recycled substantially by modifying bitumen with 0.2-0.3% CBs [18].

Problem Statement

Heavy traffic loads are repetitively imposed to pavements causing distresses and damages that leads to fatigue cracks, and permanent deformation. The earlier researchers have tried to enhance mechanical properties but there is still limitation in determining the best type and content of fiber. Cigarette butt fibers and encapsulated cigarette butts had been used in asphalt concrete but its comparative analysis had never been checked with each other. High strength pavements are required

for today's traffic density. This research intended to increase the strength of Asphalt Concrete incorporating CB fibers and Encapsulated CBs which would ultimately increase the service life of the pavements.

Research Objectives

The main objectives of this research work were:

- To find the correct dose of CBs fiber contents, and encapsulated CBs for asphalt concrete used by the local industry.
- To study the permanent deformation resistance of the modified mixtures.
- To study the stiffness characteristics of the modified mixtures.
- To carry out comparative analysis of asphalt mixtures prepared using CBs fiber and encapsulated CBs.

Materials

Aggregate

Aggregate are taken from Margalla Quarry, which produces limestone i.e. calcium carbonate ($CaCO_3$) based on petrography. NHA Class B wearing coarse gradation is used for asphalt mix design.

Binder

Attock Oil Refinery's 60/70 pen-grade binder is used on which softening, penetration, and ductility tests are performed.

Fibers

The collection of cigarette butts was done from the local industry. About 95% of cigarette butts are made of cellulose acetate (a plastic), while the remaining 5% are paper and rayon. The cellulose acetate fibers that form butts are narrower than stitching thread, white in color, and densely packed; they are like cotton. Dried Cigarette Butts were shredded into ground fiber with a grinder and converted into CBs fiber. When cigarette butts are coated with bitumen, they are called encapsulated cigarette butts.

Methodology

Research comprises of three phases. Material selection was made in the first phase. The second phase consists of testing of bitumen softening, penetration, and ductility with fiber addition in dosages of 0.2%, 0.4%, and 0.6% by weight of bitumen. The asphalt samples prepared with cigarette butts include the extraction of fiber from cigarette butts, then oven-dried at 105 degrees Celsius. The CBs Fiber was then combined with bitumen at 160°C. The aggregate mixture was then poured with hot asphalt. After completing the asphalt mixing procedure, the mixture was poured into various test-specific molds. After adding Cigarette Butt fibers, asphalt samples were tested using Marshall Stability, Wheel tracker and indirect tensile stiffness techniques. In the third phase, the asphalt mix was prepared with Encapsulated CBs. First, Cigarette Butts were oven-dried at 110°C for 24 hours. Then bitumen heated to 160 degrees Celsius was gathered in a thick aluminum tray, and CBs were kept in the tray for one hour. The aggregates and Encapsulated CBs were then covered with hot asphalt. After completing the asphalt mixing procedure, the mixture was poured into various test-specific molds. Then Marshall Stability, Wheel tracker, and indirect tensile tests were done on asphalt modified with 1%, 2%, and 3% Encapsulated Cigarette Butts, which were taken by weight of the mix. The Marshall test a sample of 101.6mm-diameter, 76.2mm-tall cylindrical mold held the mix. Each specimen face received 75 compaction blows. Hydraulic jacks de-molded the specimen after 24 hours. The obtained specimen had a diameter of 101.6mm and a height of 63.5mm. The specimens were conditioned in a 60°C water bath for 1 hour. In wheel tracker test Square slab, Mold Size 300mm X 300mm, Height 50mm. The mixture was compacted with the help of a roller compactor. The roller compactor compacts the specimen in 4 phases. 1st phase 2.1 bar pressure was applied for 10 passes. 2nd phase 2.5 bar pressure for the next 10 passes. 3rd phase 3.5 bar pressure was applied for 5 passes. 4th phase 4 bar pressure was applied for 5 passes. A total number of 30 passes were given. In the indirect tensile test, a cylindrical mold with a diameter of 101.6mm and a height of 76.2mm was filled with the mixture. Each face of the specimen was subjected to 75 numbers of compaction strikes. After twenty-four hours, the specimen was demolded using a hydraulic jack. The obtained specimen measured 101.6mm in diameter and 63.5mm in height. Then, tests were conducted.

Figure 1: Cigarette Butts, Cigarette Butt fibers, Wheel Tracker sample

Experimental Test results

Bitumen Tests results

The penetration of bitumen with varying percentages of Cigarette Butt fibers decreases as the percentage of fiber increases while softening point value increases. Cigarette Butt fibers reduce ductility because the CBs fiber reinforces the sample and does not allow it to stretch, so the fiber breaks it instead of stretching.

Table 1: Bitumen Tests results with different Cigarette Butt fibers percentages

Sr. No.	Sample	Penetration (0.1mm)	Softening (°C)	Ductility (cm)
1	Base-binder + 0.00% of Cigarette Butt fibers	63	49	104
2	Base-binder + 0.2% of Cigarette Butt fibers	62	53	86
3	Base-binder + 0.4% of Cigarette Butt fibers	57	54	55
4	Base-binder + 0.6% Cigarette Butt fibers	53	56	35

Marshall Stability

First, we prepared Marshall Specimen without asphalt binder additives. Then the specimen are made from Cigarette Butt fibers with varying percentages (0.2%, 0.4%, and 0.6%) taken by weight of bitumen at 4.5% OBC. Initially the Cigarette Butts fiber were oven dried at a temperature of 105°C. CBs Fiber were then mixed with bitumen at a temperature of 160° C. After the completion of mixing procedure, the mix were poured into different molds required for different tests. After that, Encapsulated Cigarette Butts are added to asphalt at 1%, 2%, and 3% by weight of asphalt mix at 4.5% OBC and same procedure is repeated for sample preparation. The Marshall Stability increases gradually with an increase in CBs fibers percentage because the CBs fiber mix well and reinforce the asphalt. The CBs fiber performs well at 0.6%. The Marshall Stability increases with Encapsulated Cigarette Butts up to 1%. Then it decreases because as the percentage of Encapsulated Cigarette Butts increases, the quantity of Encapsulated CBs in one place also increases as it sticks together, so Marshall Stability decreases. Encapsulated CBs are also compactable and more compressible under load, so stability decreases.

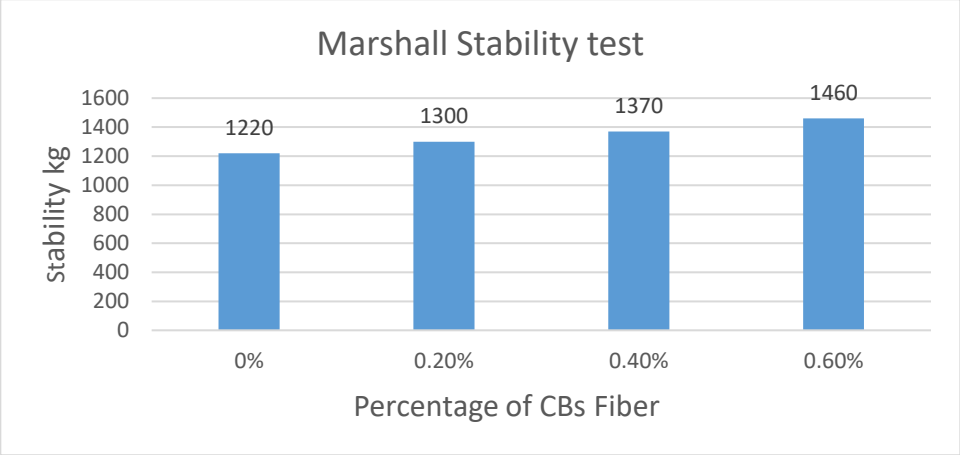

Figure 2: Marshall Stability and Percentage of CBs Fiber graph

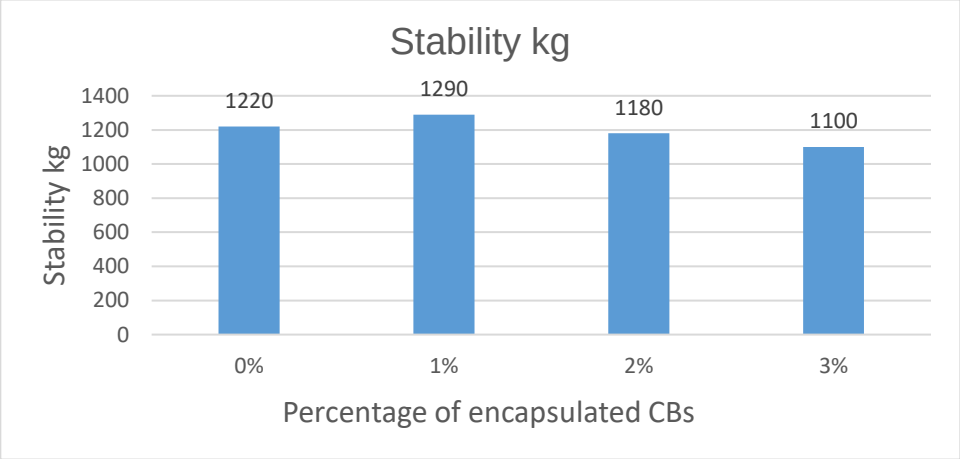

Figure 3: Marshall Stability and Percentage of encapsulated CBs graph

Wheel tracker test

The wheel tracker test is performed on samples modified with Cigarette Butts fibers (0.2%, 0.4%, and 0.6% dosages) in order to measure rutting resistance at 55°C for 10000 cycles with 12mm maximum permissible rutting depth. Similarly, rut depth is determined for asphalt samples modified with encapsulated cigarette butts (1%, 2%, and 3% dosage by weight of mix). The rut depth of samples modified with Cigarette Butt fibers decreases as we increase the Cigarette Butt fibers percentage. At 0.6% of cigarette butt fibers, the rut depth is small, so at 0.6%, the rut resistance is high. For Encapsulated Cigarette Butts, the rut depth decreased at 1% Encapsulated Cigarette Butts and then started increase by adding more percentages of Encapsulated CBs, and the samples failed at 3%. The 1% Encapsulated Cigarette butts showed good rut resistance. The Encapsulated Cigarette butts have low rut resistance because it is a spongy material immersed in bitumen, so it has absorbed the bitumen. So when the wheel passes on it, the absorbed bitumen may come out of the Cigarette Butts when compressed, so the rut depth increases.

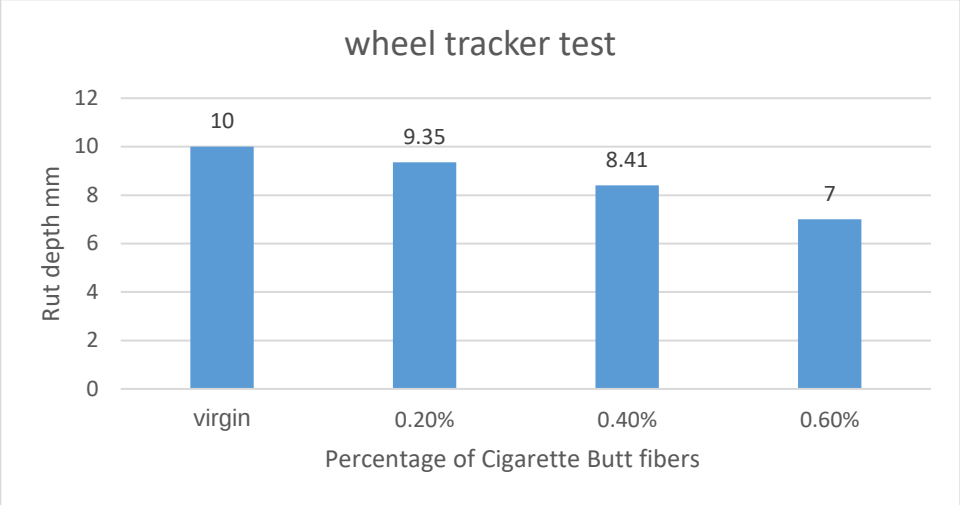

Figure 4: Rut depth and Percentage of Cigarette Butt fibers graph

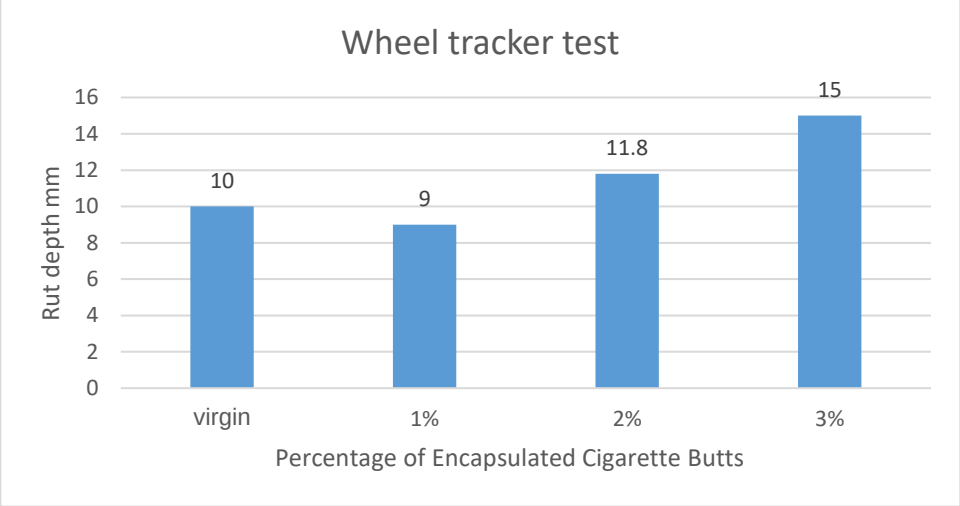

Figure 5: Rut depth and Percentage of Encapsulated Cigarette Butt fibers graph

Indirect tensile modulus test

Specimen were made from Cigarette Butts fibers with varying percentages (0.2%, 0.4%, 0.6%) Taken by weight of bitumen at 4.5% OBC. Then specimen were made for Encapsulated Cigarette butts and Encapsulated Cigarette butts are added to asphalt with a percentages of 1%, 2% and 3% by weight of asphalt mix at 4.5% OBC. Then the indirect tensile test were conducted on all the samples. Asphalt samples modified with Cigarette Butts fibers have shown a higher resilient modulus as compared to the ones modified with Encapsulated CBs. Resilient modulus value is low for 0.2% addition of Cigarette Butt fibers, then by increasing the percentage of CBs fibers to 0.6%, MR value showed an increase and at 0.6% CBs fibers it give best results. The Resilient modulus value increases

up to the 1% dosage for Encapsulated Cigarette Butts and then by increasing the percentages up to 3% Encapsulated Cigarette Butts the MR value goes decreases.

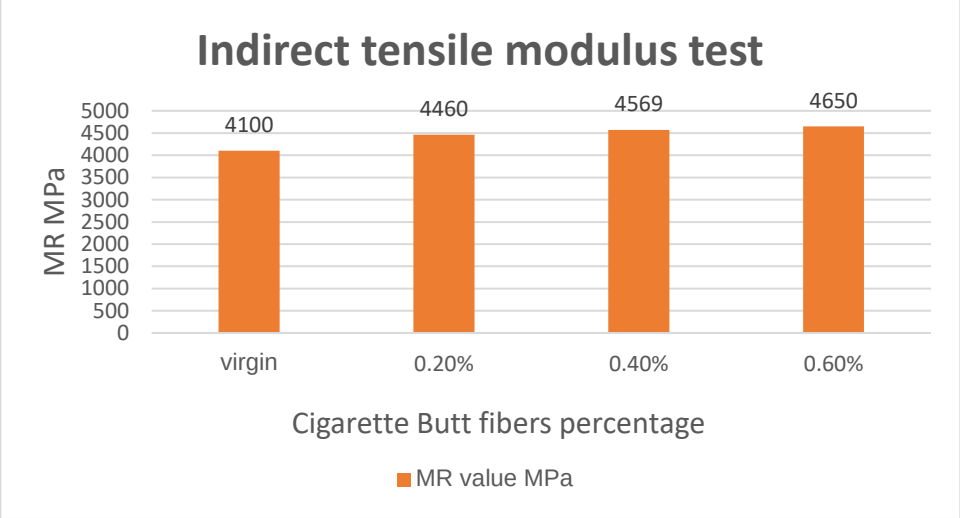

Figure 6: MR values and Cigarette Butt fibers percentage graph

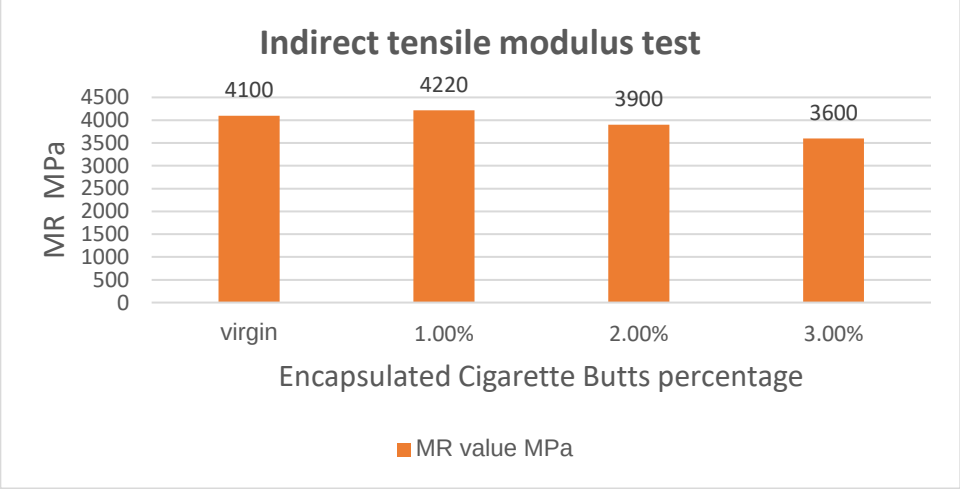

Figure 7: MR values and Encapsulated Cigarette Butt fibers percentage graph

Comparison at optimum contents for both Additives

The Cigarette Butt fibers have performed well in asphalt mix compared to Encapsulated Cigarette Butts in all three tests. Cigarette Butt fibers mix uniformly and form good bonding with asphalt. So it reinforces the asphalt and increases the stability, stiffness, and rut resistance as the percentage of CBs fiber increases. The Encapsulated Cigarette Butts cannot mix uniformly in asphalt, and many

Encapsulated Cigarette Butts may present in numbers in one place, as it stick together so it does not contribute much to the asphalt performance improvement.

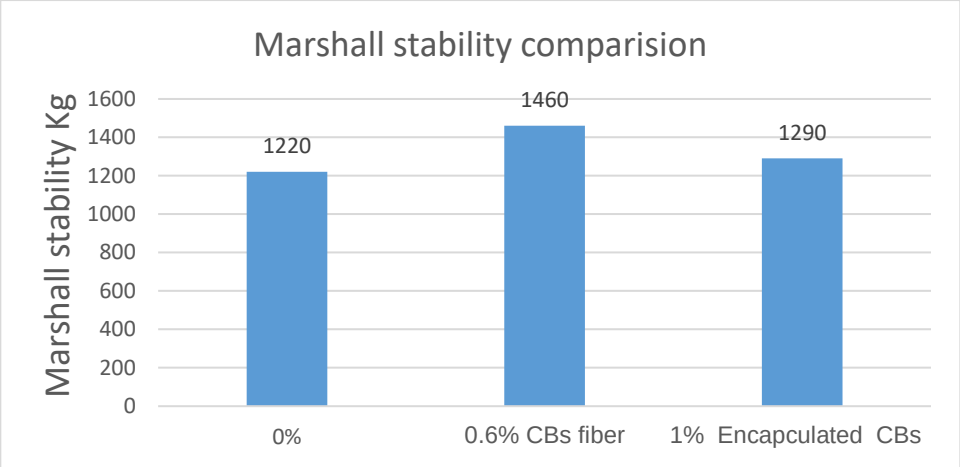

Figure 8: Marshall Stability comparison of optimum content of both additives

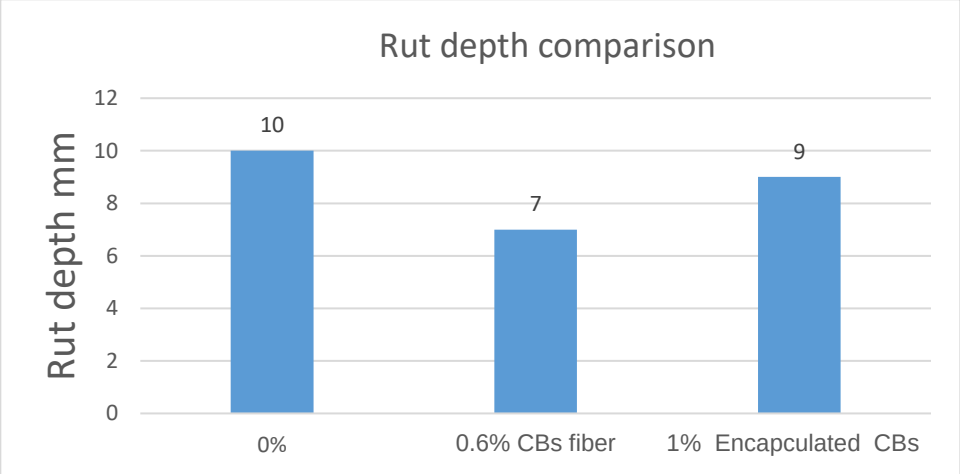

Figure 9: Rut depth comparison at 0.6% CBs and 1% Encapsulated CBs

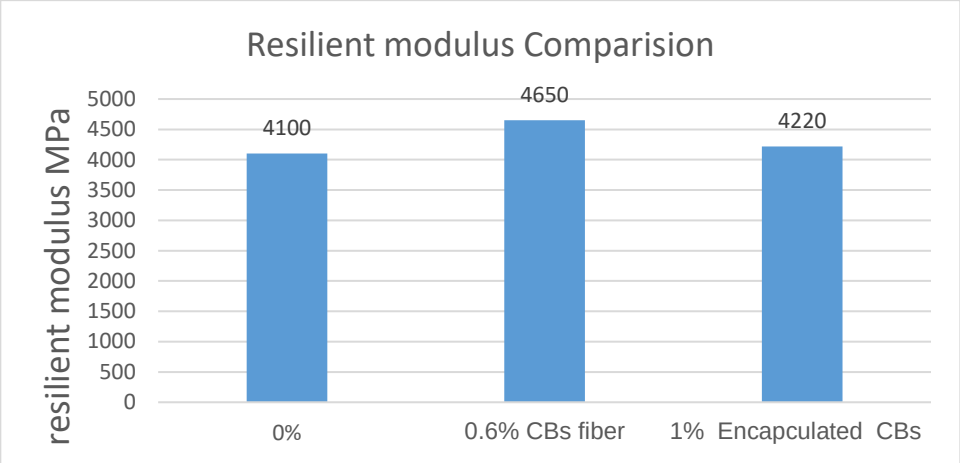

Figure 10: MR value comparison at 0.6% CBs and 1% Encapsulated CBs

CONCLUSIONS

The conclusions drawn from this study are provided below:

- The recommended dosage for Cigarette Butt fibers is 0.6% by weight of bitumen.
- For Encapsulated Cigarette Butts optimum dosage is 1% by weight of asphalt mixture.
- Addition of 0.6% CBs fiber increases the Marshall stability value by 19.67% while addition of 1% encapsulated Cigarette butts increases the Marshall stability by 5.73%
- Addition of 0.6% CBs fiber in asphalt mixture reduced the rut depth by 30% while addition of 1% encapsulated CBs reduced the rut depth by 10%.
- Presence of 0.6% Cigarette butts fiber in asphalt mixture enhance the stiffness by 13.41% while 1% encapsulated CBs increase the stiffness by 2.92%.
- At optimum dosage CBs fibers performing better in comparison to Encapsulated CBs. Therefore it is recommended that Cigarette butts can be converted into fibers and then use in asphalt mixture instead of using them in encapsulated form.

References

1. De Fenzo A, Giordano M, Sansone L. A Clean Process for Obtaining High-Quality Cellulose Acetate from Cigarette Butts. *Materials*. 2020; 13(21):4710. https://doi.org/10.3390/ma13214710
2. Tataranni, P.; Sangiorgi, C. A Preliminary Laboratory Evaluation on the Use of Shredded Cigarette Filters as Stabilizing Fibers for Stone Mastic Asphalts. *Appl. Sci*. 2021, 11, 5674. https://doi.org/10.3390/app11125674

3. N. Akmal, A.M. Usmani, Application of asphalt-containing materials, *Polym.News* 24 (1999) 136–140.

4. K.J. Murali, K.R. Rajagopal, Review of the uses and modeling of bitumen from ancient to modern times, *Appl. Mech. Rev.* 56 (2) (2003) 149–214.

5. Mohajerani, Abbas, Yasin Tanriverdi, Bao Thach Nguyen, Kee Kong Wong, Harin Nishamal Dissanayake, Lachlan Johnson, Damian Whitfield, *et al.* "Physico-Mechanical Properties of Asphalt Concrete Incorporated with Encapsulated Cigarette Butts." *Construction and Building Materials* 153 (2017): 69-80. /https://doi.org/10.1016/ j.conbuildmat.2017.07.091.
6. Jin, Jimei, Zhaorong Wu, Jin Song, and Xue Liu. "Research on the Road Performance of Cigarette Butts Modified Asphalt Mixture." *Journal of Physics: Conference Series* 1168, no. 2 (2019): 022053. https://doi.org/10.1088/1742-6596/1168/2/022053
7. R.L. Fitzgerald, Novel Applications of Carbon Fiber for Hot Mix Asphalt Reinforcement and Carbon–Carbon Pre-Forms MSc Thesis, Department of Chemical Engineering, *Michigan Technological University*, 2000.

8. H. Hassan, S. Al-Oraimi, R. Taha, Evaluation of open-graded fiction come mixture containing cellulose fibers and styrene butadiene rubber polymer, *J. Mater. Civ. Eng*. 17 (4) (2005) 415–422.

9. Rahman MT, Mohajerani A, Giustozzi F. Possible Recycling of Cigarette Butts as Fiber Modifier in Bitumen for Asphalt Concrete. *Materials*. 2020; 13(3):734. https://doi.org/10.3390/ma13030734

10. P. Peltonen, Wear and deformation of characteristics of fiber reinforced asphalt pavements, *Constr. Build. Mater.* 5 (18) (1991) 22.

11. A. Goel, A. Das, Emerging road materials and innovative applications. in: *National conference on materials and their application in civil engineering, Hamipur, India*, August 2004.

12. S. Tapkın, The effect of polypropylene fibers on asphalt performance, *Build. Environ*. 43 (2008) 1065–1071.

13. Serfass JP, Samanos J. Fiber-modified asphalt concrete characteristics, application and behavior. *J Assoc Asphalt Paving Technol* 1996; 65:193–230.

14. Kim, M.-J., et al., Enhancing mechanical properties of asphalt concrete using synthetic fibers. *Construction and Building Materials*, 2018. 178: p. 233-243.

15. Rahman, Md Tareq, and Abbas Mohajerani. "Thermal Conductivity and Environmental Aspects of Cigarette Butt Modified Asphalt." *Case Studies in Construction Materials* 15 (2021): e00569. https://doi.org/https://doi.org/10.1016/j.cscm.2021.e00569.

16. A. Mohajerani, Y. Tanriverdi, B.T. Nguyen, K.K. Wong, H.N. Dissanayake, L.Johnson, D. Whitfield, G. Thomson, E. Alqattan, A. Rezaei, Physico-mechanical properties of asphalt

concrete incorporated with encapsulated cigarette butts, Constr. Build. Mater. 153 (2017) 69–80

17. J. Rebbechi, L. Petho, (2014) Guide to Pavement Technology Part 4B: Asphalt. Austroads. Sydney, Australia. Retrieved from https://austroads. com.au/ publications/ pavement/ agpt 04b (2020)

18. Rahman, Md Tareq, Abbas Mohajerani, and Filippo Giustozzi. "Possible Use of Cigarette Butt Fiber Modified Bitumen in Stone Mastic Asphalt." *Construction and Building Materials* 263 (2020): 120134. https://doi.org/https://doi.org/10.1016/j.conbuildmat. 2020. 120134.

2nd International Conference on Advances in Civil and Environmental Engineering (ICACEE-2023)

University of Engineering & Technology Taxila, Pakistan

Conference date: 22nd and 23rd February, 2023

Effect of using Warm Mix Asphalt Technology on Performance of Asphalt Concrete

Salman Khan[1], Naveed Ahmad[2], Taimur Shah[3]

[1]MSc. Scholar, Department of Civil Engineering, University of Engineering and Technology UET Taxila, Pakistan, salmankhan68t@gmail.com

[2]Associate Professor, Department of Civil Engineering, University of Engineering and Technology Taxila, Pakistan, n.ahmad@uettaxila.edu.pk

[3]MSc. Scholar, Department of Civil Engineering, University of Engineering and Technology UET Taxila, Pakistan, Taimurshah1255@gmail.com

ABSTRACT

Pavement construction uses old hot mix asphalt technology. HMA's normal mixing temperature is 140–160°C, which requires much fuel, emits CO_2, and harms the environment. With increasing interest in the use of HMA in the paving industry, more study in this field for improvement of HMA performance seems to be necessary. Hence the main objective of this study is to compare warm mix asphalt concrete using varying sasobit ratios in typical HMA samples. The 60/70 penetration grade bitumen was separately modified with sasobit at different percentage ranging from 0% to 3.5%. Penetration and softening point test of modified bitumen shows that penetration value decreases while softening point increases with increase in modifier dosage. OBC was determined using the Marshall Mix Design method and came out to be 4.5%. The mix's wheel tracker test showed rut depths of 3.46mm, 3.41mm, and 3.3mm for 2.5%, 3.0%, and 3.5% of Sasobit (percent by weight of binder) respectively, satisfying rut depth failure criteria. Stripping and coating technique tested moisture susceptibility at 2.5%, 3.0%, and 3.5% of Sasobit dosages and modified samples performed well. Furthermore, addition of sasobit also improved the modulus of stiffness.

KEY WORDS: Warm Mix Asphalt, Greenhouse Gases, Emission Reduction, Sasobit.

Introduction

Identifying the application of WMA technology to asphalt pavement will enable the creation of mixture designs and surface treatments with greater environmental benefits. To guarantee that the State's transportation development is of the greatest quality feasible, certain asphalt pavement construction enhancements might be mandated as part of publicly funded roadways. Warm mix asphalt can decrease blending and laying temperatures more significantly than hot mix asphalt (HMA), which is also friendlier to the environment [1,2]. The WMA methods decrease the bitumen viscosity and improve its workability and density [3]. As concerns about global warming increase, the asphalt industry strives ceaselessly to cut its emissions. This is accomplished by reducing the mixing and compacting temperatures of asphalt mixes [4]. Warm mix asphalt (WMA) can be combined and packed at temperatures lower than hot mix asphalt (HMA). WMTs provide numerous environmental and economic benefits by reducing energy use and fuel costs. [5]. The WMA combinations can be created using a variety of foaming, organic, and chemical additives that

permit a thorough coating between the binders and aggregates under appropriate workability conditions [6]. Sasobit reduces the viscosity of asphalt binder at elevated temperatures, decreasing building temperatures and aging while boosting rutting resistance at ambient temperature for a specific bitumen type and supply. At intermediate and low temperatures, Sasobit may enhance the likelihood of fatigue and low-temperature cracking [7]. By melting below the binder's melting point and lowering its viscosity during mixing, organic additives in waxes and fatty amides operate as flow modifiers, enhancing the coating and workability of the mixture [8]. For both HMA and WMA combinations' MR values are significantly impacted by aging. However, the impact on HMA mixtures is more significant. This can result from the fact that HMA combinations age more quickly than WMA mixtures [9]. Compared to the control HMA sample, the asphalt mixture modified with WMA had better rutting resistance [10]. Indirect tensile strength (ITS) and Marshall Soundness (stability), along with other favorable Marshall metrics, were high in the DBM warm mix with the Sasobit addition. In such heated mixes, stability and tensile strength are observed to be likely to be sufficient. Additionally, it is observed that the resulting heated mixes are comparable to the control HMA [11]. The wax network topologies in Sasobit-modified asphalt lead to better rheological responses [12]. In both HMA and WMA combinations, adding liquid anti strip and hydrated lime improved their moisture susceptibility properties [13]. Pull-off test findings revealed that the bond energy for the polymer modified binder class performed better than that for the Pen 60-70 binder group (about six times bigger) [14]. WMA methods were created to make asphalt at somewhat higher temperatures than 100℃ with performance and attribute comparable to, or often even better than, those of traditional HMA. Using various additives, WMA technologies primarily concentrate on the binder (bitumen) to enhance its qualities [15-17]

Materials

Aggregates and binder

Based on rock petrography, Margalla quarry aggregate is taken. The National Highway Authority (NHA) Class B grading formulated asphalt mixtures. Pakistan's Attock Oil Refinery (ARL) supplied the 60/70 penetration grade Asphalt Binder utilized in this study.

Sasobit

The Sasol Company's Sasobit is a finely crystalline, long-chain aliphatic hydrocarbon. At first, it was manufactured from coal, but it was too costly, so they changed the manufacturing process. It is in the form of solid having three types i.e., with prill (5mm dia), small pirll (1mm dia), and flaked form (3mm chips).

Methodology

Material selection was made in the first step. The selected ideal binder was added in several Sasobit dosages of 2.5%, 3% percent, and 3.5% percent by weight of base binders. Different tests on bitumen softening, penetration, ductility, and flash and fire are performed with different percentages of

Sasobit. Asphalt Mix design specimens were created in the second step to find the stability, flow, and OBC, which can be used to prepare specimens for other tests. The specimens for the wheel tracker test and the indirect tensile test are prepared based on OBC with different Sasobit content. Then to check moisture sensitivity, the stripping and coating test is performed. During the last phase of the experimental investigation, the performance testing is carried out and the results are analyzed.

Figure 1: Indirect test apparatus, Marshall Specimen, Sasobit

Experimental Test results and discussions

Bitumen Tests results

The result of the tests performed on bitumen with the addition of different percentages of Sasobit shows that penetration decreases as we increase Sasobit percentages. While softening temperature increases and ductility decreases as Sasobit dose increases. The flash and fire temperatures increase Sasobit addition. The values are given table 1.

Table 1: Bitumen test result with sasobit percentages

Sr. No.	Sample	Penetration (0.1mm)	Softening (°C)	Ductility (cm)	Flash and Fire test (°C)
1	Base-binder + 0.00% of Sasobit	63	49	104	240
2	Base-binder + 2.5% of Sasobit	58	69	87	270
3	Base-binder + 3% of Sasobit	49	76	79	281
4	Base-binder + 3.5% of Sasobit	44	78	76	292

Penetration Test:

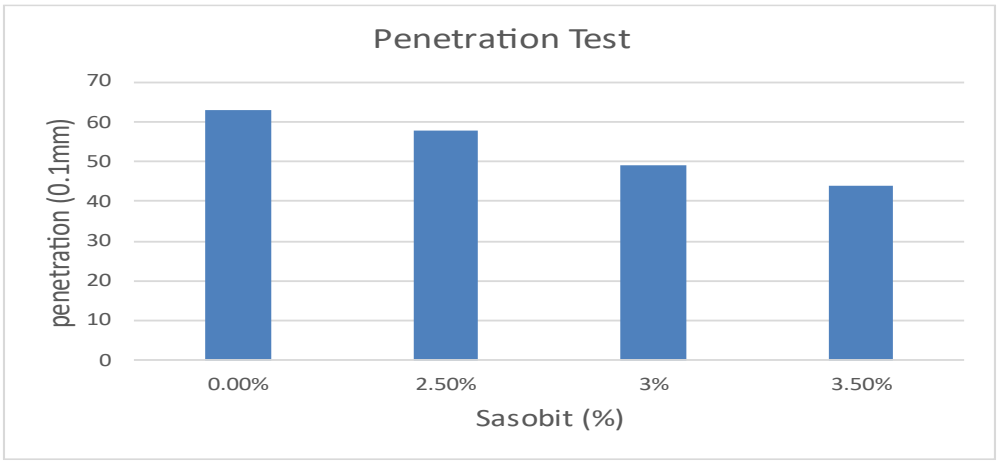

Figure 1: penetration test

Softening Point Test

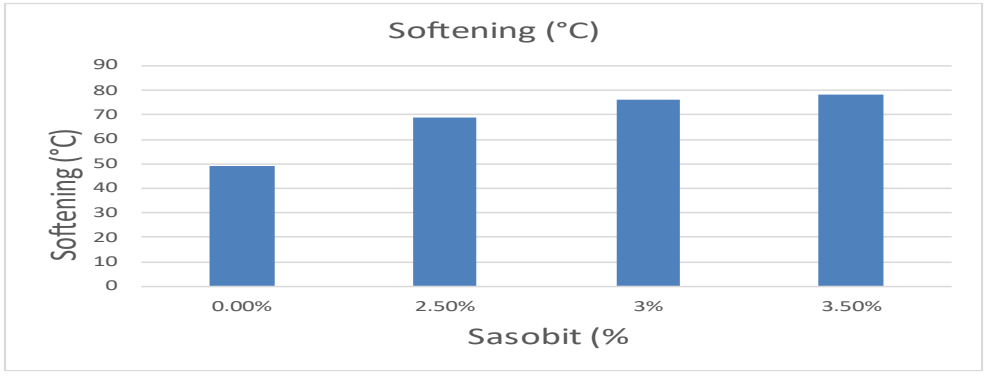

Figure 2: softening point test

Marshal Mix Design

First, Marshall Specimen were prepared without adding additives to asphalt binder. Sasobit dosage is by the percentage of bitumen in the mix. WMA specimens were prepared using different percentages, i.e., 2.5%, 3%, and 3.5%. The stability values increase as Sasobit content is increased as shown in Figure 2 below.

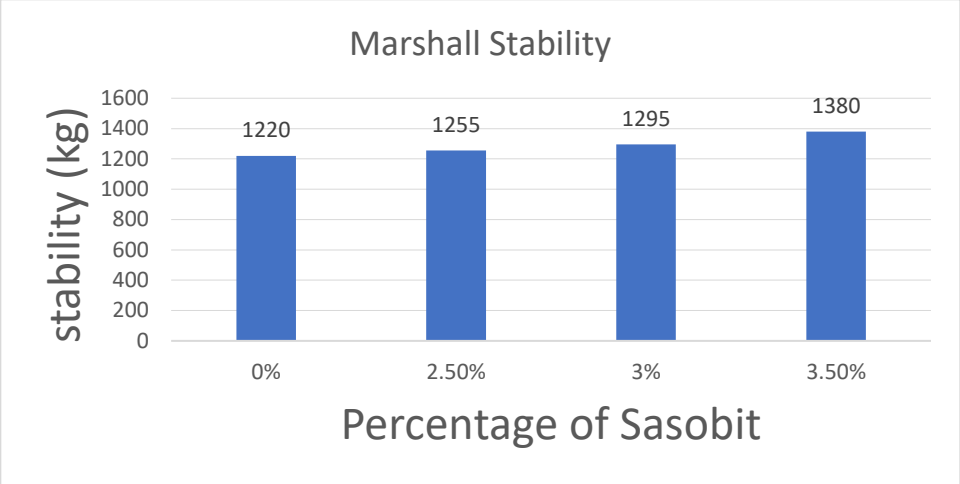

Figure 3: Marshall Stability and flow with sasobit percentage

Wheel Tracker Test

The wheel tracker test is performed for the asphalt mix to determine its rutting resistance at 10000-wheel passes. The rut depth decreases with increase in Sasobit percentage. The rutting resistance is maximum at 3.5% which is a suitable value for the Sasobit percentage to be added to asphalt to give good results.

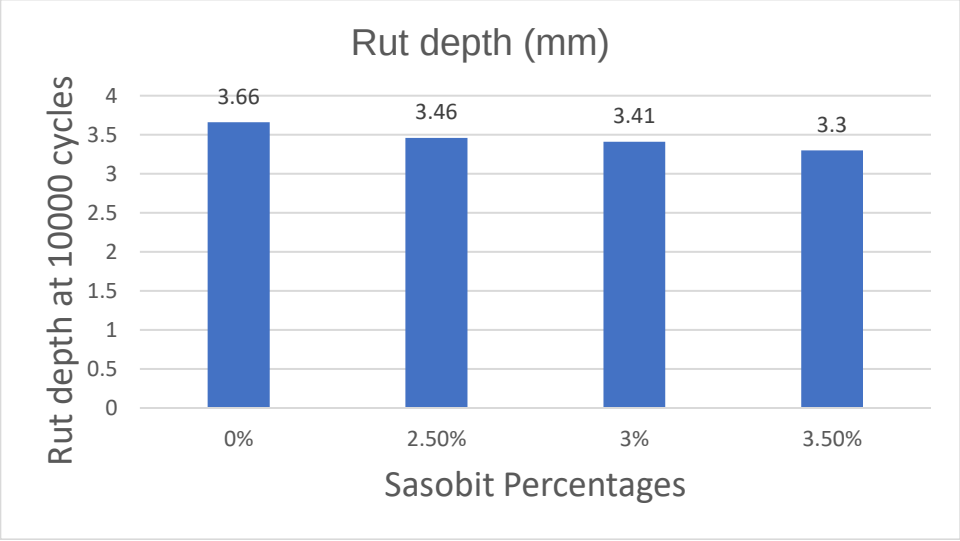

Figure 4: Rut depth with different percentages of sasobit

Stripping and Coating Test (AASHTO T182)

The stripping and coating test is performed for bitumen with 0% Sasobit and, 2.5%, 3%, and 3.5% Sasobit, and their results are obtained through visual observation by checking percent coating of samples. The value of stripping and coating for 0% Sasobit in bitumen is 97%. For 2.5% Sasobit, the value is 98%; for 3%, it is 98%; for 3.5% Sasobit, the coating is 99%. The bitumen aggregate has good coating at 3.5% Sasobit percentage.

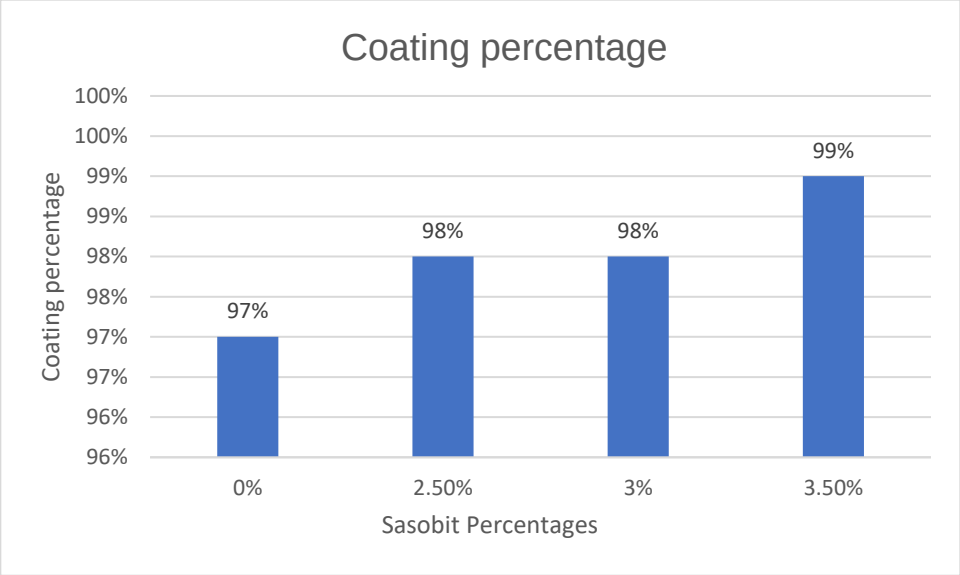

Figure 5: Coating percentage and sasobit Percentages graph

Figure 6: Stripping and coating Test sample before and after test

Indirect Tensile Modulus Test

At 25 °C, the indirect tensile modulus test was conducted on mixtures containing varying percentages of Sasobit to examine the reaction of the mixtures to loading at intermediate temperature. As shown in the Figure 6, from 0% to 3.5%, the resilient modulus of asphalt mixtures increases.

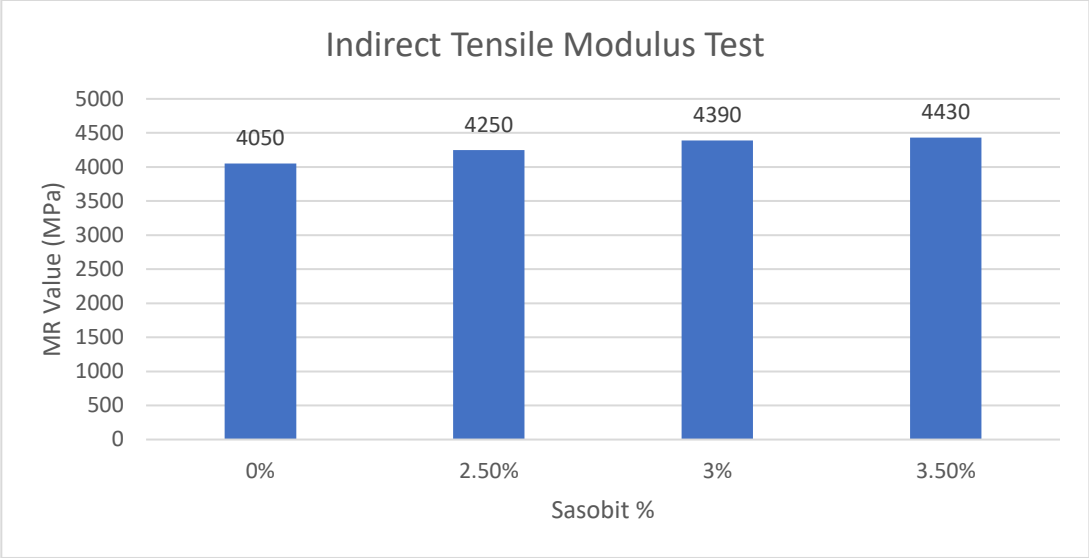

Figure 7: MR value and Sasobit percentages

CONCLUSIONS

The following conclusions are drawn from the study:

- Addition of 3.5% SASOBIT increases the Marshall stability value by 13.11% as compared to the conventional HMA.
- The wheel tracker test at 3.5% SASOBIT has minimal rut depth and resists rut better as compared to other dosages. Addition of 3.5% SASOBIT in asphalt mixture reduced the rut depth by 9.83%.
- The resilient modulus increases with the increase in modifier percentage. Presence of 3.5% SASOBIT in asphalt mixture enhanced the fatigue resistance by 9.38% as compared to regular HMA.
- By stripping and coating test of WMA, it is evident that all three percentages of SASOBIT have shown good moisture resistivity, with 3.5% dosage showing 99% coating as compared to 97% for conventional HMA.

- This research study concludes that asphalt performance parameters generally keeps on improving with increasing dosage of sasobit. However, the modifier manufacturer (sasol) recommends a dosage 3% (https://www.sasolgermany.de). As per manufacturer, dosage beyond 3% may affect the laying and compaction temperature requirement. It would be difficult to properly place the modifier asphalt mixture in the field at warm temperature which is counterintuitive as the main reason of using sasobit is reduction temperature from hot to warm.
- The test findings demonstrate that the WMA has greater resilient modulus, moisture resistivity, and rutting capability than the control HMA.

REFERENCES

1. Hui Ma, Zhigang Zhang, Xia Zhao, and and Shuang Wu. "A Comparative Life Cycle Assessment (Lca) of Warm Mixasphalt (Wma) and Hot Mix Asphalt (Hma) Pavement: A Case Study in China." *Hindawi Advances in Civil Engineering* (2019). https://doi. Org / https://doi.org/10.1155/2019/9391857.
2. Oner J, Sengoz B Utilization of Recycled Asphalt Concrete with Warm Mix Asphalt and Cost-Benefit Analysis. "*PLoS ONE 10(1):* (2015) e116180. https: // doi. org /10 .1 37 1/ journal. pone.0116180
3. Ali Behnood, A review of the warm mix asphalt (WMA) technologies: Effects on thermo-mechanical and rheological properties, *Journal of Cleaner Production* (2020), https://doi.org/10.1016/j.jclepro.2020.120817. Presence of 3.50% sasobit in asphalt mixture enhance the fatigue resistance by 9.38%.
4. Kheradmand, Behnam, Ratnasamy Muniandy, Law Teik Hua, Robiah Bt Yunus, and Abbas Solouki. "An Overview of the Emerging Warm Mix Asphalt Technology." *International Journal of Pavement Engineering* 15, no. 1 (2014): 79-94. https:// doi. Org / 10.1080/10298436.2013.839791.
5. Mayank Sukhija, Nikhil Saboo "A Comprehensive Review of Warm Mix Asphalt Mixtures-Laboratory to Field." *Construction and Building Materials* 2020.
6. Abdullah, Mohd Ezree, Kemas Ahmad Zamhari, Rosnawati Buhari, Siti Khatijah Abu Bakar, Nurul Hidayah Mohd Kamaruddin, Nafarizal Nayan, Mohd Rosli Hainin, Norhidayah Abdul Hassan, Sitti Asmah Hassan, and Nur Izzi Md. Yusoff. 2014. "Warm Mix Asphalt Technology: A Review". *Jurnal Teknologi* 71 (3). https:// doi.org /10. 1111 3/jt.v71.3757.
7. Jamshidi, Ali, Meor Othman Hamzah, and Zhanping You. "Performance of Warm Mix Asphalt Containing Sasobit®: State-of-the-Art." *Construction and Building Materials* 38 (2013): 530-53. https://doi.org/https://doi.org/10.1016/j.conbuildmat.2012.08.015.
8. Caputo, P.; Abe, A.A.; Loise, V.; Porto, M.; Calandra, P.; Angelico, R.; Oliviero Rossi, C. The Role of Additives in Warm Mix Asphalt Technology: An Insight into Their Mechanisms of Improving an Emerging Technology. *Nanomaterials* (2020), *10*, 1202. https://doi.org/10.3390/nano10061202

9. Hassan Ziari, Ali Moniri, Reza Imaninasab & Mostafa Nakhaei: Effect of copper slag on performance of warm mix asphalt, *International Journal of Pavement Engineering*, (2017): DOI: 10.1080/10298436.2017.1339884.
10. Syed, I.A., Mannan, U.A. & Tarefder, R.A. Comparison of rut performance of asphalt concrete and binder containing warm mix additives. *Int. J. Pavement Res. Technol.* **12**, 162–169 (2019). https://doi.org/10.1007/s42947-019-0021-4
11. Gunti, Uma shanker, and Javedali M Jalegar "A Performance Evaluation of Warm Mix Asphalt Mixture by Incorporating Sasobit Additive." *International Research Journal of Engineering and Technology (IRJET)* 4, no. 11 (2017).
12. Zhongkai Xu, Jingtao Shi, Lei Zhao, Ye Yuan, Nimrah Akram, Da Shan, Long Chen, Jianxin Li & Shi-Zhong Luo: A viscoelastic model and structural properties of Sasobit-modified asphalt, *Petroleum Science and Technology*, (2020) DOI: 10.1 080/ 1091 6466 .2020.1767646
13. Mogawer, Walaa S., Alexander J. Austerman, and Hussain U. Bahia. "Evaluating the Effect of Warm-Mix Asphalt Technologies on Moisture Characteristics of Asphalt Binders and Mixtures." *Transportation Research Record* 2209, no. 1 (2011): 52-60. https:// doi.Org/10.3141/2209-07.
14. Yang, Shih-Hsien, Firmansyah Rachman, and Hery Awan Susanto. "Effect of Moisture in Aggregate on Adhesive Properties of Warm-Mix Asphalt." *Construction and Building Materials* 190 (2018): 1295-307. https://doi.org/https://doi.org/10.1016/j.conbuildmat.2018.08.208.
15. Rossi, C.O.; Caputo, P.; Baldino, N.; Lupi, F.R.; Miriello, D.; Angelico, R. E ects of adhesion promoters on the contact angle of bitumen-aggregate interface. Int. J. Adhes. Adhes. 2016, 70, 297–303.
16. Baldino, N.; Gabriele, D.; Lupi, F.R.; Rossi, C.O.; Caputo, P.; Falvo, T. Rheological e ects on bitumen of polyphosphoric acid (PPA) addition. Constr. Build. Mater. 2013, 40, 397–404.
17. Caputo, P.; Porto, M.; Calandra, P.; De Santo, M.P.; Rossi, C.O. E ect of epoxidized soybean oil on mechanical properties of bitumen and aged bitumen. Mol. Cryst. Liq. Cryst. 2018, 675, 68–74.
18. Cover: STILPUNKT3 Designbüro, p. 2: Fotolia / Cmon, p. 5: Fotolia / surawutob, p. 9: V. / Rosauer. / Schäfer, p. 12: iStock / chinaface, p. 14: Fotolia / 06photo, p.15: Fotolia / surawutob, agenda / Michael Kottmeier

2nd International Conference on Advances in Civil and Environmental Engineering (ICACEE-2023)

University of Engineering & Technology Taxila, Pakistan

Conference date: 22nd and 23rd February, 2023

Effect of Temperature & Moisture Exposure Time on Binder-Aggregate Bond Strength

Adnan Khan[1], Imran Hafeez[2],

[1] Msc Scholar, Department of Civil Engineering, University of Engineering and Technology Taxila, Pakistan,engradnan2017@gmail.com

[2] Professor, Department of Civil Engineering, University of Engineering and Technology Taxila, Pakistan,ImranHafeez783@yahoo.com

ABSTRACT

This study was carried out to explore the effect of moisture exposure under varying temperature on binder-aggregate bond strength. Nanoclay (organophilic clay) modification, and different aggregate types were used for a broad range of chemical and physical conditions of the asphalt–aggregate interface. Nanoclay were blended in an asphalt binder in various percentages (starting from 3% to 5%). The result showed that aggregate type, moisture& temperature condition mainly affect the binder-aggregate bond strength.The bitumen bond strength of nano clay modified binders was enhanced at all percentages by a comparison with both virgin binders under dry & wet condition. The best improvements in the modified binders were obtained with 4.5% nanoclay..

KEYWORDS: asphalt binder, nanoclay, bitumen bond strength, pots, bbs, moisture damage, organophilic clay

INTRODUCTION

The Road network is the basic requirement for transportation facilities. Therefore, pavement should be strengthened and stabilized to withstand against any kind of distresses. The Situation most road engineers are familiar with the terms "adhesion" and "stripping". The surface phenomenon of adhesion of the bituminous binder to the aggregate is related to the physicochemical properties of the two components. The two main reasons for the lack of adhesion of a bituminous mixture are insufficient bond formation and loosening of the aggregate binder in the presence of water.

The main causes of these problems are traffic loading and moisture damage. Moisture damage in an asphalt mixture is the loss the bond strength and stiffness. Moisture damage increases failures such as bleeding, cracking, rutting, and raveling, diminishing the asphalt pavement's integrity. As a result, it is critical to understand the failure of moisture damage mechanisms of asphalt pavements and to evaluate the best material combination to resist moisture damage.

M. El-Shafie(2012) used both macroclay and modified nanoclay, blended in an asphalt binder in various percentages. The results of the study indicated that tensile strength of modified clay binders was enhanced. Raul Velasquez (2013) studied the changes in the mechanical properties of asphalt binder after water conditioning for extended periods of time.it was observed that after nine months of water conditioning the rheological properties of the binder changes significantly. The asphalt binder becomes stiffer as function of conditioning time. Lorenzo Paolo Ingrassia (2019) performed BBS test on bio-binders and different aggregate substrate, the main results show that the bio-binders exhibit a good adhesion with limestone both in dry and wet conditions. Andrea Graziani (2018)

evaluated the bond strength between a bitumen emulsion, a cold mastic prepared using limestone filler and two aggregate substrates (limestone and basalt), The results demonstrated that, both emulsion and mastic showed good affinity with the aggregate substrates, the adhesion bond between emulsion and basalt substrate was the most durable and that the use of a limestone filler penalised the moisture sensitivity of the systems. The BBS test was also able to show the positive effect of curing time and temperature on the bond strength. According to Preeda Chaturabong (2016), that surface area and mineralogy of mineral fillers have significant effects on moisture damage resistance. He also mentioned that there is a significant effect of asphalt modification on moisture damage measurements. Reza Bionghi (2021) studied the effects of the aging and stiffness of the asphalt binder, aggregate type, and their interactions on the bond strength and moisture susceptibility of the asphalt binder-aggregate systems, the results indicated that the changes in the adhesive and cohesive failures in the asphalt binder-aggregate compositions highly depend on the SFE properties.

Objectives

• Evaluation of the effect of conditioning period & temperature on bond strength of asphalt binder. • Evaluation of the effect of modifier (organophilic clay) on bond strength of asphalt binder and different aggregate types.
• To compare the adhesive strength of modified and virgin asphalt binder.

Materials & Testing Procedure

The material employed in this study are asphalt binder, aggregate substrates, organophilic clay. One type of bitumen (ARL 60/70 pen) and two aggregate types (limestone& granite) and organophilic clay modification were used for this study.

Materials

In this research study, two aggregate type, granite (acidic in nature) and lime stone (basic in nature) were selected. Asphalt binder from Attock Refinery oil limited (ARL 60/70), were used. The basic physical properties of the asphalt binder were quantified by following the ASTM standards in Table 1.

Table 2: Physical properties of the asphalt binder (ARL 60/70)

Properties	**Standard Code**	**Unit**	**ARL 60/70**	**Specification Limit (minimum)**
Penetration 0.1 mm at 25°	ASTM D5	1/10 mm	62	80
Softening Point	ASTM D36	°C	49	46
Ductility at 25°C	ASTM D36	cm	102	100
Dynamic Viscosity	ASTM D4402	cP	384.5	300
Specific gravity at 25°C	ASTM D113	-	1.02	1.01

Nano material:

In this study nano clay (organophilic clay) were used as shown in figure 1. It is generally prepared from smectite clay such as sodium bentonite having moisture content up to 10% are sprayed within activator substance that is ammonium sulphate and compacted mechanically. Pretreated clay is reground to provide organophilic clay.

Fig.1 Organophilic clay

BBS Test

BBS test is used to determine the bonding properties between aggregate and bitumen in the dry conditioning and after moisture conditioning. The BBS test involves subjecting a pull stub adhered to an aggregate substrate to a normal force created by increasing pneumatic pressure. The BBS device consists of metallic pull-off stub, reaction plate, pressure hose, piston, and a portable pneumatic adhesion tester. During the testing, pull-off force is used to separate metallic stub from aggregate surface.

POTS is calculated as

$$POTS = \frac{(BP \times A_g) - c}{A_{ps}}.$$

Where:

POTS = Pull off tensile strength (kPa)

BP = Burst pressure (kPa)

AG = Contact Area of Gasket with Reaction Plate (mm2)

C = Piston Constant (Provided by manufacturer)

APS = Area of pull-off stub (mm2)

Fig.2 BBS DEVICE

Sample Preparation

Aggregate plates were cut with size of 10" x 6" x 2" then it were immersed in distilled water in an ultrasonic cleaner for 60 min at 60°C in order to remove residue from the cutting process and to neutralize the surface of aggregate into its original condition. The surface of pull-off stub was degreased with acetone/carbon tetrachloride to remove any dust which might affect the bond. These clean stubs were placed in an oven in order to eliminate water from its surface. Bitumen Samples were prepared by modifying base bitumen with 3%, 3.5%, 4%, 4.5and 5% organophilic clay by weight of bitumen in accordance to AASHTO-T91 recommendation. Before testing, for dry conditioning samples were left at room temperature for 24 hours and for wet conditioning samples were first left at room temperature for 1 hour to allow for the aggregate-bitumen-stub system to reach a stable temperature. Then samples were submerged into a water tank at 20°C, 28°C & 40°C for 24,48, and 96 hours.

Fig.3 Lime Stone (aggregate substrate)

Fig.4 Granite (aggregate substrate)

RESULTS AND DISCUSSION

Effect of Temperature on Bond Strength

BBS test was performed on prepared samples after dry conditioning at 20°C, 28°C and 40°C .the results for the effect of temperature are presented in Fig 5 as combined bar charts for granite & limestone aggregate. It was observed that Nano clay modified bitumen have higher dry average pull-off tensile strength in comparison to the neat bitumen for both granite and limestone aggregates. The POTS values for all modified binders were increased with increasing nano clay content up to 4.5% compared with virgin binder. The maximum dry average pull-off tensile strength was recorded with 4.5% nanoclay content for both granite and limestone aggregates Decrease in bond strength was observed as conditioning temperature increases, due to a lower asphalt binder stiffness. The decrease in POTS is not consistent for aggregate/asphalt binder combinations, the drop in bond strength was low in case of granite aggregate when the conditioning temperature was increased.

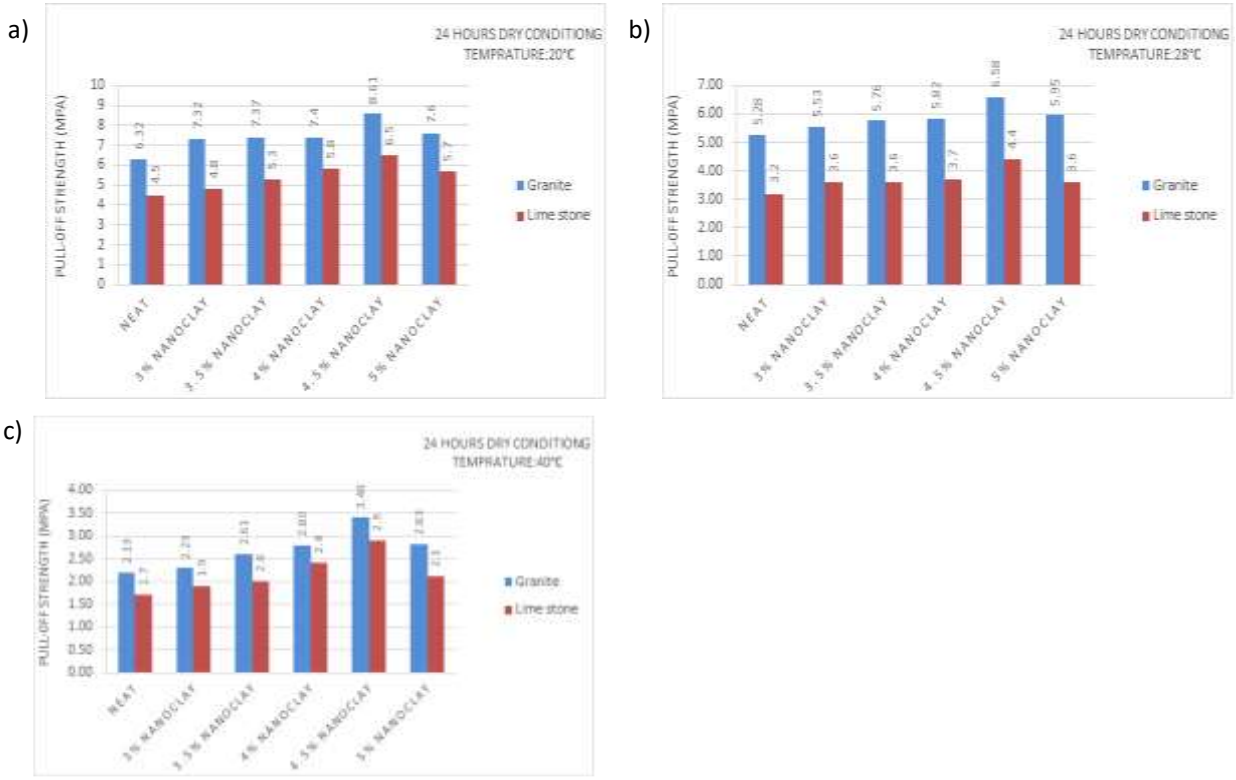

Fig 5: BBS TEST RESULTS

Effect of Moisture Exposure on Bond Strength

In this research study, samples were conditioned in water for 24, 48 and 96 hours at 20°C, 28°C & 40°C. The effect of conditioning time on bond strength can be observed in Fig 6.the conditioning of samples in water caused a significant reduction in the pull-off tensile strength .As water penetrates through the aggregate, it weakens the bond at the interface. The longer the conditioning time in water, the weaker the interface bond and the lower the pull-off tensile strength. The samples were initially conditioned in water for 24 hours at 20°C, As it can be seen from Fig.(8-10) the reduction in bond strength was observed for both limestone and granite aggregate however the maximum improvement in moisture damage resistance is realized with nanoclay content upto 4.5%.the average POTS value for neat binder with granite & lime stone aggregate is 2.82 & 3.63MPa.however with nanoclay dosages, POTS values were increased ,In wet condition, the maximum bond strength values were obtained at 4.5% nanoclay content, which are 3.69MPa for granite &5.82MPa for limestone. When the conditioning temperature was increased to 28°C, Further reduction in bond strength was observed, the drop in bond strength was high in case of granite aggregate as compare to limestone aggregate, irrespective of nanoclay modification. By further increasing the conditioning temperature to 40°C, similar trend were followed.

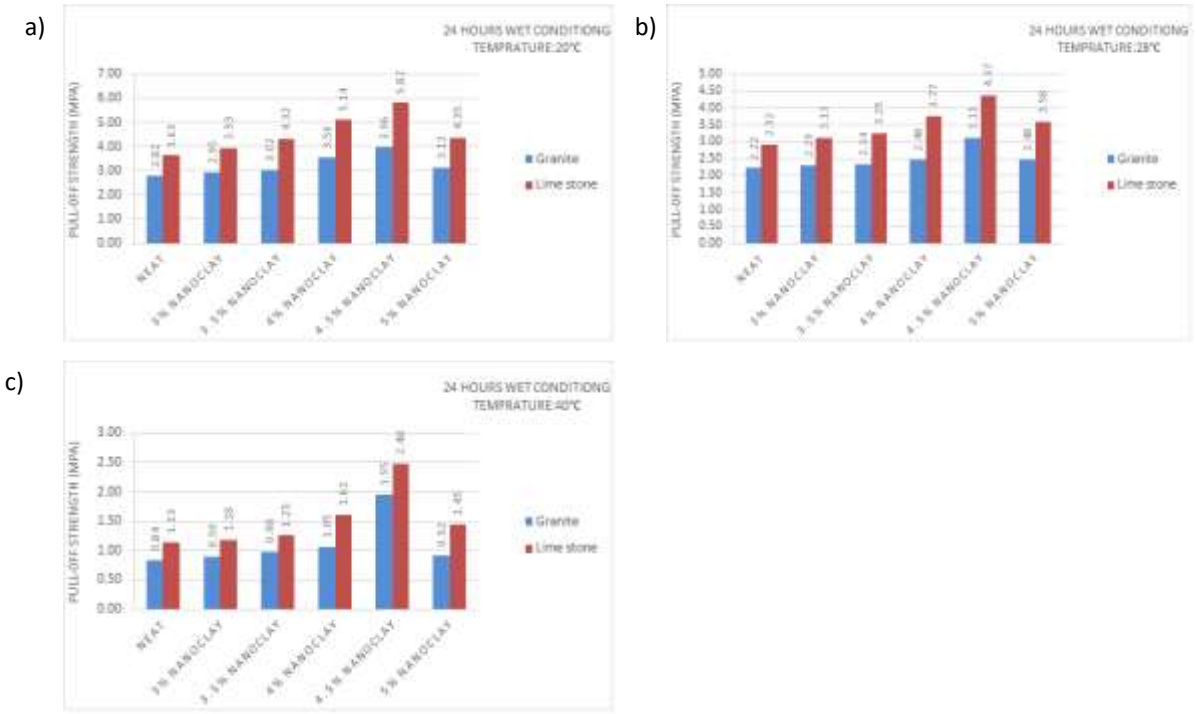

Fig 6: BBS TEST RESULTS

EFFECT OF NANOCLAY MODIFICATION:

According to Fig.(5-6), the interesting finding is that the increase of nanoclay dosage from 3% to 4.5%, the POTS keep increasing, further increase in nanoclay dosage reduces bond strength. The optimum dosage for nanoclay modification can be selected at 4.5%,Since at this concentration nanoclay modified binder shows higher POTS at both dry condition & wet condition in all cases I-e varying temperature and conditioning time.

EFFECT OF AGGREGATE TYPE

The nature and chemical characteristics of aggregates greatly affect the bitumen bond strength, different types of aggregates have different chemical composition and thus behave differently especially under different moisture conditions. In this research study two aggregate types were used I-e granite & lime stone. From Fig.(5-6), it can be clearly observed that granite had higher bond strength in dry condition but when it was exposed to wet conditioning, due to its high moisture sensitivity, bond strength values drastically dropped. Similarly, it can also be observed that lime stone has also high bond strength in dry condition but when it was subjected to wet condition, bond strength was dropped but not as much as in the case of granite due to its hydrophobic nature.

CONCLUSION

This research study was mainly conducted to investigate the effect of temperature & moisture on bitumen-aggregate bond strength under varying condition, the following conclusion can be with drawn.

1. Pull-off tensile strength mainly depend upon aggregate type, chemical composition, porosity & surface texture.
2. Limestone & Granite both exhibit better bonding characteristics in dry condition, limestone has the lowest decrease in bond strength in wet condition.
3. The POTS values were decreased under wet condition irrespective of aggregate type and binder modification.
4. Nanoclay modification enhanced POTS values irrespective of aggregate type and testing condition, 4.5% is the optimum nano clay dosage on which high bond strength is obtained.

REFERENCES

[1] M. El-Shafie, I.M. Ibrahim, A.M.M. Abd El Rahman (2012). The addition effects of macro and nano clay on the performance of asphalt binder

[2] Raul Velasquez Reyes, Lizcano Fredy, Hussain Bahia (2013). Effect of Water Conditioning for Extended Periods on the Properties of Asphalt Binders

[3] Lorenzo Paolo Ingrassia, Fabrizio Cardone, Francesco Canestrari (2019). Experimental investigation on the bond strength between sustainable road bio-binders and aggregate substrates.

[4] Andrea Graziani . Amedeo Virgili . Fabrizio Cardone(2018). Testing the bond strength between cold bitumen emulsion composites and aggregate substrate

[5] Mohammad Ali Khasawneh , Dania Mohammad Al-Oqaily, Anas Hisham Abu Alia and Aslam Ali Al-Omari(2020). Evaluation of aggregate-binder bond strength using the BBS device for different road materials and conditions

[6] Sara Anastasio, Inge Hoff, Hussain Bahia (2015).Laboratory Testing Methods for Evaluating the Moisture Damage on the Aggregate-Asphalt System.

[7] Jorge Lucas Junior, Lucas F. A. L. Babadopulos, J. B. Soares (2020). Influence of Aggregate–Binder Adhesion on Fatigue Life of Asphalt Mixtures.

[8] Lu Zhou, Weidong Huang ,Yuan Zhang , Quan Lv , Chuanqi Yan, Yi Jiao (2020). Evaluation of the adhesion and healing properties of modified asphalt binders

[9] Raquel Moraes, Raul Velasquez, Hussain Bahia (2015). The Effect of Bitumen Stiffness on the Adhesive Strength Measured by the
Bitumen Bond Strength Test.

[10] Weidong Huang and Lu Zhou(2017). Evaluation of Adhesion Properties of Modified Asphalt Binders with Use of Binder Bond Strength Test

[11] Preeda Chaturabong & Hussain U. Bahia (2016). Effect of moisture on the cohesion of asphalt mastics and bonding with surface of aggregates

[12] Syeda Aamara Asif, Naveed Ahmed, Aneeqa Hayat, Sabahat Hussan, Faisal Shabbir and Khalid Mehmood (2018). Study of adhesion characteristics of different bitumen aggregate combinations using bitumen bond strength test.

[13] Reza Bionghi , Dariush Shahraki , Mahmoud Ameri , Mohammad M. Karimi (2021). Correlation between bond strength and surface free energy parameters of asphalt binder-aggregate system.

2nd International Conference on Advances in Civil and Environmental Engineering (ICACEE-2023)

University of Engineering & Technology Taxila, Pakistan

Conference date: 22nd and 23rd February, 2023

Laboratory Evaluation of Asphalt Mixture properties modified with Biomass Ash and Waste Engine Oil

Sana Tehseen[1], Dr. Syed Bilal Ahmed Zaidi[2], M Raheel Rashid[3], Ayesha Ali[3]

[1]Research Scholar, Department of Civil Engineering, University of Engineering and Technology, Taxila. sana.tehseen85@gmail.com

[2]Associate Professor, Department of Civil Engineering, University of Engineering and Technology, Taxila. bilal.zaidi@uettaxila.edu.pk

[3]Co-Research Scholar, Department of Civil Engineering, University of Engineering and Technology, Taxila. raheelz111@gmail.com, ayesky83@gmail.com

ABSTRACT

The need for ongoing study on the utilization of waste materials has arisen as a result of the fact that the profession of road building today is more challenged than ever due to limited and rising cost of resources for component ingredients of asphalt mixes. The performance of an asphalt mixture is affected by its constituent parts. This study shows the effectiveness of asphalt mixes when biomass fillers such as RHA (rice husk ash), WSA (wheat straw ash) and WEO (waste engine oil) are incorporated. Moreover, addition of these components not only help in enhancing qualities of asphalt but also their use in asphalt mixtures helps to lessen environmental issues. In this research, Waste engine oil (2% and 4%), as well as biomass ashes (2%, 4%, and 6%), are utilized. Thus, virgin bitumen is modified using WEO with 2% and 4% ratios, RHA with 2% 4% 6% ratios, and WSA with 2% 4% 6% ratios. Moreover, the modified binder specimens are examined for asphalt mixture properties by performing adhesion and mixture testing along with the conventional testing. Semi-circular tests and wheel tracking tests are conducted using 12 distinct combinations for the laboratory evaluation of asphalt mixture properties modified with biomass ash and waste engine oil. Results show significant improvement in binder and asphalt mixture performance by adding certain percentages of bio ashes in comparison to virgin binder. RE-3 showed the best performance in all 12 combinations considering binder, mixture, and adhesion test results. There is need to perform more mixture testing to evaluate exact behaviour of these mixtures.

KEYWORDS: Asphalt mixture, WEO **(**Waste Engine Oil), RHA (Rice Husk Ash), WSA (Wheat Straw Ash),

INTRODUCTION

Mankind has been continuously depleting capacity of our planet to meet his needs and recklessly discards garbage at the cost of environmental damage. As a result, the necessity to reduce usage of finite primary resources is becoming ever more critical in most industries. This also applies to the transportation sector. The need for improved road paving materials arises from rising traffic density and increasing permissible axial loads. The goal of highway authorities is to provide affordable, secure, and long-lasting pavements to support the expected loads [1]. Flexible

pavements have been constructed with hot mix asphalt since a very longer period of time. With the help of this standard mix formula (hot mix asphalt), several stress-related challenges arise, leading to rutting, damage due to moisture content and fatigue cracking. These issues are caused by overloading, changing climate, hot and cold temperature and moisture [7-8]. Due to its high in-service performance, asphalt mixture is the most often utilized material in road paving. The asphalt mixture is a blend of filler, asphalt binder, and aggregate. Filler is a crucial component because the basic dispersed system in an asphalt mixture, known as asphalt mastic, is created by combining binder and filler. Filler is used in hot mix asphalts to improve the rutting behavior, wearing performance, and prevention of damage due to moisture [2-4]. To address every issue connected to stress in road structure, modification of binder is the prime choice. In order to prevent cracking, wear as well as tear, and damage due to moisture, various asphalt mixture alterations and modifications are made [9].

Increase in population resulted in rapidly growing solid wastes. Consequently, huge dumping sites are created which pose a threat to environment and human health. Scarcity of land for dumping these wastes is also an important issue [10]. Growth in Industrial sector and increased raw material usage are to blame for fast depletion of the natural resources. Waste disposal methods and recycling procedures are insufficient to deal with widespread resource extraction and shortage of raw materials. [5-6].

The world's overall economic growth is significantly influenced by the agricultural sector. Agriculture-related waste production has increased as a result of increased agricultural disposal and farming activities. Considerable quantity of wastes is generated due to harvesting of crops. Straws, husks, and bagasse are among the agricultural wastes that are harvested in enormous volumes each year. These wastes are mainly burned by industries, mills and plants to fulfil their energy demands which results in tons of biomass ash. Also, environmental effects, such as an increase in the emissions of greenhouse gases that contribute to global warming, have also been caused by the open burning of crop waste [13]. Data collected from FAO research shows that about 7.82E + 08 tons of rice and 7.34E + 08 tons of wheat are produced every year respectively. Thus, 200 kg of rice husk carries one ton of rice [11] and 1-ton grains of wheat produce almost 1300kg to 1400 kg straws of wheat [12].

Waste engine oil is generally a petroleum product. Waste engine oil is defined as any petroleum-based or synthetic oil that has undergone contamination and has lost its initial qualities or is no longer appropriate for its intended use. It goes through physical and chemical processes thus picking up contaminants. Waste engine oil includes difficult-to-decompose non-biodegradable components. Waste engine oil might harm the environment irreparably if it is dumped carelessly. The need set forth in European Directive 2009/28/EC [2] to produce 20% of the energy from renewable sources by 2020 has prompted a rise in the construction of biomass-fuelled power stations in recent years. In order to conserve finite resources, to save cost of construction, and to address environmental contamination, numerous academics have attempted to evaluate the possibility of using agriculture wastes and fuel by-products in the asphalt business. These by-products and end products, including palm oil, sugarcane bagasse, ashes from palm oil fuel, rice husk ash, wood waste and wheat husk ash, are viewed as potential raw materials for generating substantial products [14].

However, there has been relatively little research on applications in asphalt binder and asphalt concrete. It has been discovered that adding 50% RHA and 50% lime stone filler to Hot Mixed Asphalt Concrete (HMA) significantly increases the Marshall stability of the asphalt concrete [15].

RHA's primary impact on rutting and fatigue was determined by Arabani and Tahami's evaluation of the mechanical properties of the asphalt mixture modified by RHA [16]. A systematic examination of how HL disruption affected the amount of moisture in bitumen mastic and asphalt mixtures was carried out by Zaidi et al. RBT, BBS tests, among other methods, can be used to evaluate moisture damage, and asphalt concrete modified with HL has shown improved adhesion and resistance to moisture damage [17].

In 2016, researchers looked into how RHA as a filler affected asphalt mixes' resistance to moisture and Marshall stability. The study's findings suggested that adding RHA might boost mix stability by 65%. In addition, RHA asphalt mixes outperformed standard mixes in terms of indirect tensile strength and moisture resistance. [18]. Later, in another study (by Muhammad Huzaifa), the results were improved by adding waste engine oil in addition to biomass ashes in "EVALUATION OF ASPHALT BINDER PROPERTIES MODIFIED WITH BIOMASS ASH AND WASTE ENGINE OIL."

As RHA and WSA are dumped in large quantities, it creates a problem with land filling. Also, WEO is dumped in rivers where it is carelessly littered. Thus, endangering reservoirs of water and causing harm to habitat, nature and health of human beings. On the other hand, the natural resources are swiftly running out due to the constant rise in demand for petroleum goods. Utilizing as much waste as possible in the asphalt mixture can assist in resolving these issues. As a result, different bio ashes (RHA and WSA) and WEO combination will now be used for testing asphalt mixtures. So, using this waste, bitumen save will be evaluated. With the addition of this waste material to the asphalt mixture, bitumen usage will also be monitored.

MATERIALS

The materials used in this research are bitumen, wheat straw ash (WSA), rice husk ash (RHA), waste engine oil and natural limestone aggregate form local source.

Asphalt binder

All mixture types were created using the ‘Attock oil refinery's asphalt binder, grades 60 to 70. In Pakistan, 60-70 Pen grade bitumen is a widely utilized form of binder which was made by ‘Attock refinery limited (ARL) situated near Rawalpindi, Pakistan. The elementary properties of the base binder comprised the softening point of 49°C, the mean penetration (1/10 mm) of 64, ductility is 108 cm.

Aggregates

The aggregates are obtained from local quarries which are natural limestone in occurrence. The mechanical properties of collected aggregates are as follows: 30.67% Elongated, 4.30% Water

absorption, 23.20% Los Angeles abrasion, 84.30% Sand equivalent, 43.78% Flakiness, 100% Fractured particles and OBC is 4.30%.

Rice husk ash (RHA) and Wheat straw ash

Agriculture waste ashes (RHA and WSA) were collected from local mills based in Pakpattan, Pakistan. Rice husk and wheat straw were heated in a furnace, at 500-800 ^{o}C for 2h, to get ashes.

Waste engine oil (WEO)

Waste engine oil includes difficult-to-decompose non-biodegradable components. Waste engine oil was collected from local auto-repair shop. WEO was filtered, to remove solid impurities to ensure usefulness.

Figure 3: Images of materials used

Figure 2: Semi-circular test.

Figure 3: Cooper Wheel tracking

METHODOLOGIES

RHA with 2%, 4% and 6% is added with WEO (2% & 4%) in asphalt binder. WSA with 2%, 4% and 6% is added with WEO (2% & 4%) in asphalt binder. By taking a percentage of the asphalt binder's weight, modified asphalt is prepared. To achieve effective mixing of RHA (rice husk ash) and WSA (wheat straw ash) with WEO (waste engine oil) to get altered asphalt, a shear mixer with a 1500 rpm speed is employed. The mixing takes place for 45 minutes at 140°C. Mixture of bitumen blend and limestone accumulation was heated at 145 °C throughout the sample preparation to ensure the strong bond. Thus, virgin bitumen has been modified using WEO with 2% and 4%, RHA with 2% 4% 6%, and WSA with 2% 4% 6%. In addition to conventional testing, the modified binder specimens are examined for mixture and adhesion testing. Different binder combinations are utilized to address rutting, fatigue, and moisture damage. Material combinations are shown in table 1.

By executing the penetration and softening point tests in accordance with ASTM D5[19][20], ASTM D36[21], respectively, the effects of RHA and WSA in WEO binder were identified. The softening point test simulates the bitumen's deformation properties under high temperatures. The ductility value provides an insight into the asphalt binder's tensile capabilities. The penetration value is a measure of the asphalt binder's stiffness at room temperature The degree of fluidity (viscosity) is graded. The higher grade indicates stiffer bitumen.

Table 1: Ratio of Material Combination

Sr. no	Material Combinations	Material ratios
1	RE-1	2%WEO+2%RHA
2	RE-2	2%WEO+4%RHA
3	RE-3	2%WEO+6%RHA
4	RE-4	4%WEO+2%RHA
5	RE-5	4%WEO+4%RHA
6	RE-6	4%WEO+6%RHA
7	WE-1	2%WEO+2%WHA
8	WE-2	2%WEO+4%WHA
9	WE3	2%WEO+6%WHA
10	WE-4	4%WEO+2%WHA
11	WE-5	4%WEO+4%WHA
12	WE-6	4%WEO+6%WHA

RESULTS AND DISCUSSSION

CONVENTIONAL TESTING RESULTS

The softening point is higher than average at RE-3, resulting bitumen is stiff. A lower penetration number suggests a stiffer binder. Since its penetration value is lower than that of other combinations, Table 2 demonstrates how RE-3 in bitumen stiffens the binder. RE-3 has a lower ductility value than other combinations. The bitumen's increased stiffness was the cause of the decrease in ductility. According to the experimental findings, all adjusted binder percentages behave

more viscously than base binder. The findings indicate that the value of 249 CPs at RE-3 is the highest value (optimum) when evaluated against all altered and basic binder samples.

Table 3: Conventional Testing Results

Sr no	material combinations	Softening Point	Ductility	Penetration	Viscosity (CPs)
1	RE-1	50	98	60	235
2	RE-2	53	80	57	240
3	***RE-3***	***55***	***75***	***54***	***249***
4	RE-4	49	101	62	211
5	RE-5	51	83	60	217
6	RE-6	53	79	57	222
7	WE-1	49	96	65	220
8	WE-2	54	82	58	228
9	WE3	53	77	56	240
10	WE-4	48	100	65	212
11	WE-5	49	88	61	215
12	WE-6	51	82	58	222
13	Virgin	48	103	65	210

Mixture testing

Semi-circular Bending test (ASTM D8044-16)

The specimen is positioned beneath a loading rig, and after the standard frequency/temperature sweep, the material's modulus can be ascertained. The specimen can then be loaded repetitively until failure takes place. Figure 4 and 5 shows results for different combinations of WSA, RHA and waste engine oil. The results show improved behaviour and better resistance to cracking for all the combinations as compared to virgin combination. RE-3 shows failure load of 258KN, which is the highest load when compared to each sample of a basic and changed binder.

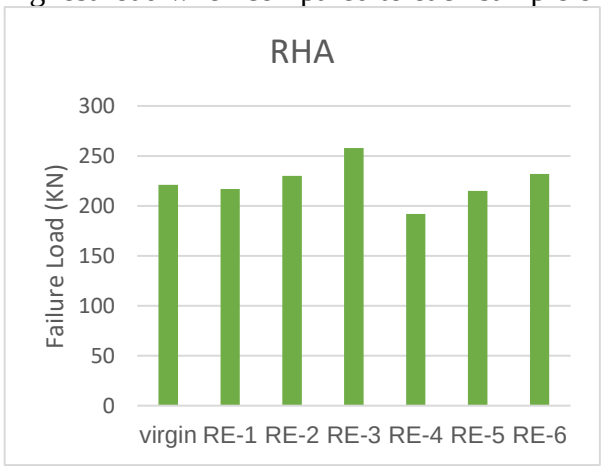

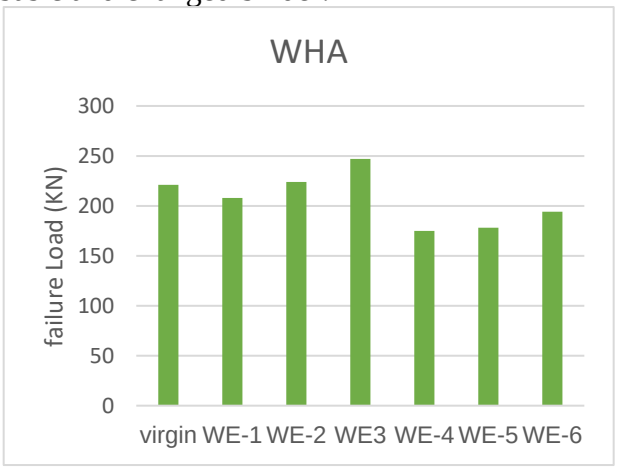

Figure 4: Semi-circular bending test for RHA *Figure 5: Semi-circular bending test for WSA*

Cooper Wheel tracking test (AASHTO T 324)

Wheel tracker test was performed at 55 ◦C for 10000 cycles with 15mm maximum allowable rutting depth. The test temperature was maintained throughout the test. Specimen thickness was taken as 50mm. Dynamic stability, rate of deformation, and maximum rut depth were all determined from the test data. Figure 4 and figure 5 shows results for wheel tracking test for different combinations of WSA, RHA and waste engine oil. RE-3 and WE-3 show the lowest rut depths compared to virgin and all other combinations. In Figure 6 it can be seen that with the increase of RHA in 2% oil the rut depth in decreasing gradually and similar trend has been observed with 4% WEO. In Figure 7 the addition of WSA in WEO has also improve the rut performance with the increase in WSA percentage. So from the results it can be concluded that addition of RHA and WSA can improve the rut resistance of the asphalt mix modified with WEO.

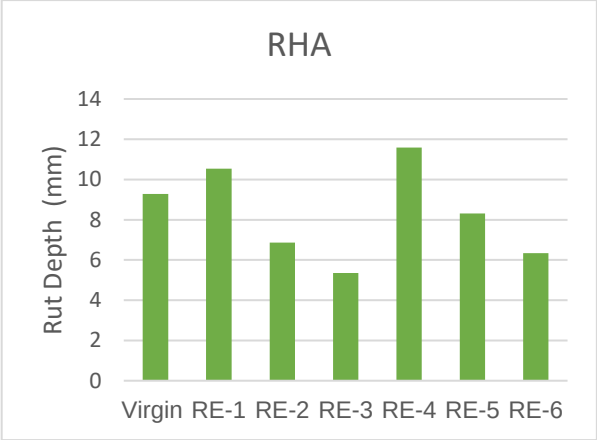

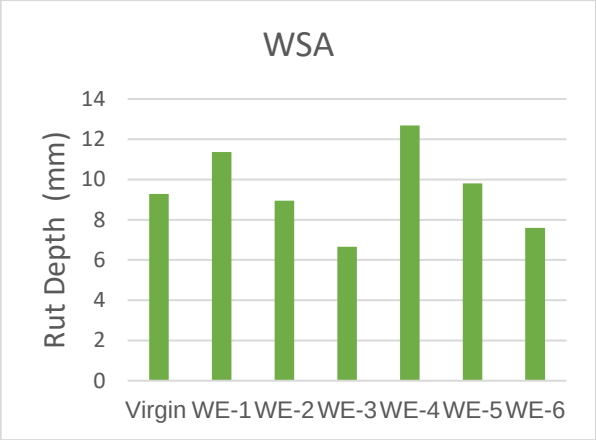

Figure 6: Wheel Tracking Test for RHA *Figure 7: Wheel Tracking Test for WSA*

Adhesion testing

Bitumen bond strength test (BBS) (ASTM D 4541)

Pneumatic Adhesion Tensile Testing Instrument (PATTI) was used according to BBS test and in keeping with ASTM D-4541 to explore mentioned bituminous bonding with aggregate incorporation under dry and wet conditions [19]. It is clear that adding more RHA and WSA to selected blends while the samples were being dried enhanced the POTS (Pull-Off Tensile Strength) values of the RHA & WSA modified specimens significantly. The decline in POTS values under moist conditions is due to the bond weakening caused by water activity at the bitumen-aggregate interface.

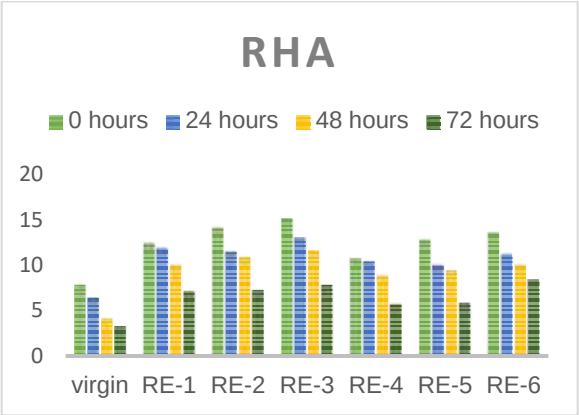

Figure 8: Bitumen bond strength test for RHA

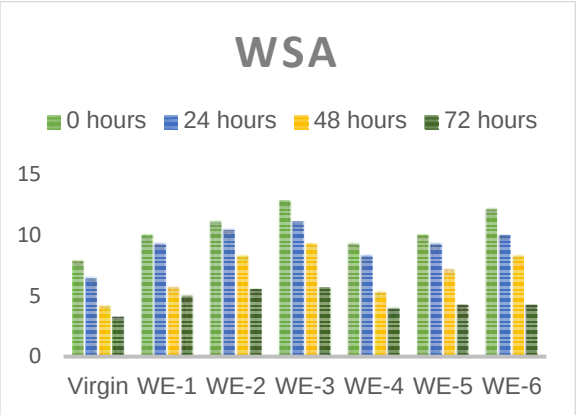

Figure 9: Bitumen bond strength test for WSA

Rolling Bottle Test (BS EN 12697-11:2012)

A qualitative test to assess the loose, compacted asphalt mix's sensitivity to moisture is the rolling bottle test. The purpose of the test is to measure the bitumen-aggregate adhesive bond during mechanical water abrasion. RBT in accordance with BS EN 12697-11 was carried out to examine the sensitivity to moisture. A mixture of 170g aggregate and 8g bitumen was used to prepare the sample. After rolling for 6, 24, 48, and 72 hours, samples of the bitumen coating on those samples were obtained. When exposed to wet conditions for a variety of times, the percentage coating around aggregates improved in comparison to base binder. At 6, 24, 48, and 72 hours, RE-3 combination was found to have a better coating than other combinations.

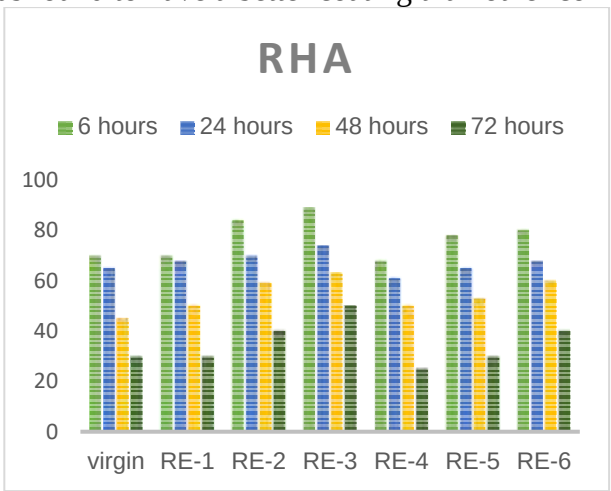

Figure 10: Rolling bottle test for RHA.

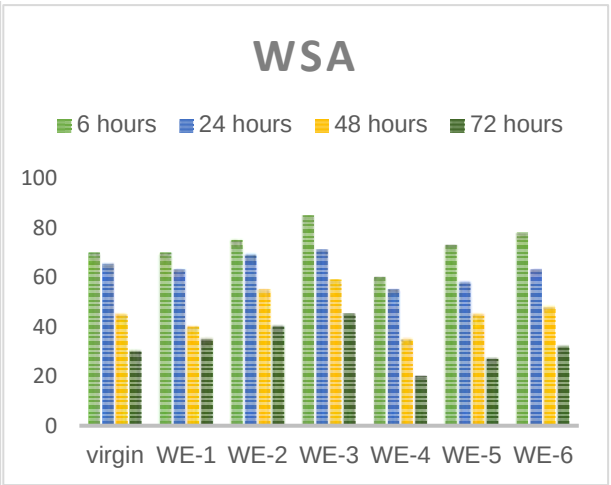

Figure 11: Rolling bottle test for WSA.

CONCLUSION

- Conventional bitumen testing involves softening point, penetration, ductility and viscosity. The outcomes of the research suggests that the inclusion of RHA (rice husk ash) and WSA

(wheat straw ash) in aforementioned bitumen modified with WEO stiffens the binder and bring back its viscosity to the required level which was declined due to waste oil.

- In semi-circular bending test for mixture evaluation, RE-3 shows failure load of 258KN as compared to failure load of 221KN for virgin combination, which shows that RE-3 shows better behaviour.
- In wheel tracking test RE-3 gave 5.35 mm rut depth which is minimum in all combinations. This depicts clear improvement against rutting due to induced stiffness by adding RHA+WEO (2%+6% respectively).
- Adhesion testing involves BBS (bitumen bond strength) test and RBT (rolling bottle test). Under dry conditions significantly enhanced POTS (Pull-Off Tensile Strength) values were observed of the RHA & WSA modified specimens. But the POTS values for each wet conditioned specimen were lower. This is because water impact at the bitumen-aggregate interface weakens the connection, resulting in a decrease in POTS values. Similar trends were observed in RBT testing.
- Overall, these 12 combinations show better behaviour in conventional bitumen testing, mixture testing and adhesion testing in comparison with virgin binder with RE-3 give the best performance.
- There is need to perform more mixture testing to evaluate exact behaviour of these mixtures.
- In order to achieve, understand and check high temperature biomass ashes behaviour on a large scale, an extensive and in-depth study is required which involve investigation of carbon emissions in environment. Thus, this investigation is a large-scale project which is out of scope for this research.

REFERENCES

1 G.D. Airey, M.M. Rahman, A.C. Collop, Absorption of bitumen into crumb rubber using the basket drainage method, Int. J. Pavement Eng. 4 (2) (2003 Jun 1) 105–119.

2 M. Arabani, S.A. Tahami, M. Taghipoor, Laboratory investigation of hot mix asphalt containing waste materials, Road Mater. Pavement Des. 18 (3) (2017 May 4) 713–729.

3 M. Chen, J. Zheng, F. Li, S. Wu, J. Lin, L. Wan, Thermal performances of asphalt mixtures using recycled tyre rubber as mineral filler, Road Mater. Pavement Des. 16 (2) (2015 Apr 3) 379–391.

4 Y.R. Kim, D. Little, I. Song, Effect of mineral fillers on fatigue resistance and fundamental material characteristics: mechanistic evaluation, Transp. Res. Rec.: J. Transp. Res. Board 1 (1832) (2003 Jan) 1–8.

5 M. Arabani, S.A. Tahami, Assessment of mechanical properties of rice husk ash modified asphalt mixture, Constr. Build. Mater. 15 (149) (2017 Sep) 350–358.

6 A. Blasl, M. Khalili, G. Canon Falla, M. Oeser, P. Liu, F. Wellner, Rheological characterisation and modelling of bitumen containing reclaimed components, Int. J. Pavement Eng. 4 (2017 Jun). 1 1.

7 M. J. Khattak and N. Peddapati, "Flexible Pavement Performance in relation to In Situ Mechanistic and Volumetric Properties Using LTPP Data," vol. 2013, 2013.

8 A. Ebrahim and A. E. Behiry, "Laboratory evaluation of resistance to moisture damage in asphalt mixtures," Ain Shams Eng. J., vol. 4, no. 3, pp. 351–363, 2013

9 M. Porto, P. Caputo, V. Loise, S. Eskandarsefat, B. Teltayev, and C. O. Rossi, "Bitumen and Bitumen Modification : A Review on Latest Advances," pp. 1– 35, 2019

10 Y. Hefni, Y. A. El Zaher, and M. A. Wahab, "Influence of activation of fly ash on the mechanical properties of concrete," Constr. Build. Mater., vol. 172, pp. 728–734, 2018.

11 S. A. Zareei, F. Ameri, F. Dorostkar, and M. Ahmadi, "Rice husk ash as a partial replacement of cement in high strength concrete containing micro silica: Evaluating durability and mechanical properties," Case Stud. Constr. Mater., vol. 7, pp. 73–81, 2017.

12 X. Pan and Y. Sano, "Fractionation of wheat straw by atmospheric acetic acid process," Bioresour. Technol., vol. 96, no. 11, pp. 1256–1263, 2005.

13 Zhenqiang Han , Aimin Sha , Zheng Tong a. study on the optimum rice husk ash content added in asphalt binder and it modification with bio-oil .construction and building material, 147 (2017) 776–789

14 Isak Rajjak shaikh, Alamghir Abdullah Shaikh. utilization of wheat usk ash as a silica source for the synthesis of MCM-41 type mesoporous silicates.Research journal of chemical sciences.2231-606

15 S_. Sargın, M. Saltan, N. Morova, S. Serin, S. Terzi, Evaluation of rice husk ash as filler in hot mix asphalt concrete, Constr. Build. Mater. 48 (2013) 390–397

16 M. Arabani and S. A. Tahami, "Assessment of mechanical properties of rice husk ash modified asphalt mixture," Constr. Build. Mater., vol. 149, pp. 350–358, 2017

17 S. Bilal and A. Zaidi, "The influence of hydrated lime on moisture susceptibility of asphalt mixtures," no. February, 2018

18 Al-Hdabi, Laboratory investigation on the properties of asphalt concrete mixture with Rice Husk Ash as filler, Constr. Build. Mater. 15 (126) (2016 Nov) 544–551.

19 ASTM, "Standard test method for penetration of bituminous materials," USA, ASTM Int., 2013

20 ASTM, "Astm D 36," "Standard Test Method Softening Point Bitumen", ASTM Int. West Conshohocken, PA, USA., vol. 1, no. d, pp. 3–6, 2006.

21 A. Standard, "Standard Test Method for Pull-Off Strength of Coatings using Portable Adhesion Testers (ASTM D4541)," ASTM Int. West Conshohocken, PA, 2009.

22 Xue, S. Wu, J. Cai, M. Zhou, and J. Zha, "Effects of two biomass ashes on asphalt binder: Dynamic shear rheological characteristic analysis," Constr. Build. Mater., vol. 56, pp. 7–15, 2014.

2nd International Conference on Advances in Civil and Environmental Engineering (ICACEE-2023)

University of Engineering & Technology Taxila, Pakistan

Conference date: 22nd and 23rd February, 2023

Impact of traffic composition on highway mobility based on speed categorization of vehicles

Asim khan[1], Jamal Ahmed Khan[2], Muhammad Bilal Khursheed[3]

[1]Department of Civil Engineering/UET Taxila, asimkhanpgc7@gmail.com

[2]Department of Civil Engineering/UET Taxila, jamal.ahmed@uettaxila.edu.pk

[3]Frontier Work Organization/FWO, dirtn@fwo.com

ABSTRACT:

This study was conducted to examine the effect of traffic composition on the mobility of four lane divided highway based on the speed categorization of vehicles. spot speed and traffic composition data were gathered at ten different sites during peak hours in the morning and evening. The vehicles were categorized based on their speed into three categories i.e., slow moving vehicles (SMV), medium moving vehicles (MMV), and fast-moving vehicles (FMV). The analysis shows that SMVs consists of trucks, rickshaws, and tractor-trolleys with more than 50% of vehicles operating at speed of less than 40 km/h. MMV comprises hiaces, suzuki/carries, and bikes. Whereas FMV comprises trucks and buses. The analysis also shows that as the percentage of SMVs increased in the traffic stream highway mobility decreases in terms of speed of cars. On the other hand, when there are more MMVs and FMVs in the traffic stream overall mobility of highway in terms of speed of cars is found to be increased.

Keywords: Mobility, Slow Moving Vehicles (SMV), Medium Moving Vehicles (MMV), Fast Moving Vehicles (FMV), Spot speed

INTRODUCTION

A country's ability to grow economically largely depends on its transportation infrastructure. An enormous sum of money and time is required for the building of a new transportation infrastructure. The ideal strategy in a growing nation like Pakistan is to improve the traffic system that are already in place [1]. Knowledge of traffic composition is very vital and needed for the planning, analysis, design, and operation of roadway systems [2]. Contrary to affluent nations, the traffic in developing nations like Pakistan is characterized by mixed traffic conditions comprising vehicles of wide-ranging static and dynamic characteristics and the presence of weak/loose lane discipline [3]. The traffic conditions become chaotic when all these vehicles of different operational capabilities are allowed to share and operate on a common carriageway width [4]. The traffic mix includes the vehicle of different classes there is no specific categorization for these

vehicles based on speed, so vehicle categorization is vital based on spot speed according to Pakistani roadway conditions where flow is heterogeneous. Under this heterogeneous flow when the vehicles moving at slow speed comes in front of other vehicles operating at the high-speed overall flow of the traffic is disturbed which ultimately impact the mobility of multilane highway. SMV is considered any vehicle that cannot keep up a constant speed of 25 mph (40 km/h) or greater [5]. Slow moving vehicle (SMV) is one of the crucial factors responsible for the traffic problems and congestion affecting the transport network. The most significant problem with SMVs on public roadways is the speed differential between SMVs and regular vehicles on the roadway. Shoulders are often not large enough to safely accommodate SMVs while simultaneously allowing other vehicles traveling in the same direction sufficient space to overtake without entering into the other travel lane which impacts the traffic flow. The extensive diversity of vehicles and the difference in their dimensions and speed generate several difficulties for traffic operations. Vehicles do not obey the lane markings and tend to utilize every possible lateral or longitudinal gap [6]. We must thus classify vehicles and research how the makeup of the traffic affects highway mobility.

RESEARCH METHODOLOGY

Study Area

Data is collected on National Highway(N5) which is a multilane highway. The geographic location for data collection is selected between Chongi No 26 and Burhan. A total of ten sites were decided for the data collection based on traffic flow in both northbound and southbound directions.

Figure I: Google imagery of Study Area

Data Collection Plan

The full-scale field data collection activity was conducted on ten selected sites. A total of 20 field hours were obtained at an average of 2 hours per site.

TABLE 1: Details of Data collection at Different Sections

Road Location (Coordinates)	**Site**	**Field Data Collection**		**No Of Lanes**	**Flow Direction**
		Collection Time(hrs.)			
		Morning	**Evening**		
33.822610,72.669494	1	0700-0800	1600-1700	2	NB
33.823211,72.664997	2	0730-0830	1630-1730	2	NB
33.824789,72.658550	3	0730-0830	1630-1730	2	NB
33.680434,72.847543	4	0730-0830	1630-1730	2	NB
33.822155,72.673073	5	0730-0830	1630-1730	2	NB
33.825176,72.655927	6	0715-0815	1645-1745	2	SB
33.820849,72621077	7	0715-0815	1645-1745	2	SB
33.667073,72.876044	8	0715-0815	1645-1745	2	SB
33.638844,72.926618	9	0715-0815	1645-1745	2	SB
33.822565,72.669459	10	0715-0815	1645-1745	2	SB

*NB= Northbound *SB=Southbound

Data Collection Technique

After studying different techniques and going through their pros and cons and according to our data needs, we decided to go with a radar gun to collect speed data. The flow and vehicle types were observed in the field by using the video recording technique, (mobile video recording using a tripod stand). We retrieved the required data from the recorded video to measure traffic composition.

Figure II: Measurement of spot speed and traffic composition

Vehicle Categorization

Based on the speed data collected on various sites at a four-lane divided highway. Vehicles are classified into three main speed categories

1) Slow-moving vehicles (0-40 km/h speed range)
2) Medium moving vehicles (40-60 km/h speed range)
3) Fast-moving vehicles (>60 km/h speed range)

The mean speed data of each class of vehicle tell us about which of the above category it falls into. The relationship of each category of vehicle is then checked with the traffic composition to get us an idea about the impact of traffic composition on highway mobility.

RESULTS AND DISCUSSION

After gathering all the data from different sites this data is formatted and analysis is performed in Microsoft excel. The analysis performed on collected data gave us following results.

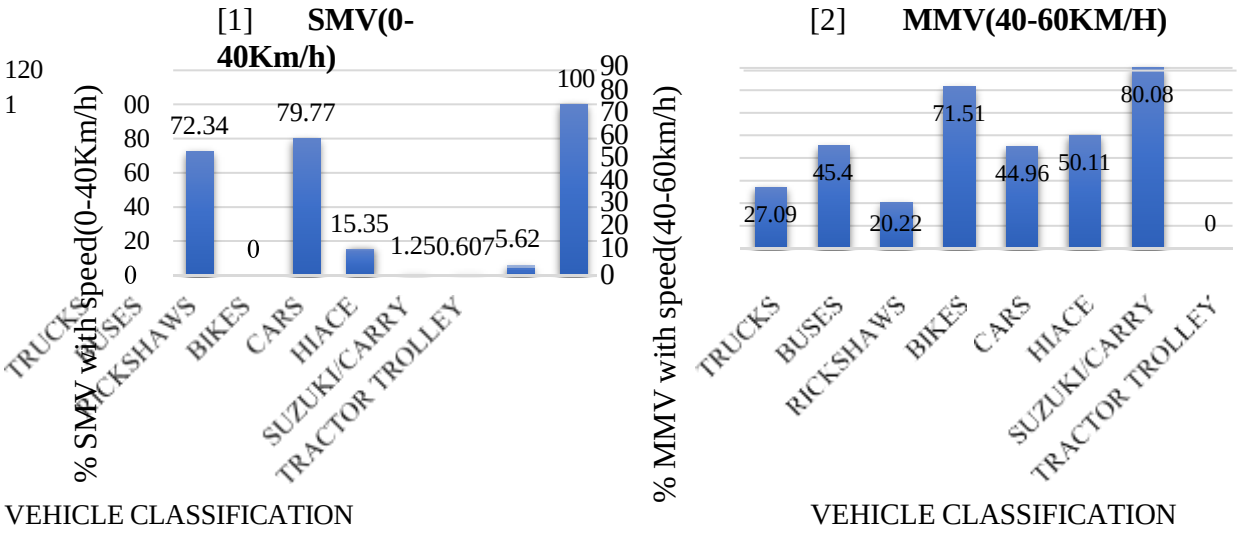

Figure III: Graph shows the percentage of SMV & FMV w.r.t vehicle type

As it is evident from figure III more than 50% of trucks, rickshaws, and tractor-trolleys are traveling at speeds less than 40 km/h so these are classified as SMVs. Trucks and rickshaws form an important part of SMV here. When trucks are loaded, they cannot keep their speed high and travel below 40km/h. In the case of rickshaws, they always try to pick up a passenger from the roadside, that's why travel at low speeds.

It is also depicted by the figure that more than 50% of bikes, hiaces, and Suzuki's/carries are traveling at a mean speed between 40-60 km/h and hence they fall into the category of medium moving vehicles. Some of the trucks also lie in the category of MMV because when they are unloaded, they keep their speed high.

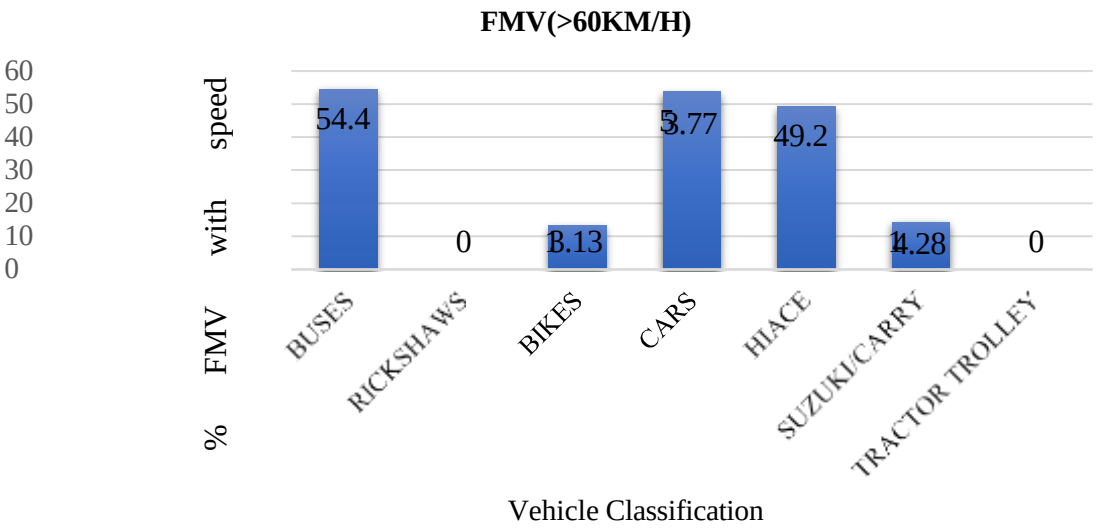

Figure IV: Graph shows the percentage of fast-moving vehicles w.r.t vehicle type

The graph shows that 53% of cars and 54% of buses are traveling above 60 km/h and can be called fast-moving vehicles. The mean speed of cars is more than all types of vehicles. Higher the speed of cars higher the mobility of the highway. So, the relationship between the speed of cars and different categories of vehicles is also drawn to check the impact of traffic composition on highway mobility.

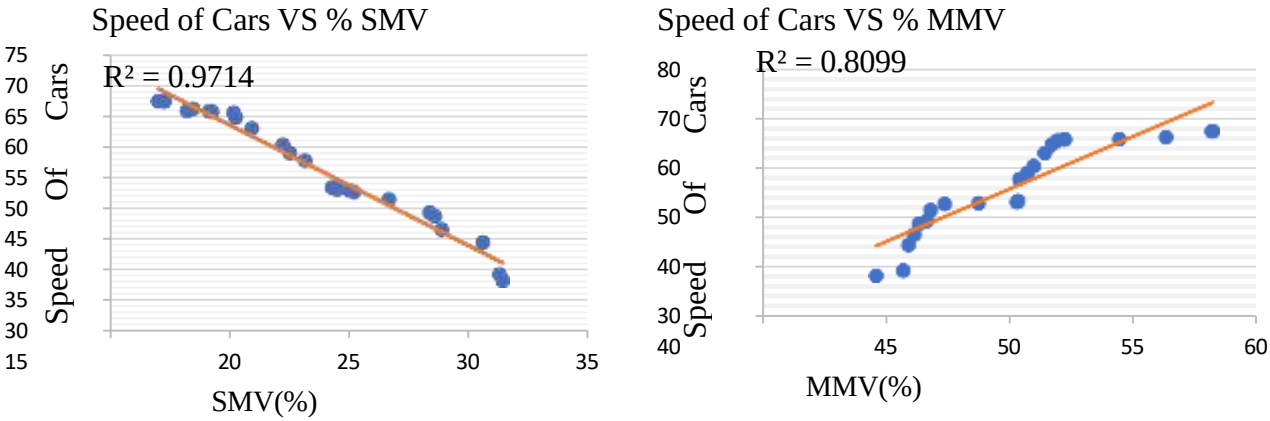

Figure V: Graph shows relationship b/w speed of cars and %age of SMV & MMV

Figure V shows that the speed of cars inversely relates to a percentage of slow-moving vehicles in the traffic stream. As is evident from the graph when the percentage of the slow-moving vehicles increases in the traffic stream the mean speed of the car decreases. The value of $R^2 = 0.9714$ shows that a strong relationship exists between both. Here $\beta = -1.9634$ shows the negative impact of SMV on the speed of cars. Further, it explains that one unit increase in the percentage of SMV causes to decrease in the speed of the car by approximately 2 km/h. Figure 6 also shows that a direct relationship exists between the speed of cars and the percentage of medium-moving vehicles. As the percentage of medium-moving vehicles increases, the traffic stream speed of cars also improve. The value of $R^2 = 0.8099$ shows a relatively less strong relationship between both as compared to the relationship between SMV and speed cars. The positive value of $\beta = 2.1221$ shows that one unit increase in the percentage of medium-moving vehicles causes approximately a 2 km/h increase in the speed of cars.

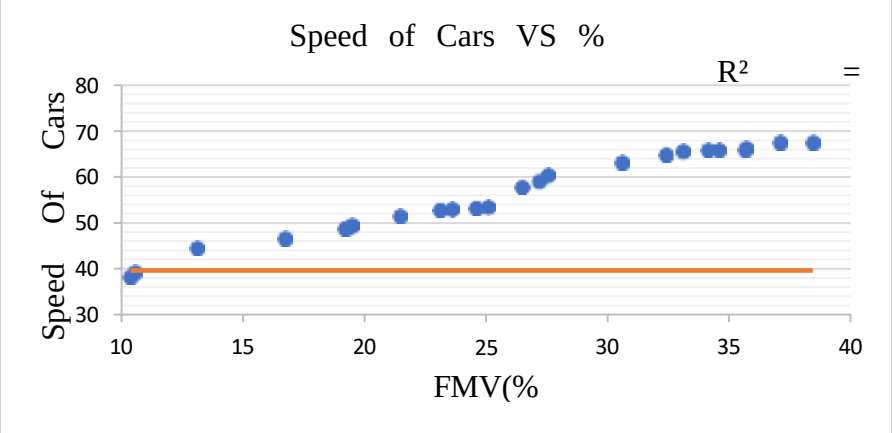

Figure VI: Graph shows relationship b/w speed of cars and percentage of FMV

The figure shows that the speed of cars is directly proportional with the percentage of fast-moving vehicles in a traffic stream. As the fast-moving vehicles increase in the traffic stream speed of cars also increases. The value of R^2 shows that a strong relationship exists between both. Furthermore, one unit increase in the percentage of fast-moving vehicles also causes approximately a 1 km/h increase in the speed of cars which is less increase as compared to medium-moving vehicles. The main reason for this is that cars are already at formidable speed when the percentage shift from medium towards fast-moving vehicles.

CONCLUSIONS:

This study was conducted to study the impact of traffic composition on highway mobility based on the speed categorization of vehicles. The analysis shows that SMVs mostly consist of truck

and rickshaws. The possible reason for a high percentage of trucks in SMVs category is when trucks are loaded. The relationship drawn between the speed of cars and SMVs shows that as the percentage of SMVs increases in the traffic stream it negatively impacts the speed of cars. The main reason for this decrease in the speed of cars is due to the fact that when SMV try to overtake another vehicle traveling at a lower speed they block the traffic lane and platoons are formed the frequency of which increases with the number of slower vehicles in the traffic stream. The analysis also shows that a direct relationship exists between the speed of cars and percentage of MMVs and FMVs and the overall mobility of highway in terms of speed of cars is found to be increased. The main reason for this increase in speed of cars is due to the reason that that there are no lane blockages and platoons' formation, and cars can maneuver and travel fast when there are more MMVs and FMVs in the traffic stream.

ACKNOWLEDGEMENTS

The authors thank the Taxila institute of transportation engineering for providing a research-oriented environment and NH&MP for allowing us to collect data on N-5.

REFERENCES

[3] Saha AK, Ahmed B, Rahman M, Nahar TT. Analysis of Traffic Congestion and Remedial Measures at Traffic Mor in Pabna City, Bangladesh. Biography Md. Jakirul Islam Jony Prothan graduated from Pabna University of Science and Technology (PUST), Pabna, Bangladesh in Urban and Regional Planning in. 2017.

[4] Arkatkar, Arasan. "Micro-simulation study of vehicular interactions on upgrades of intercity roads under heterogeneous traffic conditions in India." (2012).

[5] Arasan, V. Thamizh, and Reebu Zachariah Koshy. "Methodology for modeling highly heterogeneous traffic flow." *Journal of Transportation Engineering* 131.7 (2005): 544-551.

[6] Chandra, Satish, Arpan Mehar, and Senathipathi Velmurugan. "Effect of traffic composition on capacity of multilane highways." *Ksce journal of civil engineering* 20, no. 5 (2016): 2033-2040.

[7] Hawkins, Neal, Cari Kinzenbau, and Shauna Hallmark. "Improving Safety for Slow Moving

Vehicles on Iowa's High-Speed Rural Roadways." (2009).

[8] Chandra, Satish, and Upendra Kumar. "Effect of lane width on capacity under mixed traffic conditions in India." *Journal of transportation engineering* 129.2 (2003): 155-160.

2nd International Conference on Advances in Civil and Environmental Engineering (ICACEE-2023)

University of Engineering & Technology Taxila, Pakistan

Conference date: 22nd and 23rd February, 2023

Improvement of Self-healing capabilities of asphalt mixture by enhancing Temperature

M.Farhan Zaheer, Fahad Nabi,Moazam Sattar, Talha Naseer, Muhammad Saif Ullah, Hafiz Sami Ullah, Muzamil Usman

[1]NUML Rawalpindi, fzaheer465@gmail.com
[2] NUML Rawalpindi, fahadnabi4987@gmail.com
[3] NUML Rawalpindi,moazam.malik59@gmail.com
[4]NUML Rawalpindi, naseertalharana490pk@gmail.com
[5]NUML Rawalpindi, saifmansha898391@gmail.com
[6]NUML Rawalpindi, muhammadsamiu7@gmail.com
[7]NUML Rawalpindi, muzamilrana152@gmail.com

ABSTRACT

Asphalt pavement frequently gets micro cracks over time, mostly because of the weather and traffic. Microwave progression could be an elective procedure to help the self-healing of asphalt mixture. Initially, cracks in asphalt mixture have micrometric size but it may grow very fast due to traffic circulation and environmental stresses. Self -healing of asphalt mixture occurs under high temperature. The main mechanism of this healing process is capillary flow of the bitumen through the cracks. However, it is not clear how much healing will be done with respect to time and temperature via microwave heating of mixture. For these reasons, healing recovery was tested via Marshall Stability Test, semi cylinder asphalt samples were get fractured till the crack occurs then presented to microwave machine to warm them up to various time with moderate temperature. The principal results demonstrated that the best healing recovery was accomplished at temperature ranging from 37 ºC to 40 ºC recovery percentage were 85 %, 65 %, 65% and 50% for the first, second, third and fourth samples with first 80 sec, second 60 seconds, third 40 seconds, and fourth 20 seconds individually, heating the combination up to 80 seconds was not sufficient to reach to the greatest healing. That was a demonstration that microwave heating may repair cracking in asphalt mixture; higher time more than 80 seconds did not promote healing, in fact healing was lower.

KEYWORDS: Asphalt mixture, Microwave radiation heating, Crack healing.

INTRODUCTION

Asphalt pavement frequently gets micro cracks over time, mostly because of the weather and traffic. These fissures eventually worsen into more serious problems including potholes, ravelling, and cracking. Additionally, the fatigue life of asphalt pavement will be shortened. Asphalt pavements therefore require preventative maintenance techniques to increase their longevity. Asphalt-mixture fissures may eventually mend on their own, but it is a difficult process that could take several days to finish. The combination of steel wool and graphite was added to make it more susceptible to electromagnetic induction [1]. However, it was found that microwave devices use less power to achieve similar results compared to electromagnetic induction [2]. Temperature control during microwave heating is difficult [3]. Overheating the binder can cause its chemical makeup to be destroyed, so heating time must be kept short [4]. Incorporating self-healing microcapsules into the asphalt binder is another effective method to allow it to heal micro cracks and increase fatigue life [5]. The impact of ferrite on the rheology of asphalt binder was studied using microwave absorbers and substituting some limestone filler [6]. Pre-processed ground tire rubber enhanced binders showed reduced composite viscosity and improved rutting resistance after exposure to microwave radiation [7]. The effectiveness of thermo mechanical treatment in improving hot asphalt mixture's self-healing capacity was also studied [8]. Steel wool, waste metals, Nano modifiers, and microcapsules have all been used to improve asphalt's self-healing ability [9]. However, the main limitations of electromagnetic induction for field use are the long heating time and difficulty in mixing the fibres. Temperature control during microwave heating is also challenging [10]. More research is needed to improve the duration and temperature of the microwave induction approach [11]. Electromagnetic induction requires more power to achieve similar results compared to microwave devices [12].

Materials

Aggregates:

Strength of aggregate has the major contribution for road pavement construction, so in order to achieve high strength we have used the Margalla Crush (aggregate). Selection of aggregate source plays an important role and provides a guarantee towards the pavement performance. Different test was performed on selected aggregate, following are specific gravity, bulk density, aggregate impact value and aggregate crushing values.

Binder type:

Bitumen from the Attack Oil refinery's 60/70 and 80/100 penetration grade aggregates were utilized. In order to check the binder performance following tests were made on asphalt binder to meet binder requirements. Firstly, it was tested for penetration. Secondly, it was tested for ductility, and last was for viscosity and softening point.

Methodology

In methodology, we made the Combined Aggregate Grading Requirements as per ASTM D 3515 class B. Attack Oil refinery's asphalt binders and Margalla aggregates were chosen to make preparation of the asphalt mixture. Then specimens were made ready for both qualitative as well as quantitative tests. First test on asphalt mixture was Marshall Stability and flow. The primary tests were a four-point beam fatigue test. The test self-healing of asphalt mix was performed utilizing microwave induction method. Tests were performed during self-healing to compare the asphalt material beam's fatigue resistance. Which indicates the Healing Index. Analysing the data was the last step in the study technique. The flowchart of research Methodology is given below in Figure

Table 4: Laboratory tests used in Experimental work

Test type	Test Name	Standard	Sample Dimensions	Test Conditions	Test samples
Asphalt Mixture Tests	Marshall Mix Design test	ASTM D1559	Dia = 4inch Height= 2.5inch	Conditioning time= 30minutes Conditioning Temp= 60°C Deformation rate= 5mm/minute	15×2=30

	Four-point beam fatigue test	AASHTO T321-03 (TP8)	15×2×2 (Inches)	Controlled Stress Temperature= 20°C&25 °C Frequency= 5Hz &10Hz Target stress =600Kpa	20×2=40

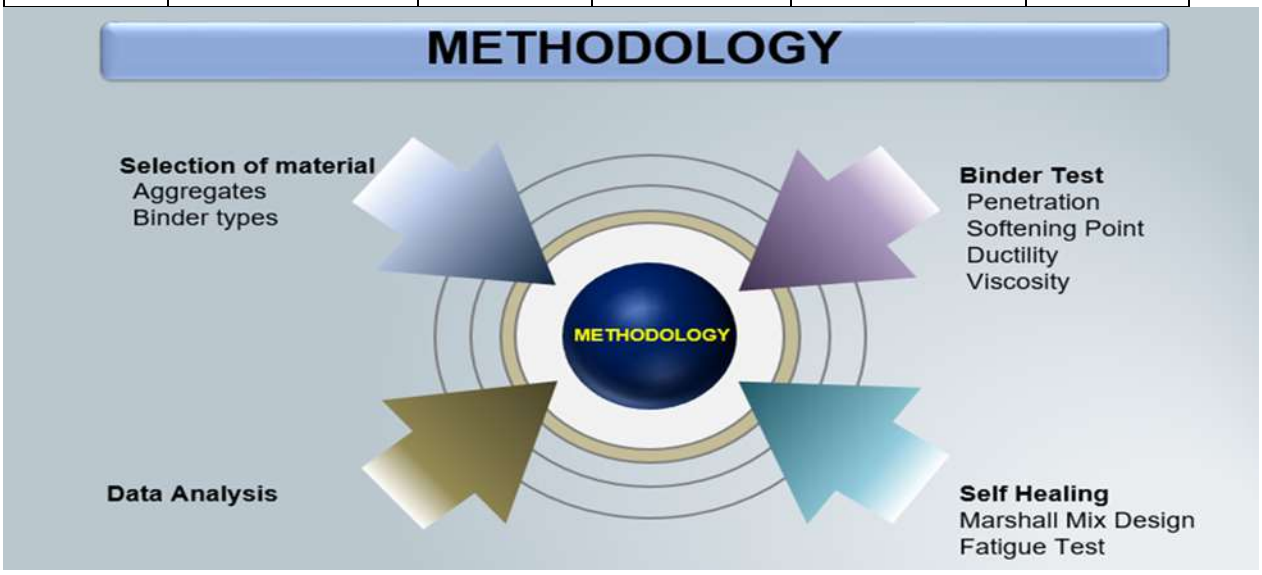

Figure 4: Flowchart of Methodology

Result and Discussion

As we break the specimen for the First time, we get the Bending Strength which is about (1.4 KN) and then we put the specimen into the microwave and heat the specimen. Then after 24 hours of heating the specimen we break the specimen for the second time and there is a difference in strength. The strength will decrease. Again, we put the sample into the microwave oven and heat the sample for the third time and we break the specimen and cracks are produced and there is a difference in the strength. The strength will decrease more than the second one. Now there is a temperature factor. As we move from left to right the temperature will increase and the second bending strength and the third bending strength will be increase. We increase the temperature from 25 degree centigrade to 40 degrees centigrade. The bending strength or recovery ratio will be increased. It means the healing capability of the specimen or recovery ratio is increasing with respect to temperature.

Table 5: Effect of Temperature on bending strength of asphalt mixture

Temperature	1st Bending Strength	2nd Bending Strength	3rd Bending strength
25-27	1.4	0.25	0.1
28-30	1.4	0.3	0.18
31-33	1.4	0.4	0.19
34-36	1.4	0.45	0.21
37-38	1.4	0.55	0.3
39-40	1.4	0.55	0.3

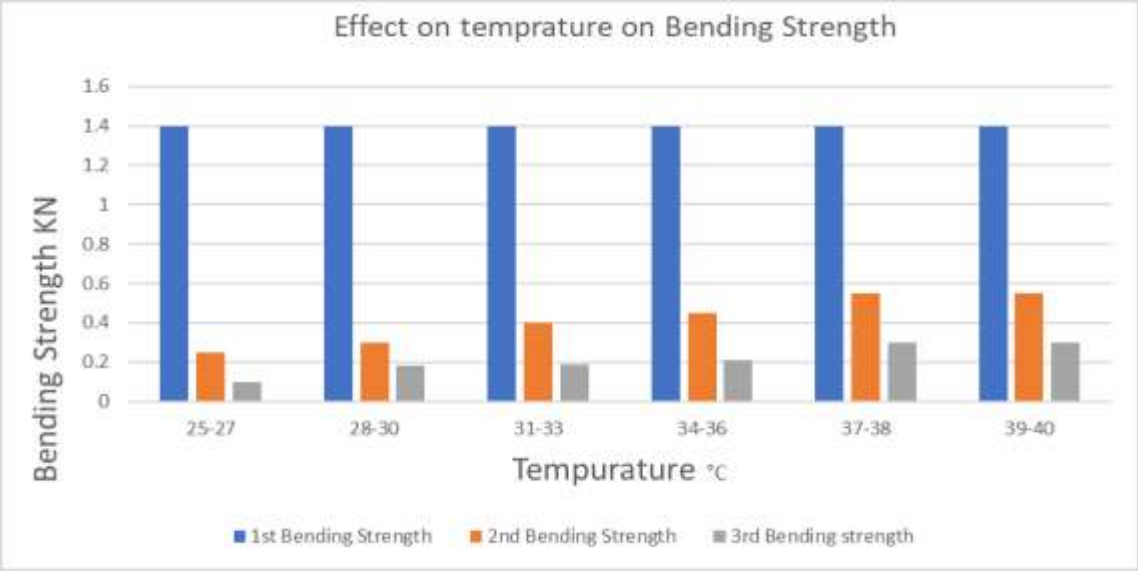

Figure 5: Effect of temperature on bending strength

CONCLUSION

- By raising temperature, asphalt's self-healing properties can be improved.
- Heating temperature has been shown to be the key factor in the self-recovery of asphalt material. The healing index peaked between 37 and 40 °C.
- Because asphalt material cracks mend at high temperatures, raising the temperature can lengthen the fatigue life of a pavement.
- This method is limited to laboratory and further research is required to use this method in field.

REFERENCES

[1] Y. Sun, S. Wu, Q. Liu, W. Zeng, Z. Chen, Q. Ye, et al., Self-healing performance of asphalt Mixtures through heating fibers or aggregate, Constr. Build. Mater.150.

[2] Y. Sun, S. Wu, Q. Liu, W. Zeng, Z. Chen, Q. Ye, et al., Self-healing performance of asphalt

Mixtures through heating fibers or aggregate, Constr. Build. Mater.150

[3] J. Norambuena-Contreras, I. Gonzalez-Torre, Influence of the Microwave Heating Time on The Self-Healing Properties of Asphalt Mixtures, Applied Sciences-Basel. 7 (10) (2021) 1076.

[4] J. Norambuena-Contreras, I. Gonzalez-Torre, Influence of the Microwave Heating Time on The Self-Healing Properties of Asphalt Mixtures, Applied Sciences-Basel. 7 (10) (2021) 1076.

[5] Z. Liu, Preparation of microcapsule and its influence on self-healing property of asphalt, Petrol. Sci. Technol. 37 (9) (2019) 1025–1032.

[6] B. Lou, A. Sha, D.M. Barbieri, Z. Liu, F. Zhang, W. Jiang, Improved microwave heating uniformity and self-healing properties of steel slag asphalt containing ferrite filler, Mater. Struct./Materiaux et Construct. 54 (2021) 1–14.

[7] O. Xu, M. Li, D. Hou, Y. Tian, Z. Wang, X. Wang, Engineering and rheological properties of asphalt binders modified with microwave preprocessed GTR, Constr. Build. Mater. 256 (2020) 119440.

[8] J. Gallego, F. Gulisano, V. Contreras, A. Pa´ez, The crucial effect of re-compaction energy on the healing response of hot asphalt mortars heated by microwaves, Constr. Build. Mater. 285 (2021) 122861.

[9] E. Yalcin, Effects of microwave and induction heating on the mechanical and self-healing characteristics of the asphalt mixtures containing waste metal, Constr. Build. Mater. 286 (2021) 122965, h.

[10] J. Norambuena-Contreras, I. Gonzalez-Torre, Influence of the Microwave Heating Time on

the Self-Healing Properties of Asphalt Mixtures, Applied Sciences-Basel. 7 (10) (2019) 1076.

[11] J. Norambuena-Contreras, I. Gonzalez-Torre, Influence of the Microwave Heating Time on the Self-Healing Properties of Asphalt Mixtures, Applied Sciences-Basel. 7 (10) (2017) 1076.

[12] G. Amin, A. Esmail, Application of nano silica to improve self-healing asphalt mixes, J. Central South Univ. 24 (5) (2017) 1019–1026.

2nd International Conference on Advances in Civil and Environmental Engineering (ICACEE-2023)

University of Engineering & Technology Taxila, Pakistan

Conference date: 22nd and 23rd February, 2023

Effect of shear rate on shear thinning behavior of asphalt binder modified with organophilic clay

[a] Safia kousar*, [b] Imran hafeez

a. Department of Civil Engineering, University of Engineering & Technology Taxila, Pakistan, Safiakousar16@gmail.com

b. Department of Civil Engineering, University of Engineering & Technology Taxila, Pakistan, Imran.hafeez@uetaxila.edu.pk

Abstract

This research was done to explore the Effect of shear rate on shear thinning behavior of asphalt binder modified with organophilic clay. Blending asphalt with nano material was carried out using melting process. An asphalt binder is a liquid that is not Newtonian, being a Non-Newtonian liquid exibites shear-thinning behaviour. The dependence of shear viscosity on shear rate is a characteristic of an asphalt binder's shear-thinning or pseudo-plastic behaviour. By adding organophilic nano clay as an asphalt binder modifier in bitumen with different percentages 0%,1%,2%,3%,4%,5%, it was concluded that nano clay improves the asphalt performance. Two type of bitumen grade ARL 60/70 and ARL 80/100 were used for experimental work by rotational viscometer test to check the response of shear thinning behavior of asphalt binder. Experimental results shows that shear rate and viscosity inversely proportional to each other. By increasing shear rate apparent viscosity decreases.

Keywords: Brookfield Rotational Viscometer, Modified Asphalt, Organophillic clay, Viscosity, Shear rate, shear stress, shear thinning.

Introduction

Asphalt use as a binder in the construction of highway in great extent all around the world. Most organophilic polymeric matrices require the hydrophilic clay to be changed in order to achieve acceptable interfacial adhesion and mechanical qualities. Clay modification is often accomplished through ion exchange reactions between sodium ions that naturally exist between the clay layers and organophilic cations. (Garcia-Lopez et al 2019). Rubber composite-modified asphalt can have its high-temperature stability, ageing resistance, and despite an improvement in storage stability, its low-temperature performance can be decreased due to the varying contents of nano-organic montmorillonite (NOMMT). (Tian et al. 2018).

The penetration value and temperature sensitivity of nano-aluminum oxide (nano-Al 2 O 3) and nano-silica oxide (nano-Si 2 O 3) were decreased, while the ductility value and softening point temperature were enhanced, respectively, by the addition of 5% modifier. (Hussein et al. 2021). The addition of 1%–5% nano zinc oxide (nano-ZnO) can increase the characteristics of asphalt that make it resistant to ageing, and it can interact physically and chemically a stable modified asphalt system with the base asphalt and raise the base asphalt's softening point and consistency. (Xu et al. 2019). Bitumen is a common binder used in road construction that is produced from crude oil at refineries. It is a complex chemical combination of molecules composed mostly of hydrocarbons, with a small amount of structurally related heterocyclic species and functional groups containing sulphur, nitrogen, and oxygen atoms. (Morgen and Mulder, 2013). The characteristics of bitumen can alter during the course of its service life according to climatic conditions and vehicle loads. The passage of oxygen and UV rays is what ages bitumen. Due to tiredness, carrying loads repeatedly will cause strength to decline. Water may have an impact on how well bitumen adheres to the aggregate. All these factors may cause an early failure. (Petersen, Halstead, 2012). In present research work organophilic clay with asphalt binder modified to investigate the impact of shear rate on the modified asphalt binder's shear thinning behaviour.

Material

Bitumen

Bitumen of ARL 60/70 grade & ARL 80/100 (Attock Refinery limited) is collected from MKA Asphalt plant near Margalla stop, Islamabad. Bitumen stored at room temperature, store in 2.5kg containers. Conventional testing of bitumen was carried out using penetration, ductility, softening points etc tests. **Table 1** represents data obtained from the conventional tests.

Table 1: physical properties of virgin bitumen

Properties	Standard code	unit	ARL 60/70	ARL 80/100	Specification limit (minimum)
Penetration 0.1mm @ 25°C	ASTM D5	1/10 mm	62	91	60
Softening point (°C)	ASTM D36	°C	49	44	43
Ductility at 25°C	ASTM D36	cm	102	112	100
Dynamic viscosity	ASTM D4402	cp	385.5	340.4	300

Organophilic clay

Organophillic clay is taken from the PCSIR lab in Islamabad. sodium bentonite, which is typically made from smectite clay and has a moisture level of up to 10%, is sprayed inside an activator substance made of ammonium sulphate and mechanically compacted. To create organophilic clay, the previously treated clay is reground.

Figure 1: Organophilic clay

Experimental work

Three samples were prepared for each of the nano clay content (0%, 1%,2%,3%,4%,5%) for all type of binders in order to perform experiment according to specifications. The asphalt was heated up to 160 °C .A percentage of nano clay was added in a mixer to ensure uniform dispersion of the particles. Then introduced to the rotational viscometer to evaluate its effect on viscosity, shear thinning.

Brookfield rotary viscosity test

According to ASTM D4402, a Brookfield viscometer was used to measure the viscosity of asphalt treated with nano clay. Throughout the test, temperature, rotational speed, shear stress, shear rate, and viscosity were noted. The conditions under which the viscosity tests were conducted mentioned in Table 2.

Table 2: Test conditions for Brookfield rotary viscosity

Organophilic clay (%)	Test temperature (°C)	Shear rate (1/s)
0% , 1% , 2% , 3% , 4% , 5%	135	3.4, 6.8, 10.2, 13.6, 17, 20.4, 23.8, 27.2, 30.6, 34

Results & Discussion

It is evident from Figs. 02(a) and (b) that the viscosity is connected to shear rate. With an increase in shear rate, the asphalt's viscosity will decrease. The organophilic clay modified asphalt binder shows shear thinning behavior. As shear rate rises, the structure rearranges itself in a way that is more suited to causing the asphalt to flow and distort , which reduces asphalt viscosity. It can be seen from Figs. 03(a) and (b) that different shear rates, ranging from the lowest shear value to the highest shear value, were used to assess the impact of shear rate on the shear stress of the asphalt binder. Which shows that as the speed of rotation increases, stress value is also increases. This behaviour between shear rate and shear stress specify that they are directly proportional to each other. It can be observed from Figs. 05(a) and (b) that that by the increase of shear rate the value of torque is also increasing which show when the velocity of rotation is increased, the shear rate is increased and therefore the torque increases, unless the fluid is sufficiently shear thinning to compensate this effect.

ARL 60/70 ARL

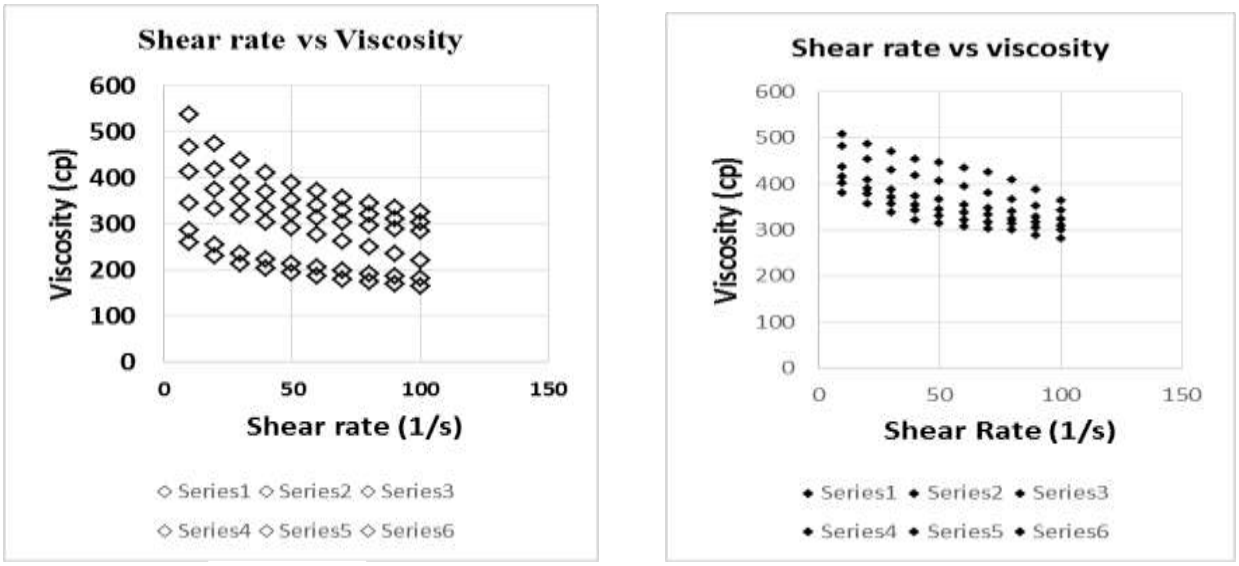

(a) (b)

figure 02: Effect of shear rate on viscosity of asphalt binder

ARL 60/70 ARL 80/100

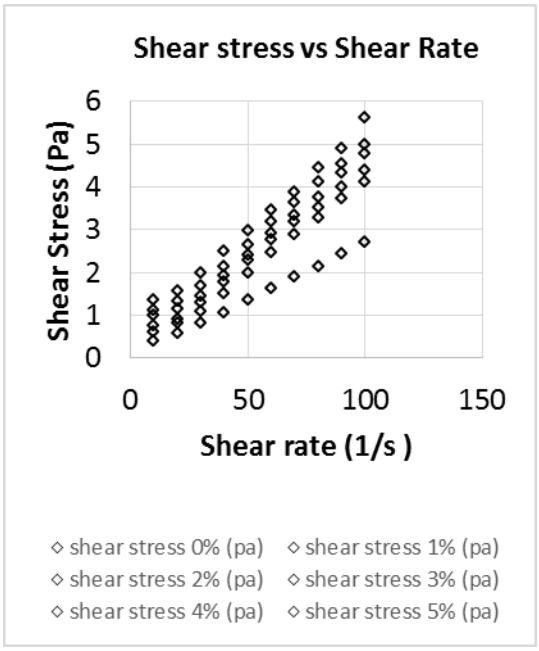

(a)

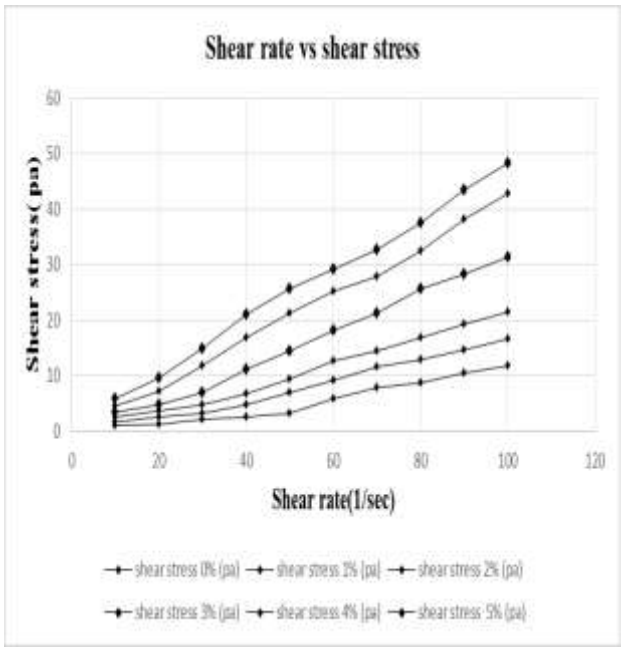

(b)

Figure 03: Relationship between shear rate & shear stress

ARL 80/100 ARL 60/70

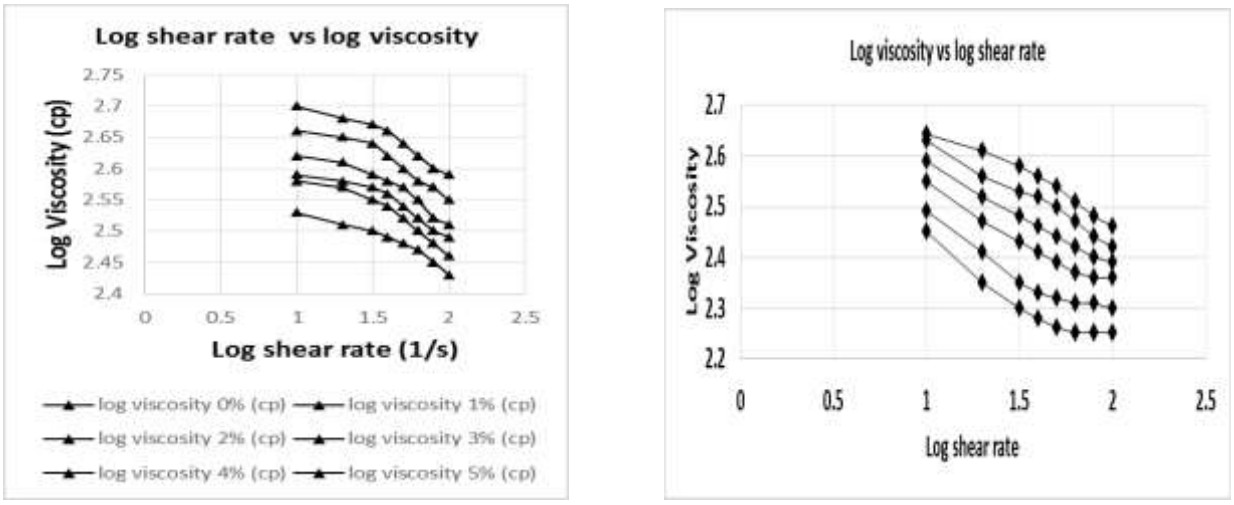

(a) (b)

Figure 04: effect of log of shear rate on log of viscosity

ARL 60/70 ARL 80/100

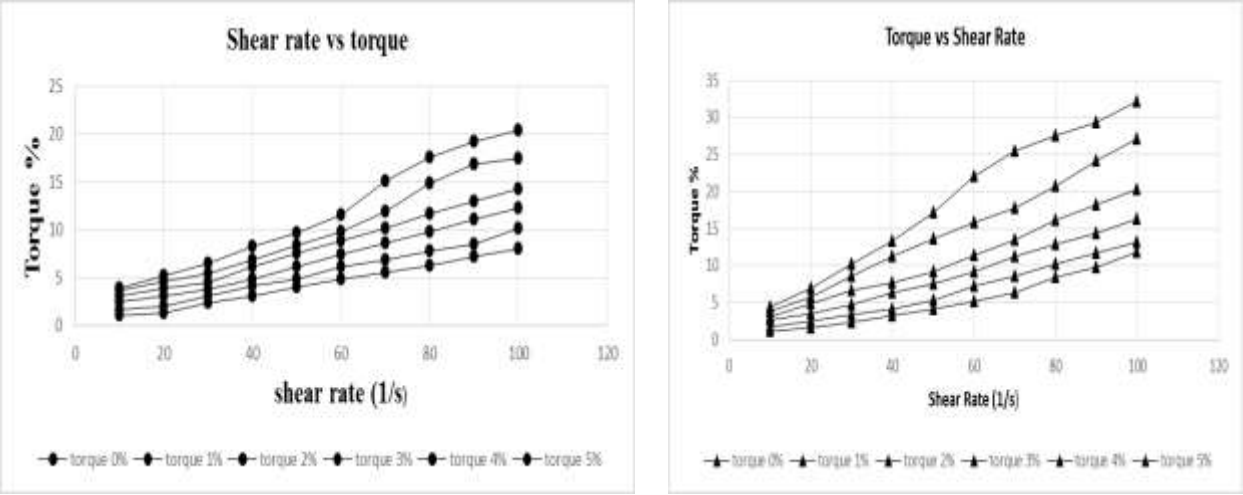

(a) (b)

Figure 05: Effect of shear rate on torque

Conclusions

Two type of asphalt binder (ARL 60/70 and ARL 80/100) were used in this study using Rotational Viscometer to evaluate the properties such as apparent viscosity and shear thinning behavior. This study investigated the influence of shear stress on the viscosity of modified asphalt binder with nano clay percentages.

- When compared to other concentrations, organophilic clay in asphalts had a high 5% viscosity increase on average.
- As the shear rate rises, the asphalt's viscosity will decrease. The Organophilic clay modified asphalt display the shear thinning characteristics that represents they are non-Newtonian fluid.
- When the shear rate increases, the percentage of torque is also increases. Which indicates that as the input speed of the rotational viscometer increases, the output torque increases proportionately.

- In comparison to virgin bitumen, the rate of microstructure rearrangement increased with the treatment of organophilic clay.

Limitations

Different shear rates are applied to modified asphalt binder to investigate the effect of viscosity at temperature of 135℃. Modified binders shows shear thinning behavior up to a shear rate of 100 1/s. As the shear value increases upto120 1/s the viscosity value become constant.

Acknowledgments

The author acknowledges the support and cooperation of the Department of Civil Engineering in the research activity and thanks the University of Engineering and Technology for funding the project.

Reference

[1] Kamiya S, Tasaka S, Zhang X, Dong D, Inagaki N. Compatibilizer role of styrene–butadiene–styrene triblock copolymer in asphalt. Polym J 2001; 3(33):209–13.

[2] Krishnan JM, Rajagopal KR. On the mechanical behavior of asphalt. Mech Mater 2005;37:1085–100.

[3] Garcia-Lopez D,Gobernado-Mitre I, Fernandez JF, Merino JC, Pastor JM. Influence of clay modification process in PA6-layered silicate nanocomposite properties. Polymer 2005;46:2758–65.

[4] Enieb M, Diab A. Characteristics of asphalt binder and mixture containing nanosilica. Int J Pavement Res Technol. 2017;10(2):148–157.

[5] Mazumder M, Kim H, Lee SJ. Performance properties of polymer modified asphalt binders containing wax additives. Int J Pavement Res Technol. 2016;9:128–139.

[6] Yu R, Fang C, Liu P, et al. Storage stability and rheological properties of asphalt modified with waste packaging polyethylene and organic montmorillonite. Appl Clay Sci. 2015;104:1–7.

[7] Zare-Shahabadi A, Shokuhfar A, Ebrahimi-Nejad S. Preparation and rheological characterization of asphalt binders reinforced with layered silicate nanoparticles. Constr Build Mater. 2010;24:1239–1244.

[8] Abolfazl Zare-Shahabadi, Ali Shokuhfar, Salman Ebrahimi-Nejad, Preparation and rheological characterization of asphalt binders reinforced with layered silicate nanoparticles, Construction and Building Materials 24 (2010) 1239–1244.

[9] E. Iskender (2016); P.K. Ashish, D. Singh, Evaluation of rutting, fatigue and moisture damage performance of nanoclay modified asphalt binder, Constr. Build. Mater. 113 (2016) 341–350.

[10] A. Kavussi, (2020) P. Barghabani, The influence of nano materials on moisture resistance of asphalt mixes, Study Civ. Eng. Archit. 3 (2014) 36–40.

[11] J.M.L. Crucho, J.M.C. Neves, S. Capitão, L. Picado-Santos, Characterization of bituminous mixtures modified with organophilic nanoparticles, in: World Conf. Pavement Asset Manag., 12–16 June, Milan, Italy, 2018.

[12] Akbari, Abbas, and Amir Modarres. "Evaluating moisture susceptibility of asphalt mixes Containing Modified Bitumen with Nano-Clay."Road Materials and Pavement Design (December 5, 2018): 1–24.

[13] D. Wingard, Y.K. Yap, X. Shi, S.W. Goh, Rheological Properties and Chemical Bonding of Asphalt Modified with Nanosilica, J. Mater. Civ.Eng. 25 (11) (2013)

[14] West Conshohocken, PA, ASTM International. Shear-rate dependent viscosity of dilute polymer solutions. Rheology, and physical properties of polymer-modified asphalt binders. Euro Polymer J. 2019;112:766–791. (2010)

[15] Zahedi, Arabani M, Haghi AK, Mottaghitalab V. Carbon Nanotubes modified Asphalt Binder: Preparation and Characterization. Int J Pavement Res Technol 2015;8(2017)

[16] Behnam, Golestani B, Nam BH, Nejad F, El Rahman AMMA (2020) The addition effects of macro and nano clay on the performance of asphalt binder, Egypt. J Pet. 2013;21:149–154. characterization of polymer and linear nanocomposite-modified asphalt binder and mixture. Constr Build Mater. 2015;91:32–38.

[17] Kennedy, Goodrich, J. L. 2019. "Asphalt and Polymer Modified Asphalt Properties Related to the Performance of Asphalt Concrete Mixes." Proceedings of the Association of Asphalt Paving Technologists, Vol. 57, 116-175.

[18] Amirkhanian, Thomas W.Johnson, PH.D, Sidharth Patra, Application of nano material is asphalt pavement, University of Alberta, Engineering and Technology Session of the 2018 TAC-ITS Canada Joint Conference.

[19] Marwa M, João Miguel Lopes Crucho, José Manuel Coelho das Neves, Silvino Dias Capitão, Mechanical performance of asphalt concrete modified with nanoparticles: Nanosilica, zero-valent iron and nanoclay, Construction and Building Materials 181 (2018) 309-318.

[20] Qiao Dong, Jiao Jin, Yanqing Tan, Feipeng Lin, Structure characteristics of organic bentonite and the effects on rheological and aging properties of asphalt, Powder Technology 329 (2020) 107–114.

2nd International Conference on Advances in Civil and Environmental Engineering (ICACEE-2023)

University of Engineering & Technology Taxila, Pakistan

Conference date: 22nd and 23rd February, 2023

USE OF GEOGRID IN PAVEMENTS AND MSE WALLS: "COMBINED APPLICATION"

Muhammad Saroosh, Dr. Naveed Ahmad

University of Engineering & Technology Taxila, Pakistan

18-ce-118@students.uettaxila.edu.pk ; n.ahmad@uettaxila.edu.pk

ABSTRACT

In this research, combined application of Geogrid is studied in the pavement structure along with MSE walls. The reinforcement of Geogrid on the roads and highways is proved to be quite efficient not only in enhancing the strength of pavements but also as a key element of the MSE wall. The fundamental idea was that the reinforcement embedded in the soil provides tensile strength to the soil thus enhancing the load carrying capability of pavements. This embedded reinforcement would also help to hold retaining walls on both sides of the pavement structure. Geogrid reinforcement tends to reduce tensile strains in pavement systems. Mechanically Stabilized Earth retaining walls have been increasingly used as a design alternative to the traditional reinforced concrete retaining walls for supporting earth fills in civil infrastructure projects. A field project was selected as a case study for the above-mentioned analysis. Subgrade soil samples were collected from the field and analysed using sieve analysis, liquid limit, and plastic limit tests. Subgrade soil strength was determined using CBR test. AASHTO design technique was used to determine the service life of pavement under study. Cost analysis of the pavement structure was also carried out. Tensar geogrid software was used for the analysis of a 7.2m high retaining wall and its stability was also checked against various loads. Cost-benefit analysis of the MSE and RC walls was also carried out. Combined application of geogrid in pavements and retaining walls not only help to enhance the load carrying capability of pavement foundations but also helps to save a lot in costs.

KEYWORDS: Tensar geogrid, MSE Walls, Unreinforced Soil, Reinforcement, Tensile Strain.

INTRODUCTION

Geogrids are typically solid nets with large openings called apertures. These apertures are large enough to aid in the interlocking with the surrounding soil and rocks, allowing the reinforcement function to be performed. It is incorporated into the main layers of finished surfaces and the surface layers of walls and slopes and acts as a stabilizing force within the soil structure. This stabilization occurs when the fill interlocks with the grid. The strength of the geogrid determines the effect of interlocking, mesh size, and essential materials used [1]. In the case of pavement design, standard strengthening materials like sugarcane bagasse ashes, plastics, coal ashes are required to fulfil strength behaviour strength requirements. Similarly, very expensive retaining wall structures are required for soft soils to provide high tensile resistance to dynamic and seismic loading [2]. Geogrids have this unique capability where their combined application in structural and transportation Engineering can provide solution to both above-mentioned problems. Geogrids can enhance the strength by up to six times compared to standard unreinforced soil [3]. Along with gaining high pavement strength, the MSE (Mechanical Stabilize Earthen) wall can be built with high stability and cost-effectiveness compared to RC walls. The design life of an MSE wall with the help of geogrid increases up to 120 years, and on the other hand, the RC wall has only 40 to 50 years of design life. MSE walls can be used for soft soils and can also provide high tensile strength [4].

PROBLEM STATEMENT

Sustainability, stability, serviceability, design life, and cost, are the key factors in every engineering project. Strength is the primary concern in the case of pavements, and stability is the factor while designing the retaining walls. As in many cases like our field case study Ammar Chowk Rawalpindi Remodelling Project, pavement design and retaining wall design are interconnected, which affects the whole project. So, there is a need to get some unique elements that gives us a combined application of transportation and structural engineering. Using traditional techniques can make a project very expensive.

OBJECTIVES

- To evaluate the effectiveness of geogrid as a reinforcement for sustainable strength of soil respective to unreinforced soil.
- Serviceability and Cost benefit analysis of the pavement.
- Dual application of geogrid in pavement along with MSE wall.
- Strength parameters of MSE wall as comparison with RC wall.
- Cost benefit analysis of MSE wall and RC wall.

MATERIALS AND METHODS

Materials

- **Soil**

We get the soil sample from our case study field Ammar Chowk Rawalpindi. By AASHTO soil classification we get soil type which is A-2-6 (Silty or Clayel Gravel Sand) with the help of Liquid Limit, Plastic Limit and by sieve analysis.

- **Geogrid**

As Tensar Biaxial geogrid is used in the Ammar Chowk Rawalpindi project, therefore we get the samples of geogrid from the field. A biaxial geogrid is a bi-directional structure with two-way stretch which provides the mechanical properties in two directions, both longitudinal and transverse.

- **Tensar Blocks**

Tensar Blocks are the concrete blocks used in both sides of the reinforced pavement and perform the action of MSE retaining wall.

- **Connectors**

Connectors are made up with polyfibers and helps to bind geogrid and tensar blocks. Connectors are provided for securing soil reinforcing elements to the face panels of a retaining wall for an earthen formation. The connectors comprise rigid eyes fixed to the panels and extensions formed on the elements for extension through the eyes. The eyes and extensions are selectively locked together and serve to orient the reinforcing elements in a horizontal disposition within the soil embankment being reinforced.

Figure 1. Tensar Geogrid

Figure 2. Tensar Block

METHODOLOGY

We classify the soil using the sieve analysis, liquid and plastic limit tests. Several laboratory experiments were conducted to investigate the possibilities of employing geogrid to improve soil strength in the pavement. The Standard Proctor test is performed as a compaction test, which yields Maximum Dry Density (MDD) and Optimum Moisture Contents (OMC) values for which samples are produced for testing. The CBR test provides the soil specimen's CBR values, which are necessary for pavement design. Sieve analysis, liquid limit tests, and plastic limit tests were carried out. The modulus of resilience is found by CBR value, and by using AASHTO empirical equation, we find the W18 and design life of the pavement. The cost estimation is done according to the rates of NHA pavement design. For geogrid reinforcement, different checks are applied on Tensar Geogrid Software. E.g., design life, ultimate strength, creep factor, durability factor, installation damage, tensile resistance, and design strength. Connection strength, e.g., block length, block height, and width, weight incline, infill, an inclination of forces, Max. Grid spacing. Grid coordination and serviceability result, e.g., level, left end, right end, length, coverage, pullout interaction factor, post-construction strain. For the MSE wall, the test on tensar block of size 4"x4"x4" to find dry weight and ultimate load and stress. We checked various stability factors (Verification of external stability, Verification of internal stability, Reinforcement layout, applied partial load factors and a resistance factor) and used partial material and a resistance factor. The cost comparison of the RC and MSE walls follows standard local rates.

ANALYSIS AND RESULTS

Table 1. Geogrid vs. Conventional method pavement design

Parameters	Unreinforced Soil	Reinforced Soil
Initial Cost	34 million	30.7 million
Life Cycle Cost	129.26 million	21 million
Total Cost	163.3 million RS.	51.7 million RS
Design Life	20years	65years
W18	14X10^6	45X10^6
Wearing course	4in	2in
Sub-base	6in	6in
Base	6in	6in
Rutting	20mm	5mm
Economical	68% more expensive	68% less expensive

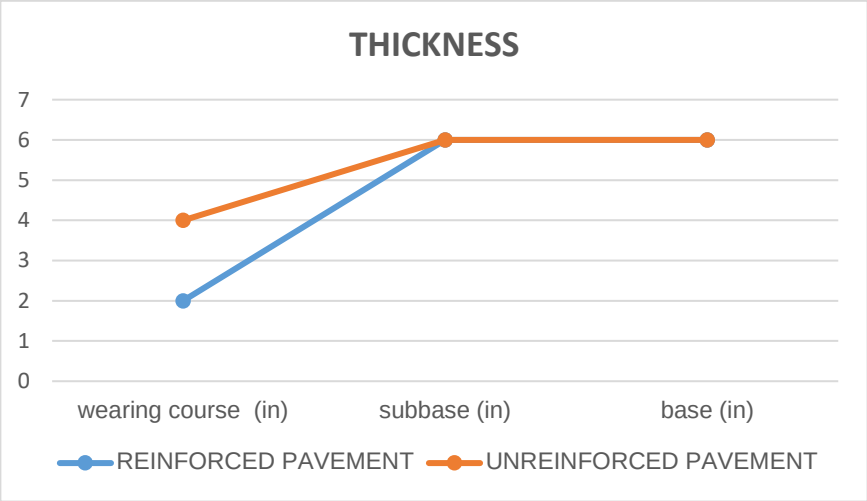

Figure 3. Geogrid vs. Conventional method pavement thickness

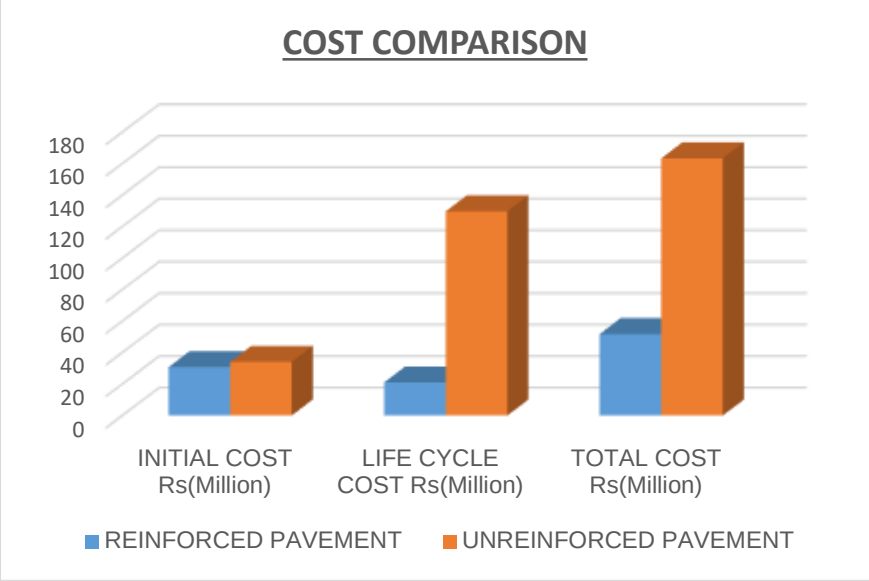

Figure 4. Geogrid vs. Conventional method pavement cost

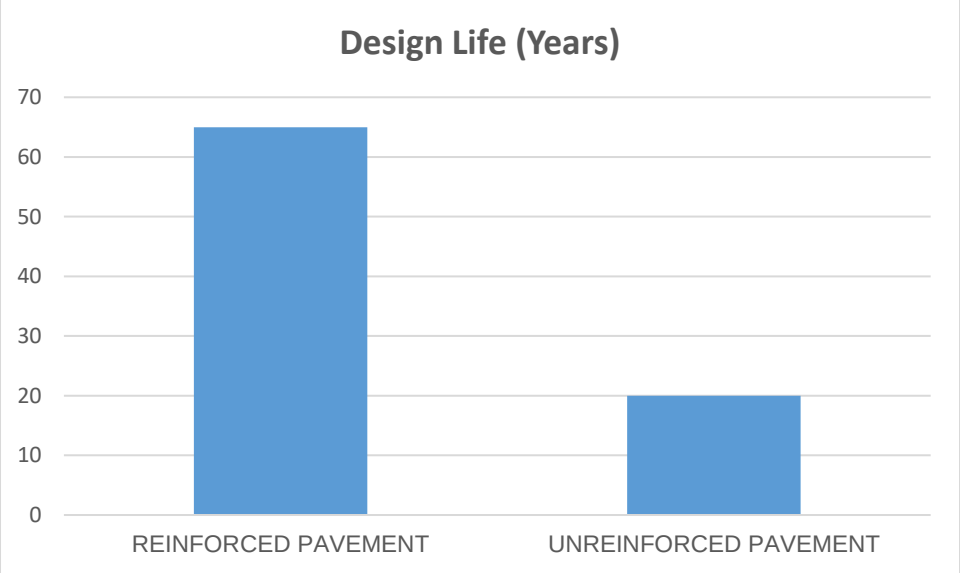

Figure 5. Geogrid vs. Conventional method pavement design life

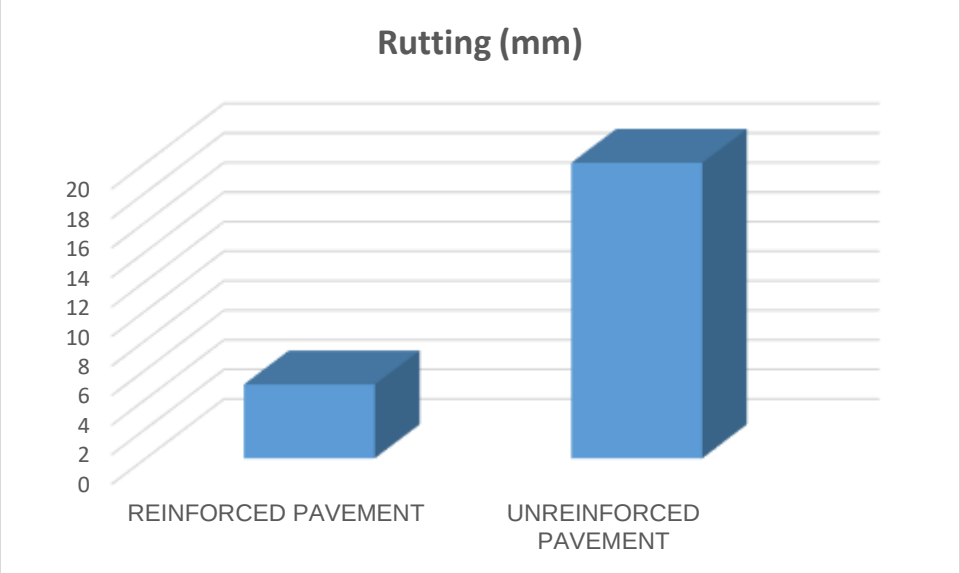

Figure 6. Geogrid vs. Conventional method pavement design Rutting

Our results show that the cost of the reinforced system is much more economical than the conventional system. The number of repetitions in reinforced is three times more than the unreinforced pavement by taking all the parameters constant except the modulus of resilience while flexible pavement design. The design life and the serviceability of the reinforced system are three times more than the conventional pavement. The design life of unreinforced pavement is twenty years, and the design life of reinforced pavement is sixty-five years. The thickness of the wearing course in reinforced pavement reduces to half of the thickness of the unreinforced wearing course. The process of rutting, deterioration, potholes, and cracks is also critical and plays a vital role while designing pavement. The geogrid reduces the rutting up to 90%, and this process is about negligible in reinforced soil.

Table 2. Strength Parameters of MSE Wall

Tensar Geogrid	Ultimate Strength (kN/m)	Creep Factor	Durability Factor	Installation Damage	Tensile Resistance Factor	Design Strength	Sliding Coefficient
	52.80	2.09	1.1	1.07	0.9	21.43	0.8

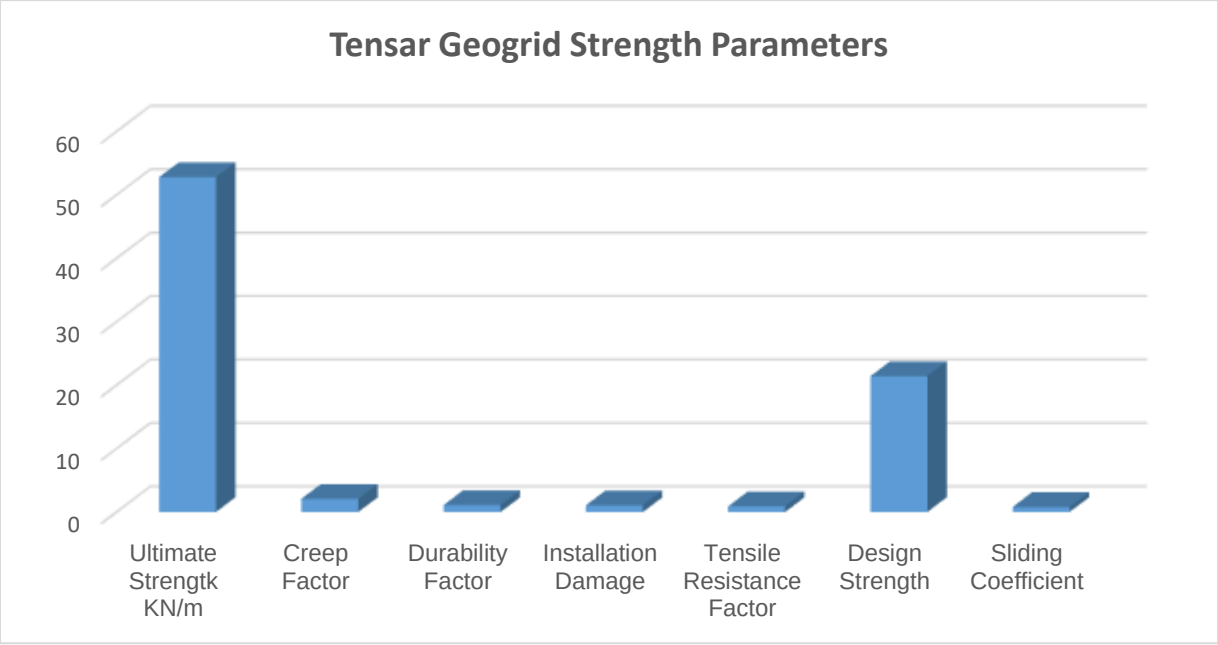

Figure 7. Geogrid Strength Parameters

Geogrid reinforcement design for static loading is to be checked and designed for 100 years, and the ultimate strength is 52.80, creep factor 2.09, durability factor 1.1, installation damage 1.07, tensile resistance factor is 0.9, design strength 21.43, and sliding coefficient is 0.8, and the serviceability factor is 4.82.

Table 3. Cost comparison of RC and MSE wall

Des.	MSE Wall	RCC R/W
Cost Estimate Rs. (Million)	**81.28**	**99.61**

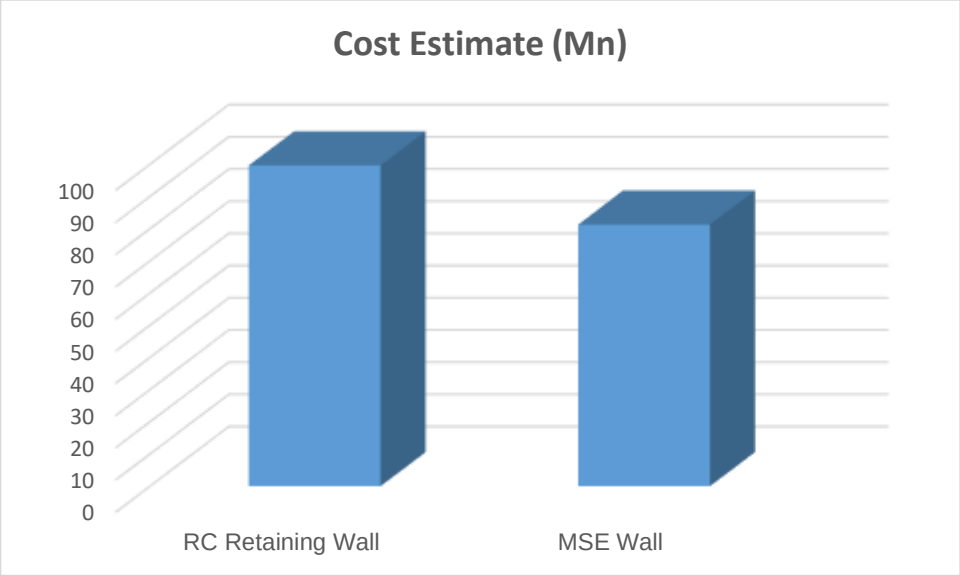

Figure 8. Cost comparison of RC and MSE wall

The total cost for the MSE wall is 81.28 million, and the RCC retaining wall is 99.61 million. MSE wall saves 18.4% cost in comparison to RC retaining wall.

CONCLUSIONS & RECOMMENDATIONS

The following conclusions are drawn from the given study:

- The number of vehicles passing through the geogrid reinforced pavement is three times more than unreinforced pavement. The design life of reinforced pavement could be fourty times more than the unreinforced pavement.
- The thickness of the wearing course in reinforced pavement reduces to half of the thickness of the unreinforced wearing course, and the geogrid reduces the rutting up to 90%, which is about negligible in reinforced soil.
- The life cycle cost of geogrid reinforced pavement is 68% less expensive than conventional pavement.
- MSE walls have no wedge and shear failure. MSE walls have a design life of 100 years, whereas RC walls are only for 40 years. MSE wall is more stable against tension failure and Earthquake forces and mainly resists more lateral forces acting on it. It is well durable against pull-out and push-out.
- And the cost of the MSE wall is 81.28 Mn, whereas the RC wall is 99.61Mn.

Some of the Recommendations are Geogrid Reinforced pavements should be in practice instead of conventional methods and that Local labour should be trained. There should be local industries for promoting geogrid locally. Awareness should be provided to local and primary contractors to install geogrid on local projects. MSE walls should replace RC walls because they are much better in all aspects.

ACKNOWLEDGEMENTS

Almighty Allah, the considerate, the most merciful, and the source of all knowledge and wisdom, deserves all praise and gratitude. All due respect to his holy prophet (PBUH), who will always be

a lighthouse for us all. I'm grateful to my supervisor for his wise advice and support throughout my academic endeavor.

REFERENCES

1. Suku, L., Prabhu, S.S. and Babu, G.S., 2017. Effect of geogrid reinforcement in granular bases under repeated loading. Geotextiles and Geomembranes, 45(4), pp.377-389. https://www.researchgate.net/publication/267990573_Improvement_of_Flexible_Pavement_Wit h_Use_of_Geogrid

2. Allen, T.M. and Bathurst, R.J., 2019. Geosynthetic reinforcement stiffness characterization for MSE wall design. Geosynthetics International, 26(6), pp.592-610. https://www.constructionspecifier.com/mechanically-stabilized-earth-walls/

3. Cardile, G., Pisano, M. and Moraci, N., 2019. The influence of cyclic loading history on soil-geogrid interaction under pullout condition. Geotextiles and Geomembranes, 47(4), pp.552-565. https://apps.ict.illinois.edu/projects/getfile.asp?id=9779

4. Saride, S., Baadiga, R., Balunaini, U. and Madhira, M.R., 2022. Modulus Improvement Factor-Based Design Coefficients for Geogrid-and Geocell-Reinforced Bases. Journal of Transportation Engineering, Part B: Pavements, 148(3), p.04022037.

5. Baadiga, R., Saride, S., Balunaini, U. and Madhira, M.R., 2021. Influence of tensile strength of geogrid and subgrade modulus on layer coefficients of granular bases.

2nd International Conference on Advances in Civil and Environmental Engineering (ICACEE-2023)

University of Engineering & Technology Taxila, Pakistan

Conference date: 22nd and 23rd February, 2023

The Study of Intermolecular Bonding of Bituminous Material using Compositional Analysis

H M Nouman[1], Shahzaib Farooq[1], Rana Ehtisham[2], Ali Ahmad[3], Aziz ur Rehman[4]

[1]Department of Civil Engineering, University of Engineering, and technology Taxila, nomankhan12364@gmail.com

[1]Department of Civil Engineering, University of Engineering and Technology Taxila, shahzaibfarooq010@gmail.com

[2]Department of Civil Engineering, University of Engineering and Technology Taxila, Rana.Ehtisham@students.uettaxila.edu.pk

[4]Department of Civil Engineering, University of Engineering and Technology Taxila, azizkhan5541@gmail.com

ABSTRACT

Bitumen is amorphous, black-coloured visco-elastic material, composed principally of hydrocarbons having high molecular weight characterized by “asphaltenes, resins and oils”

Investigation on the composition of Bitumen having same grade taken from different Refineries i.e., NRL, ARL as Virgin Binder (VB) and RAP (extracted from the pavement). Also the careful examination of the Intermolecular Bonding of the Bitumen Microstructure by a review of studies and correlation with its composition.

In research methodology, firstly SARA analysis was performed by Column chromatography on each type of bitumen. Secondly, microstructure intermolecular bonding was investigated theoretically from the literature of methods Scanning Electron Microscopy (SEM), ESEM etc. and its critical analysis was conducted.

From the research results, it has been found out that there are solid and liquid phases having different percentage compositions of the bitumen that are Saturate, Aromatic, Resin, and Asphaltene (SARA) according to their polarizability and polarity of each type of bitumen. Asphaltene is a solid phase while the other three are in liquid phases that are basically taken from Maltene. Then Compared SARA Results of VB with RAP. Data obtained from compositional analysis of asphalt help us to handle the problems related the stability of bitumen structure. While microstructure intermolecular bonding study theoretically from the literature using techniques like SEM, ESEM etc helped to understand the internal nature of the bitumen when it is aged, unaged and modified by many modifiers like CNF, SBS, SBR latex fibre etc

KEYWORDS: SARA Analysis, Scanning Electron Microscopy (SEM), Bitumen, Microstructure

INTRODUCTION

Bitumen has been used in road construction and engineering since the days of early Babylon [1]. Currently, it's one of the main road transportation infrastructure products. Approximately 95 percent of worldwide bitumen supply (approximately 100 Mt/year) is utilized as asphalt mixtures for the paving business[2]. Bitumen is a complicated substance, and its characteristics appear to be different based on source, process of production, contaminants, and additional chemical-physical treatment. The complicated chemical composition of bitumen makes most analytical approaches difficult beyond the point of applicability.

A commonly known analytical method is to classify bitumen into a Saturated, Aromatic, Resin, and Asphaltene fraction (SARA) due to same chemical behaviour. SARA methodology of analysis which separates elements of crude oil according to their polarity and polarization. SARA research is a very wide area for studying bitumen and related properties of bitumen compositions. Asphaltene is the insolvable n-heptane and toluene dissolve portion of bitumen while in n-heptane this portion is called maltene. Maltene consists of the Saturates, Aromatics and Resins that are separated by column Chromatography. It is the procedure of bitumen isolation which is most accepted and effective.

Scholarly work on bitumen as well as its bonding demonstrates and provides strong proof that bitumen really has a significant composition and micro-structure that can be evaluated and visualized using different techniques. Such methods are “Small Angle X-ray Scattering (SAXS)”, and studies with “Small Angle Neutron Scattering (SANS)” have shown beyond doubt that there are organized structures and configurations in bitumen. Although Atomic Force Microscopy (AFM) and Scanning Electron Microscopy (SEM) showed a distinctive and reproducible presence morphology that is sometimes defined as 1–5 μm "bee-like" structures [3].

“Confocal Laser Scanning Microscopy (CLSM) has uncovered the existence of fluorescent centres in bitumen of 1–10 μm size [4]. CLSM is effective of monitor highly localised fluorescence emission as well as enables for comprehensive examination of the asphalt bitumen [5]. This may be utilised to accurately visualise bitumen microstructure as well as the structural impacts of bituminous alteration [6]. In this research, SARA compositional analysis of given bitumen have been performed in details and their correlation with the literature investigation of intermolecular bonding of bitumen have been explained.

LITERATURE REVIEW

SARA analysis is crucial for examining how the bitumen and crude oil's characteristics relate to composition. SARA fractions effects rheology properties like dynamic modulus rises by increase in asphaltene or resins. Also, SARA analysis helps to make an approach for the study of microstructure of bitumen. A Scientist [7] researched the impact of fractions in 1979 by introducing asphaltene in varying proportions to the original asphalt. This study revealed that asphalt binder viscosity increased with the increase in asphaltene content and reduced with the increase in maltene content.

SARA fractions in correlated with microstructure of bitumen by fluorescent approach [4]. They had taken the five different grade bitumen and did CLSM on it. They used the excitation radiation of wavelength 488 mm and after that they observed the emission radiation from bitumen of wavelength 500-530 and by these radiations, they got the image that was showing the microstructure image of the bitumen. In the study, they separated the bitumen in the Asphaltene and Maltene and Maltene further separated in Saturates, Aromatics, Resins and found that resin and aromatic phases are the only elements able to produce adequately intense fluorescent emissions. It is a clear justification for a complicated internal micro-structure which consists of an aromatic mantle covering an inner core [8].

Various microscopic techniques, such as optical microscopy, SEM, ESEM etc used in past and now a days for microscopic intermolecular analysis. Gaskin, et al. used ESEM not just to asphalt binder but also bitumen percentage fraction including asphaltene, maltenes, and waxes . The network structuring has been seen at varying temperatures [9].

Bitumen is the typical kind of rheological material. When comparing the rheological properties with the SARA fraction of modified asphalt binders shown that they have a greater impact on dynamic modulus and Phase Angle. The dynamic modulus increases when frequency increase and achieves a steady value whenever the frequency is relatively high [10].

Asphalt is usually considered to be a colloidal structure consisting of fractions of SARA. Various asphalt fractions obey a colloidal rule [11]. The colloidal instability index (CII) is an approach to determine the instability of heavy oil which is based on the chemical composition of crude oil. It is reflecting or showing the stability index of the bitumen Fractions like Maltene or Asphaltene. Stability of crude oil can be analysed by the equation (1).

$$Colloidal\ instability\ index\ (CII) = \frac{Saturates + Asphaltenes}{Aromatics + Resins} \quad (1)$$

The crude oil or bitumen stability can also be evaluated by using the SARA fractions. When the CII is lesser than 0.7 then it is recognized as stable while when CII value is 0.9 then the bitumen is unstable [12].

METHODOLOGY

The methodology includes the material selection and specific experimental testing that are used for investigation purpose. In This study comprises on two phases, first describes the materials and second is related to experimental work.

Materials

Three types of asphalt binders were used. They are RAP (Reclaimed asphalt pavement) that are extracted from detritus Road of Taxila, and its Grade is checked during testing by penetration grade and compared with the virgin binder (penetration grade 60/70) (PG-58-22) from Attock (ARL) & Karachi (NRL) refineries.

RAP was extracted according to ASTM D2172 and ASTM D5404. The aggregates and asphalt binder has been separated from RAP by centrifuge extraction method using the trichloroethylene (TCE) solvent according to ASTM D2172. TCE was vaporized from the extracted material by rotary evaporator in accordance with ASTM D5404.

Experimental Program:

Analysis of bitumen fractions using SARA analysis test according to ASTM D4124 is shown in Figure 1. While rheology study would be done by DSR tests and critically analysis from literature and investigation of the microstructural behaviour of bitumen would also be done by Scanning Electron Microscopy (SEM) and ESEM literature study theoretically and then would correlate them by compositional analysis (SARA) testing data.

SARA Analysis:

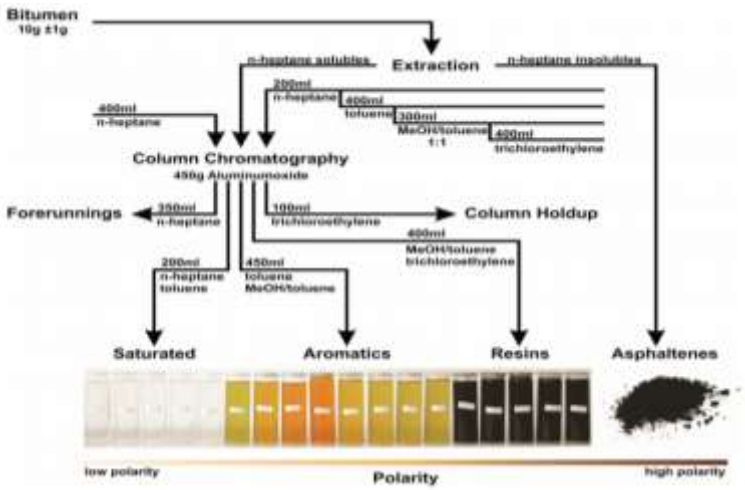

Figure 6: Schematic SARA analysis Procedure according to ASTM D4124

Rheological Analysis:

Rheological Properties test was carried out on the Anton Paar Peltier dynamic shear Rheometer (DSR) by which the program investigates the Performance Grading (PG) of the bitumen and also Frequency sweep test (FST). Using this test, the stiffness or resistance of the bitumen against deformation under the repetitive load according to ASTM D7175− 15 can be evaluated. The samples for all three types of asphalt were made that were then used in the experimental study. The sample made is 25 mm in diameter and 1 mm thick. To determine the time / temperature responsiveness Frequency sweep test have been performed. This analysis expresses the oscillatory shear stress at a constant strain level as well as calculates the volume and failure modulus at a specified frequency and temperatures scale.

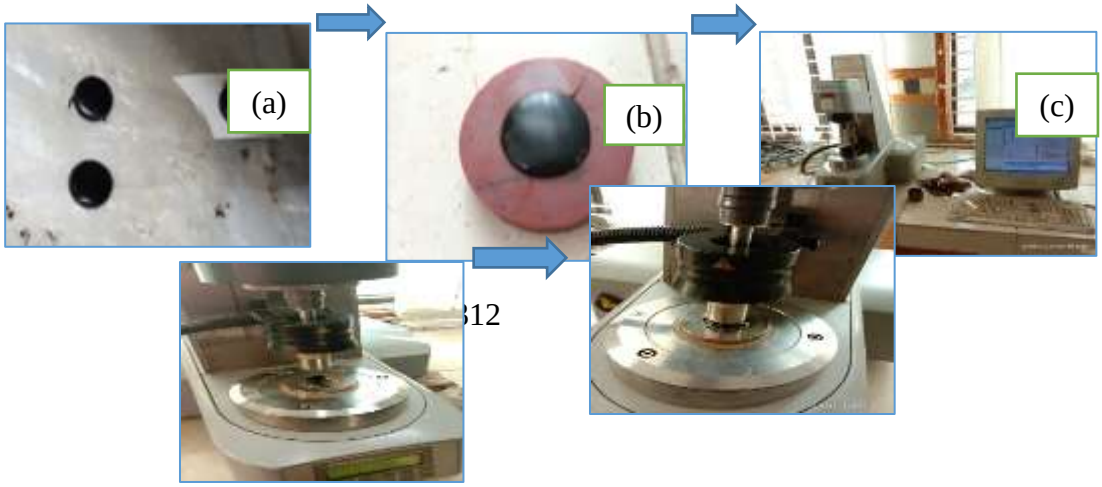

(d) (e)

Figure 7: From left to Right (a) Asphalt Samples, (b) Mould for making specimens, (c) DSR, (d) sample placing , (e) Applying Loading

SEM Analysis:

The region that has been micro-analysed is treated by a SEM equipment with a closely aligned electron ray, which might have travelled across the surface or dynamically in a raster. The whole SEM Analysis technique is depicted in the schematic image below.

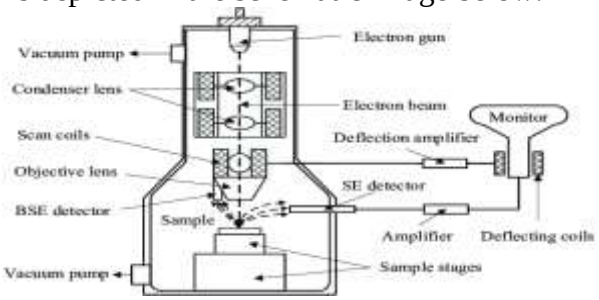

Figure 8: schematic diagram of SEM Analysis [13]

RESULTS AND DISCUSSIONS

ARA fractions of the Asphalt binder were isolated by using the method of Column Chromatography. The Results of SARA fraction and their stability index according to ASTM D4124 are shown in the following charts. The value of Saturates in all three binders approximately near each other and it is also decreasing from ARL to RAP. While aromatics values of VB have almost equal and a significant change in the RAP value that make RAP less viscous. Also, the RAP has maximum value of Asphaltene that make the RAP stiffer than ARL and NRL. From CII curve it can be seen that the RAP is unstable in nature as compared to VB because of the high value of asphaltene content. This high value asphaltene also showed that the dispersion/scattering of the asphaltene is week. Rheology properties of RAP has higher performance Grading temperature that was about the 88 ^{0}C. As far as microstructural analysis investigation of bitumen concerns, it has been done by reviewing the past studies of many researchers. A lot of researchers

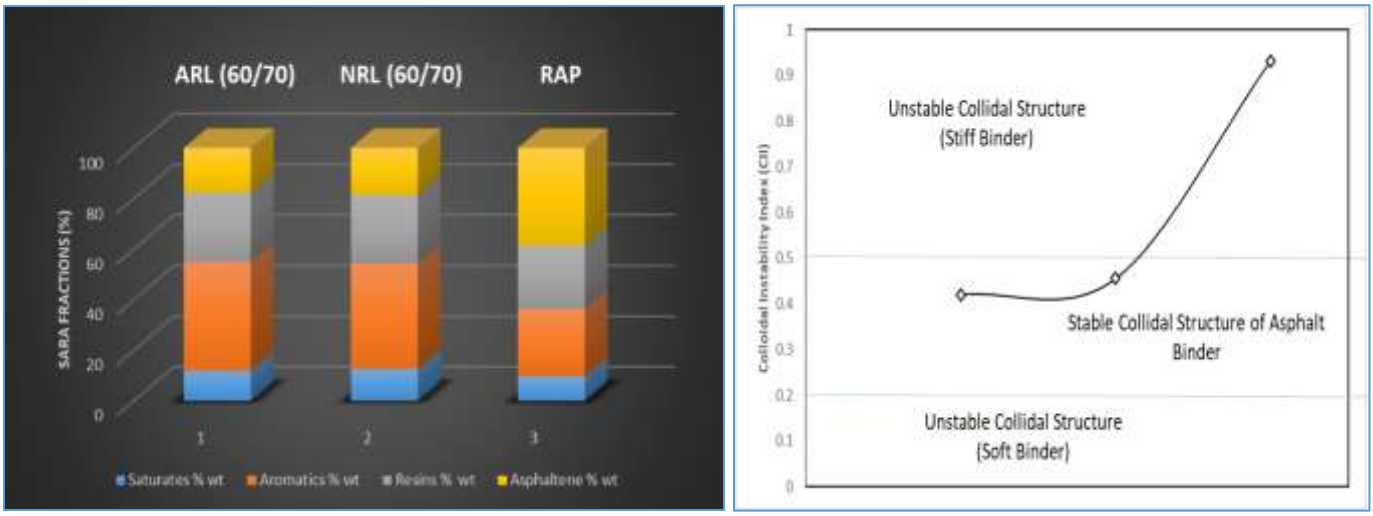

Figure 9: Left to Right Bar Chart of SARA Fraction of Virgin Binder (60/70) ARL, NRL & RAP Binder and CII Chart

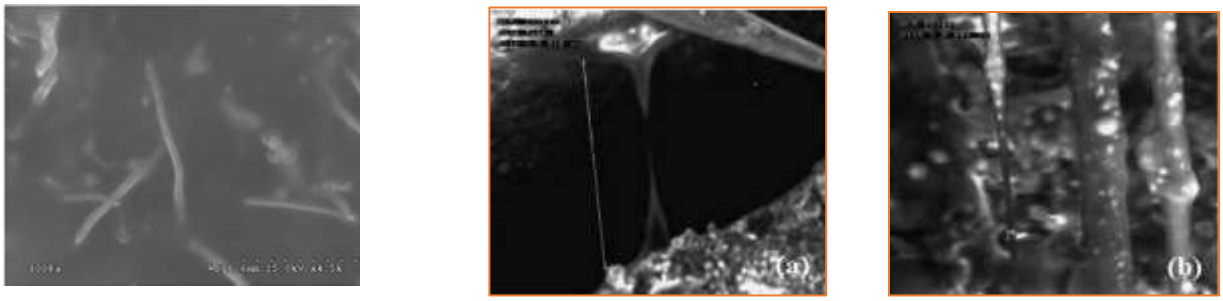

Figure 10: (a) deformation mechanism of necking with fibril and
(b) Deformation mechanism of Elongation with fibril [15]

did study from last 20 to 30 years on the microstructure of the bitumen of different grades using SEM and ESEM techniques.

In 2013, A researcher used SEM analysis to investigate CNF (Carbon Nano-modifiers) modified HMA. The results shows that when CNF amount increases the binder density increases. That

means the interconnectivity would strong and good internal structure would be made. This is showing in Fig. 5 in the form of the linear CNF structure. But at the root of the CNF, SEM shows the cone shaped structure of the modified binder. This shows that the high adhesion in the Binder [14]. The study carried out in 1997 by modifying bonder using SBS, SBR latex polymer was investigated using ESEM. They noted that the fibril or small slender fibre type structure have been made due to the concentration of the fibre. Due to the SBR addition a significant change in the microstructure of binder. Because of this, the density of the fibril structure grows, and a particularly special type of deformation called elongation rather than necking results as shown in Figure 6. These types of morphology are very helpful in the asphaltic concrete to which the cracks that are producing can be healed easily [15].

Theoretical investigation on the Rheological properties like PG, FST etc was conducted. The results showed that when the binder in its original form they have the extreme high and low temperature. Like change of PG ‘80-16’ to PG ‘70-10’ But with the addition of the rejuvenator like sulphur, etc. the PG can be set on the standard range. While Asphaltene has greater impact on FST property of the binder that dynamic modulus rises with the rise in quantity of asphaltene. At low frequencies the differences between various modulus curves are greater than at higher frequencies [7].

CONCLUSIONS

- RAP has maximum value of Asphaltene compared to Virgin Binders that makes RAP solid in nature and unstable than Virgin Binders. While CII of RAP is 0.931 that make its stiffer binder. This high value of asphaltene shows that the dispersion/scattering of the asphaltene is week.
- Temperature for Rheology characteristics such RAP greater performance grade was about 88 C. The quantity of asphaltene has an effect on rheological parameters such as PG and FST, among others. With more asphaltene present, the FST property of the binder is more significantly affected, and the dynamic modulus increases.
- When an asphalt binder is altered and artificially aged, the bonding structure of the material manifests itself differently. SEM, ESEM, CLSM, AFM, and other techniques and apparatus have a stronger influence on the binder's microstructure.

- Using the modifiers like CNF, SBS, SBR latex fibre, increases the density of asphalt binder by making the network and fibre thread like structure. These types of morphology are very helpful in the asphaltic concrete to which the cracks that are producing can be healed easily

1 REFERENCES

1. Abraham H (1920) Asphalts and allied substances, 4th edn. D. Van Nostrand Company Inc., New York.
2. Lesueur D (2009), The colloidal structure of bitumen: consequences on the rheology and on the mechanisms of bitumen modification, Adv Colloid Interface Sci, 145:42–82. doi:
3. Wilson A, Champion-Lapalu L, Fuchs G, Martin D, Planche JP (2002) Cryo-scanning electron microscopy: a new tool for interpretation of fracture studies in bitumen/polymer blends. Energy Fuels 16:143–147. doi: 10.1021/ef010122s
4. Bearsley S, Forbes A, Haverkamp RG (2004) Direct observation of the apshaltene structure in paving-grade bitumen using confocal laser-scanning microscopy. J Mi-crosc 215:149–155
5. Lackner R, Spiegl M, Blab R, Eberhardsteiner J (2005) Is low-temperature creep of asphalt mastic independent of filler shape and mineralogy? Arguments from multiscale analysis. J Mater Civ Eng 17:485–491
6. Sengoz B, Isikyakar G (2008) Analysis of styrene-butadiene-styrene polymer modified bitumen using fluorescent microscopy and conventional test methods. J Hazard Mater 150:424–432. doi:10.1016/j.jhazmat.2007.04.122
7. John M. Dealy (1997), Rheological properties of oil sand bitumen, The Canadian Journal of Chemical EngineeringVolume 57, Issue 6 p. 677-683
8. Florian Handle et al. (2016), The bitumen microstructure: a fluorescent approach, Materials and Structures 49:167–180
9. Gaskin J. On bitumen microstructure and the effects of crack healing. UK: University of Nottingham; 2013. Ph. D thesis.
10. “Yongli Xu, Ph.D.Enhao Zhang and Liyan Shan, Ph.D”, “Effect of SARA on Rheological Properties of Asphalt”, “Binders Materials in Civil Engineering”, (June 2019)
11. Lesueur, D. 2009, The colloidal structure of bitumen: Consequences on the rheology and on the mechanisms of bitumen modification, Adv. Colloid Interface Sci. 145 (1 –2): 42–82.
12. S. Verdier, Experimental study and modelling of asphaltene precipitation caused by gas injection (Ph.D. thesis), Technical University of Denmark, 2006.

13. Yao, Sheng & Hai, Li &Shuiquan, Pang & Zhu, Benliang& Zhang, Xianmin&Fatikow, Sergej. (2021). A Review of Computer Microvision-Based Precision Motion Measurement: Principles, Characteristics, and Applications. IEEE Transactions on Instrumentation and Measurement. PP. 1-1. 10.1109/TIM.2021.3065436.
14. Khattak, A. Khattab, P. Zhang, H.R. Rizvi, T. Pesacreta, Microstructure and fracture morphology of carbon nano-fiber modified asphalt and hot mix asphalt mixtures, Mater. Struct. 46 (12) (2013) 2045–2057.
15. A. Bhurke, E. Shin, L. Drzal, Fracture morphology and fracture toughness measurement of polymer-modified asphalt concrete, Transport Res Record J Transport Res. Board 1590 (1997) 23–33 .

2nd International Conference on Advances in Civil and Environmental Engineering (ICACEE-2023)

University of Engineering & Technology Taxila, Pakistan

Conference date: 22nd and 23rd February, 2023

EFFECT OF POLYETHYLENE ON THE VISCOSITY AND SHEAR RATE OF BITUMEN

Naveed Ahmad[1], [1]UET Taxila, naveedahmad7630@gmail.com
Imran Hafeez[2] , [2]UET Taxila, imranhafeez@yahoo.com

ABSTRACT

Several research studies in the past have focused on the development of modified asphalt materials to enhance the overall performance of pavements. One of the approaches was to utilize waste plastic in the asphalt materials. Utilizing waste materials in the construction of roads is an environmentally sustainable solution. This study discusses the addition of various plastic types to petroleum bitumen. The bitumen used in the construction of the pavement was modified using plastic components. Pure bitumen and five modifications with modifier contents of 0%,2%, 3% ,4%, and 5% were evaluated. Rotational viscosity on 60/70 grade PARCO and ARL bitumen was measured to investigation the effect of plastics on bitumen properties. At 5% Polyethylene the value of absolute viscosity is maximum in both ARL and PARCO samples. In case of apparent viscosity both ARL binders and PARCO binders at 135 °C And 165 °C it increases as the proportion of polyethylene content rises from 0%, 2%, 3%,4%, and 5%.
At 135 °C PARCO shows maximum shear thinning at 4% Polyethylene and ARL shows maximum shear thinning at 4%. At 165°C the PARCO shows maximum shear thinning at 2% of Polyethylene while ARL shows maximum shear thinning at 2% Polyethylene.

KEYWORDS: Waste plastic, modified bitumen, and a rotational viscometer

INTRODUCTION

Asphalt roads can be made from a sizable portion of the garbage generated in metropolitan and peri-urban areas. It has been demonstrated that asphalt roadways technically have the ability to recycle a variety of waste items, including glass, asphalt, concrete, wood, and used tyres. Estimates were made of the available volumes of European waste that would otherwise be burned or dumped in landfills. Additionally, it was demonstrated that Europe has a large potential for recycling in the field of road construction, particularly in the case where 33% of new roads are constructed utilising the target waste materials [1].

The results show that the specimen with 20% cement and 4% bentonite had a high initial, cured strength and a high cracking resistance at low temperatures. This study replaced mineral filler with cement and bentonite using 20%, 40%, and 60% cement according with 4%, 8%, and 12% bentonite in cut back asphalt. The results also showed that the 40% cement content group had the highest unconditioned IDT strength and the 20% group had the highest unconditioned Marshall stability. [2].

Due of their resistance to rutting, polyolefins are desirable possibilities for modifying asphalt. Polyethylene (PE) is used to represent plaster. In new studies there is addition of low-density polyethylene (LDPE) to concrete mixtures containing asphalt, and the effect on fracture toughness was investigated. The asphalt mixture received LDPE additions that were weighted. The three different LDPE concentrations (1.5, 3, and 4.5%) were combined with the asphalt binder before being used to make the asphalt mixture. It was determined fracture toughness using the J-integral concept. The results of the study showed that LDPE-modified asphalt binders have better physical properties and greater fracture toughness than unmodified asphalt binders. With regard to fracture toughness, mixes treated with 4.5% LDPE exhibited the highest levels. [3].

As large concentrations of the polymers were applied, the polymer-modified binders significantly changed from having a reduced dependence on shear rate to having an increased dependence on shear rate, with non-Newtonian behaviour predominating. Since the viscosity behaviour changes on time, concentration, and the type of polymer used, the theory of the viscous fluid for determining the mixing and compaction temperature of such modified binders is broken. [4]

There is also replacement of Trinidad Lake Asphalt (TLA) and Trinidad Petroleum Bitumen (TPB) with PE and examined its rheological properties. Three different LDPE percentages—0.5, 2 and 3% of LDPE by weight—were used to make TPB-LDPE and TLA-LDPE. The results of the investigation demonstrated that the G* value increased as the fraction of LDPE increased. [5].

There is also examination of the properties of asphalt mixtures incorporating HDPE and LDPE additives using the Marshall Mixture design approach. The heated asphalt mixture contained both intact and ground polymers. It was found that adding PE to asphalt mixtures increased stability and VMA levels when compared to asphalt mixtures without the addition. Asphalt mixtures changed with HDPE have superior engineering properties as compared to those treated with LDPE. The asphalt mixtures with 12% ground HDPE had the greatest stability. Asphalt mixtures with PE modifications frequently offer greater rut and fatigue resistance. [6].

The effects of using recycled polyethylene into asphalt binders is also evaluated. To change the asphalt binder, recycled LDPE and PE with a low molecular weight were both employed. It was shown that asphalt binders changed with recycled LDPE components performed better than those modified with low molecular PE. [7].

The thixotropy of four types of binder hysteresis loop is also determined which is, stepwise test, single shear rate, dynamic modulus, and structural kinetic method in order to develop thixotropy models. and found that the asphalt binder's thixotropic tendencies depend on the maximum shear rate applied, that the stepwise test using an 8-mm parallel plate does not accurately reflect the thixotropy of asphalt binder, that the viscosity of asphalt binder changes under a single shear rate according to a general exponential function, and that the structural kinetic method and dynamic modulus method reflect the long-term thixotropy of asphalt binder. [8].

Two different penetration grades of bitumen, PEN 70/100 and PEN 160/220, were utilised on reversible changes in microstructure after mechanical loading to see the manifestation of the loss and recovery of microstructure. The varying penetration grades of bitumen have microstructural differences that affect the crack forms and damage levels. In the presence of thermal energy or rest periods, the molecular structures change, reorganise, and adopt new configurations. The reversible formation of the bitumen microstructure is thought to be the main cause of thixotropy [9].

PROBLEM STATEMENT

At a particular temperature range, an asphalt binder can behave in a non-Newtonian manner. Asphalt binder is of the shear-thinning type of non-Newtonian liquid. The dependence of shear viscosity on shear rate is a characteristic of an asphalt binder's shear-thinning or pseudo-plastic behavior. A thorough understanding of these binders' viscosity at manufacturing and construction temperatures (often above 135°C) offers crucial knowledge regarding their pumpability, mixability, workability, and placement.

OBJECTIVES

- To investigate the absolute viscosity of an asphalt binder with a range of Polyethylene content.
- Studying the impact of shear stress on the viscosity of various binders with various Polyethylene content ratios.
- Analyze how Polyethylene affects the viscosity of the asphalt binder at various temperatures and shear rates

METHODOLOGY

Five Phases are used to evaluate the research methodology of this research study. In Phase 1, There is investigation of shear thinning behavior of bitumen as well as the relationship b/w viscosity and shear rate for modified bitumen related to past studies.

In Phase 2 and 3, there is selection and preparation of bitumen samples of five replicants made from ARL and PARCO bitumen will be prepared for each polyethylene modified asphalt content (0%, 2%,3%, 4%, and 5%), as well as control samples. In Phase 4, Testing was carried out to ascertain the modifier's impact on bitumen after it has been mixed with the asphalt binder and chosen. This test matrix is displayed

In final Phase the analysis is done with respect in which the asphalt binder is defined by its rotational viscosity in terms of its workability during mixing and pumping. AASHTO T316 standard test method, was used to conduct the Rotational Viscometer (RV) test. [At] a temperature of 135°C and 165°C, the asphalt binder sample was poured into the RV test samples and put into the RV container. A 20-rpm rotating speed is applied as the spindle is inserted into the asphalt binder sample. The rotational viscosity is determined by calculating the torque necessary to achieve this speed.

c. The rotational viscosity was provided by the RV device in (c P or m Pa. s). A total of five readings were taken at every single minute. The test materials include [virgin] asphalt binder and PE/A mastics with percentages of 0%, 2%,3% ,4%, and 5% by [volume] of asphalt binder.

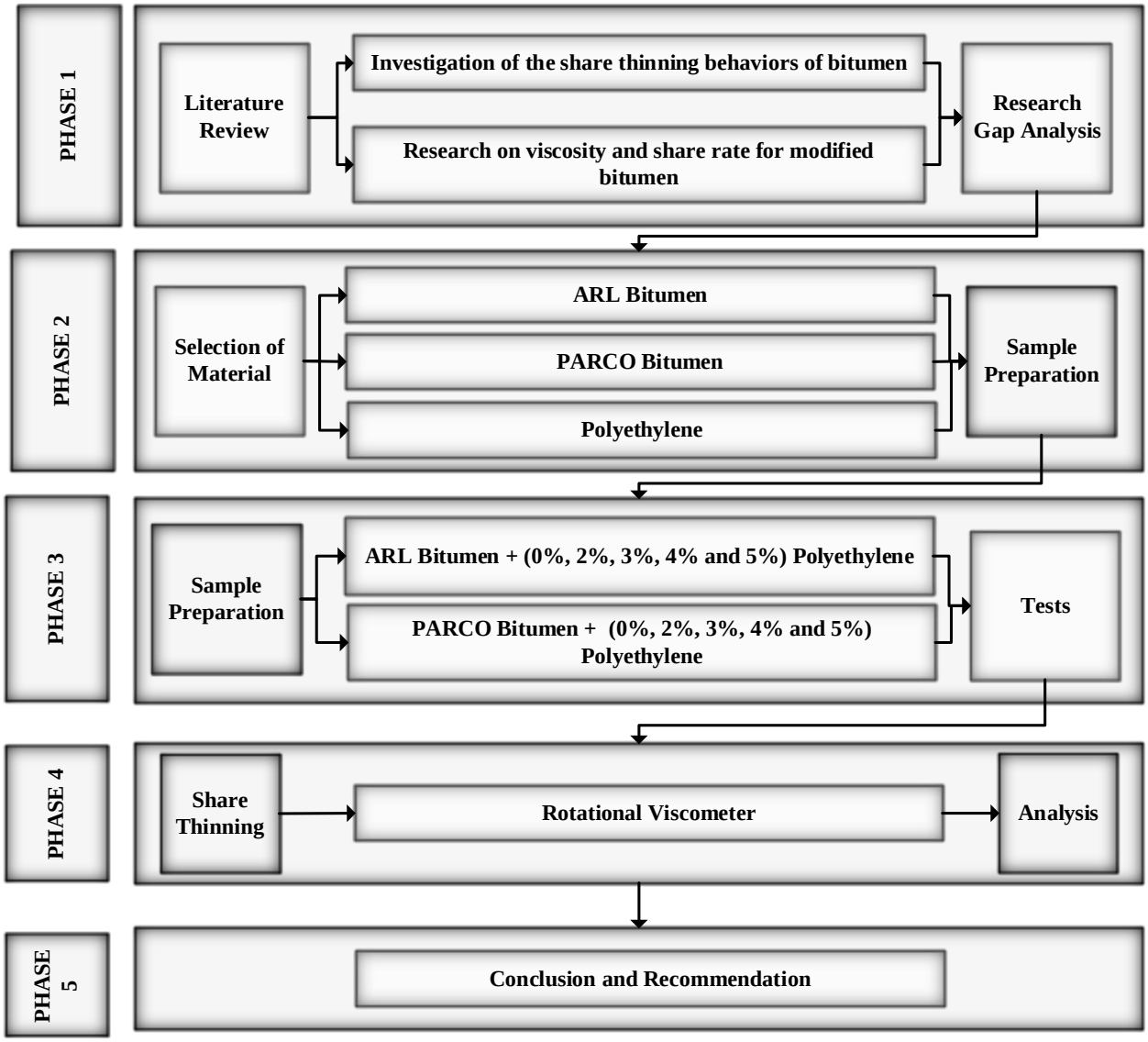

Figure 1: Flow Chart of Methodology

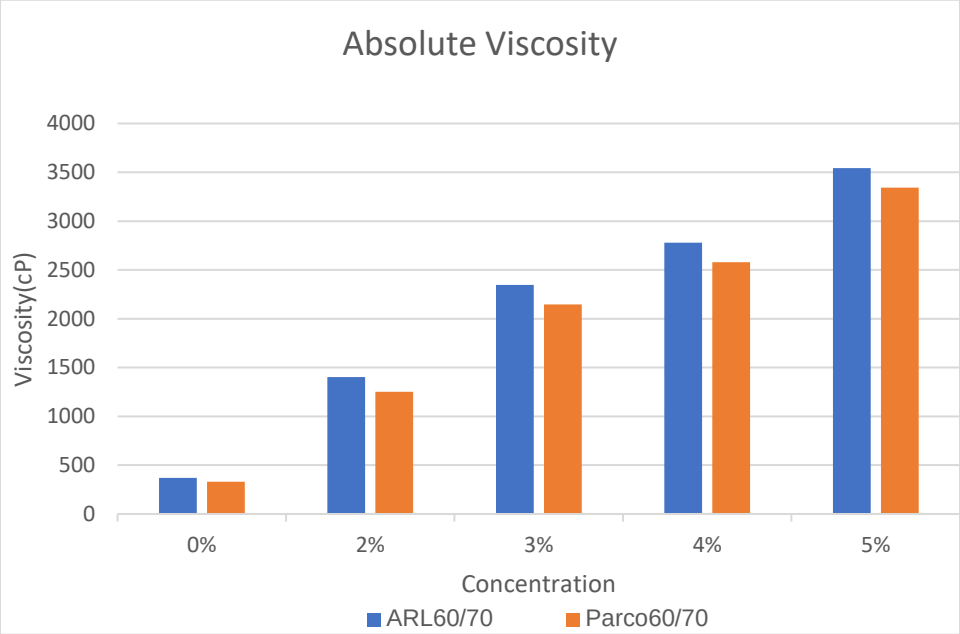

Figure 2: Absolute viscosity Value Graph

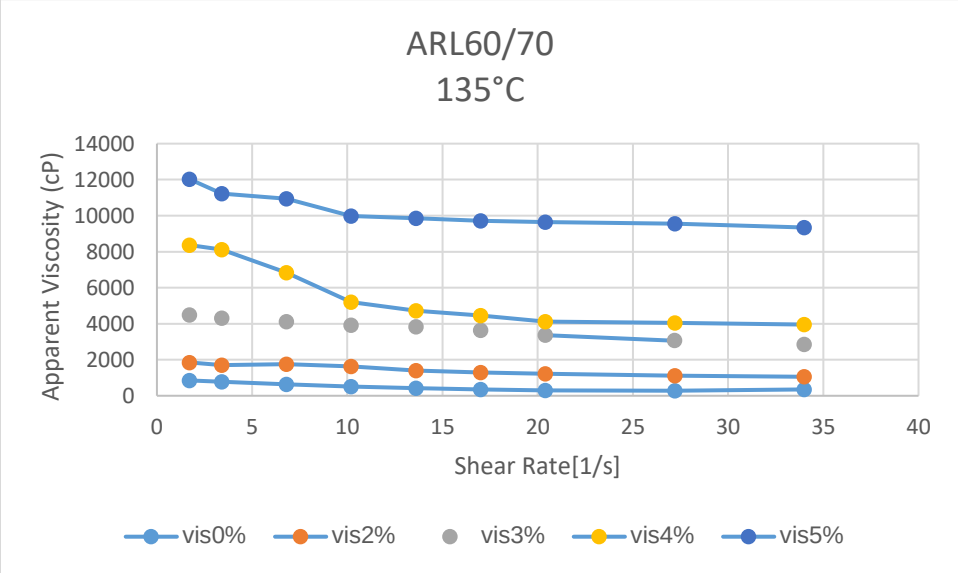

Figure 3: Apparent viscosity value Graph

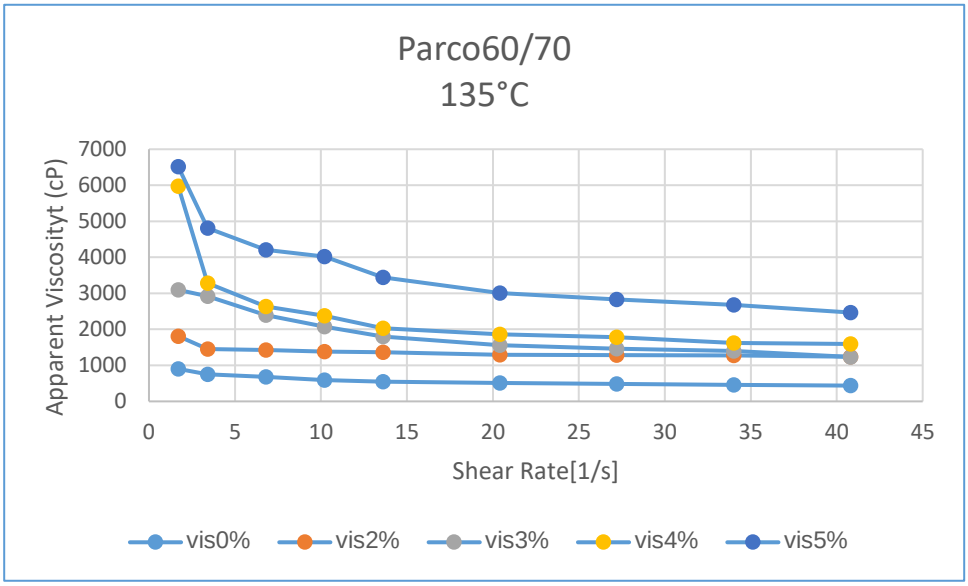

Figure 4: Apparent viscosity value Graph

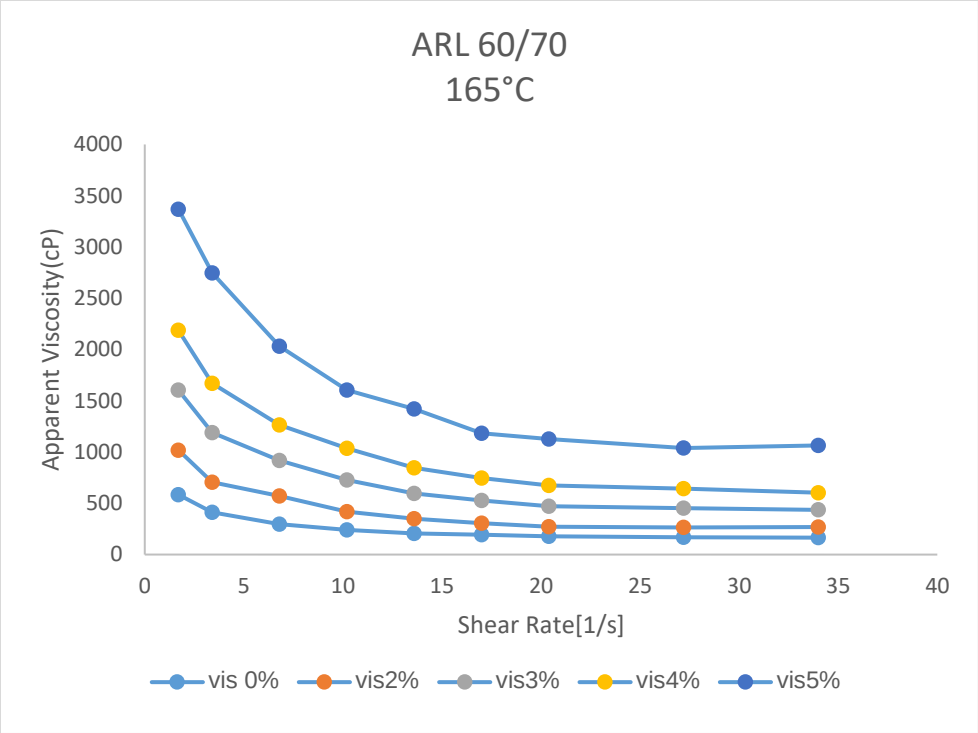

Figure 5: Apparent viscosity value Graph

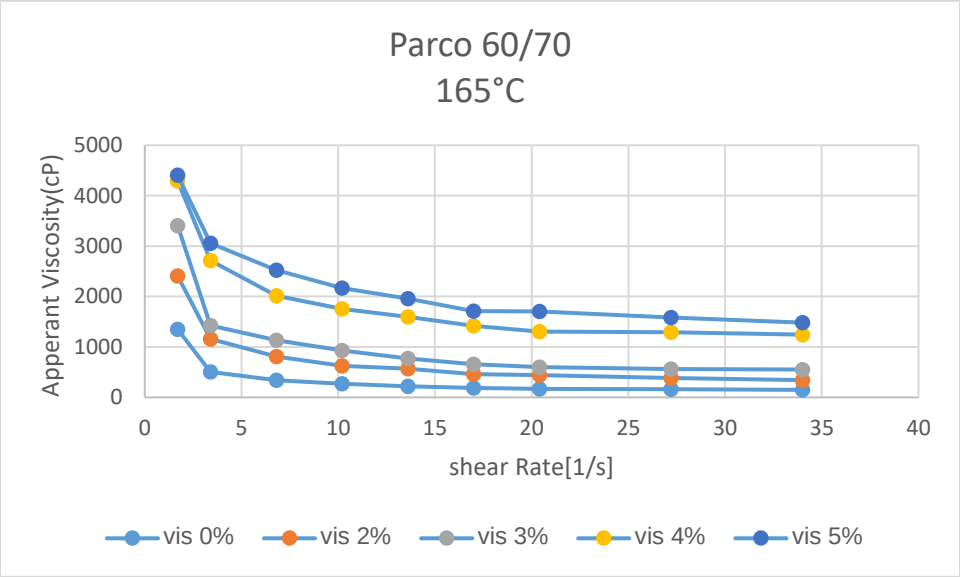

Figure 6: Apparent viscosity value Graph

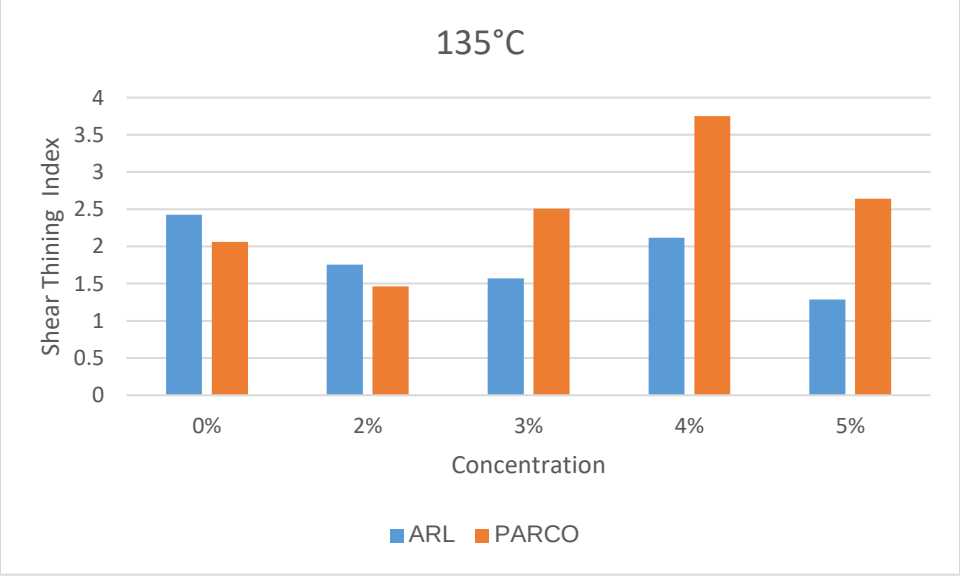

Figure 7:Shear Thining Index value Graph

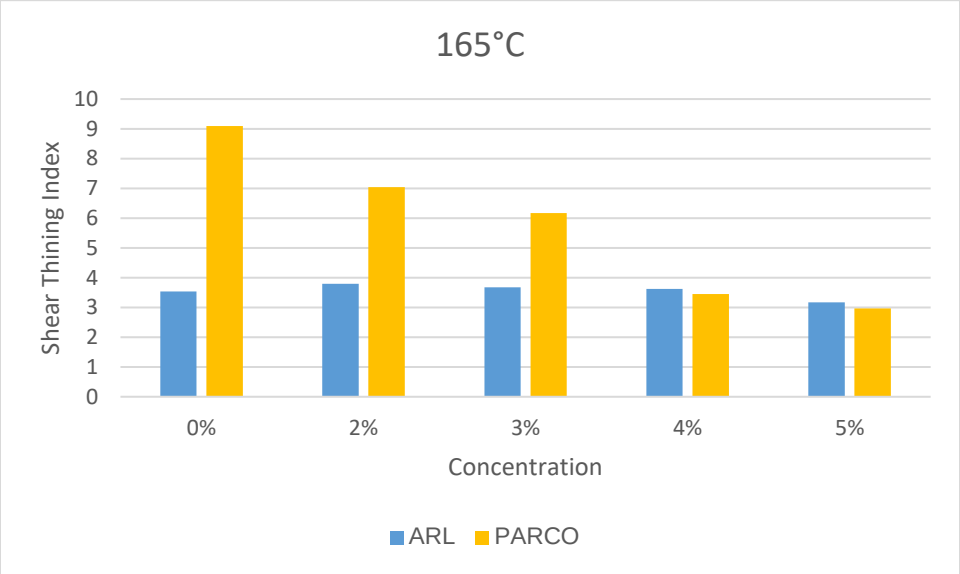

Figure 8: Shear Thining Index value Graph

RESULT AND DISCUSSION.

Absolute viscosity is calculated at 20rpm speed with different interval time difference of 60 sec. From Figure 2 it is clear that with increase in concentration of Polyethylene the absolute viscosity also increases for both ARL and PARCO bitumen. At 0% the value of absolute viscosity is minimum and at 5% the value of absolute viscosity is maximum in both ARL and PARCO samples.

According to the Figure 3 and Figure 5 Apparent viscosity is calculated at different shear rates values from 1.7, 3.4, 6.8, 10.2, 13.6, 20.4, 27.2, 34 and 40.8s-1 for ARL binders at 135 °C And 165 °C From this it is clear that apparent viscosity increases as the proportion of polyethylene content rises from 0%, 2%, 3%,4%, and 5%. When compared to the binder modified with, the values for the viscosity virgin binder ARL are smaller (PE) with Various Percentages 0%, 2%, 3%,4%, and 5%.

For PARCO Binders at 135 °C And 165 °C Apparent viscosity is calculated in the similar manner as shown in Figure 4 and Figure 6. In this apparent viscosity has maximum value at 5% addition of Polyethylene at both temperatures.
Shear thinning is calculated by taking ratio of value of viscosity at low speed to the value of viscosity obtained at high speed at different percentages of modifier which is Polyethylene. From all the percentages the ratio which is maximum shows the shear thinning behavior. At 135 °C PARCO shows maximum shear thinning at 4% Polyethylene of value 3.8 and ARL shows maximum shear thinning at 4% of value 2.1 as shown in Figure 7. At 165 °C the PARCO shows maximum shear thinning at 2% of Polyethylene of value of about 6.4 while ARL shows maximum shear thinning at 2% Polyethylene of value 3.9 as shown in Figure 8.
The viscosity of both ARL and PARCO reduces at a consistent rate as temperature rises. The nearly identical viscosity measurements for Virgin Binder ARL 60-70 and PARCO 60-70 demonstrate the similar composition of bitumen obtained from several refineries.

CONCLUSION

It has been investigated whether adding various waste polymers to ARL and PARCO bitumen can enhance its performance in pavement applications. The RV test findings, on the other hand, demonstrated that viscosity values rose with increasing concentrations of modifier at both temperature values 135 °C And 165 °C. When all of these findings are taken into account, it is clear that the waste window-based additives produced the best results when used at the recommended ratio of 2% in the modification of pure bitumen with waste materials.

REFERENCES

[1] ho, s., church, r., klassen, k., law, b., macleod, d., and zanzotto, l., "study of recycled polyethylene materials as asphalt modifiers", canadian journal of civil engineering, vol. 33, 2022, pp. 1-26.

[2] maharaj, r., balgobin, a., and singh-ackbarali, d., "the influence of polyethylene on the rheological properties of trinidad lake asphalt and trinidad petroleum bitumen", asian journal of materials science, vol. 1,2022; pp 36-44.

[3] othman, a. "effect of low-density polyethylene on fracture toughness of asphalt concrete mixtures", journal of materials in civil engineering, vol.2021, pp. 951-966

[4] qiao dong, jiao jin, yanqing tan, feeing lin, structure characteristics of organic bentonite and the effects on rheological and aging properties of asphalt, powder technology 329 (2021) 107–114.

[5] west conshohocken, pa, astm international. shear-rate dependent viscosity of dilute polymer solutions.properties
of polymer-modified asphalt binders. euro polymer j. 2019;

[6] liyan shan, yiqiu tan, b. shane underwood, thixotropic characteristics of asphalt binder, american society of civil engineers, doi: 10.1061/(asce)mt.1943-5533.0000328.

[7] s. n. nahar, g. leegwater, reversible molecular structuring and thixotropy in bitumen, road materials and pavement design, doi: 10.1080/14680629.2021.1911835.

[8] Yu R, Fang C, Liu P, et al. Storage stability and rheological properties of asphalt modified with waste packaging polyethylene and organic montmorillonite. Appl Clay Sci. 2019;104:1–7.

[9] Youtcheff, J., Stuart, K., Al-Khateeb, G., and Shenoy, A., "Understanding the Performance of Polymer Modified Binders", Proceedings of the 3rd Eurasphalt & Eurobitume Congress (EEC), Papers Technical Sessions 5-8, Vol. 2, Vienna, Austria, May 12-14, 2018, pp. BookII-2268-2278.

[10] American Association of State Highway and Transportation Officials (AASHTO), AASHTO Standards, AASHTO T315 "Standard Method of Test for Determining the Rheological Properties of Asphalt Binder Using a Dynamic Shear Rheometer (DSR)", 2018

2nd International Conference on Advances in Civil and Environmental Engineering (ICACEE-2023)

University of Engineering & Technology Taxila, Pakistan

Conference date: 22nd and 23rd February, 2023

Vehicle Headway Distribution Models for Srinagar Highway and Islamabad Expressway

Muhammad Ziad Bacha[1], Jawad Hussain[2,] Abid Rahman[3]

[1]Department of Civil Engineering, University of Engineering & Technology Taxila, Pakistan

ziadbacha001@gmail.com

[2]Department of Civil Engineering, University of Engineering & Technology Taxila, Pakistan

jawad.hussain@uettaxila.edu.pk

[3]Department of Civil Engineering, International Islamic University Islamabad, Pakistan

Engr.ark2020@gmail.com

ABSTRACT

The safety, driver behavior, capacity, and level of service of transportation systems are influenced by flow characteristics like time headway between vehicles. To find suitable probability distribution models for vehicle headways on the Srinagar Highway and the Islamabad Expressway, this study collected data from two locations in Islamabad - G-10 intersection (Loc. 1) and Iqbal Town (Loc. 2) - and grouped vehicle headways into 0.2-second intervals. Different mathematical distributions - Gen. Pareto, Johnson SB, Gen. Extreme Value, Pareto 2, Gamma, and Log-Logistic - were proposed, and the Kolmogorov-Smirnov test was used to assess their goodness of fit. The study found that traffic flows were high at the selected locations, with traffic volume ranging between 4000 and 5800 vehicles per hour per lane, and that the Johnson SB distribution provided the best fit at all locations under study with a 90% confidence level. The study recommended using the Johnson SB distribution to generate traffic for traffic analysis at highway sections with traffic volumes under 5000 vehicles per hour.

Keywords—headway, traffic flow, probability distribution, goodness of fit.

INTRODUCTION

Characterizing progress conveyance work is, subsequently, considered as essential in rush hour traffic jam stream learning and its recreation issue. A key segment of deciding the exhibition of a renewal model is the age between appearance times as a contribution to the recreation procedure. Although there have been numerous inquiries conducted on the subject of traffic congestion, a

large portion of them have primarily concentrated on situations involving consistent or low-to-medium levels of traffic. However, there exists a paucity of research that has specifically examined the efficacy of managing heavy or congested traffic flow, especially when dealing with mixed traffic environments. Likewise, there is a need to build up a fitting progress model, particularly under blended traffic circumstance while taking choices on transportation framework improvement. Simultaneously, the issue of traffic congestion has emerged as a significant challenge in numerous western nations, prompting transportation professionals to take decisive action to mitigate its impact. They are, along these lines, looking for having a brought-together strategy for portraying types of progress with the end goal of traffic portrayal and displaying at the blocked condition of the stream; this is because of the way that the traditional methodology doesn't show similarity under such stream regardless of whether the traffic is homogeneous in character.

Time progress is a significant minute traffic stream boundary what's more, characterized as the time stretch, typically estimated in seconds, between progressive vehicles in the rush hour traffic jam stream. Study on this boundary is significant especially in setting to limit investigation, security contemplates, vehicle following and path changing conduct displaying and level of administration assessment. The boundary of a street and the interest stream speed of convergence is equal to the least time progress; in a way, that a backside crash doesn't happen even in case of a sudden stop of driving vehicles. Further, appraisal of LOS on highways is overwhelmingly founded on the level of vehicles that move in following with shorter types of progress. Characterizing progress conveyance work is, along these lines, considered as principal in rush hour traffic jam stream study and its recreation issues. A key part of deciding the presentation of a recreation model is the age between appearance times as a contribution to the reenactment procedure. In any case, a large portion of the past concentrates regarding this subject emphasize on homogeneous traffic what's more, viewed as low and medium progression of traffic. In setting to blended traffic, there have been not several explorations that engaged on displaying degrees of progress under overwhelming traffic stream in up until now.

Understanding the scientific description of vehicle progress is necessary as input for traffic flow simulation models on a computer, such as in modeling intersections, vehicle tracking, highway entry ramps, and other road traffic situations.

Two methods can be used to obtain traffic data as input for simulation models. The first is to collect

actual data in the field, but this has two disadvantages: it takes a long time to collect and process the data, and the ability to examine extreme conditions is limited. The second method is to generate internal data on a computer. This eliminates both disadvantages of the first method but requires an accurate mathematical model to generate data that accurately fits the real situation.

The aim of this study was to identify the probability distribution model of vehicle progress on the Islamabad Expressway and Srinagar Highway in Islamabad, using six mathematical distributions: Gen. Pareto, Johnson SB, Gen. Extreme Value, Pareto 2, Gamma, and Log-Logistic, with vehicle headway as the variable.

LITERATURE REVIEW

Over the past few decades, researchers have proposed various theoretical models to describe degrees of progress. When it comes to urban traffic, hyperlang distribution is the ideal model to depict progress attributes under mixed traffic conditions [9]. Conversely when traffic primarily comprises smaller vehicles, such as bicycles or mopeds, the negative exponential distribution demonstrates similarities across a broad range of traffic flow rates. [5]. The research of Khasnabis and Heimbach [10] in North Carolina established progress distribution models for two-lane rural roadways with different traffic flow levels. In their study, they tested six alternative progress distribution models and found that the GEV distribution was the most effective for depicting various forms of progress. These findings align with those of Panichpapiboon [11], who examined and characterized the time-progress distributions of cars on an urban motorway in Bangkok, Thailand. In contrast, the exponential distribution was determined to be the least effective distribution model. In a study by Al-Ghamdi [4], various types of progress were identified in traffic flow rates for different traffic densities. The findings revealed that the negative exponential distribution was a good fit for data at low traffic flow rates (below 400 cars per hour), while the moving exponential and gamma distributions were more suitable for medium traffic flow rates (400-1200 vph). At high traffic flow rates (over 1200 vph), the Erlang distribution was found to be the best fit. Luttinen [12] suggested the lognormal distribution as a traffic flow model for low to moderate traffic volumes, where shorter progress periods are less frequent. In contrast, Riccardo, and Massimiliano [8] found that the reverse Weibull distribution provided an excellent fit for traffic flow data on rural two-way highways. Abtaehi et al. [13]

conducted an analysis of different traffic flow models on congested urban highways, focusing on passing and center lanes. They found that lognormal and gamma models with shifts of 0.25 and 0.68 seconds, respectively, provided the best fits. Ren and Qu [14] studied three different progress distributions, including exponential, backward Gaussian, and lognormal, and found that most progress samples exhibited a reverse Gaussian distribution. When these progress samples were considered as following and independent-after components, mixed models were found to be more flexible in accommodating various types of progress. Griffiths and Chase [15] recommended the double-negative exponential distribution as a suitable model for vehicular development. Zhang et al. [16] compared the performance of various progress-blending models. To evaluate the quality of fit, the K-S test was used, and the Q-Q plot was used to illustrate it. The results indicated that the general-purpose lane progress data is best modeled by the shifted lognormal distribution, while the double-truncated negative exponential distribution model provides the best fit for the urban road progress data. Over time, several blended models have been created and tested to predict progress distributions, including the combination of normal and shifted negative exponential distributions, the combined negative exponential and shifted negative exponential distribution, and the semi-Poisson distribution. Several blended distributions have been constructed to forecast progress distributions based on the presumption that progress consists of two parts, following and free [17]. These include the generalized linear model, the semi-Poisson model, the Cowan models M1-M4, and other significant models. Cowan's M3 model is widely investigated and used due to its simplicity and ease of estimation for longer types of development [18]. To identify freely moving vehicles in traffic, various studies have explored vehicle tracking systems [19]. According to research, vehicle independence can be considered after 6 seconds on Swedish roads, as there is often no vehicle interaction [20]. Similar results have been found in studies conducted on two-way roadways [21, 22]. Dey and Chandra [23] proposed two statistical distribution models, gamma and lognormal, to simulate the appropriate delay and time progression of drivers in a constant vehicle-following state on two-way highways with mixed traffic. The models were developed to accurately represent the delay and progression behavior of drivers, and they have been shown to be effective in simulating real-world traffic scenarios on two-way highways with mixed traffic. Mei and Bullen [24] observed that time progressions when a vehicle is being followed are log-normally distributed and converge to a shifted lognormal

distribution with a shift of 0.3-0.4 seconds at higher traffic volumes. Kumar and Rao [25] found that the positive exponential distribution accurately reflects progress levels at low to moderate flow rates. A correlation was found between the frequency of gaps and mean progress when cars traveling at progress levels below 2.0 are in gaps. A study on mixed traffic [26] showed that the progression between two vehicles in vehicle-following states depends on the length of the lead vehicle. The papers discussed in the previous paragraphs highlight various statistical distributions that can be utilized to model time progressions. However, since most of these models are based on homogeneous traffic, it is important to investigate the effects of heterogeneity in distribution models. This becomes even more critical in scenarios where there is a large stream of traffic, and communication between the vehicles is strong. To address this gap, the current study was designed to develop accurate models that consider an effective investigation of progress information under "blended traffic."

METHODOLOGY

The research was conducted in Islamabad, with data being collected from two locations: Srinagar Highway (Loc. 1) and Islamabad Expressway (Loc. 2). The data collected included traffic volume and vehicle headways, with each location being observed for a two-hour period during peak hours (one hour in the morning and one hour in the evening). Six headway distribution models were evaluated, specifically the Gen. Pareto, Johnson SB, Gen Extreme Value, Pareto 2, Gamma, and Log-Logistic models. Traffic volume was collected in one direction at both locations, with Srinagar Highway having a total length of 25 km, two lanes, and five interchanges, while Islamabad Expressway is a straight road with two to ten lanes. The methodology employed involved data collection, extraction, and statistical analysis.

Data Collection:
To collect data, a location was chosen after visiting several sites, and a video camera was installed there. Traffic peak periods were recorded at the chosen location for Srinagar Highway during morning hours (7:45 am - 8:45 am) and in the evening (4:40 pm - 5:40 pm), and for Islamabad Expressway during morning hours (7:30 am - 8:30 am) and in the evening (4:45 pm - 5:45 pm). The chosen section was free of hindrances such as parking lots, gradients, and bus-stops, and both locations had four lanes. An iPhone with a 12-megapixel camera, phase detection autofocuses, and dual LED was used to capture the traffic, ensuring high video quality. Data was collected on a sunny working day from a 15 ft high roadside vantage point to record traffic in both directions of the entire road width. Due to high traffic volume during most of the survey time, overtaking by vehicles (excluding two-wheelers) was limited.

Data Extraction:
Two locations were used for the video filming, which was split into four 15-minute segments each. For further examination, the period with the largest vehicle traffic was picked. Raw data regarding the movement of traffic, different kinds of vehicles, passage times, and events were gathered and entered into computer systems. The Kolmogorov-Smirnov test and standard statistical methods were used to evaluate the theoretical distributions' fit to the actual data. The team's findings will advance knowledge in the area and facilitate further investigations into the relationship between theoretical and actual distributions in traffic studies.

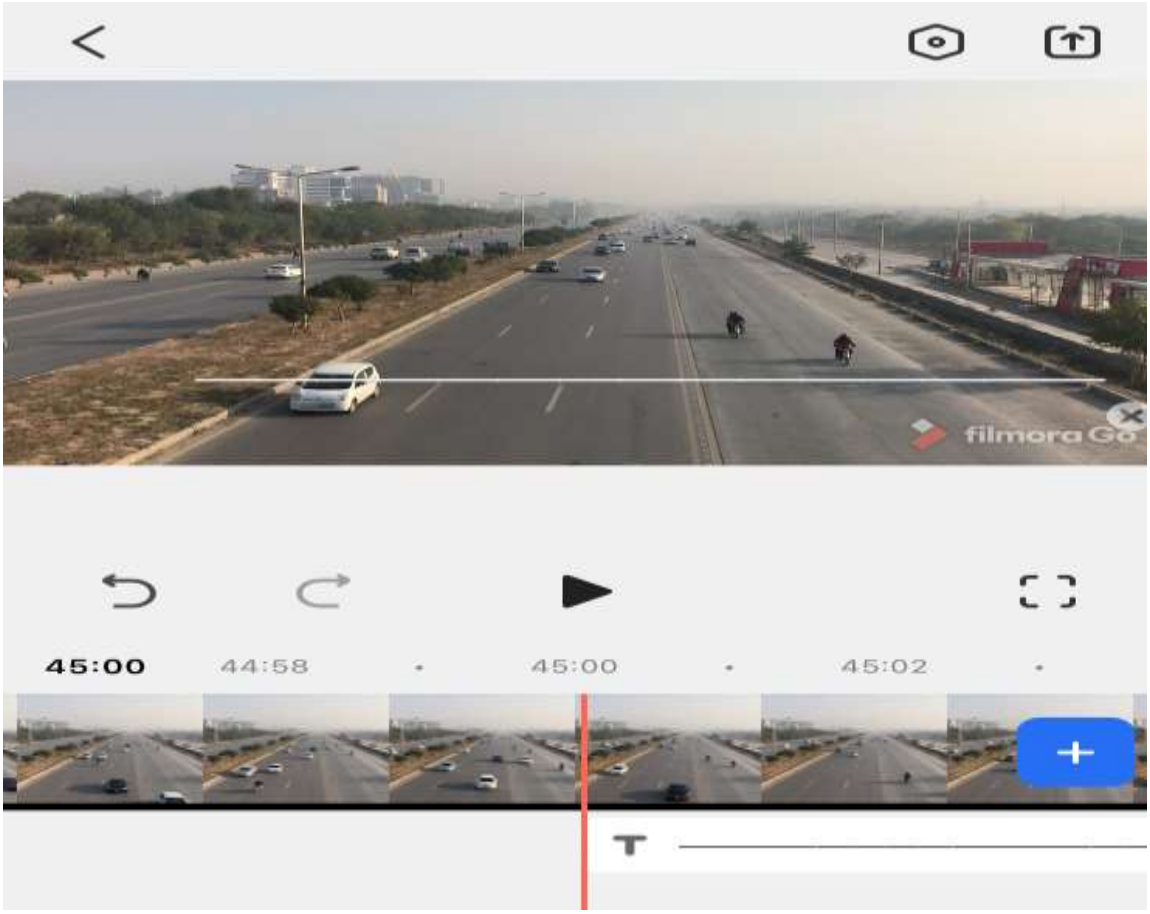

Figure 3. 1: *Data Extraction using Filmore9 Software*

RESULTS AND DISCUSSION

The unique characteristic of road traffic in Pakistan, common to many underdeveloped countries, is the presence of a diverse mix of vehicles using the same highway sections. This includes passenger cars, buses, lorries, motorbikes, and other types of vehicles, as well as non-motorized modes such as bicycles, tricycles, and wagons. In this context, the present study aimed to estimate the model of vehicle headway on three to five-lane roadways, focusing on three specific vehicle types: passenger cars, station wagons, and multi-purpose vehicles (MPVs). Motorcycles and bicycles were excluded from the analysis, as they often form a single traffic flow, and the number of other vehicle types investigated was also limited. By narrowing the scope in this way, the study was able to provide a more focused and in-depth analysis of the headway patterns of the selected vehicle types, contributing to our understanding of the dynamics of road traffic in this context.

Two specific locations were identified as having significant traffic volumes. Location 1, situated on the Srinagar Highway, recorded a traffic volume of 4628 cars per hour or 77 vehicles per minute, while Location 2, located on the Islamabad Expressway, had a higher traffic volume of 5794 vehicles per hour or 97 vehicles per minute. These findings highlight the significant congestion and traffic flow in these two areas, which can have important implications for traffic management and infrastructure planning. The data collected in this study can be used to inform strategies aimed at improving traffic flow and reducing congestion in these locations, ultimately leading to a more efficient and safe road network

Figure 4.1 4.2 4.3 4.4 shows the observed vehicle headways for the two locations, with headways grouped in 0.2 second intervals. The majority of headways at both locations fell within the 1-2 second interval group. At Location 1, out of the total 1198 observed headways, approximately 29.22% fell within the 100-200 second interval group, while only about 14.27% had values greater than 500 seconds. At Location 2, a total of 1602 headways were observed, with about 40.82% falling within the 1.00-2.00 second interval group and only about 5.31% having values greater than 5 seconds.

The frequency distribution of vehicle headways at different intervals is presented in Figures 4.1and 4.2, as well as in Figures 4.3 and 4.4. The majority of vehicles have headway intervals ranging from 1.00 to 2.00 seconds, indicating that most vehicles have a flow rate within this range. Figures 4.1, 4.2 and 4.3 and 4.4 show the measured headway probability distributions for

Locations 1 and 2, while Figures 4.5, 4.6, 4.7 and 4.8 display the theoretical headway probability distributions for both locations. The probability for each headway interval is depicted in these figures, with six mathematical distributions presented as theoretical distributions, namely Gen. Pareto, Johnson SB, Gen. Extreme Value, Pareto 2, Gamma, and Log-Logistic. To perform a qualitative evaluation of the measured probability distribution, a comparison was made with various theoretical probability distributions. The analysis revealed that the Johnson SB distribution was a closer match to the measured distribution when compared to other theoretical distributions. This observation was consistent across both Location 1 and Location 2, indicating that the Johnson SB distribution may be a more accurate model for the data in question.

Vehicle headway distribution models were found to vary according to the amount of traffic flow, as a result of the interaction between vehicles. As traffic flow increases, so does the interaction between vehicles. In rare traffic conditions, vehicles move freely without interacting with other vehicles, meaning that each vehicle can appear at any time, except for the required minimum headway for safety purposes. The model fit tests were conducted for each location using the Kolmogorov-Smirnov (K-S) procedure, and the results showed that the Johnson SB distribution fit the headway distributions at all studied locations. The distribution of headways in traffic can be characterized using Johnson SB conditions.

Traffic flow can be high and low. Low flow represents one of the two boundary conditions, while the other occurs as traffic flow approaches capacity. In high flow situations, almost all vehicles interact with one another, leading to a more or less constant headway. In contrast, an intermediate situation exists between these two boundary conditions, where some vehicles move autonomously while others interact with their surroundings. This intermediate situation reflects a more complex and dynamic traffic environment, where the behavior of individual vehicles can be influenced by a range of external factors, such as the density of other vehicles on the road, the speed of traffic, and the presence of traffic signals. Understanding the dynamics of traffic flow in different scenarios can provide valuable insights into traffic management, infrastructure planning, and road safety.

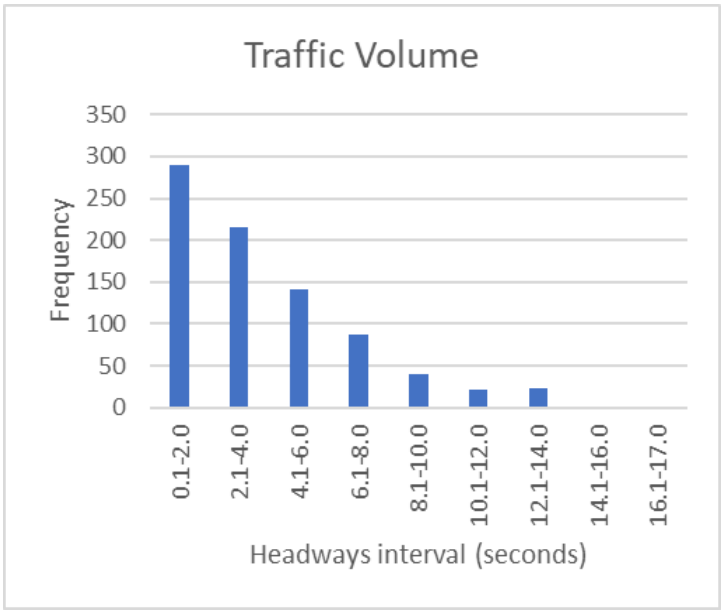

Figure 4. 2: Measured Vehicle Headway at selected location 1 (Evening)

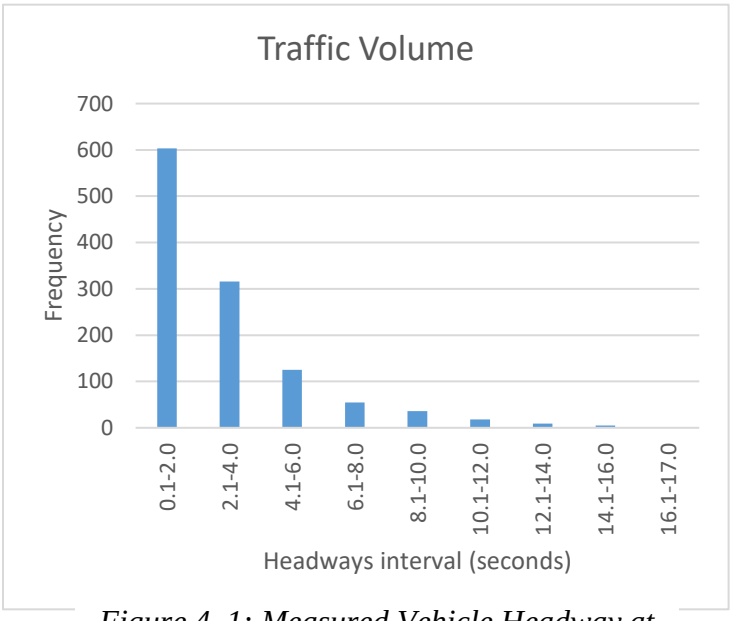

Figure 4. 1: Measured Vehicle Headway at selected location 1 (Morning)

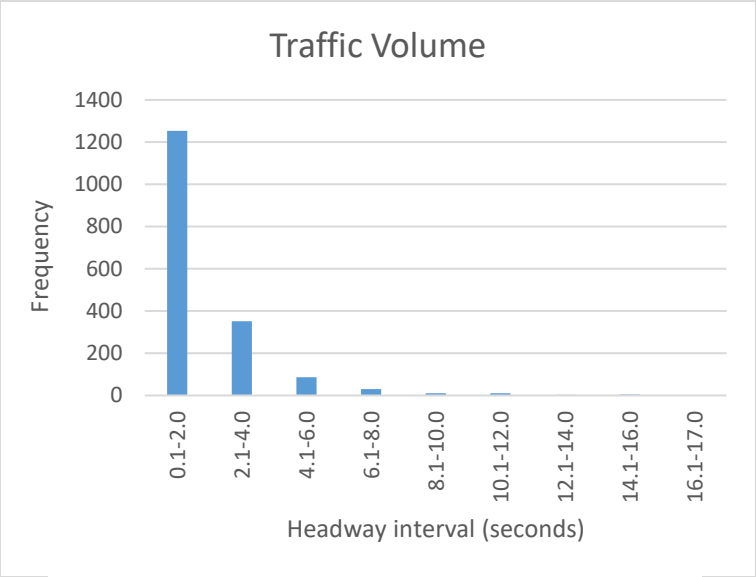

Figure 4. 3: Measured Vehicle Headway at selected location 2 (Morning)

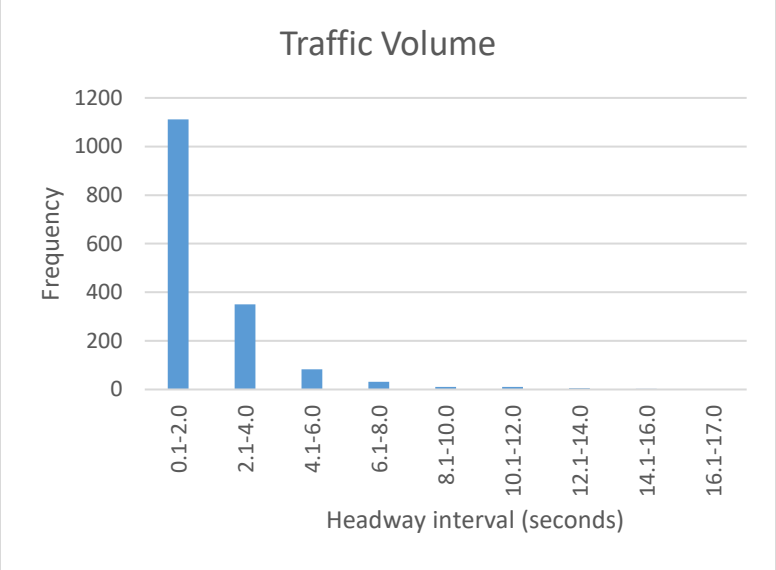

Figure 4.4: Measured Vehicle Headway at selected location 2 (Evening)

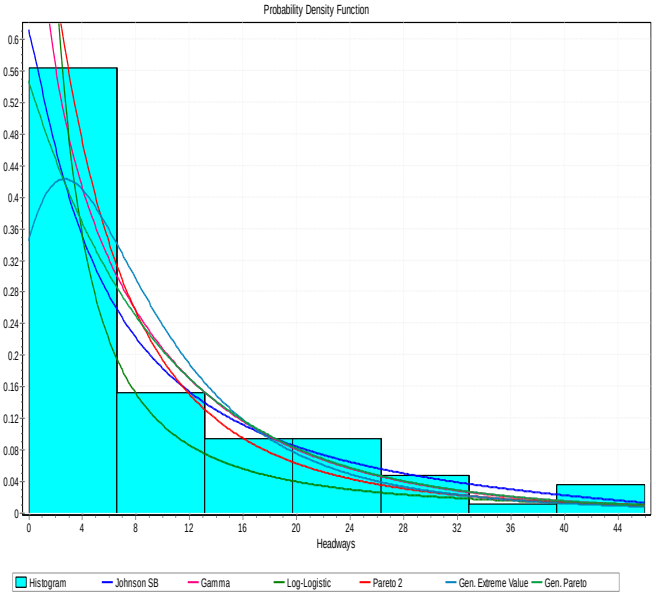

Figure 4.5:probibality of theoritical vehicle headways at location 1 (Morning)

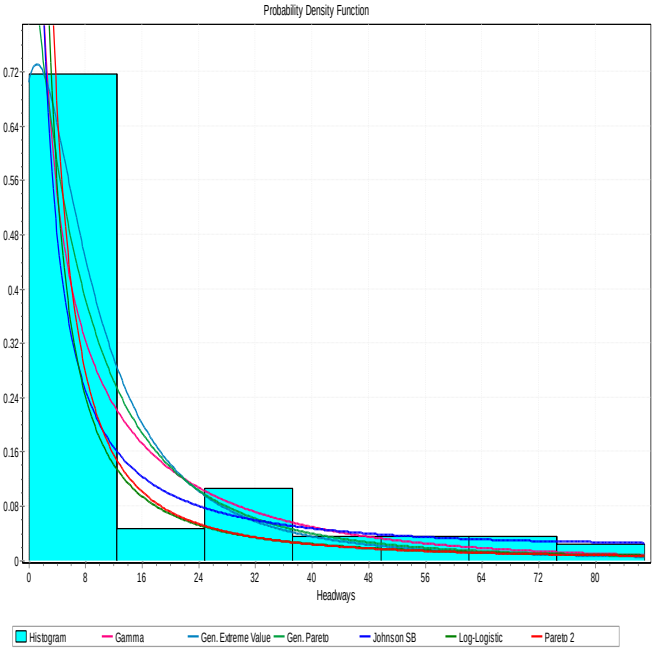

Figure 4.6: probability of theoretical vehicle headways at location 1 (Evening)

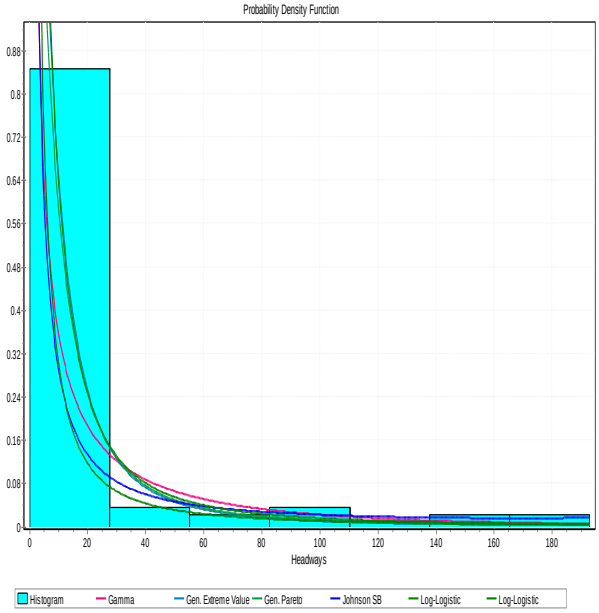

Figure 4.7: :probability of theoretical vehicle headways at location 2 (Morning)

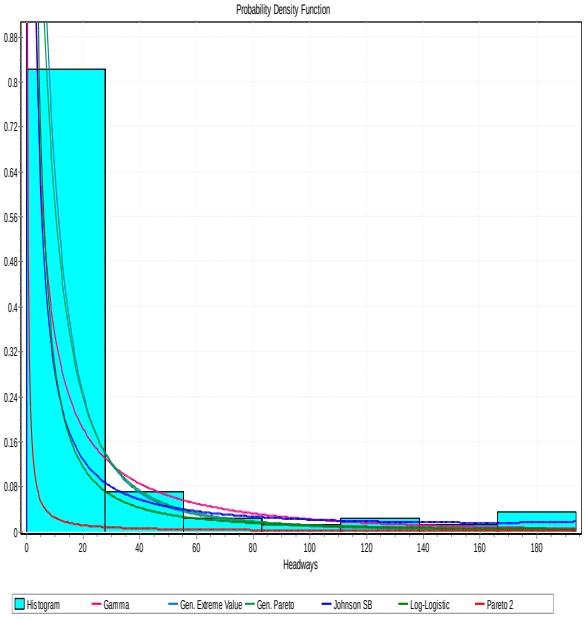

Figure 4.8 :probability of theoretical vehicle headways at location 2 (Evening)

The road segments that were examined in this study have a capacity of approximately 5000 passenger car units (pcu) per hour. However, the actual traffic volume observed at the two locations was found to be 4298 cars per hour at Location 1 and 5796 vehicles per hour at Location 2, which exceeds the capacity of the route. As such, the traffic in these areas can be classified as high volume. The results of the Kolmogorov-Smirnov goodness of fit tests, as presented in Table-I, demonstrate that the vehicle headway distributions at all selected locations fit the data. These findings are consistent with the results of previous research conducted by Muhammad Ziad Bacha and Abid Rahman, who also found that the traffic distributions followed theoretical models. As an example, Smirnov's asymptotic formulae proposed in 1948, which rely on a value of N greater than 35, are applicable in our scenario. Therefore, we have used the relevant asymptotic critical values for D in our analysis. These results provide valuable insights into the dynamics of traffic flow and can inform future research on traffic management and infrastructure planning.

Table 6: Critical Values

Asymptotic Critical Values for D (N>35)	
Alpha	Critical Value
0.01	1.63 / √N
0.05	1.36/ √N
0.1	1.22/ √N
0.15	1.14/ √N
0.2	1.07/ √N

As we assume (alpha=0.05) then the critical value is 1.36 /√N, the value of N is 85, as shows that in above tables that we take the no. of sample as 85.By calculating (1.36 /√85), we get that the critical value is equal to 0.1475 ≅ (0.15). Now the check of acceptance and rejection, the Kolmogorov-Smirnov test is defined as, "If the value of Dmax > Do the condition is rejected, and if Dmax < Do then the Condition is accepted."

TABLE I. KOLMOGOROV-SMIRNOV GOODNESS OF MODEL FIT TESTS RESULT

Locations	Rank	Distributions	D_{max}	D_o	Remark
1. (Morning)	1	Gen. Pareto	0.12391	0.15	Accept H_o
	2	Johnson SB	0.12847	0.15	Accept H_o
	3	Gen. Extreme Value	0.14305	0.15	Accept H_o
	4	Pareto 2	0.15294		Reject H_o
	5	Gamma	0.15294	0.15	Reject H_o
	6	Log-Logistic	0.15917	0.15	Reject H_o
(Evening)	1	Johnson SB	0.14888	0.15	Accept H_o
	2	Gen. Extreme Value	0.17365	0.15	Reject H_o
	3	Gen. Pareto	0.17418	0.15	Reject H_o
	4	Gamma	0.18824	0.15	Reject H_o
	5	Log-Logistic	0.18824	0.15	Reject H_o
	6	Pareto 2	0.18824	0.15	Reject H_o
2. (Morning)	1	Gen. Pareto	0.23346	0.15	Reject H_o
	2	Gen. Extreme Value	0.24348	0.15	Reject H_o
	3	Johnson SB	0.30481	0.15	Reject H_o
	4	Log-Logistic	0.30588	0.15	Reject H_o
	5	Gamma	0.30588	0.15	Reject H_o
	6	Pareto 2	0.62010	0.15	Reject H_o
(Evening)	1	Johnson SB	0.13758	0.15	Accept H_o
	2	Gen. Extreme Value	0.21232	0.15	Reject H_o
	3	Gen. Pareto	0.23586	0.15	Reject H_o
	4	Gamma	0.32941	0.15	Reject H_o
	5	Log-Logistic	0.32941	0.15	Reject H_o
	6	Pareto 2	0.59564	0.15	Reject H_o

CONCLUSION

Upon careful analysis of the data presented in the table and considering the results obtained, it can be inferred that all the locations that were examined had a significant level of traffic. However, the Johnson SB model was the only one that showed conformity to all four selected sites based on the Kolmogorov-Smirnov goodness of fit tests. Therefore, the Johnson SB distribution is recommended for generating traffic data that can be used to simulate traffic flow on highway sections with a volume of 5000 cars per hour or less. These findings have significant implications for traffic management and infrastructure planning, as accurate traffic flow simulations can provide valuable insights into traffic patterns and help in the design of more efficient transportation systems.

REFERENCE

[1] Dewen Kong and Xiucheng Guo Analysis of vehicle headway distribution on multi-lane freeway considering car–truck interaction. (2016)

[2] Pavel Hrabáka, Milan Krbáleka Distance- and Time-headway Distribution for Totally Asymmetric Simple Exclusion Process . (2017)

[3] Rupali Roy & Pritam Saha Headway distribution models of two-lane roads under mixed traffic conditions: a case study from India. (2011)

[4] Jinhwan Janga, Changsoo Parkb, Byunghwa Kimc, Namkuk Choid.Modeling of Time Headway Distribution on Suburban Arterial: Case Study from South Korea. (2016)

[5] Rattaphol Pueboobpaphan, Dongjoo Park, Youngchan Kim, and Sangho Choo Time Headway Distribution of Probe Vehicles on Single and Multiple Lane Highways. (2011)

[6] Chandra S, Kumar R Headway modeling under mixed traffic on urban roads. Road Trans Res (2001); 10(1):61–7

[7] Riccardo R, Massimiliano G An empirical analysis of vehicle time headways on rural two-lane two-way roads. Proc Soc Behav Sci (2012) 54:865–87.

[8] Panichpapiboon S Time-headway distributions on an expressway: case of Bangkok. J Trans Eng-ASCE (2014); 141(1): 0501400.

[9] Kumar Molugaram, G Shanker Rao Statistical Techniques for Transportation Engineering. (2011)

[10] Zhang G, Wang Y, Wei H, Chen Y Examining headway distribution model with urban freeway loop event data. Transp Res Rec J Trans Res Board:141–149; (2007).

[11] Cowan RJ Useful headway models. Trans Res 9(6):371–375; (1975).

[12] Zhang G, Wang YA Gaussian kernel-based approach for modeling vehicle headway distributions. Trans Sci 48(2):206; (2013).

[13] Mei, Minje, Bullen, A Graham R. LOGNORMAL DISTRIBUTION FOR HIGH TRAFFIC FLOWS Issue Number: 1398 Publisher: Transportation Research Board ISSN: 0361-1981

[14] Al-Kaisy A, Karjala S Car-following interaction and the definition of free- moving vehicles on two-lane rural highways. J Transp Eng 136(10):925–931; (2010).

[15] Saha P, Roy R, Sarkar AK, PalM Preferred time headway of drivers on two-lane highways with heterogeneous traffic Transportation Letters: The International Journal of Transportation Research. (2017)

[16] Penmetsa P, Ghosh I, Chandra S Evaluation of performance measures for two-lane intercity highways under mixed traffic condition. J Transp Eng-ASCE 141(10):04015021–04015028; (2015).

[17] Sai Kiran M, Verma A Review of studies on mixed traffic flow: perspective of developing economies. Transp in Dev Econ. (2016)

[18] Saha P, Sarkar AK, Pal M Evaluation of speed-flow characteristics on two-lane highways with mixed traffic. Transport. (2015)

[19] Adams WF Road traffic considered as a random series. Inst. Civ Eng. 4(1):121–130; (1936).

[20] Zwahlen HT, Oner E, Suravaram KR Approximated headway distributions of free-flowing traffic on ohio freeways for work zone traffic simulations. (2007)

[21] Krbalek M, Seba P, Wagner P Headways in traffic flow: remarks from a physical perspective. Phys Rev E 64(6):1–7; (2001).

[22] Al-Ghamdi AS Analysis of time headways on urban roads: case study from Riyadh. J Transp Eng. 127(4):289–29;(2001).

[23] S. Khasnabis, C. L. Heimbach. Headway-distribution models for two-lane rural highways.

2nd International Conference on Advances in Civil and Environmental Engineering (ICACEE-2023)

University of Engineering & Technology Taxila, Pakistan

Conference date: 22nd and 23rd February, 2023

EXPERIMENTAL STUDY OF SOIL STABILITY AND EROSION OF EMBANKMENT BY USING SISAL FIBER

Sardar Faisal Abbas[1],
[1]UET Taxila, faisal.abbas@nets-international.com

ABSTRACT

Natural fibers are thought to be an attractive alternative to enhance these features since soil embankment slopes are vulnerable to erosion, especially during rain, offer the easiest path against erosion, and rapidly deteriorate in strength. This study is focused on research into how sisal fibers may be used to change the soil's stability and erosion properties in soil embankments. By performing various analysis tests such as Sieve analysis, Liquid limit, Plastic limit, Hydrometer test, Modified Proctor test, and Surface erosion test on the natural and treated soil, the effect of the Sisal Fibres as additives were determined. The findings demonstrated that the soil's stability improved as seen by the liquid and plastic limits. The decrease in soil's dry unit weight and rise in moisture content are both caused by this addition. The primary benefit of sisal fibers was also demonstrated by the decrease in soil surface erosion.

KEYWORDS: Soil embankment, stability, erosion

INTRODUCTION

The naturally occurring process that affects all the landforms is commonly known as Soil Erosion. A process called soil erosion involves the separation and movement of soil by wind and water. Large quantities of fine-grained soils can be found in Pakistan, particularly in the Punjab Province, at shallow depths and are typically utilized to build soil embankments [1]. The term "stabilization" mostly refers to chemical modifications in the soil characteristics by adding chemical admixtures. The qualities of soil can be improved physically or mechanically [2]. Construction of rail and road infrastructure, foundations, berms, backfill for bridges, and retaining walls, among other civil engineering projects, all make extensive use of soil stabilization.

The topsoil of the fined-grained slope could be eroded. The topsoil is weak in water stabilization so during rainfall slope surface suffers from soil erosion. The effect could easily have been through the affected growth of plants available at that slope surface. So, the slope designed for the railway, highway, and earthen lands becomes unstable which ultimately affects its stability as well as drainage issues. Erosion of embankments is a significant issue that can lead to the failure of a building. The problem statement is to identify and prevent the causes of erosion to protect nearby properties and infrastructure. Mitigating the erosion of embankments is crucial to ensure the safety of communities and prevent costly repairs[3]. Sisal fibers are used for soil stability because of their high tensile strength, flexibility, and biodegradable nature. They can withstand pulling forces and conform to soil shape,

providing long-term stability while being environmentally friendly and cost-effective[4]. Significant issues with rehabilitating outdated and aging infrastructure have been successfully overcome by the use of Sisal fiber composites in engineering infrastructures[5].

LITERATURE REVIEW

With a change in moisture content, expansive soils may experience a volume change. These soils can rise, and the differential settlement they experience might result in infrastructure damage[6].

Wang et al. examined the mutual interaction of lime stabilization and wheat straw fiber reinforcement on the mechanical behavior of Hefei clayey soil [7]. Suggested that the addition of Kenaf fiber to the soil evolves volume change by reducing initial contraction up to 34% and subsequent dilation of specimen up to 40% [8]. Examined how Nano-Silica may be used in a novel way to enhance the mechanical qualities of soil samples and recyclable polypropylene fiber (PPF), which is created during the production of plastic chairs[9, 10]. Experimented to determine the contact erosion of a dispersive levee and an embankment that had been treated with Nano silica and allowed to cure for up to 28 days [11, 12]. Described that, he used as a waste material in many engineering applications, silica fume (SF) offers a significant advantage examined how Nano-Silica may be used in a novel way to enhance the mechanical qualities of soil samples and recyclable polypropylene fiber (PPF), which is created during the production of plastic chairs [13, 14]. Algadwi et al. investigated how polymers function during the stabilization process. Natural soils' mechanical properties and buildability were enhanced by the addition of polymer [15]. Investigated the effect of cornsilk fiber on the mechanical properties of soft clay [16]. Nano calcium carbonate which was reinforced with fibers of the waste carpet also used as material to improve the mechanical properties of soil [7, 17]. Waste tire textile fibers are also used as soil reinforcement[18].

METHODOLOGY

The soil is obtained from a slope and put through several tests to see how sisal fibers affect the soil's stability and erosion. A variety of tests are performed on the untreated and treated soil and the results are compared to check the properties of the soil after the addition of the additives (sisal fibers). Following are the tests which are performed on the soil for the study.

Sieve analysis

Sieve analysis is frequently used to identify and categorize soil. The study was conducted using a set of ASTM sieves that included sieves # 4, 8, 16, 40, 50, 100, and 200. While using the oven-dried sample, the set of sieves is arranged such that sieves with the widest apertures are on top and gradually smaller in size below.

Hydrometer analysis

Hydrometer analysis may be used to identify the distribution of fine-grained soil's particle sizes. If less than 10% of the sample passes through the No. 200 sieve, the test is not valid.

Specific gravity Test

The specific gravity of fined-grained soil could be determined by the density bottle method. It might be used for medium and coarse-grained soils provided that the soil is pulverized and passed through the No. 4 sieve.

Liquid Limit

The level of wetness at which fine-grained dirt ceases to flow like a fluid is considered as liquid limit (LL) of soil. A soil sample was taken from sieve No. 40 pass into a dish and water was added slowly to make a thick paste with continuous mixing.

Plastic Limit

The plasticity index (PL) of the soil is the relative humidity during which fine-grained soil can neither longer be molded without cracking. The soil sample was taken from sieve No. 40 pass into a dish and water was added to make enough plastic to mould into a ball shape.

Modified proctor test

Compaction is the removal of air and increasing the density to attain the moisture density relationship for a given compaction effort on the soil. The soil sample retained on sieve no. 4 was taken and mixed with 2 to 3 % of the water of the weighted sample.

Unconfined compression test

The laboratory test is used for the determination of the unconfirmed compressive strength of a soil sample. It is the highest amount of axial compressive strength a soil specimen may support in the absence of any constriction stress. Both a soil sample without and one with reinforced sisal fiber underwent testing.

Surface erosion test

To ascertain the pace at which the soil in the embankment erodes, a slope erosion test was performed. Literature has shown that soil compaction and the growth of many plant species were typical practices in the past. Since the embankment is made of fine-grained soil, vegetation is not a long-term solution since heavy rainfall causes soil erosion to happen quickly. The main goal was to stop soil erosion to prevent slope or shear collapses. The slope

model was needed to determine the erosion rate in the lab; for this, basic hydrology equipment with a fixed slope angle was used.

RESULTS

The results of all the analyses after the addition of sisal fibers are given below.

Sieve analysis

Percent passing through sieve number 200 was 83% showing the study material falls in the category of fine-grained soil with clay dominancy as the percentage passing through sieve # 200 is more than 50%.

Hydrometer analysis

For hydrometric analysis, 29 a dispersing agent like sodium hexa-meta-phosphate was used for the dispersion of soil particles. The standard test method for particle size analysis of soil samples is shown in table 1.

Table 1: Hydrometer Test Analysis

Time Elapsed (min)	Temperature (ºC)	Actual Reading (Ra)	Corrected Reading (Rc)	% Finer	Correction for meniscus	L (cm)	L/t	K	D (mm)
2	22	28	23.4	46	29	11.7	5.85	0.013	0.0317
4	22	26	21.4	42	27	12	3	0.013	0.0227
8	22	23	18.4	36	24	12.5	1.56	0.013	0.0164
16	22	21	16.4	32	22	12.9	0.80	0.013	0.0118
30	22	19	14.4	29	20	13.2	0.44	0.013	0.0087
60	22	18	13.4	27	19	13.3	0.22	0.013	0.0062
120	22	16	11.4	23	17	13.7	0.11	0.013	0.0044
330	22	14	9.4	19	15	14	0.04	0.013	0.0027
1440	22	13	8.4	17	14	14.2	0.1	0.013	0.0013
2880	22	10	5.4	11	11	14.7	0.005	0.013	0.0009

Specific gravity test

The value for the specific gravity of fined-grained soil is 2.710 concluded from table 2.

Table 2: Specific gravity of soil

Test No.	1	2
Volume(ml)	500	500

W1(g)	266.5	266.4
W2 (g)	391.5	391.4
W3(g)	963.26	963.36
W4(g)	883.8	884.7

Liquid Limit

Standard test method (AASHTO T 89-10, ASTM D 4318 -10) used for liquid limit determination. The liquid limit is determined from the graph as shown in figure 1.

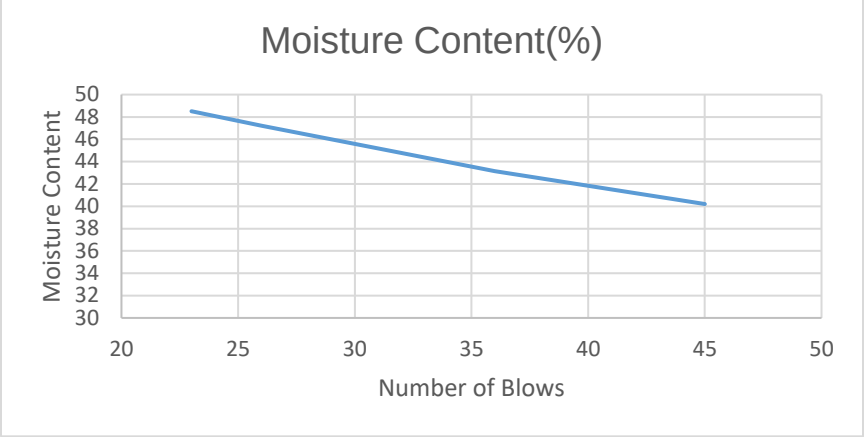

Figure 1: Liquid Limit

Liquid Limit from the graph=47.8%

Plastic Limit

The plastic limit is determined by experiment and the values are given in table 3.

Table 3: Plastic limit values

Sample No	1	2
Container No	17	18
Weight of empty container, W1 (g)	14.9	15.2
Weight of wet soil + container W2 (g)	19.65	19.85
Weight of dry soil + container W3 (g)	18.7	18.89
Weight of water (g)	0.95	0.96
Weight of dry soil (g)	3.8	3.69
Moisture content (%)	25	26.02

Plastic Limit=25
Plasticity Index=Liquid Limit-Plastic Limit
=47.8-25
=22.8%

Modified proctor test

The standard test procedure for measuring soil compaction properties in a laboratory (56000 Ib./ft3) (AASHTO T 180-10, ASTM D 1557-12). The maximum unit weight and ideal moisture content for the natural soil are 18.8 kN/m3 and 12.9%, respectively. As additives are added, the total dry unit weight rapidly declines while the ideal soil moisture content rises, as seen in the graph (Figure 2).

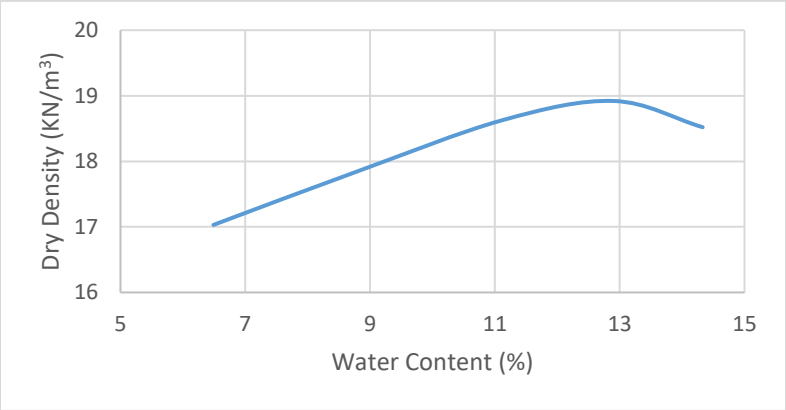

Figure 2: Compaction curve of natural soil

Unconfined Compression test

The soil sample was tested without and with reinforced sisal fiber. The different percentages (5%, 10%, 15%, 20%, and 25%) of sisal fiber were reinforced by weight having a constant length (6.5mm observed through previous literature**)**. At 15% the optimum unconfined compressive strength was achieved.

Surface erosion test

Results of soil-treated samples with varied RH and SD fractions in terms of the pace of land degradation 32.3% of the untreated soil eroded as a result of weathering. The soil degradation rate was reduced by 55%, and the optimum RH value was calculated to be 15%, giving a value of 14.65%. The optimal SD value was discovered to be 5%, but the real value was 12.1%, resulting in a 62% decrease in the rate of soil deterioration. Both of these additions provided resistance to erosion because the interaction here between additives and soil particles produced a physical link.

ACKNOWLEDGEMENTS

All praise and thanks are directed toward the All-Mighty Allah. I am grateful to my supervisor Engr. Rameez Sohail for providing both guidance and assistance during this study effort. I am also thankful to Engr. Zafar Ali Shah helped me a lot in experimental works during my whole tenure.

CONCLUSION

In this work, a soil slope reinforced by sisal fibers is evaluated for stability and degradation characteristics. Several tests are carried out in this regard, including those using sieve analysis, moisture content analysis, dry density test, liquid limit test, plasticity index test, the compatibilizer proctor test, maximal dry density test, increased moisture content test, the ground erosion test. The sample material is classified as fine-grained soil with a predominance of clay, as seen by the 83% percent passing through sieve number 200, which is more than 50%. The Liquid limit of the soil is found to be 47.8% and the Plastic limit is 22.8 % when Atterberg's limit tests are performed. The specific Gravity of the fine-grained soil is 2.710 when determined by the Specific Gravity Analysis Test. The specific gravity of the Sisal fibers is less than the grained soil.

- Standard method of hydrometer analysis is performed to examine the particle size of the gained soil. The fine-grained nature of the soil is also confirmed by this method.
- The maximum unit weight and ideal moisture content for the natural soil are 18.8 kN/m3 and 12.9%, respectively. The dry density unit steadily declines when additives are added, but the soil's ideal moisture level rises. Because of the flocculation and agglomeration of fine-grained soil particles, the maximum dry unit weight has decreased.
- The specific gravity and density of Sisal Fibre are also less as compared to soil, which is also another reason for the reduction in this dry unit weight. Now, it is quite natural that the larger surface area needs more water for the lubrication of colloid particles, which alternately increases the water contents.
- The percentage figure for the land degradation rate of stabilized soils is 32.3%. With the inclusion of sisal fibers, surface erosion is reduced.

REFERENCES

1. Farooq, M.U., et al., *Evaluation of stability and erosion characteristics of soil embankment slope reinforced with different natural additives.* Iranian Journal of Science and Technology, Transactions of Civil Engineering, 2020. **44**(1): p. 515-524.
2. Afrin, H., *A review on different types soil stabilization techniques.* International Journal of Transportation Engineering and Technology, 2017. **3**(2): p. 19-24.

3. Mizal-Azzmi, N., N. Mohd-Noor, and N. Jamaludin, *Geotechnical approaches for slope stabilization in the residential area.* Procedia Engineering, 2011. **20**: p. 474-482.
4. Pranjal, U., M. Pratiksha, and V. Singh, *Experimental investigation on strength characteristics of Sisal fiber reinforced soil stabilized with sugar cane bagasse ash.* International Journal for Research in Applied Science and Engineering Technology, 2017. **5**(11): p. 5000-5007.
5. Navaratnam, S., et al., *Applications of natural and synthetic fiber reinforced polymer in infrastructure: A suitability assessment.* Journal of Building Engineering, 2023: p. 105835.
6. Vardon, P.J., *Climatic influence on geotechnical infrastructure: a review.* Environmental Geotechnics, 2015. **2**(3): p. 166-174.
7. Wang, Y., et al., *Behavior of fiber-reinforced and lime-stabilized clayey soil in triaxial tests.* Applied Sciences, 2019. **9**(5): p. 900.
8. EsmaeilpourShirvani, N., et al., *Improvement of the engineering behavior of sand-clay mixtures using kenaf fiber reinforcement.* Transportation Geotechnics, 2019. **19**: p. 1-8.
9. Tomar, A., T. Sharma, and S. Singh, *Strength properties and durability of clay soil treated with a mixture of nano silica and Polypropylene fiber.* Materials Today: Proceedings, 2020. **26**: p. 3449-3457.
10. AL-Soudany, K.Y., *Improvement of expansive soil by using silica fume.* Kufa Journal of Engineering, 2018. **9**(1).
11. Vakili, A.H., et al., *Contact erosional behavior of foundation of pavement embankment constructed with nano-silica-treated dispersive soils.* Soils and Foundations, 2020. **60**(1): p. 167-178.
12. Mirzababaei, M., et al., *Stabilization of soft clay using short fibers and polyvinyl alcohol.* Geotextiles and Geomembranes, 2018. **46**(5): p. 646-655.
13. Türköz, M., S.U. Umu, and O. Öztürk, *Effect of Silica Fume as a Waste Material for Sustainable Environment on the Stabilization and Dynamic Behavior of Dispersive Soil.* Sustainability, 2021. **13**(8): p. 4321.
14. Tiwari, N., N. Satyam, and K. Singh, *Effect of curing on micro-physical performance of polypropylene fiber reinforced and silica fume stabilized expansive soil under freezing thawing cycles.* Scientific reports, 2020. **10**(1): p. 1-16.
15. Algadwi, M.B., E. Spyropoulos, and B.A. Nawaz. *Erosion protection by polymer additive*. in *Proceedings of the 2nd International Conference on Civil Engineering Fundamentals and Applications (ICCEFA'21) Seoul, South Korea Virtual Conference*. 2021.
16. Tran, K.Q., T. Satomi, and H. Takahashi, *Effect of waste cornsilk fiber reinforcement on mechanical properties of soft soils.* Transportation Geotechnics, 2018. **16**: p. 76-84.

17. Choobbasti, A.J., M.A. Samakoosh, and S.S. Kutanaei, *Mechanical properties soil stabilized with nano calcium carbonate and reinforced with carpet waste fibers.* Construction and Building Materials, 2019. **211**: p. 1094-1104.
18. Abbaspour, M., E. Aflaki, and F.M. Nejad, *Reuse of waste tire textile fibers as soil reinforcement.* Journal of cleaner production, 2019. **207**: p. 1059-1071.

2nd International Conference on Advances in Civil and Environmental Engineering (ICACEE-2023)

University of Engineering & Technology Taxila, Pakistan

Conference date: 22nd and 23rd February, 2023

Relation Between Resilient Modulus Evaluated from UPV And Dynamic Triaxial Testing Machine

Abdus Saboor Khan[1], Kashif Riaz[2], Naveed Ahmad[3]
University of Engineering and Technology Taxila Department of Geotechnical EngineeringEngsaboor87@gmail.com

ABSTRACT

Roads are the most widely used geotechnical structures in land transportation system throughout the world constructed on compacted sub grade. In a pavement, properties of sub grade and method of calculation defines the quality of pavement. Resilient modulus (M_r) is the most important parameter in pavement design which defines quality of pavement but Lack of equipment and consistency to calculate M_r adversely affects the pavement design. All major correlations to calculate resilient modulus are derived from different index and strength properties of sub grade soil. The aim of this investigation was to establish a correlation between resilient modulus evaluated from ultra-sonic pulse velocity and triaxial test. To achieve this, 24 soil samples were collected from Pakistan. Index Properties, Ultra-sonic Pulse Velocity, and triaxial tests were conducted on these soil samples. Trend of resilient modulus from group A-2-4, A-2-6, A-4, and A-6 indicated that higher percentage finer leads to the lower value of resilient modulus. Triaxial test results gave higher value of resilient modulus as compared to the UPV test values. Results of UPV test highlighted that higher density leads to the higher velocity hence the higher value of resilient modulus. The correlation can be used to accurately predict the resilient modulus from UPV data of groups A-2-4,A-2-6 A-4, and A-6without performing triaxial test.

KEYWORDS: Ultra-sonic Pulse velocity, Resilient Modulus, Triaxial, Correlation**.**

INTRODUCTION

A well-developed road system is extremely important for smooth, comfortable, and sustainable land navigation. A well-constructed road is the key for high quality transportation system around the world. .[1]The resilient modulus M_r is fundamental property of the sub grade that governs the sustainability of the sub grade soil and determines the quality of the pavement Resilient modulus is the most important parameter in pavement design which defines quality of pavement but Lack of equipment and consistency to calculate M_r adversely affects the pavement design. [2, 3]. The Exponential rate of urbanisation in past decades demands novel techniques to measure the resilient modulus with a focus on lowering the time consumption and construction costs [4]All major correlations to calculate resilient modulus are derived from different index properties such as mean particle diameter, liquid limit, plastic limit, optimum moisture content, maximum dry density, void ratio relative density and specific gravity of the sub grade soil. The resilient modulus is also derived from

strength properties of sub grade soil[5][2, 6].Pavement failure has been a major issue worldwide for many years. The recently built or repaired roads are degrading quickly. Following construction, there were numerous road problems in Pakistan every year.[7] Rutting, cracks, potholes, sinking, corrugation, shove, and other failures are the most frequently seen. High-quality materials and building methods must be used to increase the condition of pavement [5].

Most of Pakistan's roads are fast degrading because of inadequate methods to calculate the resilient modulus and low-quality materials [7]. These obsolete methods force national highway authority NHA to spend a large portion of their development funds on road repair and maintenance. However, the burden on Pakistan's national highway system is growing because of growing population, economic expansion, and greater dependence on roadways.[8] The resilient modulus also serves a significant part in describing the characteristics of the materials in different pavement layers in the new mechanistic-empirical design guide NCHRP 2004. Cohesive soils' resilient modulus is not a constant stiffness feature but is strongly influenced by the stress condition, the soil's structure, and the water content [9]. George numerous attempts have been made to create predictive equations by including state factors such confinement stress, bulk stress, deviator stress, and soil physical parameters due to the difficulty of conducting resilient modulus testing.[3, 7]
Hveem 1998 first used the phrase "resilient modulus," which is the ratio of repetitive axial deviator stress to recoverable axial strain. However, responses to various materials are affected in different ways by test conditions (such as stress state, amount of stress treatments).[10, 11]
One of the key material characteristics in the mechanical analysis and structural planning of road pavements is resilient modulus (MR). In order to measure the resilient modulus of sub grade soils, repetitive load triaxial experiments are often carried out in the lab on remoulded or undisturbed specimens.[1].The nonlinear stress-strain behaviour of pavement materials under cyclic loadings is described by the resilient modulus, a fundamental feature of engineering materials.[12] According to the recoverable strain under cyclic load, it is described as the elastic modulus [13]. The term "resilient modulus of a material" was first used by Signes in 2002 [14] who described it as "the ratio of applied dynamic stress (σ_d) to the resilient or elastic strain component (ε_r) under a transient dynamic pulse load." [15].Resilient modulus (M_r) is the most important parameter in pavement design which defines quality of pavement but Lack of equipment and consistency to calculate M_r adversely affects the pavement design. All major correlations to calculate resilient modulus are derived from different index and strength properties of sub grade soil. The aim of this investigation was to establish a correlation between resilient modulus evaluated from ultra-sonic pulse velocity and triaxial test.

METHODOLOGY

The research was carried out as a qualitative study following cross sectional pattern. Methodology part consists of two major components classified as experimental program and regression analysis. Figure1 is the representation of flow chart of the methodology.

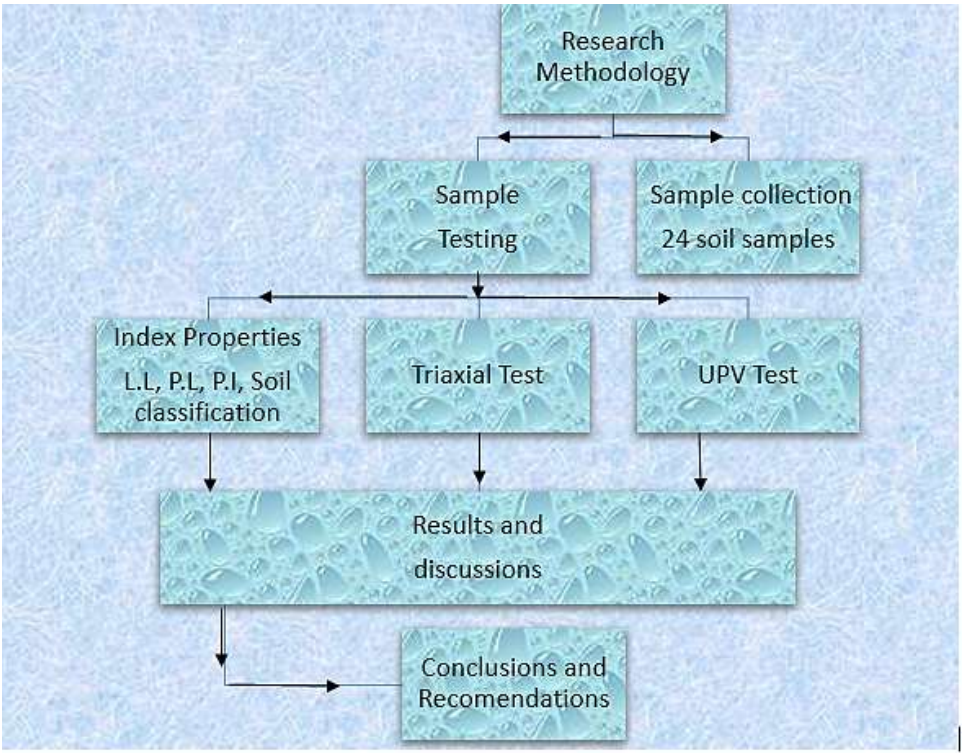

Figure 1 Flow Chart of the research

Experimental Program

The experimental program included index properties testing which consisted of Atterberg limits test, standard proctor test to calculate optimum moisture content and maximum dry density, and sieve analysis. It also included ultrasonic pulse velocity UPV test and triaxial test on all soil samples. Unconsolidated Undrained (UU) triaxial test was carried out in accordance with ASTM D 4767.Triaxial test is used to determine compressive strength, angle of internal friction of soil, cohesion, shear strength, modulus of elasticity, pore water pressure and Poisson's ratio of soil.[16] Different trails were carried out using different moisture contents to determine stress- strain relationships of loaded soil. Apparatus from UET Taxila Geo-technical engineering laboratory was used to conduct Tri-axial compression test. Great care was considered while noting down readings of load at different increments of time and pore pressure. The UPV test was performed on moulded soil samples in accordance with ASTM-C597[17]. Cylindrical Soil samples were placed under UPV apparatus, and an ultrasonic wave was allowed to pass from the samples. The pulse velocity

can be noted down from display screen. The further evaluation of the wave velocities gave us the predicted values of resilient modulus.

RESULTS AND DISCUSSIONS

In this section the results evaluated from all tests carried out on soil samples and discussion of the results is given. Results from experimental program included, Triaxial compression test, Ultra Sonic Pulse velocity test, Resilient modulus, and correlations between resilient modulus from UPV and resilient modulus from triaxial test.

Index Test Results and Shear Wave Primary Wave Velocities:

Table 1 shows the results of index testing as well as primary wave velocity and shear wave velocity calculated by performing ultrasonic pulse velocity test on collected soil samples. The index properties such as liquid limit, plastic limit, plasticity index, mean particle size, optimum moisture content, and maximum dry density play an important role in determination of resilient modulus of any sub grade soil sample. The variation of resilient modulus is significantly dependent on the index properties of the soil. [18]. According to Muhammad et al 2019, the mean particle size directly affects the value of resilient modulus. The coarser cohesive soils tend to have high resilient modulus as compared to fine soils.[7] Similarly, the liquid limit and plastic limits also control the value of resilient modulus. Soil samples with high liquid limit and high plasticity index tend to have low value of resilient modulus. The results in figure 2 shows a downward trend from group A-2-4 towards group A-6. It is because of the fact that coarse grained cohesive soils tend to have low plasticity index and high resilient modulus while fine grained soils have high plasticity index and low resilient modulus.[19]. The shear wave and primary wave velocity is purely dependent on the soil skeleton. If the compaction is good and density is higher shear wave velocity will be higher. The coarser soil samples tend to have good relative compaction and higher densities that is why the shear wave and primary wave velocities.[20].

Table 1 Results of index properties and shear primary wave velocities.

A-2-4								A-4							
Soil sample	**L.L**	**P.L**	**P.I**	**Density**	**OMC**	**Vs**	**Vp**	**Soil sample**	**L.L**	**P.L**	**P.I**	**Density**	**OMC**	**Vs**	**Vp**
Ghazi kohali to jlala	31	20	11	120.15	5.5	5.97	3	Kohistan enclave	49	29	20	117.85	6.5	4.31	2.2
Maegewali Attock	34	27	7	121.54	6	6.24	3.1	Kohat KPK	51	33	18	118.54	6.5	4.28	2.1
Village new house	32	22	10	120.34	4.5	5.84	2.9	Behrain Upper Swat	49	32	17	117.64	7	4.05	2
Stadium Bajour	37	28	9	119.42	5	5.65	2.8	HMC farooqia Taxila	52	32	20	117.98	6.5	3.98	2
Daman Shah Bajour	32	24	8	120.35	5.5	6.05	3	Khalool	55	36	19	118.24	7	3.67	1.8
Attock sample 2	35	24	11	121.32	5	6.28	3.1	Balousar Area	54	33	21	117.32	7.5	3.51	1.8
A-2-6								**A-6**							
Soil sample	**L.L**	**P.L**	**P.I**	**Density**	**OMC**	**Vs**	**Vp**	**Soil sample**	**L.L**	**P.L**	**P.I**	**Density**	**OMC**	**Vs**	**Vp**
Civil Col Malaknd	41	25	16	119.25	6.5	4.98	2.5	Khalool to swari	59	33	26	116.15	7	3.57	1.8
Ghazi Kohali Taxila	45	28	17	119.28	6	4.65	2.3	B17 Islamabad	58	35	23	117.54	7	3.65	1.8
Shahkot Malakand	43	29	14	118.24	6.5	5.51	2.8	Gujranwala	61	38	23	117.67	7.5	3.07	1.5
Takht bai mardan	42	29	13	118.84	6.5	4.52	2.3	Swabi	60	34	26	118.36	6.5	3.27	1.6
Chakdara Dir	44	28	16	119.16	7	4.87	2.4	Wah Model Town	58	36	22	117.25	7	3.29	1.6
Wah cantt	45	29	16	118.04	6.5	4.59	2.3	Karak KPK	61	39	22	116.58	7.5	3.18	1.6

Resilient Modulus from Triaxial Test:

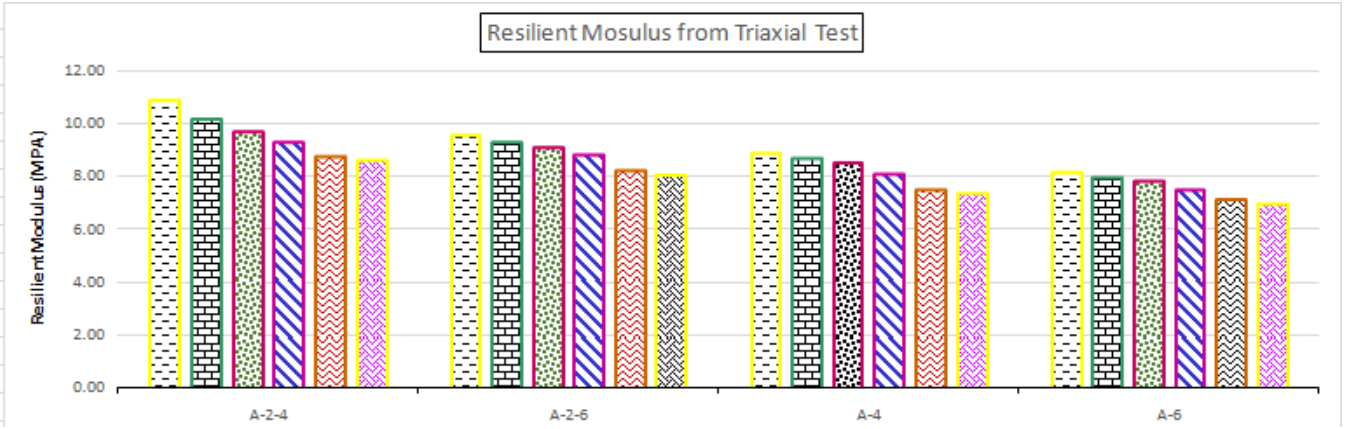

Figure 2 is a graphical representation of resilient modulus from Triaxial test of Group A-2-4, A-2-6, A-4, and A-6

The above given figure 2 represents the resilient modulus calculated from triaxial tests. In the graph on the X-axis there are group numbers and on Y-axis resilient modulus calculated from Triaxial test. The graph indicates that the maximum resilient modulus of all groups is 11.02MPa, 10.21MPa, 9.2MPa, and 8.67MPa respectively. Resilient modulus is directly related to the density of soil sample.[14, 19, 21, 22] Higher values of density of soil samples result in higher values of resilient modulus. Resilient modulus also depends on the particle size of soil samples. The higher value of resilient modulus in group A-2-6 indicates that the particle size of this group is comparatively coarser than other groups which resulted in higher value of resilient modulus.[18, 22].

Resilient Modulus from UPV

The given figure 3highlights the resilient modulus calculated from Ultrasonic Pulse Velocity Test. In the graph on the X-axis group numbers from A-2-4 A-2-6 A-4 and A-6 are given and, on the Y-axis, resilient modulus from UPV test. Ultrasonic pulse velocity test is carried out to predict the resilient modulus of soil samples based on shear wave and primary wave velocities of the soil samples.[18] The resilient modulus calculated from this test entirely depends on the density of soil samples and velocity of shear waves and primary waves[23, 24]. Following are the results given in graphical form.[1, 7, 20]. The graph in fig 2 and fig 3 solidify the fact that experimental values of the resilient modulus calculated from triaxial test are higher than UPV values. Hence a model is developed to predict MR from UPV by finding a correlation factor but the experimental values are more reliable than the predicted values through UPV test.[10, 16, 25].

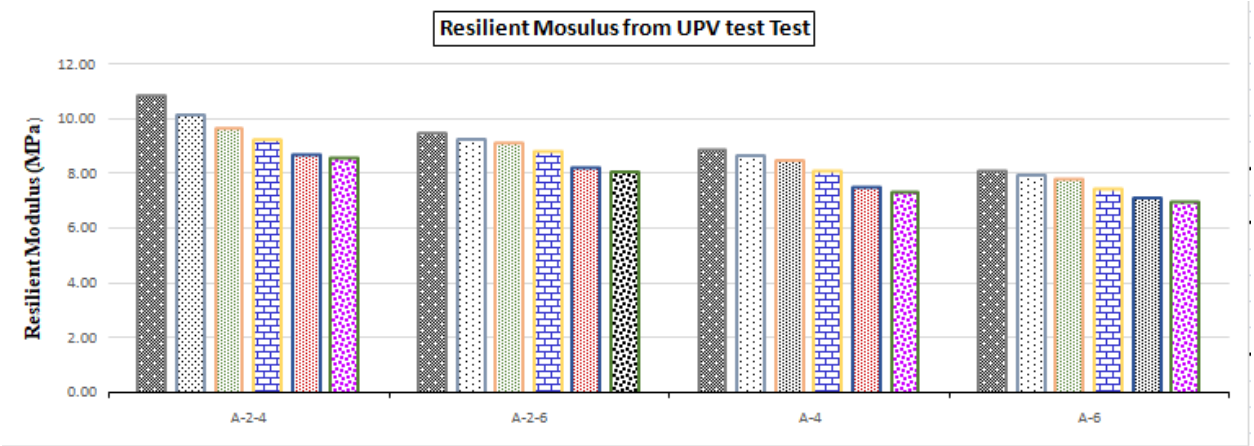

Figure 3 showing the results of resilient modulus from UPV for groups A-2-4, A-2-6, A-4, and A-6 respectively.

Regression Analysis

Below given figure 4 represents the linear correlation between ultrasonic pulse velocity test and dynamic triaxial test results. On the x axis there is UPV resilient modulus and y axis is resilient modulus from dynamic triaxial.[15, 19, 26] The resilient modulus from UPV depends on the density of the samples. Black dots indicate resilient modulus of 24 samples plotted. The red line highlights the trend line of plotted data. [8, 27]. An equation is also given which is a numerical representation of this regression model. This equation shows that the predicted resilient modulus from UPV is a linear function of Experimental resilient modulus calculated from triaxial test involving some constant values.[18, 28, 29]. The correlation model can be used to accurately measure the experimental resilient modulus from UPV data by help of this equation.

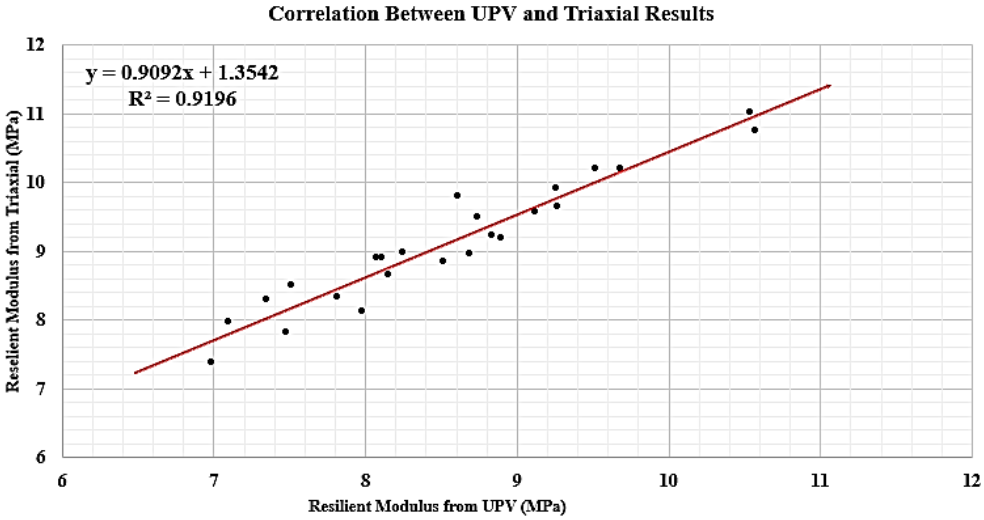

Figure 4Relation between predicted UPV on x-axis and Experimental Triaxial values on y-axis

CONCLUSIONS

- Triaxial test results indicate that resilient modulus is directly affected by mean particle size of the soil. As the graph shows higher value of resilient modulus for group A-2-4 and lower values for group A-6.
- Group A-2-4 tends to show higher values of resilient modulus as compared to group A-2-6, A-4, A-6 because of its coarse mean particle size and potentially easy compaction.
- The triaxial test results are best representation of the resilient modulus of sub grade due to low number of variables and correlations involved.
- UPV values tend to have error in the results as compared to triaxial tests. The correlation model is the best possible way to correlate the resilient modulus calculated from both tests.
- The regression equation or correlation can be used to predict the resilient modulus of groups A-2-6 A-2-4 A-4 and A-6.

ACKNOWLEDGEMENTS

We prostrate before Allah (SWT) and greet his beloved Prophet Muhammad (peace be upon him) in remembrance of all the bounties. We would like to thank the supervisor Engr. Kashif Riaz of UET Taxila, without his guidance this work would have never been completed. We also appreciate the efforts of technical staff and lab staff of UET Taxila Geotech lab.

REFERENCES

1. Abdollahi, M. and F. Vahedifard, *Predicting Resilient Modulus of Unsaturated Subgrade Soils Considering Effects of Water Content, Temperature, and Hydraulic Hysteresis.* International Journal of Geomechanics, 2022. **22**(1): p. 04021259.
2. Afkhamy Meybodi, P., et al., *Effect of crushed glass on skid resistance, moisture sensitivity and resilient modulus of hot mix asphalt.* Arabian Journal for Science and Engineering, 2019. **44**(5): p. 4575-4585.
3. Azam, A., et al., *Modeling resilient modulus of subgrade soils using LSSVM optimized with swarm intelligence algorithms.* Scientific Reports, 2022. **12**(1): p. 1-20.
4. Alnunu, M.Z. and Z. Nalbantoglu, *Performance of Using Waste Marble Dust for the Improvement of Loose Sand in Deep Soil Mixing.* Arabian Journal for Science and Engineering, 2022. **47**(4): p. 4681-4694.
5. Bastola, N.R., et al., *Artificial neural network prediction model for in situ resilient modulus of subgrade soils for pavement design applications.* Innovative Infrastructure Solutions, 2022. **7**(1): p. 1-12.
6. Çöleri, E., *Relationship between resilient modulus and soil index properties of unbound materials*. 2007, Middle East Technical University.
7. Arshad, M., *Development of a correlation between the resilient modulus and CBR value for granular blends containing natural aggregates and RAP/RCA materials.* Advances in Materials Science and Engineering, 2019. **2019**.
8. Du, J., et al., *Experimental Study on Stiffness Degradation of Organic Matter-Disseminated Sand under Cyclic Loading.* Sustainability, 2022. **14**(18): p. 11793.
9. Kardani, N., et al., *Prediction of the resilient modulus of compacted subgrade soils using ensemble machine learning methods.* Transportation Geotechnics, 2022. **36**: p. 100827.
10. El-Ashwah, A.S., et al., *Advanced characterization of unbound granular materials for pavement structural design in Egypt.* International Journal of Pavement Engineering, 2022. **23**(2): p. 476-488.
11. George, K., *Prediction of resilient modulus from soil index properties*. 2004, University of Mississippi.
12. Hanandeh, S., et al., *Prediction of the Resilient Modulus of Stabilized Weak Subgrade for Pavement Design Structure.* Transportation Geotechnics, 2022: p. 100856.
13. Singh, A.P., et al., *Studies on Design of Flexible Pavement Using Resilient Modulus: A Review.* Optimization of Industrial Systems, 2022: p. 101-109.
14. Signes, C.H., et al., *An Experimental Study of a New Soil-Rubber Mix for Railway Embankment.*
15. Haj, E.Y., et al., *Resilient modulus prediction models of unbound materials for Nevada*. 2018, SOLARIS Consortium.

16. Kim, S.S., et al., *Prediction of Resilient Modulus From the Laboratory Testing of Sandy Soils*. 2019, Georgia. Department of Transportation. Office of Performance-Based ….
17. Kuttah, D., *Determining the resilient modulus of sandy subgrade using cyclic light weight deflectometer test.* Transportation Geotechnics, 2021. **27**: p. 100482.
18. Yao, Y., et al., *Model for predicting resilient modulus of unsaturated subgrade soils in south China.* KSCE Journal of Civil Engineering, 2018. **22**(6): p. 2089-2098.
19. Patel, A., et al., *A methodology for determination of resilient modulus of asphaltic concrete.* Advances in Civil Engineering, 2011. **2011**.
20. Ji, R., et al., *Evaluation of resilient modulus of subgrade and base materials in Indiana and its implementation in MEPDG.* The Scientific World Journal, 2014. **2014**.
21. Zhang, J., et al., *Rapid estimation of resilient modulus of subgrade soils using performance-related soil properties.* International Journal of Pavement Engineering, 2021. **22**(6): p. 732-739.
22. Zhang, J., et al., *Predicting resilient modulus of fine-grained subgrade soils considering relative compaction and matric suction.* Road Materials and Pavement Design, 2021. **22**(3): p. 703-715.
23. Jamsawang, P., et al., *Mechanical and microstructural properties of dredged sediments treated with cement and fly ash for use as road materials.* Road Materials and Pavement Design, 2021. **22**(11): p. 2498-2522.
24. Burra, S.G., *Resilient modulus of stabilized subgrade soil using commercial products and industrial by-products.*
25. Nantung, T.E. and D. Kim, *Evaluation of Resilient Modulus of Subgrade and Base Materials in Indiana and Its Implementation in MEPDG.*
26. Ševelová, L., A. Florian, and P. Hrůza, *Using Resilient Modulus to Determine the Subgrade Suitability for Forest Road Construction.* Forests, 2020. **11**(11): p. 1208.
27. Muhammad, N. and S. Siddiqua, *Moisture-dependent resilient modulus of chemically treated subgrade soil.* Engineering Geology, 2021. **285**: p. 106028.
28. Yuan, H., et al., *Resilient modulus—physical parameters relationship of improved red clay by dynamic tri-axial test.* Applied Sciences, 2019. **9**(6): p. 1155.
29. Qian, Y., et al., *Determination of resilient modulus of subgrade using cyclic plate loading tests.* Geo-Frontiers, 2011. **2011**: p. 4743-4751.

2nd International Conference on Advances in Civil and Environmental Engineering (ICACEE-2023)

University of Engineering & Technology Taxila, Pakistan

Conference date: 22nd and 23rd February, 2023

Numerical Simulation of response of footing resting on Sandy Soil against Impact Loading

Hamza Alam Khan [1], Irshad Ahmad[2]

[1]University of Engineering & Technology Peshawar, 15pwciv4275@uetpeshawar.edu.pk

[2]University of Engineering & Technology Peshawar, irspk@yahoo.com

ABSTRACT

Industrial vibrations are frequently caused by impact stresses on machine foundations. These foundations frequently create ground vibrations and vertical dynamic loads that can harm neighbouring structures or buildings. The main objective of this work is to use ABAQUS finite element software to simulate the dynamic reaction of the foundation under impact load at various depths. Previous experiments used a dynamic load created by an impactor on a plate resting on dense sandy soil medium. At several depth, the responses of various soils were assessed. The falling weight deflectometer (FWD) and accelerometers are used to measure displacements, velocities, and accelerations that occur as a result of the impact acting at different depths inside the soil. This problem is discretized by using solid 3D element to model the impact load, soil, and the aluminum plate. Soil, impact mass and plate parameter were used the same as in experimental work. It is observed that the finite element analysis correlates well with the experimental results. Furthermore, it can be concluded that ABAQUS program is suited well for simulating the dynamic behavior of structures and soil.

KEYWORDS: Impact loading, Sandy soil, Numerical Simulation

INTRODUCTION

The dynamic reaction of an elastic plate lying on sand is a useful topic for research that can be used to a variety of situations. For instance, the plate can be considered as a structure's footing, which is important for foundation vibration research. Second, the reaction of a finite plate to an impact force is a fundamental structural design problem. Furthermore, analyzing the impact force is vital and intriguing since knowing the live load on the impacted structure allows for better design and prediction of the structure's damage. Finally, it's critical to comprehend how impact loads are transmitted through the soil. Impact is described as a collision occur between two bodies in a very short period of time. In such collision, the bodies exerts very high forces on each other, known as impact loads, that are dependent on the collision bodies' velocity, mass, shape, elastic and plastic properties. Many structures that were intended just to resist their own dead loads in addition to the traditional static living loads may be subjected to impact loads. It's a good idea to test the impact resistance of buildings that are meant to withstand static stresses. Some structures, such as nuclear plant facilities and buildings, must be designed to withstand impact loads. (H. L. Chen et al., 1988) experimentally worked on plate that rested on the sand and experienced an impact load.

Strain of plate and acceleration of sand were observed. The experimental results measured had good agreements with the analytical solution. (H. L. Chen et al., 1990) in one of his research works developed a cylindrical model buried inside a sandy soil experiencing an impact load on its top. It was observed that higher the Poisson's ratio, the lower the rigidity. In addition, analytical and numerical models were developed that shows good agreement with experimental results. (H.-L. Chen & Chen, 1996) has worked on buried structures and target plates resting on soil experimentally. A small scale model was developed and impact load of known weight was drop on target plate. Analytical and experimental results in the form of time histories of force and displacement shows good agreement. The results demonstrate that the separation of plate from the soil is less in case of stiffer plate as evidenced by higher loading magnitudes and longer loading durations. Furthermore (Fattah et al., 2017) numerically worked on the square concrete foundation with dimensions of 3×3×0.3 m placed on the foundation sandy soil 15m deep and 9 m away from the edge of the plate subjected to impact load. Parameters including foundation thickness, load eccentricity and amplitude of impact load were taken as variables. The load eccentricity was found to enhance displacement while decreasing stress at the foundation center. This is due to non-uniformly distributed pressures on the loaded surface, where the loads are concentrated locally. The foundation displacements and stresses are significantly reduced when damping is present. At all damping ratios, increasing the damping ratio reduces the vertical displacement of the foundation at the same moment. (Ali et al., 2018) uses dry dense sand in his experimental study, and measured sand behavior under impact load. The response of sand against the footing area and embedment depth were studied. The obtained result were in the form of stress, acceleration and displacement time histories. It was observed that the force-time history grow with the footing embedment. Due to an increase in the degree of confinement, time history has increased by around 10%-30% that results in decrease in displacement. When the embedment depth was raised, the overburden pressure increased by about 40-50 percent, causing the rigidity of sandy soil to increase.

Methodology

The numerical work is done entirely in ABAQUS. According to the experimental study, all dimensions and material qualities are utilized (Ali et al., 2018). To model soil, target plate, and impact mass, a solid 3D element is used. The soil model's dimensions are 1.2mx1.2mx0.8m. A circular plate with a thickness of 0.02m and a diameter of 0.1m was used. The impact mass is 100 kg with a diameter of 0.1m and is employed as a falling weight from a height of 0.05m on the target plate. The impact response will observed for four models: Model 1 (plate is placed at the top of soil), Model 2 (Plate is placed at 0.05m depth buried in soil), Model 3 (Plate is placed at 0.1m depth buried in soil and Model 4 (Plate is placed at 0.2m depth buried in soil).

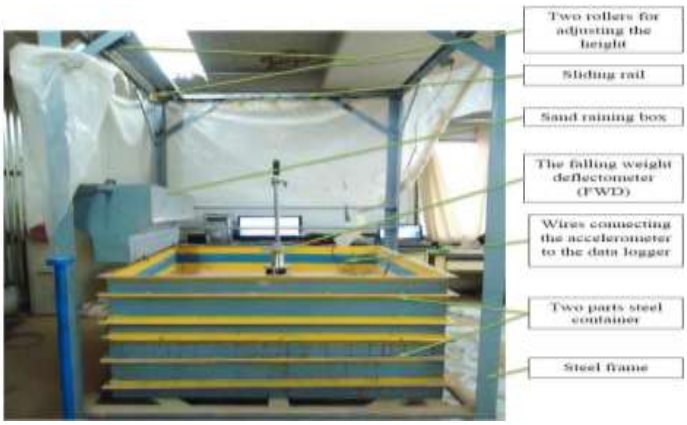

Figure 0.1 Experimental Setup for soil placement

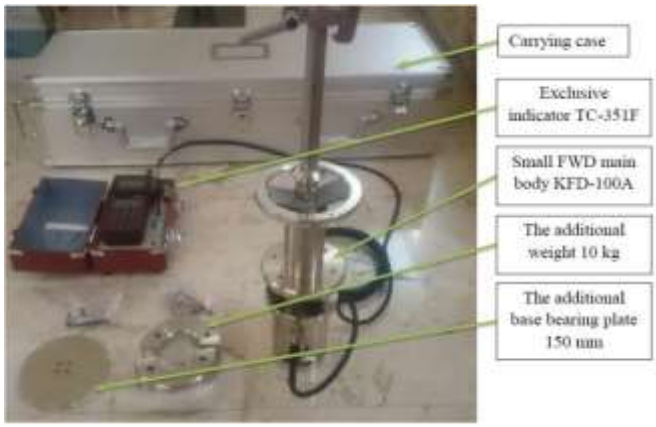

Figure 0.2 Plate and Impact load and other accessories

Table 1 shows the material parameters of the soil. The impact mass and target plate properties are shown in Table 2 and Table 3 respectively. Impact mass and plate are taken as elastic materials, whereas the soil is taken as an elasto-plastic medium. The problem is solved using the Mohr Columb Model. While simulating the model, dynamic explicit analysis was used. The soil has been given a fixed boundary condition while the impact mass and target plate are allowed to displace only vertically. The impact load is applied in a vertical direction at a velocity of 1m/s. The velocity is calculated through free fall weight formula:

$$V = \sqrt{2}gh \quad (1)$$

Where h equals 0.1m and g equals 9.8m/s^2. The impact mass and surface-to-surface contact between the soil and the target plate have been provided. The contact interaction between the soil and the target plate is given a coefficient of friction 0.502, whereas the interaction between the target plate and the impact mass is given a coefficient of friction 0.47.

Table 2 Soil Properties

Mass Density (kg/m^3)		**1720**
Angle of friction		37
Elastic Modulus (N/m^2)		6.00E+10
Poisson ratio		0.25
Specific Gravity		2.65
Dilation Angle		1

Table 3 Plate Properties

Mass Density (kg/m^3)	**2821**
Elastic Modulus (N/m^2)	6.89E+10
Poisson ratio	0.33

Table 4 Impact load properties

Mass density (kg/m^3)	**7800**

Elastic Modulus (N/m^2)	2.1E+11
Poisson ratio	0.28

.

RESULTS

Model 1

In model 1, Plate is placed at the top of soil the displacement and force time histories developed are shown in figure 3.1 and figure 3.2 respectively.

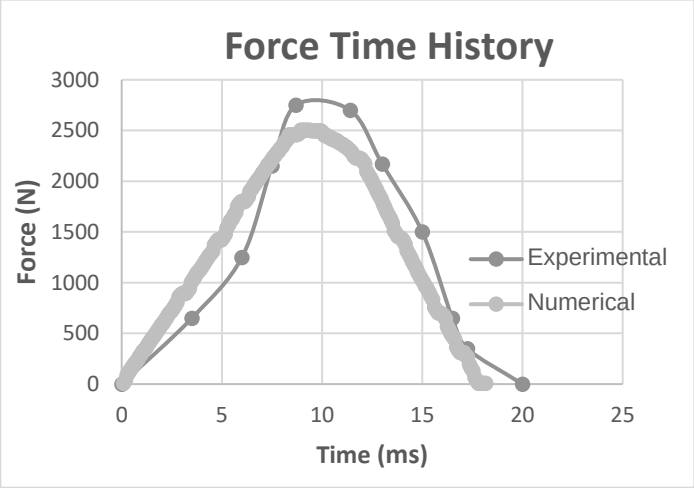

Figure 0.3 Force Time History of plate resting at the top of soil

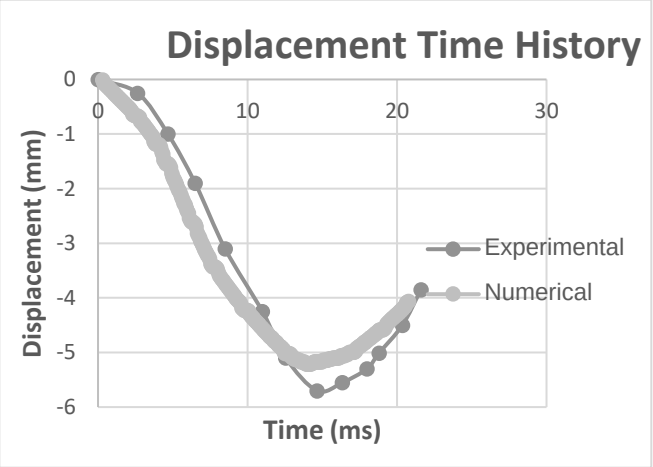

Figure 0.4 Displacement Time History of plate resting at the top of soil

Model 2

In model 2, Plate is placed at the depth of 0.05m buried in the soil, the force and displacement time histories developed are shown in Figure 3.3 and Figure 3.4 respectively.

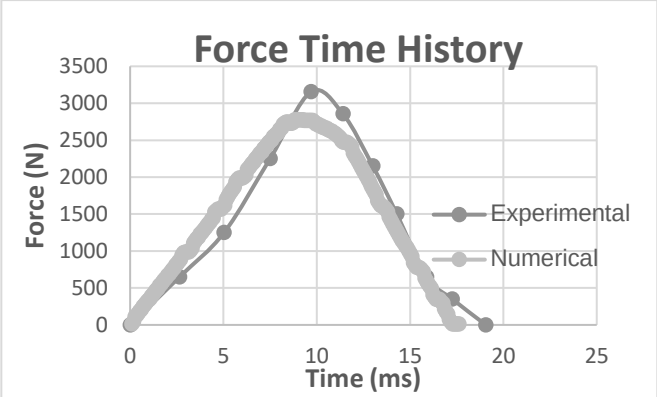

Figure 0.6 Force Time History of plate at 0.05m depth

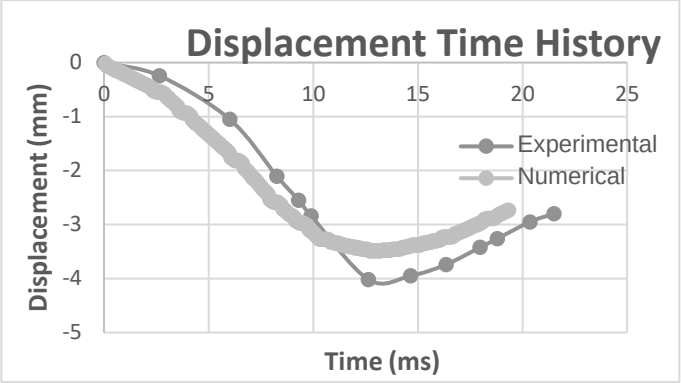

Figure 0.5 Displacement Time History of plate at 0.05m depth

Model 3

In model 3, Plate is placed at the depth of 0.1m buried in the soil, the displacement and force time histories developed are shown in Figure 3.5 and Figure 3.6.

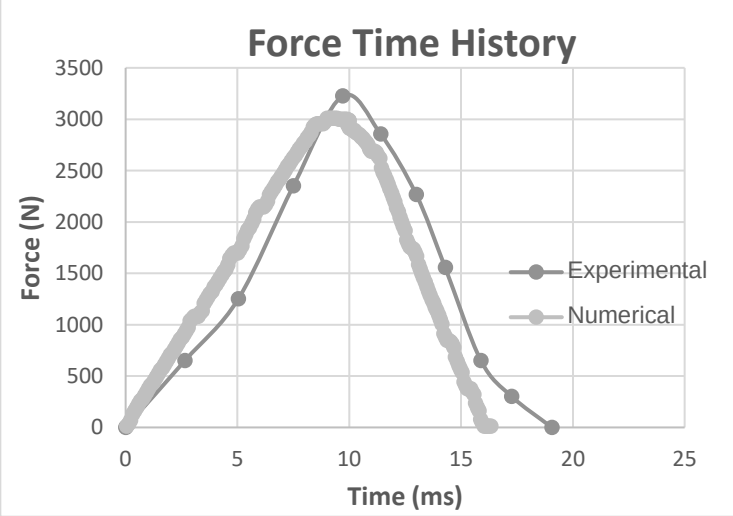

Figure 0.8 Force Time History of plate at 0.1m depth

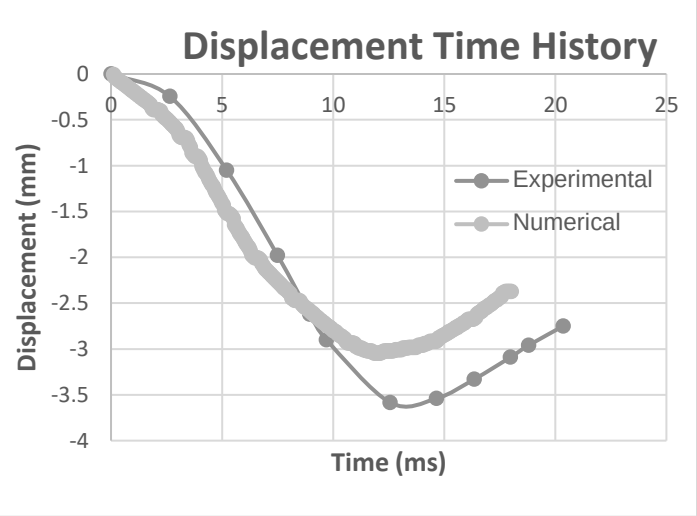

Figure 0.7 Displacement Time History of plate at 0.1m depth

Model 4

In model 4, Plate is placed at the depth of 0.1m buried in the soil, the displacement and force time histories developed are shown in Figure 3.7 and Figure 3.8.

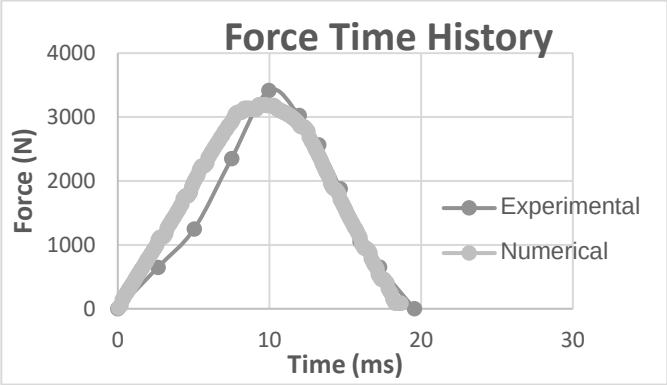

Figure 0.10 Force Time History of plate at 0.2m depth

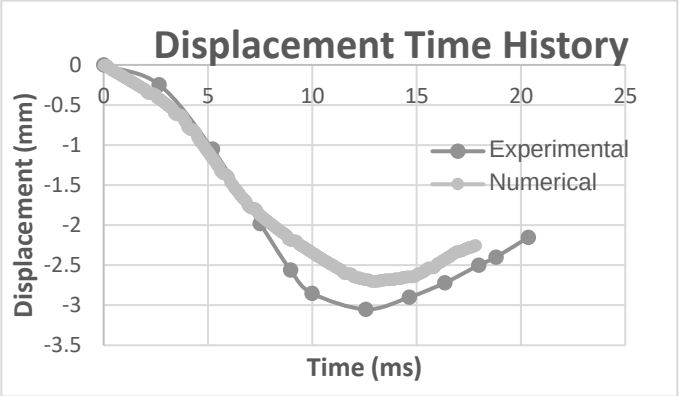

Figure 0.9 Displacement Time History of plate at 0.2m depth

Conclusions

1. The experimental results of (Ali et al., 2018) has been verified numerically. The force and displacement time histories shows good agreement with the experimental results.
2. The surface displacement decreases while the response force increases when the impact plate is placed in deeper locations; the maximum displacement always occurs when the impact plate is placed at the top soil surface. When the plate is immersed at 2B as opposed to when it is positioned at the top soil surface, the values of displacement are typically reduced by 35–40% while the value of response force increases by 20-30%.
3. The foundation's embedment depth has a considerable impact. The peak response happens very quickly after the peak impulse occurs when the impact plate is embedded 2B below the top of the soil (with a time lag of 25% to 30% of the time of peak impulse). When the impact plate is positioned at the soil's top surface, the greatest phase angle (time lag) always happens. The time lag is discovered to be between 25% and 35% of the peak impulse time.

REFERENCES

Ali, A. F., Fattah, M. Y., & Ahmed, B. A. (2018). Response of circular footing on dry dense sand to impact load with different embedment depths. *Earthquakes and Structures, 14*(4), 323–336.

Chen, H.-L., & Chen, S.-E. (1996). Dynamic responses of shallow-buried flexible plates subjected to impact loading. *Journal of Structural Engineering*, *122*(1), 55–60.

Chen, H. L., Lin, W., Keer, L. M., & Shah, S. P. (1988). *Low velocity impact of an elastic plate resting on sand*.

Chen, H. L., Shah, S. P., & Keer, L. M. (1990). Dynamic response of shallow-buried cylindrical structures. *Journal of Engineering Mechanics*, *116*(1), 152–171.

Fattah, M. Y., Hamood, M. J., & Abbas, S. A. (2017). Dynamic response of plates on elastic foundation under eccentric impact load. *MATEC Web of Conferences*, *120*, 6006.

2nd International Conference on Advances in Civil and Environmental Engineering (ICACEE-2023)

University of Engineering & Technology Taxila, Pakistan

Conference date: 22nd and 23rd February, 2023

Numerical study on basement wall contribution in lateral load resistance in pile raft foundation

Abdus Salam[1], Muhammad Hamza Sheikh[2], Mehtab Ahmad[3], Irfan Jamil[4]

[1]University of Engineering and Technology Peshawar, abdussalamhajiabad@gmail.com

[2]University of Engineering and Technology Peshawar, hamzasheikh0341@gmail.com

[3]University of Engineering and Technology Peshawar, 19pwciv5234@uetpeshawar.edu.pk

[4]University of Engineering and Technology Peshawar, engrirfan@uetpeshawar.edu.pk

ABSTRACT

The population of the world is increasing exponentially day by day, and to facilitate them with shelter we need more land which is limited. Therefore, high-rise buildings are a better solution to this problem, these high-rise buildings are exposed to lateral loads caused by wind and earthquakes so, we need a sound foundation. In this case, Pile Raft is the most efficient foundation in which the lateral and vertical loads are resisted by piles and raft. Practically in high-rise buildings, there are multiple basement stories, which increases the ratio of floor area to height that can be used to fulfil the storage and parking facilities requirement. Conventionally during the design of the foundation, the lateral load capacity of the basement wallis ignored by engineers, but in reality, basement walls can resist lateral loads. In this research study, a parametric study is performed on small-scale models, in order to study the sensitive parameters which are affecting the lateral contribution of the basement wall in the pile raft foundation.It was concluded that basement height is one of the major parameter affecting the lateral contribution of piled raft system.

INTRODUCTION

The growth of population and the scarcity of land has beenneeded to build many high–rise building. And these high-rise buildings are exposed to lateral load from wind and earthquakes. The most critical structural component of a tall building is its foundation and it's very important to design it for safety and economic reasons. The basement's contribution to lateral loads is usually not taken into account during foundation design even though, in reality, it can resist lateral loads and increase the lateral stiffness of the foundation.[2]

Most researchers have worked on the settlement behaviour and capacity of the foundation of tall buildings to make them more economical, and safer, satisfying the desired lateral and vertical loading conditions. The common types of foundations for tall buildings are raft foundations, pile foundations, and piled raft foundation.A raft foundation is used when isolated footings cover 50%–70% of the building area under a superstructure.[1]Such a foundation supports a building of moderate height but for very tall buildings it is not feasible due to large lateral and bending moment loadings that the raft foundation cannot resist. So, for taller buildings, pile foundations are provided to resist lateral and bending moment

loadings.Piles also reduce settlement by transferring the load from soft strata to hard strata but in most cases, an increased number of piles result in an uneconomical foundation.[3]

Most researchers referred to the use of pile raft foundations instead of Pile foundations. Recently Irfan et al. performed and experimental study on a small-scale model of piled raft foundation under lateral loading and concluded that the raft contributes to resist the lateral loads. So, it shows that Pile raft foundation is more suitable than a pile foundation.[4]

In most of the high-rise buildings, we have multiple basement stories. Recently an experimental study was performed by Irfan Jamil et al, that basement wall contribution in resisting lateral load ranges from 50%–80%, which is a major contribution. So, it means that Pile Raft Foundation with a basement wall is more efficient than Pile Raft Foundation.

No parametric study has yet been performed on the pile raft foundation with a basement wall. In this study, different parameters of the Pile raft Foundation with the basement wall will be studied, in order to find out the sensitive parameter which are affecting the lateral load capacity of the basement wall**.**

METHODOLOGY

Soil Condition

All the Properties of the soil is taken from the experimental study performed by Irfan et al.[1]

Table 1. Property of soil.

Property	**Value**
effective diameter, D_{10}	0.32 mm
coefficient of uniformity, C_u	2.56
coefficient of curvature, C_c	0.70
classification (USCS)	SP
specific gravity, G_s	2.63
maximum dry unit weight	17.60 kN/m^3
minimum dry unit weight	14.50 kN/m^3
test dry unit weight	16.40 kN/m^3
relative density, D_r	60%
angle of internal friction	34°
soil type	poorly graded sand (SP)

Modelling of Pile Raft Foundation with Basement Wall

Modelling of piled raft foundation with a basement wall has been performedby using the finite element software Plaxis 3D. Toinvestigate the behaviour of pile raft foundation with basement, raft and basement wall are modelled as a plateand piles are treated as embedded beams

Table 2. Properties of materials.

component	material	Young's modulus (GPa)	unit weight (kN/m³)	Poisson's ratio
Raft	aluminium	69	26.54	0.33
Piles	galvanized iron	200	26.70	0.30
basement wall	aluminium	69	26.54	0.33

Parametric Study

Parametric studies are performed to determine sensitive parameters which are affecting the lateral load capacity of the basement wall in piled raft foundation with basement wall. Different parametersare basement wall height, basement wall thickness, raft thickness, pile length, pile diameter and number of piles. In this study, six cases study were taken into consideration to analyze the behavior of piled raft foundation with basement wall behavior.

Case 1:

The effect of basement wall height was analysed in "Case 1" with constant other parameters, basement wall height varies as 5.08cm, 10.16cm, 15.2cm, 20.3cm, 25.4cm, and 30.4cm were analysed to find the maximum lateral load capacity of the basement wall with raft.

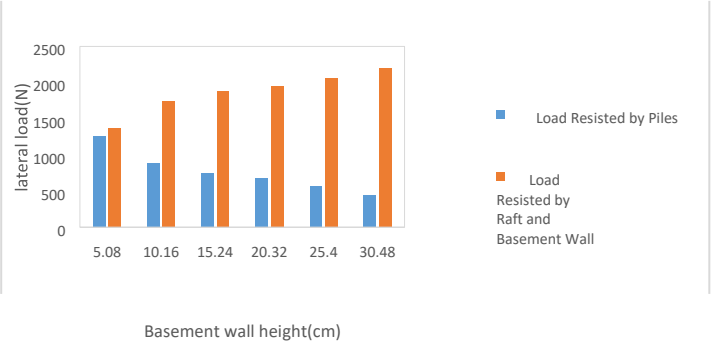

Figure 2. variation of basement wall height

By increasing basement wall height from 5.08cm to 30.4cm, the lateral loads resisted by basement wall and raft increase from 52% to 83%.

Case 2:

In this case, the basement wall thickness is focused without changing other parameters, basement wall thickness varies as 0.25cm, 0.5cm, 0.76cm, 1cm, 1.27cm, 1.52cm, 1.78cm, 2.03cm, 2.29cm, and 2.54cm were analyzed to find the maximum lateral load capacity of basement wall with the raft.

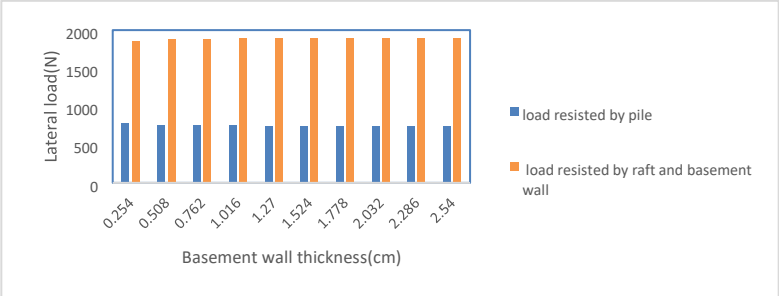

Figure 3. Variation of basement wall thickness.

When we change basement wall thickness from 0.25cm to 2.54cm the lateral load resisted by basement wall and raft are increases from 70% to 72%

Case 3:

This case is mainly focusing the raft thicknesswithout changing other parameters, the various raft thickness areas 0.635cm, 1.27cm, 1.905cm, 2.54cm, 3.175cm, and 3.81cm were analyzed to find the maximum lateral load capacity of the basement wall with the raft.

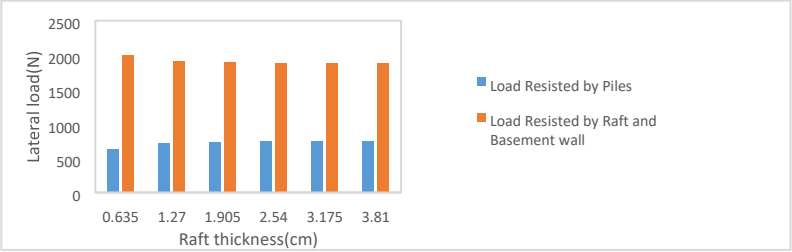

Figure 4: Variation of raft thickness

By varying the raft thickness from 0.635cm to 3.81cm the load resisted by basement wall and raft is decreased from 76% to 71%.

Case 4:

In this case, we studied various pile lengths without changing other parameters, which are as 15.24cm, 25.4cm, 35.56cm, 45.72cm, 55.88cm, 66.04, and 76.2cm were analyzed to find the maximum lateral load capacity of basement wall with the raft.

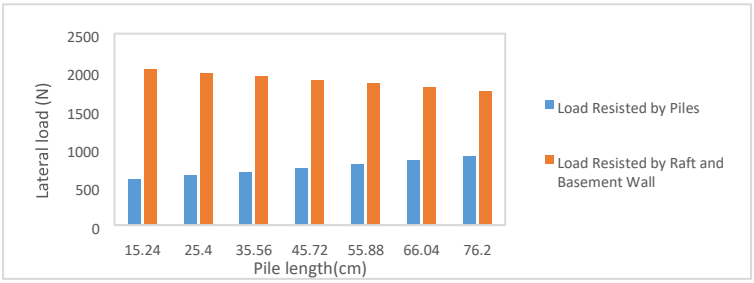

Figure 5: Variation of pile length.

When the pile length is increased from 15.24cm to 76.20cm the load taken by basement wall and raft is decreased from 77% to 61%.

Case 5:

Case 5 deals with the effect of changing pile diameter without changing other parameters, various pile diameter isas 0.635cm, 0.889cm, 1.43cm, 1.397cm, 1.651cm, 1.905cm, 2.159cm, and 2.413cm were analyzed tofind the maximum lateral load capacity ofbasement wall with raft.

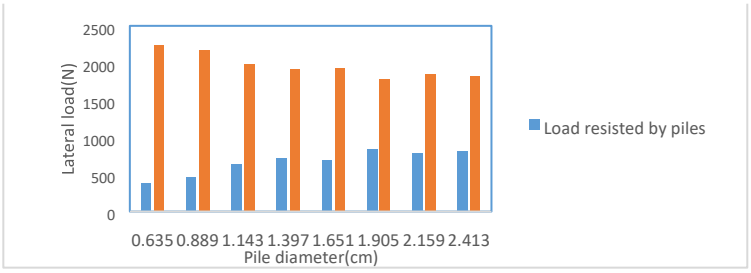

Figure 6: Variation of pile diameter.

When diameter of pile is increased from 0.635cm to 2.413cm the combine load taken by basement wall and raft change from 85% to 69%.

Case 6:

In this case the pile number is varied without changing other parameters, various pile numbers areas 1, 2, 3, 4, 6, 9, 13, 17, and 21were analyzed tofind the maximum lateral load capacity of the basement wall with raft.

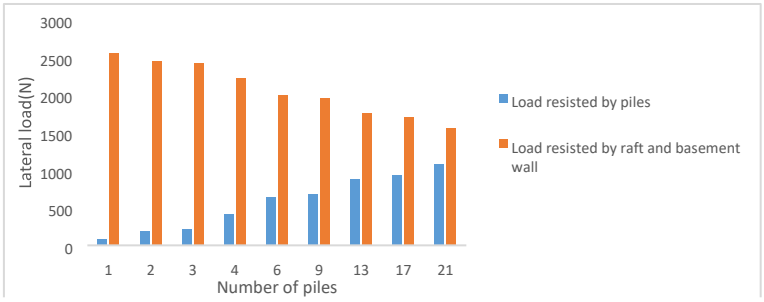

Figure 7: variation of number of piles.

By changing pile numbers from 1 to 21 the load taken by basement wall and raft is decreased from 97% to 59%

CONCLUSION

Conventionally in design of high-rise building the lateral load contribution of basement wall is ignored. In this research study, we have performed a parametric study to find sensitive parameters which contribute to the lateral load capacity of basement wall with raft. The parameters which were varied are height of basement wall, thickness of basement wall and raft, pile length and diameter and number of piles. From the results, it is consulted that by increasing basement wall height the lateral load capacity of basement wall with raft increase from 52% to 83%.By increasing the number of pile the lateral load capacity of basement wall decreases from 97% to 59%. The other parameters have no significant effect on lateral capacity of basement wall with raft. It is strongly recommended to include the lateral load capacity of basement wall in lateral load resisting system as it will results in an economical design and will also reduce the number of piles and bending moments in piles.

REFERENCE

1. Jamil, I., et al., *Response of basement wall in tall buildings foundation under lateral loading.* 2022: p. 1-9.
2. Chow, H. and H. Poulos. *Effects of basement resistance on tall building foundation behaviour*. in *Proc. 13 th ANZ Conf. on Geomechanics*. 2019.
3. Aung, P.W.W. and K.L. Htat, *Parametric Study on the Settlement of Piled Raft Foundation for High-Rise Building.*
4. Clancy, P., M.J.I.J.f.N. Randolph, and A.M.i. Geomechanics, *An approximate analysis procedure for piled raft foundations.* 1993. **17**(12): p. 849-869.

2nd International Conference on Advances in Civil and Environmental Engineering (ICACEE-2023)

University of Engineering & Technology Taxila, Pakistan

Conference date: 22nd and 23rd February, 2023

An Experimental Study for Quantification of Lateral Contribution of Piles and Raft in a Piled Raft Foundation

Engr.Abrar Ullah[1], Dr.Naveed Ahmad[2], Dr. Irfan Jameel[3], Engr.Zia Ullah[4]

[1]Civil Engineering, University of Engineering and Technology Taxila,
abrar.cordaid@gmail.com

[2]Civil Engineering, University of Engineering & Technology Taxila,
naveed.ahmad@uettaxila.edu.pk

[3]Civil Engineering, University of Engineering and Technology Peshawar,
irfanuop@hotmail.com

[4]Civil Engineering, Islamic International University Islamabad,
engr.ziamarwat@yahoo.com

ABSTRACT

In high rise building, piles are provided underneath the raft to satisfy the serviceability requirement in problematic soil. The combination of piles and raft makes a new type of foundation which is called piled raft foundation. In piled raft foundation, both of the foundation components i.e. piles and raft contributes in resisting structural/ vertical and lateral loads. The Piled raft foundation was used for the first time in the construction of 182m high Latin American Tower designed by Dr. Leonardo Zeevaert in 1956. The vertical contribution of piles and raft in piled raft foundation has been widely researched but the lateral contribution of the piles and raft under lateral load are still unclean and needs further research. In order to find the lateral contribution of piles and raft due to increase in number of piles, a small scale instrumented piled raft foundation with different pile numbers are subjected to lateral load under constant vertical loading in sand having 35% of relative density. It was observed during experimental study that by increasing the number of piles, the lateral contribution of raft is decreasing and the piles lateral load resistance are increasing. It was also observed that when the number of piles increases, the contact between the soils underneath the raft is decreases. The results shows that the rear piles take more load than the front piles.

KEYWORDS: Piled raft foundation, High rise building, Lateral load contribution

INTRODUCTION

For high rise building built and weak and compressible strata, piles are usually provided under the raft and this new type of foundation is call piled raft foundation (PRF). The PRF was firstly used by Dr. Leonardo Zeevaert in Latin American Tower in 1956. The Latin American Tower withstood an earth quick of 7.9 and 8.5 magnitudes in 1957 and 1985 respectively and showed that the piled raft foundation is one of the most suitable type of

foundation for high rise building resisting vertical and lateral loads. A lot of researchers have studied the vertical loading carry capacity of piles and raft in piled raft foundation while the lateral load contribution of piles and raft in piled raft under lateral loading is still unclear.

The piled raft and pile group were modelled in ABAQAS software in order to compare the lateral deflection of piled raft and pile group. The lateral deflection of the piled raft was 25% less than the pile group of same pile configuration also it was found that subsoil underneath the raft in piled raft played significant role in increasing the lateral resistance of the piled raft [1]. The effect on the lateral resistance due to piles spacing and length in piled raft model placed in dry sand is experimentally studied and found that the pile length and spacing significantly affect the bearing capacity, settlement and lateral deflection of the piled raft foundation [2]. The vertical and lateral load response of the pile group and piled raft in sandy soil with the same pile configuration and length is experimentally studied and it was found that the piled raft response to vertical and lateral load was much stiffer than the response of the pile group [3]. The behaviour of the piled raft under vertical and lateral load in two layers soil is studied and found that there is positive as well as negative impact of vertical loading on the lateral load resisting capacity of piled raft foundation [4]. The performance of piled raft foundation under static horizontal loads is studied and concluded that the resistance of single pile in piled raft is different from those observed in isolated single pile of same size due to difference in the confining stresses around the pile. It was also noted that the pile connect rigidly with raft resisted more horizontal load than the piled raft with hinged pile head connection [5]. In another experimental study, it was found that lateral resistance changes with changing the pile spacing due to change in group interaction [6, 7]. In the presence of combined loading, the lateral resistance of piled raft increases [8, 9].

According to the aforementioned and available literature, most of the researchers have measure the lateral deflection of the piled raft or piled group with concluding remarks that the pile and raft are contributing in resisting lateral loading but none of them has quantified the piles and raft contribution.

The main aim of this experimental research is to quantify lateral contribution of piles & raft and study the change in lateral contribution of piles and raft when the number of piles are increased in piled raft model. In this study three number of small scale instrumented piled raft models with four, five and six piles are examined.

TEST SETUP

First small scale instrumented piled raft models having four, five and six piles were fabricated in laboratory as shown in Figure 1. The 2.54cm thick model raft made of aluminium was square in shape with dimension of 30x30cm. Total 25nos holes were drilled in raft with 1.3cm dia and 6.35cm c/c spacing for installation of 1.905cm dia galvanized hallow circular iron piles having 45cm length in different configuration. The piles were attached to the raft with nut and bolt assembly.

To measure the lateral load contribution, calibrated strain gauges were installed on each pile. Vertical load cell having 8ton capacity was installed on the top of piled raft to measure the applied vertical load. To measuring the applied lateral load, a lateral load cell having 5ton

capacity was installed perpendicular to raft of the piled raft model. The entire three piled raft model were first placed exactly in the centre of rectangular soil container as shown in Figure 3. The soil container was the filled with sand by sand raining technique using mobile pluviator to achieve the required 35% relative density. The properties of the test sand are given in Figure 1. When the piles were buried in the sand then the raft was attached through nut and bolt assembly. Linear Variable Displacement Transducers (LVDT) was installed perpendicular to the raft of the model on the opposite side to the lateral load application. The schematic and pictorial view of the experimental setup is shown in Figure 5, 6. Lateral load was applied concentrically and at right angle to the raft under 5000N vertical load and all the date is recorded in data logger attached with computer.

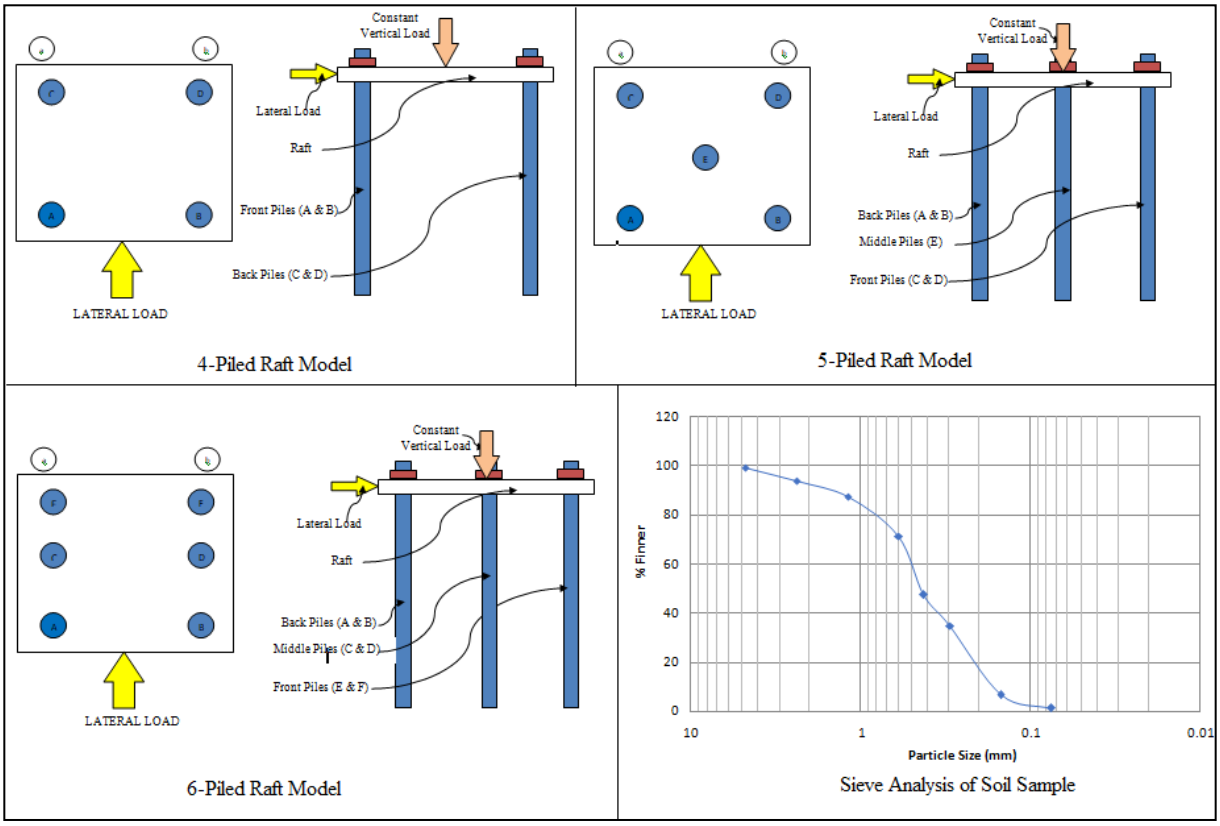

Figure1. Plan and sectional view of 4-piled raft, 5-piled raft & 6-piled raft model and sieve analysis of test soil.

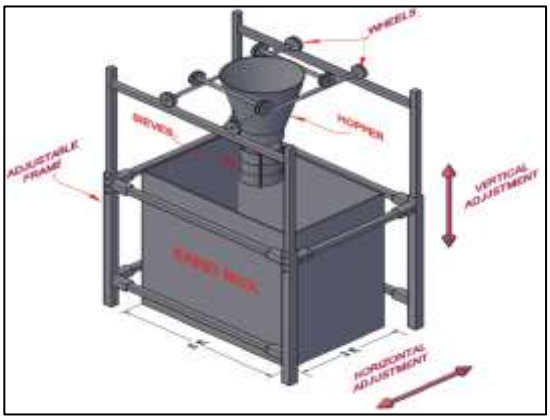

Figure2. Schematic view of Experimental setup

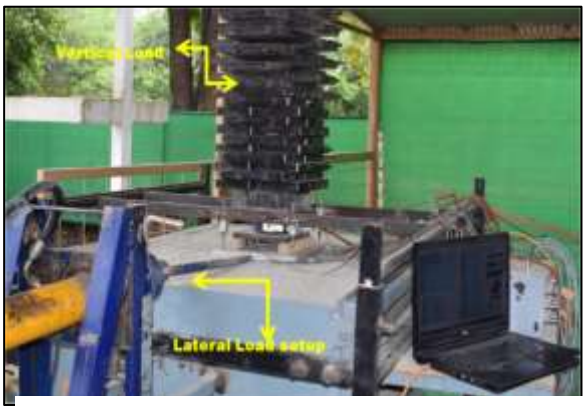

Figure3. Experimental setup in laboratory

RESULTS AND DISCUSSION

Piled Raft Model

Lateral load was applied on 4-piled raft model under a constant vertical load of 5000N.It was observed that initially the raft resisted the lateral load and with the passage of time the piles also started taking load. After 2mm lateral deflection, the piles were carrying more load than the raft as shown in Figure 5. Figure 4 shows that the lateral contribution of the piles and raft is 54% and 45% while Figure 5 shows that back piles took more lateral load than the front piles due to more contact pressure in front of the back piles than the front piles due to constant vertical loading.

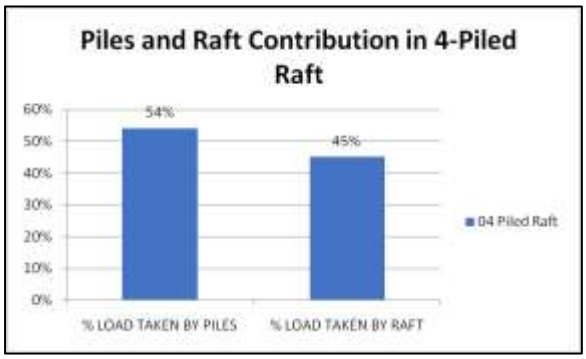

Figure 4.Percentage of lateral load contribution of piles and raft in 4-piled raft model

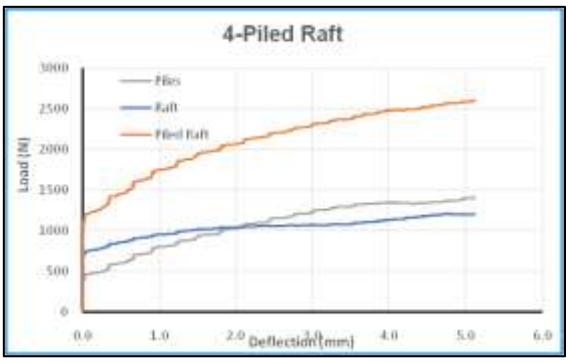

Figure 5.Lateral load distribution of piles, raft and piled raft in 4-piled raft model

5-Piled Raft Model

Lateral load was applied on 5-piled raft model under a constant vertical load of 5000N as shown in Figure 1. Contrary to 4-piled raft model, the piles and raft start taking load simultaneously just after the application of lateral load as shown in Figure 6. The lateral contribution of the piles increase and found 59% while the raft contribution decreased to 41% as shown in Figure 7 as compared to 4-piled raft model. The back piles took more lateral load than the middle pile and the middle pile took more load than the front piles due to different contact pressure in front of the piles due to constant vertical loading as shown in Figure 6.

6-Piled Raft Model

Lateral load was applied on 6-piled raft model under a constant vertical load of 5000N as shown in Figure 1. Initially the applied lateral load was resisted by piles and then the raft also started resisting lateral load as shown in Figure 8. Due to addition of piles, the contact between the raft and underneath soil further decreased that's why the piles start taking load from the start and the raft start taking load after some time. The lateral contribution of the piles increase and found 62% while the raft contribution decreased to

38% as shown in Figure 9 as compared to 4-piled raft and 5-piled raft model. The back piles took more lateral load than the middle pile and the middle pile took more load than the front piles due to different contact pressure in front of the piles due to constant vertical loading as shown in Figure 8.

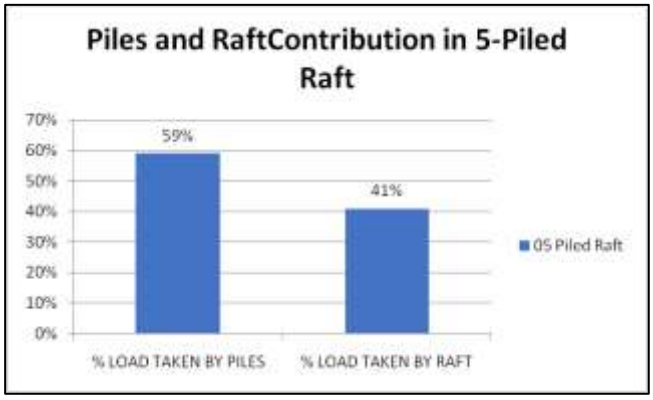

Figure 7. Percentage of lateral load contribution of piles and raft in 5-piled raft model

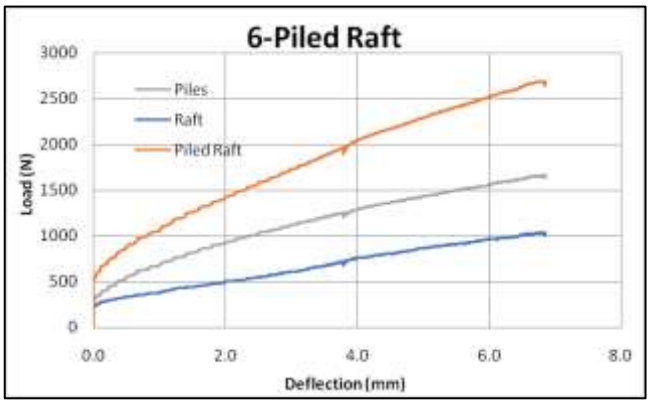

Figure 8. Load distribution of piles, raft and piled raft in 6-Piled raft model

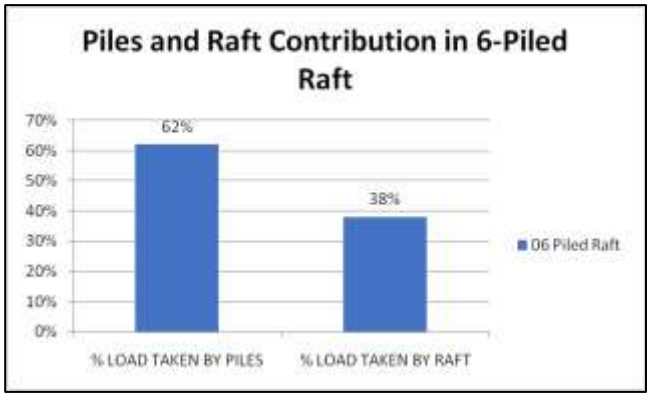

Figure 9. Percentage of lateral load contribution of piles and raft in 6-piled raft model

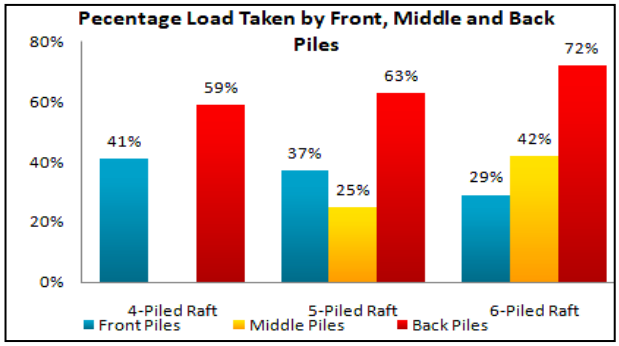

Figure 10. Percentage of lateral load taken by front, middle and back piles

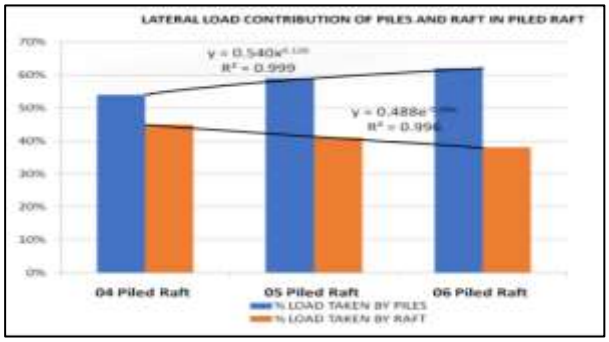

Figure 11. The effect of lateral load contribution of piles and raft due to increase in number of piles

CONCLUSION

The piles and raft in piled raft foundation are resisting lateral loads combinedly. The lateral contribution of raft decreases when the number of piles increases and the back piles takes more load than the front piles due to less confining pressure in front of the front piles.

ACKNOWLEDGEMENTS

I am very thankful to Dr. Irfan Jameel of Civil Engineering Department, University of Peshawar for allowing me to use his established experimental setup for this research work.

REFERENCES

1. Alsanabani, N., AL-Refeail, T., & Alshenawy, A. (2017). Contribution Of Raft On Lateral Resistance Of Piled Raft On Sandy Soil. In *17th International Multidisciplinary Scientific Geoconference Sgem 2017* (pp. 167-174).
2. Chandiwala, A., & Vasanwala, S. (2023). Experimental Study of Lateral Loading on Piled Raft Foundations on Sandy Soil. *International Journal of Engineering*, *36*(1), 28-34.
3. Jamil, I., Ahmad, I., Ullah, W., Ahmad, M., Sabri, M. M. S., & Majdi, A. (2022). Experimental Study on Lateral and Vertical Capacity of Piled Raft and Pile Group System in Sandy Soil. *Applied Sciences*, *12*(17), 8853.
4. Deb, P., & Pal, S. K. (2021). Nonlinear analysis of lateral load sharing response of piled raft subjected to combined VL loading. *Marine Georesources & Geotechnology*, *39*(8), 994-1014.
5. Horikoshi, K., Matsumoto, T., Hashizume, Y., Watanabe, T., & Fukuyama, H. (2003). Performance of piled raft foundations subjected to static horizontal loads. *International Journal of Physical Modelling in Geotechnics*, *3*(2), 37-50.
6. Comodromos, E. M., & Pitilakis, K. D. (2005). Response evaluation for horizontally loaded fixed-head pile groups using 3-D non-linear analysis. *International Journal for Numerical and Analytical Methods in Geomechanics*, *29*(6), 597-625.
7. Kim, B. T., & Yoon, G. L. (2011). Laboratory modeling of laterally loaded pile groups in sand. *KSCE journal of Civil Engineering*, *15*(1), 65-75.
8. Davisson, M. T., & Robinson, K. E. (1965). Bending and buckling of partially embedded piles. In *Soil Mech & Fdn Eng Conf Proc/Canada/*.
9. Stacul, S., & Squeglia, N. Analysis of Laterally Loaded Piled Raft Foundation.

2nd International Conference on Advances in Civil and Environmental Engineering (ICACEE-2023)

University of Engineering & Technology Taxila, Pakistan

Conference date: 22nd and 23rd February, 2023

EVALUATION OF DYNAMIC PROPERTIES AND LIQUEFACTION POTENTIAL OF SOILS USING SPT-N VALUES

Tasawar Abbas[1], Hammad Raza[2], Naveed Ahmad[3], Haseeb Yaqoob[4]

University of Engineering and Technology, Taxila, Pakistan, tasawarabbas121@gmail.com

University of Engineering and Technology, Taxila, Pakistan, hammad.raza@uettaxila.edu.pk

University of Engineering and Technology, Taxila, Pakistan, naveed.ahmad@uettaxila.edu.pk

University of Engineering and Technology, Taxila, Pakistan, haseebyaqoob101@gmail.com

ABSTRACT

Pakistan lies in a seismically active and earthquake prone region of the world where Indian, Eurasian, and Arabian plates are interacting at different rates of movement. On September 24, 2019, Mirpur - a northeastern city of Pakistan was struck by an earthquake of magnitude 5.8. The earthquake was small and relatively shallow, which means that a significant area will have experienced peak ground accelerations. According to report published by USGS in 2019, at least 450 people were injured, and more than 30 individuals have been declared dead. A field analysis of Mirpur's infrastructure failures revealed that major damage was caused by earthquake induced soil liquefaction. During an earthquake, soil liquefaction is caused by an increase in pore water pressure (PWP) and this rise has significant effect on cohesionless soil with shallow water table. In order to evaluate the dynamic response and development of pore water pressure in seismically active zone, a generalized/Hyperbolic constitutive model was combined with PWP development model in a one-dimensional seismic site response to evaluate PWP development beneath the soil layer. Soil columns in the nearby regions close to the cities of Jhelum and Mirpur were investigated and analyzed using DEEPSOIL software. The liquefiable layers at different depths were analyzed and documented. The developed attributes can be helpful to the design engineers for seismic resistant design of newly proposed or requalification of existing civil engineering structures considering soil dynamic response and pore water development.

KEYWORDS: Mirpur, Soil Liquefaction, DEEPSOIL, Seismic Resistant Design, Seismic Requalification

INTRODUCTION

Soil liquefaction is a complex phenomenon that has been observed in numerous earthquakes in its various aspects [1]. When a soil deposit is liquefied, the excess pore pressures in the soil equals the effective stress of soil then the strength and stiffness of the soil starts reducing dramatically. Different consequences of soil liquefaction may be seen during and after an earthquake similar as excessive settlements, tilting, and lateral spreading [2]. These consequences are the main reasons behind the massive damage to structures and life.

Mirpur earthquake, unlike Kashmir Earthquake (2005), affected the alluvial deposits overlying sandy soil, having tendency to liquefy and is the base of inducing wide liquefaction settlements. The Mirpur earthquake affected the civil engineering structures, utility lines, road networks, causing severe damage (NDMA, 2019). HFT is located in veritably close proximity to the epicenter of the Mirpur earthquake occurred on 24 September, 2019 of magnitude 5.8.

A wide range of case studies, experimental tests, or numerical models have been employed in recent years to highlight soil liquefaction and its effects on structures. Evaluation of liquefiable soil behavior with experimental tests may be thought an ideal method under realistic earthquake conditions. However, these tests are generally costly and too complex to put into practice. On the other hand, numerical analysis or modeling offers an economical solution to simulate soil behavior with different parametric variables. Reliable prediction of the behavior of a liquefiable soil profile (i.e., excess pore pressures, accelerations, and deformations) remains a major challenge in geotechnical earthquake engineering. In this regard, numerical modeling is an efficient tool for practitioners to predict liquefiable soil behavior and prevent liquefaction-induced failures in the future. Provided that constitutive soil models sufficiently cover the real soil behavior under seismic loading, the liquefiable soil behavior can be reasonably simulated via numerical studies. In other words, considerable attention is needed during the calibration of constitutive soil models in order to properly represent the soil nonlinearity[3, 4].

METHODS

Soil profile

In order to evaluate soil liquefaction potential using SPT-N values, sub surface soil investigation has been carried out for the areas near Jhelum and Mirpur marked in Figure-1. followed by nonlinear seismic site response analysis (NL GRA) of the explorated soil data. The sites chosen for evaluation of dynamic properties and liquefaction potential are near the center of bridges in Chenab River and Jhelum River.

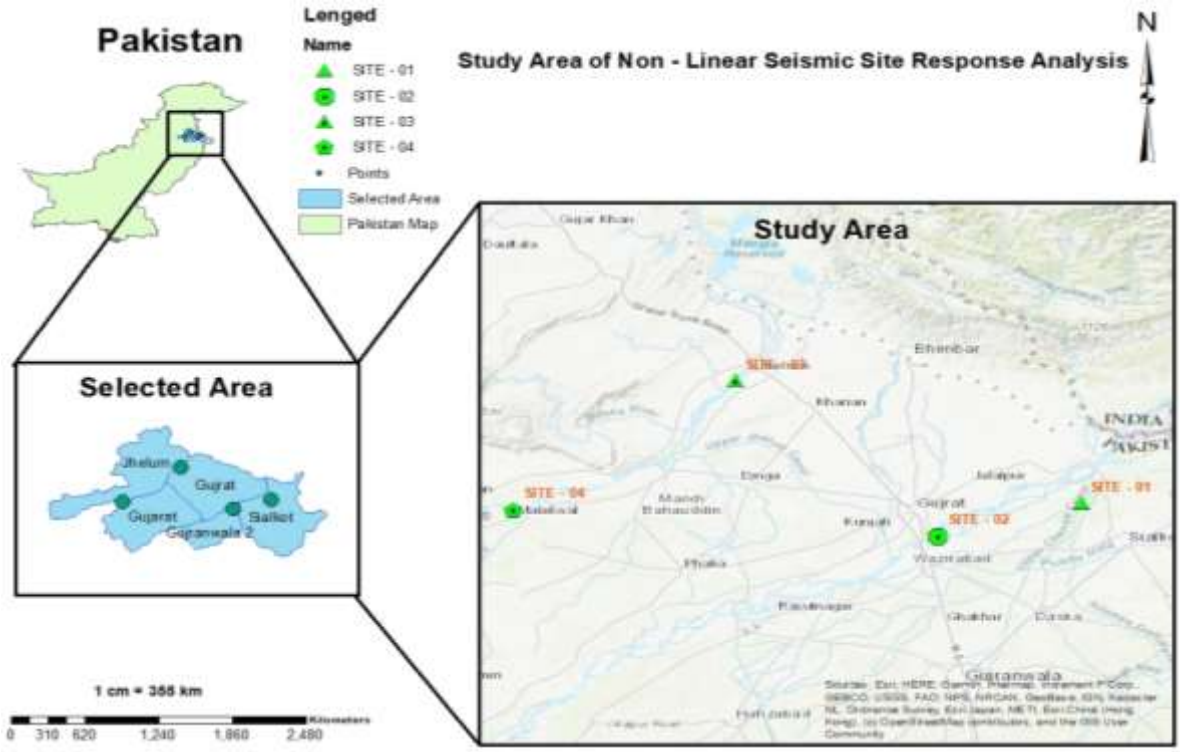

Figure-1 Study area of nonlinear seismic site response analysis (Courtesy google maps)

As the selected profile is near the river side, therefore the soil columns mainly consists of sand with varying shear wave velocity (Figure-2).

Earthquake induced liquefaction failure that occurred during 2019 Mirpur earthquake motivated the researchers to evaluate the dynamic response of soil. Therefore, evaluation of dynamic properties and liquefaction potential of soil in one of the active seismic zone will be helpful in performing seismic requalification of existing structures or seismic resistant design of new structures. The water table depth for Site 1-4 are 1 m, 1.5 m, 2 m, and 3 m respectively.

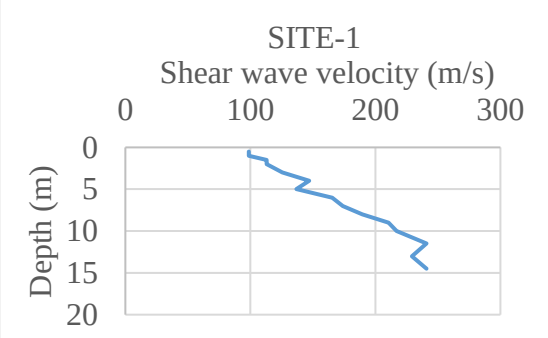

Figure 2a.

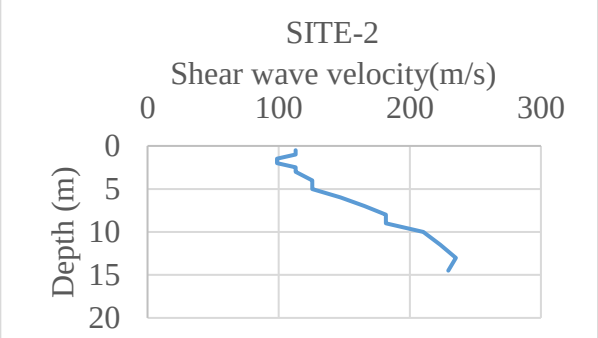

Figure 2b.

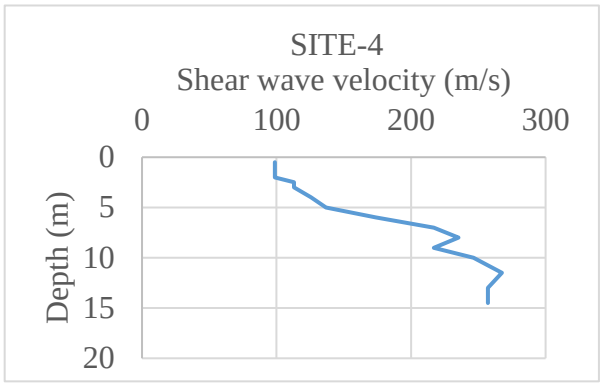

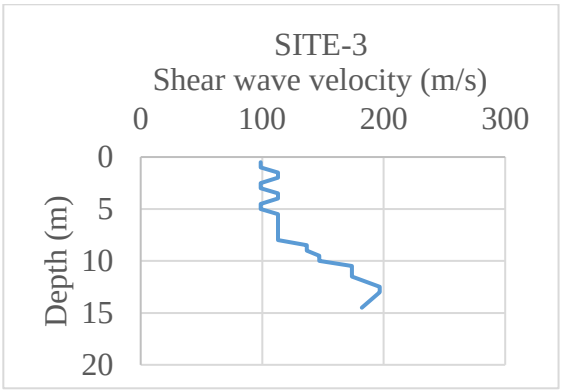

Figure 2c. *Figure 2d.*

Figure-2 (a,b,c, and d) Shear wave velocity of sites with varying depth

Considered ground motions

Several ways of choosing a strong ground motion includes recorded motions, spectrum-compatible produced motions, scaling recorded motions, synthetic motions etc. However, recorded accelerograms as available option is more realistic than both artificially generated and spectrally matched [5]. For this study, the recorded Kobe motion was chosen for NL GRA. Massive liquefaction in Kobe city and nearby areas was caused by the enormous 6.9 *M*w Kobe earthquake [6].

Nonlinear GRA & Dynamic Soil Response Parameters

Nonlinear seismic site response analysis in comparison with the equivalent linear approach, because of its realistic approach is widely used nowadays. This study considered the same for evaluating increased pore water pressure ratio for the soil columns considered. The analysis has been performed using DEEPSOIL software version 7.0 [7]. Standard curves proposed by [8] available in software, are used for evaluation of dynamic properties. For all exploration data, the thickness of the layers is so adjusted that the maximum frequency at which a layer may propagate is more than 30Hz [9]. The bed rock is modelled as an elastic half space with 2% damping value, 25 kN/m^3 density and 760 m/s as value of shear wave

velocity [10]. Due to the lack of in situ measured shear velocity (V_s) data, the required input parameter for the study is evaluated based on SPT-N values in accordance with [11-12] as follows:

$$Gmax = 650N^{0.94}$$

$$Gmax = \rho Vs^2$$

The input parameters for analysis were imported form the real soil investigation data, MRDF-UIUC pressure dependent, hyperbolic procedure implemented in DEEPSOIL was used for fitting the provided data points. In order to evaluate the increased PWP generation and dissipation of soil columns considered in this study, soil model proposed by [13-14] was used. The required input parameters for PWP model (p,F,s, m_v, k, and C_v) were evaluated using [15].

RESULTS AND DISCUSSIONS

The DEEPSOIL software v7.0 was applied for evaluation of dynamic properties and soil liquefaction potential. According to the findings of different researchers [16-17], liquefaction occurs at a threshold value for $r_u > 0.8$. Figure-3 presents the PWP ratio (r_u) profiles for considered ground motion with depth. For Kobe event, a liquefiable depth of 2.5 m - 7.5 m and 12.25 m was observed for Site-1 (Figure 3a). Similarly for other sites, the liquefiable depths were shown in Figure 3b, 3c, and 3d respectively.

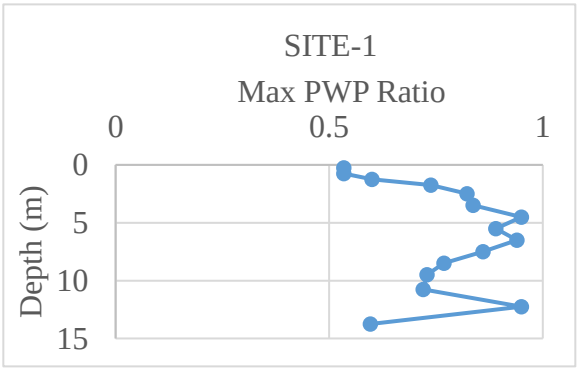

Figure 3a.

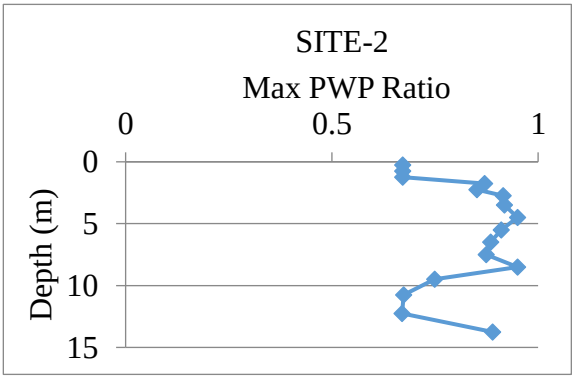

Figure 3b.

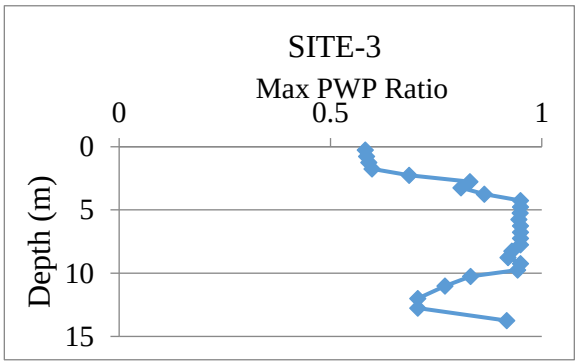

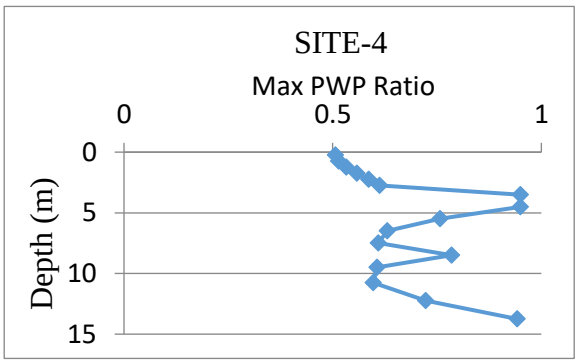

Figure 3c. *Figure 3d.*

Figure 3 DEEPSOIL results for pore water pressure development in soil layers

It can also be observed that vulnerability of liquefaction has increased with intensity of shaking. For each site, PWP gets increased with time (Figure-4). The profile plots for PWP Ratio Vs time are shown in Figure 4a, 4b, 4c, and 4d respectively.

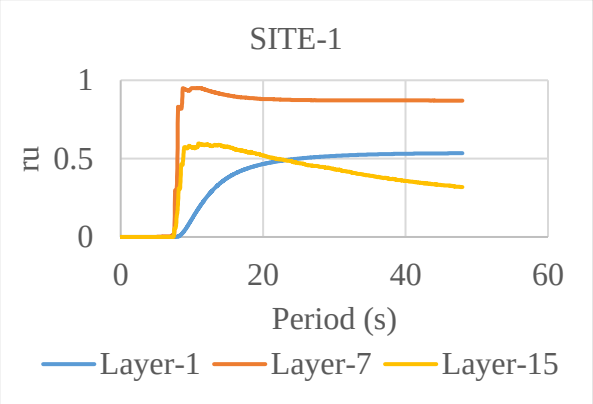

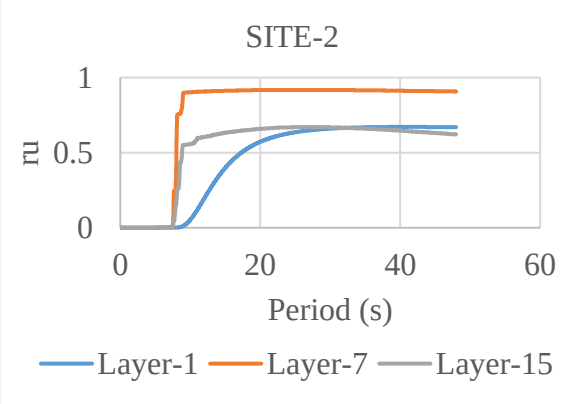

Figure 4a. *Figure 4b.*

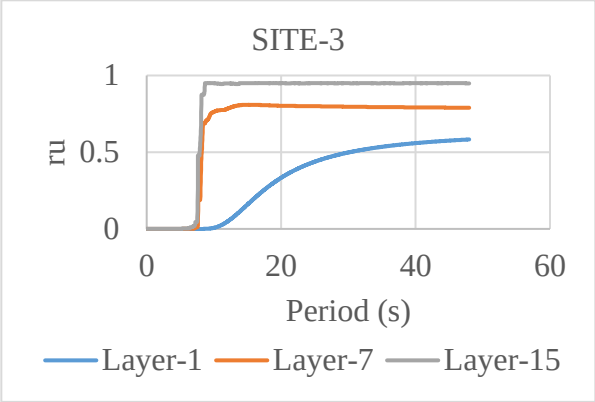

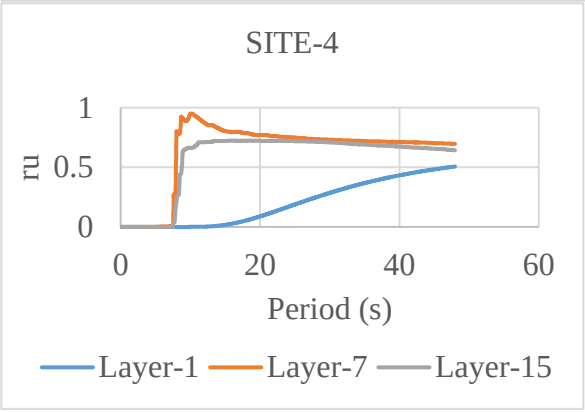

Figure 4c. *Figure 4d.*

Figure-4 DEEPSOIL results for pore water pressure development in soil layers (1,7,15)

CONCLUSION

This paper evaluated liquefaction potential of layered soil from sub surface soil investigation data using one dimensional non-linear ground response analysis with development of pore water pressure for typical sites (in northeastern region of Pakistan) considering the recorded Kobe strong ground motions. The loose surficial soil columns experienced high pore water pressure development at different depths. The pore water pressure (r_u) obtained from results were greater than the threshold value (i.e., 0.8) defined by different researchers that fell in different layers near the ground surface. The analysis is shown to be a good evaluation of the sites to be liquified with the vibrations and this model can calculate soil V_s for layered soils with different relative densities based on established correlations. Furthermore, from the history, the northeast Pakistan region frequently witnesses mild to moderate seismic events, such high amplifications and excessive PWP development for random motions should be comprehensively investigated. This study will be helpful for seismically resistant design of civil engineering structures.

REFERENCES

[1] Khan, M. Y., Turab, S. A., Riaz, M. S., Atekwana, E. A., Muhammad, S., Butt, N. A., ... & Ohenhen, L. O. (2021). Investigation of coseismic liquefaction-induced ground deformation associated with the 2019 Mw 5.8 Mirpur, Pakistan, earthquake using near-surface electrical resistivity tomography and geological data. *Near Surface Geophysics*, *19*(2), 169-182.

[2] Youd, T. L., & Garris, C. T. (1995). Liquefaction-induced ground-surface disruption. *Journal of Geotechnical Engineering*, *121*(11), 805-809.

[3] Gottardi, G., & Galli, E. (2012). *Natural zeolites* (Vol. 18). Springer Science & Business Media.

[4] Bannister, S., & Gledhill, K. (2012). Evolution of the 2010–2012 Canterbury earthquake sequence. *New Zealand journal of geology and geophysics*, *55*(3), 295-304.

[5] Bommer, J. J., & Acevedo, A. B. (2004). The use of real earthquake accelerograms as input to dynamic analysis. *Journal of Earthquake Engineering*, *8*(spec01), 43-91.

[6] Towhata, I. (2022, September). Coseismic and post-seismic slope instability along existing faults. In *Proceedings of the 4th International Conference on Performance Based Design in Earthquake Geotechnical Engineering (Beijing 2022)* (pp. 195-213). Cham: Springer International Publishing.

[7] Hashash, Y. M. A., Musgrove, M. I., Harmon, J. A., Ilhan, O., Xing, G., Numanoglu, O., ... & Park, D. (2020). DEEPSOIL 7.0, user manual. *Urbana, IL, Board of Trustees of University of Illinois at Urbana-Champaign*.

[8] Darendeli, M. B. (2001). *Development of a new family of normalized modulus reduction and material damping curves*. The university of Texas at Austin.

[9] Gürtürk, C. C., & Selçuk, M. E. (2021, July). Investigation of parameters affecting the soil amplification by means of 1-D analysis. In *IOP Conference Series: Materials Science and Engineering* (Vol. 1141, No. 1, p. 012030). IOP Publishing.

[10] Puri, N., Jain, A., Nikitas, G., Dammala, P. K., & Bhattacharya, S. (2020). Dynamic soil properties and seismic ground response analysis for North Indian seismic belt subjected to the great Himalayan earthquakes. *Natural Hazards*, *103*, 447-478.

[11] Ohsaki, Y., & Iwasaki, R. (1973). On dynamic shear moduli and Poisson's ratios of soil deposits. *Soils and Foundations*, *13*(4), 61-73.

[12] Panjamani, A., Manohar, D. R., Moustafa, S. S., & Al-Arifi, N. S. (2016). Selection of Shear Modulus correlation for SPT N values based on site response studies. *Journal of Engineering Research*, *4*(3).

[13] Matasovic, N. (1993). *Seismic response of composite horizontally-layered soil deposits*. University of California, Los Angeles.

[14] Matasović, N., & Vucetic, M. (1993). Cyclic characterization of liquefiable sands. *Journal of Geotechnical Engineering*, *119*(11), 1805-1822.

[15] Carlton, B. (2014). *An improved description of the seismic response of sites with high plasticity soils, organic clays, and deep soft soil deposits*. University of California, Berkeley.

[16] Hazirbaba, K. (2005). *Pore pressure generation characteristics of sands and silty sands: a strain approach* (Doctoral dissertation).

[17] Olson, S. M., Mei, X., & Hashash, Y. M. (2020). Nonlinear site response analysis with pore-water pressure generation for liquefaction triggering evaluation. *Journal of Geotechnical and Geoenvironmental Engineering*, *146*(2), 04019128.

2nd International Conference on Advances in Civil and Environmental Engineering (ICACEE-2023)

University of Engineering & Technology Taxila, Pakistan

Conference date: 22nd and 23rd February, 2023

ROLE OF PILES IN A PILED RAFT FOUNDATION SYSTEM

Muhammad Zubair[1], Dr. Naveed Ahmad[2], Dr. Irfan Jamil[3], Muhammad Lateef[4], Haris Uddin Qureshi[5]

[1]University of Engineering and Technology Taxila, xubikhan.edu@gmail.com
[2]University of Engineering and Technology Taxila, Naveed.ahmad@uettaxila.edu.pk
[3]University of Engineering and Technology Peshawar, irfanuop@hotmail.com
[4]University of Engineering and Technology Taxila, lateefismail30@gmail.com
[5]Sir Syed University of Engineering and Technology, Karachi cvv003.haris@ssuet.edu.pk

ABSTRACT

With the increase in population, construction has also been carried out in Problematic or reclaim soil. In the case of problematic or reclaim soil, piled raft foundation is the best option for construction. The term piled raft foundation" refers to foundation system that combines the custom of pile and raft. When high-rise buildings are constructed on soil of low bearing capacity, piled raft foundation system have proven to be cost-effective without compromising serviceability and bearing capacity requirements. The use of strategically positioned piles beneath a raft can increases the raft's load resisting capacity and decreases differential settlements. This paper presents an experimental study to predict role of piles in a piled raft foundation system. For this purpose, a small scaled piled raft model was fabricated in the laboratory. The experimental testing was carried out at a relative density of 35%. Before applying vertical load LVDT's are installed at the edges of raft for the observation of settlement against applied vertical load. It was found that piles not only resist vertical load but can also act as settlement reducer.

KEYWORDS: Piles, Raft, Settlement, Piled Raft

INTRODUCTION

The major and crucial component of civil engineering structures is foundation. To meet structural stability and serviceability criteria foundation should be designed with due diligence. The primary purpose of foundation system is to transfer load from the superstructure into the underlying soil. Foundation is one of the most crucial and significant components, hence it needs to be carefully designed because its failure will lead to failure of whole structure. Raft foundations, pile foundations, and piled raft foundations are the three main types of foundations for high rise buildings. Raft foundation systems are the most cost-effective choice for high-rise buildings when the subsoil has strong bearing capability, such as gravel or dense sand. Examples are the Trianon Tower in Frankfurt, which is around 190 metres tall, and the Main Plaza Tower, which is about 90 metres tall in which tilt is less than 1:800 and the settlement is less than 100 mm [1]. Skin friction, end bearing, or a combination

of end bearing and skin friction are used to transfer stress from superstructure to the underline soil. In a piled raft foundation, the load is distributed between the raft, which is referred to as a shallow foundation, and the piles, which are deep foundation. In order to increase the soil's ability to support the load and decrease structural settlement piled raft foundation are provided. To decrease differential settlement of the foundation system and increase the raft's capacity for carrying load, the pile arrangement might be designed accordingly. In conventional design of piled raft, it is assumed that the total load from superstructure is supported by piles, ignoring the contribution of the raft [2]. Pile foundations are provided to transfer the load to hard strata when the upper soil layer is weak, and cannot support the load from the superstructure and may result excessive settlements. Since the raft is in close contact with the soil, it carries a significant percentage of the load from the superstructure, making the traditional method of piled raft design too conservative. The design will become uneconomical if the raft's contribution is disregarded, increasing the number and length of piles. In addition to supporting the load from superstructure, piles also serve to prevent settlements [3]. A piled raft foundation has composite soil structure interaction. Care must be practised in the Analysis of pile-soil interaction, raft-soil interaction, pile-pile interaction, and pile-pile raft interaction [4]. Majority of piled raft foundations for tall buildings were built on Frankfurt clay with settlement-reducing piles [5]. The raft's ability to support load and tendency to experience less differential settlements can both be improved by arranging piles [6]. Since a few decades ago, high-rise structures, particularly in the Gulf region, have been built using a piled-raft foundation technique. A few of them are the QIPCO tower in Doha and the Burj Khalifa in Dubai [7]. Based on the available research data it is concluded that piles contribute to load. The present study aims to evaluate how piles act as settlement reducer under different piles configuration at applied vertical load.

EXPERIMENTAL STUDY

Scope

The primary objective of this study is to investigate role of piles in poorly graded soil within a piled raft foundation system under vertical load. A small scale model was manufactured in the laboratory for this purpose, and subjected to vertical load to forecast pile's behavior. The calculation of piled raft settlement against applied vertical load is goal of this study.

Test Equipment

A small scale piled raft model was manufactured in the laboratory and embedded it in loose sand to predict the function of piles in a piled raft foundation system. The raft was squarely modelled and has dimensions of 30 x 30 cm and thickness of 2.54 cm. Aluminum was used to manufacture the raft and having an elastic modulus of 69 GPa. Within the raft surface, holes were made for the insertion of piles in various designs. A total number of 25 holes were provided at the raft surface. Each hole has 1.3 cm in diameter and spaced 6.35 cm apart. The piles were fabricated from 200 GPa galvanized iron. The piles were made in circular

shape and are hollow from inside. The piles' diameter was 1.905 cm, and they were joined to the raft by nut and bolt assemblies. In the laboratory, nine (09) piles with a 45 cm length were manufactured. Each pile is instrumented with strain gauges. To confirm the load taken by the piles as shown by the strain gauges, a calibrated vertical load cell with a maximum capacity of 8 tons was also installed on the raft top. On each side of the raft, LVDTs (Liner Variable Displacement Transducers) were fitted, with the tips of the devices placed vertically on the raft to measure settlement as observed under vertical load. The objective of LVDTs was to measure vertical displacements (Settlements) and rotation of piled raft in the event of differential settling. LVDTs precision was 0.01 mm. Testing arrangements has shown in figure 1,2 and 3 below. The piled raft model was loaded both vertically and concentrically, and vertical displacements (settlements) were measured using LVDTs mounted at the raft surface of raft. The soil container had a rectangular shape with 1.50 m in height, 1.20 m in length, and 0.90 m in width. The size of the sand container is sufficient to meet the boundary constraint. In order to prevent the container from expanding when applying load to the pile raft model, additional supports were provided to sand container. The model of the piled raft was precisely positioned in the middle of the sand container for the application of vertical load.

Figure 1: Installation of Raft and LVDTs after Pluviation

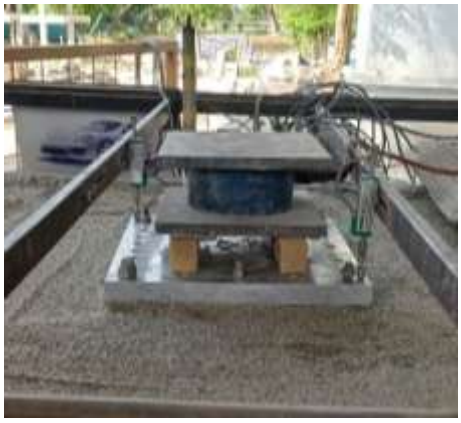

Figure 2: Arrangements for Installation of Load cell

Figure 3: Overall arrangements for vertical load application

EXPERIMENTAL PROCEDURES

Sand that was poorly graded used in this study. A set of sieves were used to perform an assessment of the grain size distribution in accordance with ASTM D-422. Figure 4 illustrates the grain size distribution curve. The calculated uniformity coefficient (Cu) and coefficient of curvature (Cc) were 0.72 and 3.12, respectively. The sand is considered to be poorly graded. Table 1 lists the characteristics of sand. The minimum and maximum unit weights, calculated according to ASTM D-4254 and D-4253, were 106 pcf and 92 pcf, respectively. Testing was carried out at a relative density of 35%. Mobile pluviator was used to achieve this density. Sand was dropped from a sand cone at various heights to calibrate the mobile pluviator. By allowing sand to fall from a height of 9.5 inches, the required density was accomplished. The sand container was filled in 10 layers, with a thickness of 15 cm each, due to its 1.50 m height.

Table 5: Properties of sand

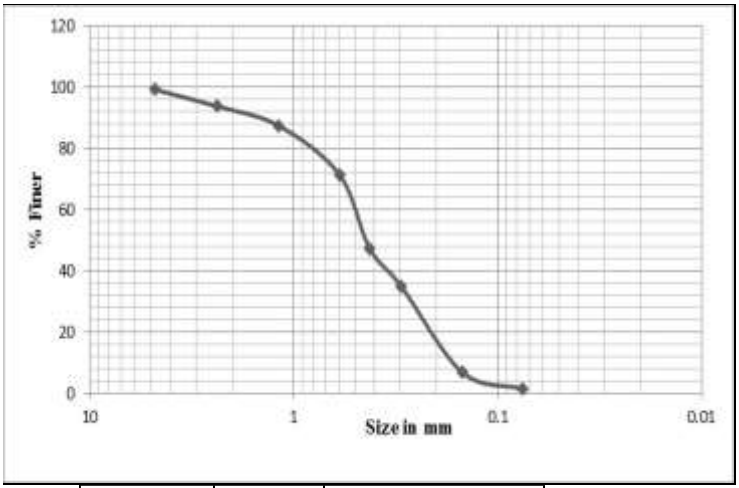

Parameter	Value	Remarks
D60	0.5	SP because $C_u < 6$ and $C_c < 1$
D50	0.46	
D30	0.24	
D10	0.16	
Coefficent of Uniformity (CU)	3.12	
Coefficent of curvature (CC)	0.72	
Maximum unit weight	106 PCF	
Minmum unit weight	92 PCF	

Figure 4: Gradation curve of soil

RESULTS AND DISCUSSIONS

The following configurations were made as shown below.

a. Raft Only
b. 04 Piled Raft
c. 06 Piled Raft

Raft Only

The raft was placed in the centre of the sand container after pluviation for the purpose, to evaluate how the raft responds to vertical loading. Figure 5 shows the load verse settling curve after applying a vertical load of 5000 N. Figure 5 clearly shows that the raft settles 7.6 mm under a load of 5000 N. The settlement observed at corresponding load is too high, and not to be permitted.

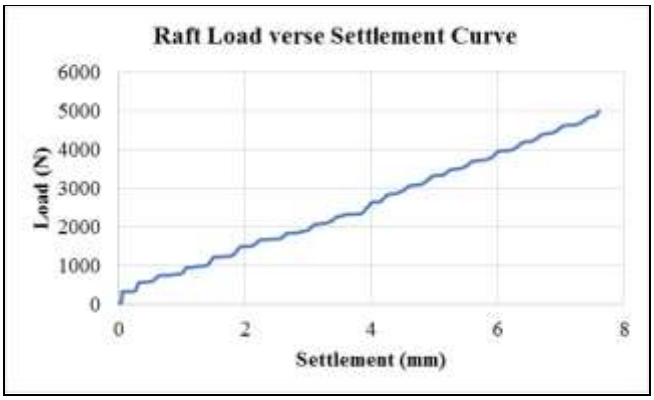

Figure 5: Load verse Settlement curve of Piled Raft

04 Piled Raft

With the help of nuts and bolts, four piles were firmly attached to the raft with a centre-to-centre distance of 25 cm, and placed at the centre of sand container. A total of 5000 N load was applied to piled raft model. Figure 6 illustrates how piles act as settlement reducer to vertical loading. The graph clearly shows that the piled raft received a total vertical load of 5000 N. At this load, approximately 3.6 mm settlement was recorded. At the start of loading, the raft's contribution is minimal, but as the vertical stress increases the soil beneath the raft becomes compacted and stiff, increasing the raft's load-sharing capacity. Therefore, it is predicted that, piled raft foundation system built on loose sand, the raft initially shares less of the load but as the load increases, the soil becomes compacted beneath the raft tend to increase raft contribution.

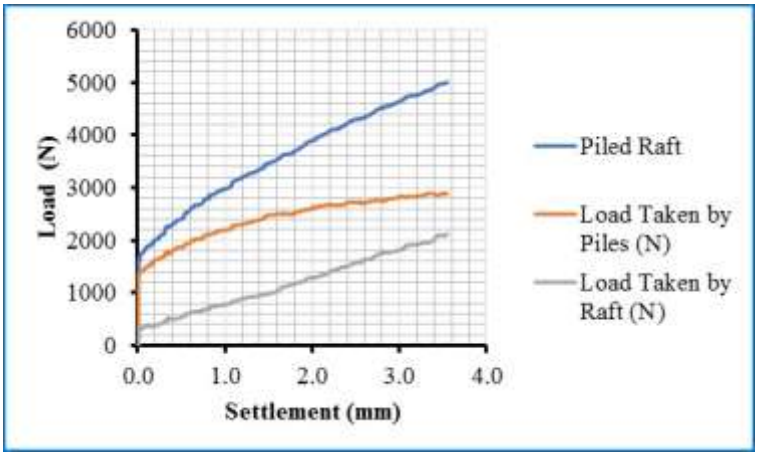

Figure 6: Load verse Settlement curve of 04 Piled Raft

06 Piled Raft

With the help of nuts and bolts, six piles were attached to the raft, and vertical load of 5000 N was applied. According to figure 7, the load resisted by the raft was 39%, but the load resisted by the piles was 61%. The contribution of the piles tends to rise as the number of piles increases, whereas the load carried by the raft tends to decrease. Furthermore, the settlement dropped from 3.6 mm (in the case of the 04 piled raft) to 2.6mm. So it is predicted that roles of piles are, to act as settlement reducer.

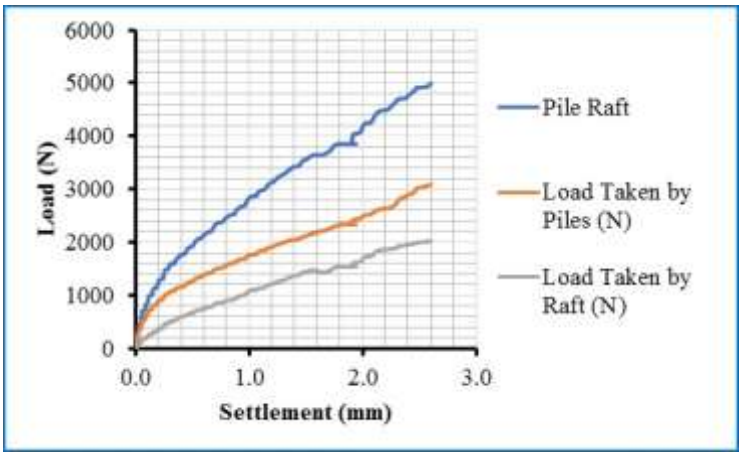

Figure 7: Load verse Settlement curve of 06 Piled Raft

CONCLUSIONS

1. In a piled raft foundation, the piles operate as a settlement reducer in addition to taking on the load transferred by the raft.
2. Raft without a pile can support a load of 5000 N at a settlement of 7.6 mm, however the settlement was decreased to 3.6 mm by adding 4 piles to the same raft under the same loading conditions. Four additional piles lowered the settlement by around 50%.

REFERENCES

[1] Phung Duc Long. "Piled raft - A new foundation design philosophy for high rises" Geotechnics for Sustainable Development- Geotech Hanoi 2011, Phung. Construction Publishing House ISBN 978-604-82-000-8.

[2] J.B. Burland, B.B. Broms, V. Demello, "Behavior of Foundation and Structures" in: Proc. 9th. ICSMFE, Tokyo, 1977, pp. 495–546

[3] Burland, J.B, Broms, B.B, De Mello, V.F.B. (1977). Behavior of foundations and structures. Proc. 9th ICSMFE, Tokyo, Vol. 2, 495-546

[4] Yilmaz, B., (2010), "An Analytical and Experimental Study on Piled Raft Foundations", MSc. Thesis, Middle East Technical University, Ankara.

[5] Katzenbach, R., Schmitt, A., Turek J (2003) Reducing the costs for deep foundations of high-rise buildings by
advanced numerical modeling. ARI The Bulletin of the Istanbul Technical University, Vol. 53, No.2.

[6] A.Z. Elwakil, W.R. Azzam 2015. Experimental and numerical study of piled raft system. Alexandria Engineering Journal (2016) 55, 547–560

2nd International Conference on Advances in Civil and Environmental Engineering (ICACEE-2023)

University of Engineering & Technology Taxila, Pakistan

Conference date: 22nd and 23rd February, 2023

Utilization of Rice Husk Ash for Strength Enhancement of Clayey Soil

M. Umair[1], Shahzad Ahmad[2], Noman Ali[3], Naveed Ahmad[4]

[1,2,3,4] Civil Engineering Department

University of Engineering and Technology Taxila, Pakistan.

Gmail:muhammadumair7321@gmail.com

Abstract

Several studies have been performed to find out how adding waste products can change the properties of soil. The current study shows how adding locally available material like rice husk ash, can change the properties of the soil. By replacing a significant amount of the stabilizer agent with rice husk ash, the cost of stabilization may be decreased. For this study, a Soil sample collected from the Taxila region of Punjab, classified as an A-6 soil on AASHTO classification was stabilized with 3-15% Rice Husk Ash (RHA) by weight of the dry soil. The results obtained indicate a general decrease in the maximum dry density (MDD) and an increase in optimum moisture content (OMC) with an increase in RHA content. There was alsoa slight improvement in UCS and Plasticity Index decrease using RHA content at particular ratios. The peak UCS values were recorded at between 6-9% RHA, indicating a little potentialof using 6-9% RHA for strength improvement of A-6 clayey soil. The various tests were conducted on different proportions and the optimized proportion is arrived at.

Keywords: Soil stabilization, Rice Husk Ash (RHA), Plasticity Index (PI), Unconfined Compression Strength (UCS).

Introduction

If the waste has desirable qualities that allow it to be used for various geotechnical applications, such as land reclamation, the construction of embankments, etc. The amount of solid waste disposed of in landfills can be reduced. The geotechnical properties of problematic soils can be improved using a variety of techniques, including densification (using techniques like shallow compaction, dynamic deep compaction, and pre-loading), drainage, inclusions (such as geo- synthetics and stone columns), and stabilizations [1]. Many researchers attempt to use industrial wastes like rice husk ash (RHA) and fly ash (FA) are used to revamp the geotechnicalproperties of soil [1]. The process of improving the soil's engineering properties and making it more stable is known as soil stabilization. When the soil available for construction is not stable, soil stabilization is necessary.

Compaction, consolidation, drainage, and several other similar processes are all part of it. For instance, fly ash, a solid waste product from thermal power plants, is used in a number of geotechnical building projects as well as cement and brick making [2]. In the current experiment Rice Husk Ash (RHA), a type of solid waste is used to explore the effects of the index and engineering characteristics of problematic soil. Pakistan has produced 1.7 million tons of rice husk in 2021. Which is used as a fuel, the resulting ash can be used economically in various ways in the construction sector, it is chemically stable and its physical properties are similar to natural sand. The High angularity and friction angle (up to 530) contributes to excellent stability and load-bearing capacity. With a specific gravity ranging from 2.2 to 2.8, rice husk aggregates are heavier than conventional granular materials. Rice husk tends to dry freely and is not frost susceptible. Plasticity Index, compaction, shear strength, and UCS tests have been carried out on problematic clay and alluvial soil with increasing percentages of rice husk ash in order to use it for the improvement of problematic clay [3].

Natural Soil

A natural soil sample (clay soil) was collected from a site in the Taxila region by making an open trench at a depth of 1.5 m from the ground surface. The collected soil was stored in the laboratory at room temperature. Physical properties of natural soils were identified and classified using Sieve Analysis and Atterberg Limits. 95.8% of the soil sample passed the 75- micron size sieve and had a plasticity index value of 13 which is classified as A-6 soil in the AASHTO classification.

Table 1. Properties of natural soil

Characteristics	**Descriptions**
Optimum Moisture Content (%)	20
Percentage IS sieve #200	95
Specific Gravity	2.58
Liquid Limit (%)	33
Plasticity Index (%)	12
Maximum dry density (g/cm^3)	1.68
Unconfined Compression Strength (KN/m^2)	255

Rice Husk Ash (RHA)

Rice husk is an agricultural waste obtained from the milling of rice. About 108 tons of rice husk is generated annually in the world. Meanwhile, the ash has been categorized under

pozzolana, with about 67-70% silica and about 4.9% and 0.95%, Alumina and iron oxides, respectively [3]. Rice husk was collected from Taj Rice Mill, Sargodha, Punjab. It was burnedin the open air for 24 hours, yielding ash that was 20% of the husk by weight. The constituents of RHA are listed in Table 2.

Table 2. Oxide composition of Rice Husk Ash

Constituent	Composition (%)
SiO2	66.8
Al2O3	5.1
Fe2O3	0.98
CaO	1.34
MgO	1.89
Loss Of Ignition (LOI)	18.3

Sample Preparation and Testing

The laboratory tests carried out on the natural soil include particle size distribution, Atterberg limits, Proctor test, and UCS. The geotechnical properties of the soil as well as the stabilization tests were determined in accordance with ASTM standards. Specimens for unconfined compressive strength (UCS) were prepared at the optimum moisture contents (OMC) and maximum dry densities (MDD). In the second phase of the study, five different percentages of RHA, 3%, 6%, 9%, 12%, and 15% mixed with soil in different tests. To achieve appropriate properties of soil with RHA mix them properly. For the above five different ratios, tests are carried out to observe changes in the properties of soil i.e. maximum dry density, maximum moisture content, and Unconfined compressive stress of soil.

Liquid limit: The liquid limit test was conducted on samples passing 0.425 mm (No. 40) sieve; clayey soils and soil mixed with (0, 3, 6, 9, 12, and 15%) rice husk using Casagrande's liquid limit apparatus as per the procedures laid down in ASTM D 4318-00.

Plastic limit: The plastic limit test was conducted on samples passing 0.425 mm (No. 40) sieve; clayey soils and soil mixed with (0, 3, 6, 9, 12, and 15%) rice husk, as per the specifications laid down in ASTM D 4318-00.

Specific gravity:The specific gravity test was conducted on the soil in accordance with ASTM D .

Compaction: The standard compaction tests were performed in accordance with ASTM D 1557. The specimens were 102 mm in diameter and 116 mm in height.

Unconfined Compression Test: This test was performed in accordance with ASTM D 2166-00. The sample sizes were 38 mm in diameter and 76 mm in length. At the optimum moisture content (OMC) and maximum dry unit weight, the tests were performed.

Results and Discussion

Effect of RHA on Compaction characteristics of natural soil

The variations of MDD and OMC with RHA contents mixed with soil are shown in Figure 1 and Figure 2, respectively. The MDD is decreased while the OMC is increased with an increase in the RHA content. The decrease in the maximum dry unit weight can be attributed to the replacement of soil by the RH in the mixture which has a relatively lower specific gravity (2.04)compared to that of the soil which is between 2.69 to 2.71 [3]. OMC increased with an increase in RHA contents. These processes need water to take place. This also indicates that more water is required to compact the soil-RHA mixture.

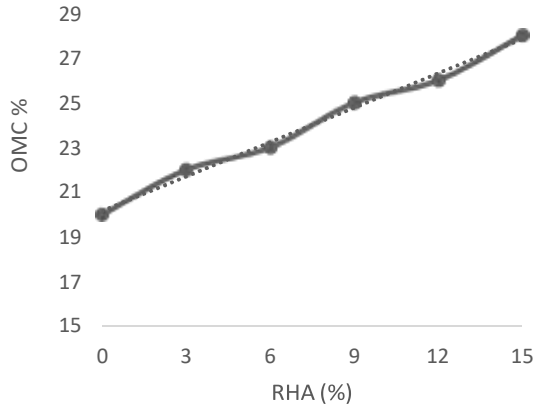

Figure 1: Variation of OMC % with RHA

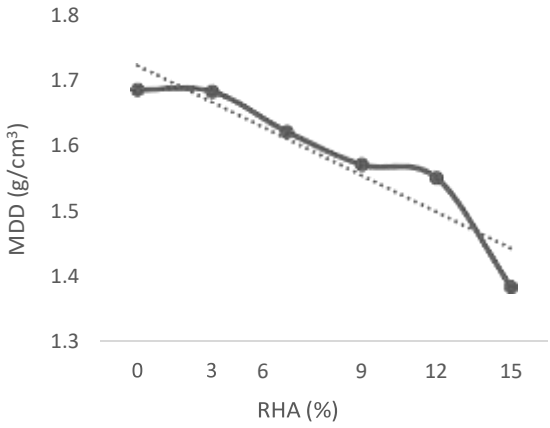

Figure 2: Variation of MDD with RHA

Effect of RHA on Liquid Limit and Plasticity Index

Significant addition of rice husk ash to soil Changes the Atterberg limits. Increasing the content of rice husk ash, the mixture causes an increase in the liquid limit shown in Figure 3. But italso observed to decrease in Plasticity Index due to the increase in the plastic limit shown in Figure 4.

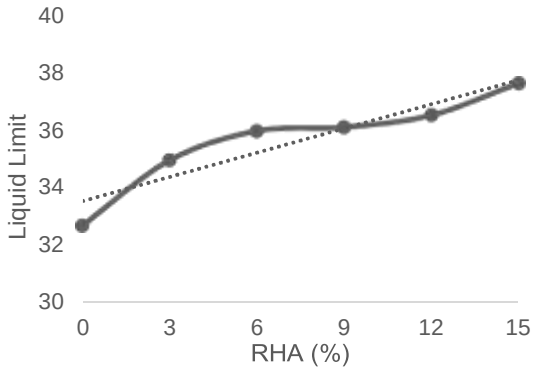

Figure 3: Variation in Liquid Limit

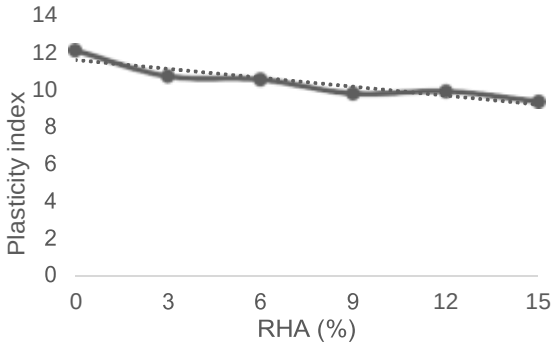

Figure 4: Variation in Plasticity Index

Effect of RHA on Unconfined Compression Strength

Unconfined compressive strength (UCS) is the most common and adaptable method of evaluating the strength of stabilized soil. It is the main test recommended for the determination of the required amount of additive to be used in the stabilization of soil [1]. The variation was found in UCS with an increase in RHA from 0% to 15% content to the dry weight of soil. Therewas a UCS value of 255.7kN/m2 recorded for the natural soil.

UCS values increase with the increase in RHA to its maximum between 6–9% RHA after whichit falls from 12–15% RHA. The subsequent increase in UCS is due to the formation of cementitious compounds between CaOH and RHA in the soil and pozzolanic in RHA. This reduction in UCS values after the addition of 9% RHA may be due to the additional RHA entrained in the soil and hence the formation of weaker bonds between the soil and the cementitious composites. The maximum UCS value recorded was 284.72 kN/m2 at 9% RHA content respectively shown in Figure 5. These values are slightly higher than the natural soil UCS of 255kN/m2.

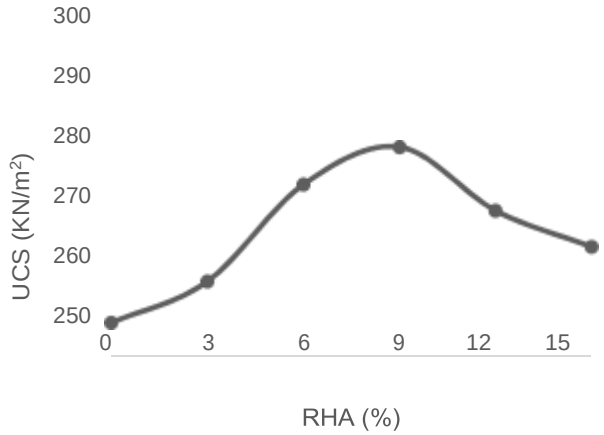

Figure 5. Variation in UCS with RHA

Conclusion

From the result of this study, the following conclusions can be drowned:

- The soil was identified as A-6 (clayey soil) on AASHTO (1986) classification system.Also, it is a clay of high plasticity (CH) according to USC.
- Treatment with RHA shows an increase in OMC % and a decrease in MDD with RHA content.
- The Atterberg Limits altered with RHA content. Liquid limit and plastic limit increasewhile the Plasticity Index of soil decreases respectively.
- The unconfined compression strength is maximum increased at 9% RHA content andalso slightly changed with the variation of RHA content.

Recommendation

The result of the study shows little potential for using RHA only for soil improvement, it is recommended under the literature review that it should be employed more with cement or lime to improve the compressive strength of the soil.

References

[1] S. A. 1. K. J. 2, "POTENTIALS OF RICE-HUSK ASH AS A SOIL STABILIZER," *International Journal of Latest Research in Engineering and Technology (IJLRET),* vol.2, no. 2, p. 9, 2016.

[2] M. P. B. M. V. A. Mr.Vishal Ghutke, "Stabilization of soil by using rice husk ash," *The International Journal of Engineering and Science (IJES),* p. 4, 2018.

[3] S. S. S. Anil Kumar Singhai1, "LABORATORY STUDY ON SOIL STABILIZATIONUSING FLY ASH," *IJRET: International Journal of Research in Engineering and Technology*, vol. 3, no. 11, p. 4, 2014.

[4] H. Afrin, "A Review on Different Types Soil Stabilization Techniques," *InternationalJournal of Transportation Engineering and Technology,* vol. 3, no. 2, p. 6, 2017.

[5] R. S. A. Maninder Singh1, "SOIL STABILIZATION USING INDUSTRIAL WASTE (WHEAT HUSK AND," *International Research Journal of Engineering and Technology(IRJET),* vol. 4, no. 9, p. 8, 2017.

[6] M. J. a. B. Lal, "Impact of Rice Husk Ash on Soil Stability (Including Micro Level Investigation)," *Indian Journal of Science and Technology,,* vol. 9, p. 9, 2016.

[7] F. H. R. K. Y. H. A.-S. Mohammed Y. Fattah*1, "Improvement of Clayey Soil Characteristics Using Rice Husk Ash," *Journal of Civil Engineering and Urbanism,* vol.3, no. 1, p. 8, 2013.

2nd International Conference on Advances in Civil and Environmental Engineering (ICACEE-2023)

University of Engineering & Technology Taxila, Pakistan

Conference date: 22nd and 23rd February, 2023

Prediction of Geotechnical Engineering Properties using Artificial Neural Networks: A State-of-the-Art Review and Advances

Shahrukh Abbas[1], Shaheera Sharib[2], Naveed Ahmad[3], Muhammad Junaid Zafar[4] Mudassar Munir Shah[5]

[1]engr.shahrukh.uettaxila@gmail.com
[2]shaheeramalik07@gmail.com
[3]naveed.ahmad@uettaxila.edu.pk
[4]junaidzafar1127@ gmail.com
[5]mudassarmunirshah461@gmail.com

ABSTRACT:

Artificial Neural Networks (ANNs) are extensively used machine learning simulations, that simulates the composition and function of the person brain, capable of recognizing patterns and making predictions based on input data. Numerous researchers have shown their ultimate interests to demonstrate the potential of ANNs to accurately predict soil properties and analyse geotechnical structures. However, there appears gaps in classification of studies and research concerning organised literature analysis of these approaches. The current study focus is to review the research articles published in last two decades, identifying recent advancements of ANN at various stages of geotechnical engineering and theories of the ANNs algorithms. An overview of the different types of ANNs, their architectures, as well as a discussion of the advantages and limitations of using ANNs in geotechnical engineering is made. Furthers the various types of ANN such as feedforward and recurrent neural networks have been demonstrated with supportive examples. Specific case studies on implementation of ANNs in geotechnical engineering have been deliberated for various applications including prediction of soil behaviours, modelling, and evaluation of retaining walls, prediction of soils California Bearing Ration (CBR), liquefaction assessment, earth retaining structures, pile bearing capacity. settlement of structures, slope stability, classification of soils as well as landslide vulnerability mapping and risk assessments.

KEYWORDS: Artificial Neural Network, California Bearing Ratio, Feedforward, Recurrent, Geotechnical Engineering

INTRODUCTION

Artificial Neural Networks (ANNs) is a soft computing artificial intelligence (AI) technique that have become increasingly crucial in Civil Engineering owing to their capability to model and solve complicated, nonlinear problems. ANNs is trained using a stage set of input-output pairs, where the weights of the synapses are adjusted to reduce the difference among the ANN's forecasts and the actual outputs. There are different types of ANNs, such as feedforward networks, recurrent networks, and convolutional networks, each with their own strengths and suited for specific types of tasks and data. Because of their imprecise and complicated natures, evaluating the engineering characteristics of rock and soil strata reveals unpredictable and variable behaviour. Several alternative materials used in civil engineering (for example, steel, wood, and concrete) exhibit significantly greater homogeneity as well as isotropy. ANNs are modern mathematical simulations

and computer software applications that can aid in identifying the most reliable options for achieving a particular project outcome[1].

ANNs are quite so adapted towards modelling the dynamic behaviour of majority of geotechnical engineering materials, that demonstrate great unpredictability. When compared to conventional methods, ANNs have indeed exhibited higher forecasting skills[2]. ANNs have been effectively implemented to practically most of the difficulties in geotechnical engineering since the early on 1990s. This section briefly examines the uses of ANNs in geotechnical engineering after 2001, and concerned viewers are directed to Shahin et al. covering the articles before 2001 in detail.

Deep-rooted (pile foundation) and superficial foundation behaviour in soils is complicated, unpredictable, and therefore not completely recognized. This feature has prompted numerous academics to use the ANN approach for the estimation of foundation behaviour. ANNs, for example, have been widely implemented to estimate the capacities of pile foundations under axial as well as lateral load in compression and uplift, such as drilled shafts, driven piles, and ground anchoring piles[3]. ANNs have been used to develop methodologies for estimating several soil characteristics, as well as pre-consolidation pressure[4], shear strength and stress background[5], swell tension , lateral earth pressure, compaction properties as well as permeability, soil structure and classification, and soil dynamics estates[6-8].

Liquefaction process occurring during earthquakes is indeed a catastrophic ground collapse phenomenon that can cause severe damage to numerous civil engineering infrastructure. Despite the liquefaction phenomenon is widely understood, predicting liquefaction potential is extremely difficult. Many academics have been drawn to examine the suitability of ANNs for forecasting liquefaction. Modelling and evaluation of retaining walls, liquefaction valuation, prediction of soils California Bearing Ration (CBR), pile bearing capacity prediction soil retaining structures, slope stability, settlement of structures, classification of soils and, landslide vulnerability mapping and risk assessments are the other important applications of ANN in geotechnical engineering[9].

Artificial Neural Networks (ANN)

ANNs is a few of most important application of soft computing (SC) technique. An ANN is made up of a network of interconnecting units (the neurons) that collaborate to accomplish a given problem. ANNs are encouraged by the structure and role of biologic neurons observed in the human nervous system and brain. They are simplified versions of these counterparts and can solve problems based on the information they have been trained on. To be capable of generating actual answers for a particular problem, ANNs must go through a training (calibration) procedure through which numerous input parameters are faced by the network as an feedback environment[10].

ANNs are a subclass of AI that employs automated optimization to learn the links and interdependence among many input parameters in a particular system[11]. They then predict these relationships by modelling them as mathematical operations. ANNs are implemented successfully to find patterns as well as model real problems in understanding the complex systems. Many researchers in domain of geotechnical engineering have expressed their interests[12]. ANNs can be categorised based on factors such as the understanding condition, model topography, number of hidden layers, and training algorithm. This paper aims to simplify the concepts of backpropagation ANN simulation model and explore their applicability for modelling of the stabilized clays behaviour in order to give predictions about the soil parameters, to reduce misconceptions and encourage their practice in soil stabilization complications for further accurate solutions.

Elements of ANN:

ANNs imitate the design of biological neuronal networks by consisting of a group of interconnecting nodes called neurons. Figure 1 provides a comprehensive picture of a biological brain network[13]. A network is formed when these neurons are connected by edges so that one neuron's output becomes another neuron's input. Several neurons serve as the network's data gathering or processing nodes. Important soil parameter laboratory outcomes would serve as the inputs throughout particular application. Each neuron's output is calculated by calculating the weighted total of the inputs across the associated neurons and adding a bias value. The final output is produced by passing this output via an initiation function, which may be a linear or non-linear function[14].

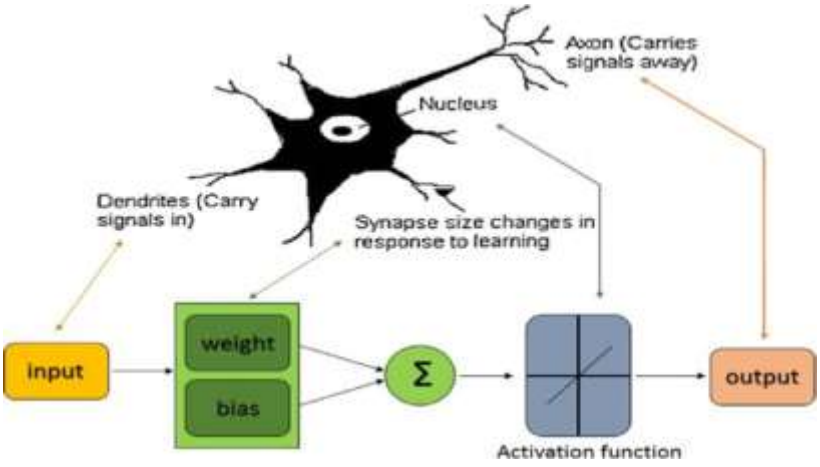

Figure 12: Representation of Biological Neural Network [13]

A complex network of interconnected neurons makes up the human brain is referred as a biological neural network (BNN). The brain's capacity for problem-solving is governed by these networks. Dendrites, soma, axons, and synapses are the four fundamental parts of individual neuron inside the brain. Several neurons send messages to the dendrites, which extend beyond the neuron cell body. The synapses, that are the locations where neurons come together, are where the axon, which extends through the cell body as well, delivers electrical pulses across its length to interact with several other neurons. Through this neuronal network which has synapses just at terminals of its axons, the brain is able to communicate and interpret information. The natural method of processing of information within human brain served as the model for the establishment of numerical programs that may offer solutions based on information already available without the requirement for existing theories, presumptions, or complicated matrices[15].

Architecture and working of ANN:

In charge to simulate functions with a large range of input variables and poorly understood or quantifiable effects, artificial neural networks (ANNs) are implemented. They are able to learn, generalise, categorise, and anticipate values, which explains why. They are effective tools because of their adaptability and capacity to "remember" information after training. They consist of several layers, with a network of interlinked "neurons" in each layer. According to the operation of synapses, each link functions similarly to dendrites inside the human brain by way of multiplying

a certain coefficient known as a weight by the values produced by the neurons. The values as of all the neurons in a particular layer are then combined with a bias value and transmitted through the connections to the next layer as presented in figure 2[16].

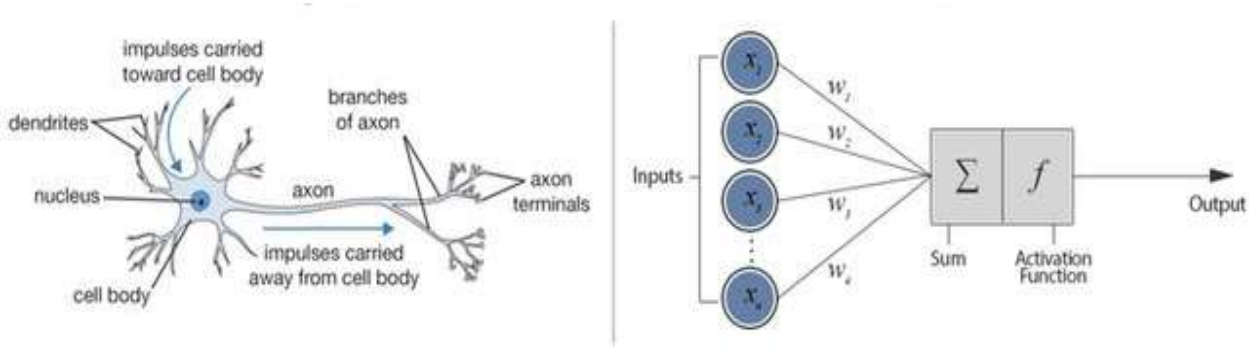

Figure 14: Biological verses Artificial Neural Network [16]

A predetermined transfer and otherwise activation function (f), which depicts the interaction among the neurons in successive layers and functions similarly to the cell body and otherwise soma within human brain, receives the entire final sum, indicated by Eq. (1). The input data for these nerve cell in the subsequent coating of the ANN are determined by the outcomes of the activation functions in a particular layer. The connections are given arbitrary weights at first, and the learning or calibration procedure uses the existing data to calculate the connections' ultimate values.

$$x_i = \sum(y_k w_{kj}) + b_j \quad (1)$$

$$y_i = f(x_j) \quad (2)$$

Here x_j is just the output of such neural network y_k, wkj remain just the weighted coefficients, b_j would be the prejudice values, f represented the start, *i* provides total number or quantity of nerve cell in a particular layer, and k denotes the amount of layers; values derived using the activation function f(xj); The parallel processing skills of its neurons are the foundation for ANNs capacity aimed at learning. The fineness of the input information determines how effectively the ANN predicts the future. Linear and non-linear activation functions using ANNs can indeed be widely categorised[17].

APPLICATIONS OF ANNS IN GEOTECHNICAL ENGINEERING:

Systematic study has been made on the number of publications representing the role of ANNs in the field of geotechnical engineering to elaborate the concerns of the researchers towards the soft computing techniques for the evaluation of complex engineering problems. Figure 3 depicts the domain of ANN implementation in geotechnical engineering according to total articles year wise and total of citations mentioned in each year. It can be noticed that publications have been increased from year 2000 to onwards with significantly increasing number per year[13].

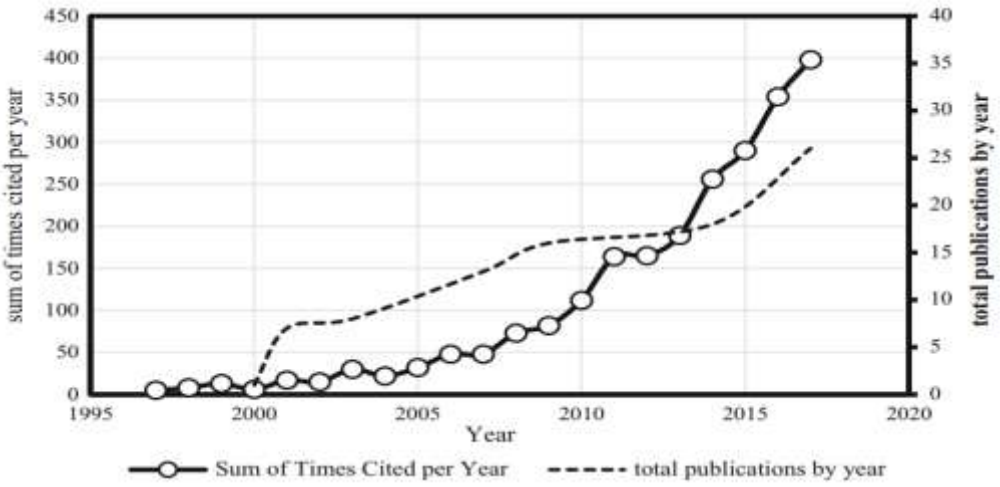

Figure 15: Graphical analysis of the research articles on geotechnical applications of artificial neural networks (ANN) from 1995 to 2020 [13]

Prediction of Soil CBR by ANN:

A study [9], presented a technique for assessing the CBR of soil using soft computing systems, which include ANNs, adaptive neuro-fuzzy inference systems (ANFIS), and support vector machines (SVMs). The authors collected data on soil properties and CBR values for various soil types and used this data to work out and test the soft computing models. They found that all three models were able to accurately predict CBR values, with the ANN and ANFIS models performing slightly better than the SVM model. The authors also discuss the advantages and disadvantages of each model and conclude that the use of soft computing systems can be an effective method for estimating CBR values. They have used approximately 124 soil data sets including soil gradation data (% fines, sand, and gravel), Atterberg limits (W_L (%), W_P (%) and PI), compaction characteristics (MDD as well as OMC), soil classification. They obtained a higher value (R^2 = 0.86) of corelation coefficient of California bearing ratio (CBR) using simple regression analysis (SRA) using gravel percentage as independent variable. Analysis further reveals that maximum dry density, optimal moisture content, and gravel then sand percentage have maximum effect on CBR.

Another study[18] have calculated the CBR value of soil by modelling in the area of artificial neural networks. To establish the optimum correlations amongst CBR and such soil properties, sub - base dataset parameters have been qualified. In perspective of simple statistical criterion, generated ANN model is legitimate. This ANN model is effective in anticipating CBR values based on genuine CBR tests. Inside the ranges of the key indices, Soluble salts represented the most significant element, with a significance percentage 39.46%, whereas the plasticity index (PI) is indeed the smallest significant influence, with a significance percentage of 2.06%. The input variable ranges are important in sensitivity analyses.

Similarly, [19] have estimated CBR value by ANNs and genetic representation programming. Genetic Expression Programming (GEP) is a genetic algorithm-based optimization technique that is used to automatically generate exact expressions or computer programs that can perform a specific task. It is a form of figurative regression where the aim is to find the mathematical interpretation that best fits a given set of data. GEP uses a symbolic symbol of the solution in the

form of a family tree-like shape called an expression tree, where the nodes of the tree represent mathematical functions and the branches represent the input variables. GEP and ANN have been attempted to estimate CBR utilising eight soil parameters including % of gravel, % Sand, liquid limit (W_L), plastic limit (W_P), fine content (FC), optimum moisture content (W_{opt}), plasticity index (IP), and maximum dry density (γ_{dmax}). The percent contribution of each of the parameters in CBR prediction is compared using ANN and GEP as presented in figure 4 of sensitivity analysis.

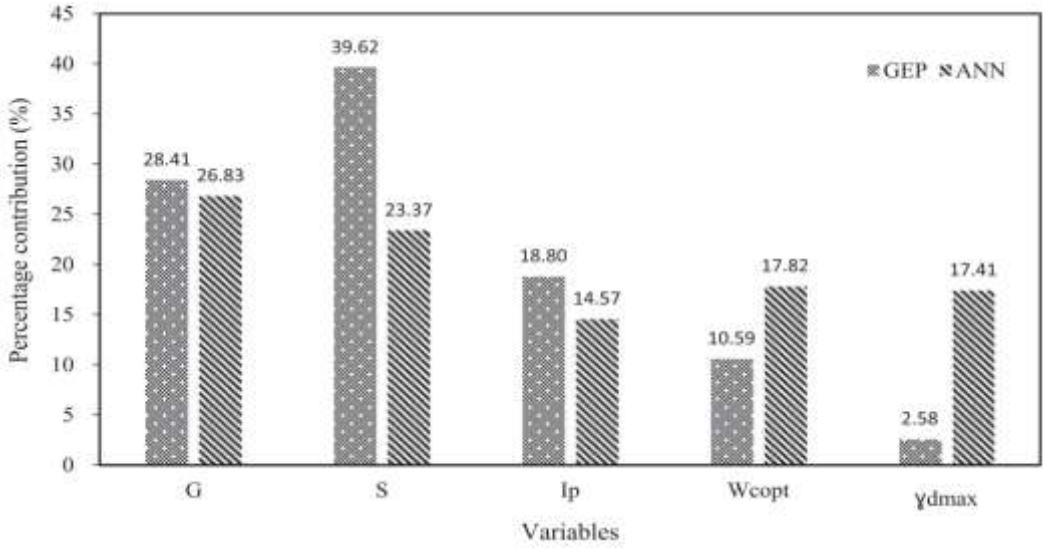

Figure 16: Comparative (Sensitivity) Analysis of ANN and GEP in prediction of soil CBR [19]

Application of ANN in Earth Retaining Structures:

A study [20] predicted and optimized factor of safety for retaining walls using ANN. To accomplish the goals of this research, a complete list was created that included 2880 dataset values of wall up elevation, wall up breadth, wall up weight, soil weight, and core friction angle as key variables and factor of safety of retaining wall as a product. Factor of safety Fs values have been predicted using an ANN model in the initial stage. To accomplish this, multiple ANN models were created and suggested, and the finest one was chosen. Finally, a Proposed model with four nerve cells in the secret layer performs better than the previous models. For the best ANN model, R2 and root mean square error (RMSE) and R^2 values of (0.0052 and 0.0049) as well as 0.998 were achieved, indicating an excellent level of sensitivity in terms of performance assessment.

R-squared (R^2) and RMSE are two frequently used statistical measures to assess the execution of a regression model. R^2, also known as the coefficient of fortitude, measures the percentage of the variation in the contingent variable that is described by the independent variable(s) in the model. It ranges sandwiched between 0 and 1, where 1 indicates a perfect fit and 0 indicates no fit. R2 is a relative measure and can be used to comparison the goodness of fit of different models.

RMSE is a gauge of the disparity between the expected values and the actual values. It is the square root of the mean of the adjusted differences between the expected and actual values. The lower the RMSE value, the well the model fits the data. It is commonly used to measure the model's performance in conditions of accuracy. Both R2 and RMSE are commonly used to assess the implementation of regression models but R2 is relative measure and RMSE is absolute measure.

Similarly, [8] developed an ANN model that estimated maximum deflections of wall in braced excavations and soft soils mostly in the wall up top. The results showed great accuracy, with correlation values of 0.984 to 0.967 for the exercise as well as assessment datasets, correspondingly.

ANN model for the prediction of Soil Behaviour:

A study [21], presented a study on employing adaptive neural networks to demonstrate the intensity characteristics of lateritic soils. They collected data on the unconfined compressive strength and Atterberg limits of several samples of lateritic soil and used this data to train a neural network. They then used the expert network to calculate the strength characteristics of additional samples of lateritic soil that were not included in the training dataset. The outcomes demonstrated that the neuronal network was able to precisely predict the strength characteristics of the lateritic soils, with a high correlation among the predicted and real values. Overall, this research provides evidence that adaptive neural networks can be a valuable tool for modelling the strength characteristics of lateritic soils.

[22] Presented a study on using recurrent neural networks (RNN) to model the trimming behaviour of a remaining soil. The authors collected data on the shear strength and stress-strain performance of a residual soil under different loading situations and used this data to train a recurrent neural network. They then used the trained system to predict the shearing behaviour of the soil in different loading situations that were not involved in the training dataset. The outcomes demonstrated that the recurrent neural network was able to correctly predict the shearing behaviour of the residual soil, with a good relationship stuck among the expected and actual values. The authors also compared the results obtained with recurrent neural networks with other methods such as multiple regression, ANNs and fuzzy logic and found persistent neural network to be more accurate. Overall, this study provides evidence that recurrent neural networks can be a valuable tool for modelling the shearing behaviour of residual soils.

Prediction of Pile Capacity using ANN:

A study [23] has developed an enhanced ANNs model to accurately estimate the maximum uplifting capability of under-reamed piles installed in dry up granular soils. They used a prediction approach and included critical elements such as under-reamed end diameter, diameter of shaft, angle of expanded base, and embedment ratio in the model. The ANN model achieved good correlation with a mean absolute error of below 0.262, outperforming previous theories.

[24], presented a technique for calculating the bearing capacity of piles using artificial neural networks (ANNs). The authors trained and tested ANN models using data from laboratory and playing field tests on full-scale piles and found that the ANN forecasts were in good understanding with the measured bearing capacities. The writers also discuss the advantages of using ANNs for pile bearing capacity predictions, including the capability to manage nonlinear and complex interactions, and the ability to incorporate uncertain and incomplete data. Overall, the study shows that ANNs can be a useful tool for predicting pile bearing capacity.

Measurement of Soil Liquefaction by ANN:

[25] used data from 105 soil samples collected from various locations in Iran and used various soil properties as input to the ANN model. The outcomes of the research demonstrated that the ANN simulation can accurately assess the soil liquefaction potential with a high-level correlation coefficient of 0.96 between the expected and observed values. The authors also found that the use of soil characteristics such as SPT-N value, relative density, and fines matter as input to the ANN model improved the model's accuracy. The authors also compared the outcomes obtained from the ANN model along with those obtained using the conventional methods and found that the results were in good agreement. The research concluded that ANNs can be effectively used to estimate soil liquefaction capability, and that the use of soil charachteristics such as SPT-N value, relative density, and fines content as input to the ANN model improves the simulation's accuracy.

[26] established various ANNs models to evaluate and forecast the potential for soil liquefaction. Soil liquefaction is a sensation that happens when soil drops its strength and stiffness in an earthquake and behaves like a liquid. The authors used data on soil properties, site circumstances, and earthquake parameters to train and test different ANN models, including feedforward neural networks, probabilistic neural networks, and circular basis function networks. They also compare the performance of these models against other machine learning algorithms. Findings of the study demonstrated that the ANN simulations are competent to correctly predict the liquefaction ability of soils, and that the best-performance simulation was the probabilistic neural network. The authors suggest that these models can be used as a means for assessing the liquefaction potential of soils in seismically active areas.

Prediction of Foundations Settlement using ANN:

[27] given a study on the use of ANNs to calculate the settlement of narrow foundations on sandy soils. Settlement is the amount of subsidence or sinking that occurs when a foundation is built on soil. The authors used data on soil properties, foundation properties, and site conditions to train and test ANN models to determine the settlement of shallow foundations. They compared the outcomes of the ANN models to those of traditional methods such as the elastic theory and the conclusions of the study demonstrated that the ANN models are competent to accurately forecast the settlement of shallow foundations on sandy soils. The authors suggest that ANNs can be an effective tool for determining settlement of shallow foundations on sandy soils.

[28] presented a study on the use of ANNs to calculate the settlement of tropical soft soils. The authors used data on soil properties, foundation properties, and site conditions to prepare and test ANN models to calculate the settlement of shallow foundations. They demonstrated that the ANN types are capable to correctly calculate the settlement of tropical soft soils and be able to be used as a tool for forecasting settlement of shallow foundations on tropical soft soils. The authors also conclude that the use of ANNs for predicting settlements of tropical soft soil is a promising approach and can be useful for geotechnical engineers.

Prediction of Slope Stability using ANN:

A research was conducted [29]in which the authors used an ANNs to calculate the slope stability of a road embankment on smooth ground that had been handled with manufactured upright drains.

The authors collected data on various parameters such as the depth of the drains, the width of the soil layer, and the water content of the soil, and used this data to train the ANN. They then used the trained ANN to make predictions of slope stability and compared these predictions to the results of a conventional method, the limit equilibrium method. The authors found that the ANN was able to accurately predict slope stability and that it had the ability to be a useful tool for assessing the stability of embankments on soft ground. Overall, the study showed the potential benefits of using ANN as a tool for evaluating the stability of embankments on soft ground.

[30] presented a study in which the writers propose a novel artificial intelligence technique for forecasting the coefficient of consolidation of soil. The approach combines a Multi-layer Perceptron Neural Network (MLPNN) and Biogeography-based Optimization (BBO) algorithm. The authors collected data on different soil factors such as the soil type, initial void ratio, and degree of saturation and used this data to train and optimize the MLPNN. They then used the optimized MLPNN to predict the coefficient of consolidation and compared the results with those obtained from a conventional method, the Terzaghi's method. The writers found that the suggested approach was capable to accurately foresee the coefficient of consolidation and had a high correlation with the Terzaghi's method. They also demonstrated that the BBO algorithm enhanced the implementation of the MLPNN. The study demonstrated the potential benefits of using this novel AI approach for predicting the coefficient of consolidation of soil.

Soil Classification Prediction by ANN Model:

[31] presented a study in which the authors propose a simulation based on ANNs to calculate the spatial distribution of soil types utilizing data from the piezocone penetration test (CPTu). The authors collected CPTu data from a site in Iran and used this data to train and validate the ANN. They also used the educated ANN to foresee the spatial distribution of soil types and compared the results to the actual soil type distribution. The authors found that the ANN simulation was capable to accurately calculate the three-dimensional distribution of soil types and had a high correlation with the actual soil type distribution. They also showed that the ANN model worked well than other conventional methods such as the k-nearest neighbour technique. The study demonstrated the potential benefits of using ANNs for predicting the spatial distribution of soil types using CPTu data.

[32] presented a study in which the authors propose a Munsell color-based methodology for soil categorization using Fuzzy Logic (FL) and ANNs. The authors collected data on the Munsell color of soil samples and used this data to prepare and substantiate the FL and ANN models. They then used the trained models to classify the soil samples and compared the results to the actual soil classifications. The writers found that the FL and ANN models were able to accurately classify the soil samples and that the ANN version performed well than the FL model. They also showed that the Munsell color-based approach was more effective than other conventional methods such as the USDA textural triangle. The study demonstrated the potential benefits of using the Munsell color-based approach and FL and ANN models for soil classification.

Landslide Vulnerability Prediction using ANN:

A study was presented [33] in which the authors propose a method for landslide susceptibility mapping make use of ANNs and Multi-approach Evaluation of Backpropagation Algorithm (BP)

using the Neuralnet package in Cuenca, Ecuador. The authors collected data on various landslide-related parameters such as topography, geology, and land use and used this data to train and validate the ANNs. They then used the trained ANNs to predict landslide susceptibility and compared the results to actual landslide occurrences. The authors found that the multi-approach analysis of the backpropagation algorithm improved the performance of the ANNs. They also found that the ANNs were able to accurately predict landslide susceptibility and that the findings were stable with the real landslide occurrences. The study demonstrated the potential benefits of using ANNs and multi-methodology analysis of the backpropagation algorithm for landslide susceptibility mapping.

Risk Management Approach using ANN:

[34] , presented a study in which the authors propose an ANNs methodology for credit risk management. The authors collected data on various credit-related parameters such as credit history, income, and employment status, and used this data to train and validate the ANN. They also used the educated ANN to foresee credit risk and compared the results to actual credit defaults. The authors found that the ANN was able to accurately predict credit risk and that the findings were consistent with real credit defaults. They also found that the ANN performed better than traditional statistical methods such as logistic regression. The study demonstrated the potential benefits of using ANNs for credit risk management.

Conclusions:

ANNs as an AI method can shape and explain complex, nonlinear complications in Civil Engineering. ANNs learn and adapt to new information through a process termed as training. Several different types of ANNs have been used for different types of tasks and data. ANNs have remained effectively cast-off in geotechnical engineering to evaluate the engineering characteristics of rock and soil strata, estimate the capacities of pile foundations, develop methodologies for estimating soil characteristics, forecast liquefaction potential, and model and evaluate retaining walls, among other applications. Following are the set of conclusions drawn from the current study.

- Artificial Neural Networks (ANNs) as a soft computing technique mimic the structure and function of biological neurons to solve complicated problems accompanied by specific training process to generate accurate answers. They have been effectively utilized in various areas with geotechnical engineering. The concepts of ANN simulation model have been simplified and their applicability is explored in modelling and simulation of soil parameters and their role is encouraged in soil stabilization problems.
- ANNs are discovered to be an efficient tool because of their adaptability and ability to "remember" information after training. As ANNs consist of several layers, each with a network of interconnected "neurons" that function similarly to dendrites in the human brain by multiplying a certain coefficient (weight) by the values produced by the neurons. The estimates from all the neurons in a particular layer are combined with a bias value and transmitted through connections to the next layer.
- Moreover, ANNs implementations in geotechnical engineering has been used with a steady increase in recent years, with a growing number of publications and citations in this field. This trend indicates that researchers are recognizing the possibility of soft computing methods, such as ANNs, to address complex engineering problems.

- Uses of soft computing practices in geotechnical engineering is a promising approach for addressing complex engineering problems, specifically in the domain of CBR prediction of soil, and it's an asset for geotechnical engineers, researchers and practitioners in their work.
- ANNs simulations have shown capacity in forecasting and optimizing structural performance in retaining walls and soft soils. Studies have demonstrated the effectiveness of ANN models in the area of civil engineering for predicting and optimizing factors such as factor of safety and maximum deflections in retaining walls and soft soils.
- ANNs models have shown to be useful in predicting the maximum uplifting capability of under-reamed piles installed in dry up granular soils and pile bearing capacity. Researchers have successfully incorporated critical components such as angle of expanded base, under-reamed end diameter, diameter of shaft, and embedment ratio in their models and achieved high accuracy in predictions.
- ANNs have been effectively utilized to estimate soil liquefaction potential. Studies have shown that ANN models can accurately estimate the soil liquefaction potential with a high correlation coefficient between predicted and observed values.
- ANNs and Multi-methodology Analysis of Backpropagation Algorithm (BP) can be effectively used to predict landslide susceptibility with a high accuracy. These techniques have been shown to be a valuable tool used for identifying areas at high risk of landslides and can help mitigate the potential impacts of landslides on communities and infrastructure.
- The studies have highlighted the potential benefits of using ANNs in credit risk management, showing its effectiveness in predicting credit defaults. The use of ANNs in credit risk management can potentially improve risk assessment and decision-making processes, leading to more effective and efficient management of credit risk.

References

1. Ahmad, I., M.H. El Naggar, and A.N. Khan, *Artificial neural network application to estimate kinematic soil pile interaction response parameters.* Soil Dynamics and Earthquake Engineering, 2007. **27**(9): p. 892-905.
2. Lee, S., S.R. Lee, and Y. Kim, *An approach to estimate unsaturated shear strength using artificial neural network and hyperbolic formulation.* Computers and Geotechnics, 2003. **30**(6): p. 489-503.
3. Adeli, H., *Neural networks in civil engineering: 1989–2000.* Computer-Aided Civil and Infrastructure Engineering, 2001. **16**(2): p. 126-142.
4. Chou, J.-S. and J.P.P. Thedja, *Metaheuristic optimization within machine learning-based classification system for early warnings related to geotechnical problems.* Automation in Construction, 2016. **68**: p. 65-80.
5. Gao, W., et al., *Study of biological networks using graph theory.* Saudi journal of biological sciences, 2018. **25**(6): p. 1212-1219.
6. Flood, I. and N. Kartam, *Neural networks in civil engineering. I: Principles and understanding.* Journal of computing in civil engineering, 1994. **8**(2): p. 131-148.
7. Lu, P., S. Chen, and Y. Zheng, *Artificial intelligence in civil engineering.* Mathematical Problems in Engineering, 2012. **2012**.
8. Goh, A.T., K. Wong, and B. Broms, *Estimation of lateral wall movements in braced excavations using neural networks.* Canadian Geotechnical Journal, 1995. **32**(6): p. 1059-1064.

9. Yildirim, B. and O. Gunaydin, *Estimation of California bearing ratio by using soft computing systems.* Expert Systems with Applications, 2011. **38**(5): p. 6381-6391.
10. Basheer, I.A. and M. Hajmeer, *Artificial neural networks: fundamentals, computing, design, and application.* Journal of microbiological methods, 2000. **43**(1): p. 3-31.
11. Stepniewska-Dziubinska, M.M., P. Zielenkiewicz, and P. Siedlecki, *Development and evaluation of a deep learning model for protein–ligand binding affinity prediction.* Bioinformatics, 2018. **34**(21): p. 3666-3674.
12. Chao, Z., et al. *The application of artificial neural network in geotechnical engineering*. in *IOP Conference Series: Earth and Environmental Science*. 2018. IOP Publishing.
13. Sharifi, Y., et al., *Study of neural network models for the ultimate capacities of cellular steel beams.* Iranian Journal of Science and Technology, Transactions of Civil Engineering, 2020. **44**: p. 579-589.
14. Kalantary, F. and A. Kordnaeij, *Prediction of compression index using artificial neural network.* Scientific Research and Essays, 2012. **7**(31): p. 2835-2848.
15. Kumar, S. and S. Barai, *Neural networks modeling of shear strength of SFRC corbels without stirrups.* Applied Soft Computing, 2010. **10**(1): p. 135-148.
16. Rout, S., V. Dwivedi, and B. Srinivasan, *Numerical Approximation in CFD Problems Using Physics Informed Machine Learning.* arXiv preprint arXiv:2111.02987, 2021.
17. Karlik, B. and A.V. Olgac, *Performance analysis of various activation functions in generalized MLP architectures of neural networks.* International Journal of Artificial Intelligence and Expert Systems, 2011. **1**(4): p. 111-122.
18. Al-Busultan, S., et al. *Application of artificial neural networks in predicting subbase CBR values using soil indices data*. in *IOP Conference Series: Materials Science and Engineering*. 2020. IOP Publishing.
19. Tenpe, A.R. and A. Patel, *Application of genetic expression programming and artificial neural network for prediction of CBR.* Road materials and pavement design, 2020. **21**(5): p. 1183-1200.
20. Gordan, B., et al., *Estimating and optimizing safety factors of retaining wall through neural network and bee colony techniques.* Engineering with Computers, 2019. **35**: p. 945-954.
21. Attoh-Okine, N. and E.S. Fekpe, *Strength characteristics modeling of lateritic soils using adaptive neural networks*. Construction and Building Materials, 1996. **10**(8): p. 577-582.
22. Zhu, J.H., M.M. Zaman, and S.A. Anderson, *Modelling of shearing behaviour of a residual soil with recurrent neural network.* International journal for numerical and analytical methods in geomechanics, 1998. **22**(8): p. 671-687.
23. Moayedi, H. and A. Rezaei, *An artificial neural network approach for under-reamed piles subjected to uplift forces in dry sand.* Neural Computing and Applications, 2019. **31**(2): p. 327-336.
24. Lee, I.-M. and J.-H. Lee, *Prediction of pile bearing capacity using artificial neural networks.* Computers and geotechnics, 1996. **18**(3): p. 189-200.
25. Pal, M., *Support vector machines-based modelling of seismic liquefaction potential.* International Journal for Numerical and Analytical Methods in Geomechanics, 2006. **30**(10): p. 983-996.
26. Abbaszadeh Shahri, A., *Assessment and prediction of liquefaction potential using different artificial neural network models: a case study.* Geotechnical and Geological Engineering, 2016. **34**: p. 807-815.

27. Luat, N.-V., K. Lee, and D.-K. Thai, *Application of artificial neural networks in settlement prediction of shallow foundations on sandy soils.* Geomechanics and Engineering, 2020. **20**(5): p. 385-397.
28. Kolay, P., A. Rosmina, and N. Ling. *Settlement prediction of tropical soft soil by Artificial Neural Network (ANN)*. in *The 12th international conference of international association for computer methods and advances in geomechanics (IACMAG)*. 2008.
29. Mamat, R.C., et al., *Slope stability prediction of road embankment on soft ground treated with prefabricated vertical drains using artificial neural network.* IAES International Journal of Artificial Intelligence, 2020. **9**(2): p. 236.
30. Pham, B.T., et al., *A novel artificial intelligence approach based on Multi-layer Perceptron Neural Network and Biogeography-based Optimization for predicting coefficient of consolidation of soil.* Catena, 2019. **173**: p. 302-311.
31. Ghaderi, A., A. Abbaszadeh Shahri, and S. Larsson, *An artificial neural network based model to predict spatial soil type distribution using piezocone penetration test data (CPTu).* Bulletin of Engineering Geology and the Environment, 2019. **78**: p. 4579-4588.
32. Pegalajar, M., et al., *A Munsell colour-based approach for soil classification using Fuzzy Logic and Artificial Neural Networks.* FUZZY sets and systems, 2020. **401**: p. 38-54.
33. Bravo-López, E., et al., *Landslide Susceptibility Mapping of Landslides with Artificial Neural Networks: Multi-Approach Analysis of Backpropagation Algorithm Applying the Neuralnet Package in Cuenca, Ecuador.* Remote Sensing, 2022. **14**(14): p. 3495.
34. Pacelli, V. and M. Azzollini, *An artificial neural network approach for credit risk management.* Journal of Intelligent Learning Systems and Applications, 2011. **3**(02): p. 103.

2nd International Conference on Advances in Civil and Environmental Engineering (ICACEE-2023)

University of Engineering & Technology Taxila, Pakistan

Conference date: 22nd and 23rd February, 2023

STUDY ON STRENGTH CHARACTERISTICS OF COLLAPSIBLE SOILS CONSIDERING VARYING MOISTURE CONTENT

Muhammad Mudassar[1], Dr. Zia-Ur-Rehman[2], Dr. Naveed Ahmad[3], Muhammad Abdul Rehman[4], Babar Khan[5]

1: MS Student-Civil Engineering Department, UET Taxila-Pakistan, muhammadmudassar195@gmail.com
2: Assistant Professor, Civil Engineering Department, UET Taxila-Pakistan, ziaur.rehman@uettaxila.edu.pk
3: Assistant Professor, Civil Engineering Department, UET Taxila-Pakistan, naveed.ahmad@uettaxila.edu.pk
4: MS Graduate-Civil Engineering Department, UMT Lahore, Pakistan, arbutt7861@gmail.com
5. CEO-Geoservices Engineering Consultants, Islamabad, Pakistan, geoservices.gec@gmail.com

ABSTRACT

The research focuses on the issue of foundation problems in the collapsible soil of Hattar Industrial Estata, Sohawa, Pasni and Eighteen Islamabad, and found Eighteen Islamabad highest collapse potential of 4.2. Most of the buildings were fractured after or even during construction. Cracks were not only in walls or beams but also in foundations. Therefore, this study was carried out to identify collapsible soil potential and develop suitable mitigation techniques for the under-study area. Collapse potential was found by Oedometer test and by index test including; grain size distribution (ASTM D422 and D4693), Atterburg's limit (ASTM D 4318), Hydrometer analysis (ASTM D 1140), Specific Gravity (ASTM D 854), UCS. Collapse potential with varying moisture content was also examined and results show that this variation causes foundation failure, which results in structure failure. Values from all tests were in ASTM ranges. It is suggested to protect that type of soil with interaction of water before and after construction.

KEYWORDS: Collapsible Soil, Collapse Potential, Single Oedometer, Double Oedometer, and Eighteen Islamabad.

INTRODUCTION

Collapsible soil is a type of soil in which volume decreases with the addition of water. Loess is a fine example of collapsible soil and is a wind-made silt deposit. Loess is normally lesser erractic than compared with other types of collapsible soil, but is usually thicker. (Coduto, 2005).The bearing capacity of these soils is particularly lesser, having high compressibility and lower density.

More precisely, collapsible soils are those that collapse on moisture, as soil fabric is unable to hold weight of the load. Soils are capable of withstanding a certain amount of stress on saturation, when saturation collapse pressure will be greater than the overburden pressure and can be considered conditionally collapsible soil.

The difference between the pressures caused by overburden and saturation collapsible is the maximum load that such soils can support. There are identified sandy, silty, and clayey kinds of these soils, with the majority falling into the silty category, typically including 50 to 90% silt particles. These soils often have a loose skeleton of grains (typically quartz) and micro-aggregates as their fabric (usually assemblages of clay particles). These often have equally distributed pores,

bonds, and bridges connecting them and a tendency to be independent of one another. Clay-sized minerals were used to create the bridges (Salley, 2005). Since grains are not in direct contact, the nature and quality of the bonds and bridges determine their mechanical behavior.

The Settlement of soil depends on the types of soil and stresses due to applied pressure. Although that type is either, compaction may complete after some time because the solids in soil may develop in a new shape. But, in a few cases of a specific type of soil, more settlement may be caused by additional wetting. (Vandanapu, 2019) term this settlement as collapsed settlement.

Although the existence of collapsible soil has long been acknowledged by several studies, the present construction of infrastructure over this type of soil as well as the issues related to it has made a detailed investigation of its weak points and mitigation strategies necessary.

Collapsible soils give high SPT N-values when dry or partially saturated, but lose a major part of their strength with an increase in moisture content, causing severe damage in terms of the settlement of structures.

Objective

The objective of this research work is to identify and evaluate collapsible soil potential in under-study area, developing a bearing capacity reduction factor for collapsible soil, evaluating the soil collapse potential indirectly by correlating it with other engineering properties such as unit weight, Atterberg's limit, or percentage of clay particles, and bearing capacity reduction factor for collapsible soils with correlating other properties.

Research Methodology

Site Identification

The understudy region was used due to building failure in Eighteen Islamabad after construction. Moreover, prior testing shows the highest collapse potential of 4.2 as shown in Table 1 in Eighteen Islamabad as compared to other study areas, Hattar Industrial Estate, Pasni, and Sohawa. Eighteen Islamabad is located in Islamabad, near Lahore-Islamabad Motorway Grand Trunk Road and 16 kilometers from New Islamabad International Airport as shown in Figure 1. This mega-housing society spreads over 572 Acres.

Figure 17: Study Area of Eighteen Islamabad

Table 6: Collapse Potential of under study areas

Sr. No.	Area	Soil Type	Plasticity Index	Bulk Density	Dry Density	Collapse potential I_c
1.	Hatter Industrial Estate	Silty Clay	7	1.9	1.7	4.1
2.	Eighteen Islamabad	Silty Clay	6	1.8	1.6	4.2
3.	Pasni	Clay	12	1.8	1.5	2.3
4.	Sohawa	Sandy Silty Clay	6	1.8	1.6	3.1

Most of the structures are single or double stories, with one multi-story structure having more than ten stories. Almost all structures possess major cracks, not only in walls or beams but also in foundations due to moisture variation underneath the soil.

Sampling of Soil

Fifteen samples from different locations were collected from Eighteen Islamabad using Hand Auger with a 6 ft depth for each sample. Samples were preserved in sampling bags (Disturbed) and shell by tube (Undisturbed) and transferred to the laboratory for further testing.

Field Testing

SPT was done in field to find N value.

Laboratory Testing

Tests performed in the laboratory on samples collected from field were; grain size distribution (ASTM D422 and D4693), Atterburg's limit (ASTM D 4318), Hydrometer analysis (ASTM D 1140), Specific Gravity (ASTM D 854), UCS, Single and Double Oedometer test (ASTM D5333-03).

RESULTS AND DISCUSSION

Single Oedometer Test

Collapse potential is measured by Oedometer (single and double) with ASTM D5333-03. One-dimensional collapse is determined using this method. Sample no 5 was taken for this test. In this test, collapse potential is determined by changing moisture content. Initial moisture content is taken as 3 showing a collapse potential of 6.57, and final moisture content is taken as 17.5, showing a 2.57 collapse potential. A graphical picture of the results is shown in Figure 2.

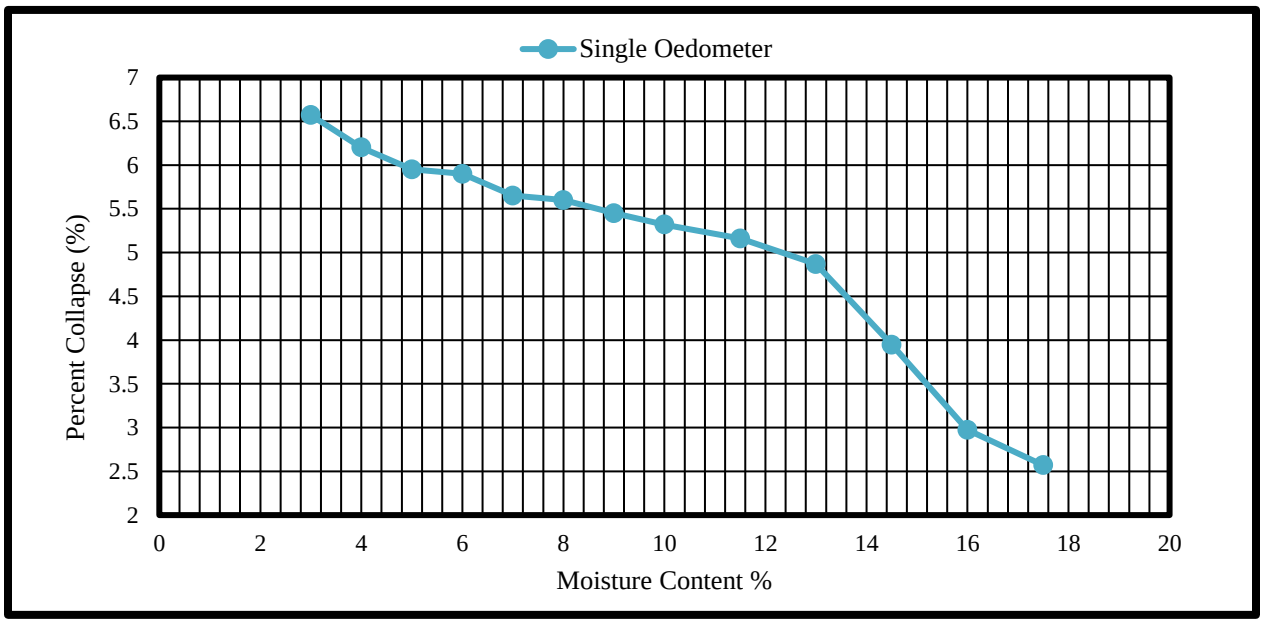

Figure 18: Collapse Potential with Varying Moisture Content in Single Oedometer.

Double Oedometer Test

Collapse potential is also measured by a double Oedometer with ASTM D5333-03. Sample no 5 was taken for this test. In this test, collapse potential is determined by changing moisture content. Initial moisture content is taken as 3 showing a collapse potential of 8.93, and final moisture

content is taken as 17.5, showing a 2.95 collapse potential. A graphical picture of the results is shown in Figure 3.

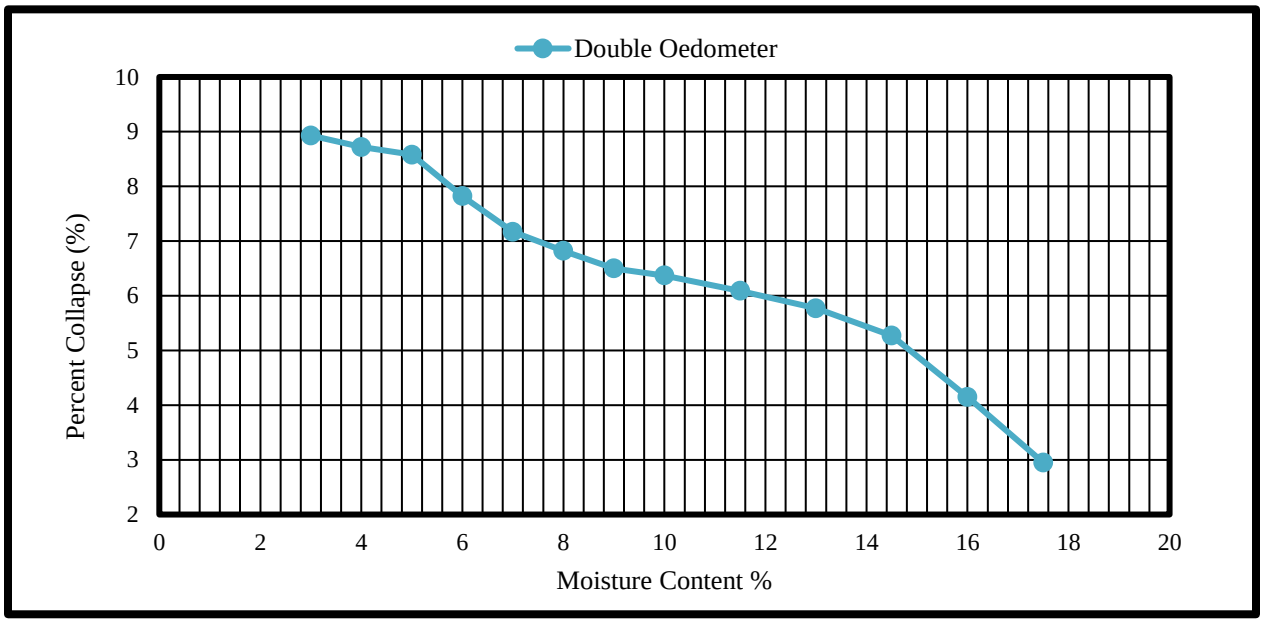

Figure 19: Collapse Potential with Varying Moisture Content in Double Oedometer.

Comparison of Collapse index from single and double Oedometer

Results from single and double Oedometer are shown in below Figure 4. Double Oedometer results shows higher value as compared with single Oedometer, but values from both lie in the ASTM range.

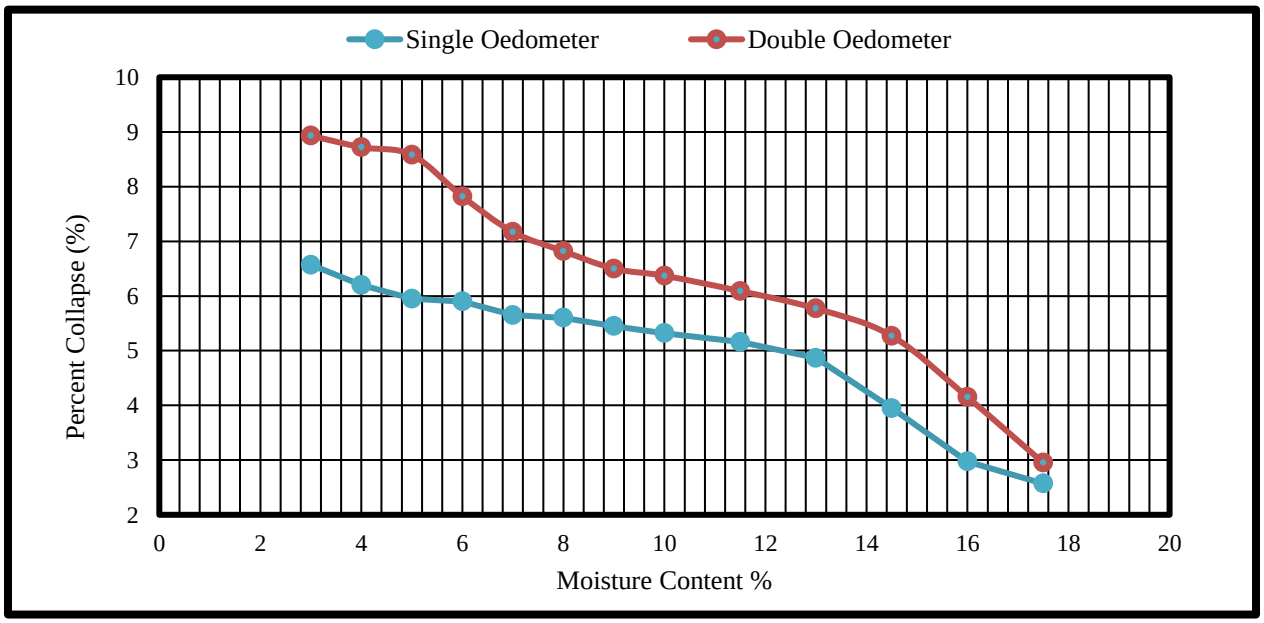

Figure 20: Comparison of Results of Single and Double Oedometer

Index Properties

Samples collected from ten locations were used to measure index properties. Sieve analysis shows fine particles in samples ranging from 70 to 81%. Liquid limit, Plastic limit, and Plasticity index ranges from 24.6 to 29.5, 17.9 to 20.7 and 6.1 to 9.9 respectively. Atterburg's limit results are shown in ASTM range. Unified Soil Classification system shows soil ranges in between CL and CL-ML. Moisture content ranges from 6.1 to 8.3. Density, specific gravity, void ratio, and saturation values are shown in Table 2.

Table 7: Index Properties Results

Borehole No.	Gravel	Sand	Fines	LL	PL	PI	USCS	Wn (%)	Density Yd (g/cm3)	Gs	Void Ratio (eo)	Saturation (%)
1	2	19	79	29.5	20.3	9.2	CL	6.9	1.6933	2.642	0.560	32.535
2	0	24	76	25.4	19.6	5.8	CL-ML	7.1	1.6677	2.614	0.567	32.705
3	1	27	72	24.9	18.8	6.1	CL-ML	7.7	1.6212	2.652	0.636	32.115
4	0	19	81	28.4	20.3	8.1	CL	6.1	1.7362	2.671	0.538	30.262
5	1	26	73	27.7	18.9	8.8	CL	6.9	1.6483	2.608	0.582	30.907
6	1	27	72	28.1	20.7	7.4	CL	6.5	1.6921	2.618	0.547	31.098
7	2	28	70	29.1	19.2	9.9	CL	8.3	1.6418	2.629	0.601	36.289
8	0	19	81	27.8	18.5	9.3	CL	7.3	1.6720	2.629	0.572	33.531
9	2	18	80	24.6	17.9	6.7	CL-ML	6.4	1.7238	2.639	0.531	31.811
10	1	24	75	25.3	19.2	6.1	CL-ML	7.9	1.6627	2.689	0.617	34.416

Particle size distributions of samples are shown in Figure 5A and 5B.

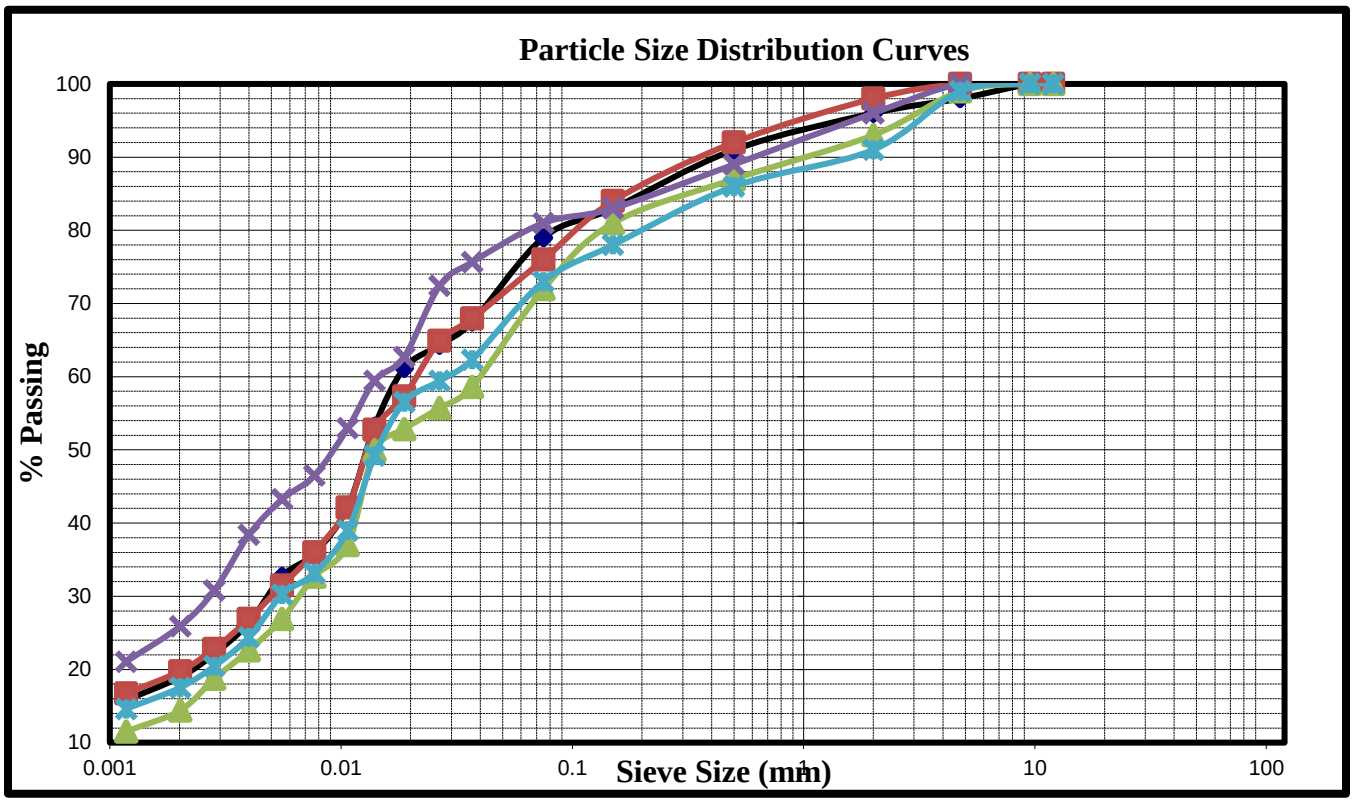

Figure 21A: Particle Size Distribution

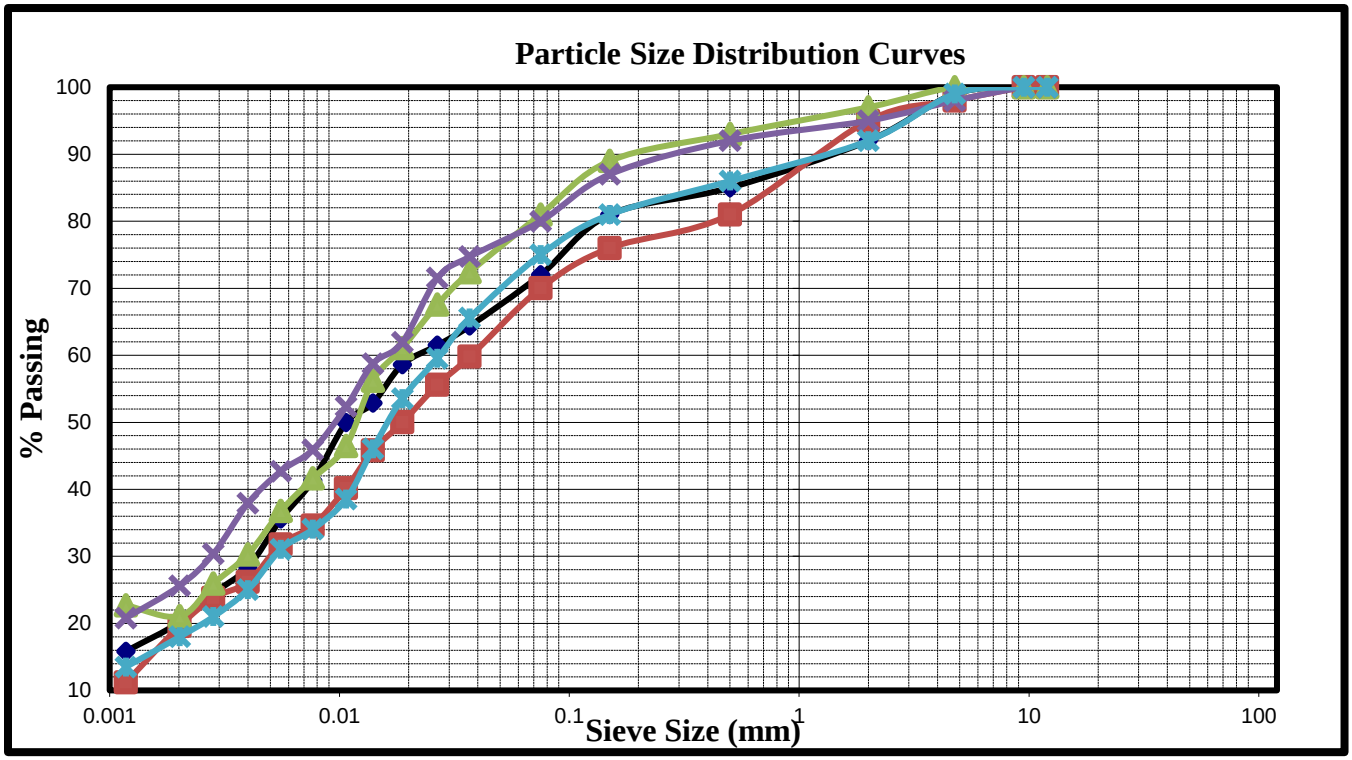

Figure 5B: Particle Size Distribution

Comparison of collapse potential with index properties

A comparison of collapse potential with specific gravity, liquid limit, and saturation are shown in Figures 6, 7, and 8 respectively. Collapse potential in all cases decreases due to variations in moisture content.

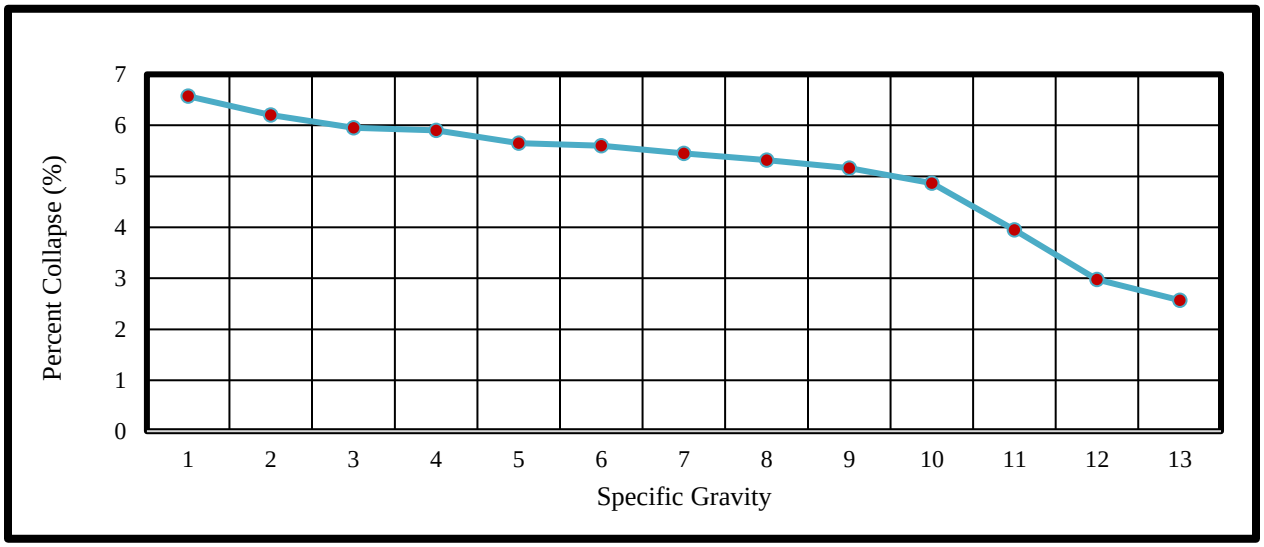

Figure 22: Comparison of collapse potential with specific gravity

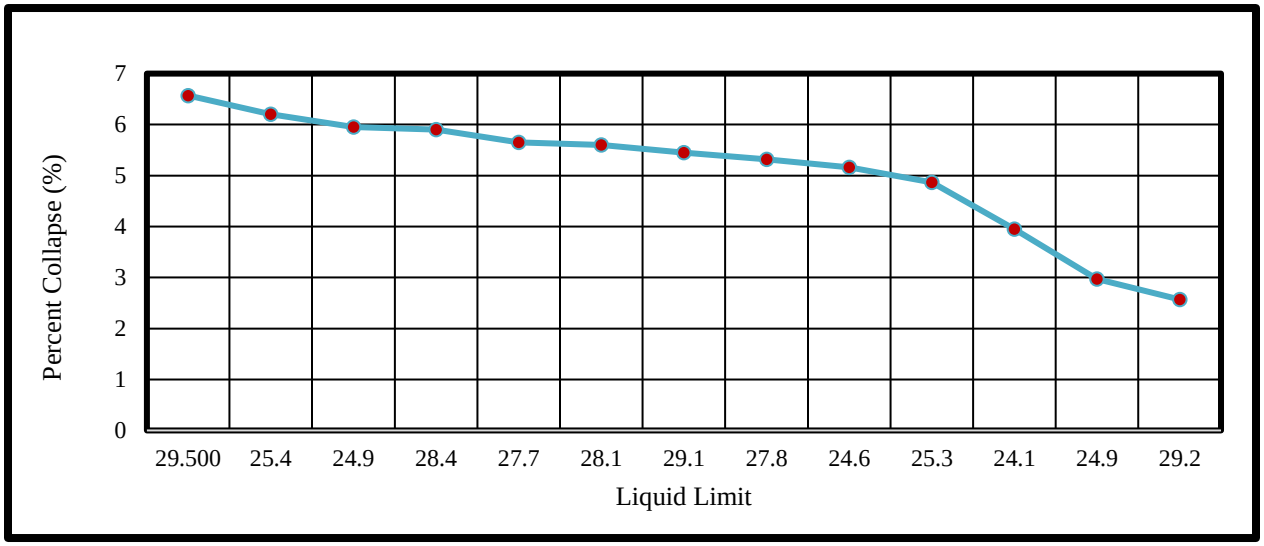

Figure 23: Comparison of collapse potential with liquid limit

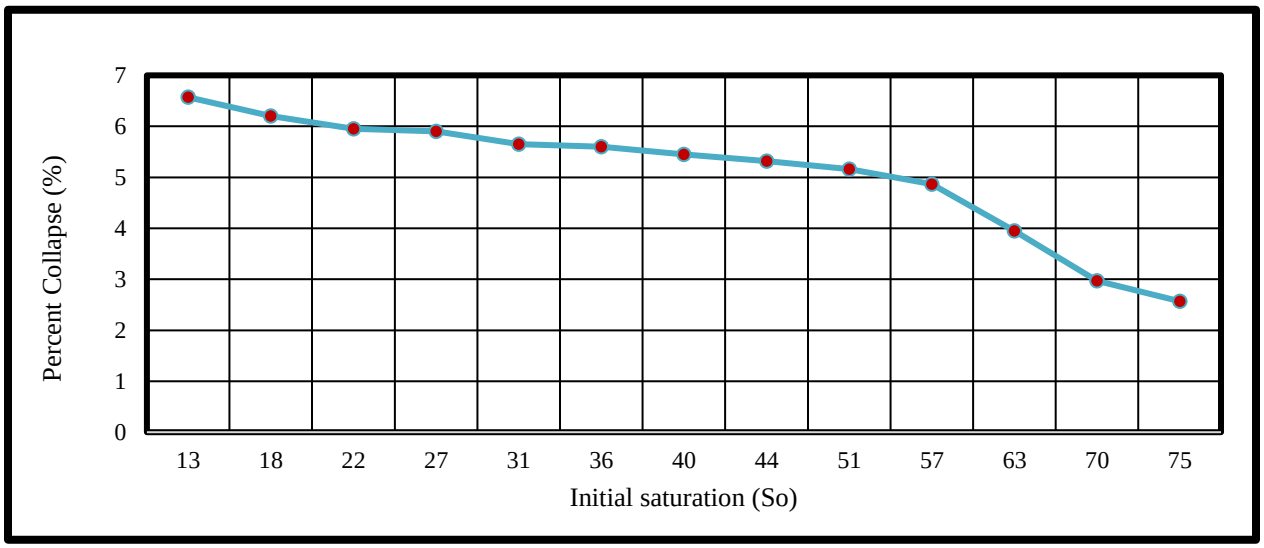

Figure 24: Comparison of collapse potential with saturation

CONCLUSION AND RECOMMENDATIONS

Detailed analysis was conducted for samples from ten locations of Eighteen Islamabad and results concluded that this location needs proper attention because this location possesses potential collapse soil. The potential of collapsible soil is average to high as per ASTM D5333 standard. Although these soils have low moisture content and appear to be relatively hard, they will eventually settle due to their ability to collapse, which causes wall cracking in light load construction as well as cracks in foundations for high-rise structures. It is recommended that bearing capacity reduction factor against different moisture content should be developed in order to minimize settlement.

ACKNOWLEDGMENT

Under the direction of the Geotechnical Faculty at UET Taxila, Pakistan, I thoroughly enjoyed this research project, which enhanced my practical knowledge. I am thankful to all who help directly and indirectly in this research.

REFRENCES

1. Coduto, D. P., Kitch, W.A. and Yeung, M. R., *Foundation Design, Principles and Practices*. 2005. 3rd Edition.
2. Selley, R. C., Cocks, L. R. M. and Plimer, I. R, *Encyclopedia of Geology*. 2005.
3. Vandanapun, R., *Laboratory simulation and finite element analysis of irrigation-induced settlements of built environment overlaying collapsible soil strata in United Arab Emirates.* Kingston University London, 2019
4. ASTM D422. *Standard Test Method for Particle-Size Analysis of Soils*.
5. ASTM D 4318. *Standard Test Methods for Liquid Limit, Plastic Limit and Plasticity Index of Soils.*

6. ASTM D1140. *Standard Test Methods for Determined the Amount of Material Finer than 75 µm (No. 200) sieve in Soils by Washing*.
7. ASTM D854. *Standard Test Methods for Specific Gravity of Soil Solids by Water Pycnometer.*
8. ASTM D5333-03. *Standard Test Method for Measurement of Collapse Potential of Soils*.

2nd International Conference on Advances in Civil and Environmental Engineering (ICACEE-2023)

University of Engineering & Technology Taxila, Pakistan

Conference date: 22nd and 23rd February, 2023

Performance enhancement of loose unsaturated soils using vertical sand drains

Muhammad Rameez Sohail[1], Naveed Ahmad[1*]

[1]University of Engineering and Technology Taxila, Pakistan, rameez.sohail@uettaxila.edu.pk
[2]University of Engineering and Technology Taxila, Pakistan, naveed.ahmad@uettaxila.edu.pk

ABSTRACT

With increase in urbanization, cities are growing and making the people to move towards unfavorable topographies for living in an unsustainable manner. The usual practice in Pakistan is to cut and fill such uneven topographies and let them settle under self-weight and rainfall percolation without proper compaction. This study is aimed to enhance preconstruction settlement in loose unsaturated soils by introducing Vertical Sand Drains (VSDs) which will contribute to the sustainable design and construction of infrastructure projects. Cylindrical models were filled with loose unsaturated indigenous soil and, settlement and shear strength were determined against different moisture contents under different situations, i.e., without sand drains, with sand drains and with combination of sand drains and surcharge loading. It was observed that provision of VSD resulted in uniform distribution of moisture within the models and cumulative soil settlement was increased with moisture content. For maximum shear strength, an optimum moisture content value ranging between 16-17% was observed. Both settlement and shear strength were increased under the combined effect of VSD and surcharge loading compared to providing the VSD alone. Hence provision of VSDs will not only reduce the postconstruction settlement of loosely dumped fill soil but will also increase its shear strength considerably.

KEYWORDS: Loose unsaturated soil, preconstruction settlement, surcharge loading, vertical sand drain, shear strength.

INTRODUCTION

Loose soils are formed because of disturbances in the natural topography of an area. These disturbances can be natural like landslides triggered due to earthquakes or rainfalls [1, 2] or they can be caused by human activities mostly during leveling of undulating ground if proper compaction is not ensured. The main characteristics of loose unsaturated soils are their low density, low moisture content, compressibility, and a potential to collapse upon wetting [3].

Most of the research has been focused on loose saturated clean granular sandy soils [4]; [5]; [6]; and [7]. During the development of residential areas on undulating ground, the soil is usually comprised of fines and is unsaturated. Some research has also been carried out on unsaturated fine-grained soils but mostly addresses compacted soils [8]; [9]; [10]; and [11].

The comparison of loose saturated and unsaturated soil at different dry densities, subjected to triaxial stress path shear test, shows that the volumetric behavior of unsaturated soil changes from dilative to contractive with increasing net mean stress. The unsaturated soil fails at a degree of saturation far below full saturation and the suction at failure decreases with an increase in the net mean stress. Saturated loose soil behaves like clean sands during undrained shearing; and strain-softening behavior can be observed in saturated loose fills. However, unsaturated loose soil, sheared at a constant water content, shows a hardening stress–strain relationship, and relatively significant volumetric contraction. This implies that the design of stabilization measures in loose

fills, slopes and geo-structures should consider the wetting and shear induced volume changes in the soil, which may lead to potential serviceability problems [12].

Wetting caused collapse mainly depends on mean net stress and initial density; higher mean net stress and lower initial density result in more decrease in volume. Moreover, wetting induced collapse can be amplified by increasing degree of saturation in unsaturated soil [13]. Therefore, proper compaction is required so that wetting induced collapse can be avoid otherwise these soils cause a lot of economic loss when construction is carried on them [14].

It has been observed by that during the development of residential areas in Islamabad, the undulating ground is levelled without proper compaction [15]. Figure 1 (a) to (e) are the satellite images taken at different dates and they show that levelling has been being carried out by spreading the soil and afterwards a house has been constructed on which cracks started to appear due to ground settlement as shown in Figure 1 (f) to (h).

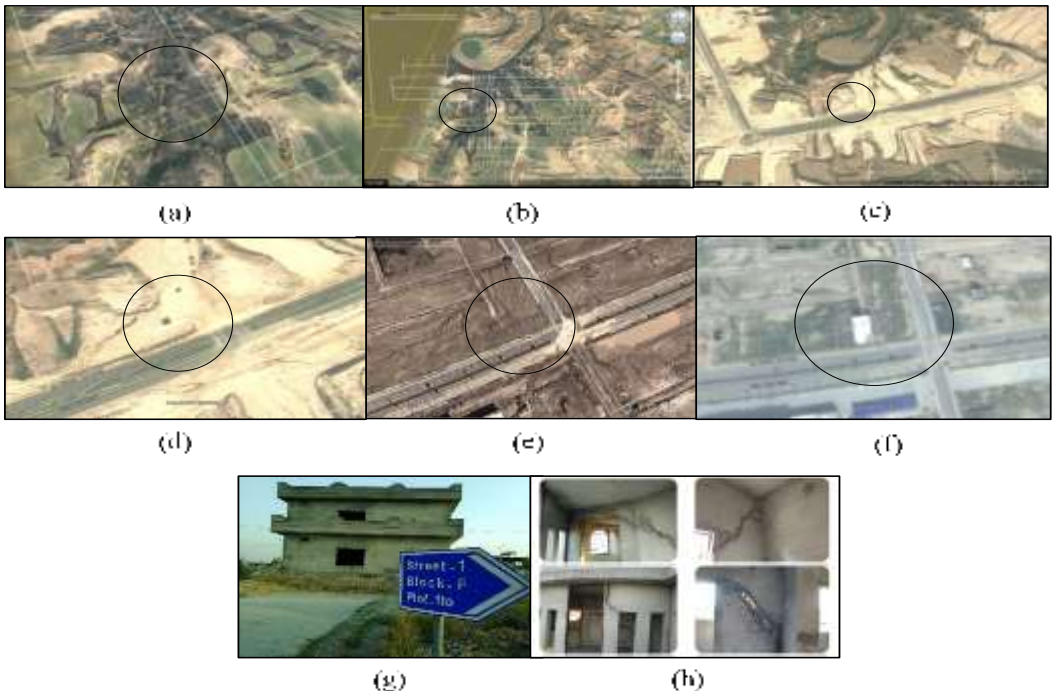

Figure 1. Inadequate compaction and appearance of structural cracks. (a) to (e) Satellite Images of leveling process without compaction. (f) Satellite image of residential building. (g) Front elevation of the building. (h) Appearance of cracks due to soil settlement.

This research has been carried out while keeping in view the current situation of housing sector in Islamabad. The soil in the vicinity is usually alluvial silty clay. In the past, ideal locations like flat plains were available for constructing residential and commercial buildings but with the passage of time these ideal locations are completely utilized. The expansion of the city can only be done on the undulating areas of Islamabad. The correct way to construct is to follow the natural topography but for modern living standards the natural topography needs to be amended. Undulating ground needs to be levelled out or made in a perfect gradient by cutting soil from higher elevations and filling in the depressions. The right way for this activity is to properly compact the soil in layers no more than 150 mm thick according to American Society for Testing and Materials (ASTM). But when preparing vast areas for housing due to rising demand, compaction is sometimes not done properly. This creates pockets of loose soils which tend to settle on its own weight and collapse when contacted with moisture.

These soils undergo settlement due to self-weight or surcharge loading, if present. This settlement is amplified if moisture comes in contact with the soil for example after rainfall. The usual soil improvement methods include excavating such soils and filled again with proper compaction. Deep footings are also laid to include basement floors in buildings. In case of deep fills, pile foundations are provided under buildings. But these methods are not economical for single or double storey residential units.

The general trend for economical treatment is to leave such areas for more than a year and hope that rainfalls cause initial settlements and as water gets drained consolidation occurs which helps in increasing shear strength of the soil. But in reality, the rainfalls cause top layers to get compacted which decrease permeability in the top 2 to feet crest. This hinders the moisture to penetrate lower soil which results in formation of a hard and less permeable crest over soft and compressible soil pockets. Buildings constructed at such locations undergo long term post-construction settlements as moisture seeps very slowly through the overlaying crest. The underlaying soil gets compressed due to added surcharge load of the building and slowly reaching moisture causes continuous settlements. Cracks start appearing in such buildings which keep on appearing and widening for years to come. Structural elements of such buildings need frequent repairs and sometimes they get damaged beyond repair.

If the moisture is introduced to deep soil, then maximum soil settlements can be achieved but this can result in loss of shear strength of the soil. Consolidation due to drainage of this moisture can increase strength but this takes a very long time. This study aims to utilize Vertical Sand Drains (VSDs) to deliberately introduce moisture to deep underlying soil uniformly and finding optimum quantity of moisture to get highest possible shear strength along with settlements before construction takes place.

TEST PROGRAM

A comprehensive test program was conducted on physical models to study the behavior of loose unsaturated soil with and without VSDs subjected to wetting by adding different quantities of water and surcharge loading. Various tests were performed to obtain moisture content, settlement, density, and shear strength before and after wetting of soil at various depths from the surface and horizontal distances from the center of the models. Tests were performed in two batches; first the effect of VSDs was observed and then surcharge loading was applied on better performing models so that the effect of VSDs along with surcharge loading could be monitored. The test program is presented in Table 1. It consists of 16 physical models; of which 9 were provided with VSDs extending the entire depth of the soil and surcharge loading was applied on 3 of them. The nomenclature of the physical models was selected as simple as possible for example 10D is a model with water added to achieve an overall gravimetric moisture content (m) of 10% and is provided with a VSD while 10N is a model with same moisture added without a VSD. Similarly, 10DS is a model with the same moisture added and provided with a VSD and surcharge load.

Table 8. Test program

Physical Model	Drain	*m* (%)	Surcharge Loading applied
Control	No	Initial	No
5D	Yes	5	No
5N	No	5	No
10D	Yes	10	No
10DS	Yes	10	Yes
10N	No	10	No

15D	Yes	15	No
15DS	Yes	15	Yes
15N	No	15	No
20D	Yes	20	No
20DS	Yes	20	Yes
20N	No	20	No
25D	Yes	25	No
25N	No	25	No
30D	Yes	30	No
30N	No	30	No

Physical Models and Soil Properties

Physical models consisted of cylindrical containers made of 1.625 mm thick galvanized steel sheet welded to the base, having diameter and height of 600 mm. The containers were provided with adequate bracing at the top and bottom rim to avoid deformation in the walls and all the joints were sealed to make them watertight. Each container was filled to the top with loose unsaturated soil having characteristic properties given in Table 9 that were determined by following the standard procedures of ASTM. The soil was classified as silty clay according to Unified Soil Classification System (USCS).

Table 9. Characteristic properties of soil used

Characteristic properties		**Standard Procedure**
Plastic Limit	20.46	ASTM D4318 [16]
Liquid Limit	26.23	ASTM D4318 [16]
Plasticity Index	5.77	ASTM D4318 [16]
Moisture Content	2.55%	ASTM D2216 [17]
Specific Gravity	2.708	ASTM D854 [18]

Filling of containers

Filling was done in four layers of 150 mm thickness with 52 kg of soil each. Settlement plates were placed on top of each layer at horizontal distances of 75 mm, 150 mm and 225 mm from the center as shown in Figure 2. These settlement plates comprised of a 1.219 mm thick steel circular base plate having a diameter of 50 mm, welded to a rigid steel wire with 2 mm diameter. The dimensions of settlement plates were chosen to minimize disturbance in homogeneity in the soil mass due to base plates as well as to minimize the friction along the wire. The settlement plates were carefully placed so that the bottom plates were horizontal and the wires were kept vertical during filling of the containers. Height of fall during the entire filling process was kept constant to ensure constant compaction energy.

Locations of settlement plates

Name	Horizontal distance from center (x), mm	Vertical distance from top surface (d), mm
A1	75	0
A2	150	0
A3	225	0
B1	75	150
B2	150	150
B3	225	150
C1	75	300
C2	150	300
C3	225	300
D1	75	450
D2	150	450
D3	225	450

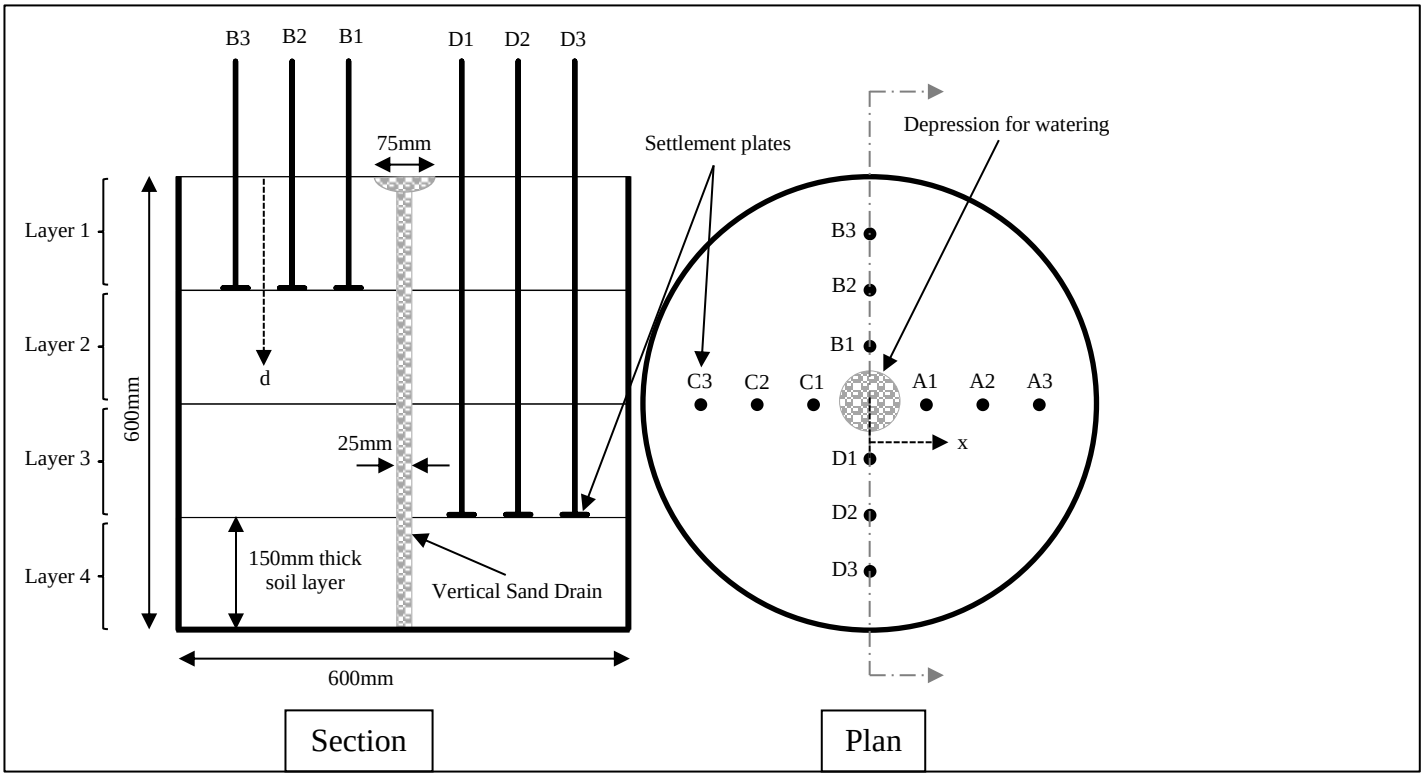

Figure 2. Physical Model with VSD and settlement plates

Providing VSDs

Smooth hollow thin-walled PVC pipes with diameter of 25 mm were utilized to provide VSDs by placing them at the center of the containers during filling. They were ensured to be kept vertical and in position during the entire filling. After filling the containers, these pipes were filled with coarse sand and were pulled out carefully without disturbing the surrounding soil. A bowl-shaped depression with 75 mm diameter, filled with coarse sand as shown in Figure 2 was provided on the top surface of the soil at the center of each physical model for watering. Soil was left in the containers for 24 hours to avoid measuring early settlements due to self-weight of soil mass. After

that water was added slowly in the depressions and was not allowed to flow out of them during the entire wetting process to avoid soil erosion and excessive saturation at the surface.

Applying surcharge loading

A surcharge load of 100 kg/ft^2 or 10.56 kN/m^2 was applied with 314 kg coarse aggregate (25 mm size) on some models before wetting. A steel wire mesh having opening size of 12 mm was used to confine the aggregates above these models. The wire mesh was properly secured in place with diameter equal to that of models. Several PVC pipes with 25 mm diameter were placed so that vertical wires of settlement gauges were kept undisturbed from surcharge. Extra PVC pipes were provided above VSDs and locations where soil samples were to be taken.

Determination of Settlement, Density, Moisture Content and Shear Strength

Soil settlements were measured from the markers drawn on wires welded to the settlement plates by taking measurements with a calibrated scale from a reference beam placed on the top rim of the containers before and after 24 and 48 hours of watering. Each settlement plate was able to provide overall cumulative soil settlement in the underlying layers therefore, individual settlement for each layer was measured by taking differences in the measurements of the settlement plates placed on subsequent layers at the same horizontal distance from center of the container. Bulk density was measured at various locations using a very smooth thin-walled hollow steel tube with sharp edges on the tip having a diameter of 25 mm and provided with longitudinal opening 10 mm from the tip as shown in Figure 3.

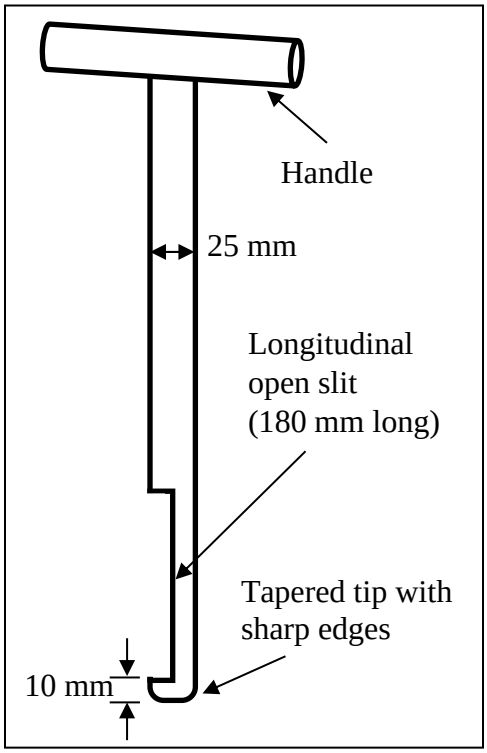

Figure 3. Soil Sampler

The tube was driven 150 mm in a single drive and pulled out to avoid compression in the soil and achieve Sample Recovery Ratio (*SRR*) of more than 95% which is calculated as

$$SRR\ (\%) = \frac{L_r}{L_d} \times 100$$

Where L_r is the length of recovered sample and L_d is the length of steel tube driven in soil in one drive.

After determining the bulk density of the samples, their moisture contents were determined by following the procedure of ASTM D2216. The holes thus formed were carefully filled with the same soil to avoid disturbance in the integrity of soil mass. Shear strength at various locations was determined using a handheld vane shear device by following the standard procedure of ASTM D8121 [19]. All the mentioned parameters were determined after 24 and 48 hours of watering and were recorded along with those determined on control model with no watering.

RESULTS AND DISCUSSIONS

Soil Settlement and Moisture Content

Loose soils having large air voids undergo settlement when subjected to wetting and the amount of moisture governs the extent of settlement i.e., the more the moisture, the more is the settlement except in expansive soils. This trend continues till the saturation of soil mass. Figure 4 shows cumulative settlements recorded from settlement plates placed on top surface of layer 1 and 150 mm thick subsequent layers beneath at horizontal distances of 75 mm, 150 mm and 225 mm from center of the containers.

It has been observed that soil settlements are more pronounced in the models with more quantity of moisture added and, even more settlements in the models, provided with VSDs and applied with surcharge for the same moisture. For example, the settlements in models with 20% moisture (20N, 20D and 20DS) are higher as compared to models with lower moisture such as 10N, 20D and 10DS. Similarly, overall cumulative settlements at a horizontal distance of 150 mm from center are 16 mm for 20N while 30 mm for 20D and 42 mm for 20DS which translates into settlement gain of 87.5% when VSD was provided and 162.5% when VSD along with surcharge loading was used for the same moisture added. This behavior can be attributed to better distribution of moisture due to VSD and increase in mean net stress due to surcharge loading. This is exactly in line with the findings of Sun et al. [13] that wetting induced volumetric changes depend on degree of saturation during wetting and mean net stress exerted on soil mass.

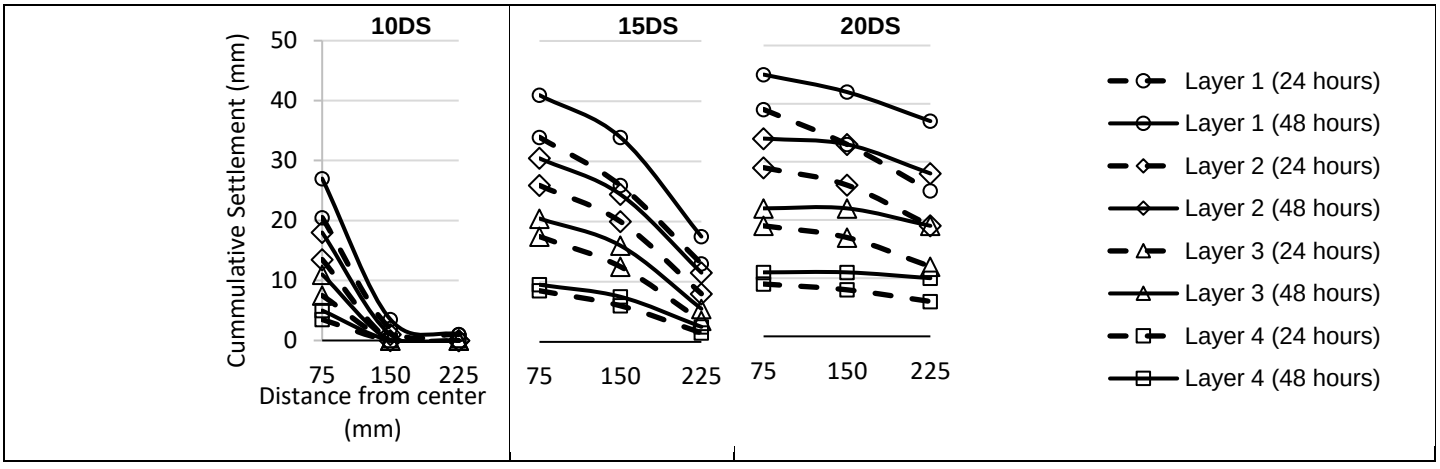

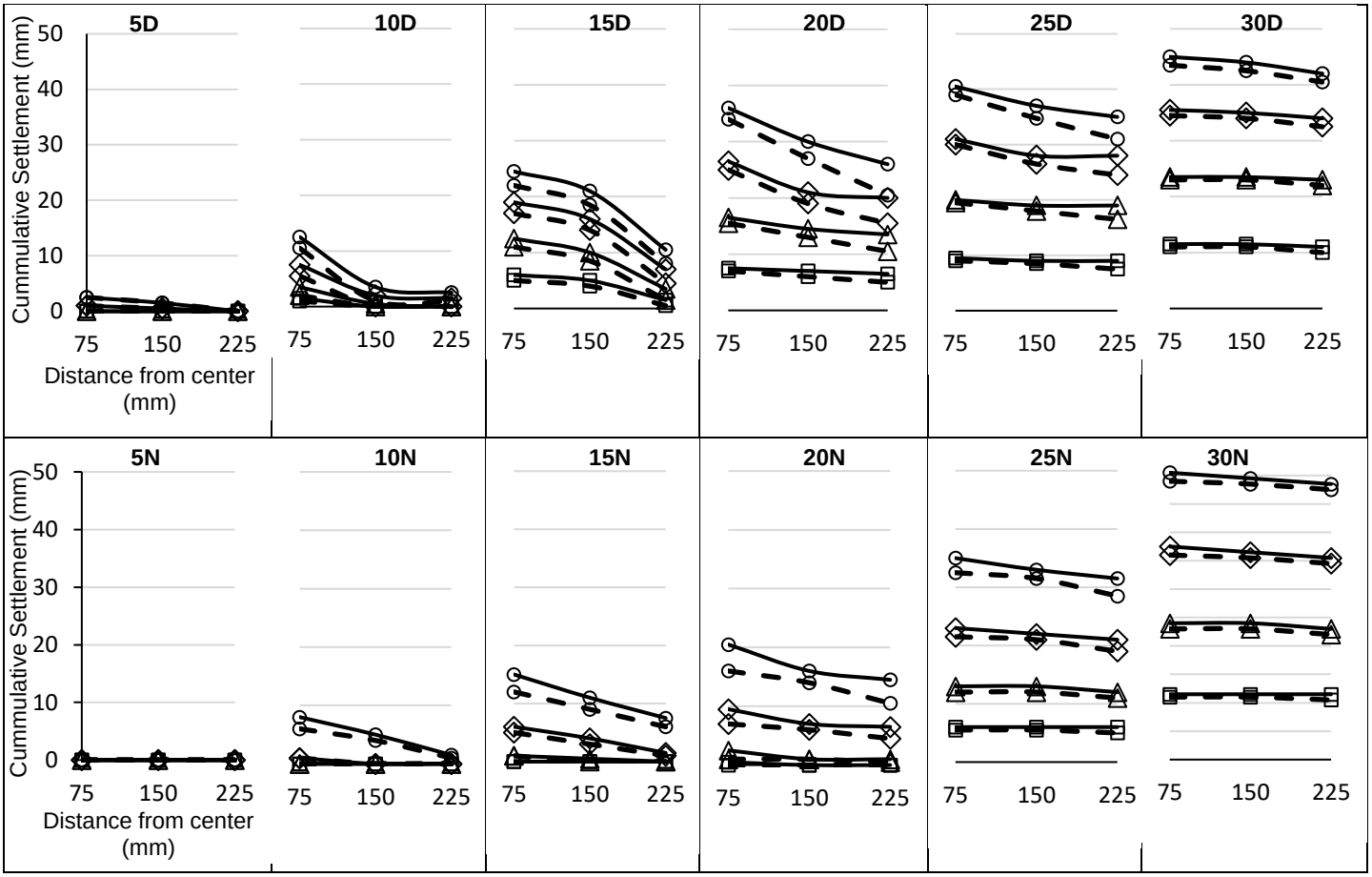

Figure 4. Cumulative settlements at different location

Table 3 shows that soil in upper layers of models without VSDs have undergone more settlements as compared to the subsequent lower layers due to the presence of more moisture while the models with VSDs show uniform settlements among all the layers which indicates better distribution of moisture through the drains. Moreover, settlements are more pronounced in the models with surcharge loading.

Table 10. Settlements in individual layers at various locations

Physical Model	Layer	Settlements in individual layers (mm)					
		After 24 hours			After 48 hours		
		x=75mm	x=150mm	x=225mm	x=75mm	x=150mm	x=225mm
5D	1	1.5	1	0	1.5	1	0
	2	1	0.5	0	1	0.5	0
	3	0	0	0	0	0	0
	4	0	0	0	0	0	0
5N	1	0	0	0	0	0	0
	2	0	0	0	0	0	0
	3	0	0	0	0	0	0
	4	0	0	0	0	0	0
10DS	1	7	2	1	9	2.5	1
	2	6	0	0	7	1	0
	3	4	0	0	6	0	0
	4	3.5	0	0	5	0	0
10D	1	5	1	1	5	1.5	1

	2	3.5	0	0	4	1.5	1.5
	3	1	0	0	2	0.5	0
	4	1	0	0	1.5	0	0
10N	1	5	4	1	7	5	1.5
	2	1	0	0	1	0	0
	3	0	0	0	0	0	0
	4	0	0	0	0	0	0
15DS	1	8	6	5	10.5	9.5	6
	2	8.5	7.5	4.5	10	8.5	6
	3	9	6.5	2	11	8.5	3
	4	8.5	6	1.5	9.5	7.5	2.5
15D	1	5	4.5	3.5	5.5	5	3.5
	2	6	5.5	3	6.5	6	3.5
	3	6	4.5	1	6.5	5	2
	4	5	4	0.5	6	5	1.5
15N	1	7	6	5	9	7	6
	2	4	3	1	5	3.5	1.5
	3	1	0	0	1	0.5	0
	4	0	0	0	0	0	0
20DS	1	10	7	6	11	9	9
	2	10	9	7	12	10	9
	3	10	9	6	11	11	9
	4	9	8	6	11	11	10
20D	1	9	8	5	9.5	9	6
	2	9.5	6	5	10	10	6.5
	3	8.5	7	5.5	9	7.5	7
	4	7	6	5	7.5	7	6.5
20N	1	9	8	6	11	9	8
	2	6	5	4	7	7	5.5
	3	1	1	0.5	2	1	1
	4	0	0	0	0.5	0	0
25D	1	9	8.25	6.5	9.5	9	7
	2	10.5	8.5	8	11	9	9
	3	10.5	9.5	9	10.5	10	10
	4	9	8.5	7.5	9.5	9	9
25N	1	11	10.5	9.5	12	11	10.5
	2	9.5	9	8	10	9	9
	3	6.5	6.5	6	7	7	6
	4	5.5	5.5	5	6	6	6
30D	1	9	8.5	8	9.5	9	8
	2	11.5	11	10.5	12	11.5	11
	3	12	12	12	12	12	12
	4	11	11	10	11.5	11.5	11
30N	1	13	13	13	13	13	13
	2	13	12.5	12.5	13.5	12.5	12.5
	3	12	12	11.5	12.5	12.5	11.5
	4	11	11	10.5	11.5	11.5	11.5

After watering, the soil at the top surface and adjacent to VSDs was observed to be more saturated as compared to rest of the soil in all the models. Figure 5 shows that the moisture in the soil at various locations within the models provided with VSDs like 20D and 25D is more uniformly distributed as compared to the models without VSDs like 20N and 25N respectively. Moreover,

no change in moisture content can be observed in bottom layers of 5D, 10D and 15D which indicates that moisture added in these models is insufficient for wetting of the entire soil mass. Complete saturation of entire soil mass can be seen in 30N and 30D.

Figure 4 and Figure 5 show that more settlements because of higher moisture content can be seen near the center of the models from where watering was done as compared to distant locations. Moreover, more settlements have been observed after 48 hours of watering as compared to 24 hours as wetting proceeded throughout the models. The relationship between moisture content and settlement throughout the entire testing has been found directly proportional as shown in Figure 6.

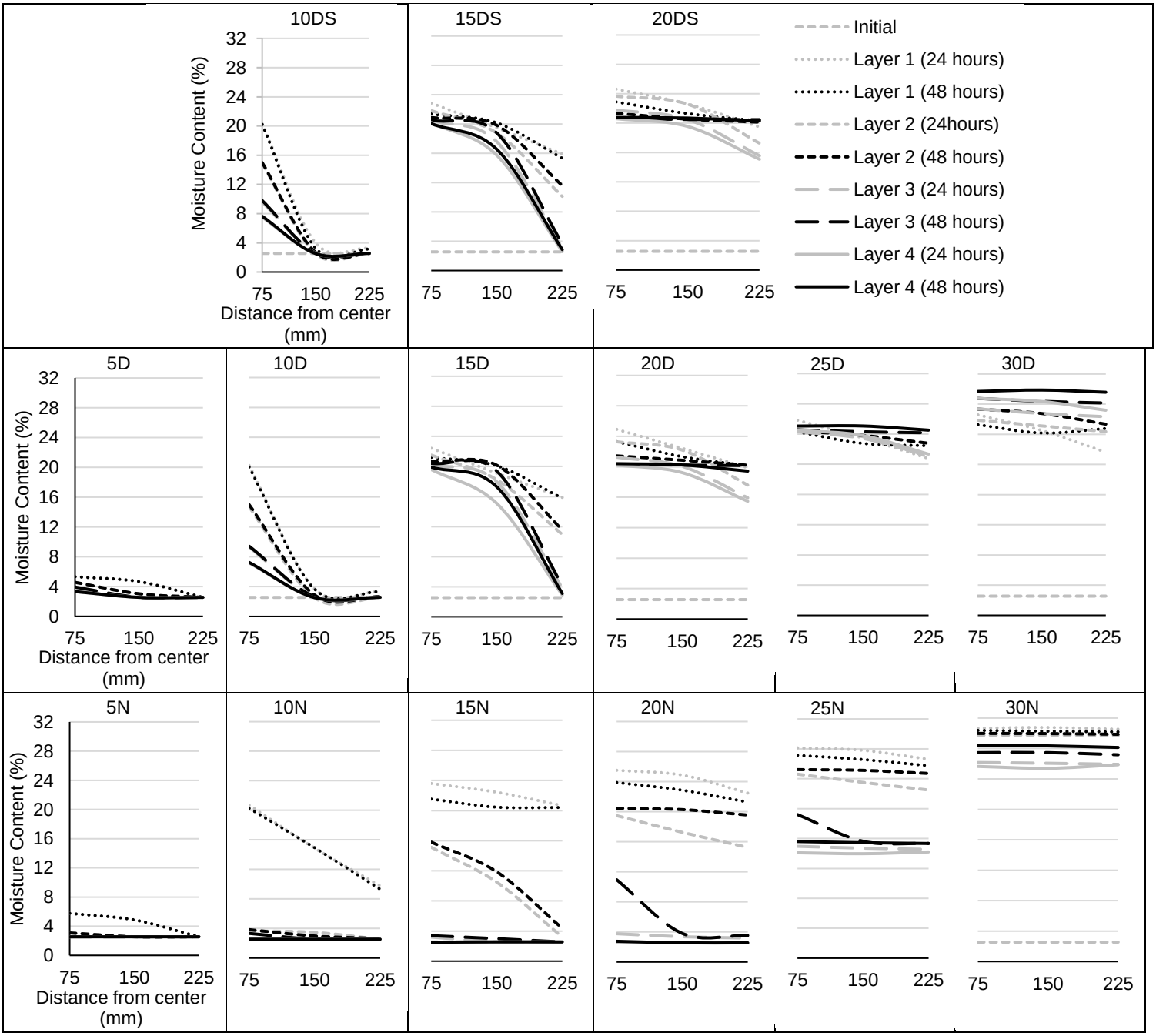

Figure 5. Moisture contents at different locations

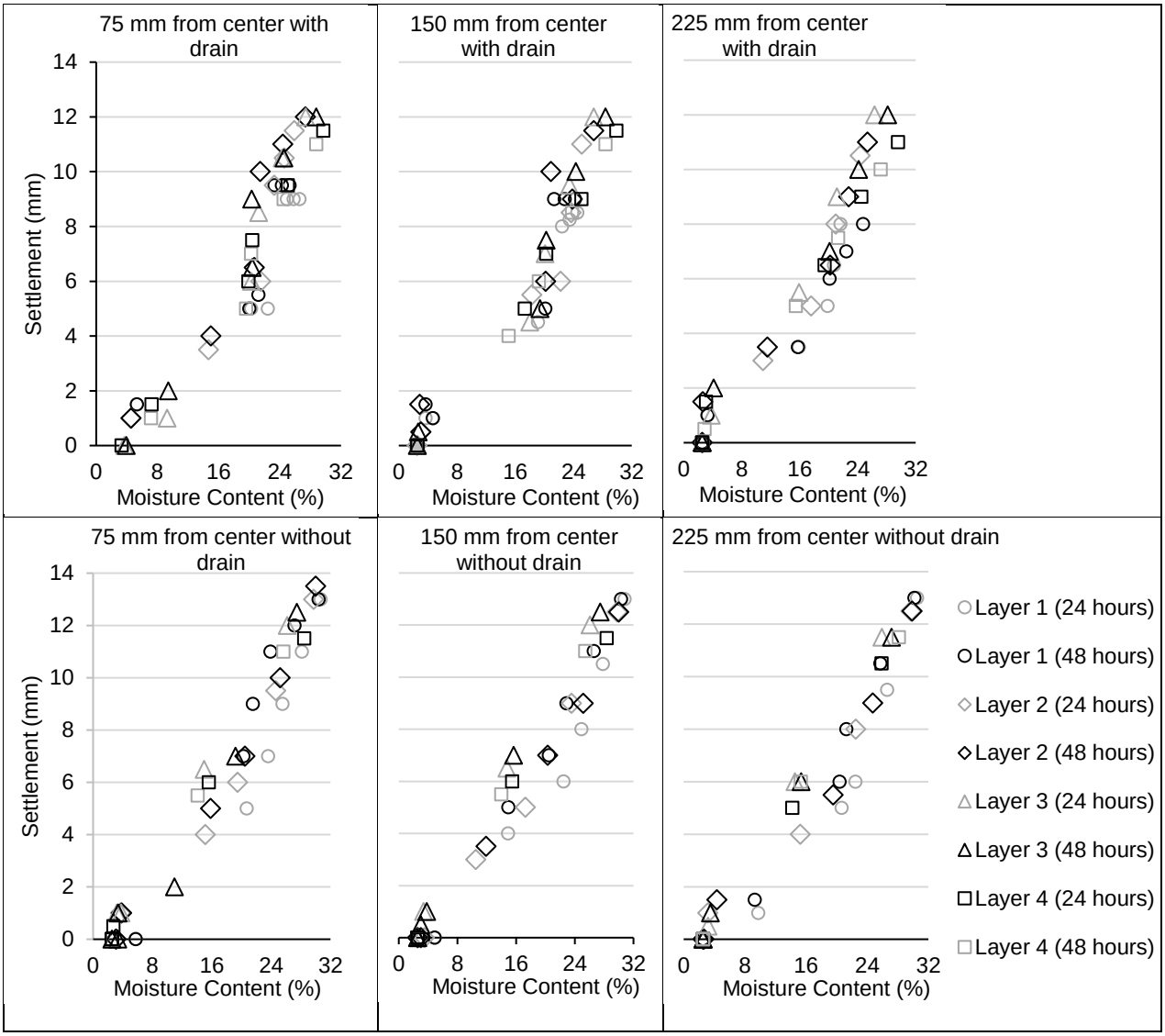

Figure 6. Moisture contents and settlements at different locations

Density

The bulk density of loose soils increases with increase in moisture content during wetting as the voids start filling with water. The initial bulk density of the soil mass before watering was found to be 1.169 g/cm^3. Figure 7 shows that higher bulk densities have been observed in the models with more moisture added. Moreover, soil has been found to be more dense at locations with higher moisture contents. The models with VSDs show more uniform densities among all the layers as compared to the other models because of better distribution of moisture and the models with surcharge loading showed even more densities for the same moisture added.

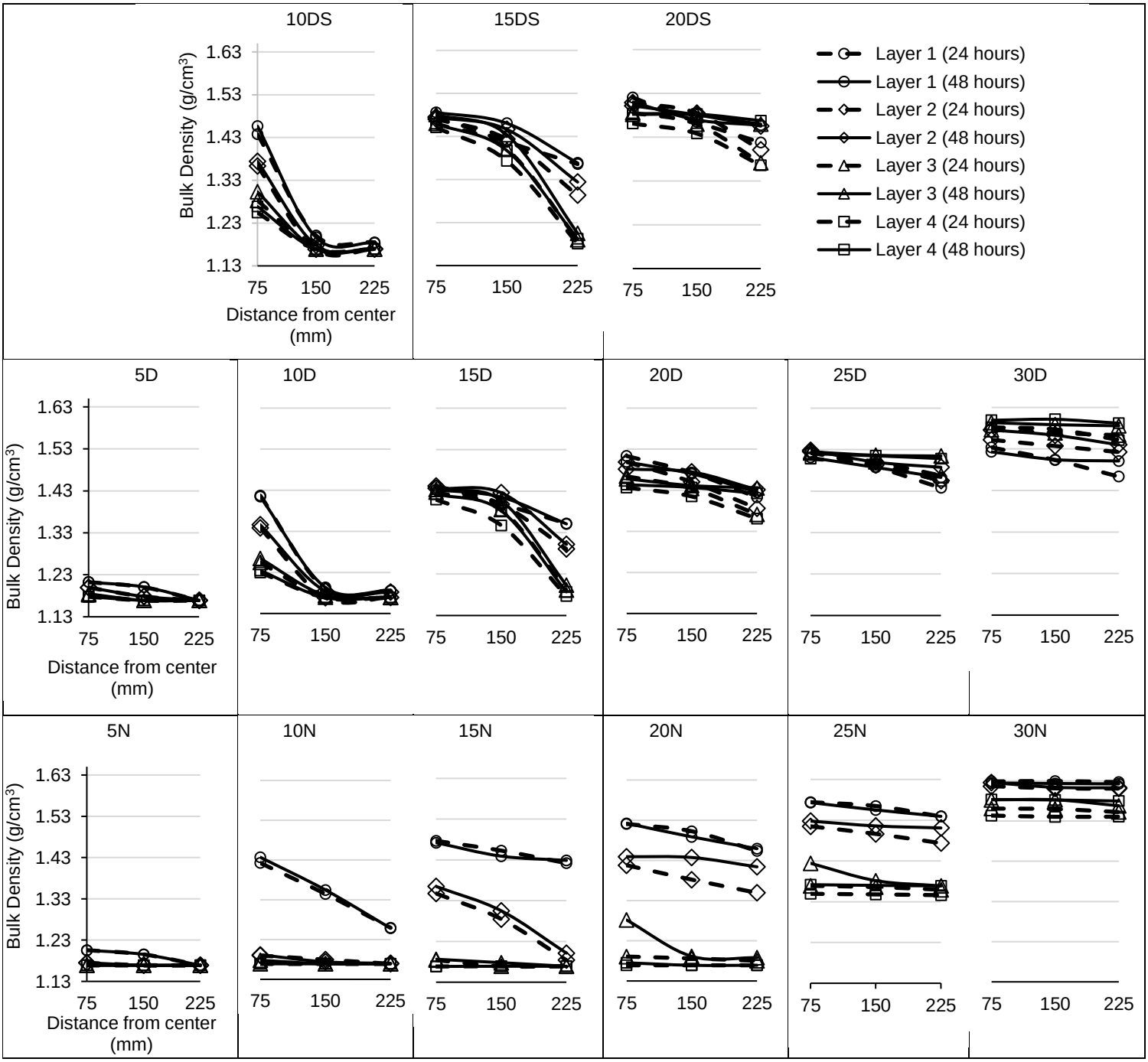

Figure 7. Bulk densities at different locations

Shear Strength

Shear strength in homogeneous soils increases with increase in depth because of higher total stress due to overlaying mass. Similar increase in shear strength has been observed during experimentation. Figure 8 shows the variation of shear strength at different locations in the models after 24 and 48 hours of wetting. These shear strengths have been compared with that of control model which have been shown as initial shear strengths before watering.

The performance of VSDs can be judged from higher and uniform gains in shear strength by the soil in the models with VSDs as compared to the models without them. Overall higher shear

strengths can be seen in models with VSDs like 5D, 10D, 15D and 20D which increased further with time, as compared to 5N, 10N, 15N and 20N, respectively. Moreover, even higher gains in shear strength can be observed in the models with VSDs and surcharge loading like 10DS, 15DS and 20DS. Very low and non-uniform gain in shear strength can be observed in 5N, 10N, 15N and 20N which is more pronounced with the passage of time, in all layers except for top layers where increase in shear strength is observed. The remaining models without VSDs exhibited overall decrease in shear strength which further diminished with time.

Here it is pertinent to note that an overall increase in shear strength has been detected in models 10D, 15D and 20D with increase in quantity of added moisture during watering. The soil in these models gained even more strength with time. The increments in strength were more amplified when surcharge loading was applied as shown by 10DS, 15DS and 20DS. The gain in shear strength in 5D, 10D and 15D is subsequently lower as compared to 20D which is due to inadequate addition of moisture in former models. The model 20DS showed highest gains in shear strength as compared to all the models. Moreover, shear strength in models 25D and 30D can be seen declining with increase in moisture added during wetting when compared with 20D. This can be attributed to the presence of excess moisture which collapsed the soil skeleton of unsaturated soils and lubricated individual particles. Therefore, the quantity of moisture added in 20D seems to be optimum to gain highest shear strength in the soil within a model.

The shear strength of bottom most layer of 20N after 48 hours remained unchanged from its initial value of 170 kPa because moisture could not reach there while the shear strength from the same location of 20D was 260 kPa showing an increment of 53%. Similarly, the shear strength of the soil at the same location of 20DS was 325 kPa which is 91% higher as compared to the initial value before watering.

The shear strengths observed at various locations in all the models have been plotted against the corresponding moisture contents at those locations in Figure 9. The soil in all the layers gained strength with increase in moisture content up to a value of ω = 16-17% after which further increase in moisture resulted in lower strengths and after ω = 20%, the soil started losing its shear strength.

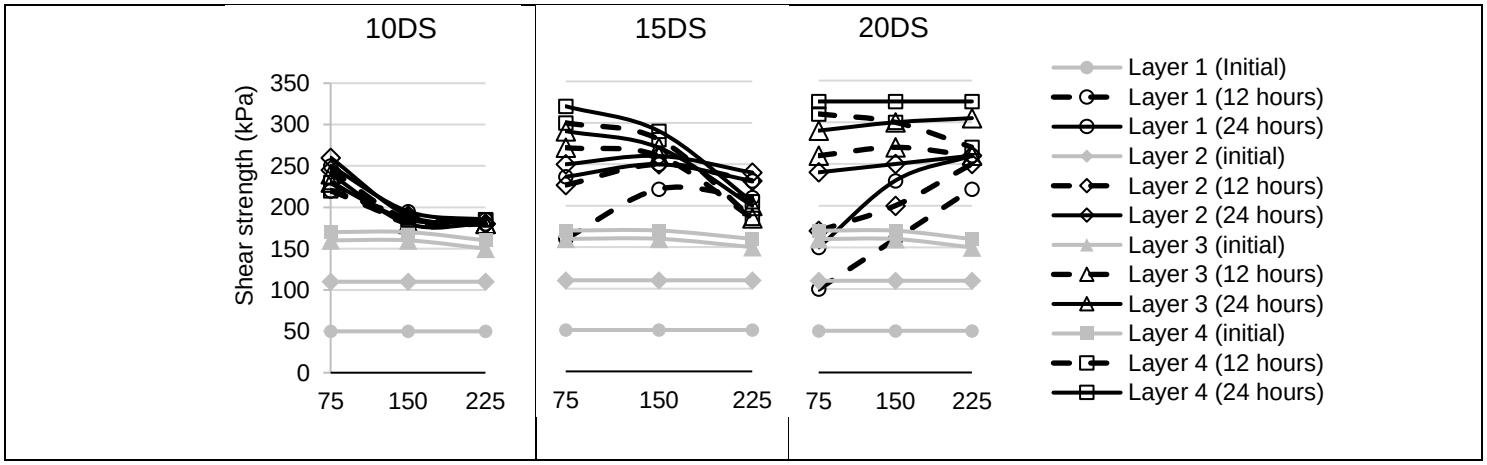

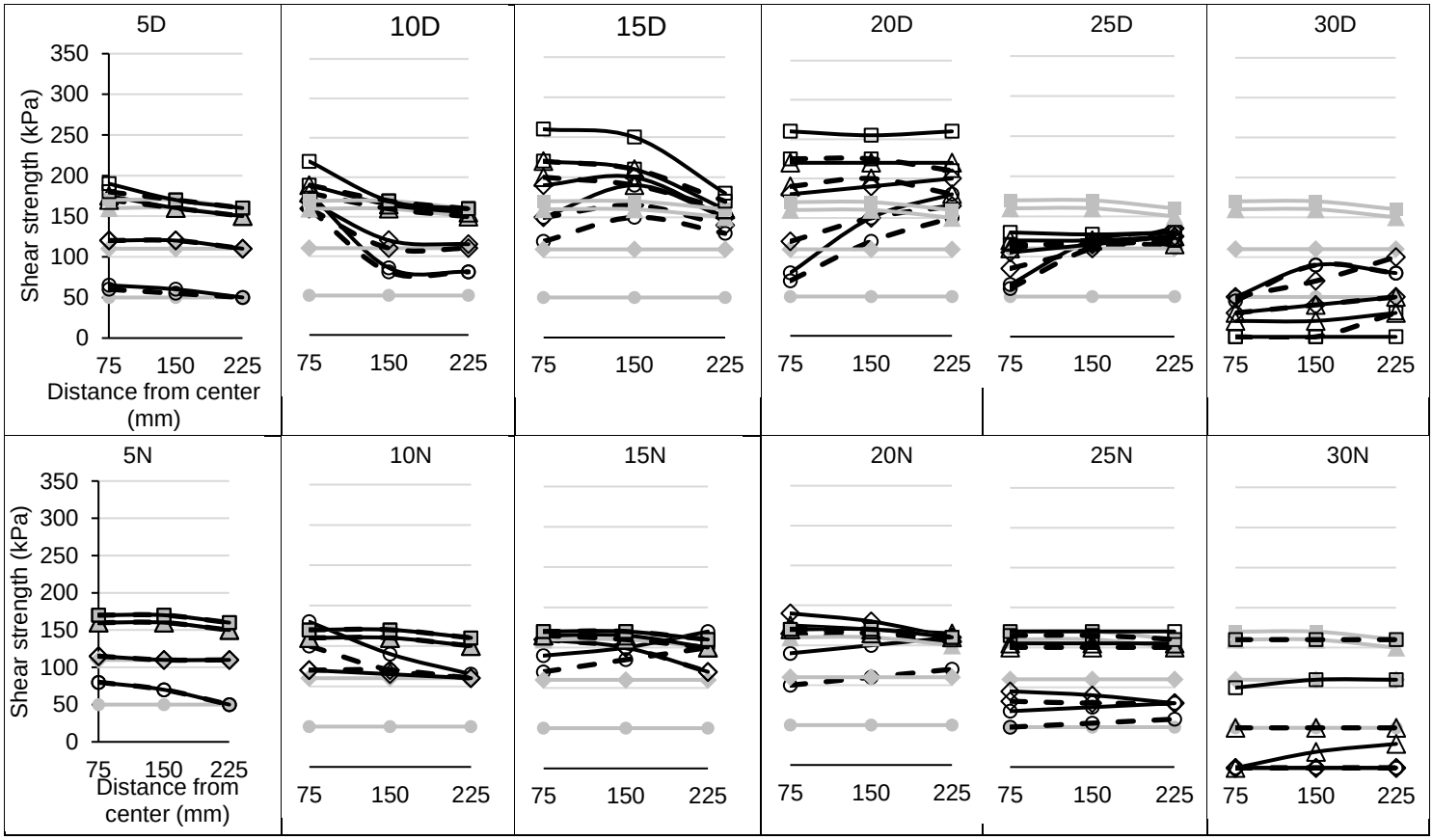

Figure 8. Shear strength at different locations

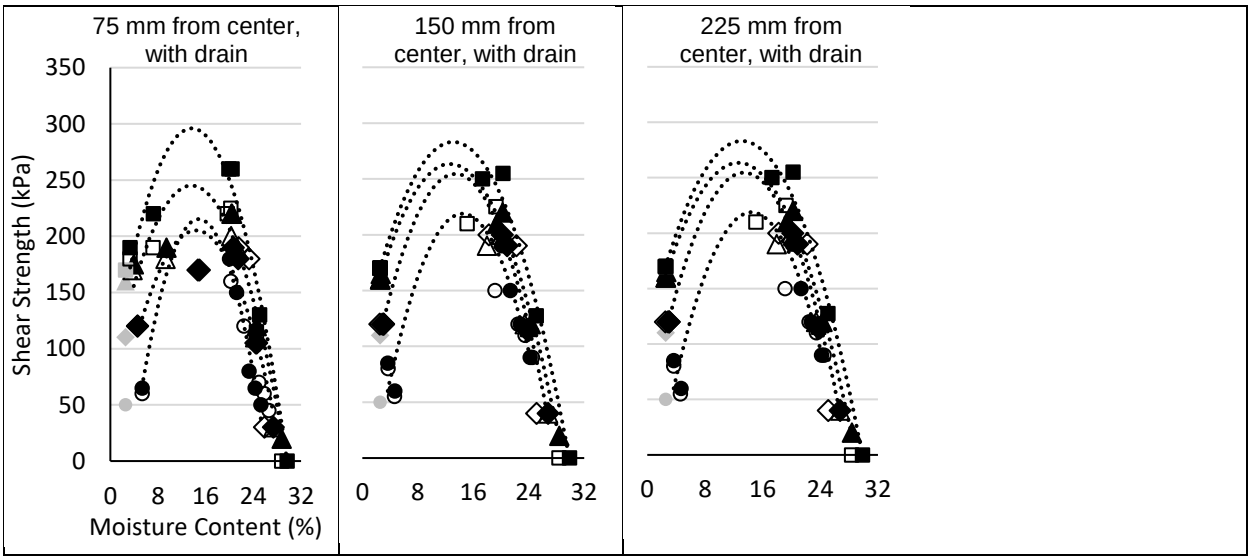

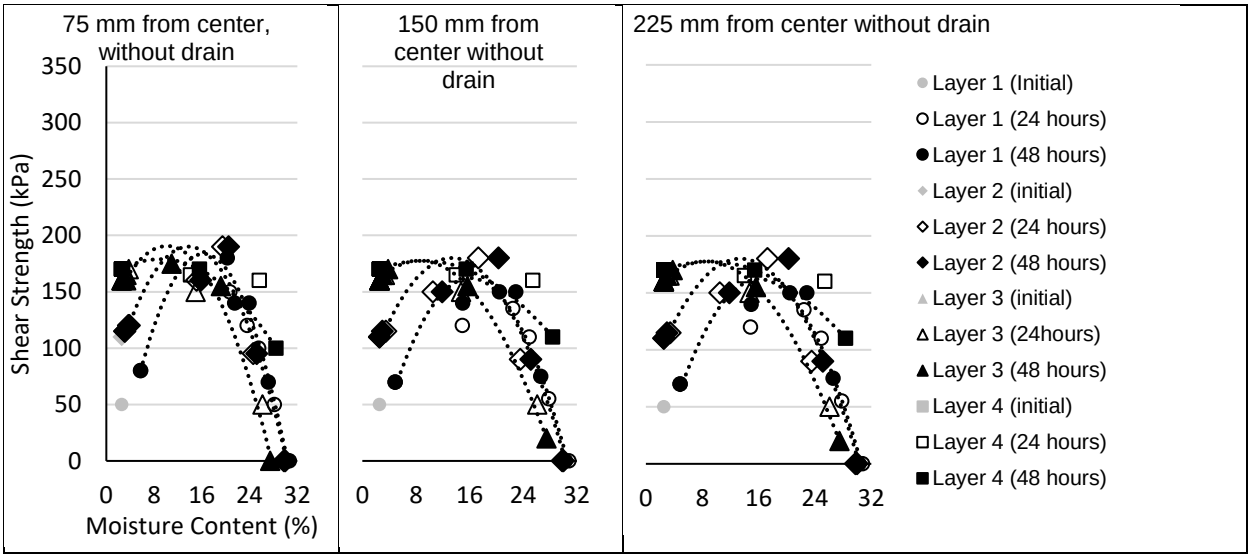

Figure 9. Shear strength and moisture contents at different locations

CONCLUSIONS

In this paper, the effect of moisture content, vertical sand drains and surcharge loading on shear strength, settlement, and densification of loose unsaturated soil at various depths and lateral distances is presented. The possibility of using VSDs along with surcharge loading have important implications for sustainable infrastructure development by achieving enhanced shear strength and maximum pre-construction settlements upon wetting. The following conclusions can be drawn from this research.

- The installation of VSDs result in uniform distribution of moisture in the soil, and hence consequently uniform and higher soil settlements in the entire soil mass.
- Installation of VSDs result in homogeneous increase of shear strength in the entire soil mass up to a certain moisture content, followed by a rapid decrease with further addition of moisture. This optimum percentage of moisture as obtained from laboratory testing was found to be in the range of 16 to 17% for different combinations. This optimum percentage of moisture was observed in 20% addition of water case (20D & 20DS), making them as best performing models.
- For best performing models, it was observed that shear strength for bottom most layer after 48 hours was increased up to 53% by using VSD. Whereas, under the combined effect of VSD and surcharge, this increase was observed up to 91% compared to model without VSD.
- For same best performing models, at a horizontal distance of 150mm from center of model, cumulative settlements for top surface after 48 hours of watering was increased up to 87.5% by using VSD and 162.5% under the combined effect of VSD and surcharge showing better densification of soil mass.

Funding

This research did not receive any funding from any institute.

Acknowledgement

The experimentation for this research has been conducted in Geotechnical Engineering Laboratory of University of Engineering and Technology, Taxila, Pakistan. The findings and outcomes of this experimental work are specific to the testing and laboratory conditions used in the study and may not necessarily apply to different field conditions or other types of soils. Further research with different testing conditions and comparison with other studies is needed to fully understand the behavior of unsaturated loose soils.

References

1. Sassa, K., et al., *Earthquake-induced-landslides: distribution, motion and mechanisms.* Soils and Foundations, 1996. 36(Special): p. 53-64.
2. Zhang, S., et al., *Assessment of risks of loose landslide deposits formed by the 2008 Wenchuan earthquake.* Natural Hazards & Earth System Sciences, 2012. 12(5).
3. Fredlund, D.G. and H. Rahardjo, *Soil mechanics for unsaturated soils*. 1993: John Wiley & Sons.
4. Casagrande, A., *Liquefaction and cyclic mobility of sands: a critical review.* Harvard soil mechanics series, 1976. 88.
5. Sladen, J., R. D'hollander, and J. Krahn, *The liquefaction of sands, a collapse surface approach.* Canadian geotechnical journal, 1985. 22(4): p. 564-578.
6. Ishihara, K., *Liquefaction and flow failure during earthquakes.* Geotechnique, 1993. 43(3): p. 351-451.
7. Yamamuro, J.A. and P.V. Lade, *Steady-state concepts and static liquefaction of silty sands.* Journal of geotechnical and geoenvironmental engineering, 1998. 124(9): p. 868-877.
8. Alonso, E.E., A. Gens, and A. Josa, *A constitutive model for partially saturated soils.* Géotechnique, 1990. 40(3): p. 405-430.
9. Maatouk, A., S. Leroueil, and P. La Rochelle, *Yielding and critical state of a collapsible unsaturated silty soil.* Géotechnique, 1995. 45(3): p. 465-477.
10. Wheeler, S. and V. Sivakumar, *An elasto-plastic critical state framework for unsaturated soil.* Géotechnique, 1995. 45(1): p. 35-53.
11. Cui, Y. and P. Delage, *Yielding and plastic behaviour of an unsaturated compacted silt.* Géotechnique, 1996. 46(2): p. 291-311.
12. Ng, C.W. and A.C. Chiu, *Laboratory study of loose saturated and unsaturated decomposed granitic soil.* Journal of Geotechnical and Geoenvironmental Engineering, 2003. 129(6): p. 550-559.
13. Sun, D.a., D. Sheng, and Y. Xu, *Collapse behaviour of unsaturated compacted soil with different initial densities.* Canadian Geotechnical Journal, 2007. 44(6): p. 673-686.
14. Lawton, E.C., R.J. Fragaszy, and M.D. Hetherington, *Review of wetting-induced collapse in compacted soil.* Journal of geotechnical engineering, 1992. 118(9): p. 1376-1394.
15. Rehman, M.U., *Geotechnical problems of residential soils in undulating topograpy* in *Civil Engineering Department*. 2018, University of Engineering and Technology, Taxila: Taxila.
16. ASTM, *Standard Test Methods for Liquid Limit, Plastic Limit, and Plasticity Index of Soils*, in *ASTM D4318-17e1*. 2017, ASTM International: West Conshohocken, PA.
17. ASTM, *Standard Test Methods for Laboratory Determination of Water (Moisture) Content of Soil and Rock by Mass*, in *ASTM D2216-19*. 2019, ASTM International: West Conshohocken, PA.
18. ASTM, *Standard Test Methods for Specific Gravity of Soil Solids by Water Pycnometer*, in *ASTM D854-14*. 2014, ASTM International: West Conshohocken, PA.

19. ASTM, *Standard Test Method for Approximating the Shear Strength of Cohesive Soils by the Handheld Vane Shear Device*, in *ASTM D8121 / D8121M-19*. 2019, ASTM International: West Conshohocken, PA.

2nd International Conference on Advances in Civil and Environmental Engineering (ICACEE-2023)

University of Engineering & Technology Taxila, Pakistan

Conference date: 22nd and 23rd February, 2023

Laboratory Reproduced Weathering of Soft Rocks and Its Application for Risk Assessment

Haseeb Yaqoob[1], Naveed Ahmad[2], Muhammad Junaid Riaz[3], Maryem Naeem[4], Tasawar Abbas[5]

[1]University of Engineering and Technology, Taxila, Pakistan, haseebyaqoob101@gmail.com
[2]University of Engineering and Technology, Taxila, Pakistan, naveed.ahmad@uettaxila.edu.pk
[3]University of Engineering and Technology, Taxila, Pakistan, maryemnaeem950@gmail.com
[4]University of Engineering and Technology, Taxila, Pakistan, mjunaidriaz59@gmail.com
[5]University of Engineering and Technology, Taxila, Pakistan, tasawarabbas121@gmail.com

ABSTRACT

Weathering of rocks is a natural phenomenon followed by disastrous events like slide, flow, topple, creep, spread, etc. Considering the considerable loss of life and property, it has become a crucial need of time to know rate of weathering and resulting strength loss for indigenous rocks. The purpose of this study was to characterize the weathering cycle of Murree for laboratory reproduced weathering (one cycle of accelerated weathering in laboratory represent weathering in one year in natural conditions) of indigenous rock samples and find out the rate of strength degradation. The indigenous samples of sandstone were collected from Murree formations. Taking into consideration the local climatic conditions, the physical weathering cycle was broken into saturation, freezing, thawing, heating, and cooling phases. Uniaxial compression test was performed after the completion of each weathering cycle and found out that there is a significant impact of weathering on strength properties of sandstone. Sandstone is present in Murree at variable depths and it is clearly visible on exposed slopes of valley side therefore, it is very important to know the rate of strength degradation with weathering in areas like Murree.
KEYWORDS: Sandstone, Weathering, Laboratory Reproduced Weathering, Murree

INTRODUCTION

Till now paramount research has been done on physical weathering of rocks as physical conditions can be more conveniently reproduced and controlled in the laboratory. These conditions are also much close to the real conditions prevailing in the field unlike chemical weathering that is difficult to replicate. Different researchers have studied weathering phenomenon by applying different process on rocks like Freeze-Thaw, Heat-Cool and Wet components of weathering cycle. The purpose of this study was to use the phases of weathering cycle which completely represents the Murree weather conditions and then study the effect of weathering on the rocks present in Murree formation.

It was observed that there are basically three major processes that necessarily contribute to overall physical weathering, namely freezing - thawing, heating - cooling, and wetting – drying, which completely represent the overall climate cycle with frost weathering being the most dominant factor of weathering against the other two. The porosity of the samples increased with increasing weathering cycle. The strength of sandstone was dominantly reduced due to freeze-thaw cycles as compared to heat-cool, wet-dry cycles.[1]

The effect of frost weathering on hard intact rock was investigated by using samples of fine sandstone and coarse sandstone. It was concluded that, the triaxial compressive strength of the two sandstones decreases with an increase in freeze-thaw cycles under the same confining pressure. [2]

METHODOLOGY

Sampling

The purpose of this study is to investigate the principal cause of disastrous events i.e landslides specially in Murree. Therefore, an accessible location is selected in Murree formation located near Lower Topa, Murree. Drilling in rock has been done with the help of straight rotary rig and rock cores have been obtained with the help of double/tripple tube core barrel. During the drilling process, sufficient sandstone specimens were collected.

Figure 1: Straight rotary rig during the drilling process

Sample Preparation

During the drilling process, collected rock samples are varied in lengths due to the presence of joints and fissures. These specimens are then modified in a way that their l/d ratio set to 2.

Weathering Cycle Phases

To reproduce physical weathering in laboratory, five (05) Phases of weathering are defined by considering the environmental conditions from past historical data of Murree.

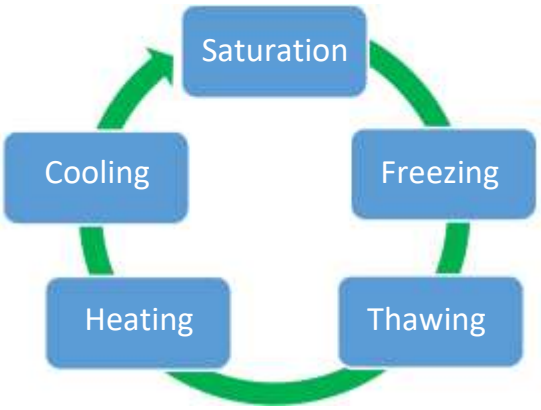

Figure 2: Phases of weathering cycle

Based on the findings of various experimental studies, Selected duration of different phases of weathering cycle are as follows.[3]

Table 1: Duration for different phases of Weathering Cycle

Weathering phases	Sandstone
Saturation	11 hours 19 min
Freezing	2 hours13 min
Thawing	1 hour 15 min
Heating	10 hours 40 min
Total Time for one complete weathering cycle	25 hours 27 Minutes

Test Procedure

To study the effects of weathering on strength degradation of sandstone, 14 weathering cycles were performed on sandstone. Unconfined Compression test were performed using compression testing machine of 5000 KN capacity on intact rock sample and after the completion of every weathering cycle. No of weathering cycles is restricted to 14 due to time constrained.

Figure 3: Uniaxial compression testing on specimens

RESULTS AND DISCUSSION

Effect of Weathering on Strength Properties of Rocks

Intact rock sample of sandstone shows 44.55 MPA strength in its natural state but it is observed that there is a significant drop in strength with the increase in no of weathering cycles and there is a sharp drop in strength in first two weathering cycles due to the development of micro cracks.

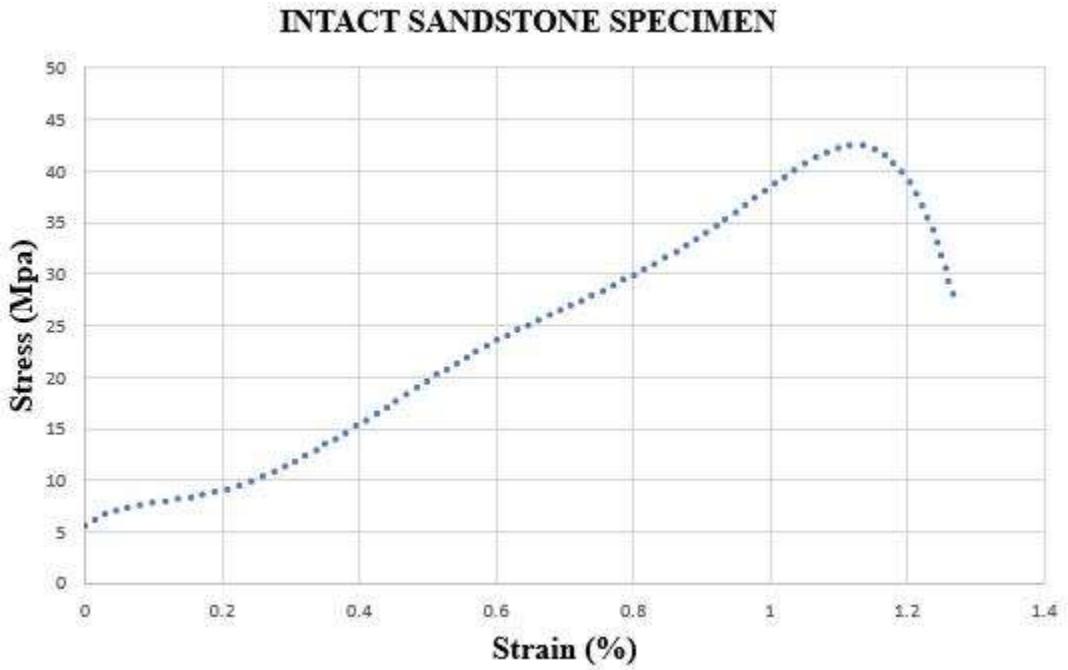

Figure 4: Stress strain relation of intact rock specimen

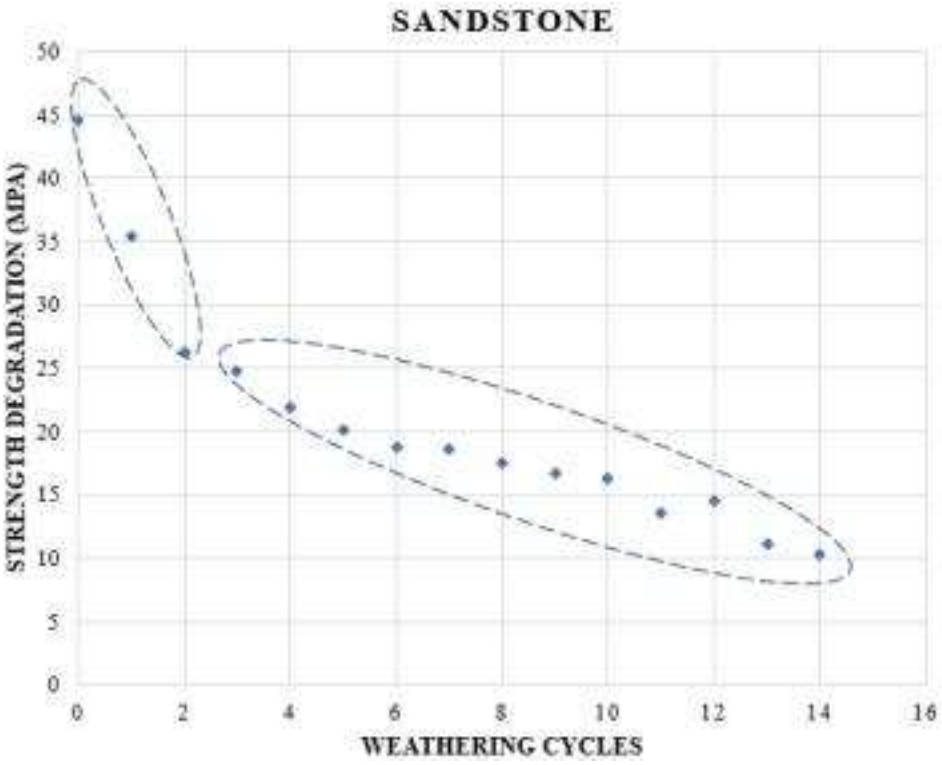

Figure 5: Strength degradation with respect to weathering cycles of sandstone

CONCLUSIONS

Intact rock sample (zero weathering cycle) of sandstone shows 44.55 MPA strength but it reduced to 10.33 with the application of just 14 weathering cycles. The rate of strength reduction was higher during first two cycles followed by gradual decrease in strength. Knowing the rate of strength reduction with weathering is extremely important in determining the stability of slopes especially in areas like Murree.

REFERENCES

1. Hale, P. A., & Shakoor, A. (2003). A laboratory investigation of the effects of cyclic heating and cooling, wetting and drying, and freezing and thawing on the compressive strength of selected sandstones. *Environmental & Engineering Geoscience*, *9*(2), 117-130.
2. Liping, W., Ning, L., Jilin, Q., Yanzhe, T., & Shuanhai, X. (2019). A study on the physical index change and triaxial compression test of intact hard rock subjected to freeze-thaw cycles. *Cold Regions Science and Technology*, *160*, 39-47.

3. Yaqoob, H,. Naeem, M,. Riaz, M, J,. Ahmad, N,. Maqsood, Z,. (2022). Characterization of weathering cycles for laboratory reproduced accelerated weathering of soft indigenous rocks. *International Conference on Recent Advances in Civil Engineering and Disaster Management, 397-402.*
4. Hamzaban, M. T., Büyüksağiş, I. S., Touranchehzadeh, A., & Manafi, M. (2021). The
Effect of Heat Shocks and Freezing–Thawing Cycles on the Mechanical Properties of Natural Building Stones. *Journal of Modern Mechanical Engineering and Technology*, *8*, 76-100.
5. Khan, A. N. (2001). Impact of landslide hazards on housing and related socio-economic characteristics in Murree (Pakistan). *Pakistan Economic and Social Review*, 57-74.
6. Khan, A. N. (1995). Landslide Hazards and Policy-Response in Pakistan: A Case Study of Murree. *Commission on Science and Technology for Sustainable Development in the South*, *35*.
7. Lamp, J. L., Marchant, D. R., Mackay, S. L., & Head, J. W. (2017). Thermal stress weathering and the spalling of Antarctic rocks. *Journal of Geophysical Research: Earth Surface*, *122*(1), 3-24.
8. Li, H., Xu, G., Luo, J., Zhou, Y., & Jiang, X. (2021, October). Effect of Freeze-thaw Cycles on Microstructure and Mechanical Properties of Limestone. In *IOP Conference Series: Earth and Environmental Science* (Vol. 861, No. 2, p. 022058). IOP Publishing.
9. Liu, X., Wang, Z., Fu, Y., Yuan, W., & Miao, L. (2016). Macro/microtesting and damage and degradation of sandstones under dry-wet cycles. *Advances in Materials Science and Engineering*, *2016*.
10. Mutlutürk, M., Altindag, R., & Türk, G. (2004). A decay function model for the integrity loss of rock when subjected to recurrent cycles of freezing–thawing and heating– cooling. *International journal of rock mechanics and mining sciences*, *41*(2), 237-244.

2nd International Conference on Advances in Civil and Environmental Engineering (ICACEE-2023)

University of Engineering & Technology Taxila, Pakistan

Conference date: 22nd and 23rd February, 2023

Understanding the impacts of land use and climate changes in the Simly Dam watershed

Muhammad Shahid[1], Muhammad Waseem[2] , Hamza Farooq Gabriel[3], Sajjad Haider[4]

[1]Department of Civil Engineering, University of Engineering and Technology, Lahore, 54890, Pakistan, m.shahid@uet.edu.pk

[2]Center of Excellence in Water Resource Engineering, University of Engineering and Technology, Lahore, 54890, Pakistan, dr.waseem@uet.edu.pk

[3,4]NUST Institute of Civil Engineering (NICE), NUST-H12 Islamabad Hamza.gabrieal@nice.nust.edu.pk, haidersajjad5@gmail.com

ABSTRACT

The present study is an attempt to quantify the impacts on land use and climate changes on water resources of the Islamabad, Capital of Pakistan. The annual trends of three variables precipitation, temperature and surface runoff has been evaluated during 1983-2012. Two conceptual hydrological models namely Chaudhry Yang equation and Climate elasticity method have been used to perform the analysis. The Man-Kendall and Pettitt's tests have been applied to the selected variables during the study period. Man-Kendall test indicated that at significant level of 0.05 the trend in annual precipitation and runoff decreases while annual temperature showed an increasing trend. The Pettitt's test showed a change point for the runoff series at 1997 and based on this change runoff series have been divided into pre-change (1983-1997) and post-change period (1998-2012). The results from Chaudhry-Yang equation and Climate elasticity method showed that land use change was the major factor for runoff variations in Simly catchment, with a contribution of 52% while the contribution of climate change is 48%. For sustainable management of the water resources it is recommended that integrated watershed management should be practiced in the study area.

KEYWORDS: Sustainable water resources**,** Climate change, Land use change, Runoff, Simly

INTRODUCTION

Water is necessary for survival of every living thing on the earth. It is limited and due to urbanization, agriculture activities this resource is under serious threat. The demand for water resources is increasing worldwide which leads toward water scarcity. Due to hydrological cycle, climatic and geographical conditions there is a gap between demand and supply in water resources of Pakistan [1]. Sixty eight percent of Pakistan has annual rainfall less than 250 millimetres (mm), twenty four percent receives 250-500 mm and only eight percent exceeds 500 mm. Water resources planning and management in arid and semi-arid region is essential for food production and ecosystem functioning [2]. The analysis and quantification of regional hydrological cycle is necessary to deal

with water resources management issues. Since beginning of 20th century the variability of global precipitation has increased. Decreasing trends in rainfall have been observed in coastal areas and arid plains of Pakistan[3]. Mostly water for domestic, industrial and agricultural use is obtained from runoff. What can be effect of change in annual average precipitation of a catchment on runoff? This question attracted attention of hydrologist and water resource managers for the last fifty years [4]. Runoff of a catchment depends upon the topography, geology, metrology, land use and hydrological cycle of the catchment. The metrological factors govern weather and climate of a catchment which determine their variations. The topography and geology remain unchanged within time scale of interest to hydrologist. Land use and human activities affect the runoff of a catchment. More over due to rising temperature pattern of precipitation changed which affected runoff in rivers [5]. Understanding of past hydrological trends is important to predict future changes. There are many methods proposed by researchers to distinguish the impact of climate change and human activities on runoff. Hydrological modelling and sensitivity analysis is used in this regard. This approach cannot be applied due to some reasons. Firstly, it is difficult to understand biological process at a catchment scale, secondly too many parameters calibration may be needed and thirdly field data with fine resolution may not be available. Therefore, this study applied conceptual hydrological models which have less data requirements and are suitable for data scare regions. The study has been carried out in the watershed of the Simly lake and study area is presented in the Figure 1.

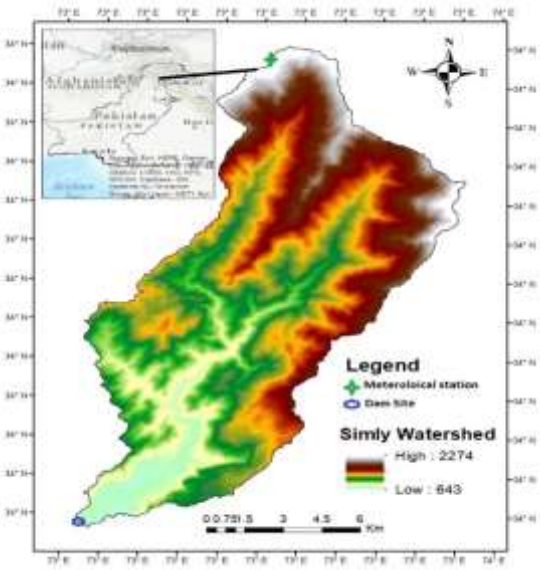

Figure 1: Location map of the study area.

MATERIALS AND METHODS

The topographic, hydrological and metrological data were collected and processed as follows: The digital elevation model (DEM), ASTER GDEM 30 obtained from global topography data base was used to simulate catchment topographic information. For flow measurement the gauging station is located about 5 miles upstream of Simly lake and it is known as Chinot gauging station. The flow data for the period 1983-2012 was collected from CDA (Capital Development Authority). The Simly catchment lies in north of Islamabad and Murree, there is only one meteorological station installed within the Simly catchment named Murree observatory. The other meteorological station which is installed near the Simly lake site is named Islamabad Zero pint observatory. The both stations rainfall and temperature data for the period 1983-2012 was obtained from PMD. As the Simly catchment lies in Islamabad and Murree so the average of both stations rainfall and temperature data was used to perform analysis. The potential evapotranspiration (PET) was calculated using FAO Penman-Monteith equation as referred by [6]. The procedure for calculation of PET with limited data was adopted as stated in [7]. The potential Evapotranspiration data of Islamabad and Murree was computed and then averaged to get the potential Evapotranspiration of catchment area). In this study the Mann-Kendall (MK) test [8] has been used it is a non-parametric test mostly used for trend identification in time series [9-10]. This test is applicable for non-normally distributed data which is mostly used in hydrology and climatology. The Budyko frame work [11] deals the partitioning of precipitation (P) between evapotranspiration (Eo) and runoff (R) as functional balance between water supply and demand. It is an excellent tool used to evaluate the relations between climate, catchment properties and the hydrological cycle . Choudhury-Yang equation is used in this study [12-13]. The Chaudhry-Yang equation can be written as:

$$E = \frac{P\mathrm{E0}}{(\mathrm{P^n}+\mathrm{E0^n})^{\frac{1}{n}}} \quad (1)$$

In this equation "n" represents the catchment properties such as soil properties, slope, vegetation curve, and climate seasonality [14] it is assumed that change in parameter "n" is due to human activities in catchment area. If P, Eo and R are given "n" can be estimated. It is assumed that runoff can be expressed as function of precipitation, potential evapotranspiration and catchment properties.

R = f (P, PET, Catchment properties) (2)

This equation can be rewritten and following equation can be drawn:

$$\mathrm{R} = \mathrm{P} - \frac{P\mathrm{E0}}{(\mathrm{P^n}+\mathrm{E0^n})^{\frac{1}{n}}} \quad (3)$$

$$dR = \frac{\partial R}{\partial P}dP + \frac{\partial R}{\partial Eo}dEo + \frac{\partial R}{\partial n}dn \quad (4)$$

$$\frac{\partial R}{\partial P} = 1 - \frac{E}{P}\left(\frac{E^n}{P^n+Eo^n}\right) \quad (5)$$

$$\frac{\partial R}{\partial Eo} = -\frac{P^{n+1}}{(P^n+Eo^n)^{\frac{n+1}{n}}} \quad (6)$$

$$\frac{\partial R}{\partial n} = -\frac{E}{n}\left(\frac{ln(P^n+Eo^n)}{n} - n\frac{(P^n \ln P + Eo^n \ln Eo)}{P^n+Eo^n}\right) \quad (7)$$

It can be concluded from equation 2:
Robs1=Rsim1=f(P1,PET1,n1)
Robs2= Rsim2=f(P2,PET2,n1)
dR=Robs2-Robs1 (8)
Where dR is the total change in runoff and according equation 11 it can be separated into climate and land use changes where:
ΔRclimtae=Rsim2-Robs1
ΔRlanduse=Robs2-Rsim2
The second method used for this study is known as climate elasticity method and its detailed description is given in Hu at al., 2012

Trends in Hydro-climatic variable

The changes in hydro-metrological variables are shown in Figure 2. This shows that precipitation has observed significant decline after 1997 and runoff is also consistent with it. The results of the trend analysis are presented in the Table1:

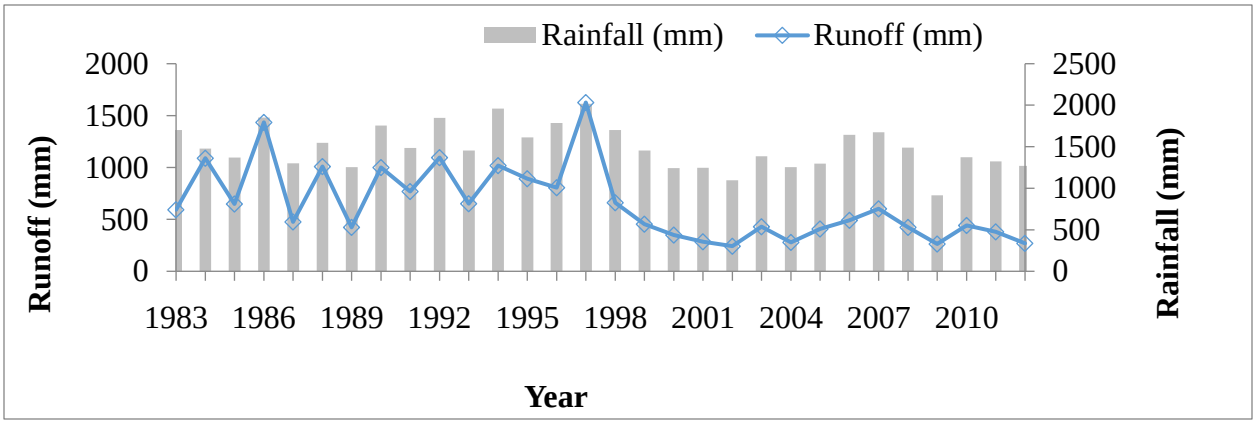

Figure 2: Annual Precipitation and Stream flow in Simly catchment

Table 1: Trend analysis of the hydro-meteorological series at the 0.05 significance level

Series	ZMK	Trend
Runoff	-3.5	⇩
Precipitation	-1.89	⇩
Temperature	3.5	⇧

These results indicated a decreasing trend in the annual runoff at 0.05 significant level, while the annual average temperature indicated an increasing trend at 0.05 significant level. The annual average

precipitation also presented decreasing trend at 0.05 significant level. The Pettit test for homogeneity at 0.05 significant level indicated significant abrupt change in runoff and changing point occurred in 1998 as shown in Figure 3:

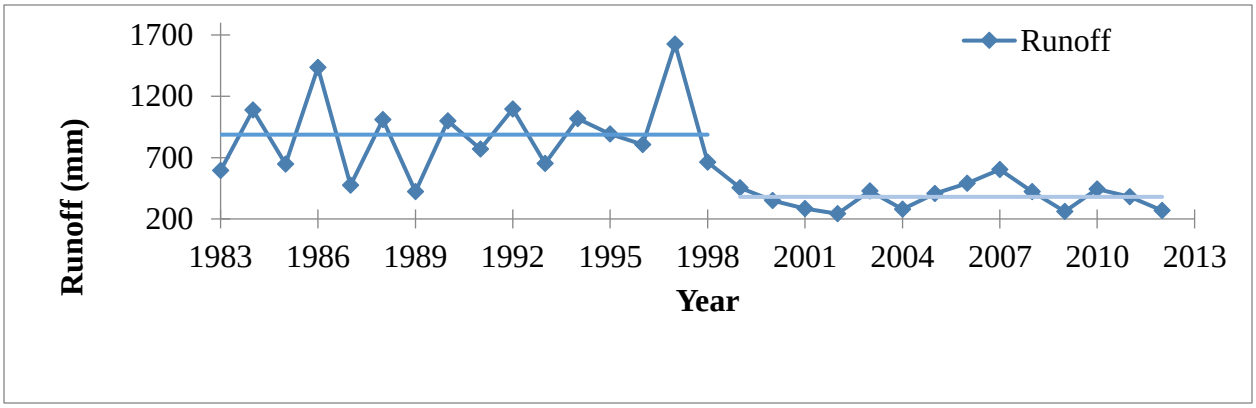

Figure 3 Pettit test for Runoff in Simly catchment

According result of homogeneity test the study period was divided into two periods, the period before the change point was regarded as period-1 (1983-1997) and the period after change point was regarded as period-2 i.e. (1998-2012). The mean annual runoff, precipitation and potential evapotranspiration were calculated for 1983-1997 (period-1) and 1998-2012 (period-2). The catchment properties 'n' for period-1 and period-2 were computed using Chaudhry-young equation. Then the change in precipitation, (dP), change in potential evapotranspiration (dEo) and change in catchment properties (dn) between period 1 and period 2 were computed the results are presented in Table 2.

Table 2: Mean annual water budget estimates during period1 and period 2

Water budget component Period 1	Water budget component Period 2	Difference
P 1 = 1628 mm	P 2 = 1358 mm	dP = -270 mm
R1 = 902 mm	R2 = 399 mm	dR = -503 mm
E01 = 1144 mm	E02 =1219 mm	dEo = 75 mm
n1 = 1.13	n2 = 2.4	dn = 1.27

The change in runoff dR as a function of climate change (P, Eo) and catchment properties (n) can be calculated using equations. if the values of sensitivity coefficients are known. During study period (1983-2012) the change in precipitation (dP), change in evapotranspiration (dEo) and change in land use parameter (dn) are presented in *Table 2*. Using equation (10a, 10b, 10c) and information in Table 3 the sensitivity coefficients were computed for Simly catchment which are: $\partial R/\partial P$= 0.77 , $\partial R/\partial Eo$= -0.42 ,and $\partial R/\partial n$= -203.87

By substituting the values of sensitivity coefficients and (dP), (dEo) and (dn) in equation 10 the total change in Simly catchment runoff dR during the study period (1983-2012) is given as:

$dR=0.77dP-0.42dEo-203.87dn$

dR= -498.33 mm where dR is the total change in Runoff and can be divided into climate and land use changes as:

$\Delta Rclimtae=0.77(-270)-0.42(75) = -239.4$

Similarly: $\Delta Rlanduse= -258.9$

Using equations runoff (Rsim1=901.80 and Rsim2=662.43) for period-1and period-2 were simulated. The runoff change due to climate change and land use change can be partitioned as:

ΔR climate =Rsim2-Robs1

= 662.43- 902

= -239.57

ΔR landuse =Robs2-Rsim2

=399 – 662.43 = -263.43

These relative contributions can be presented as given in the Figure 4

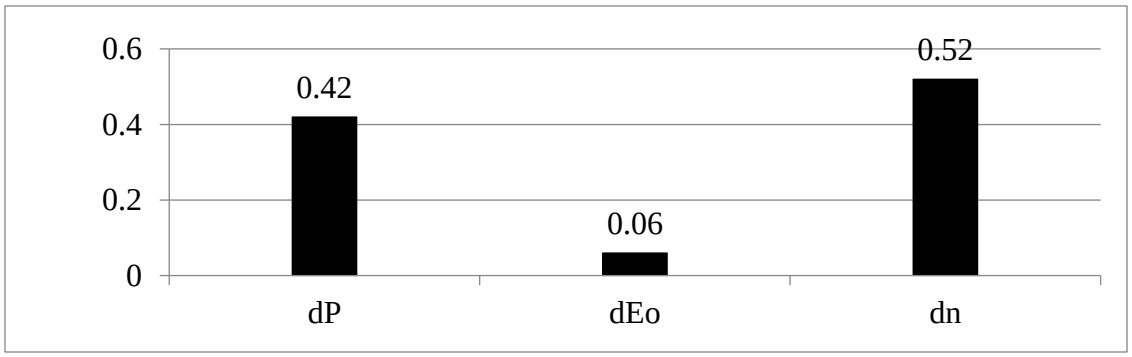

Figure 4 Relative contributions of Climate change and Land use change

CONCLUSION

The annual trends of three variables precipitation, temperature and surface runoff has been evaluated during 1983-2012. Two conceptual hydrological models namely Chaudhry Yang equation and Climate elasticity method have been used to perform the analysis. The results from Chaudhry-Yang equation and Climate elasticity method showed that land use change was the major factor for runoff variations in Simly catchment, with a contribution of 52% while the contribution of climate change is 48%.

ACKNOWLEDGEMENTS

This study has been funded by Higher Education Commission of Pakistan under China Pakistan Economic Corridor (CPEC) Grant number HEC-CPEC Project No. 161.

REFERENCES

1. Deal, J. The Nutmeg's Curse: Parables for a Planet in Crisis by Amitav Ghosh. Georgetown Journal of International Affairs, 2022. **23**(1):p. 128-131.
2. Farrokhzadeh, S., Hashemi Monfared, S. A., Azizyan, G., Sardar Shahraki, A., Ertsen, M. W., & Abraham, E. Sustainable water resources management in an arid area using a coupled optimization-simulation modeling. Water, 2020. **12**(3): p.885.

3. Hussain, A., Cao, J., Ali, S., Muhammad, S., Ullah, W., Hussain, I.,& Zhou, J. Observed trends and variability of seasonal and annual precipitation in Pakistan during 1960–2016. International Journal of Climatology, 2022. **42**(16) p.8313-8332
4. Roderick, M. L., and Farquhar, G. D. A simple framework for relating variations in runoff to variations in climatic conditions and catchment properties, Water Resour. Res.,2011 **47**,
5. Tabari, H. Climate change impact on flood and extreme precipitation increases with water availability. Scientific reports, 2020. **10**(1): p. 1-10.
6. Onoz, B., Bayazit, M.. The Power of Statistical Tests for Trend Detection. Turkish Journal of Engineering & Environmental Sciences 2012. **27** (203) p.247 – 251
7. Allen, R.G., Pereira, L.S., Raes, D., Smith, M. Crop evapotranspiration guidelines for computing crop water requirements FAO Irrigation and drainage paper 56. Food and Agriculture Organization, Rome 1998.
8. Shahid, M., Cong, Z., & Zhang, D. Understanding the impacts of climate change and human activities on streamflow: a case study of the Soan River basin, Pakistan. Theoretical and Applied Climatology,2018. **134**(1):p. 205-219
10. Love, D., Uhlenbrook, S., Twomlow, S., and Van der Zaag, P. Changing hydro-climatic and discharge patterns in the northern Limpopo Basin, Zimbabwe. Water SA 2010. **36**(3)
11. Hu, Y., Maskey, S., Uhlenbrook, S, and Zhao, H. Streamflow trends and climate linkages, in the source region of the Yellow river, China. Hydrological processes, 2011. **21**, p.2124-2134.
12. Choudhury, B.J. Evaluation of an empirical equation for annual evaporation using field observations and results from a biophysical model. J. Hydrol.1999. **216**, 99–110.
13. Yang, H. B., D. W. Yang, Z. D. Lei, and H. M. Lei , Derivation and validation of watershed coupled water-energy balance equation at arbitrary time scale , J. Hydraulic Eng, 2008. **39**(5), 610–617.

2nd International Conference on Advances in Civil and Environmental Engineering (ICACEE-2023)

University of Engineering & Technology Taxila, Pakistan

Conference date: 22nd and 23rd February, 2023

Analytical and Numerical Validation of the Drop Length of Nappe Flow

K.D.C.R. Dissanayaka[1], Norio Tanaka[2], Md. Kamrul Hasan[1]

[1] Graduate School of Science and Engineering, Saitama University, charitha871@gmail.com

[2] International Institute for Resilient Society, Saitama University, tanaka01@mail.saitama-u.ac.jp

ABSTRACT

Flow over an embankment creates nappe flow downstream when an embankment slope starts to erosion downstream, and the slope becomes steep. Coastal embankments play a vital role in controlling the tsunami flow surge/coastal flood discharge. In this research, a fixed bed model has been used with a different geometric setup over the crest of the embankment, including lowering the slope of the downstream surface to investigate the nappe flow formation. Referencing the experimental setup, developed an analytical method and numerical simulation by using the OpenFOAM software to validate the nappe flow trajectory drop length (L_d). In this CFD (Computational Fluid Dynamics) application, flow phenomena were solved by the finite element method, and the free surface fluctuations were captured using the VOF (Volume of Fluid Method). The $k-\omega$ SST turbulence model was used for the CFD simulation. CFD simulation results were compared with the available experimental and analytically obtained results for validation.

KEYWORDS: embankment, nappe flow, drop length, CFD, VOF, OpenFOAM, $k-\omega$ *SST*

INTRODUCTION

An embankment or dike in a coastal region may be overtopped and breached when a tsunami run-up/ flood discharge exceeds the designed high flood level. This overtopping flow has the potential to do significant damage in the downstream region. Tsunami causes a lot of damage like coastal structure failure, inflicting devastation on society and as well as over property [1-2]. Few of the structures may collapse for various reasons, including the fact that they can only remain within the established safety margins and/or are prone to degradation [3]. Due to the inundated flow currents caused by the 2011 Great East Japan Tsunami (GEJT) created wide, scoured holes near the toe of the coastal embankment, and the downstream surface slope was completely damaged. According to the post-tsunami survey in the Tohoku region, Japan, identified slope collapsing of coastal embankments, with scour holes spanning more than 20 meters in width [4-5]. Meanwhile, when head-cut migration begins, then the embankment overtopping flow forms a nappe flow towards downstream, which is responsible for the erosion of the embankment structure [6]. This overtopping flow from an embankment created a pond downstream due to the fluid circulation between the impact point of the falling jet with the bottom surface of the channel and the downstream surface of the embankment. Several researchers have identified by both the approach of experimentally and numerically about the overtopping flow over the broad-crested weirs in their studies [7-8]. The *RNG* $k-\varepsilon$ and $k-\omega$ *SST* models had the best performance over capturing of the free surface profile of the numerical simulation

of flow over the broad crested weir [9-10]. Therefore, the goal of this case study is to experimentally determine the nappe flow impinging jet physical properties while changing the overtopping depth, downstream surface slope, and crest geometry of a coastal embankment. Finally, based on the analytical and numerical approach, validated the experimental findings of the nappe flow drop length (L_d) for the cases considered.

MATERIALS AND METHODS

Experimental Setup and Initial Conditions

A laboratory experiment consisting of a non-erodible embankment model (EM) with a horizontal crest (EM_{HC}) was conducted in a glass-sided experimental flume that is 6.25m in length, 0.5m in width, and 1.2m in height, with a horizontal bed in the Saitama University, Japan [12]. The schematic diagram of the experimental setup is shown in Figure 1. The current study aimed to classify the flow conditions of the nappe flow and its properties when the downstream surface slope angle has changed in 5^o intervals up to the vertical position with the crest orientation of the EM. The effect of the orientation of the EM crest was investigated, with a (+)4% ascending slope (EM_{AC}) and (-)4% descending (EM_{DC}) slope (δ) towards the downstream. In Figure 1(b), the EM model setup for the (+)4% ascending (EM_{AC}) slope and (-)4% descending (EM_{DC}) slope were indicated by using dashed lines. All the experiments were conducted on a smoothly coated wooden bed to reduce the surface tension effects and replicate the existing conditions of the coastal embankment as they usually follow surface erosion protective measures. Weir was installed at downstream of the experimental setup used to create a plunge pool to identify the depth of water below the nappe bottom surface (h_p) when the jet of the nappe hit on the downstream surface following overtopping.

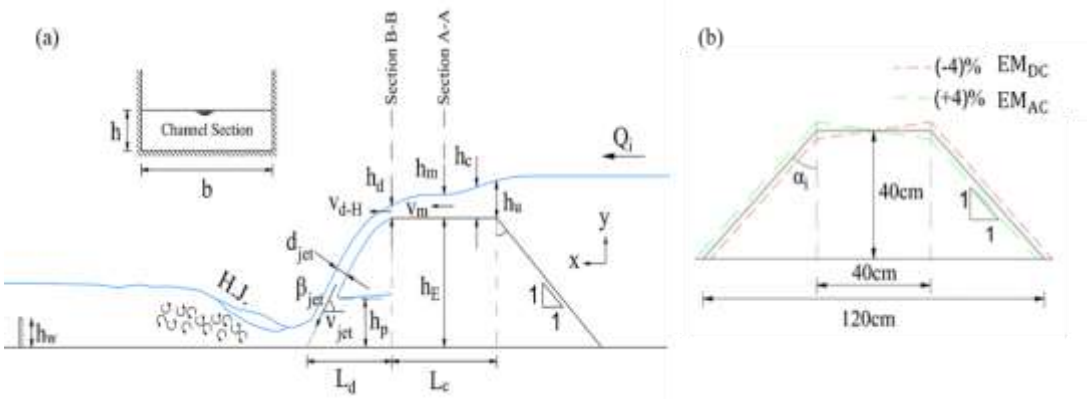

Figure 2: Schematic diagram of the experimental setup. (a) side view, (b) embankment crest slope arrangement. N.B. h_E: height of the embankment, h_d, h_m, h_u: depth of water at downstream brink edge, mid-section, and upstream brink edge over the EM crest, respectively, h_c: critical water depth, v_m, v_{d-H}: flow velocity at mid-section and downstream brink edge over the EM crest, h_p: pool water depth below the nappe bottom surface, d_{jet}: thickness of the nappe jet, v_{jet}: velocity of the nappe jet, β_{jet}: angle of the nappe jet,

which was measured concerning the vertical axis, h_w: height of the weir, α_i: downstream surface slope angle measured with respect to the vertical axis

The overtopping depth of the initial case was measured at the mid-section of the embankment with a horizontal crest (EM_{HC}) while keeping the upstream and downstream surface slopes equal to 1:1. The final overtopping depths were set as 2.0 cm, 3.0 cm, 4.0 cm, 5.0 cm, and 6.0 cm, while the equivalent Froude numbers for the initial overtopping depths recorded at the mid-section over the embankment crest were 0.928, 1.040, 1.084, 1.095, and 1.086, respectively.

Numerical Simulation and the Boundary Conditions

The overtopping flow over the coastal embankment was simulated numerically using the OpenFOAM [13]. The recorded data from the experiment were used to validate the numerical simulation results [12]. Geometry was created in the Salome open-source model builder, and CFD results were extracted using ParaView, an open-source CFD visualizer. The refinement region was used in the meshing to define finer mesh over the embankment crest and nappe flow region to capture the nappe trajectory successfully. The $k-\omega\ SST$ turbulence model was used to simulate the flow, which was a two-equation model consisting of a turbulence kinetic energy (k) and the turbulence dissipation rate (ω) with shear stressed transport terms [13]. Details of the governing equations, turbulence model, and the algorithm details can be found in the OpenFOAM User's Guide [13]. Referring to Figure 1(a), the numerical domain boundary conditions were applied. The flow depth at the upstream boundary of the embankment was divided into two parts, water, and air, with the inlet velocity boundary condition used for them. The upper boundary of the simulation domain was set as an atmospheric pressure boundary condition, and the zero-gradient boundary condition was chosen for the outlet in the simulation domain [7,9-10]. A no-slip boundary condition was used for the bed and the walls in the numerical domain. In addition to the above boundary conditions, the atmospheric pressure boundary condition was applied on the slopping downstream wall of the embankment from crest level to the free surface of the plunge pool to simulate the nappe impinging jet.

Development of an Analytical Relationship

Flow structures of the overtopping flow over the embankment in this study were similar to the flow over a broad-crested weir. This flow structure was analyzed by using the one-dimensional momentum equations and Newton's laws of motion in the smooth prismatic channel [11]. Primarily concerned about the drop length (horizontal distance between the nappe flow impinging jet impact point and the downstream brink edge of the crest) (L_d) of the nappe trajectory at the centerline. To derive an analytical relationship, the momentum equation was applied between the mid-stream section of the EM and the downstream brink section of the EM crest. Referring to Figure 1(a), to develop the following analytical equation applied the conservation of momentum in the x-direction between the sections of A-A and B-B. Finally, Equation (1), given the drop length (L_d) of the nappe trajectory.

$$L_d = 2.12 C_L \sqrt{h_c(h_E + 0.33 h_c)} \quad (1)$$

Where, C_L is the correction coefficient of a drop length used to compensate for the effects of the assumptions and the geometrical variations considered when conservation of momentum principles are applied. Value of C_L would be fixed with respect to the trial and error method.

RESULTS AND DISCUSSION

Impinging Jet Velocity and Total Head Loss

Figure 2 shows the numerical simulation results of the nappe flow trajectory for the three considered cases of EM with a horizontal crest (EM_{HC}), (+)4% ascending crest (EM_{AC}), and (-)4% descending crest (EM_{DC}) for when the overtopping depth equals to 6.0cm as described in the sub-chapter 2.1. As shown in Figure 2, when the crest geometry was changed, the velocity of the impinging jet of the nappe flow changed. At the jet impact location downstream, velocity was increased in the EM_{DC} case than in the EM_{HC} and EM_{AC} cases. But in the EM_{AC} case velocity of the impinging jet is lowered at the impact location due to the crest geometry, and jet thickness is also reduced than the other two cases.

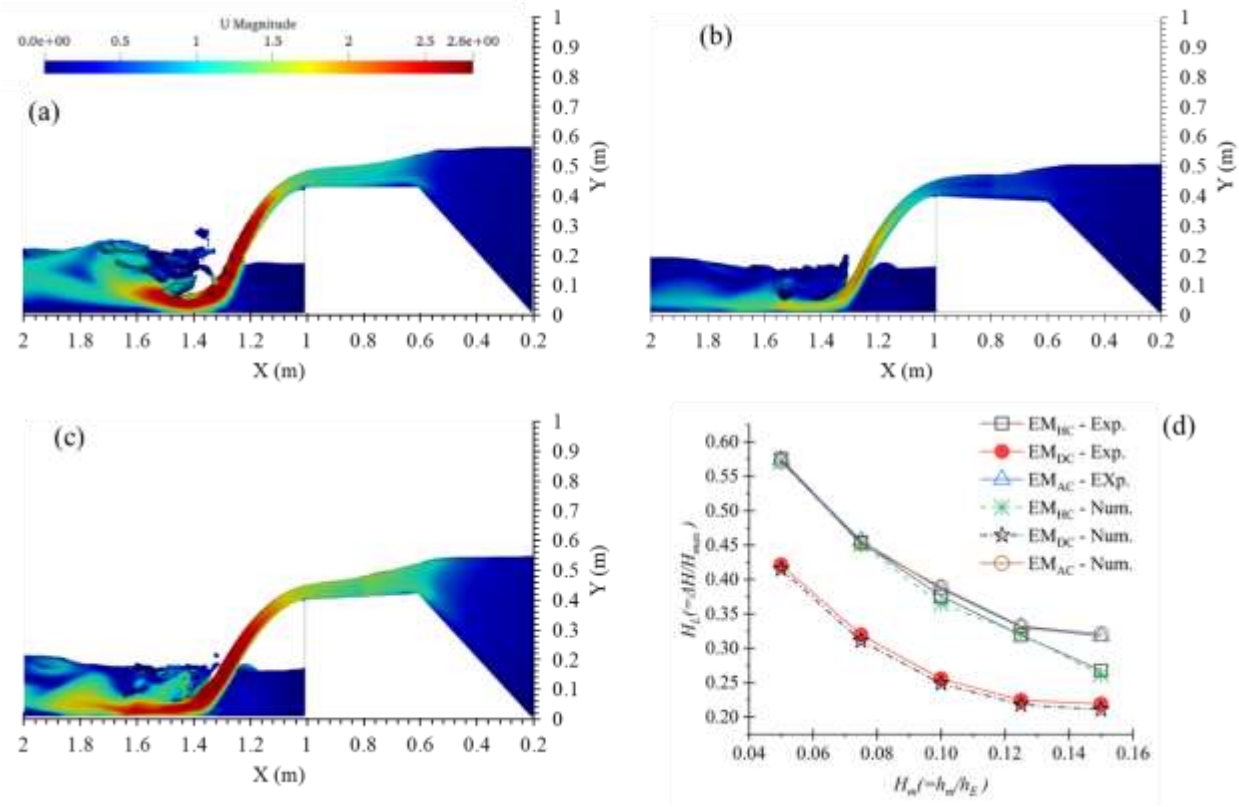

Figure 3: Numerical simulation results when α_i=0 for the EM_{HC}, EM_{AC} and EM_{DC}

Figure 2(d) shows the calculated total head loss at downstream for both the experimental and numerical cases when the downstream surface slope angle α_i=0°, relative to the non-dimensional overtopping

depth h_m/h_E [12]. Head loss was calculated with respect to the water depth at upstream of the EM and near the nappe flow jet impact location downstream. The EM_{AC} case gave the highest head loss, and the lowest head loss was given by the EM_{DC} case [12]. Also, referring to Figure 2, it can be concluded that (+)4% ascending slope EM_{AC} case delays the formation of the nappe flow and (-)4% descending slope EM_{DC} case quickly forms the nappe towards downstream.

Variation of the Nappe Flow Drop Length

Referring to the experimental results, nappe flow impinging jet drop length (L_d) was validated with respect to the numerical and predicted results given by Equation (1), as explained in the sub-chapter 2.3. Figure 3 shows the comparison of the nappe flow drop length (L_d) when the downstream surface slope angle α_i=0°, obtained by the numerical simulation and the analytical equation (Eqn. 1). Referring to Figure 3, for the (+)4% ascending slope case (EM_{AC}), predicted values of the nappe flow drop length (L_d) used by Eqn. (1) were slightly increased from the other two cases of EM_{HC} and EM_{DC}.

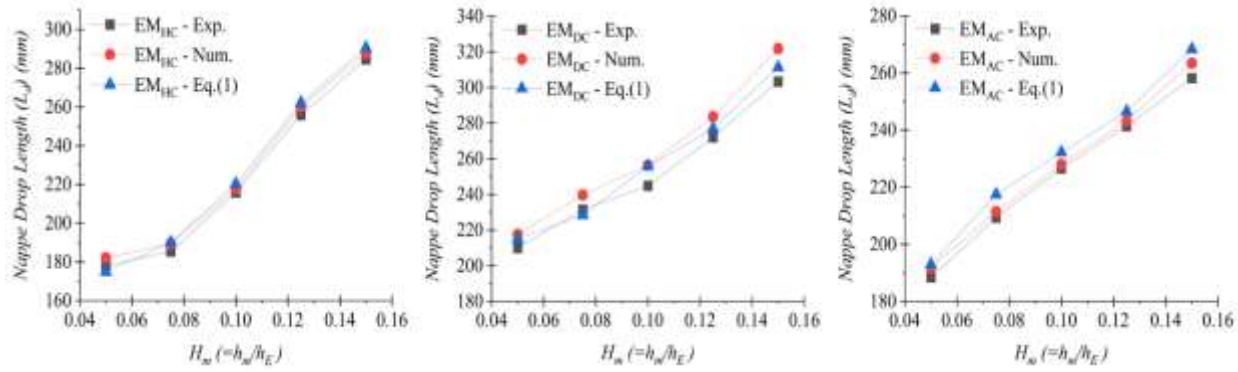

Figure 4: Comparison of the nappe flow drop length (L_d)

Referring to Figure 3, the average percentage difference of the numerical prediction of the nappe flow drop length (L_d) for each case of EM_{HC}, EM_{DC}, and EM_{AC} range between 0.87% to 2.24%, 3.41% to 5.74%, and 0.64% to 2.01%, respectively.

Figure 4 shows the correlation plot of the predicted nappe flow drop length (L_d-Analytical.) over the experimentally obtained nappe flow drop length (L_d-Exp.) for each case considered. From this correlation, the correction coefficient (C_L) was obtained. This correction coefficient (C_L) was defined by using the trial and error method to identify the optimized value as denoted in each figure. For the EM_{HC}, EM_{DC}, and EM_{AC}, the correction coefficient C_L is equal to 0.997, 0.994, and 0.993, respectively. Also, Referring to Figure 4, the average percentage error of the predicted nappe flow drop length (L_d) given by the Eqn. (1) ranged between 1.42% to 3.48%, 0.75% to 4.66%, and 0.92% to 3.74% for the EM_{HC}, EM_{DC}, and EM_{AC}, respectively.

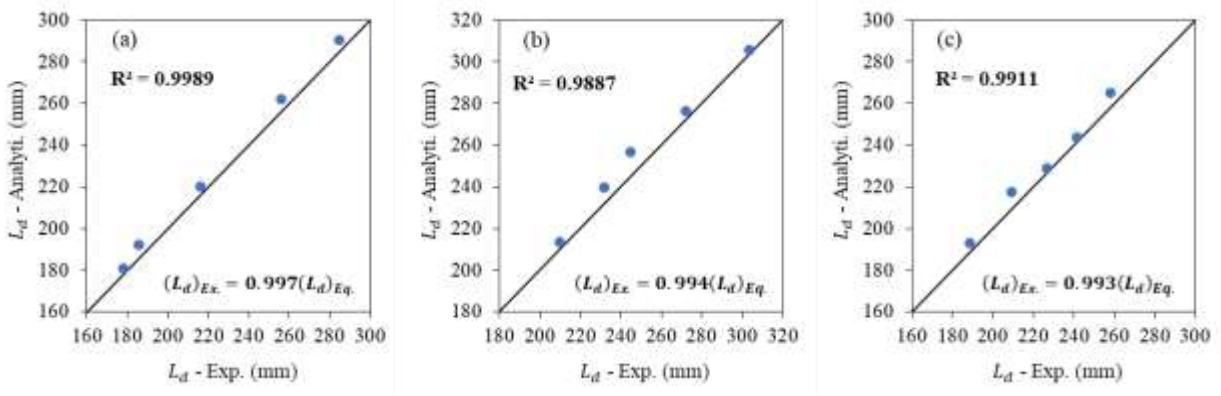

Figure 5: Correlation plot of predicted drop length (L_d-Analy.) versus experimental drop length (L_d-Exp.). (a) EM_{HC}, (b) EM_{DC}, and (c) EM_{AC}

CONCLUSION

This study concerns the experimental findings of the nappe flow formation while changing the overtopping depth, crest geometry, and downstream surface slope done by Dissanayaka et al. [12]. The developed analytical equation and numerical models evaluate the predictability of the nappe flow impinging jet property, i.e., drop length (L_d), which was horizontally measured from the downstream brink edge of the embankment crest to the nappe impinging jet impact point at the downstream plunge pool [11]. Experiments were carried out in a horizontal smooth rectangular channel with specific conditions such as subcritical approaching flow with different discharges, different model geometries, and without tail water effect. The same condition was considered when developing the numerical domain in the OpenFOAM to capture the formation of the nappe flow impinging jet accurately while lowering the downstream surface slope angle (α_i) of the EM. Based on the theoretical approach, under the specific assumptions, a developed equation can compute the average drop length (L_d) of the nappe with respect to the geometric conditions of the EM. The coefficient (C_L) used in the theoretical equation was calibrated under the requirement of the comparison between the experimental and theoretical predicted values with respect to the geometrical concerns.

ACKNOWLEDGEMENTS

The authors would like to appreciate the support of the Japanese Ministry of Education, Culture, Sports, Science, and Technology (Monbukagakusho–MEXT Scholarship). The authors also acknowledge the anonymous reviewers for their valuable comments to improve this manuscript.

REFERENCES

1. Allsop, N.W.H.A., A. Kortenhaus, and M. Morris, *Failure mechanisms for flood defense structures*. FLOODsite Rep. T04-06-01, FLOODsite Consortium, 2007.
2. Igarashi, Y., N. Tanaka, and T. Zaha, *Changes in flow structures and energy reduction through compound tsunami mitigation system with embankment and lined piles*. Ocean Eng., 164, 722–732, 2018.
3. Dissanayaka, K.D.C.R., N. Tanaka, and T.L.C. Vinodh, *Integration of Eco-DRR and hybrid defense system on mitigation of natural disasters (Tsunami and Coastal Flooding): a review*. Natural Hazards, 2021.
4. Kato, F., et al., *Mechanism of coastal dike failure induced by the Great East Japan Earthquake Tsunami*. Proc. of 33rd ICCE, 9 pages, 2012.
5. Tokida, K. and R, Tanimoto, *Lessons for countermeasures using earth structures against tsunami obtained in the 2011 Off the Pacific Coast of Tohoku Earthquake*. Soils and Foundations 54(4):523-543. 2014.
6. Zhu, T. *Breach Growth in Clay Dikes*. Ph.D. Thesis, ISBN-10: 90-9020964-6, 2006.
7. Afshar, H. and S.H. Hoseini, *Experimental and 3-D numerical simulation of flow over a rectangular broad-crested weir*. Int. J. of Eng. and Adv. Tech. 2(6), 214-219, 2013.
8. Badr, K. and D. Mowla, *Development of rectangular broad-crested weirs for flow characteristics and discharge measurement*. KSCE J. of Civ. Eng., 19(1), 136-141, 2015.
9. Hargreaves, D., H. Morvan, and N. Wright, *Validation of the volume of fluid method for free surface calculation: the broad-crested weir*. Eng. Appl. of Comp. Fluid Mech. 1(2), 136-146, 2007.
10. Daneshfaraz, R. et al., *3-D Numerical simulation of water flow over a broad-crested weir with openings*. ISH J. of Hydraulic Eng., 1-9, 2019.
11. Abdalla, M.G. and M.T. Shamaa. *Experimental Investigations of Nappe Profile and Pool Depth for Broad Crested Weirs*. Int. J. Eng. Res. & General Science, 4(1), 2016
12. Dissanayaka, K.D.C.R., and N. Tanaka, M.K. Hasan, *Effect of Orientation and Vegetation over the Embankment Crest for Energy Reduction at Downstream*. Geosciences, 12, 354, 2022.
13. OpenFOAM User Guide, OpenFOAM Foundation. Available online: https://www.openfoam.com/documentation/user-guide/ (accessed 20 June 2022).

2nd International Conference on Advances in Civil and Environmental Engineering (ICACEE-2023)

University of Engineering & Technology Taxila, Pakistan

Conference date: 22nd and 23rd February, 2023

The impact of emerged vegetation on a submerged dike; A numerical study

Sohail Iqbal[1], Norio Tanaka[1,2]

[1]Graduate School of Science and Engineering, Saitama University, 255 Shimo-okubo, Sakura-ku, Saitama-shi,Saitama 338-8570, Japan
[2]International Institute for Resilient Society, Saitama University, 255 Shimo-okubo, Sakura-ku, Saitama-shi,Saitama 338-8570, Japan

ABSTRACT

The vegetated dike has the same bank protection effect as the impermeable dike when the water level is low under normal water conditions. Only when the water level increases the upper part of the dike work as a permeable dike, providing bank protection while suppressing water level rise.The Reynolds stress turbulence modelcode FLUENT was used in this study's numerical simulations to examine the flow behavior a vegetated dike with changing permeability.This study examined impermeable and vegetated dikes with varied permeabilities (24%, 48%, and 74%) to demonstrate how they affected the flow structure, velocity, and Reynold stresses.The depth-averaged and vertical velocity were calculated at different five and two locations respectively. Various velocity and Reynold stress profiles as well as contours were examined at different chosen positions.The numerical results showed that the vegetated dike with 24% porosity can reduce 45% depth averaged velocity at the downstream side with minimum concentration of recirculation region. Moreover, high velocity flow that was splashing at the just upstream face of impermeable dike distributed uniformly toward the main flow region.

KEYWORDS: Vegetated dike, ANSYS, Flow Characteristics

INTRODUCTION

To meet the demands for both river training and restoration, different types ofstructures, such as stream barbs,weirs, and various types of dikes and vanes, were developed.In terms of the dynamic function of the bed, knowledge regarding dike has been accumulated primarily through hydrographic experiments and numerical analysis of moving and fixed beds [1].River structures called dikes are built in a way that protrudes from the riverbank to slow down the flow of the river and alter its direction. The dikes which increase the main channel's velocityare provided in emerged or submerged condition.On the other hand, dead zones between two dikes during emerged conditions or a recirculation zone during submerged flow conditions might occur. This velocity difference causes the formation of a mixing layer and the exchange of mass and momentum between the dike fields (slow) and the main channel (fast) [2,3].

Figure 6: Vegetation on the top of the dike in Punjab Pakistan

There are concerns about the risk of flooding because conventional impermeable dike raises the level of water when floods occur. It was explained that in permeable dikes, the horseshoe vortex of the dike shrinks due to flow infiltration inside the dike, and the scouring depth decreases. Various researchers concluded that permeable dikes have an advantage over impermeable dikes because they allow flow to pass through them [4]. However, there is concern that the bank protection effect will be diminished. As a result, in this study, we perform a numerical analysis using a vegetation dike as a permeable part over impermeable dike. The vegetation dike is a group of vegetation-type piles installed on top of the concrete work, and it has the same revetment effect as the impermeable dike when the water level is low during normal water conditions. The vegetation on the top of the dike can be seen in Figure 1. The upper portion of the sluice only functions as a permeable sluice when the water level rises, and it is anticipated that this will exhibit the bank protection effect while suppressing the rise of the water level. The effective form and permeability of dikes, however, are still unknown due to the paucity of research on vegetation dikes. In this study, we looked closely at the permeability of the vegetation ditch, the impact of changing the height of the concrete structure below the ditch on the flow velocity, and the evolution of the flow structures.

MATERIALS AND METHODS

Model validation

Experiments were performed in a 5 m long, 0.7 m wide and 0.5 m deep channel under critical flow condition in Saitama University Japan. In the experimental channel, a single impermeable dike with dimensions of 17.5 cm and 14 cm in length and width, respectively, in emerged condition was used.To refrain from using a large mesh structure and cut the computational cost, the geometry was simplified, i.e., channel length was decreased. While maintaining the domain width at 70 cm, a domain of 160 cm in length that contained a single impermeable dike was modelled (Figure 2a). The depth of the domain was maintained at 8 cm due to the modelled flow depth. To produce high-quality results, a trial for mesh independence was also conducted [5]. In the beginning, the mesh grids of 9.5 million for coarse, 13.33 million for medium, and 15 million for fine, were tested. The primary velocities between the

coarse and medium meshes differed by about 5%, while the results between both medium and fine meshes differed by about 1%, which was acceptable. As a result, the 13.33 million grid mesh was chosen.

Amass flow rate and outlet boundary condition were set up at the inlet and outlet of computational domain. While a non-slip wall condition was assigned to the side walls, dike, and the channel bed, a symmetry boundary condition was assigned to the channel free surface.FLUENT ANSYS, a CFD code, was used for the simulations and post-processing. The turbulence closure was accomplished using a Reynolds stress model (RSM). The validation of the numerical model at position 1 (P1) and position 2(P2) are shown in Figure 2b.

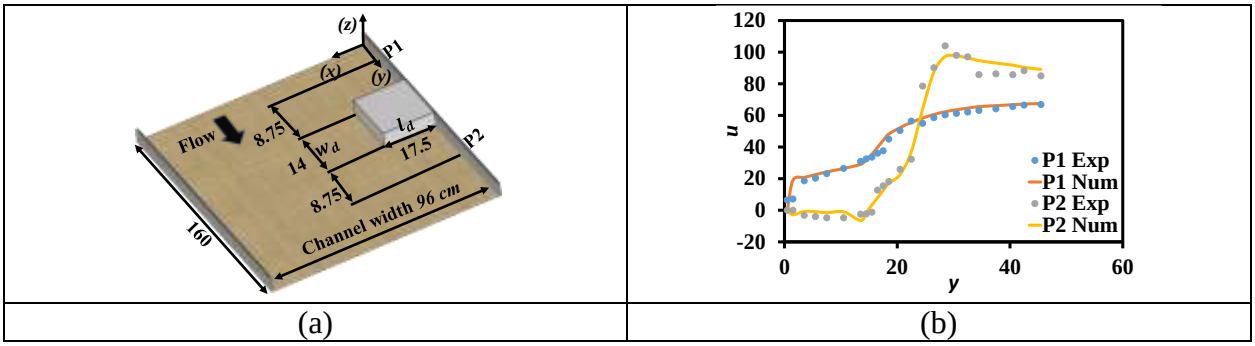

Figure 2: (a) Experimental domain used for numerical validation showing velocity measuring location P1 and P2. where l_d and w_d are dike length and width, (b) depth averaged streamwise velocity validation at P1 and P2, all the units are in cm.

Simulation setup

The goal of the current computational study was to investigate the complex flow patterns surrounding vegetated dikes with different porosities.The channel domain and dike dimensions were modelled similarly to those used for validation.In the current study, a staggered arrangement of rigid cylinders was used to create the vegetated dike, because Takemura and Tanaka's [6] research indicates that a colony-type vegetation model offers a largerdrag force in staggered compared to a grid arrangement.Figure 3a shows the computational domain used for numerical simulation while Figure 3b-3e show thevegetated dike arrangement used for different cases. The physical scale model was chosen to be 1/15. Table 1 shows four different cases that were considered.

Table 1:Geometric and Hydraulic conditions, where Pr is the porosity,ED is emerged dike Q is the discharge, *U* (m/s) is the mean velocity, *and SDEV is submerged dike with emerged vegetation,* $h_v$is vegetation height, $h_d$is dike height, *Fr is the Froude numberand Re is Reynolds number.* All the values are in cm.

Cases	Pr (%)	Dike Condition	*U*	h_v	h_d	*Fr**	*Re***
1	0	ED	0.53	0	8	0.59	34,347
2	24	SDEV	0.53	2	6	0.59	34,347
3	48	SDEV	0.53	4	4	0.59	34,347
4	72	SDEV	0.53	6	2	0.59	34,347

*$F_r = U/(gh_0)^{0.5}$; where *U* and $h_0$aremeanvelocity and original water depth respectively

**$R_e = \frac{\rho U L}{\mu}$;where *U* and *L* are mean velocity and characteristics length while ρ and μ are density and dynamic viscosity of water respectively.

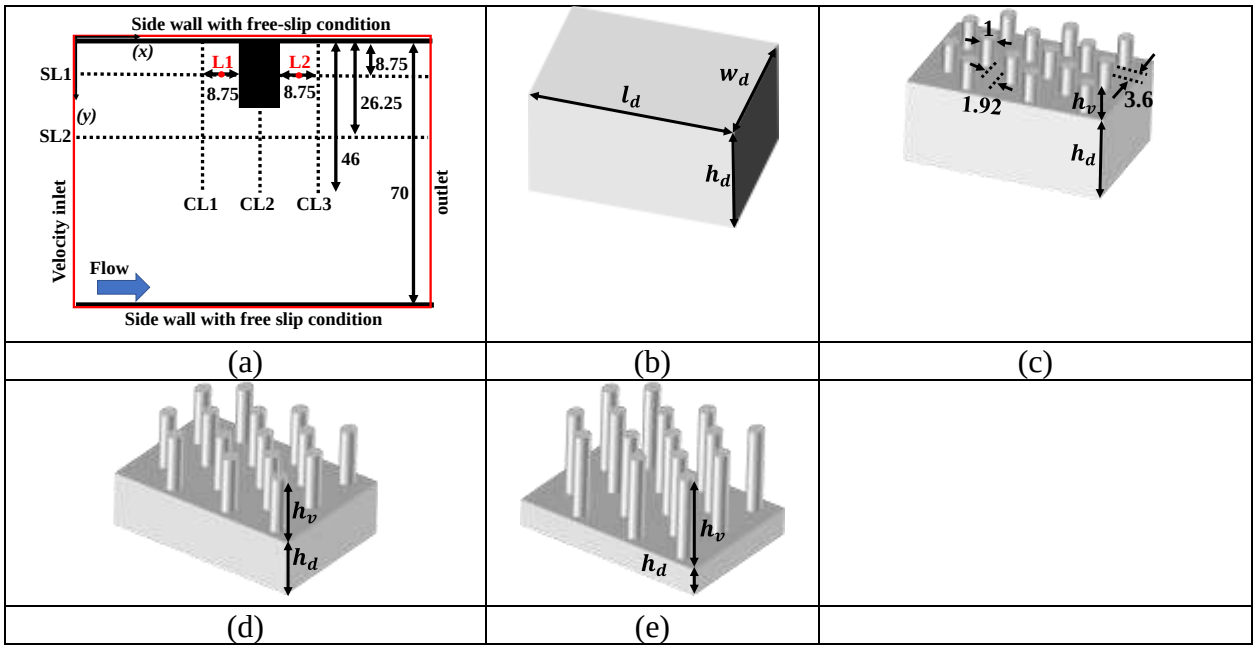

Figure 3: (a) Boundary conditions and five measuring locations (CL1-CL3 and SL1, SL2), where CL and SL represent cross sectional and streamwise location, and all the units are in cm, while dikes usedfor numerical simulation in (b) Case1, (c) Case 2, (d) Case 3, and Case 4. All the units are in cm

RESUTS AND DISCUSSION

Velocity distribution

The depth averaged streamwise velocity (*u*) was calculated at five locations (three cross sectional line (CL1-CL3) and two streamwise location (SL1 and SL2)) while vertical velocity (*w*) was calculated at

two critical locations (L1 and L2). Both velocities (*u* and *w*) were made non dimensional with the mean velocity (*U*). Since CL2 is in the middle of the dike Case 1 with 0% porosity displayed lower values there, because the impermeable dike generates significant concentrated momentum exchange at upstream corner of the dike.Because of that, the velocity near the dike's center and downstream exhibited the lowest value in Case 1 (Figure 4b.At CL3 Case 1 gives minimum velocity value at the dike head location (Figure 4c). At SL1 (Figure 4d) depth averagedvelocityincrement was not much prominent compared to Case 4 because in Case 4 h_d was very less sue to that flow resistance decreased to minimum. The flow at upstream of dike showed same behavior at downstream side. In the mainstream Case 3 and Case 4 showed velocity reduction in front of dike which is suitable for dike protection in submerged condition [7].

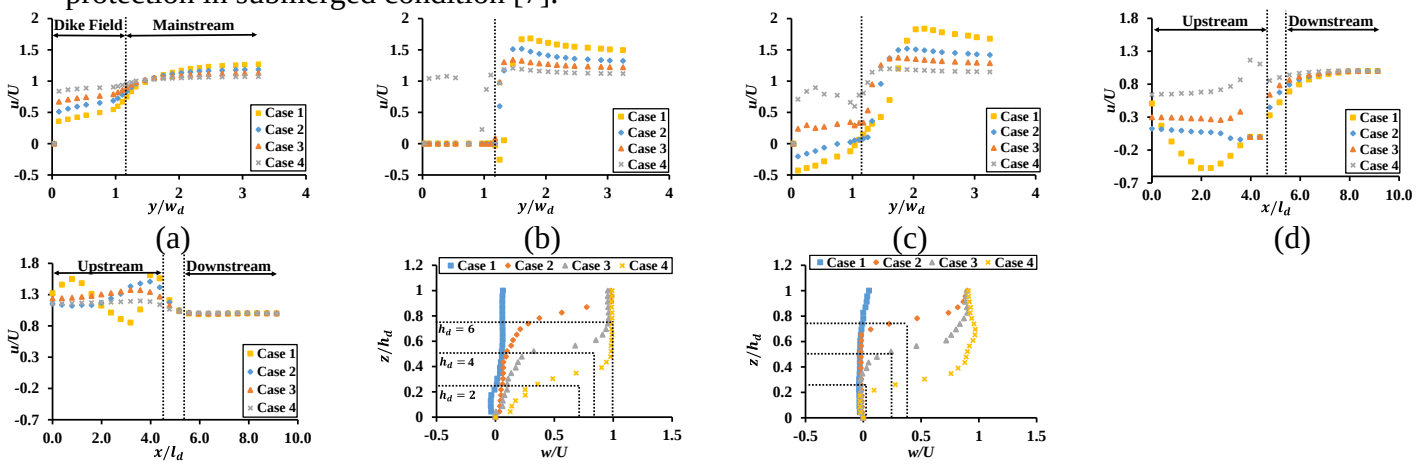

Figure 4: Distribution of depth averaged streamwise for all cases at (a) CL1, (b) CL2, (c) CL3, (d) SL1, and (e) SL2, and vertical velocity distribution at (e) L1 and (f) L2. where dashed lines shows the location of dike.

The vertical velocity distribution at L1 and L2 showed same inflation trend, as shown in Fig. 4f and 4g. The variation in velocity values was directly related to height of impermeable dike i.e., h_d= 2, 4, and 6. Case 4 showed maximum vertical velocity distribution due to 72% porosity.

Flow structure and velocity contours

Figure 5 depicts the depth averaged flow structure in streamwise direction that formed due to the presence of ED (Case 1), and SDEV (Case 2-Case 4). In Case 1, the ED (Figure 5a) showed the recirculation region formed just after the downstream side. The bank next to the dike may disintegrate due to the extremely high velocity recirculation.Therefore, after adding vegetation to the impermeable dike's crest, which can be crucial in submerged dike conditions, this phenomenon can be lessened (Figure 5b and 5c).This phenomenon completely disappeared in Case 2 and Case 3. But in Case 4 due to very small impermeable dike part high velocity flow started directly to move from upstream to downstream side. The high concentrated streamlines changed to

parallel streamlines. From Figure 5d and 5h, the upstream region becomes a high velocity region due to less flow obstruction.

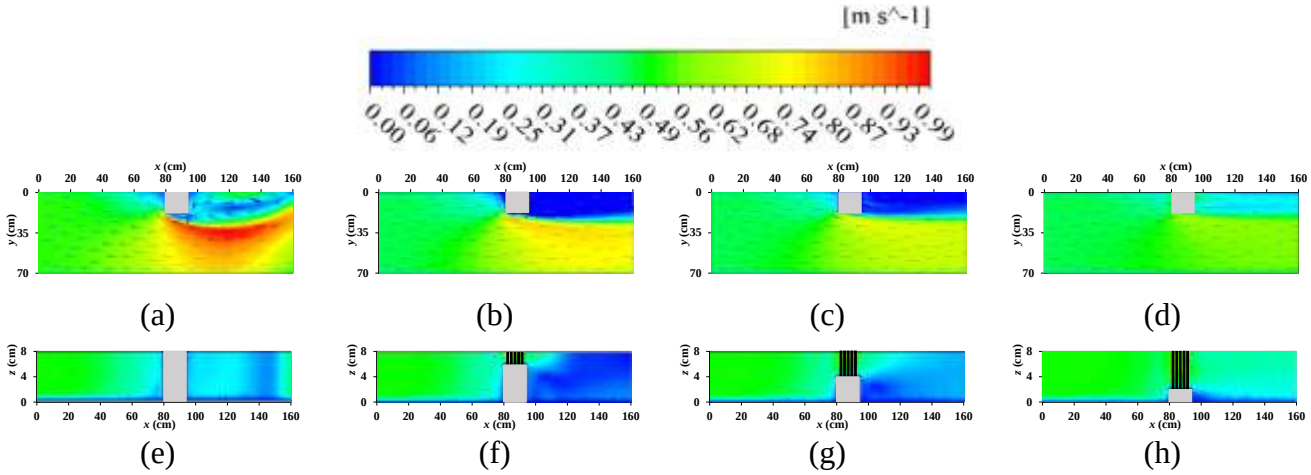

Figure 5: The depth averaged(a-d) and vertical velocity contours (e-h) for each case (a, e) Case 1, (b, f) Case 2, (c, g) Case 3, and (d,h) Case 4 where rectangle shows the location of dike.

Furthermore, the flow deflection, which was maximum in Case 1 (Figure 5a and 5e) due to the presence of a completely impermeable dike, tends to be minimum in Case 4, which contradicts the basic dike concept.In Case 1, the momentum exchange layer was completely concentrated, which can be hazardous to impermeable dike stability.But Case 2 and Case 3 provided flow deflection, divided momentum exchange layer, and low velocity region at the downstream side to protect the bank adjacent to dike [7]. Both cases (Case 2 and Case 3) satisfying the basic requirement of dike even when the dike completely submerged at high water stages.

Reynold stress distribution

Figure 6a–d depicts the vertical profiles of simulated Reynolds normal and shear stresses at L1, and L2 for all case (A–D). The *x*-axis and *z*-axis were normalized with U^2, andh_d, respectively. In these figures,$u^{/}$ and $w^{/}$represent the variations in streamwise and depth wise direction respectively. At L1 (Fig. 6a and Fig 6b) there was no fluctuations for Case 1, however maximum stresses were generated for each case (Case 2-4) at the interface of impermeable and vegetated part i.e., $h_d = 2,4, and\ 6$. The stresses were almost stable near the free surface. When compared to the other cases, Case1 had the highest and lowest values of normal and sheared stresses respectively at L2. The low velocity regions due to recirculation behavior is the responsible for negative values of shear stresses in Case 1. Stresses were reduced at this location (L2) as porosity increased [8,9]. Cases 2 and 3 had the highest stresses, while Case 4 had the lowest.

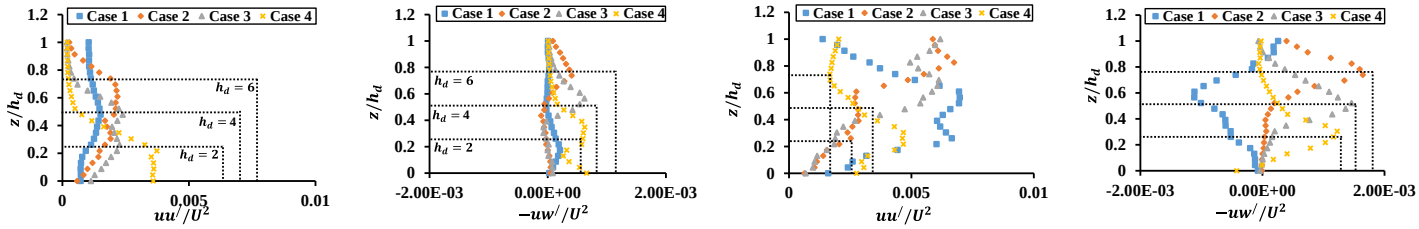

Figure 6. The vertical distribution of normal (a, c) and shear stresses (b, d) at location L1 (a, b) and L2 (c, d). where dashed lines show the location of impermeable dike head (h_d).

CONCLUSION

The purpose of the vegetated dike is to make the impermeable dike more transparent, allowing water to flow down the dike.It has been confirmed that the flow rate with the mainstream and downstream of the dike has stabilized, and it has also been confirmed that a high concentration of flow momentum that was generated in the conventional impermeable dike was maintained in the vegetated dike. Clearly, this will prevent excessive scouring and sedimentation near the dike's adjacent bank as compared to the current impermeable dike.The normal and shear stresses had a direct effect on porosity at L1 (just upstream of the dike) and a reciprocal effect on the just downstream of the dike (L2). The influence of depth averaged velocity and the recirculation zone generated at the downstream side was more clearly demonstrated for Cases 2 and 3 by paying attention to the volume ratio of the vegetation in the upper part and impermeable dike at lower portion of the vegetated dike. It was found that the vegetated groyne with the varying heights of 2 cm (24% porosity), and 4 cm (48%) exerts more influence than conventional dike (0% porosity,) due to the varying vegetation porosity.

REFERENCES

1. Pandey, M. et al.,*Experimental assessment and prediction of temporal scour depth around a spur dike*. International Journal of Sediment Research, 36(1), pp.17-28.
2. Iqbal, S., et al.,. *Flow dynamics around permeable spur dike in a rectangular channel.* Arabian Journal for Science and Engineering,2021 46(5), pp.4999-5011.
3. Iqbal, S., et al.,*Investigation of flow dynamics around a combination of different head shapes of spur dikes*. Tehnički vjesnik, 202229(6), pp.2111-2120.
4. Chauhan, V., Singhal, G.D. and Chavan, R., *A review of sediment deflection in rivers using submerged vanes*. ISH Journal of Hydraulic Engineering,2022 pp.1-17.
5. Anjum, N. and Tanaka, N., *Hydrodynamics of longitudinally discontinuous, vertically double layered and partially covered rigid vegetation patches in open channel flow*. River Research and Applications, 202036(1), pp.115-127.

6. Takemura, T. and Tanaka, N., *Flow structures and drag characteristics of a colony-type emergent roughness model mounted on a flat plate in uniform flow*. Fluid Dyn. Res. 2007 39, 694–710
8. Haider, R.et al.,*Flow Characteristics Around Permeable Spur Dike with Different Staggered Pores at Varying Angles*. Arabian Journal for Science and Engineering,2022 47(4), pp.5219-5236.
8. Pasha, et. al.,*Tsunami mitigation by combination of coastal vegetation and a backward-facing step*,2018 Coast. Eng. J. 60, 104–125
9. Pasha, G.A., et. al., F*low characteristics in a two-stage vegetated compound trapezoidal channel*. Iranian Journal of Science and Technology, Transactions of Civil Engineering,2022 pp.1-13.

2nd International Conference on Advances in Civil and Environmental Engineering (ICACEE-2023)

University of Engineering & Technology Taxila, Pakistan

Conference date: 22nd and 23rd February, 2023

Modeling of Rainfall-Runoff responses for flash flood mitigation using Nature-Based Solution (NBS)

Shees Ur Rehman[1]*, Afzal Ahmed[1], Abdul Razzaq Ghumman[2], Ghufran Ahmed Pasha[1], Rashid Farooq [3]

[1] Department of Civil Engineering, University of Engineering and Technology, Taxila 47050, Pakistan

Correspondence* sheesurrehman9@gmail.com

[2] Department of Civil Engineering, College of Engineering, Qassim University, Buraidah 51452, Saudi Arabia

[3] Department of Civil Engineering, International Islamic University, Islamabad 44000, Pakistan

ABSTRACT:

Nature Based Solutions to mitigate floods always provide an opportunity for researchers and policymakers to produce long-term solutions. In this study, a laboratory-scaled hillslope model is designed to study rainfall-runoff responses keeping in view the natural hillslope conditions prevailing in hill torrents creating flash floods. A rainfall simulator was used to perform experiments to examine the effect of flexible vegetation (grass), rigid vegetation (large trees), and their combination on runoff generation under variable rainfall intensities, and the results were compared with barren (no vegetation) conditions. Hydrographs were developed and compared for all the cases. Peak discharge (Qp), attenuation (difference between the peaks of two hydrographs), time of concentration (tc), and flow volumes in the recession limb (Vr) and falling limb (Vf) of the hydrographs were also calculated. It resulted that attenuation and tc were maximum for mixed vegetation (flexible and rigid) and Qp, Vr and Vf were maximum for no vegetation condition. The maximum tc was decreased by 24% against the double vegetation case.

KEYWORDS: Valley Model**,** Time of Concentration, Thermopore sheets, Flexible Vegetation, Rigid Vegetation

INTRODUCTION:

In the modern world, Nature-based solutions (NBS) are widely adopted by many developed and underdeveloped countries. The NBS approach is used to minimize climate change impacts, enhancing resilience in areas of meteorological risk to society such as flooding and sustainable development [1][2]. The rainfall and runoff responses are the key factors contributing to the total discharge reaching the urban drainage system [3]. The discharge at the outflow region highly depends on various factors including soil compaction, type of soil within the catchment area, morphological properties, and vegetation cover. The rainfall-runoff relation is a complex process in those areas having a variety of

above-mentioned factors. Hence, it is important to develop the quantitative and qualitative relationship between these factors and runoff generation to improve urban drainage design.

Moreover, the development of rainfall-runoff relations from green surfaces can also be used to calibrate traditional infiltration models in urban drainage engineering [4][5]. Flash floods are one of the most dangerous flood types among all types of floods. As compared to other types of floods, the impact of flash floods is naturally very sudden and high within a very short period. It was reported in the past that there were many causes of flash floods including the topography of the area, the intensity of rainfall, and exposure of the community and their assets. On the other hand, the frequency of flash floods damaged the socioeconomic environment. In recent years, an increasing trend in the frequency of floods enormously damaged the human socioeconomic environment [6].

The effect of flash floods is very high in countries like Pakistan having varied topography, steep slopes in the hilly areas, and diverse climates which is difficult to predict. The flood generated from these hill torrents has high peaks within a very short time. Hence, people usually got less time to respond to these types of flash floods resulting in the enormous loss of human lives and live stocks [7]. There are many hilly areas in Pakistan that are declared as hill torrents in all the provinces of the country. Among these, the hill torrents in Southern Punjab and Baluchistan have steep slopes and barren mountainous regions are responsible for flash floods. Due to these flash floods Layyah, Rajanpur, and Dera Ghazi Khan districts were badly affected [8].

Little knowledge exists about the nature-based solution to cope with flash floods. A laboratory-scaled rainfall simulator may be used to study the relationship between runoff and rainfall by using vegetation along the hilly areas. The rainfall simulator generates rainfall through sprinkles with variable rainfall intensities [9]. This equipment has also been used in many countries like India to study the rainfall-runoff relation in hilly terrain [10]. The Rainfall-runoff relation can be developed by physical, empirical, and conceptual models [11][12]. Based on the existing data, the empirical model can be applied to develop the relationship between the rainfall-runoff model. However, artificial neural networks [13][14] or fuzzy logic [15] have been used by researchers as a conceptual modeling technique.

Previously, a rainfall simulator was used by many researchers for generating runoff in the study area which was further used to predict erosion along the roads [16][17]. It was also used to develop a relationship between sediment yield and runoff under variable rainfall intensities in a vineyard plantation in Spain [18]. Hence, the researchers approved that the rainfall simulator could be a useful tool for representing natural rainfall conditions [19]. The runoff volume and the peak discharge estimation are important measurements to design hydraulic structures [20]. Thus, various models were previously presented to simulate the rainfall-runoff relation. Among these models, synthetic hydrographs were used to quantify runoff responses generated from the hill torrents having forests [21].

In the current study, rainfall-runoff responses were analyzed by using a rainfall simulator at a laboratory scale. The symmetrical slopy areas were modeled in the reservoir of the rainfall simulator to make similar hilly conditions of the hill torrents. Water flows in the channel at the middle of the reservoir and computerized runoff measurements were recorded from the downstream weir. Runoff was measured from the hilly model without any vegetation and results were compared by putting the flexible vegetation (grass bed), rigid vegetation (actual tree branches), and a mixture of both vegetation.

MATERIALS AND METHODS:

[1] In the current study, a Rainfall simulator in the water resources laboratory (Fig.1), University of Engineering & Technology Taxila, Punjab, Pakistan was used for experimental investigation of rainfall-runoff responses in a barren hilly area (no vegetation) and green hilly area (with vegetation). The equipment consists of networks of rainfall pipes, rainfall sprinkles (11 nos.), a discharge measuring weir, and two main control valves. The dimensions of the equipment were 1m (width) x 2m (length) x 0.12m (height). The hill model was made of polystyrene sheets with length = 1.85 m, and width = 1 m. The inclined length of the model on both sides of the rectangular channel was 0.26m, and the width of the channel was 0.23m. The remaining width of the model was horizontal as shown in Fig. 1b. The slope of the hilly area model was 27°. The dimensions of the model on each side of the channel were symmetrical with area A1=A5 and A2 = A4

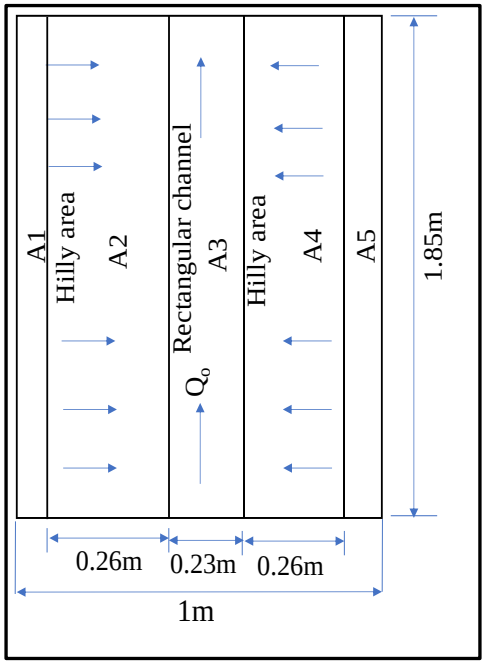

Fig. 1: (a) Isometric view of rainfall simulator (b) Line diagram of hill model

After placing the model without vegetation (Fig. 2a), the rainfall sprinkles started having uniform rainfall over the whole catchment area. There were three rainfall/precipitation spells (P1, P2, and P3) were tested against each case with P1 = 0.030 m/M, P2= 0.040 m/M, and P3 = 0.05 m/M. Hydrographs were developed by taking the runoff values from the computerized rainfall simulator. Firstly, three rainfall spells were sprinkled on the model with no vegetation (NVO). In the 2nd step, the flexible vegetation in the form of artificial grass (SVS) was placed on the polystyrene sheets (Fig.2b) to examine the effect of flexible vegetation on the runoff generation and hydrographs.
In the end, the combined effect of both flexible and rigid vegetation (DVM) was observed by placing both types of vegetation as shown in (Fig. 2c).

A video of discharge for each case was taken after starting the rainfall intensity. From that video the time of concentration was checked when the rainfall water reaches to outlet pipe of catchment area. Similarly, the time for each 1000ml was noted and checked that in which time interval the discharge was maximum (Qp). Before and after this peak value the volume of rising and falling limb was measured respectively.

In the current study, "tc" was calculated for each case. The sprinkles were run for 5 min intervals for each rainfall spell which is kept constant for all the cases to examine the difference in the hydrograph peak at the same time interval. When sprinkles were off, the runoff decreased resulting in no runoff after some time. The slope of the equipment was 0.01 for all the cases. In the current study soil erosion was not considered that's why polystyrene sheets were used for modeling because of their less permeability. The experimental conditions are shown in table 1.

Table 1: Experimental Conditions

Sr.No	Case ID	Precipitation	Vegetation type
1	NVOP1	0.030 m/M	No
2	NVOP2	0.040 m/M	No
3	NVOP3	0.050 m/M	No
4	SVFP1	0.030 m/M	Flexible (grass bed)
5	SVFP2	0.040 m/M	Flexible (grass bed)
6	SVFP3	0.050 m/M	Flexible (grass bed)
7	DVMP1	0.030 m/M	Mixed (Flexible + Rigid)

8	DVMP2	0.040 m/M	Mixed (Flexible + Rigid)
9	DVMP3	0.050 m/M	Mixed (Flexible + Rigid)

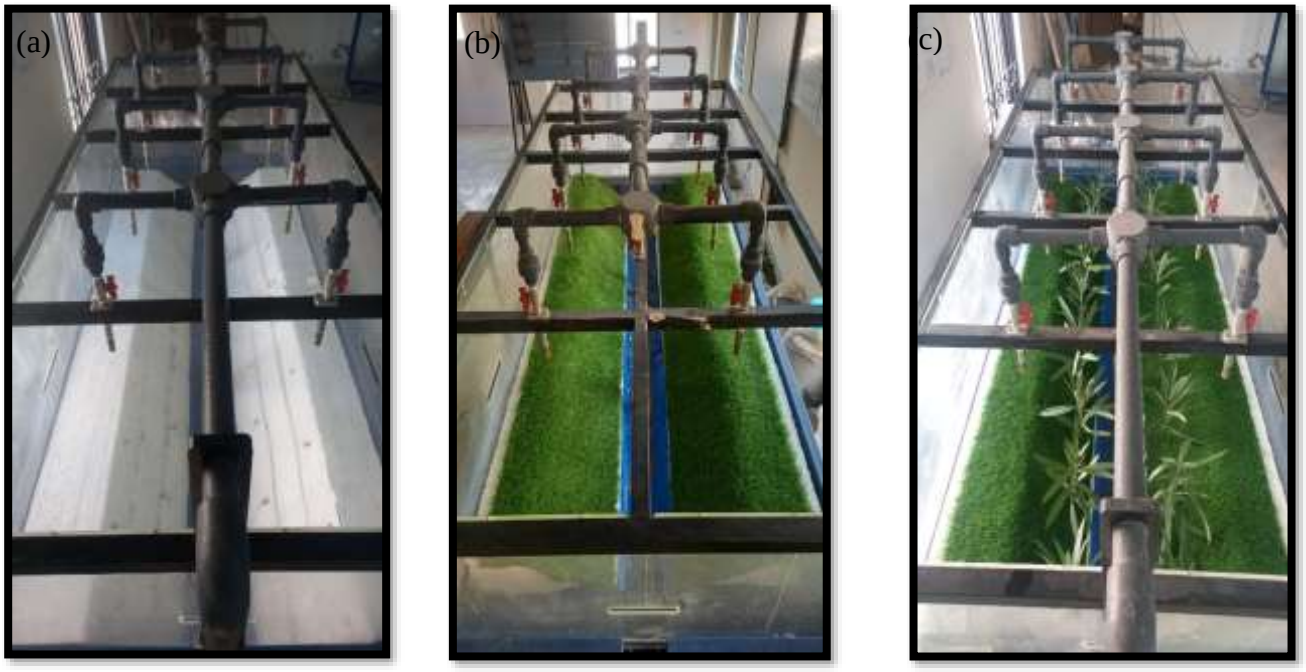

Fig. 2: (a) No vegetation model, (b) flexible vegetation model, (c) mixed vegetation model

RESULTS AND DISCUSSIONS:

HYDROGRAPHS:

The hydrograph is a graphical representation of time (x-axis) and discharge/flow (y-axis) having three main components i.e., rising limb, crest and falling limb as shown in Fig. 3a. The results obtained from the NVO model against P1, P2 and P3, showed that by increasing the intensity of precipitation, the peak of hydrograph was increased as shown in Fig. 3b. The same trend was observed for all other cases of vegetation.

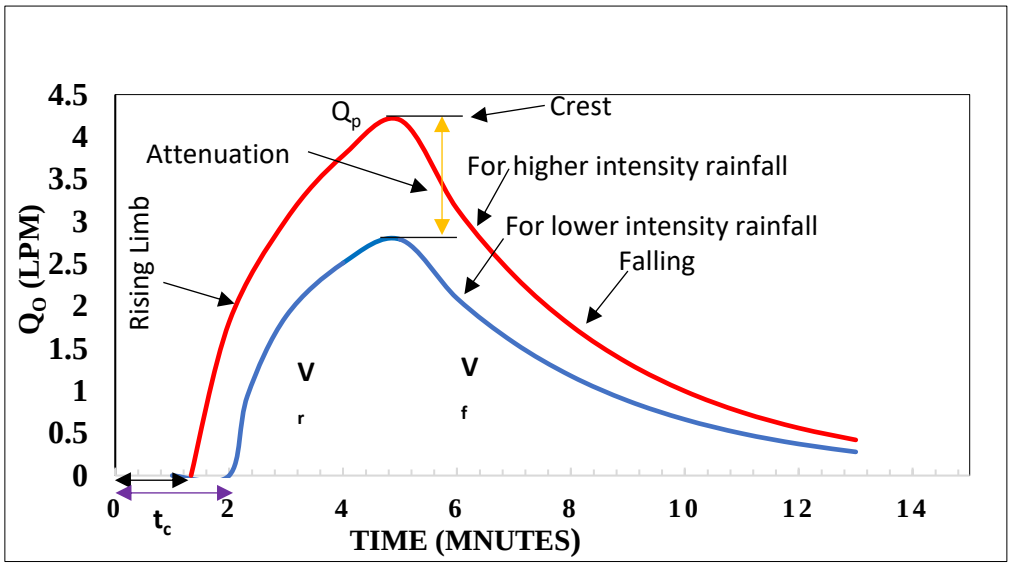

Fig. 3: (a) Components of the hydrograph

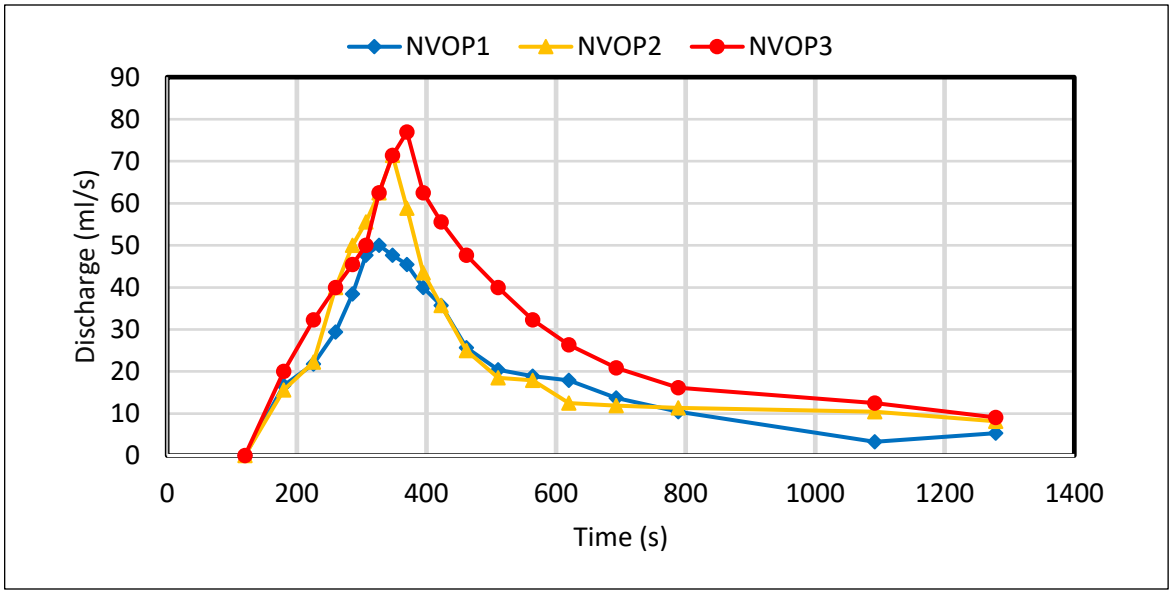

Fig. 3: (b) Discharge Hydrographs for NVO for P1, P2 and P3

The hydrograph comparison between no vegetation cases and with vegetation cases showed that for all the cases, the peak of the hydrograph was observed for no vegetation cases and the peak was decreased by placing flexible vegetation which was further decreased by placing rigid vegetation means that rigid vegetation contributed more to decrease the peak discharge as compared to flexible vegetation. The minimum peak was observed for mixed vegetation cases against P1, P2, and P3 as shown in Fig. 4 (a-c).

ATTENUATION:

The difference of peaks between the two hydrographs is termed attenuation as represented in Fig. 3a. It resulted that the attenuation of hydrographs in relation to the highest hydrograph (for NVO) was maximum in percentage for DVM because DVM cases showed maximum resistance to flow of rainwater from the hills to contribute to lateral flow in the channel (Qo). The maximum attenuation achieved in the DVM case was 63% and the minimum was 28% for the SVS case. The attenuation (%) is shown in Fig. 4d.

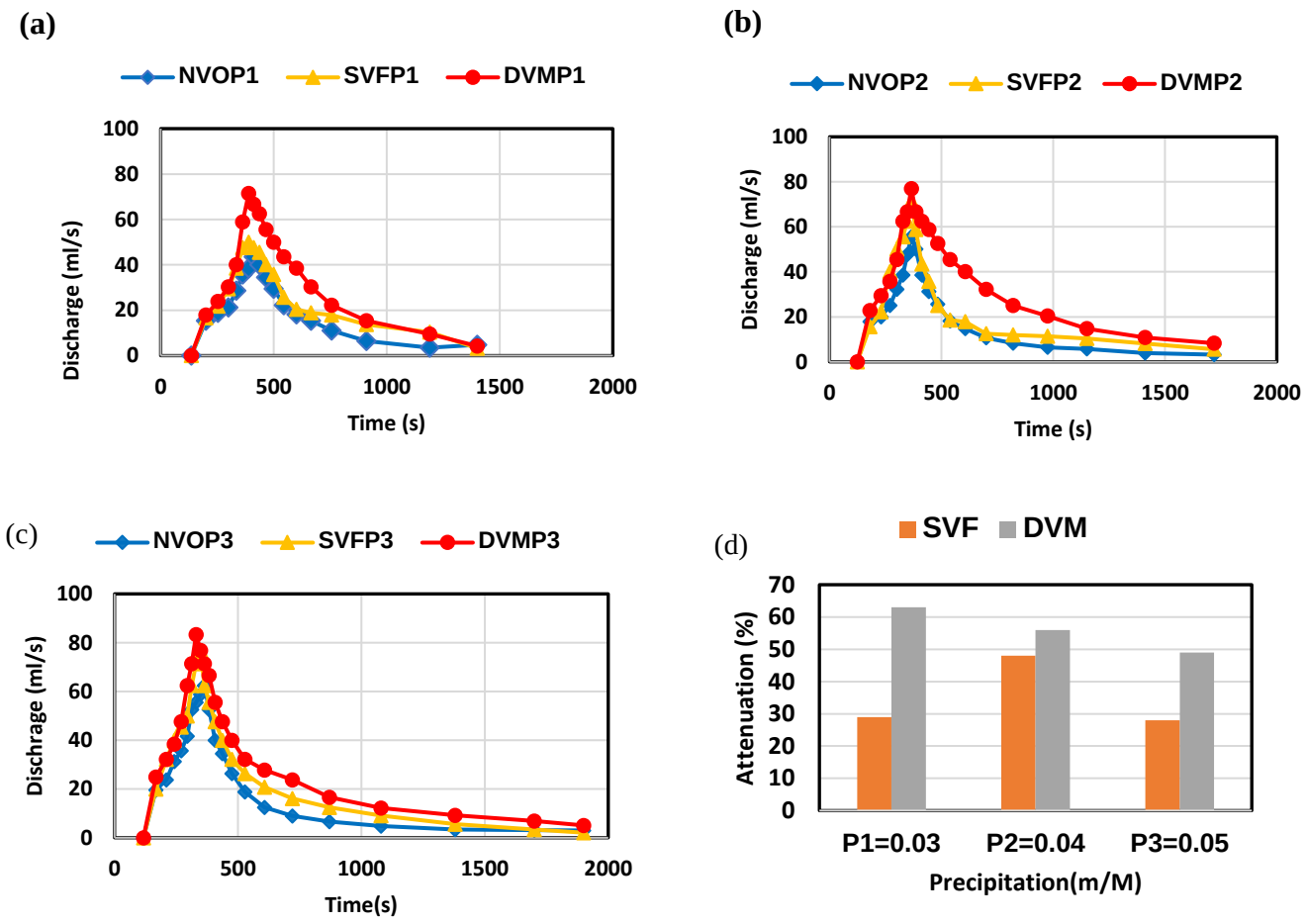

Fig. 4: (a) NVO, SVF, DVM for P1, (b) NVO, SVF, DVM for P2, (c) NVO, SVF, DVM for P3 and (d) Attenuation (%) for SVF, and DVM w.r.t NVO.

PEAK FLOW (Qp) AND TIME OF CONCENTRATION (Tc):

Peak flow is the maximum flow at the crest of the hydrograph as represented above in Fig. 3a. It resulted that the maximum peak flow (Qp) was observed for the NVO case against precipitation P1. It was also noted that the peak flow was increased by increasing the rainfall intensity from P1 to P3 as shown in Fig. 5a. The time of concentration analysis suggested that "tc" was minimum for NVO cases and maximum for DVM cases because more water was intercepted by the combined effect of flexible and rigid vegetation so more time required to reach rainwater to the outlet of the catchment. The variation of "tc" is shown in Fig. 5b. The effect of flash floods can be reduced by increasing the time of reaching water from the hill torrents to the downstream and downhill sides.

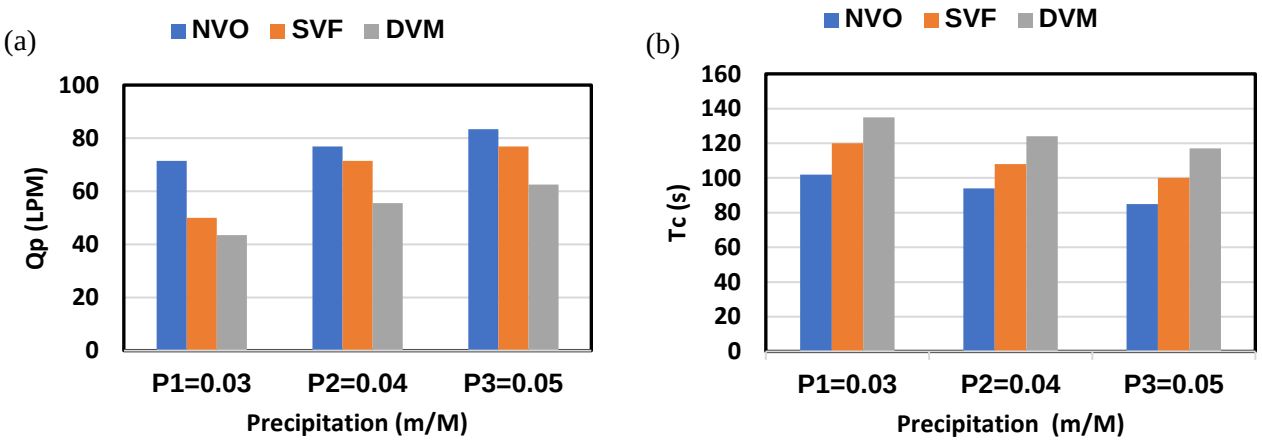

Fig. 5 : (a) Peak flow values (LPM) for all cases, **(b)** Time of concentration

VOLUME OF FLOW IN RECESSION LIMB (Vr) AND FALLING LIMB (Vf):

The impacts of flash flooding may also be reduced by decreasing "Vr" and "Vf". the flow volume under the curve of the recession limb and falling limb was calculated and it was observed that "Vr" and "Vf" were reduced by placing vegetation and minimum values were observed for DVM cases as shown in Fig. 5 c-d.

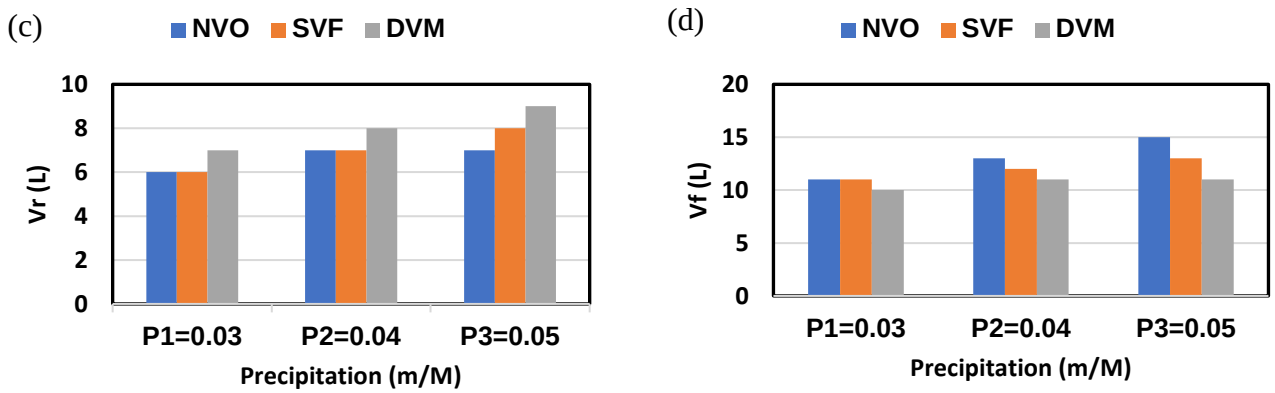

Fig. 5: (c) Vr (Volume of rising limb **(Liter)**) **(d)** Vf (Volume of falling limb **(Liter)**)

CONCLUSION:

Keeping in view the above results it is concluded that.

a. The peak of the hydrograph is directly proportional to the intensity of rainfall.
b. The peak discharge was maximum for no vegetation condition, flexible vegetation reduced the peak, which was further reduced by only rigid vegetation, and by applying mixed vegetation, the peak was minimum.
c. Time of concentration with respect to without vegetation condition was maximum i.e., 63% for mixed vegetation conditions.
d. Vr and Vf were maximum for no vegetation conditions and minimum for mixed vegetation conditions.
e. By decreasing "tc", "Qp" Vr, and Vf will reduce the impacts of the flash flood because it will provide the community more time to respond and overall impacts of flash flooding will also be minimized due to lower peak of hydrograph with mixed vegetation case.

After analyzing this model, we can check the effect of these same conditions in real field on large scale and finally can implement on different sites where flash flooding mostly take place i.e., in Taunsa villages (linked with Koh Suleiman valleys) etc. The only main limitation is that this solution (to avoid from flash flooding) is time taking as its Nature Based Solution(NBS).

REFERENCES:

[1] Cohen-Shacham, E., Walters, G., Janzen, C., & Maginnis, S. (2016).Nature-based solutions to address global societal challenges. Gland, Switzerland:IUCN. https://doi.org/10.2305/IUCN.CH.2016.13.

[2] European Environment Agency. (2017).Climate change adaptation anddisaster risk reduction in Europe. Enhancing coherence of the knowledgebase, policies and practices. Luxembourg: European EnvironmentAgency Report No 15/2017.

[3] Redfern, T. W., MacDonald, N., Kjeldsen, T. R., Miller, J. D., & Reynard, N. (2016). Current understanding of hydrological processes on common urban surfaces. Progress in Physical Geography, 40(5), 699–713. https://doi.org/10.1177/0309133316652819

[4] Gregory, J. H. (2006). Effect of urban soil compaction on infiltration rate. Journal of Soil and Water Conservation, 61(3), 117–124

[5] Quinton, J. N., Edwards, G., & Morgan, R. (1997). The influence of vegetattion species and plant properties on runoff and soil erosion: Results from a rainfall simulation study in south east Spain. Soil Use and Management, 13(3), 143–148. https://doi.org/10.1111/j.1475-2743. 1997.tb00575.

[6] van Westen C (2009) Multi-hazard risk assessment. Distance education course Guide book. Bangkok, United Nations University-ITC

[7] Ahmad H, Bokhari JI, Siddiqui QTM (2011) Flashflood risk assessment in Pakistan. In: 71st Annual Session Proceedings. Pakistan Engineering Congress, Pakistan, pp 696–708.

[8] Band, L.E.; Patterson, P.; Nemani, R.; Running, S.W. Forest ecosystem processes at the watershed scale: Incorporating hillslope hydrology. Agric. For. Meteorol. 1993, 63, 93–126.

[9] Singh VP, Woolhiser DA (2002) Mathematical modeling of watershed hydrology. J Hydrol Eng 7(4):270–292

[10] Aksoy H, Kavvas ML (2005) A review of hillslope and watershed scale erosion and sediment transport models. Catena 65:247–271

[11] Minns AW, Hall MJ (1996) Artificial neural networks as rainfall-runoff models. Hydrolog Sci J 41(3):399–417

[12] Lin GF, Chen LH (2004) A non-linear rainfall-runoff model using radial basis function network. J Hydrol 289(1): 1–8

[13] Hundecha Y, Bardossy A, Werner HW (2001) Development of a fuzzy logic-based rainfall-runoff model. Hydrolog Sci J 46(3):363–376

[14] Adams, R.; Parkin, G.; Rutherford, J.C.; Ibbitt, R.P.; Elliott, A.H. Using a rainfall simulator and a physically based hydrological model to investigate runoff processes in a hillslope. Hydrol. Process. 2005, 19, 2209–2223

[15] Sheridan, G.J.; Noske, P.; Lane, P.; Sherwin, C. Using rainfall simulation and site measurements to predict annual interrill erodibility and phosphorus generation rates from unsealed forest roads: Validation against in-situ erosion measurements. CATENA 2008, 73, 49–62.

[16] Arnaez, J.; Lasanta, T.; Ruiz-Flaño, P.; Ortigosa, L. Factors affecting runoff and erosion under simulated rainfall in Mediterranean vineyards. Soil Tillage Res. 2007, 93, 324–334

[17] Chouksey, A., Lambey, V., Nikam, B. R., Aggarwal, S. P., & Dutta, S. (2017). Hydrological modelling using a rainfall simulator over an experimental hillslope plot. *Hydrology*, *4*(1), 17.

[18] Khaleghi M.R., Gholami V., Ghodusi J., Hosseini H. (2011): Efficiency of the geomorphologic instantaneous unit hydrograph method in flood hydrograph simulation. Catena, 87: 163–171.

[19] Sapountzis M., Stathis D. (2014): Relationship between rainfall and run-off in the Stratoni region (N. Greece) after the storm of 10th February 2010. Global NEST Journal, 16: 420–431.

[20] Pradhananga, D., & Pomeroy, J. W. (2022). Diagnosing changes in glacier hydrology from physical principles using a hydrological model with snow redistribution, sublimation, firnification and energy balance ablation algorithms. *Journal of Hydrology*, *608*, 127545.

[21] Zhou, Y., Cui, Z., Lin, K., Sheng, S., Chen, H., Guo, S., & Xu, C. Y. (2022). Short-term flood probability density forecasting using a conceptual hydrological model with machine learning techniques. *Journal of Hydrology*, *604*, 127255.

2nd International Conference on Advances in Civil and Environmental Engineering (ICACEE-2023)

University of Engineering & Technology Taxila, Pakistan

Conference date: 22nd and 23rd February, 2023

Experimental Investigation of flood energy dissipation for hill torrents management

Nadir Murtaza[1], Ghufran Ahmed Pasha[1,2], Afzal Ahmed[2]

[1]UET Taxila, Nadirkhattak1122@yahoo.com
[2]UET Taxila, ghufran.ahmed@uettaxila.edu.pk
[2]UET Taxila, afzalahmed.47@gmail.com

ABSTRACT

Hill torrents in mountain regions have a very steep slope and water can't infiltrate in the region which results in a flash flood in the area that causes damage to housing crops and land. In the present investigation, for super critical condition a number of flume laboratory experiments were performed to investigate torrential flood energy dissipation through single and hybrid defense system in order of weir and vegetation. Energy dissipation through the hybrid system was investigated under five different Froude numbers by changing the flow discharge. The finding of this research was to investigate backwater rise, water surface profile and energy dissipation through single and hybrid defense system. The results show that the backwater rise increases by increasing initial Froude number while energy loss (%) decreases by increasing initial Froude number. It was observed that maximum energy loss in single and hybrid defense systems was 38% and 53% respectively.

KEYWORDS: Hills torrents, Flood, Defense system, Backwater Rise, Energy Dissipation,

INTRODUCTION

Floods are the most common type of natural event and cause an overflow of water to submerge a usually dry area. Floods are frequently the result of heavy rainfall or tsunami in coastal areas that carry serious socio-economic warning. "According to reports, floods kill 20,000 lives each year and have a damaging effect on no less than 20 million people worldwide". [1]. The previous literature predicate that damages from flood hazards can be increased in near future [2]. "According to the research analysis, 23 significant flood disasters in Pakistan from 1947 to 2015 resulted in economic damages of $38.2 billion, over twelve thousand casualties, and almost 617,000 km^2 of land area being damaged". [3]. A recent report claims that the 2022 flood in Pakistan causes Rs3.2 trillion in damages and Rs3.3 trillion in economics loss and 1739 people were killed due to this intense flood. "In recent years various researchers have worked on flood energy dissipation to derive the best possible method" [4] [5] [6]. Both artificial and natural method can be implemented to reduce the energy that is carried by flood. "Physical measure such as the construction of dam, elevated building, floodwalls, leaves, and flood proving properties" [7], [8]. "Flash floods are different from traditional riverine floods in their extent and properties" [9]. These floods are brief in duration yet devastating in terms of devastation. These floods' energy cannot be utilized as effectively as rivers floods. Weir and vegetation hydraulic resistance and water ability to reflect can lower the energy of flowing water, flooding depth, flooding area, and

hydraulic force behind the Weir and vegetation. The intensity of the water flowing through the Weir and vegetation reduces, decreasing the damage behind the Weir and vegetation. As a result, the primary goal of this research was to study the energy dissipation effects via SDS (Single defense system) and HDS (hybrid defense system). A number of tests were performed by applying laboratory models to fulfil the study's goal. The energy dissipation impacts of each test were compared, with specific emphasis paid to the upstream side of models' backwater rise. The objective of this study was to provide a hybrid defense system that sufficient reduction in flood energy.

Material and Method: -

Flume Characteristic: -

Experiment was performed in glass sided open channel of 10-m, 0.31-m, and 0.5-m length, width, and height respectively. For different flow, a flume with continuous bed slope of 1/250 was used for laboratory experiment, as shown in Table 1. the initial Froude number (Fro = V($\sqrt{gh_o}$), h_o= water depth without any obstruction, V= average-velocity of water at depth ho, and g= gravitational acceleration, 9.81m/s^2) in the channel without any obstruction was estimated from the water depth and average velocity of flow in the channel. "For generating super-critical flow" [10, 11], without any obstacle, the initial water depth (h_o) selected in the experiment were 3, 3.2, 3.6, 4.2, and 4.4cm, setting the initial Fr_o approximately equal to 1.39, 1.56, 1.59, 1.68, and 1.72. For experimental purposes all models were scaled down to 1/100.

Experimental condition: -

The Eucalyptus species was selected as vegetation model for tree species. "The peak flood from the past shows that the tree crown of such trees species was higher, that's why the circular cylinder was selected." [12]. "The trunk diameter and average height of tree in ecological zone of Punjab, Pakistan are 0.11-0.33 m and 7.6-14.6 m respectively" [13]. "Iron bar, and steel cylinder have often been used by various researcher, to ensure the dimensional similarity" [14] [15]. In current study, at a scale of 1:100 an iron bar of 0.003 m diameter were used over timber cylinder (small diameter timber cylinder were predicated to break) by keeping the previous requirement of average tree diameter in limitation. To check the effectiveness of single defense system, only weir was placed in the flume for flood energy dissipation as shown in figure 1c while for HDS, weir and sparse vegetation that have density =2.13 were used. In current study d_n=180 No.cm (d_n=$\frac{2}{D\text{^}2\sqrt{3}} Wvd\ X\ 10\text{^}2$) was selected for sparse vegetation case as shown in figure 1a b d. Point gauge was used for measuring the water level at intervals where water profile changes and the depth-averaged velocity was estimated from equation of continuity (Q=AV). The energy reduction rate [%] is calculated as

Energy reduction rate [%] = $\Delta E1 = \frac{E1-E3}{E1} x100$ & $\Delta E2 = \frac{E2-E3}{E2} x100$

Where ΔE1, ΔE2 is the energy dissipation in single and hybrid defense system and, E1 is the energy measured at the point at u/s of Weir and E3 is the energy measured at the d/s of Weir and E2 is the energy measure in front of vegetation.

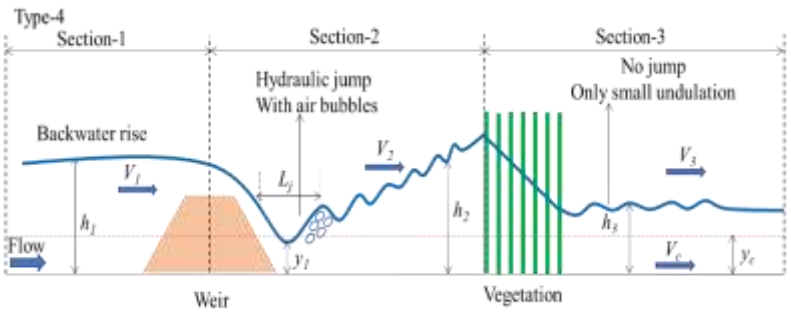

a

b

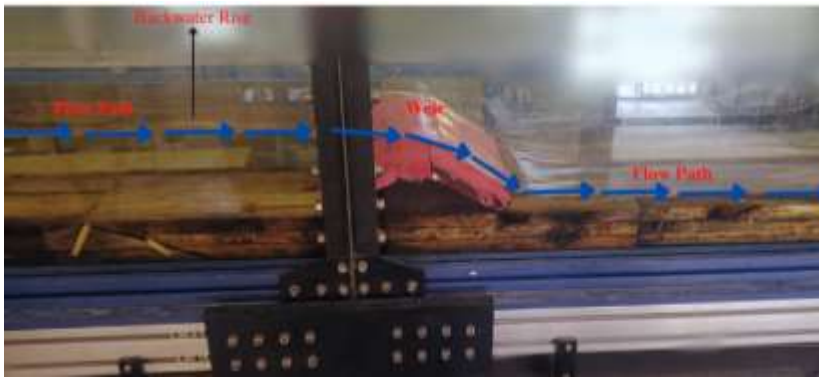

c

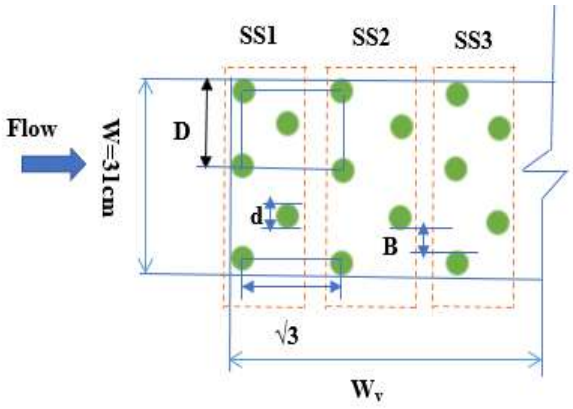

Figure 1: - laboratory trial arrangement (a) Representational diagram of the flume & hydraulic jump (b) experimental Arrangements of HDS (c) Experimental setup of SDS (d) vegetation arrangement of staggered strip (SS).

Table 1: - Experimental Conditions

CASE ID	Initial Froude Number (Fro)	Initial water depth (ho)
OW (Only Weir)	1.39, 1.56, 1.59, 1.68, 1.72	3, 3.2, 3.6, 4.2, 4.4
WV (Weir-Vegetation)	1.39, 1.56, 1.59, 1.68, 1.72	3, 3.2, 3.6, 4.2, 4.4

Results and Discussion: -

Backwater Rise: -

The weir and vegetation always provide a barrier to the flowing water which creates backwater on the upstream side and the initial water depth (ho) was raised upstream of the SDS and HDS due to the presences of weir and vegetation. The backwater rise varied linearly with increasing Froude number while relative backwater rise decrease with increasing Froude number as shown in Figure 2a,b. The decrease in relative backwater rise shows that the initial flow depth had much effect on the relative backwater rise for a given Froude number. In these figures, Δh and ho are the water depths on the upstream side of weir and weir-vegetation and initial water depth without any model placed in the channel respectively.

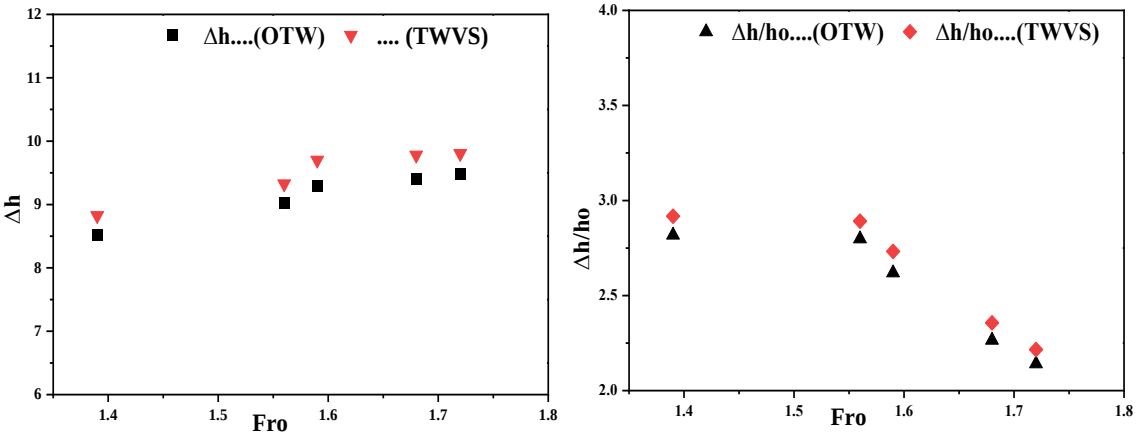

a b

Figure 2: - (a) SDS and HDS Backwater rise (Δh), (b) SDS and HDS relative backwater rise(Δh/ho).

Hydraulic Jump and water surface profile: -

When supercritical flow transforms to subcritical flow a hydraulic jump is formed [16]. The formation and classification of hydraulic jumps due to vegetation and due to dike and vegetation under sub-critical flow were investigated by various researchers [17]. For the stability of the hydraulic structure, it is essential to reduce flood energy by controlling the position of the hydraulic jump [18]. In this experimental investigation no jump were observe at upstream and downstream side of SDS as shown in figure 3b. The hydraulic jump was only observed in case of hybrid defense system (HDS) in TWVS case. The type of jump formed in the case of HDS as shown in figure 1a 3c. In figure h_1, are the mean water depth at upstream of weir, h_2 at upstream vegetation, h_3 downstream of vegetation patch and, hc critical depth respectively and V_1, are the velocity at upstream of weir, V_2 at upstream of vegetation, V_3, downstream of vegetation patch and V_c, critical velocity at the critical depth respectively. The Jump develop in section 2 with no jump in section 3 in the case of HDS. Water surface profile of SDS and HDS are shown in figure 3b c. The steep water slope in the zone of weir and vegetation are due to the transition of flow (sub-critical to super-critical and vice versa).

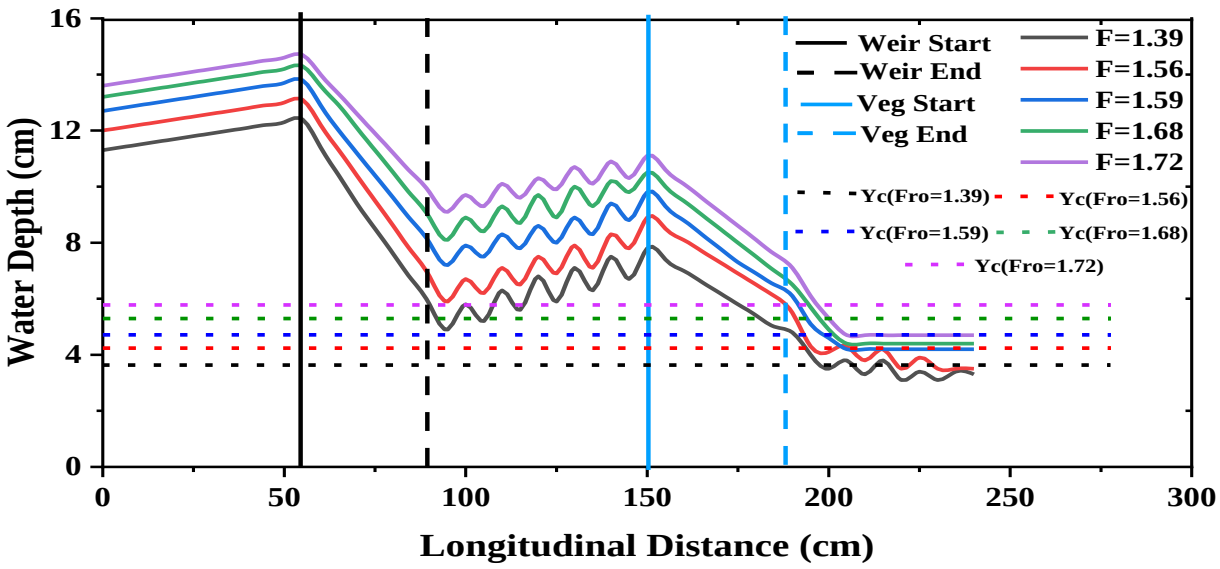

a

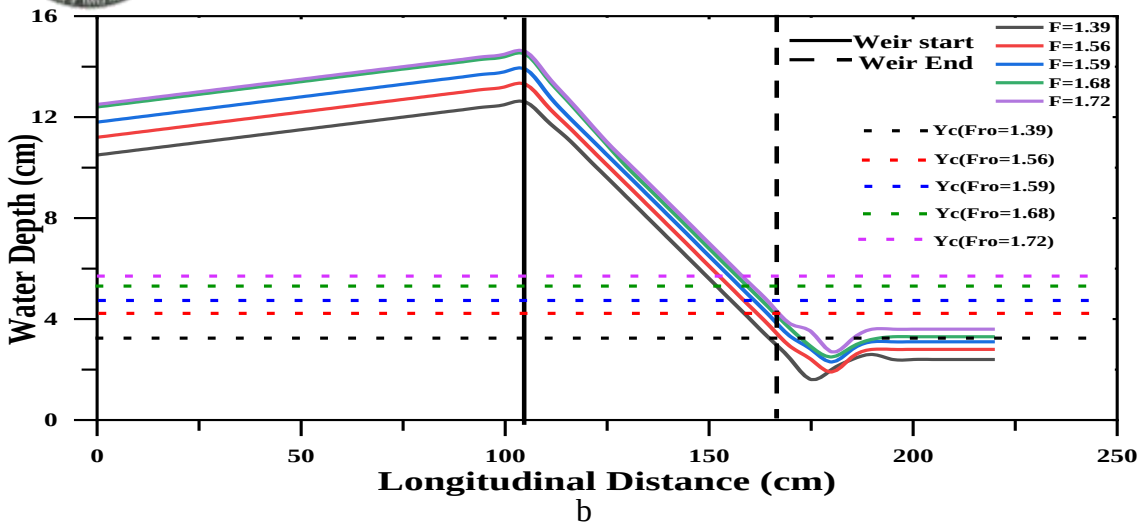

b

Figure 3: - Water Surface Profile (a) Surface profile of water for SDS (b) Surface Profile of water for HDS.

Energy Dissipation through SDS & HDS

For selected range of the initial Froude number (Fr_o =1.39-1.72), the energy dissipation through single defense system (SDS) and hybrid defense system HDS were calculated. The maximum energy reduction through SDS was 38% and it decrease with higher values of Froude number as shown in figure 4a. The energy dissipation rate decreases 15% by increasing initial Froude number from 1.39 to 1.72. The maximum energy dissipation in the hybrid defense system, case of TWVS was 53% that decreases by increasing the initial Froude number and almost 11% energy reduction was observed by increasing the initial Froude number from 1.39 to 1.72 as shown in figure 4b c. The maximum energy loss due to hydraulic jump were calculated in section 2 ($\Delta E_{j2}= (\frac{(Y2-Y1)^2}{4Y1Y2})$) for checking the effectiveness of HDS. The maximum energy loss due to hydraulic jump in the case of WV was 3%. The maximum total energy dissipation in the case of WV was 56% and the average energy reduce was 42%. From results it was observed that, factor effecting the flood energy dissipation are initial Froude number and "vegetation density (B/d)" [19] .

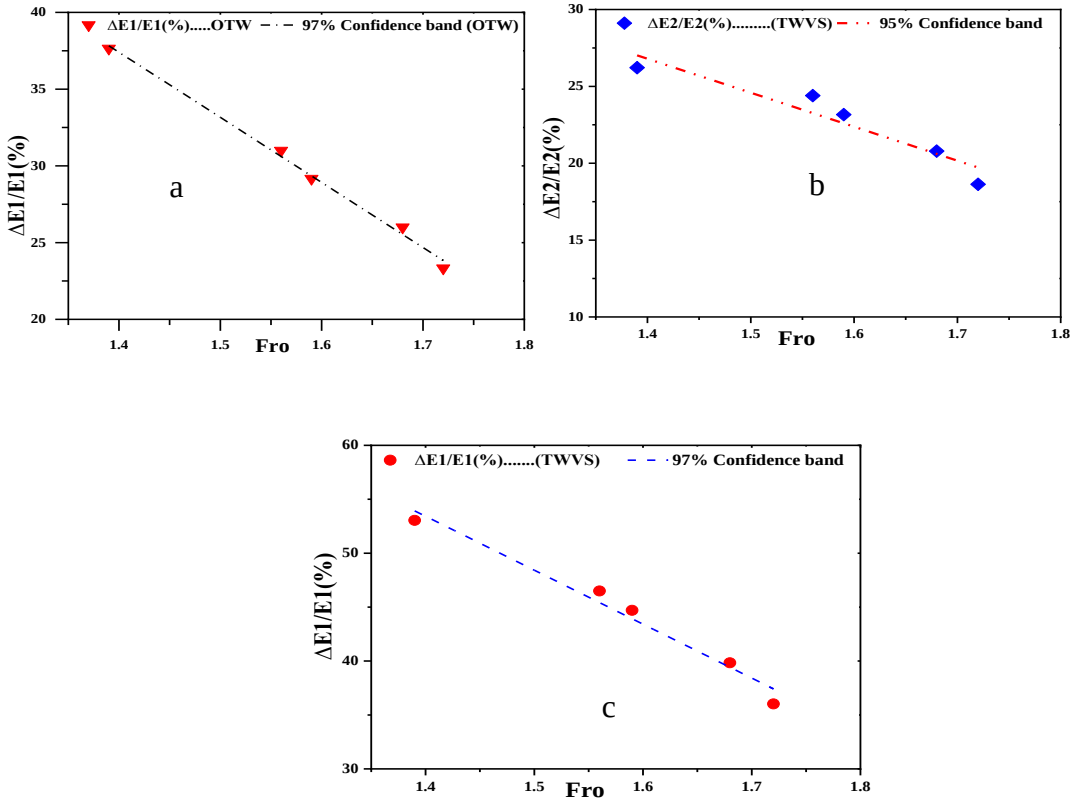

Figure 4:- Percentage energy loss for different obstruction types: (a) OW (b) WV (c) WV

Conclusion: -

For the selected range of initial Froude number (Fr_o = 1.39–1.72) a flow structure with energy dissipation was investigated experimentally in the channel. The conclusion of the study is followed:

- The backwater rise increases with increasing Fr_o while relative backwater rise decreases with increasing Fr_o.
- No hydraulic jump was observed at upstream and downstream in the case of SDS and only weak jump was observed in case of HDS in section 2.
- The maximum average energy loss (%) in the case of SDS and HDS was 30% and 45% respectively.
- The energy dissipation decreases 17% against Fr_o=1.39-1.72 in case of HDS.
- The percentage energy dissipation decreases with increase in Froude number.
- It has been concluded from the result that HDS is very effective for torrential flood energy loss as compared to SDS.

Nomenclature

h_o	Initial Water Depth
OW	Only Weir
Fr_o	Initial Froude Number
Δh	Backwater Rise
$\Delta E1/E1(\%)$ & $\Delta E2/E2(\%)$	Percentage Energy Loss
WV	weir-vegetation.

References

[1] S. K, "Environmental Hazards: Assessing Risk and Reducing Disaster.", New York, NY, USA,: Routledge:,, 2003.

[2] T. T. a. P. D. M. W. Kellens, ""Perception and communication of flood risks:A systematic review of empirical research."," *Risk Anal.,* , Vols. 33,, pp. 24-49,, 2013..

[3] T. A.-B. H. K. a. K. M. A. Abbas, ""Non-structural flood risk mitigation under developing country conditions: An analysis on the determinants of willingness to pay for flood insurance in rural Pakistan."," *Nat. Hazards.,* , Vols. 75,, pp. 2119–2135,, 2015..

[4] Nateghi, "" Statistical analysis of the of Effectiveness Seawalls and Coastal Forests in Mitigating Tsunami Impacts in Iwate and Miyagi Prefectures"," *Plos One,* , 2015.

[5] Reman, " "Experimental and numerical modeling of tsunami mitigation by canals"," *Journal of Waterway, Port, Coastal, and Ocean Engineering,* , vol. 143, no. 1, 2017.

[6] Tanaka. N, ""Effectiveness and limitations of coastal forest in large tsunami: conditions of Japanese pine trees on coastal sand dunes in tsunami caused by Great East Japan Earthquake"," *Journal of Japan Society of Civil Engineers, Ser. B1 (Hydraulic Engineering),* , vol. 68, no. 4, pp. 7-15, 2012.

[7] B. Munir and J. Iqbal, ""Flash flood water management practices in Dera Ghazi Khan City(Pakistan): A remote sensing and GIS prospective,"," *Nat. Hazards,,* vol. 81, pp. 1303–1321,, 2016.

[8] S. A. a. S. H. B. Munir, " " Integrated hazard modeling for simulating torrential stream response to flash flood events,," *Isprs Int. J. Geo-Inf*, vol. 9, no. 1, 2019.

[9] A. Petrovic, ""Challenges of torrential flood risk management in Serbia,," *J. Geogr. Inst. Jovan CVIJIC SASA,*, Vols. 65,, pp. 131–143,, 2015..

[10] N. T. Y. S. M. O. Nandasena, "Boulder transport by the 2011 Great East Japan tsunami: Comprehensive field observations and whither model predictions," *Marine Geology,* vol. 346, no. 1, pp. 292-309, 2013.

[11] M. Rahman, N. Tanaka and A. Rashedunnabi, "Flume Experiments on Flow Analysis and Energy Reduction through a Compound Tsunami Mitigation System with a Seaward Embankment and Landward Vegetation over a mound," *Geosciences,* vol. 90, no. 11, 2021.

[12] U. Fadly and K. Murakami, "Study on reducing tsunami inundation energy by the modification of topography based on local wisdom.," *J. Jpn. Soc. Civ. Eng. Ser. B3,* vol. 68, pp. I_66–I_71,, 2012.

[13] M. Tanvir, M. Siddiqui and A. Shah, " Growth and price trend of Eucalyptus camaldulensis in Central Punjab,," *Int. J. Agric. Biol,,* Vols. 4,, pp. 344-346,, 2002..

[14] W. Huai, Y. Zeng, Z. Xu and Z. Yang, "Three-layer model for vertical velocity distribution in open channel flow with submerged rigid vegetation.," *Adv. Water Resour,,* Vols. 32,, pp. 487–492,, 2009..

[15] Ž. Pavlin and N. Kuspili´c, "Reference water levels for the design of dykes and earthfill dams.," *Građevinar,,* Vols. 70,, pp. 225-233,, 2018..

[16] G. Pasha and N. Tanaka, ""Critical Resistance Affecting Sub- to Super-Critical Transition Flow by Vegetation."," *J. Earthq. Tsunami, ,* Vols. 13,, 2019..

[17]] G. Pasha and N. Tanaka, ""Undular hydraulic jump formation and energy loss in a flow through emergent vegetation of varying thickness and density,"," *Ocean Eng,,* vol. 141, pp. 308–325,, 2017..

[18] V.T Chow, "Open-Channel Hydraulics", New York, NY, USA,: McGraw-Hill,, 1959.

[19] A. A. G. A. R. A Ahmed, "Experimental Investigation of Flood Energy Dissipation by Single and Hybrid Defense System," *Water*,, vol. 11, no. 10, pp. 2073-4441, 2019.

2nd International Conference on Advances in Civil and Environmental Engineering (ICACEE-2023)

University of Engineering & Technology Taxila, Pakistan

Conference date: 22nd and 23rd February, 2023

Flood Forecasting in Pakistan using Integrated Flood Analysis System (IFAS)

Usman Ashiq[1], Muhammad Ejaz Tanveer[2], Afzal Ahmed[3]

[1]Civil Engineering Department/UET Taxila, Pakistan. usman.ashiq@students.uettaxila.edu.pk

[2]Superintending Engineer (Floods) O/o Chief Engineering Advisor/Chairman Federal Flood Commission Ministry of Water Resources, Islamabad, Pakistan. engrejaz@hotmail.com

[3]Civil Engineering Department/UET Taxila, Pakistan. afzal.ahmed@uettaxila.edu.pk

ABSTRACT

Emerging climatic changes have increased natural disasters, particularly floods. To combat the floods normally both structural and non-structural countermeasures have been utilized worldwide. In Pakistan, attention has not yet been given to precise flood forecasting in terms of non-structural measures. An Integrated Flood Analysis System (IFAS) is used in this study on one of the Indus River's basins as a non-structural countermeasure to evaluate the performance and efficacy of the model for flood forecasting in Pakistan. According to the findings, calibrated results of flood event are comparable/similar to the results of the historical flood event, as demonstrated by Nash-Sutcliffe efficiency coefficient (NSE) of 0.58, and coefficient of determination (R^2) of 0.60. This indicates that IFAS, in some respects does have the ability to forecast the flood and it can be used for the early flood forecasting as a non-structural countermeasure that ultimately contributes to the preparation of evacuation plans for communities located on floodplains, allowing decision-makers including emergency responders to take the appropriate actions and spread awareness for the mitigation of flood damages which is an emerging need for developing countries.

KEYWORDS: Hydrological modelling; Indus River System; Flood Forecasting; IFAS; Pakistan.

INTRODUCTION

Climate change has resulted in a significant increase in the magnitude and frequency of flooding events over the last decade and repeated flood events have demonstrated the developing weakness to climate change often droughts, around the world which is viewed as a major global concern[1]. Flooding is one of the most devastating natural disasters to have struck humanity, killing millions of lives and causing destruction to infrastructure and societal assets[2, 3].

To counter the flood damages in developing countries majorly structural and non-structural countermeasures have been adopted, but due to the high cost of taking adequate structural countermeasures, difficulty in obtaining real-time hydrological data in river basin and resources for authorities[4] raises the importance of developing an effective flood forecasting system based on hydrological modelling in developing countries as a non-structural countermeasure to lessen the vulnerability to flood risk[5]. Several distributed and semi-distributed hydrological models have been developed for flood modelling and forecasting in which tank modelling approach stands out among

many others with reasonable success[6, 7] because the standard precipitation runoff models struggle to account the quick rise and brief duration in rapid floods[8].

Non-structural countermeasures have not been extensively utilized in Pakistan. However in some studies IFAS is utilized and comparison showed similar results of rainfall from multiple sources to model the upper-middle Indus River[9]. The Dungun River basin in Malaysia, which produced an efficiency coefficient of 0.72, showed that IFAS performed better in large basins[10]. In the trans-boundary of Kabul River basin IFAS shows the ability to accurately simulate flood peaks in large-scale, data-scarce basins[11]. IFAS was also calibrated for the upper Indus catchment with an average NSE of 0.8[12]. In Cagayan River basin, Philippines, IFAS combined satellite and ground rainfall to predict floods with high accuracy[13]. The success of a flood modelling exercise heavily depends on the precision of the rainfall input[14] that ultimately helpful in flood forecasting, land use planning and zoning, flood plain management and provide early information which can play a vital role to counter the flood damages.

The main objective of the study is to use the IFAS model to analyse the most recent flood event of 2022 in Pakistan and check the accuracy of the model for flood forecasting.

STUDY AREA

In Pakistan five main rivers, namely, the Indus, Jhelum, Chenab, Ravi and Sutlej and their tributaries flow through the country's plains. The Indus, Jhelum and Chenab are known as the Western Rivers and Ravi, Beas, and Sutlej known as the Eastern Rivers. Flooding of the Indus River and its tributaries represents the greatest hazard in Pakistan. Floods occur usually in summer season (July - October) due to heavy rainfalls and snow melting.

In this study, analysis is carried out on the upstream reach of the Chashma basin (32.4758° N, 71.3586° E) over which the watershed has been delineated, which is located on the Indus River in Pakistan and has a catchment area of 3,40,000 Km^2. Indus River system covers all the major rivers in Pakistan and is the major cause of flooding every year. Details about the basin is shown in Figure.

DATA SETS

Digital elevation model (DEM-30M) Global Map (V2), landcover/landuse with 15 arc second resolution (ISCGM) Global Map (V2), Global soil geology (DSMW) spatial resolution of 5 X 5 arc minutes (FAO/UNESCO), and daily rainfall data are the inputs to building up a distributed rainfall-runoff analysis. Ground-based discharge data is collected from Federal Flood Commision (FFC) Islamabad Pakistan and satellite-based 24 hours with spatial resolution 0.1° X 0.1° rainfall data product (GSMaP-NRT) is obtained by the Japan Aerospace Exploration Agency JAXA.

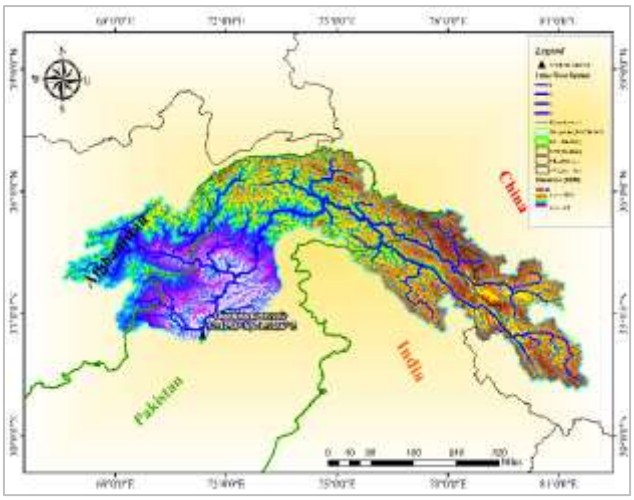

Figure 1 Study Area Map

METHODOLOGY

In this study IFAS model used consists of two layers storage tanks (surface and aquifer) and river tank for flood analysis. The analysis is performed on the flood event from August 20,2022 to August 31,2022 in which simulation model is created by utilizing the global elevation, soil, landcover data and rainfall data products. The methodology used in this study which comprises of creation of rainfall-runoff model, importing of global data, parameter estimation of 2-layers tank (Surface-Aquifer and River Course), and executing of the calculation following calibration which ultimate to runoff results. Fiqure 2 shows the schematic process.

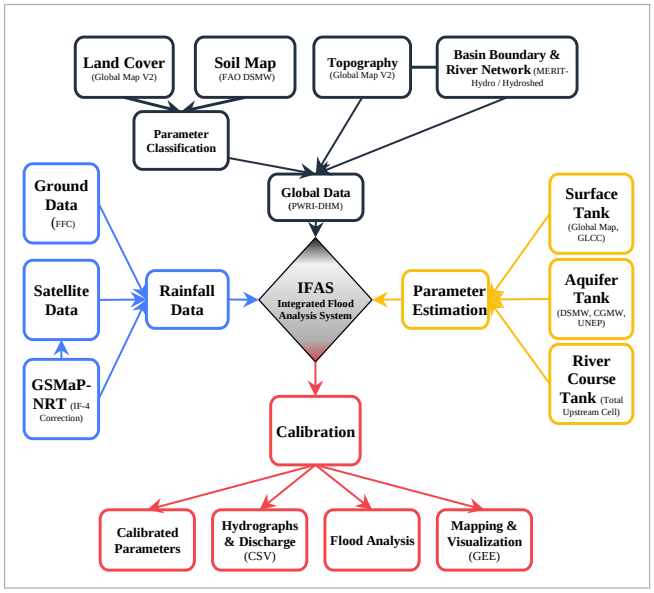

Figure 2 Adopted Methodology Diagram

Parameters (Surface, Aquifer and River Tanks)

Surface, aquifer/groundwater, and river course parameters are the three different types of parameters from Global Map that are used in the calibration process. Figure 3 shows the classification of parameters and Fiqure 4 shows the structure of the IFAS model.

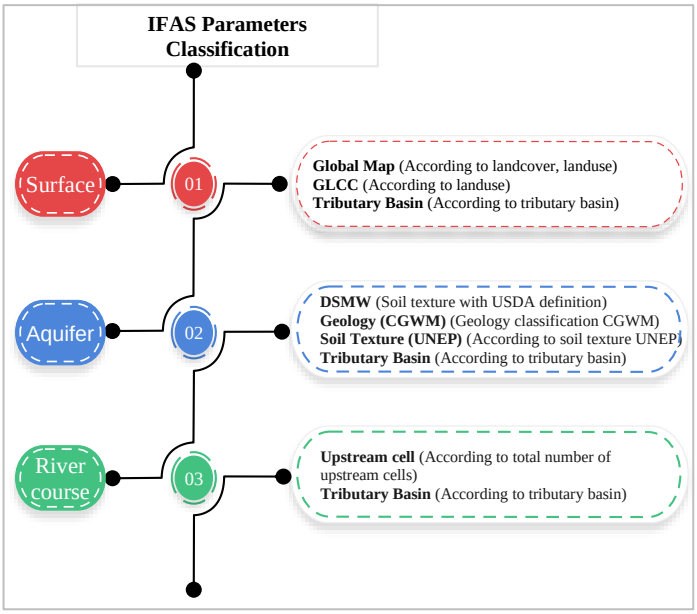

Figure 3 Parameters Sets of IFAS on each Classification

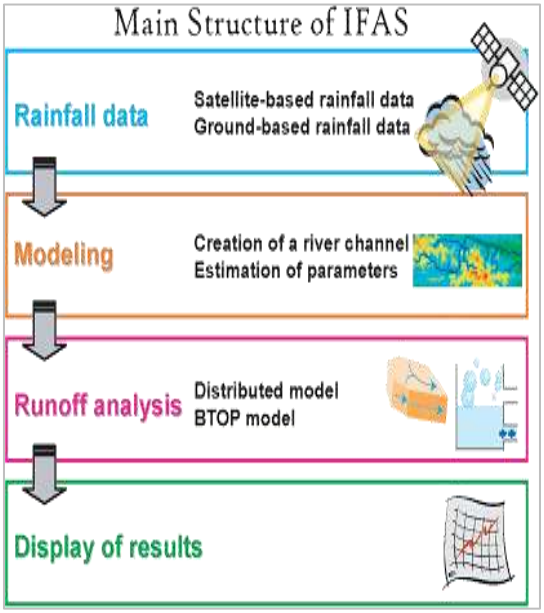

Figure 4 IFAS Model Structure

RESULTS

The observed discharge data from the river station at Chashma basin is contrasted with the calculated discharge data generated by IFAS before and after the tuning of parameters. The results calculated by the IFAS are very much like the observed discharge which means that calculated discharge is comparable with observed discharge, and comprehensive results are attained by choosing/tuning the more accurate parameters. It is essential to keep in mind that the complexity of the model and the quality and completeness of the input data influence the accuracy of IFAS model. Figure 5 and Figure 6 shows the comparison between the calculated and observed flood discharges before and after the tuning of parameters.

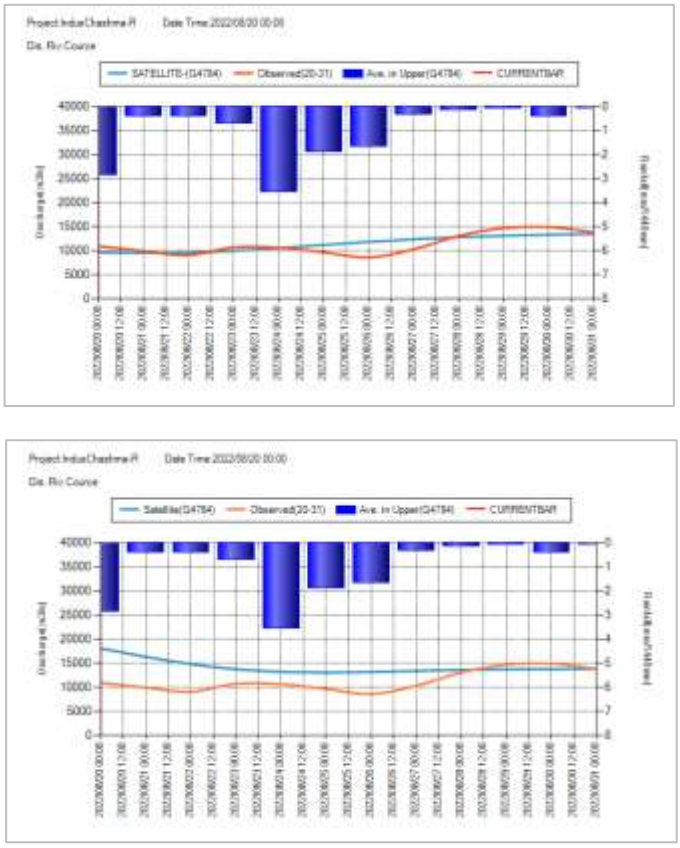

Figure 5 Comparison before tuning of parameters.

PERFORMANCE EVALUATION

The performance of IFAS model on the basin is assessed using the Nash-Sutcliffe efficiency NSE of 0.58, and coefficient of determination R^2 of 0.60. These values indicates that the model is effective and has predictive ability for flood forecasting[15, 16].

CONCLUSION

The IFAS-calculated discharge for the flood event in August 2022 is contrasted with the historical discharge at Chashma basin. However, the satellite-based GSMaP-NRT rainfall data product overestimated and underestimated the ground-based data from ground-installed stations, despite the similarities between the IFAS hydrograph and the historical discharge hydrograph. This is so that while ground-based data represents the point rainfall that originates from the designated station, and satellite-based data represents rainfall that originates from the upper atmosphere.

It is concluded from the findings that IFAS is capable of flood forecasting to some extent and the results are comparable to those of historical data. As a non-structural countermeasure, IFAS can be used for early flood forecasting, which ultimately helps in the preparation of evacuation plans for communities located in floodplains or at vulnerable locations which is a growing demand in developing country. Nevertheless, it is recommended that the results can be enhanced by adopting the appropriate parameters for the accurate flood forecasting in Pakistan.

ACKNOWLEDGEMENTS

The authors would like to acknowledge the Japan Aerospace Exploration Agency (JAXA), and Federal Flood Commision (FFC) Ministry of Water Resources Islamabad, Pakistan for providing the relevant data for this study.

REFERENCES

1. Aziz, A. and S. Tanaka, *Regional parameterization and applicability of Integrated Flood Analysis System (IFAS) for flood forecasting of upper-middle Indus River.* Pak. J. Meteorol, 2011. **8**: p. 21-38.
2. Aziz, A., *Rainfall-runoff modeling of the trans-boundary Kabul River basin using Integrated Flood Analysis System (IFAS).* Pakistan Journal of Meteorology Vol, 2014. **10**(20).
3. Chohan, K., et al., *Riverine flood damage assessment of cultivated lands along Chenab River using GIS and remotely sensed data: a case study of district Hafizabad, Punjab, Pakistan.* Journal of Geographic Information System, 2015. **7**(05): p. 506.
4. FFC, *Federal Flood Commission Annual Flood Report. Ministries of Water and Power, Islamabad.* 2016.
5. FFC, *Federal Flood Commission Annual Flood Report. Ministries of Water and Power, Islamabad.* 2018.
6. Hafiz, I., et al. *Application of integrated flood analysis system (IFAS) for Dungun River Basin*. in *IOP Conference Series: Earth and Environmental Science*. 2013. IOP Publishing.
7. Motovilov, Y.G., et al., *Validation of a distributed hydrological model against spatial observations.* Agricultural and Forest Meteorology, 1999. **98**: p. 257-277.
8. Manh Hung, N., et al., *FLOOD INUNDATION ANALYSIS USING A DISTRIBUTED TANK MODEL FOR A FLAT, LOW-LYING AGRICULTURAL AREA UNDERGOING URBANIZATION IN HANOI, VIETNAM.* Irrigation and Drainage, 2013. **62**: p. 52-62.
9. Mendoza, M.T. and R. Schwarze, *Sequential Disaster Forensics: A case study on direct and socio-economic impacts.* Sustainability, 2019. **11**(21): p. 5898.
10. Pancawati, J., et al., *Application of tank model for ungauged reservoir management: a case of Situ Cipondoh, Tangerang Indonesia.* J Environ Earth Sci, 2019. **9**: p. 52-61.
11. Samarasinghea, S., et al., *Application of remote sensing and GIS for flood risk analysis: a case study at Kalu-Ganga River, Sri Lanka.* International Archives of the Photogrammetry, Remote Sensing and Spatial Information Science, 2010. **38**(8): p. 110-115.
12. Sugiura, A., et al., *Challenges on modelling a large river basin with scarce data: A case study of the Indus upper catchment.* Journal of Hydrology and Environment Research, 2014. **2**(1): p. 59-64.
13. Shi, W., et al., *A hydrological model modified for application to flood forecasting in medium and small-scale catchments.* Arabian Journal of Geosciences, 2016. **9**(4): p. 1-15.

14. Shahzad, A., et al., *Development of a flood forecasting system using IFAS: a case study of scarcely gauged Jhelum and Chenab river basins.* Arabian Journal of Geosciences, 2018. **11**(14).
15. Suryaningtyas, L.S., S. Ery, and R. Rispiningtati, *Hydrological analysis of TRMM (Tropical rainfall measuring mission) data in lesti sub watershed.* 2020.
16. Wi, S., et al., *Calibration Approaches for Distributed Hydrologic Models in Poorly Gaged Basins.* 2015.

2nd International Conference on Advances in Civil and Environmental Engineering (ICACEE-2023)

University of Engineering & Technology Taxila, Pakistan

Conference date: 22nd and 23rd February, 2023

Disaster Management Plan for Flood Affected Areas - A GIS Based Prediction Model

Abaid Ullah[1], Noor ul Huda[2], Ishwa Azhar[3], Muniba Hameed[4], Laiba Choudhary[5], Fiza Numan[6]

[1]Department of Environmental Engineering, University of Engineering & Technology Taxila, Pakistan
abaid.ullah@uettaxila.edu.pk
[2]Department of Environmental Engineering, University of Engineering & Technology Taxila, Pakistan
19-env-03@students.uettaxila.edu.pk
[3]Department of Environmental Engineering, University of Engineering & Technology Taxila, Pakistan
19-env-18@students.uettaxila.edu.pk
[4]Department of Environmental Engineering, University of Engineering & Technology Taxila, Pakistan
19-env-19@students.uettaxila.edu.pk
[5]Department of Environmental Engineering, University of Engineering & Technology Taxila, Pakistan
19-env-27@students.uettaxila.edu.pk
[6]Department of Environmental Engineering, University of Engineering & Technology Taxila, Pakistan
19-env-33@students.uettaxila.edu.pk

ABSTRACT

Floods usually happen due to heavy rains, melting snow and malfunction of dams, and cause damage to infrastructure and human life. Various types of floods include flash floods, river floods, coastal floods, and urban floods. The impact of floods can be predicted through the use of early warning systems such as Arc GIS. Possible flood control measures include building levees, creating floodplains and developing disaster management plan. However, due to climate change and development, floods are becoming more frequent and severe. In this paper, a simulation-based study has been conducted by using Arc GIS. Moreover, a disaster management plan has been proposed to minimize the negative impacts of floods. The main components of this plan include (i) risk assessment, (ii) early warning and evacuation, (iii) search and rescue, (iv) medical assistance, (v) relief and recovery, (vi) public information and communication, (vii) coordination and cooperation, and (viii) drills and exercises. This plan is capable to minimize the loss of life, reduce the economic impact of flood and quick revival of the flood affected area.

KEYWORDS: Disaster management plan; Flood; Geographical information system; Prediction model.

INTRODUCTION

Globally, floods are one of the most common and widespread natural disasters causing significant damage to property, infrastructure, and human life. They are caused by a variety of factors including heavy rainfall, snowmelt, hurricanes, and tsunamis. In recent years, climate change has led to an increase in the frequency and severity of floods in many regions of the world. Between 80-90% of all documented disasters from natural hazards during the past 10 years have resulted from floods, droughts, tropical cyclones, heat waves and severe storms [1]. Due to rapid unplanned urbanization, particularly the cities in South Asia and Africa have experienced the equivalent increases in the number of fatalities related to floods [2].

Recent record-breaking floods in Pakistan are the worst natural disasters in the country's history. Climate activists and experts reported that while Pakistan contributes only 1% to global carbon emissions, however, its share in the devastating impacts of climate change is enormous. The flood-hit areas suffer from the scarcity of clean drinking water along with the outbreak of various diseases such as diarrhoea, cholera, typhoid fever, gastroenteritis, dengue fever and malaria [3]. In Pakistan, 20 million people were affected by the flood of 2010, 17-million-acre crops were eliminated and destroyed, economic damage were 10 billion [4]. In Pakistan, the flood of the year 2022 killed 1717 people and it has been declared as the worst in the country's history. The government of Pakistan has estimated losses worth US$40 billion from the flooding [5]. According to the World Health Organization (WHO) around 890 health facilities were damaged,15 cases of wild poliovirus were reported in KPK, 1.8 million sample collecting kits and water washing tablets were supplied for the detection of infection [6].

In 2008, participatory geographical information system (PGIS) or participatory mapping was used for the identification of hazards and associated risks [7]. The applications of PGIS are countless even local people repeatedly gather information about flood risk. For instance, it has been used for disaster risk reduction (DRR) in medical centres, dangerous infrastructure, mapping flood protection plan, mapping hazard characteristics and future disaster prediction. Especially, the government must impose emergency alertness and awareness at the national level [8]. Although several attempts have been carried out to overcome the consequences of floods by using flood modelling and risk assessments, however, real-time implementation of health and safety measures is very limited due to lack of planning and poor management. To address this issue, an attempt has been made to study the impact the flood through simulation by using Arc GIS. Moreover, a disaster management plan has also been proposed for pre, during and post flood management. This will help to minimize the losses, ensure immediate and appropriate support to victims, and achieve a quick and efficient recovery.

ArcGIS is a geographic information system (GIS) software developed by Esri, which has been used to simulate floods. The software includes tools for creating digital elevation models, analyzing hydrologic and hydraulic processes, and creating flood maps. The Flood Analysis Extension ArcGIS can be used to model flood inundation and estimate flood depths, velocities, and water surfaces. Users can also create scenario-based flood simulations and perform risk analysis [9]. Risk assessment model were also applied in household communities for evaluating hazards [10]. Previously, ArcGIS and Remote sensing were used to accurately describe flooded areas, flood-risk regions, and adequate flood shield areas to decrease the impact of flood. The collected information can be helpful for flood arrangements, flood designing, future prediction, crisis reaction and flood alertness [11].

Moreover, HEC-RAS 2D model was developed to investigate flood characteristics including duration, arrival time, flood velocity and recession time [12]. In addition risk management was also supported by public, policy makers and scientific communities where policy maker and researchers manage the risk models through their knowledge and practices [13]. Furthermore, flood

management solutions including structural (e.g. wetlands) and non-structure measures (e.g. promote flood prediction, promote warning system) were recommended to manage flood [14]. Previously, GIS-based multi-criteria model for landscape was developed to better manage rainwater runoff by increasing rainwater infiltration rates through installation of green infrastructures [15].

METHODOLOGY

Firstly, a comprehensive literature review was carried out to study the practices and plan use for disaster management. this stage helped in identifying the gap present in the field thereafter a GIS based simulation is carried out predict the impact of floods in the study area (i.e., Sindh, province of Pakistan). For this purpose, a 3D elevation map of Sindh was used in the software. Considering the results of simulation, a disaster management plan was proposed for the flood affected areas which was further validated by the help of experts. The stepwise methodology used for this study is shown in Figure 1.

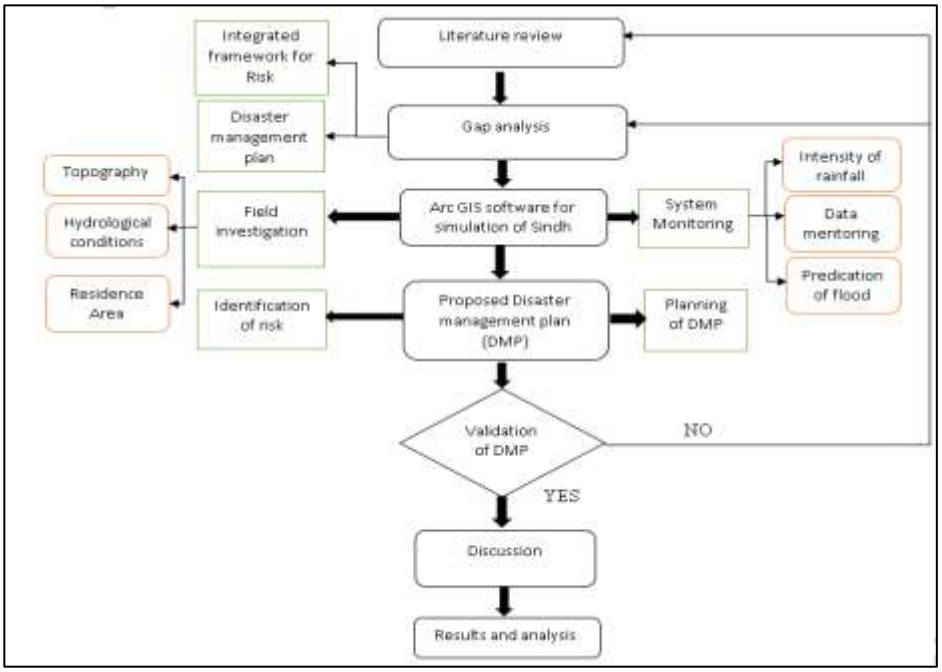

Figure 7: Methodology used for the proposed disaster management plan.

FLOOD RISK SIMULATION

The imported 3D elevation map of Sindh is shown in Figure 2. The legend shows the elevation in meters starting from -15m to 2025m. The reading of -15m shows that the surface is already in the water body due to the presence of Indus River at the specified location.

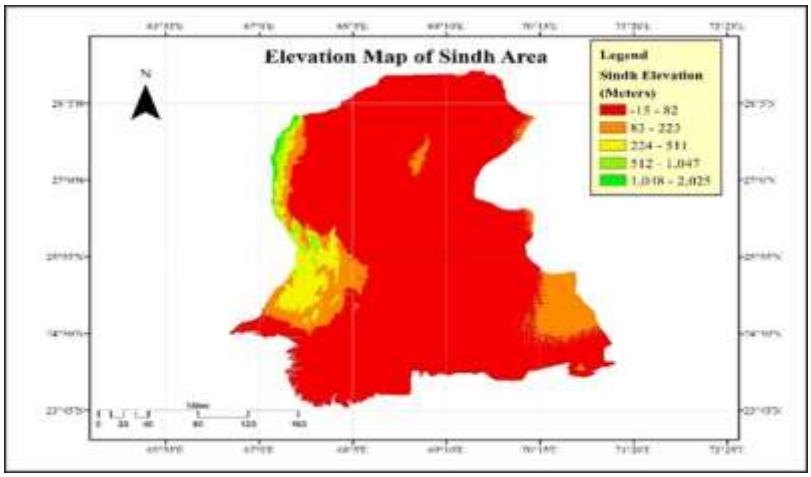

Figure 8: 3D elevation model of Sindh.

Flood risk simulation was carried out by adding the shape file of study area. Later, elevation and water level were added in study area attribute table. Figure 3 shows the simulation results of area under study.

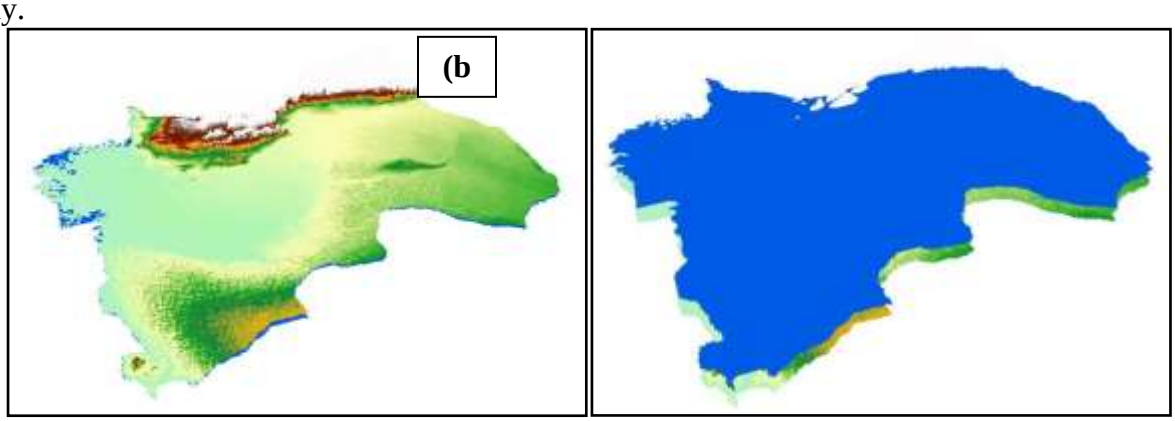

Figure 9: Simulation results for (a) pre and (b) post flooded area of Sindh.

It is important to determine the topography of the study area (i.e., mountain and plains). This map was imported in Arc scene for Arc GIS and then converted to raster. Figure 3a shows a 3D elevation model of the area of Sindh under consideration in Arc Scene without flooding. Figure 3b shows the risk simulation of area under flooding having water level 650m above sea level the automation control in Arc scene was varied from sea level to 650m above sea level to conduct flood risk simulation. Results indicate that flooding up to this level is capable to affect the whole area of Sindh specially those areas that are near to Indus River.

PROPOSED DISASTER MANAGEMENT PLAN FOR FOOD AFFECTED AREAS

The first step of flood disaster management is to assess and verify the situation under consideration. If a situation requires risk assessment or use of disaster management plan it should be followed. However, if situation is not fitting any of these scenarios, then help from disaster management team can be sought. Risk assessment for the disasters include the identification of hazards [16]. After all the hazards are identified, evaluate the hazards and resources required (i.e., time, money, manpower etc.) for the elimination of risk and hazards. Later, disaster management plan is developed after risk assessment. This plan consists of prevention, preparedness, response, and recovery. Prevention includes identification and elimination of hazards. Preparedness for disaster includes drills and trainings for emergency situations, planning of escape routes in case of floods. For instance, if the sea level is rising preparedness includes opening of flood gates and if sea level is not rising fresh pond outlets can be opened. In DMP, the response is for the situations when the flood has already occurred. To overcome this, a detailed damage assessment is carried out. If any damage occurs, then rescue and relief is provided. However, if there is not any damage to infrastructure or people then precautionary measures can be taken for the future. After the flood, restoration and rehabilitation can be done in the affected areas to overcome the damage.

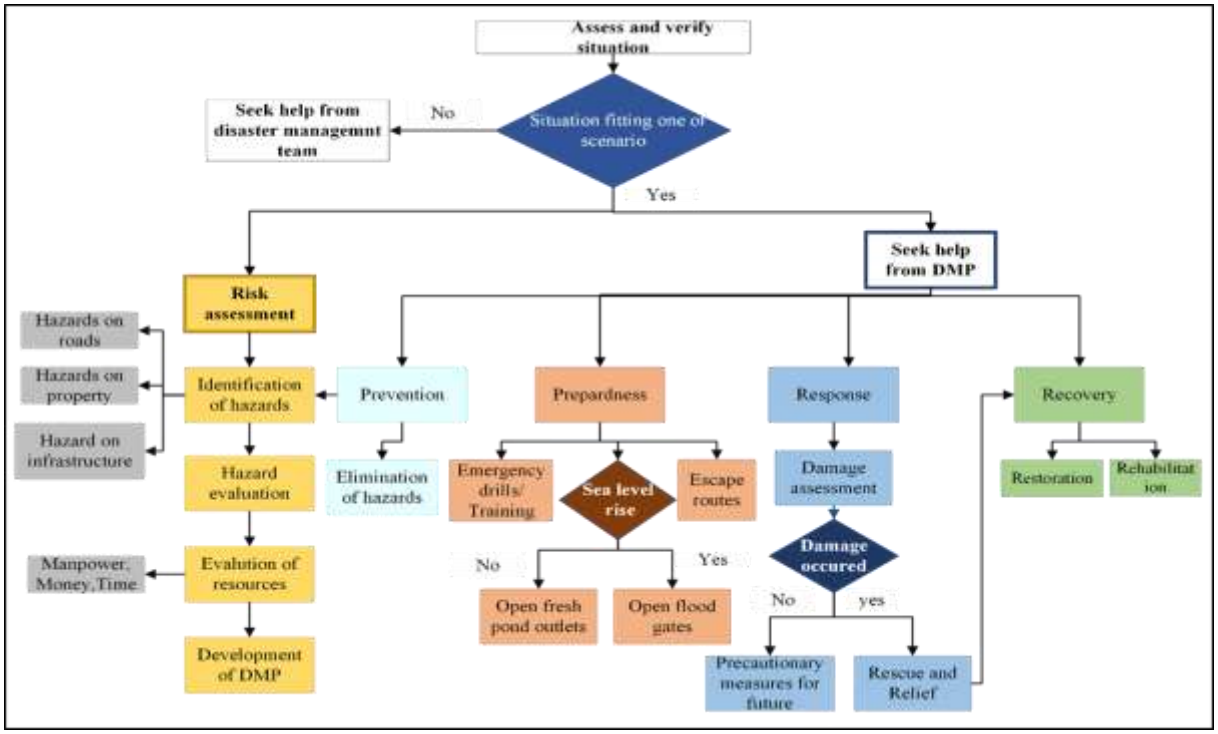

Figure 10: Proposed disaster management plan (DMP) for flood preparedness.

DISCUSSION

Several disaster management models were identified from the literature including integrated, logical, and cause models. Integrated models depict the several stages of a disaster by tracing the development of various tasks. The main events and behaviour that make up a disaster are highlighted in logical models, whereas the cause models offer some underlying causes of disasters. The typical type of integrated disaster management model includes Manitoba and Weichsel Gartner model. The Manitoba integrated model has altogether six independent elements including strategic plan, risk management, hazard management, mitigation, preparedness, monitoring and review. This model offers a balance between readiness and adaptability to enable quick response to the unique requirements of disasters [17]. The Weichsel Gartner model assesses possible damage and planning of future actions to reduce this possible damage [18]. Similarly the typical type of the pre disaster risk reduction and post disaster recovery makeup the traditional process of disaster management [19]. The expand and contract model is a continuous process in which different disaster management phases occurs concurrently [20]. The Kimberly's model describes mitigation, preparation, response, and recovery as four stages of disaster management. This model portrays response as the most important phase of disaster management. It emphasizes preparation and mitigation at the core, implying that these two factors will ultimately lead to an effective response. Because recovery phase is what remains after response it has been given top priority [21]. The Tuscaloosa model is an open-ended emergency management process and the four phases of this begin and end with mitigation to limit the effects of a disaster [22]. Cause models include crunch model and release model. The crunch model offers a framework for understanding the causes of a disaster. In this model the growth of community's variability and the reasons why the needs of people are not met are highlighted [23, 24]. The pressure and release model can be considered as the reverse of the crunch model. It demonstrates the implanting mitigation and prevention measures to lower the likelihood of disasters [25].

According to Alexander current methods for disaster management do not address (i) death tolls, (ii) transfer of technology; and (iii) disaster relief , mitigation and economic development [26]. There is not a single framework that consists of all the major activities of disaster management. The design of the majority of models consists of four main phases of disaster management i.e., (i) prevention, (ii) mitigation, (iii) recovery and (iv) response. The current models do not effectively take evaluation and analysis into account. Disaster management model should include recognizing and exploiting these resources because different conditions, activities, and resources are engaged during catastrophes. The proposed model is capable to address these issues through risk assessment, risk management and implementation of disaster management actions. The proposed model is a simple framework that consists of all the manager activities of disaster management, no expert knowledge is needed for its

comprehension. The proposed model is a simple comprehensive framework that is understandable to know expert users and address all the activities of disaster management collectively.

CONCLUSION

The study aimed at proposing the DMP for the flooded affected areas. To this purpose, a comprehensive methodology has been formulated for pre-, during-, and post- floods management while focusing on monitoring system, field investigation, mitigation measures and recommendations.

In this study, Sindh has been considered as a study for the future prediction of flood. It has been identified that Sindh is already -15% under water and a rainfall of high intensity and duration causing water level to rise to 650m above sea level can affect whole Sindh. Since psychological distress, psychosocial distress and mental health may be provoked due to floods or the fear of floods, therefore, it should be the first priority of policy makers, emergency planners, health care services and social care services. Moreover, evidence-based policy in the flooded areas is necessary to promote the management system. In future, the proposed disaster management plan can be implemented to assess its tendency to reduce the impact of floods.

REFERENCES

1. Mekuria, T., *The effects of flooding and drought on clean water accesibility in Ethiopia.* 2022.
2. Shah, S.M.H., et al., *A review of the flood hazard and risk management in the South Asian Region, particularly Pakistan.* Scientific African, 2020. **10**: p. e00651.
3. Bhamani, S., *Record flooding in Pakistan poses major health risks*. 2022, British Medical Journal Publishing Group.
4. Hashmi, H.N., et al., *A critical analysis of 2010 floods in Pakistan.* African Journal of Agricultural Research, 2012. **7**(7): p. 1054-1067.
5. *2022 Pakistan floods.* july 2022.
6. Sarkar, S., *Pakistan floods pose serious health challenges*. 2022, British Medical Journal Publishing Group.
7. McCall, M., *Participatory mapping and Participatory GIS (PGIS) for CRA, community DRR and hazard assessment.* ProVention Consortium, CRA Toolkit, Participation Resources, Geneva, 2008.
8. Deen, S., *Pakistan 2010 floods. Policy gaps in disaster preparedness and response.* International journal of disaster risk reduction, 2015. **12**: p. 341-349.
9. Oubennaceur, K., et al., *Flood Risk Communication Using ArcGIS StoryMaps.* Hydrology, 2021. **8**(4): p. 152.
10. Rana, I.A. and J.K. Routray, *Integrated methodology for flood risk assessment and application in urban communities of Pakistan.* Natural Hazards, 2018. **91**: p. 239-266.
11. Uddin, K., et al., *Application of remote sensing and GIS for flood hazard management: a case study from Sindh Province, Pakistan.* American Journal of Geographic Information System, 2013. **2**(1): p. 1-5.

12. Onubi, H.O., N.A. Yusof, and A.S. Hassan, *Green construction practices: ensuring client satisfaction through health and safety performance.* Environmental Science and Pollution Research, 2022. **29**(4): p. 5431-5444.
13. Anilkumar, S., *Urban Flood Management Under Changing Climate.* 2022.
14. Kansal, M.L. and S. Singh, *Flood Management Issues in Hilly Regions of Uttarakhand (India) under Changing Climatic Conditions.* Water, 2022. **14**(12): p. 1879.
15. Doorga, J.R., et al., *GIS-based multi-criteria modelling of flood risk susceptibility in Port Louis, Mauritius: Towards resilient flood management.* International Journal of Disaster Risk Reduction, 2022. **67**: p. 102683.
16. Plate, E.J., *Flood risk and flood management.* Journal of hydrology, 2002. **267**(1-2): p. 2-11.
17. Nojavan, M., E. Salehi, and B. Omidvar, *Conceptual change of disaster management models: A thematic analysis.* Jàmbá: Journal of Disaster Risk Studies, 2018. **10**(1): p. 1-11.
18. Weichselgartner, J., *Disaster mitigation: the concept of vulnerability revisited.* Disaster Prevention and Management: An International Journal, 2001.
19. Asghar, S., D. Alahakoon, and L. Churilov, *A comprehensive conceptual model for disaster management.* Journal of Humanitarian Assistance, 2006. **1360**(0222): p. 1-15.
20. Atmanand, *Insurance and disaster management: the Indian context.* Disaster Prevention and Management: An International Journal, 2003. **12**(4): p. 286-304.
21. Cyganik, K.A., *Disaster preparedness in virginia hospital center-arlington after Sept 11, 2001.* Disaster Management & Response, 2003. **1**(3): p. 80-86.
22. Kelly, C., *Simplifying disasters: developing a model for complex non-linear events.* Australian Journal of Emergency Management, The, 1999. **14**(1): p. 25-27.
23. Heijmans, A., *'Vulnerability': A Matter of Perception.* 2001.
24. Wisner, B., et al., *At risk: natural hazards, people's vulnerability and disasters*. 2014: Routledge.
25. Dube, E., *Using Models to Deal with Hazards and Disaster: A Trajectory toward Effective Disaster Management in Zimbabwe.* People: International Journal of Social Sciences, 2018. **4**(1): p. 111-132.
26. Alexander, D., *The study of natural disasters, 1977–97: Some reflections on a changing field of knowledge.* Disasters, 1997. **21**(4): p. 284-304.

2nd International Conference on Advances in Civil and Environmental Engineering (ICACEE-2023)

University of Engineering & Technology Taxila, Pakistan

Conference date: 22nd and 23rd February, 2023

Experimental study of scouring around compound bridge pier with Geo-bags

Muhammad Shakeel Anjam[1], Naeem Ejaz[1], Ghulam Abbas[1], Muhammad Imran[1]

1: University of Engineering & Technology Taxila, Pakistan gakhank251@gmail.com

1: University of Engineering & Technology Taxila, Pakistan naeem@ uettaxila.edu.pk

1: University of Engineering & Technology Taxila, Pakistan ghulamabbas696@yahoo.com

ABSTRACT

The major threat responsible for bridge impairment is the local scour around the bridge pier. Reducing scouring by applying different countermeasures is one of the major concerns in the design of piers. In this work, the experimental reduction of scouring is studied around different types of bridge piers with garbage. To reduce the scouring, garbages are placed above the streambed level around the different types of bridge piers, so that we can conclude maximum scour reduction. We got the best results by garbage around the circular bridge pier. After 48 hours of experiment, showing a maximum of 52% reduction in scouring for circular pier compared with others bridge piers. By using circular, sharp nose and Square bridge pier scouring was reduced by 52% and 34%, and 25% respectively. So, the more efficient bridge pier with garbages is circular.

KEYWORDS: Geobages, Local scouring, Piers, Bridge

INTRODUCTION

Most hydraulic structures like bridges lie in the water with the help of Piers and piles. Anything that comes across a river flow decreases the water flow cross-section affecting the morphology of rivers causing the flow to strike the piers, diverting streams, and giving rise to vortices, a leading cause of local scouring around bridge piers[1].

Scouring around bridge piers in the flow is an inevitable issue and a potential hazard to the structural safety of bridges[2]. Scouring around the bridge piers is an inevitable issue in the flow and one of the main reasons for bridge failure[3]. Despite widespread work being done on local scouring around circular bridge piers, different methods have been attempted to control scouring around bridge piers, such as using riprap, slots through the pier, groups of small piles in front of the pier, collars, and weir, little work has been found on the garbages effect on the bridge pier scouring. Since there is no study so far conducted on such a garbage type of method used with compound bridge type pier[4].

Investigated more than 1000 bridges failure in the United States and demonstrated that the scour was responsible for 60% of these failures. Several studies have been conducted to assess and develop countermeasures into flow altering and bed armoring techniques[5]. Bed attachments such as riprap blocks, gabions, or cabled-tied blocks were employed to protect the movable canal bed. The construction of sequences of sills is a widely applied countermeasure to control excessive erosion. Although bed-sills can control the riverbed souring problem, they also harm the downstream channel stability[6].

They recommended that further investigations are required to identify the optimum and safest methods to control local scour. Geobages are used around bridge piers to reduce local scouring. Garbage diverts the down flow and protects the river bed from impact[7].

According to previous experimental work, manually dropping 126 kg bags into place from the riverbank or dumping pontoons located on the river produces typical revetment side slopes of 1V:2H. However, it seems reasonable to assume that the existing (pre-revetment) side slope of any riverbank will play a significant role in the final revetment side slope and that the final revetment slope may influence the overall stability of a global revetment[1].

Armoring devices include cable-tied blocks, tetrapods, placed riprap rocks, flexible mattresses, grout mats, bags, anchors, and high-density particles around the piers 'foundations. Flow-altering devices that have been used to protect piers against local scour include sacrificial piles placed upstream of the pier, Iowa vanes, and flow deflectors such as collars and slots[8]. This study addresses the effectiveness of collars and geo bags around bridges' piers. Experimentally examined a new method of a flow-altering countermeasure to decrease pier scour using a roughened height with uniform grain sizes that are glued around the surface of the circular piers. The idea of using a roughness height as a scour countermeasure arises from results obtained from research that employ roughened horizontal aprons behind the hydraulic structures to dissipate more energy and reduce the corresponding downstream scouring. The down flow in front of the bridge pier, the horseshoe vortex created at the pier base, and the wake vortex developing inside the scour pit are the main causes of local scour at the bridge piers[9].

Conducted a range of bag-drop and launch tests using a 1:20 scale in a laboratory. The launch tests highlighted that "standard" 126 kg bags are the optimum, and feasible. bags for revetment stability under high flow velocities (up to 4.5 m/s); locally,126 kg bags are considered the largest geo bags safe to handle by two people[10].

EXPERIMENTAL SETUP

The experimental study will be performed at the Hydraulics Laboratory, Civil Engineering Department, University of Engineering and Technology, Taxila. An open channel of rectangular dimensions, that is, 0.96m wide, 0.75 m depth of the channel, and 20 m long with glass side walls and concrete bottom will be used for experimental setup as shown in the figures. The channel flow will be measured by using a compound rectangular trapezoidal sharp-crested weir provided at the end of the channel. Through the centrifugal pump, discharge is supplied to the tank and then enters into the main channel by an aligned honeycomb diffuser in the direction of flow for smooth and uniform distribution of flow crosswise. At the tail of the channel, water enters the sediment tank after filling and trapping the flowed sediments, and the flow discharges in the main channel. Plan view of the Laboratory channel and experimental setup shown in Figure 1: Plan View of Channel a false bottom of uniform, medium size (d50=0.06m) bed material and T-shaped spurs dyke is introduced, sand size considered in this study stood in compliance to the condition of $D/d50 > 50$ to dominate the sediment size effect on the scour evolution process guaranteeing non-ripple-forming sand. The thickness of the compound bridge pier was 10 mm which is not more than 10% of the channel width to prevent the effect of walls on scouring. The trapezoidal broad crested weir (TBCW) was modeled by wood material, the weir width was equal to

the full width of the channel, the crest length was 0.5m, the weir was 0.05m above the flatbed, and the side's slope of the TBCW was 1V:2H, which is more stable and seepage control.

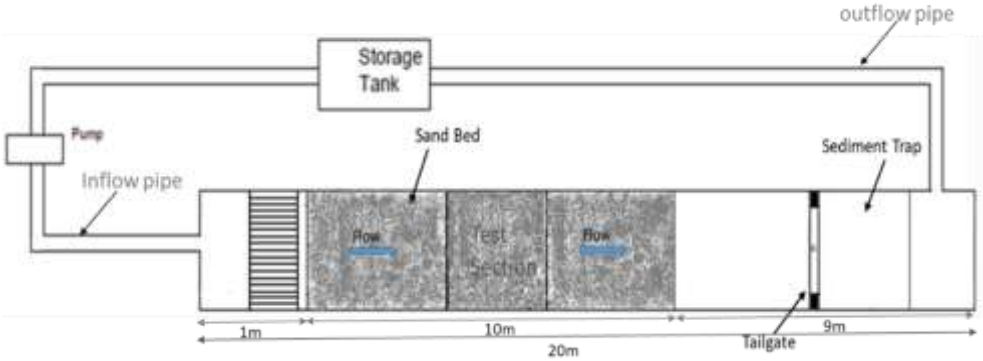

Figure 1: Experimental setup

Research Methodology

An open channel in a hydraulic lab will be used for the experimental setup and the shape of a compound bridge pier made of wood will be used. So that the evaluation of scouring around the different shapes of compound bridge pier will be placed in the flume. The slope of the channel bed will be uniform and have sediments of an average diameter of 0.00071m. Scour depth will be measured around the compound bridge pier with scour gauge or laser distance meter. After that, the Geobages will be installed at the sediment bed level around the piers with an effective width that will be three times the diameter of the piers for all experiments. The Geobages made up of Woven polyester material and vegetation mixed clay type material will be used globally for scouring countermeasures. Vegetation will be mixed with clay for strong bonding of garbage material. Each geobages size will be of 0.15m x 0.075m.

Figure:2 Geobag

Equation

Experimental work was carried out in the Hydraulics lab of the civil engineering department, theoretical discharge equation was used for measuring Discharge value.

$$Q = \frac{2}{3} crd2\sqrt{2g}\ b_2 h_2^{3/2} + \frac{2}{3} crd1\sqrt{2g}\ (2b1)h1\ h_1^{3/2} + ctd\sqrt{2g}\ \tan(\theta/2)\ h1^{3/2} \quad \text{Equation 1}$$

Where θ = Notch angle, b = Width of the weir, Crd= Coefficient of discharge of the rectangular sharp-crested weir, Ctd= Coefficient of discharge for triangular sharp-crested weir, g = gravitational acceleration, h = Water head on the weir crest, he = Effective head.

Tables and Figures

Table 1: Experimental data

Pier shape	**Q (m^3/s)**	**T (hr)**	**h (m)**	**ys_f (cm)**	**ys_ f/D**
Circular Pier with geobag	0.020	2	0.15	6.3	0.75
	0.029	2	0.15	6.8	0.78
	0.038	2	0.15	7.4	0.81
Sharp nose Pier with geobag	0.020	2	0.15	4.3	0.88
	0.029	2	0.15	5.0	0.90
	0.038	2	0.15	5.7	0.94
Square pier with geobag	0.020	2	0.15	5.1	1.03
	0.029	2	0.15	5.6	1.09
	0.038	2	0.15	6.2	1.17

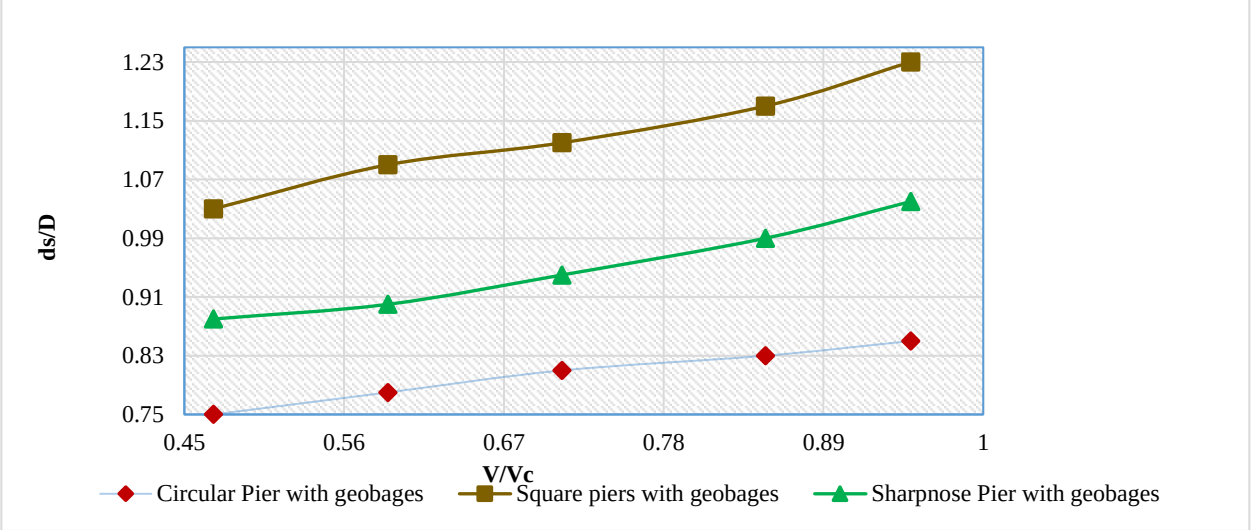

Figure: 3 Relationship between effective velocity and effective depth of the different pier

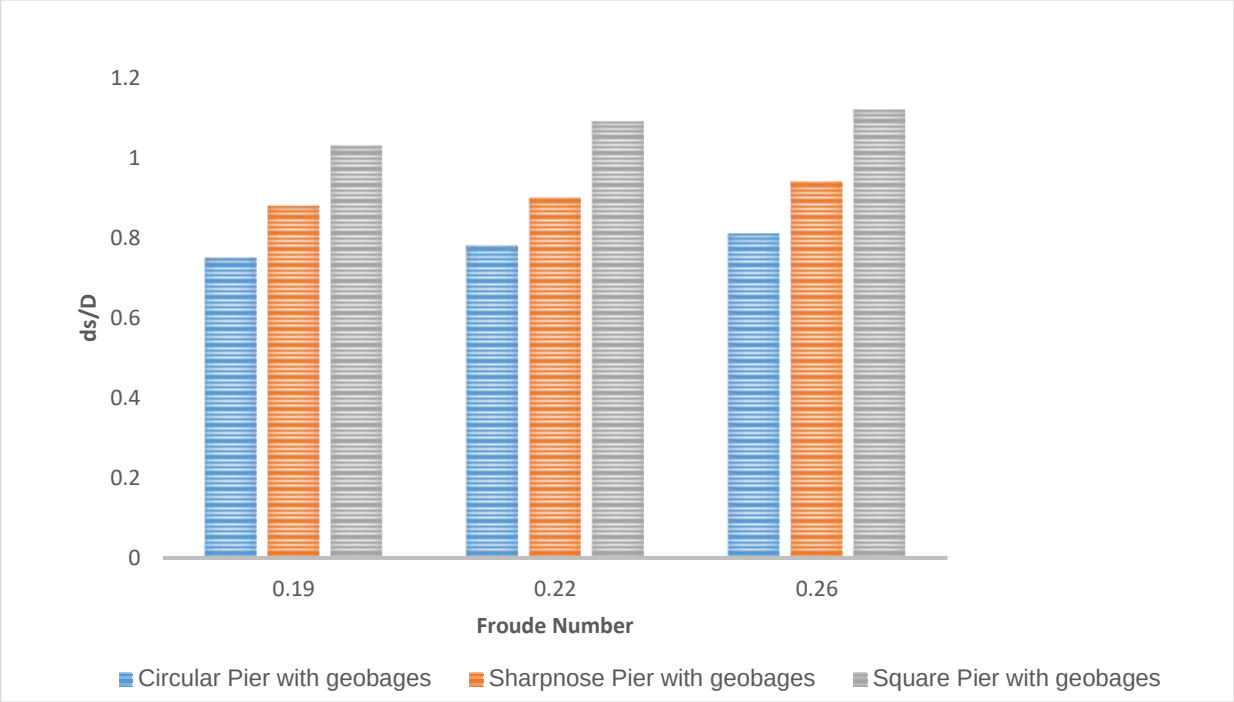

Figure 4: Relationship between scouring depth with different Froude number

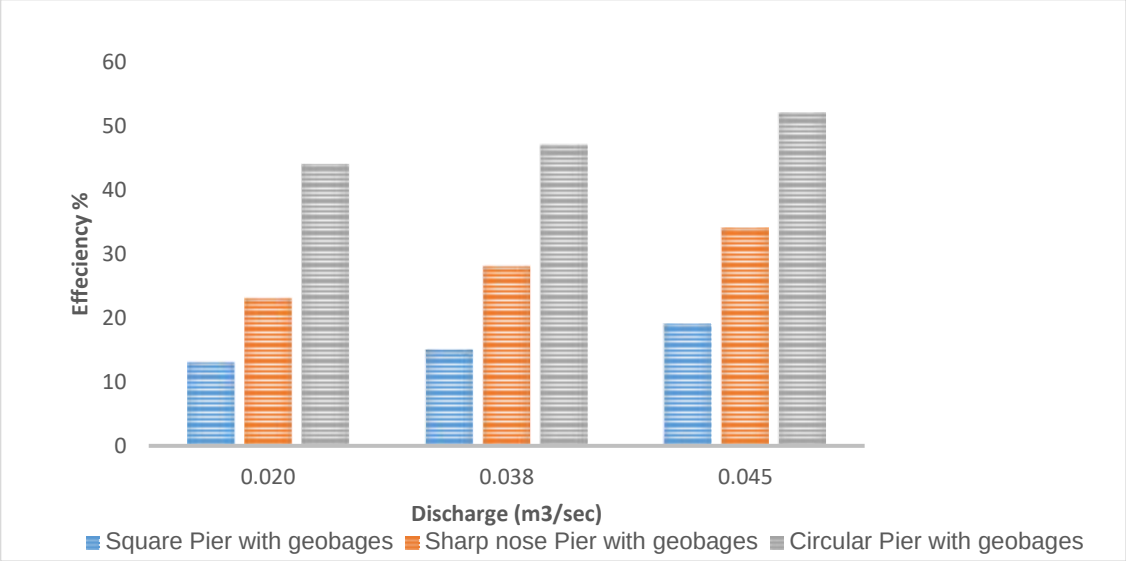

Figure 5: Relationship between Efficiency vs different discharge with geobags

Fig 3 shows the scouring around the different shapes of compound bridge piers it shows the effective velocity increases as the scouring depth around the piers increases. The scouring depth is maximum for the Square shapes bridge piers i.e., 1.23, and minimum for the circular shapes pier i.e., 0.75

Fig 4 shows the relationship between the Froude number and the depth of scouring of different shapes of bridge piers Fig 4 that as the Froud number increased the scouring depth around the bridge pier increased mean Froude number has a direct relation with the Scouring depth. From this Fig 4 observe that the Scouring depth is minimum for the circular shape pier for each Froude number and the Scouring depth is maximum for the square-shaped pier for each Froude number.

Fig 5 shows that the percentage reduction in scouring is maximum for the circular i.e., 52%, the sharp nose 34%, and the square 25%. Hence the most efficient pier with geobags is the circular pier. Scouring can be minimized by using geobags for the circular pier.

Contour Maps

To develop a contour map for all three geometry, Golden SURFER Software surveyed the bed topography surrounding the pier. For planning and building countermeasures against scouring in varied flow circumstances, contour maps for the scour depth give important information regarding scour, the size of the scour hole, and its topography. When it comes to contour maps, each trial's scour profile is shown in its final form (after 2h).

Context maps of the scour hole that surrounds the pier model were developed as a result of the inquiry. This inquiry yielded data that was used to create contour maps for the scour hole area. The maximum and lowest scouring depths of the pier were measured at eight points around the pier that's shown in fig 6.

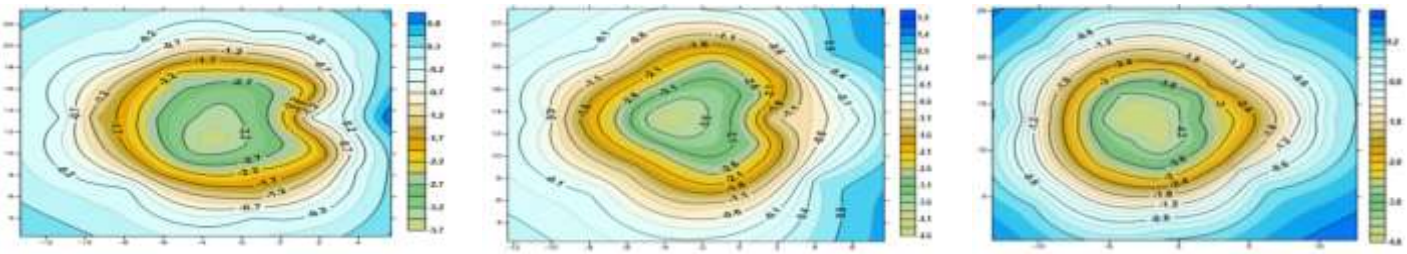

(a) (b) (c)

Figure 6: (a) Contour map of circular pier with geobag, (b) Contour map of sharp nose pier with geobag, (c) Contour map of square pier with geobag

CONCLUSION

In this work, the efficiency of different shapes of bridge piers using the geobags was studied experimentally on different shapes of bridge piers placed in an open *channel.*

The following conclusions were drawn from this experimental work

1. Scouring depth decreases with the use of geobags around the piers
2. The scouring around the compound bridge piers of different shapes with geobags decreased with increasing the discharge in the channel.
3. The efficiency of the circular bridge, square bridge pier, and Rectangular Bridge pier with geobags at the bed level was 52 % and 34 % and 25%respectively. The circular bridge pier is the most efficient that's reduced scouring by up to 52% as compared to the bridge pier.

ACKNOWLEDGEMENTS

All praise and thanks are directed toward the All-Mighty Allah. I am grateful to my supervisor for providing both guidance and assistance during this study effort. I'd want to express my gratitude to my supervisor, PROF. DR. Naeem Ejaz, instilled in me the values of perseverance and efficiency in my work. I would want to offer my most sincere gratitude to him since he allowed me to work on this project, which I am hoping would be beneficial to me in my future professional endeavours as well conclusion. I am also thankful to Engr. Ghulam Abbas helped me a lot in experimental works and during my whole tenure.

REFERENCES

1. MARTIN MOYA, M.F., *The use of geosynthetics as a countermeasure for scour at piers in rivers: experimental small case investigation.* 2021.
2. Akib, S., et al., *Reducing local scouring at bridge piles using collars and geobags.* The Scientific World Journal, 2014. **2014**.
3. Hosseinjanzadeh, H., et al., *Experimental investigation into the use of collar for reducing scouring around short abutments.* ISH Journal of Hydraulic Engineering, 2021. **27**(sup1): p. 616-632.
4. Craswell, T. and S. Akib, *Reducing bridge pier scour using gabion mattresses filled with recycled and alternative materials.* Eng, 2020. **1**(2): p. 188-210.
5. Elnikhely, E., *Minimizing scour around bridge pile using holes.* Ain Shams Engineering Journal, 2017. **8**(4): p. 499-506.
6. Memar, S., et al., *Influence of collars on reduction in scour depth at two piers in a tandem configuration.* Acta Geophysica, 2020. **68**(1): p. 229-242.
7. Hataf, N. and M. Javahery, *Numerical study on uniaxial compression behavior of geobags.* Journal of Civil Engineering and Construction, 2019. **8**(4): p. 137-148.
8. Khajenoori, L., G. Wright, and M. Crapper, *Simulating Geobag Revement Failure Processes.* 2017.
9. Thompson, A., Y. She, and K. Oberhagemann, *Geobag stability for riverbank erosion protection structures: Numerical model study.* Geotextiles and Geomembranes, 2020. **48**(5): p. 703-712.
10. Thompson, A., *Geobag Stability for Riverbank Erosion Protection Structures.* 2019.

2nd International Conference on Advances in Civil and Environmental Engineering (ICACEE-2023)

University of Engineering & Technology Taxila, Pakistan

Conference date: 22nd and 23rd February, 2023

Study of Flow Characteristics for an Oblique Compound Weir

Kainat Jabeen[1], Usman Ghani[2], Mujahid Iqbal[3]

[1]University of Engineering & Technology Taxila, Pakistan, kainat.rana234@gmail.com

[2]University of Engineering & Technology Taxila, Pakistan, usman.ghani@uettaxila.edu.pk

[3]University of Engineering & Technology Taxila, Pakistan, mujahid.iqbal@uettaxila.edu.pk

ABSTRACT

The broad crested weir is a commonly used and accurate discharge flowmeter in open channels. One way to improve the performance of a weir is to position it at a slant relative to the flow direction. This increases the effective length of the weir, resulting in a greater discharge for a given water height and channel width. In the present research work, compound trapezoidal broad crested weir (CTBCW) models were investigated in the hydraulic laboratory of Civil Engineering Department UET Taxila. A series of experiments were carried out on CTBCW models having an oblique angle 60° to the direction of flow with different weir step heights (z = 5 cm, 7.5cm, and 10 cm). The aim of this study is to experimentally evaluate the influence of geometry on the coefficient of discharge (Cd) and energy dissipation (ΔE) of a CTBCW. In each experiment, flow depths were measured at upstream and downstream of weir to calculate the Cd. From the obtained results, it was observed that Cd is largely influenced by varying geometric parameter i.e. step height. Lowest value of Cd was observed for 5 cm step height and highest value was observed for 10 cm step height. As far as the energy dissipation is concerned, the ΔE decreases as the Cd increases. Highest value of ΔE was observed in case of 5 cm step height, and lowest value of ΔE was observed in case of 10 cm step height.

KEYWORDS: Compound weir, Discharge, Coefficient of Discharge, Energy Dissipation.

INTRODUCTION

Weirs are used to measure, divert, or control the flow of water in canals, rivers, and reservoirs. They typically operate under free-flow conditions and are placed in the direction of the flow. In certain canal systems, the need for water diversion may conflict with the limited freeboard available. Traditional linear weirs may not have the capacity to handle necessary flood discharge in these cases. One solution is to extend the length of the weir, but widening the canal to accommodate a longer linear weir is not always possible. An alternative approach is to use an oblique weir, which is a longer linear weir installed at an angle less than 90 degrees to the channel centreline. This design allows for an increase in discharge capacity without the need for widening the canal [1]. Göğüş (2006) conducted a study on the effects of the width of the lower crest and step height of broad-crested weirs of rectangular compound cross-sections on discharge coefficient. The results showed that the values of discharge coefficient obtained from experiments on broad-crested weirs with compound rectangular cross-sections were found to be lower in comparison to those obtained from experiments on broad-crested weirs with rectangular cross-sections of the same crest height and length. [2]. Jan (2009) proposed a method for estimating discharge in compound broad-crested weirs. The study found that the proposed method provided accurate

discharge estimates, with differences between the calculated discharges and the measured ones being less than 3% under the experimental conditions used [3]. Kabiri-Samani et al. (2010) conducted a series of experiments on oblique weirs to study the effects of the angle of obliqueness on hydraulic flow parameters. The results showed that as the angle of obliqueness increased, the effective weir length also increased significantly [4]. Salmasi et al. conducted a study in 2011 to explore the impact of different step heights on the discharge measurement of broad-crested weirs with compound rectangular cross-sections. The results of the study revealed a disruption in the correlation between head and discharge at the point where the flow transitioned into the compound section. This was likely caused by the sudden alteration in shape and slope. [5]. In 2012, a study was conducted by M.M and their team on compound weirs. Experiments were conducted using four different oblique angles (90°, 60°, 45°, and 30°). The results showed that the compound weir with an oblique angle of 30° had the highest discharge coefficient (Cd) [6] . An experiment on a near full-scale compound sharp-crested weir was performed by Jung-Tai (2012) which was composed of a combination of different types of weirs, including a trapezoidal weir, sloping crests and a rectangular weir. The study also suggested that the discharge coefficient could be simplified by using the relative head P/H, based on the experimental data collected [7]. In 2014, Al-Khatib conducted a study to investigate the flow of water over 9 broad-crested weirs with rectangular compound cross-sections of different lower crest widths and step heights. The study utilized experimental results to create models for predicting the discharge rate. The objective of the research was to analyze the flow characteristics of these weirs and develop accurate models for forecasting discharge. [8]. In this study, the effects of different geometric factor on the discharge coefficient and energy loss of an oblique weir were examined and presented in graphical form.

EXPERIMENTAL PROCEDURE

All the experimental work was executed in the hydraulics laboratory of civil engineering department, University of Engineering and Technology Taxila. The computer-controlled channel was used in the experimental work. It was a glass walled channel having a rectangular section. The dimensions of the channel were 12.5 m long, 0.30 m wide and 0.45 m deep. The flow channel has been shown in Figure 1.

Figure 1: Computerized flow channel used in the research work

DISCHARGE MEASURMENT

Discharge of the channel was measured using sharp crested weir placed at the downstream end of channel. The discharge was calculated using Eq (2) suggested by Bos.

$$Q = \frac{2}{3} C_d \sqrt{2g} L H^{1.5} \quad (1)$$

Where;
L = Crest length of sharp crested weir
C_d = Discharge coefficient
g = Acceleration due to gravity
H = Static head on the u/s of the crest

Discharge coefficient depends upon the discharge properties and dimensions of channel and weir is given as (Brater and King 1976) as shown in Eq (2).

$$C_d = 0.611 + 0.08 \frac{H}{W} \quad (2)$$

Where;
H = Static head over the crest
W = Height of sharp crested weir (W = 12 cm)

According to Bos (1976), a theoretical discharge equation for CTBCW was derived by incorporating the discharge relationships of both rectangular and triangular weirs. The equation is expressed as a linear combination, as demonstrated in Eq (3)

$$Q_t = \frac{2}{3} C_{DRB1} \sqrt{\frac{2g}{3}} (2b_1) H_1^{\frac{3}{2}} + \frac{2}{3} C_{DRB2} \sqrt{\frac{2g}{3}} (b_2) H_2^{\frac{3}{2}} + \frac{16}{25} C_{DTB1} \sqrt{\frac{2g}{5}} \tan\left(\frac{\theta_1}{2}\right) H_1^{\frac{5}{2}} \quad (3)$$

Where;
Q_t = Theoretical discharge
C_{DRB} = Rectangular broad crested weir discharge coefficient
C_{DTB} = Triangular broad crested weir discharge coefficient
H = Static head over the upper weir crest
b = Crest width of weir
θ = Notch angle
Subscripts 1 for upper part of compound weir and 2 for the lower part of the compound weir.

Water depth at upstream and downstream side of compound crested weir was measured with the help of point gauge.

MODEL DESCRIPTION

Three different compound broad crested weirs were used in this research work. The division of these weirs was based on the various step heights i.e. z = 5 cm, 7.5 cm, and 10 cm. Weir models were prepared with wooden material. The compound weir has been shown in Figure 2.

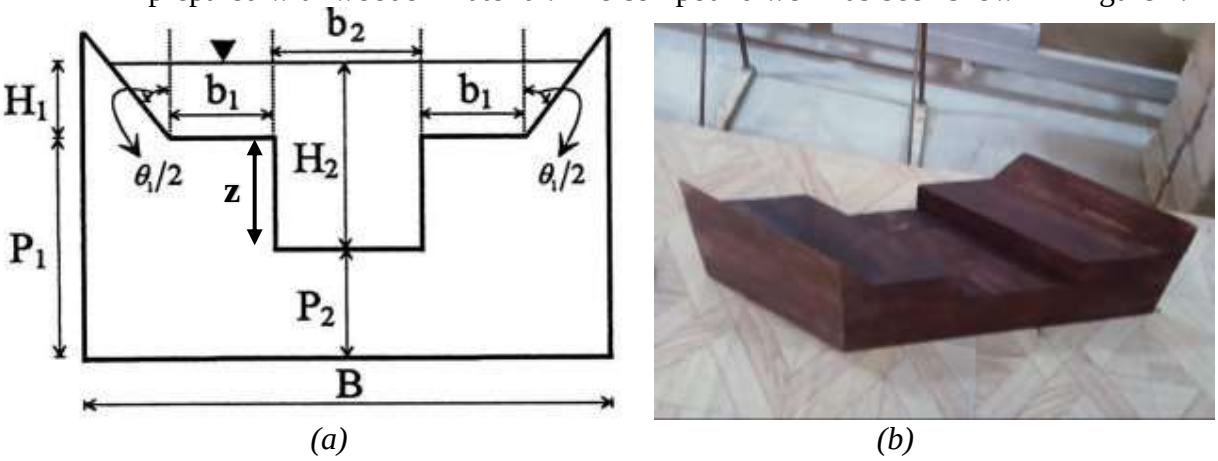

(a) *(b)*

Figure 2: Compound Weir (a) Schematic Diagram (b) Actual Diagram

RESEARCH METHODOLOGY

Three models of CTBCW at an oblique angle of 60° with the flow direction were used in this research work. The step height was 5cm, 7.5cm and 10cm in the three cases.

For each case, six different flow rates (Q) were used. These flow rates were 1.68 litre/sec, 2.33 litre/sec, 3.05 litre/sec, 4.69 litre/sec, 6.78 litre/sec, and 8.03 litre/sec.

Flow depth measurements were taken at 1-meter intervals on both the upstream and downstream ends of the weir. Point gauges were used to measure these depths. After setting up of experimental model, number of trials with varying discharge was carried out. The geometric factors for various weir models have been explained in Table 1.

Table 2: Geometric Factors of Weir Models

Model No.	**Weir Length (cm)**	**Width b_1 (cm)**	**Width b_2 (cm)**	**Crest Height P_1 (cm)**	**Crest Height P_2 (cm)**	**Angle $\theta_1/2$**	**Step Height z (cm)**
A ($\alpha = 60°$)	60	15	20	15	10	45	5
B ($\alpha = 60°$)	60	15	20	15	7.5	45	7.5
C ($\alpha = 60°$)	60	15	20	15	5	45	10

RESULTS AND DISCUSSION

By measuring the flow depths at u/s and d/s of an oblique CTBCW, the Cd and head losses were calculated for all the three step heights against various discharge values. Results of all the three step heights were compared and following graphs were plotted.

Figure 3 (a) shows the variation of Cd for different step heights of weir. As the step height changes from min. to max., the values of Cd increases. Hence it is concluded that Cd is directly proportional to the step height. Cd has lowest values for 5cm step height of an oblique CTBCW at the corresponding depths, and highest values for 10cm step height.

Figure 3 (b) shows that for non-submerged condition of weir, overflow head increases with increasing discharge values which justifies the results.

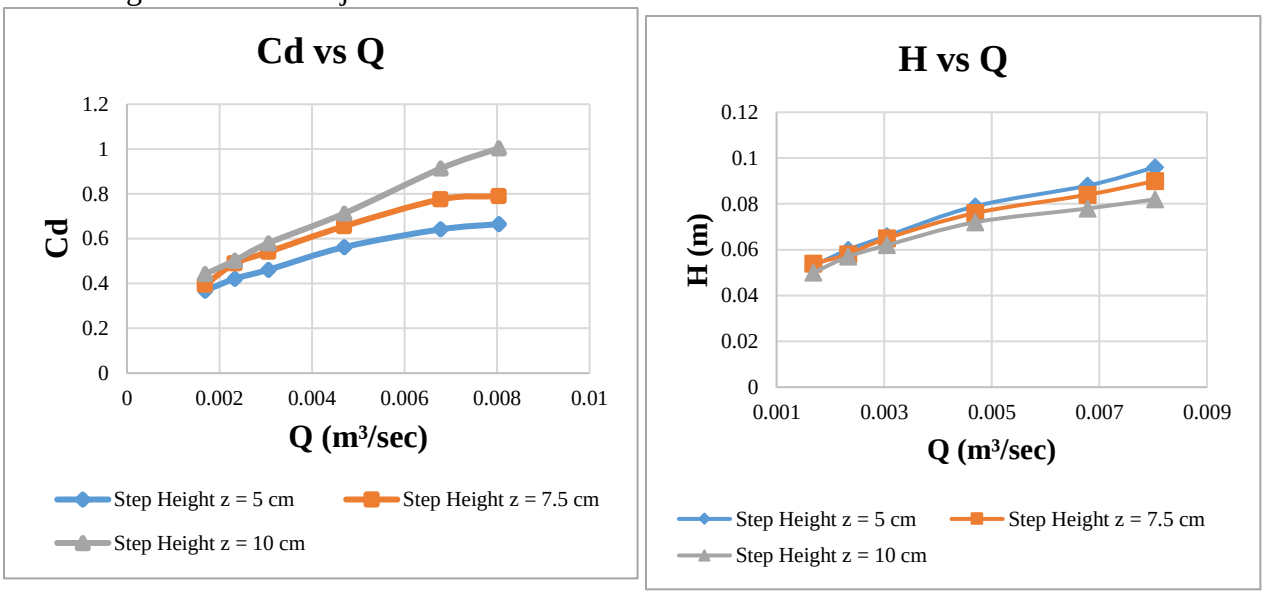

(a) *(b)*

Figure 3: (a) Cd vs Q for different step heights (b) Over flow head vs Q for different step heights

The graph in Figure 4 depicts the relationship between the discharge coefficient and the ratio of upstream head to crest length (H/L). The illustration clearly indicates that an increase in the value of H/L leads to a corresponding rise in the discharge coefficient.

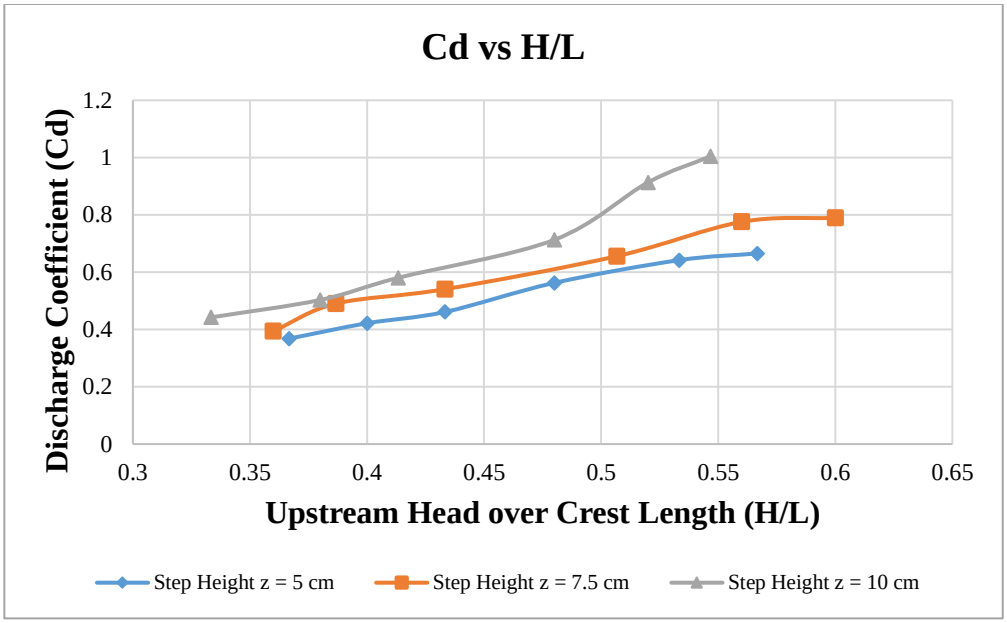

Figure 4: Cd vs H/L for all tested models

Following diagram shows the relationship between energy dissipation and downstream water depth (Y2). It is clear from the graph that head loss decreases with the increase in downstream water depth. Furthermore, the graphs which are comparing the head loss with the downstream water depth for the varying geometric parameter i.e. step height. Weir with the 5 cm step height has highest head loss and the weir with 10 cm step height has the lowest head loss. Therefore, from these results, we may say that by keeping the lower step height, upstream head increases and velocity of the flow decreases. And as a result, head loss increases.

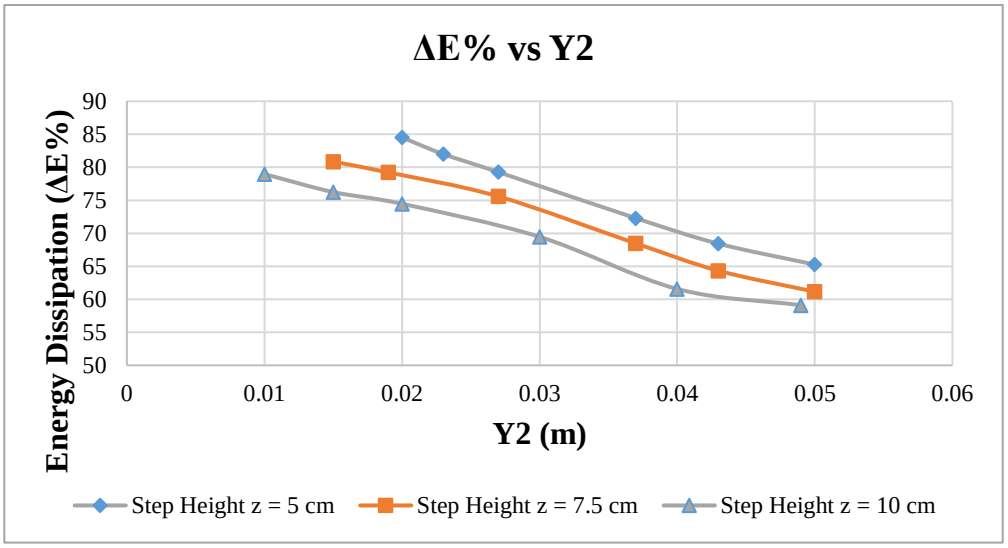

Figure 5: Effect of varying step height on ΔE

CONCLUSION

Following conclusions could be drawn from this research work:

1. Cd values were maximum for 10 cm step height and were minimum for 5 cm step height.
2. It was also observed that for non-submerged flow condition, the overflow head (H) increases with increasing discharge. The weir model with a step height of 10 cm will result in a lower stage (H) compared to the other models. The reason being, a weir with a higher step height can accommodate more discharge, leading to a lower stage.
3. The discharge coefficient values tend to increase as the ratio of head to length (H/L) increases, particularly with an increase in step height.
4. Maximum value of energy dissipation was observed for 5 cm step height and it decreases as the step height increases

ACKNOWLEDGEMENTS

The authors would like to thank every person who helped throughout the research work. The careful review and constructive suggestions by the reviewers are gratefully acknowledged.

REFERENCES

1. Borghei, S. M., Vatannia, Z., Ghodsian, M., & Jalili, M. R. (2003). Oblique rectangular sharp-crested weir. *Proceedings of the Institution of Civil Engineers - Water and Maritime Engineering*, *156*(2), 185–191.

2. Göğüş, M., Defne, Z., & Özkandemir, V. (2006). Broad-Crested Weirs with Rectangular Compound Cross Sections. *Journal of Irrigation and Drainage Engineering*, *132*(3), 272–280.
3. Jan, C.-D., Chang, C.-J., & Kuo, F.-H. (2009). Experiments on Discharge Equations of Compound Broad-Crested Weirs. *Journal of Irrigation and Drainage Engineering*, *135*(4), 511–515.
4. Kabiri-Samani, A., Ansari, A., & Borghei, S. M. (2010). Hydraulic behaviour of flow over an oblique weir. *Journal of Hydraulic Research*, *48*(5), 669–673.
5. Farzin; POORESCANDAR, S. (2011). Discharge relations for rectangular broad-crested weirs. *Tarım Bilimleri Dergisi*, *17*(4), 324–336.
6. M. M. Muhammad, A. Ismail, J. A. Otun, D. B. Adie, S. B. Igboro, & S. A. Abdullahi. (2012). HYDRAULIC PERFORMANCE OF FLOW OVER NORMAL AND INCLINED COMPOUND CRESTED WEIR MODELS. *Special Publication of the Nigerian Association of Hydrological Sciences*, *19*(1), 55–67.
7. Jung-Tai Lee. (2012). Experiments on hydraulic relations for flow over a compound sharp-crested weir. *International Journal of the Physical Sciences*, *7*(14). https://doi.org/10.5897/IJPS11.1695
8. Al-Khatib, I. A., & Gogus, M. (2014). Prediction models for discharge estimation in rectangular compound broad-crested weirs. *Flow Measurement and Instrumentation*, *36*, 1–8.

2nd International Conference on Advances in Civil and Environmental Engineering (ICACEE-2023)

University of Engineering & Technology Taxila, Pakistan

Conference date: 22nd and 23rd February, 2023

EXPERIMENTAL STUDY ON LOCAL SCOUR AROUND A COMPLEX PIER HAVING SUBMERGED PILE CAP WITH VARYING THICKNESSES

Noor Elahi[1], Usman Ghani[1]

[1]Department of Civil Engineering, University of Engineering & Technology Taxila, Pakistan

elahin988@gmail.com usman.ghani@uettaxila.edu.pk

ABSTRACT

A complex bridge pier is a combination of a column and foundation such as pile foundation with a pile-cap, partially or totally exposed to the flow. Bridges mostly fail due to local scouring around pier. The flowing water tends to cause local scour around the complex pier with the passage of time and finally leads towards the failure of the structure. The objective of this research work is to investigate and compare local scour depth around complex piers having different thickness of the pile cap. The pile cap is submerged and bed is comprised of non-uniform gravel particles. A total of nine experiments were conducted in the flume using different thickness of pile cap with varying discharges. Three pile cap thicknesses with three discharge values for each case were studied. It was results showed that maximum scour depth occurred with the maximum pile cap thickness 6cm and least scour depth occurred with the pile cap thickness of 2cm.

KEYWORDS: Complex bridge pier, Scour depth, Pile cap at different thickness.

INTRODUCTION

A complex pier is a combination of piles, pile cap and column [1]. Complex bridge pier is most desirable to be construct in river now days because of its financial and material condition. All over its period, the various parts of a complex pier exposed to the flow because of different quantity of sand deposition or scouring near to the complex pier installation. Therefore, it's essential for the hydraulics and engineers to study different changes in vortex pattern is produced by the changing pile cap thickness in gravel bed to study what alteration in vortex pattern is produced as an effect of the changing complex pier thickness comparative to the gravel bed level, and consequently the scour depth around it [2] . Due to hydraulic force of flowing water Local scour around the complex bridge pier occur. Local scour is the common cause of a collapsed foundation which leads to failure of bridge around the complex bridge pier horse shoe vertex is formed due to redirected water flows [3]. The complex pier assemblies are more frequently built as bridge piers in recent time because they are more inexpensive and structurally superior to simple piers. Complex pier is a combination of three components that is column constructed above the pile cap and pile cap is supported by numbers of pile that is called pile foundation. The vortex, which is typically responsible for the scour hole surrounding the pier. The sediment particles are subsequently moved downstream of the pier [4]. In order to find the depth of the scour around the complex piers, numerous research have been conducted. But there are very few studies available on pile cap of complex pier above bed level submerged in water

The purposes of research to calculating equilibrium scour depth around complex pier in non-uniform gravel bed. Different thickness of pile cap was studied which are fully exposed to flow. All parts of complex pier are exposed to flow which are column, pile cap and number of piles.

METHODOLOGY

This research focuses on Experimental study of local Scour around a complex pier in Non-uniform gravel bed. Experimental investigation of scour depth around Complex Bridge Pier for different pile cap thickness. About Nine experiments were done for such study in the Hydraulics Laboratory. Procedure adopted to attain these objectives is discussed in following section.

Channel Preparation

The channel shown in Fig.1 is installed in the Hydraulic Laboratory of Civil Engineering Department University of Engineering and technology (UET) Taxila, is used for performing experiments. The channel had a length of 20m, Width of 1.0m and Depth of 0.75m. The Flume assembly consist of centrifugal pump with inflow valve, water tanks, main flume, and outflow control valve Water is pumped from the re circulation tanks to the flume. The water flows into the tank after entering the flume and passing through the test section. While the valve at the upstream end of the channel was used to control the flow rate into the channel. Point gauge was used for measuring scour depth. A Rectangular weir was fixed at the end of test section to trap the sediment from flowing water into the tank and then into the pump which could stop the pump from working from tank pump took water and transfer it to the flume. Before water reach to the flume a flow control valve is installed it the upstream side of the flume. Valve are used to control the discharge. The test section was prepared for installing complex pier model. The test section was two-meter length and one meter wide. For smooth entry of flow and to prevent turbulence at the beginning of the flume slightly sloped was given in the bed.

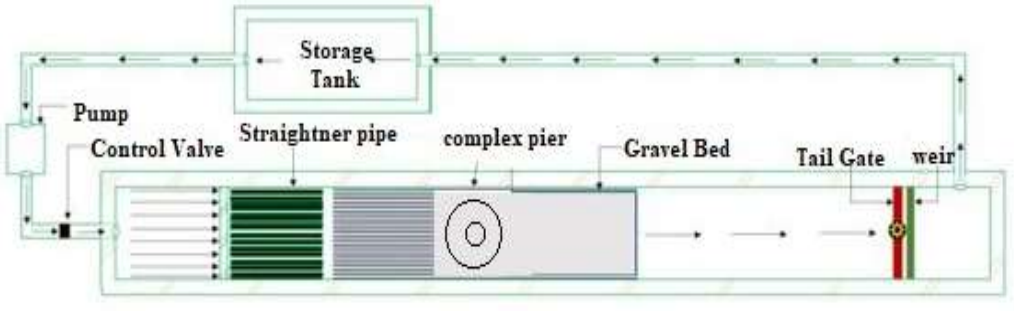

Figure 11: Top View of Laboratory Channel

Experimental Procedure

The experiment was conducted in an open channel. After cleaning the channel, the gravel with median size of 4.1mm were added to the test section. At the beginning of each experiment, the gravel was appropriately leveled

after being placed in the test region. Before the first experiment began, the water might stay for a while in order to fill the air voids in the test section with water. The dimension of complex pier is the height of piles was 15cm,the thickness of pile cap was 6cm,the diameter of pile cap was 30cm, the height of column was 25cm and the diameter of column was 6cm. The complex pier was installed in the middle of channel when the gravel was fully saturated. Care was taken when building complex pier in the middle of the test section so that it would not be twisted or bent to one side. Such misalignment significantly affect the outcomes of the scour range [5]. After turning on the pump, water was permitted to pass through the test area over the gravel bed and scouring started. After conducting the experiment for a particular period of time, the water was drained, and the scour depth was measured using the point gauge. All experiment was conducted for various pile cap thickness and discharges. To measure the discharges, a compound rectangular-trapezoidal sharp-crested weir was used. Nine experiments were performed using these parameters. Three different thickness were used and experiment were performed for 3 hours on three different discharges. For each experiment bed was leveled and prepared as shown in the figure 2.

Figure 12: Pile cap above bed level submerged in water having different thicknesses.

RESULTS AND DISCUSSION

Scour depth was measured after performing various number of experiments. They are shown in the figures below.

Scour depth variation around the complex pier having pile cap thickness 6cm by varying discharges.

It is clear from the figure 3 that maximum scour depth around the complex pier occur when the pile cap was above bed level submerged in water having discharge 0.043m^3/s is 7.8mm. by reducing discharge 0.032m^3/s scour depth reduces to 6.4mm and 3.8mm.

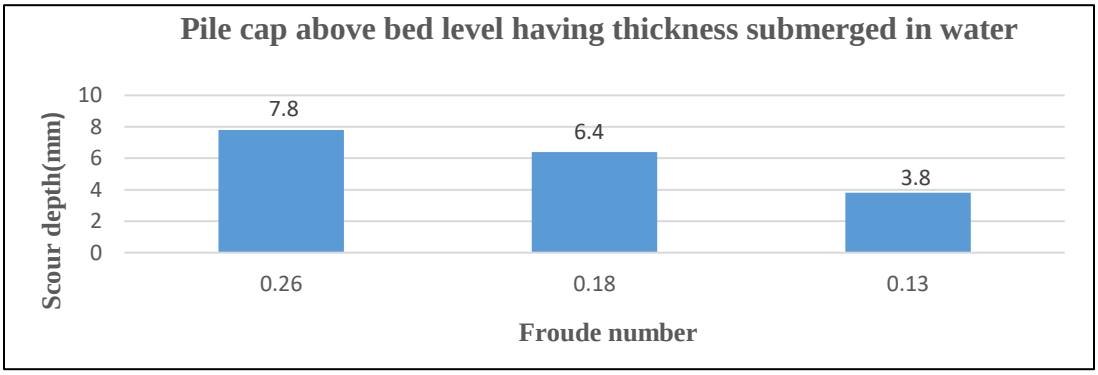

Figure 13: Pile cap above bed level having thickness 6cm submerged in water

Scour depth variation around the complex pier having pile cap thickness 4cm by varying discharges.

It is shown in the figure 4 that maximum scour depth around the complex pier occur when the pile cap was above bed level submerged in water having discharge 0.043m^3/s is 6.4mm, by reducing discharges 0.032m^3/s to scour depth reduces to 4.3mm and 2.8mm respectively.

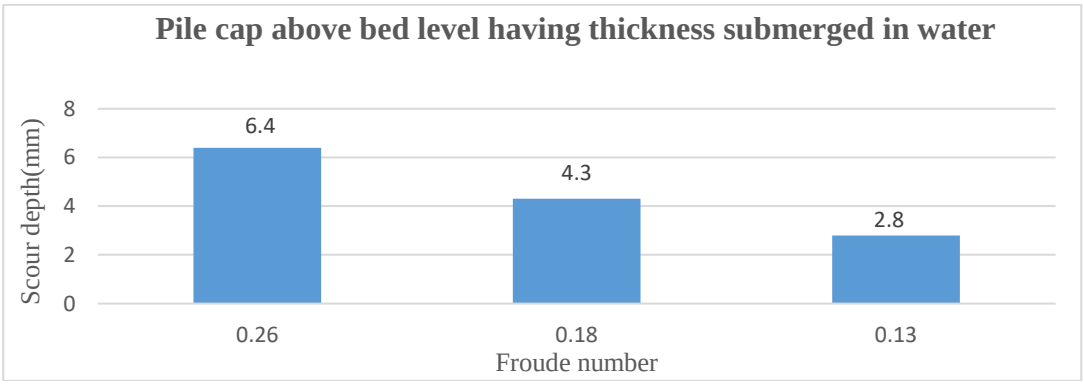

Figure 14: Pile cap above bed level having thickness 4cm submerged in water

Scour depth variation around the complex pier having pile cap thickness 2cm by varying discharges.

It is shown in the figure 5 that maximum scour depth around the complex pier occur when the pile cap was above bed level submerged in water having discharge 0.043m^3/s is 4.66mm by reducing discharge 0.032m^3/s scour depth reduces to 3.6mm and 2.63mm respectively.

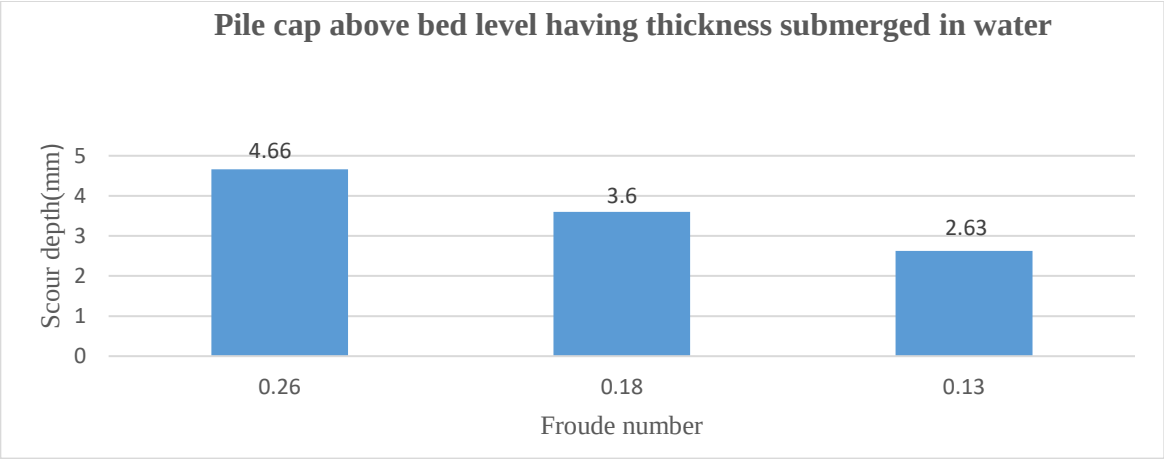

Figure 15: Pile cap above bed level having thickness 2cm submerged in water

Scour depth variation around the complex pier having different thickness of pile cap by varying discharges.

By keeping all other parameter constant scour depth increase as the discharge increase. Fig (3.4) show greater scour depth around the complex pier when the pile cap thickness 6cm Fr1(0.26) which is above bed level and submerged in water scour depth was 7.8mm when we reduce thickness of pile cap to 4cm scour depth reduces from 7.8mm to 6.4mm, and then reduce thickness of pile cap to 2cm scour depth reduce from 7.8mm to 4.66mm. Hence scour depth reduces maximum in case of when the pile cap thickness was 2cm.
Similarly, maximum scour depth around the complex pier at pile cap thickness fr_2(0.22) discharge was 6.4mm, when we reduce thickness of pile cap to 4cm, scour depth reduces from 6.4mm to 4.3mm, while using further reduce thickness of pile cap to 2cm scour depth reduce from 6.4mm to 3.6mm.

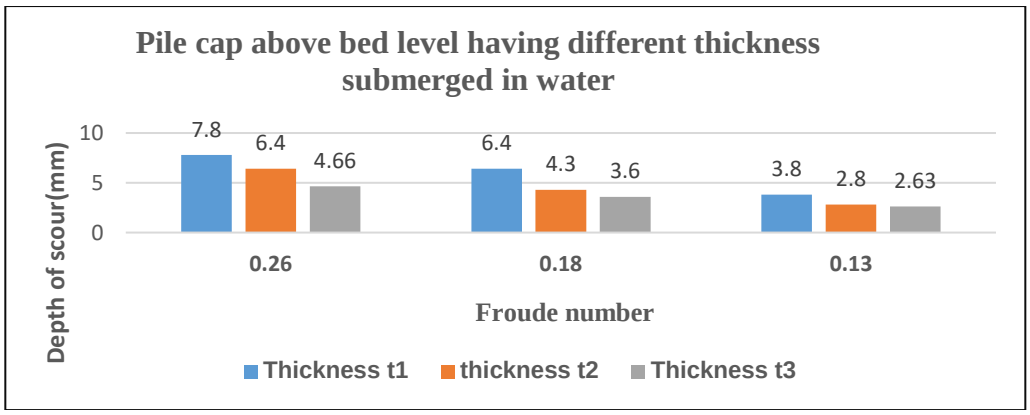

Figure 16: Pile cap above bed level having different thickness submerged in water

CONCLUSION

In this study the effect of different thickness of pile cap in reducing scour depth with respect to gravel bed was studied. For different complex pier elevation, the scour patterns were different. The scour depth was greater for pile cap at thickness 6cm > pile cap at thickness 4cm > pile cap at thickness 2cm. For case 1 fully developed vertices was observed and it had greater impact on scour depth. When the pile cap thickness was reduced it showed minimum scour depth. The results study in this paper show the importance of different thickness of pile cap. Complex pier shows different effect on the flow when the pile cap thickness is varied. When the pile cap thickness is 6cm or 4cm it exhibited greater scouring depth around it.

REFERENCES

[1] S. E. Coleman, "Clearwater Local Scour at Complex Piers," 2000, doi: 10.1061/ASCE0733-94292005131:4330.

[2] D. Ferraro, A. Tafarojnoruz, R. Gaudio, and A. H. Cardoso, "Effects of Pile Cap Thickness on the Maximum Scour Depth at a Complex Pier," *Journal of Hydraulic Engineering*, vol. 139, no. 5, pp. 482–491, May 2013, doi: 10.1061/(asce)hy.1943-7900.0000704.

[3] "gautam 2016," 2016.

[4] M. Pandey, G. Oliveto, J. H. Pu, P. K. Sharma, and C. S. P. Ojha, "Pier scour prediction in non-uniform gravel beds," *Water (Switzerland)*, vol. 12, no. 6, Jun. 2020, doi: 10.3390/W12061696.

[5] Wajahat and Naseem Khan, *UET ADB PROCEEDINGS SPONSORS 1ST INTERNATIONAL CONFERENCE ON RECENT ADVANCES IN CIVIL AND EARTHQUAKE ENGINEERING*, 1st ed. Peshawar: UET Peshawar, 2021. [Online]. Available: https://sites.google.com/uetpeshawar.edu.pk/iccee21/home

2nd International Conference on Advances in Civil and Environmental Engineering (ICACEE-2023)

University of Engineering & Technology Taxila, Pakistan

Conference date: 22nd and 23rd February, 2023

To study the effect of vegetation on acceleration of a house model againstflood by using accelerometer

Imran Qadir[1a],AfzalAhmed[1b], Saqib Mahboob[1c], Ghufran Ahmed Pasha[1d],Talha Zahid[1e]
[1]University of Engineering and Technology Taxila, Pakistan,
[1a] imrankhosa462@gmail.com , [1b] afzal.ahmed@uettaxila.edu.pk, [1c] Syed.saqib@uettaxila.edu.pk
[1d] gufran.ahmed@uettaxila.edu.pk, [1e] talhazahid7894@gmail.com

ABSTRACT

Extreme flooding causes massive amounts of property damage and human casualties, making it the most destructive natural disaster. There has been an increase in the numberof devastating floods that occur in Pakistan due to global warming. Although flood protection structures lessen the risk of flooding, these structures may collapse if flow conditions are higher than their design threshold. Therefore, aim of this research is to determine the effect of vegetation on acceleration (g) of house model and arrival time of flood water at a particular point. Acceleration of house model installed on the downstream side of vegetation is measured by attaching X2-2 accelerometer with house model. The vegetation model is placed perpendicular to the direction of flow. Two vegetation densities were considered in an experimental flume under varied flow conditions: a) intermediate vegetation (G/d = 1.09) and b) sparse vegetation *(Gld=* 2.13), where G=spacing of each cylinder in cross-stream direction, d = diameter of vegetation and seven different values of Froude numbers (Fr_o) are tested for each case. The pressure exerted by water on the upstream face of house model is also calculated. The maximum value of acceleration reduction for sparse vegetation and intermediate vegetation i.e.; S90 and I90 are 21.9% and 22.08% respectively. The range of average water pressure reduction for S90 and I90 are 5.78% and 7.43% respectively. The maximum value of arrival time I90 is higher than S90.

KEYWORDS: Vegetation, USB accelerometer, house model, pressure, acceleration

INTRODUCTION

As far as Pakistan is concerned, flooding is one of the most regular natural disasters. The nature of flooding varies by geographical region. In terms of structural and economic damages, the frequency of flood-related catastrophes has increased during the previous three decades. Consequently, there is a growing consensus that climate change is a significant contributor to the increasing frequency and severity of floods [1]. According to a recent study on floods, Pakistan was severely damaged by twenty-eight catastrophic floods that caused extensive structural damage and a large loss of life. Different emergent vegetation densities and thicknesses were discovered to reduce energy under subcritical and supercritical flow conditions in the laboratory [1][2].In the past, different defence system like moat, dikes (embankments) and riparian zones were used as a flood protection system. Even though such defences have been thoroughly investigated, most of the researchers have regarded the location of vegetation perpendicular to the direction of flood flow[2]. Previously, under subcritical and supercritical flow conditions, conducted laboratory experiment to investigate the energy loss by emerging plants of different densities and thicknesses[3].

In addition, laboratory assessments of the impacts of rapidly shifting flow on the main channel flow and the floodplain have been conducted [4]. Vegetation is a highly effective method for minimizing flood damage and the effects of flood pressures. The impact of vegetation at various angles in relation to the flow direction was also investigated in a rectangular channel[5]. The numerical study of a uniform trapezoidal compound channel with vertically piled vegetation covering the floodplains. As a result of the failure of tsunami defence measures in recent years, the majority of researchers have devised hybrid or composite tsunami mitigation techniques that use both manmade and natural structures[4]. Safety of structures is one of the global challenges facing floodplain. Continuous exposure to natural hazards, such as flooding, seismic activity, and weathering, are the greatest threat to the structuralintegrity. Due to the importance of structures in human life, it is very important to assure on-goingmonitoring of their safety and performance [6][7]. Accelerometer model X2-2 includes a high sensitivity, rotating acceleration sensor under given data. The vibration characteristics of a housecan provide enough data to calculate its acceleration. Using a USB accelerometer, a building's acceleration history may be recorded. The accelerometer work as a sensor and data collector[8][9][10]. The most important discovery of this study is the behaviour of house model on the downstream side of vegetation model against acceleration of house model, pressure force of water on house model and the arrival time of water from the inlet to the position of house modelare investigated. The effect of density of

vegetation on these parameters are also analysed.

1 METHODOLOGY

At the Water Resources laboratory at UET Taxila, experiments were conducted using a glass-sided, rectangular channel measuring 10m in length, 0.31m in width, and 0.5m in height with a constant bed surface at a mean slope of 1/1000[4][5]. The slopes in a real case are often horizontal to rising, however certain naturally occurring coastal sand dunes or the defence buildings built on a sand dune existed with a falling slope, where the energy of the flowing water increases [1][5]. Where tsunami characteristics were observed in general and not for a specific location [1]. As depicted in Figure, (2.a) a channel layout diagram illustrating the positioning of vegetation and house model in an open channel flume. The flow was supplied to the channel from a tank. Head of water at different location can be measured by using rail-mounted point gauge.

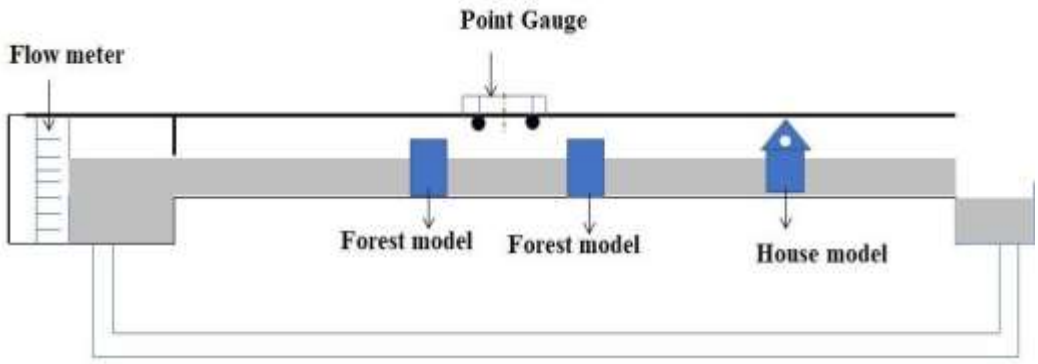

Fig 2.a: schematic diagram of laboratory channel

Figure (2.b) shows the vegetated flow pattern and experimental models with perpendicular vegetation. In every circumstance, the flow was subcritical (Fro< 1) A range of seven Froude numbers was selected (0.18-0.25). Flow properties can be observed using vegetation in the form of 0.003m-diameter steel cylinders. The vegetation can be planted in two patches at an angle of 90 degrees to the direction of flow along the half width of the flume. The house model was positioned in the middle of the channel width, placed at a distance of 243.8cm(2.438m) from the start of vegetation.

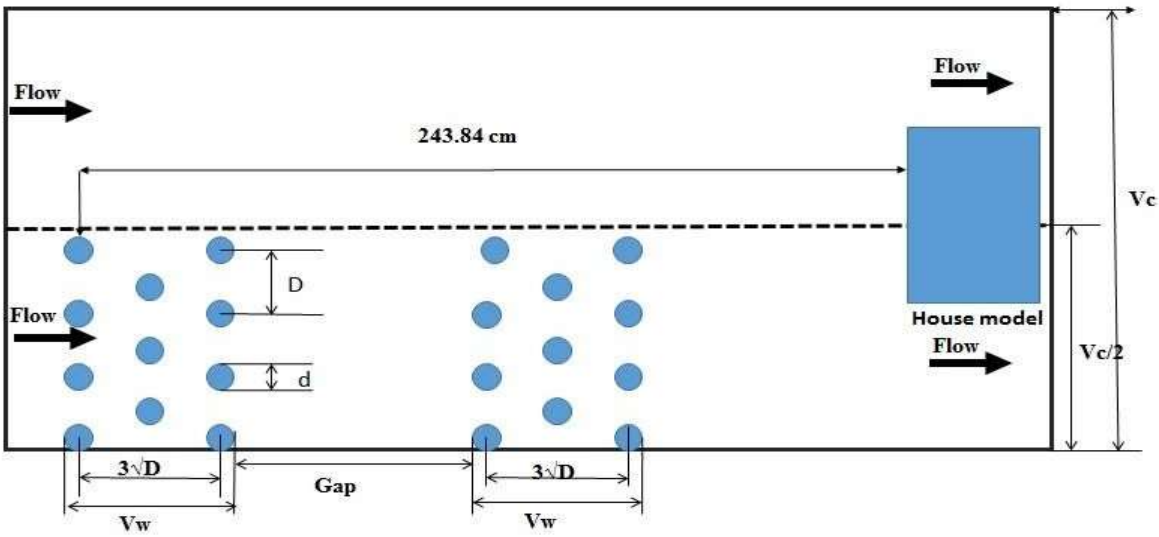

Fig 2.b: Arrangement of cylinder in a model

Acceleration of house model installed on the downstream side of vegetation is measured by attaching X2-2 accelerometer with house model. For low and high gain, it can collect acceleration data at ± 1.25g and ±2g, respectively [6]. To record the acceleration data 32 values per second with which the water strikes the home, it can be put at the back of the house. It can provide us with data at low or high gain, and the low gain data can be converted into Seismo Signal software for baseline correction.

1.1 MATERIAL

The Eucalyptus tree was considered to use as a model of vegetation in experimental work [4]. It is preferable to do this than to use wooden rods with such a small diameter that they might break or bend a lot throughout the experiment. By maintaining the geometrical consistency of the actual models, this design choice is consistent with other writers who employed steel cylinders as well, while some have used plastic dowels or metal rods, for vegetation modelling [1][4]. In Pakistan, the typical height of the tree is between 7.6 and 14.6 meters, and its average diameter is between 0.11 and 0.33 meters [11]. In this study, trees were reduced to 1/100 scale with an average diameter of 0.003 m. The G/d represents the density of a forest, with a value of 1.09 for an intermediate layout and 2.13 for sparse arrangements of the vegetation, where G is the distance between each cylinder in the cross-stream direction and d is the diameter of each cylinder as shown in Figure 2.b as also used in the literature [3][4]. The density (G/d) and thickness (dn) of vegetation are held same for all cases of sparse and intermediate vegetation with angles of 90° as shown in

Figure (2.1(a)&(c)). H_{Nv} is the depth of water when no vegetation placed in front of house model. A model of house was used to performed experiments having length = 16.5cm, width = 15.5cm and height = 23cmof the real house was designed with a small scale of 1/45. This provides the equivalent length of a real building length 742cm, width 698cm and 1035cm height as shown in in Figure (2.1(d)).The experiments were performed by varying the vegetation thickness and density.

(a)

(b)

(c)

(d)

Fig: 2.1: Experimental models; (a,c) vegetation place in the channel, (b) USB Accelerometer and (d) House model

Table 1. experimental conditions of vegetation

Case#	Case Identity	Angle	Initial Froude# (Fro)	d (cm)	H_{NV} (cm)	D (cm)	dn	W_V (cm)
1	I90180	90	0.18,0.19,0.20,0.22, 0.23,0.24,0.25	0.3	7.6,8.3,9,10.4, 11,11.7,12	1.254	180	18.32
2	I90380	90	0.18,0.19,0.20,0.22, 0.23,0.24,0.25	0.3	7.6,8.3,9,10.4, 11,11.7,12	1.254	380	38.69
3	S90180	90	0.18,0.19,0.20,0.22, 0.23,0.24,0.25	0.3	7.6,8.3,9,10.4, 11,11.7,12	1.878	180	18.32
4	S90380	90	0.18,0.19,0.20,0.22, 0.23,0.24,0.25	0.3	7.6,8.3,9,10.4, 11,11.7,12	1.878	380	38.69

2. RESULTS AND DICUSSION

2.1. HYDROSTATIC PRESSURE

The depth on the upstream face of the house model increases as the Froude number increases keeping all parameters constant. As depth increases then hydrostatic pressure increase. Figure 3.1 shows maximum depth of water against the highest Froude number i.e.; 0.25. So, pressure force will act maximum without vegetation at Fro = 0.25 was 1187.01 Pa, when we use vegetation at the I90180, I90380, S90180 and S90380 (Figure 3.1) pressure force reduces from 1187.01 Pa to 1128.15Pa, 1098.72Pa, 1147.77Pa and 1118.34Pa respectively. Hence hydrostatic pressure force reduces maximum in case of S90380 and I90380 i.e. ;5.78% and 7.43% respectively.

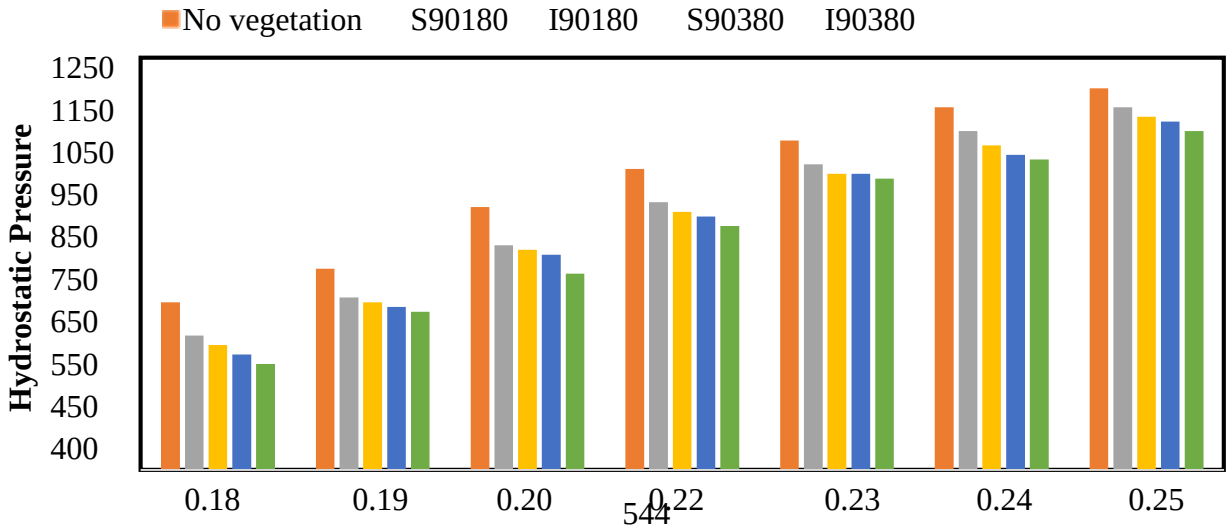

Fig 3.1 Relationship b/w Fro and Pressure Effect

TIME OF APPROACH

The time of approach is noted as the time required to reach water from the inlet of the channel to the upstream face of the house model. The time approach was determined against different Froude numbers with and without placing vegetation model in the channel. The value for different vegetation models at I90180, I90380, S90180 and S90380 are 37 to 52 sec, 47 to 60sec, 37 to 55 sec and 46 to 58 sec respectively. The maximum time delay was 1minute for I90380 i.e.; time of approach increases 21.66% against Fro 0.18. The time approach for different vegetation model as shown in Figure 3.2.

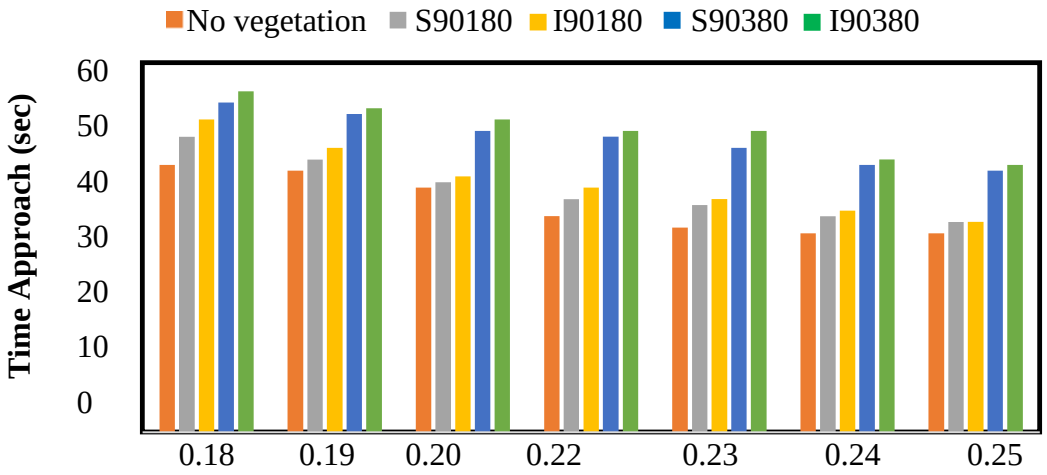

Fig 3.2 Relationship b/w Fro and Time of approach

ACCELERATION EFFECT

As Froude number increases then produce more acceleration. So, acceleration effect produce maximum without vegetation at Fro = 0.25 was 0.0833 m/sec^2, when we use vegetation at I90180 and I90380 (Figure3.3(a)) acceleration effect reduces from 0.0833m/sec^2 to 0.0659 and 0.0650 respectively. When we use vegetation at S90180 and S90380 acceleration effect reduces from 0.0833m/sec^2 to 0.0659 m/sec^2 and 0.0650 m/sec^2 respectively. Hence acceleration effect reduces maximum in case of S90180 and I90380 i.e. ;21.9% & 22.08% respectively.

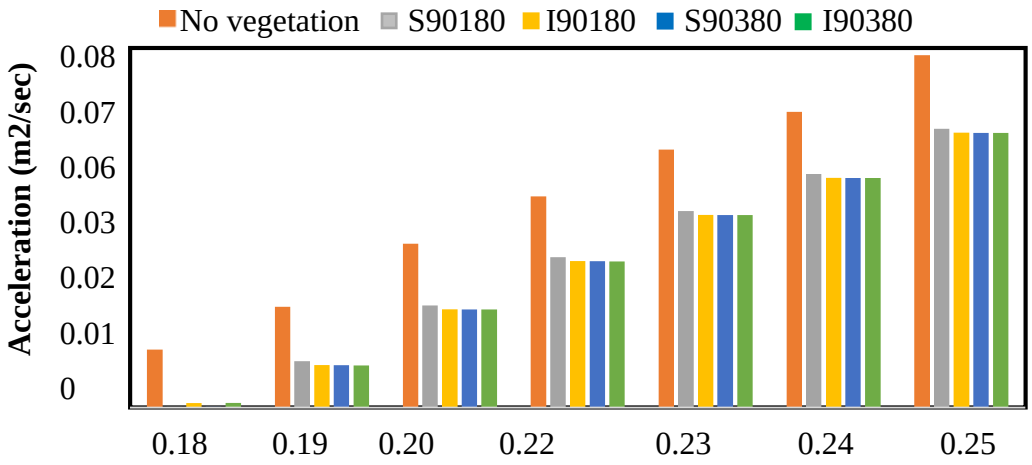

Fig 3.3 Relationship b/w Fro and acceleration

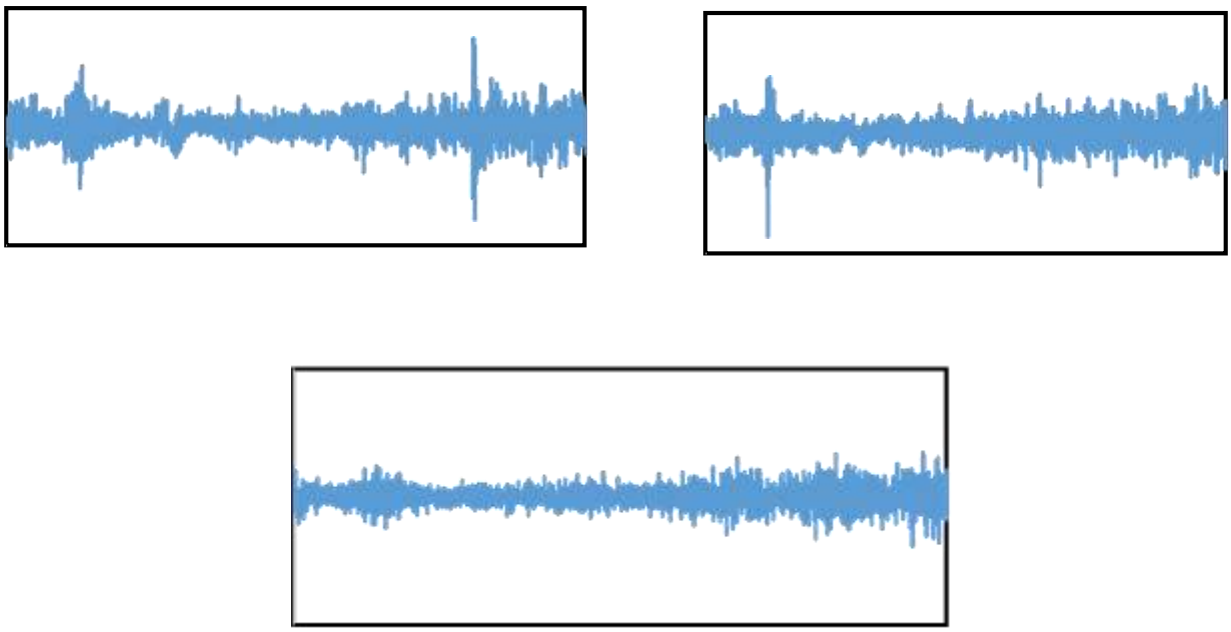

Conclusion and Recommendation

In evaluating the flood-induced risk structure stability is the main concern in floodplain areas. Detail experiments were done to investigate the effect of pressure on house model, arrival time

and acceleration of house with or without vegetation at different conditions. The place of vegetation in front of house and vegetation density has a significant role on hydrostatic pressure force reduction and the acceleration of house. According to experimental finding the hydrostatic pressure force and house acceleration dissipation was maximum I90380 in intermediate vegetation configuration. The range of maximum hydrostatic pressure and house acceleration reduction for I90380 are 7.43% and 22.08% respectively. The maximum value of arrival time I90 is higher than S90. The maximum value of time approach increasing 21.66% and 14.54% respectively. This will help to protect the house in the floodplain area. In future, this research can be extended by changing the slope of channel and submerging the forest. Also for better results can be achieved if the trees are planted at full width of channel.

5 REFERENCES

[1] N. Anjum and N. Tanaka, "Investigating the effectiveness of discontinuous and layered coastal forest defense system against the inundating tsunami current," Landsc. Ecol. Eng., vol. 18, no. 2, pp. 171–190, 2022, doi: 10.1007/s11355-021-00490-7.

[2] A. Ali, G. A. Pasha, U. Ghani, A. Ahmed, and F. M. Abbas, "Investigating Role of Vegetation in Protection of Houses during Floods," Civ. Eng. J., vol. 5, no. 12, pp. 2598–2613, 2019, doi: 10.28991/cej-2019-03091436.

[3] N. Anjum and N. Tanaka, "Changes in the flow structure and energy loss of a Tsunami current through forest with a gap," 22nd Congr. Int. Assoc. Hydro-Environment Eng. Res. Pacific Div. IAHR-APD 2020 "Creating Resil. to Water-Related Challenges," no. 2017, pp. 1–7, 2020.

[4] A. Ahmed and A. R. Ghumman, "Experimental investigation of flood energy dissipation by single and hybrid defense system," Water (Switzerland), vol. 11, no. 10, Oct. 2019, doi: 10.3390/w11101971.

[5] A. Ahmed, M. Valyrakis, A. R. Ghumman, G. A. Pasha, and R. Farooq, "Experimental investigation of flood energy reduction through vegetation at various angles," River Res. Appl., vol. 37, no. 4, pp. 644–655, May 2021, doi: 10.1002/rra.3777.

[6] R. E. Martínez-Castro, S. Jang, and R. E. Christenson, "Rapid cable tension estimation using dynamic and mechanical properties," Sensors Smart Struct. Technol. Civil, Mech. Aerosp. Syst. 2016, vol. 9803, no. 860, p. 98030E, 2016, doi: 10.1117/12.2219425.

[7] A. Ali, T. Y. Sandhu, and M. Usman, "Ambient vibration testing of a pedestrian bridge using low- cost accelerometers for shm applications," Smart Cities, vol. 2, no. 1, pp. 20–30, 2019, doi: 10.3390/smartcities2010002.

[8] T. Echnique, "Mass distribution effect on the finite model updating using operational model analysis," pp. 2–6.

[9] G. Ahmed and N. Tanaka, "Undular hydraulic jump formation and energy loss in a fl ow through emergent vegetation of varying thickness and density," Ocean Eng., vol. 141, no. June 2016, pp. 308–325, 2017, doi: 10.1016/j.oceaneng.2017.06.049.

[10] E. Irtem, N. Gedik, M. S. Kabdasli, and N. E. Yasa, "Coastal forest effects on tsunami run-up heights," Ocean Eng., vol. 36, no. 3–4, pp. 313–320, Mar. 2009, doi: 10.1016/j.oceaneng.2008.11.007.

[11] N. Anjum, U. Ghani, G. A. Pasha, A. Latif, and T. Sultan, "To Investigate the Flow Structure of Discontinuous Vegetation Patches of Two Vertically Different Layers in an Open Channel," 2018, doi: 10.3390/w10010075.

2nd International Conference on Advances in Civil and Environmental Engineering (ICACEE-2023)

University of Engineering & Technology Taxila, Pakistan

Conference date: 22nd and 23rd February, 2023

IMPACT OF URBANIZATION ON RIVER WATER QUALITY BY USING ANN MODELING APPROACH

Muhammad Taha Husssain[1], Naeem Ejaz[1], Ghulam Abbas[2], Muhammad Imran[1], Muhammad Asad Ullah[1]

1**:** Department of Civil Engineering University of Engineering and Technology Taxila,Muhammadtaha786@hotmail.com

1 : Department of Civil Engineering University of Engineering and Technology Taxila, naeem@uettaxila.edu.pk.

2 : Swedish College of Engineering and Technology Wahcantt,ghulamabbas696@yahoo.com

ABSTRACT

Water is essential for the existence and wellness of both humans and ecosystems. As a result, its quality is equally crucial. A water sample's composition is referred to as its quality. Data interpretation could be challenging and time-consuming. To improve the efficiency of an assessment operation and create a better strategy for managing water resources, evaluations of water quality characteristics are required. Predictive modeling approach such as Artificial Neural Network (ANN) has been worth the critical analysis of static data. Quality of Indus River located in Punjab, Pakistan is constantly deteriorating as a result of local human activity and urbanization. The goal of the current study is to apply ANN to evaluate the water quality characteristics of the Indus River. The model proposes the prediction model for physical, chemical, and biological parameters. The Liebenberg Marquardt algorithm (LM), one of the best neural network training techniques, was utilized to represent the nonlinear connection.The model was trained, tested, and validated producing a best-fit regression with R of 0.99 for training, 0.86 for validation, and 0.98 for testing giving an average of 0.98 indicating a close relationship between the input and output values.The results indicate that the model has great potential in determining the impact of urbanization on water quality by analyzing the parameters.

KEYWORDS: Urbanization, River water quality, ANN

INTRODUCTION

Water is a vital component of human existence and activities such as industry, farming, and others, yet it is also one of the environment's most fragile components. Because of the differences in cover-land around rivers, the water of rivers is characterized by a high level of variation in time and space [1]. This frequently makes it difficult to determine water temperatures and contamination, which is required to properly regulate pollution and develop viable methods for reducing contaminating resources.

Rapid population expansion, land along river basins, urbanization, and industry have put rivers under more stress, causing pollution and environmental degradation [2, 3]. The greatest concern of stream flow management in Pakistan is urban overflow and industrial effluents in water catchment regions [4]. As indicated by various studies, especially urbanization has extreme negative impact on river water quality in Layyah [5, 6] , Muzaffargarh [7] and Bhakkar [8]. Pollution from urban runoff and industrial discharges degrades water resources, lowers crop productivity, and harms public health. Runoff from polluted agricultural fields, such as pesticide and fertilizer residues, conveys large amounts of salts washed off from nearby agricultural regions [9]. Various approaches are utilized to analyse the impact of urbanization on river water quality. Artificial neural networks are an extremely helpful method in a large number of scientific fields, including ecology, analytical chemistry, and water management. The findings of different investigations demonstrated that ANN models outperform the linear MLR model and offer strong and trustworthy predictions [10].

LITERATURE REVIEW

Water pollution is becoming a more serious worldwide issue that threatens human health, environmental services, and agricultural productivity [11]. Artificial intelligence (AI) based model's distinguishing traits can provide a thorough understanding of growing water quality challenges. Shah et al. looked at how well gene expression programming (GEP), artificial neural networks (ANN), and linear regression models (LRM) predict monthly total solids (TDS) and specific conductivity (EC) in the middle Indus River at two outlet stations [12]. TDS and EC are significant factors in assessing the quality of the water for consumption and agricultural water since they are specifically connected to the quantity of salt in water, and hence high values of parameters result in a low water quality index[13, 14]. Analysed the water quality of Kabul, Afghanistan by using the LAB MAN instrument, and Water Quality Index was modeled by using the GIS tool [15]. The specific characteristics of machine learning (ML)-based simulation can give a thorough grasp of the escalating problems with water quality. In another study, 360 monthly data were used to create a statistical model based on multi-expression programming (MEP) for the variables of EC and TDS in the upper Indus River at two separate outlet points [16]. To forecast the river quality of the water using four strategic situations with various urban population and layouts, Random Forest (RF) machine learning model was utilized. To demonstrate the significance of urban growth patterns in affecting stream water quality, Shapley Additive explanations (SHAP) was employed. Geographically Weighted Regression (GWR) was used to examine how these patterns' effects varied depending on where they occurred [17]. In hydrological terms, ANN models are termed black box models since they are mostly data-driven [18]. Because of its tremendous processing capacity and ability to quickly and easily simulate future scenarios, the ANN model is seen to be a viable alternative to mathematical models [19]. ANN is one of the most helpful strategies for predicting groundwater level among the several methodologies

accessible, and it is especially suggested when multiple data quantities are available [20]. Studied the combined impact of urbanization and climate change by using an integrated modelling study [21]. Remote sensing technique and GIS also combined to evaluate the parameters of quality of water over tempo-spatial scale [22].

METHODOLOGY

The study area and applied methodology for the analysis of urbanization's impact on water quality is briefly described in this section.

Study Area

The river Indus system has been one of Asia's most important rivers. This river system, which runs from north to south in a north-western direction, has been running for thousands of years. The Indus River water quality evaluation along the Layyah, Muzaffargarh, and Bhakkar Districts of Pakistan is identified in this study. The study focused on a 70-kilometer stretch of the left bank of the Indus River between the Layyah Muzaffargarh Districts. The geographical coordinates of the location are 31°4'0.321"N, 70°49'41.066"E, and 30°31'32.086"N, 70°51'16.301"E. Indu's water samples are taken from three separate Layyah, Bhakkar, and Muzaffargarh locations demonstrated in Figure 3.1.

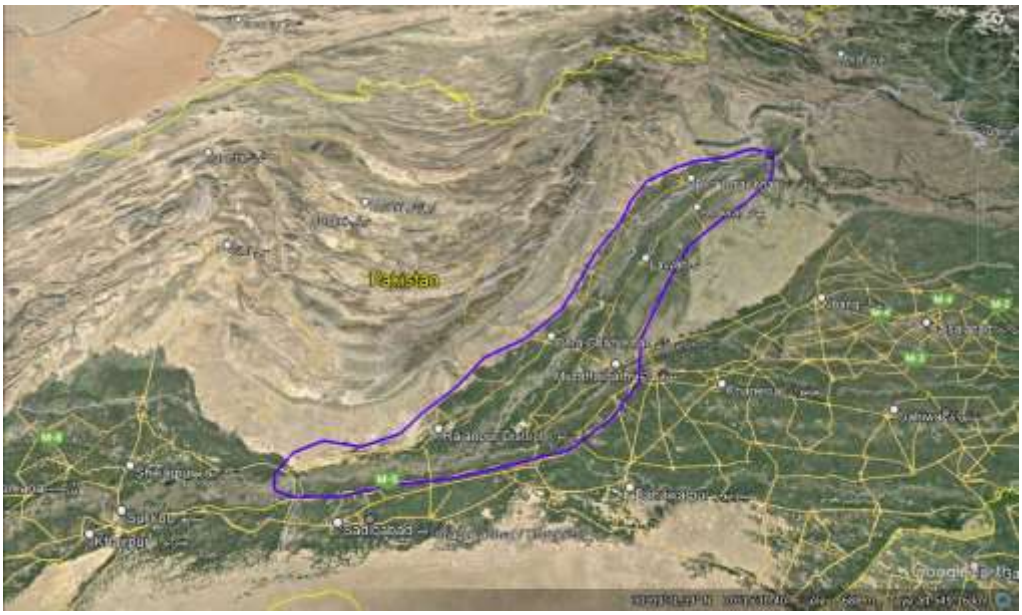

Figure 3.1: Location of Sample Sites

Predictive Modelling Approach

This modeling approach is based on Artificial Neural Networks. Model development, evaluation, validation, and robustness analysis are all steps in the process. The water quality data utilized in this investigation came from Pakistan Environmental Protection Agency and the Punjab health department. The complete data set included 40 yearly records data from Bhakkar city to Layyah city and Muzaffargarh city at a different locations. The dataset included biological, Chemical, and physical parameters as indicated in table 3.1.

Table 3.1: River Quality Parameters

Sr #	Physical Parameters	Chemical Parameters	Biological Parameters
1	Turbidity	PH	Phytoplanktons
2	Temperature	Total Dissolve Solids (TDS)	Zooplanktons
3	Color	Toxic Metals	
4	Taste and Odour	Biological oxygen Demand (BOD)	
5	Density	Chemical Oxygen Demand (COD)	
6	Electrical Conductivity	Dissolved oxygen (DO)	
7		Hardness	
8		Sulphates	
9		Carbonates	

The basis for this work is the forecast of river water quality effected by urbanization. Finding the model input variables that have a substantial impact on the output factor is one of the key challenges in an ANN (s). A priori knowledge of the causative variables, visual inspections, and statistical analysis of prospective inputs and outputs are typically used to choose the input variables. We see that there are links between the various parameters, as would be predicted. We are aware that the number of dissolved particles in the water determines its electrical conductivity (which are mostly salts). Additionally, the measurement of turbidity is directly impacted by the rise in suspended solids in water, which makes water turbid. The model of the ANN approach is shown in figure 3.2.

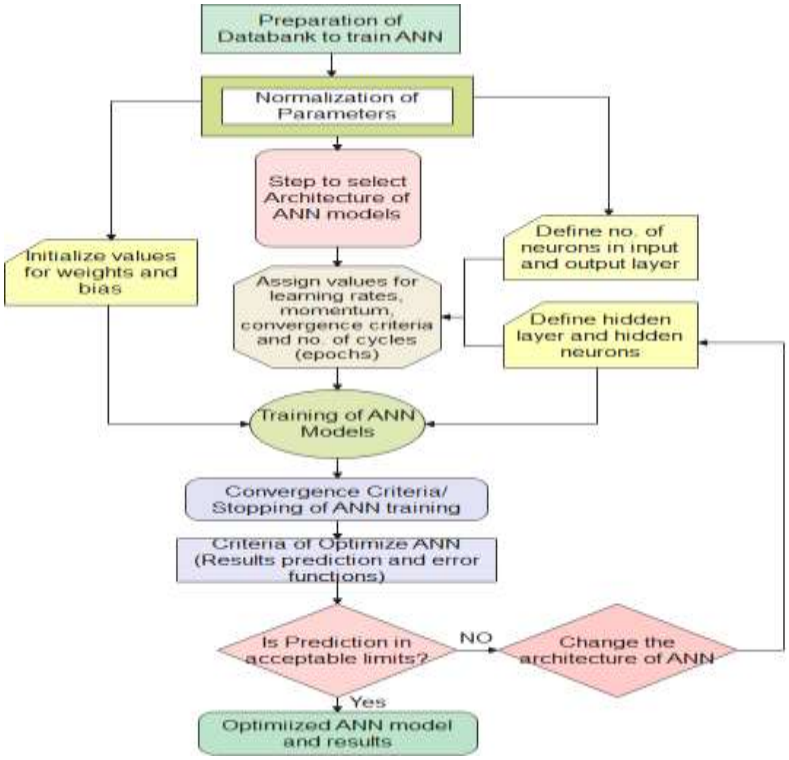

Figure 3.2: ANN Model setup

In this paper, the Levenberg-Marquardt (LM) approaches were used. The network was designed and run using the MATLAB programme.The network is divided into three phases: training, validation, and testing. Table 3 depicts the data segmentation for model training, validation, and testing. Seventy percent of the data is used for training, with the remaining 10 percent and twenty percent used for validation and testing, respectively. Ten neurons were picked for the buried layer in the first step. The network randomly picked 260 samples for training, 50 samples for validation, and 90 samples for testing based on its percentage.

$$R = \frac{\sum_{i=1}^{n}(exi - \overrightarrow{xi})(moi - \overrightarrow{moi})}{\sqrt{\sum_{i=1}^{n}(exi - \overrightarrow{exi})\sum_{i=1}^{n}(moi - \overrightarrow{moi})}} \qquad (1)$$

N is the number of data sets, Yi denotes the actual values, and I denotes the forecasted values. Regression is widely considered as the most essential indicator for measuring the overall accuracy of a network. R values are employed to evaluate the connection between outputs and planned goals. A strong link has an R-value of 1, whereas a random relationship has an R-value of zero.

RESULTS

The results of the ANN methodology to estimate the impact of urbanization on river water quality are given below. The water quality parameters (WQP) must be satisfied with the values of the numerical indicators of the relevant distribution according to the statistical approaches employed in this paper to determine the relationship between variables.

Physical Factors

The numerical information regarding the physical properties of the river water of Layyah, Muzaffargarh, and Bhakkar is presented and analyzed in the form of a graphs as shown in Figure 4.1.

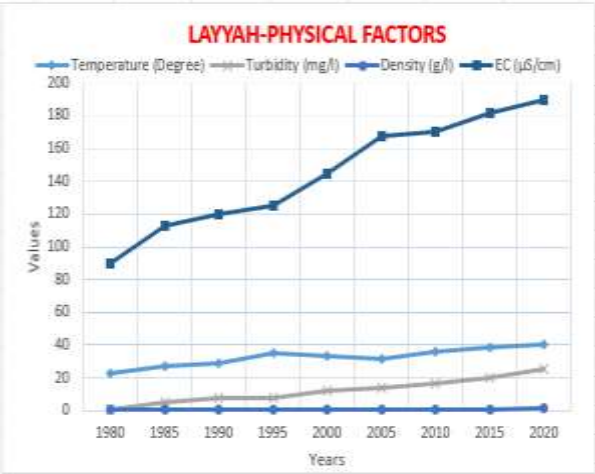

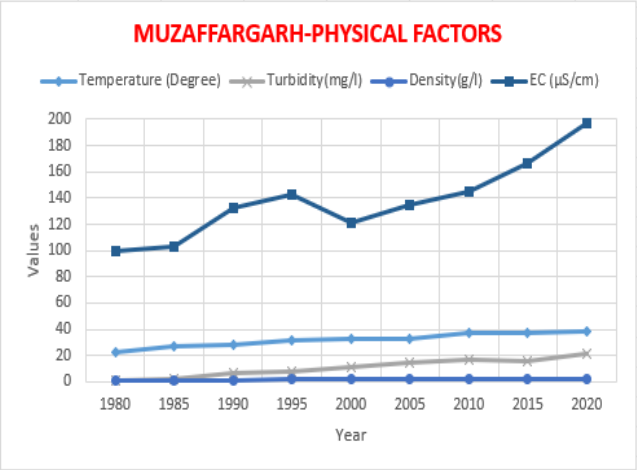

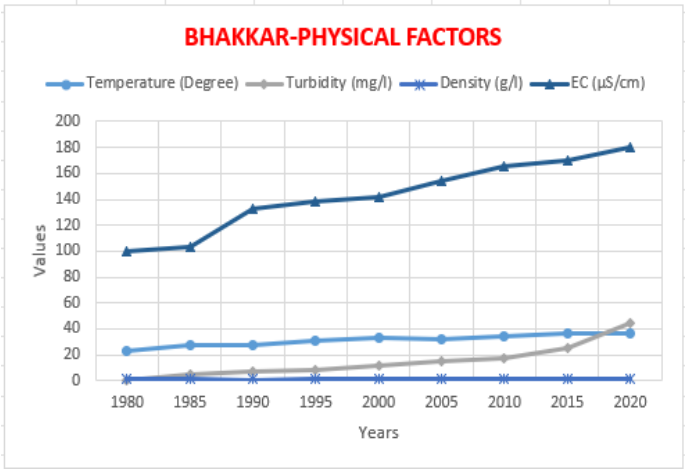

Figure 4.1: Physical Factors for Water Quality

These graphs depicts that the physical properties of Indus river water are continuously changing over the years due to the pollution and environmental effects caused by urbanization. The temperature of the river water continues to increase due to the increase in temperature of the environment by global warming caused by traffic, household appliances, and industrialization. The turbidity increases due to pollution caused by the spillage of chemicals from households, shops, and industries. The density of water has little change from 1980 to 2020 but then varies due to greater pollution in cities. The very rapid increase in electrical conductivity (EC) indicates the increase of metal content in river water. This analysis demonstrates the drastic effect of rapid urbanization on river water quality.

Chemical Factors

The static data for the chemical properties of river water from Layyah, Muzaffargarh, and Bhakkar is shown in figure 4.2.

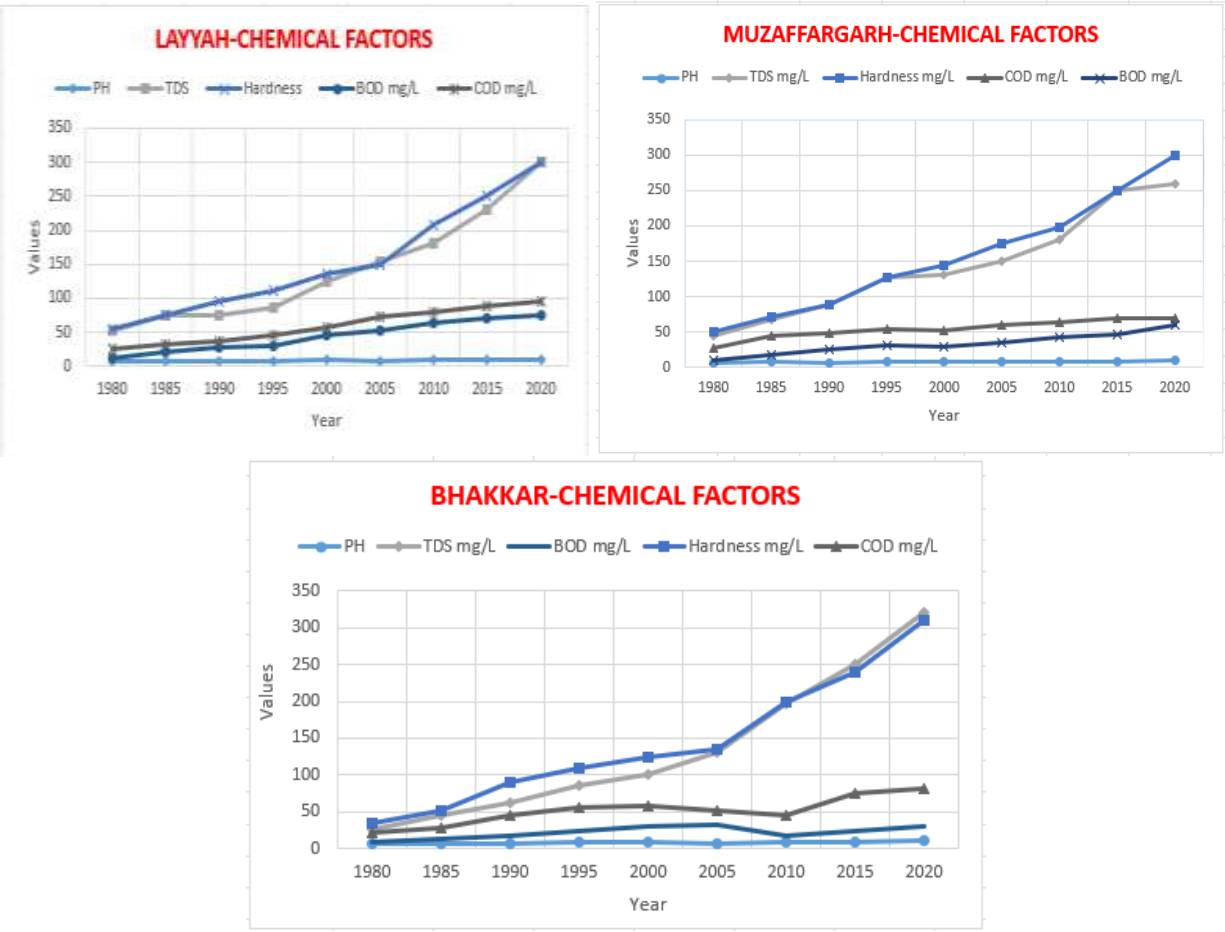

Figure 4.2: Chemical factors for Water Quality

The data from the chemical parameters of river water indicates that the river quality drastically changes from 1980 to 2020. As shown by the graphs, the PH of the river water is mostly in the 7-8 range during the early years but, in recent years PH moved towards the basic range. This is due to the increase in the carbonate and bicarbonate content of the river water. These chemicals greatly discharge from households, industries, laundries, and shops in the form of soap and detergents into the river and increase PH. The maximum hardness is 300 mg/L in all the district's samples. The population growth over time and in turn urbanization is responsible for the spillage of waste into water that results in an unexpected increase in Total Dissolve Solids (TDS). The increase is very rapid after 2020 due to very greater urbanization rate. A sharp increase can be seen in Layyah and Bhakkar. The BOD and COD also increase over time as shown in the graph of Layyah,

Muzaffargarh and Bhakkar, which also indicates the increase in the concentration of chemicals and microorganisms. This confirms the diverse impact of urbanization and population growth on the quality of the river.

Biological Factors

The data related to the biological factors of the river quality is also collected and analyzed with the help of ANN methodology and the following results are obtained as shown in figure 4.3.

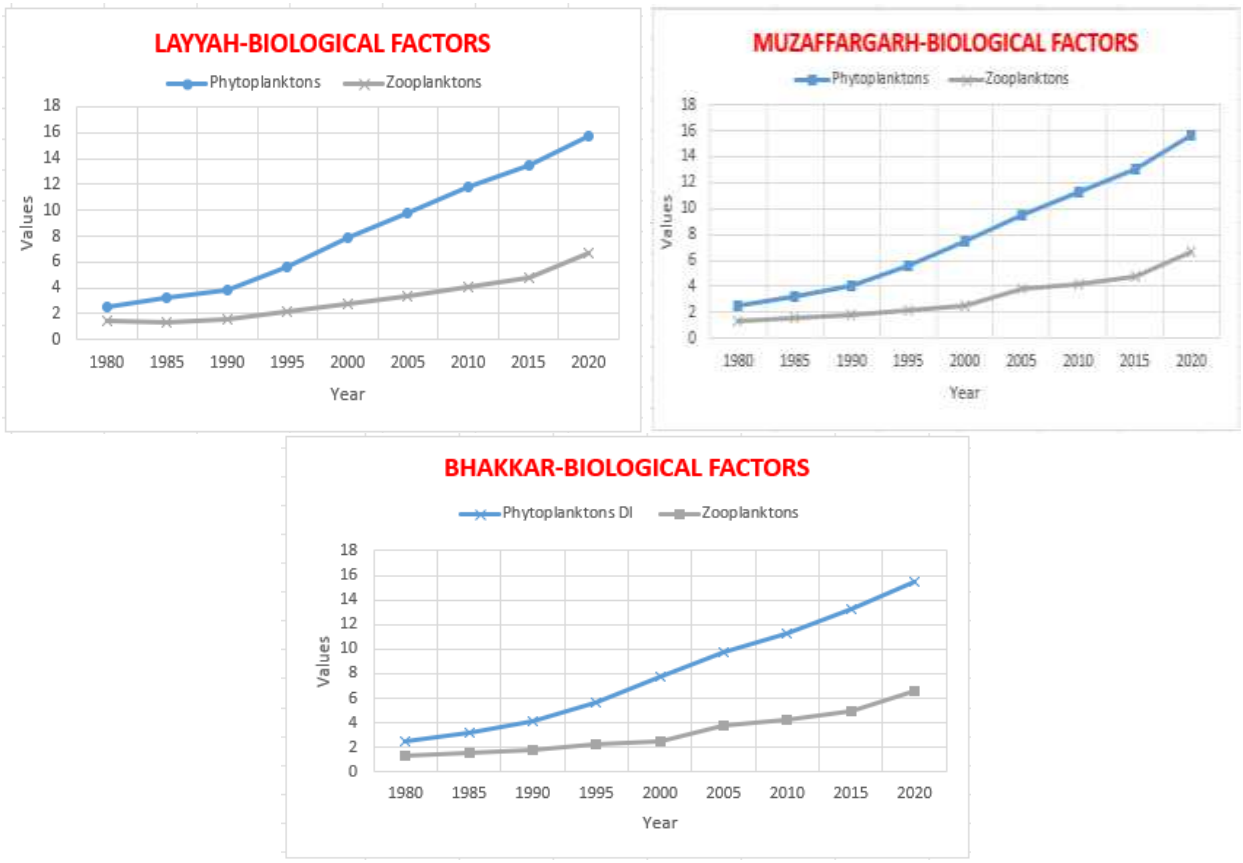

Figure 4.3: Biological factors for Water Quality

The results regarding the phytoplanktons and zooplanktons in river water showed that their population increases from 1980 to 2020. This increase in nutrients is due to the availability of the Population. Phytoplanktons grow faster in the presence of the nutrients like sulphates, nitrates, phosphates, silicate, iron, and calcium. Due to rapid urbanization over the past years, there is an increase in households, commercial shops, and industries, and from these, large amounts of

chemicals discharge directly into the river water and are responsible for the growth of the biological species.

Regression analysis of water quality data:

By using water quality data , regression analysis is carried out. Figures 4.4 (a), 4.4 (b), and 4.4 (c) show the correlation of training, validation, and testing between both the model's input and output parameters. Figure 4.4 (d) displays the overall correlation of the model. In each scenario, a red-colored linear line is shown. The overall R-value of 0.96 suggests that the correlation is reasonably close to the linear fit.

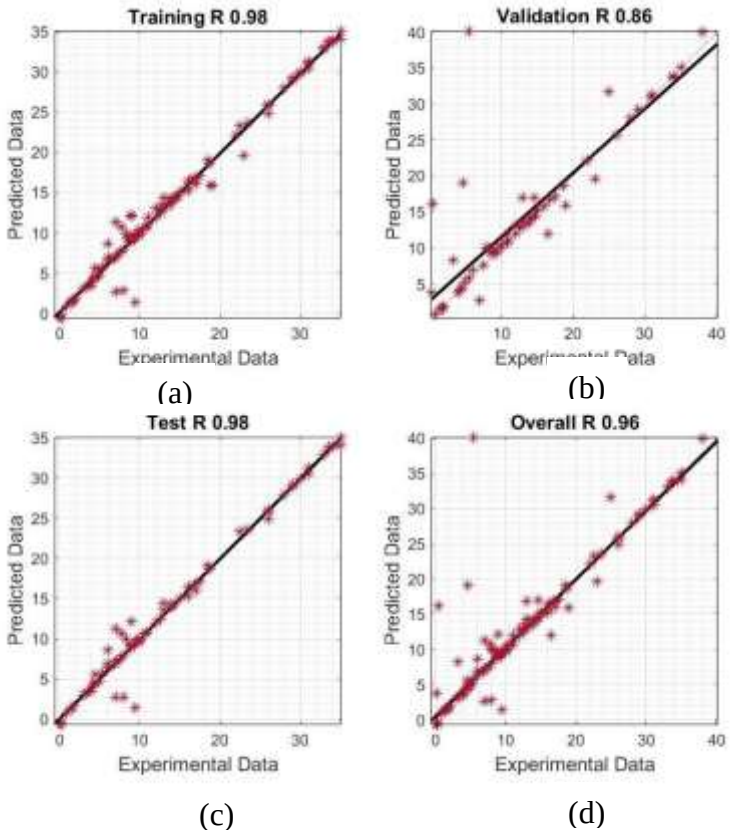

Figure 4.4:Regression analysis of water quality data through (LM algorithum)()Trainning (b) Validation (c) Testing (d) overall data set

ACKNOWLEDGEMENTS

The authors would like to express their gratitude to all individuals and departments that contributed to the study process, in particular Prof. Dr. Naeem Ejaz and Engr. Ghulam Abbas. We appreciate the anonymous reviewer's thorough analysis and helpful recommendations.

CONCLUSION

Population growth and urbanization are the main concern all over the world owing to their negative impact on the environment. This also contributes to the decline in river water quality. For Indus River, this manuscript suggested the Artificial Neural Network (ANN) based parameters as a Predictive Modeling Approach for determining the impact of urbanization on the water's quality at three different district locations (Layyah, Muzaffargarh, and Bhakkar). The physical, chemical and biological factors are taken as variables to apply the methodology and results are analyzed. The changes in the physical properties of the river water from the past years such as an increase in temperature, turbidity, and EC demonstrate the impact on river quality. The clearer indication is the chemical parameters which show the unexpected change in the river water with time such as an increase in hardness, TDS, BOD, and COD and a decrease in dissolved oxygen (DO). These parameters are directly related to the rapid discharge of chemicals from the cities and fields. The increase in biological parameters like phytoplanktons and zooplankton validated the presence of various chemicals as nutrients in the water. Thus, this demonstrates that urbanization has severely detrimental effects on the quality of the river water.

REFERENCES

1. Peng, F., et al., *Urbanization drives riverine bacterial antibiotic resistome more than taxonomic community at watershed scale.* Environment international, 2020. **137**: p. 105524.
2. Wang, L., et al., *Effects of urbanization on water quality and the macrobenthos community structure in the Fenhe River, Shanxi Province, China.* Journal of Chemistry, 2020. **2020**.
3. Freeman, L.A., et al., *Impacts of urbanization and development on estuarine ecosystems and water quality.* Estuaries and Coasts, 2019. **42**(7): p. 1821-1838.
4. Ilyas, M., et al., *Environmental and health impacts of industrial wastewater effluents in Pakistan: a review*. Reviews on environmental health, 2019. **34**(2): p. 171-186.
5. Sajid, M., et al., *Spatio-Temporal Analysis of Land Use Change and its Driving Factors in Layyah, Punjab, Pakistan.* The Nucleus, 2023. **60**(1-2): p. 15-23.
6. Riaz, M., et al., *Assessment of avifaunal diversity in riverine and urban areas of Layyah along the River Indus, Punjab-Pakistan.* Ornithological Science, 2019. **18**(2): p. 149-160.

7. Hussnain, M., et al. *Application of the online WhatIf? Planning support system in Peri-urban spatial planning; case study of Muzaffargarh, Pakistan*. in *Proceedings of the 24th International Conference on Urban Planning and Regional Development in the Information Society*. 2019.
8. Sohail, M., et al., *Freely dissolved organochlorine pesticides (OCPs) and polychlorinated biphenyls (PCBs) along the Indus River Pakistan: spatial pattern and risk assessment.* Environmental Science and Pollution Research, 2022. **29**(43): p. 65670-65683.
9. Jehan, S., et al., *Hydrochemical properties of drinking water and their sources apportionment of pollution in Bajaur agency, Pakistan.* Measurement, 2019. **139**: p. 249-257.
10. Benzer, S. and R. Benzer, *Modelling nitrate prediction of groundwater and surface water using artificial neural networks.* Politeknik Dergisi, 2018. **21**(2): p. 321-325.
11. Zafar, S., et al., *Conserve Water Resources and Reduce Water Pollution.* Multidisciplinary Current Research, 2022: p. 91.
12. Shah, M.I., et al., *Predictive Modeling Approach for Surface Water Quality: Development and Comparison of Machine Learning Models.* Sustainability, 2021. **13**(14): p. 7515.
13. Asadi, E., et al., *Groundwater quality assessment for sustainable drinking and irrigation.* Sustainability, 2019. **12**(1): p. 177.
14. Ram, A., et al., *Groundwater quality assessment using water quality index (WQI) under GIS framework.* Applied Water Science, 2021. **11**(2): p. 1-20.
15. Singh, S. and A.R. Noori, *Groundwater quality assessment and modeling utilizing water quality index and GIS in Kabul Basin, Afghanistan.* Environmental Monitoring and Assessment, 2022. **194**(10): p. 1-19.
16. Aldrees, A., et al., *Multi-Expression Programming (MEP): Water Quality Assessment Using Water Quality Indices.* Water, 2022. **14**(6): p. 947.
17. Wang, R., J.-H. Kim, and M.-H. Li, *Predicting stream water quality under different urban development pattern scenarios with an interpretable machine learning approach.* Science of The Total Environment, 2021. **761**: p. 144057.
18. Zhu, M., et al., *A review of the application of machine learning in water quality evaluation.* Eco-Environment & Health, 2022.
19. Iqbal, M., et al., *Relating groundwater levels with meteorological parameters using ANN technique.* Measurement, 2020. **166**: p. 108163.
20. Zaji, A.H., et al., *Application of optimized Artificial and Radial Basis neural networks by using modified Genetic Algorithm on discharge coefficient prediction of modified labyrinth side weir with two and four cycles.* Measurement, 2020. **152**: p. 107291.

21. Salerno, F., V. Gaetano, and T. Gianni, *Urbanization and climate change impacts on surface water quality: Enhancing the resilience by reducing impervious surfaces.* Water research, 2018. **144**: p. 491-502.
22. Carstens, D. and R. Amer, *Spatio-temporal analysis of urban changes and surface water quality.* Journal of hydrology, 2019. **569**: p. 720-734.

2nd International Conference on Advances in Civil and Environmental Engineering (ICACEE-2023)

University of Engineering & Technology Taxila, Pakistan

Conference date: 22nd and 23rd February, 2023

CRITICAL BARRIERS AND IMPLEMENTATION STRATEGIES FOR ADOPTION OF GREEN BUILDING TECHNOLOGY IN CONSTRUCTION INDUSTRY OF PAKISTAN.

Khushal khan[1], Suliman Khan[1*], Shehroze Ali[1], Ali Rabah[1], Shawal Khan[2]

[1]Lecturer, Department of Civil Engineering, NFC Institute of Engineering and Fertilizer Research (IE&FR), Faisalabad 38090, Pakistan

[2]Department of Civil Engineering, University of Engineering and Technology (UET), Peshawar 25120, Pakistan

*Corresponding author

Suliman Khan

Lecturer, Department of Civil Engineering

NFC Institute of Engineering and Fertilizer Research (IE&FR), Faisalabad

Email: Suliman.khan@iefr.edu.pk

Abstract-

Green building technology (BIM) is a step towards sustainable development, and it provides a reliable solution for green infrastructures in terms of bringing innovations in environmentally friendly and energy efficient buildings. The research was carried out to investigate the probable critical barriers to the adoption of BIM in the construction industry of Pakistan, and to recommend effective strategies for their implementation. A statistical analysis of 50 responses to questionnaire survey comprising of 12 contractors, 10 designers, 7 administrative authorities, 9 acidemias, 7 consultants, and 5 clients showed the results that the major hindrances to BIM adoption and implementation in Pakistan are due to lack of awareness and lack of promotion about the green building technology (GBT). Moreover, high initial cost of GBT and lack of green building codes is also one of the major barriers for the adoption of GBTs in construction industry of Pakistan. In addition, the critical barriers to the adoption of GBT was categorized in five groups including, governmental, financial, awareness, innovational and market issues which make it clear that awareness and educational issues are the most critical ones followed by financial and market issues. The technique used for the analysis of questionnaire survey responses is mean score ranking. To overcome these barriers, it was concluded that public awareness towards green initiatives, promotion of successful green building practices and applying mandatory GB policies, codes and regulations will be the effective implementation strategies for adoption of GBT in construction industry of Pakistan.

Keywords- Green building technologies (GBTs), Pakistan, construction industry, critical barriers

INTRODUCTION

In recent times, there is an increase pressure of human activities on the built environment. Although the blame has been shifted to the wide range of industrial activities, yet the construction industry is not left out of this quagmire. It has been discovered that the construction industry is directly responsible for a large portion of emission of pollution, energy consumption, biodiversity loss, and waste generation. Global warming and climate changes occur due to the emission of Greenhouse gas. However, buildings play a main role in causing Greenhouse gas emissions. Green building technology is defined as "the act of creating designs and utilizing processes that are naturally responsible and asset effective all through a structure's life-cycle" (Albert et al., 2017).

The adoption of GBT was essential for the building industry's continued growth because of its long-term benefits. The use of GBT is a solution to the issues of environmental pollution and climate change. The construction industry has attempted to generate new paradigms for development by integrating various green practices, such as green building (GB) and green construction (GC) [Yujing et al., 2021]. Adopting GBTs, GC, and GBs all aim to achieve the same objectives of environmental protection, resource conservation, and ultimately, sustainable growth of the construction industry. Most of the developed countries have stepped into the reign of sustainable development by adopting green practices. In developing countries such as Pakistan, adopting sustainable development faces different obstructions like lack of innovation, awareness, etc (Sara et al., 2018. Therefore, the need of hour is to understand that what are the major hurdles for the implementation of GBT in Pakistan and how Green building technology can be effectively adopted in the construction industry of Pakistan. Therefore the objectives of research are:

1. To induct the Technology by generating a model of Green Building on Autodesk Revit.
2. To identify the major obstacles to GBT adoption in Pakistan's construction sector.
3. To outline the practical methods for implementing GBT in Pakistan's construction sector.

LITERATURE REVIEW

With the revolution of the construction industry methods which are environment friendly, and eco-friendly are prescribed to be adopted. Green building reduces the construction related environmental effects while creating satisfying and healthier places for people to live. Governments from all over the world have embraced the idea of green building as a means of enhancing the sustainability of the construction industry. "Green building" is the practice of utilizing methods and developing buildings that are resource-efficient and environmentally responsible throughout a building's lifecycle. According to the research study, green building is a potent replacement for conventional buildings and plays a significant part in eradicating and minimizing the detrimental impacts of construction activities on climate and environmental change.

It is well known that the construction industry has detrimental consequences on society, the economy, and the environment. The United Nations Environment Program (UNEP) estimates that while using 40% of all energy, the building sector is responsible for up to 30% of all global greenhouse gas emissions (2011). Building is frequently recognized as the most resource-intensive industry because to its consumption of 25% of steel products and 70% of the 17 different types of cement (Kibert et al., 2008).

It is widely acknowledged that the biggest barrier to green construction is cost (Chan et al., 2017). Cost is still a crucial financial factor in programs promoting sustainable development. Using green materials on GB projects is more expensive because they are frequently more expensive than their conventional counterparts (Hwang & Tan, 2012). The organization might not have the money to employ green technology. Overall, employing green technology and materials can increase productivity by 2 to 7% (Jilong et al., 2017). The introduction of green innovations is also certain to increase the whole project cost, not just the underlying cost (Shi et al., 2013). This is because partners may be required to bear the increased capital expenses that may be associated with such innovations.

Time is yet another key financial factor in development efforts. Similar to expense, time is primarily utilized to compare project performance and is extremely important to almost all project participants (Chan et al., 2017) fought that any undertaking delay brought about by utilizing green practices might have genuine financial ramifications. This is on the grounds that undertaking delays typically make harm gatherings and result in expanded expense; moreover, they influence the standing of corporations (Arditi & Pattanakitchamroon, 2006). Delays in GB projects are brought about by a few elements, for example, longer time expected to endorse new green advances inside a firm and extensive implementation season of on location innovations (Chan et al., 2017).recognized that the apprehension about project delays is a significant obstruction deflecting partners from taking on green practices.

The achievement of carrying out green development significantly de pends on the kind of agreement embraced to convey the undertaking (Chan et al., 2017). Not having the option to decide the potential performance of GB innovations, the need to change site practices and rehearses, and the use of various acquirement and agreement types of venture conveyance recommend that partners would need to embrace new advances and practices notwithstanding vulnerabilities and dangers(Zhang, Shen, et al., 2011)(Zhang, Platten, et al., 2011).(Shi et al., 2013) placed that this regularly decreases the proficiency of GB and may push partners back to ordinary development techniques.

METHODOLOGY

A quantitative questionnaire based on the refined factors from the literature was created with the goal of ranking the important factors preventing the successful and widespread adoption of GB technologies in the construction industry. To questionnaire survey, first we have to know that how actually green building look likes, and what are the main distinctions between a conventional construction and a green building. For the purpose of letting us identify the critical barriers for the adoption of GBT in the construction industry of Pakistan by our expert respondents first we have to induct that what basically this technology is meant by, how actually green building look likes, what are the components of green building, what are the benefits of green building and what are the major differences between an ordinary building and a green building. For this purpose, a Generic model of Green Building is created on Revit. The basic purpose of this model is to get lore about the basic features and characteristics of a building constructed on the standards of GBT. In green building the materials are used which are energy efficient, resource efficient and environmental friendly e.g. fly ash bricks are used which is a thermal insulator, reflector glass is used in window panes, because it only receives light from the sun and the temperature of room is not affected by the heat rays coming from sun.

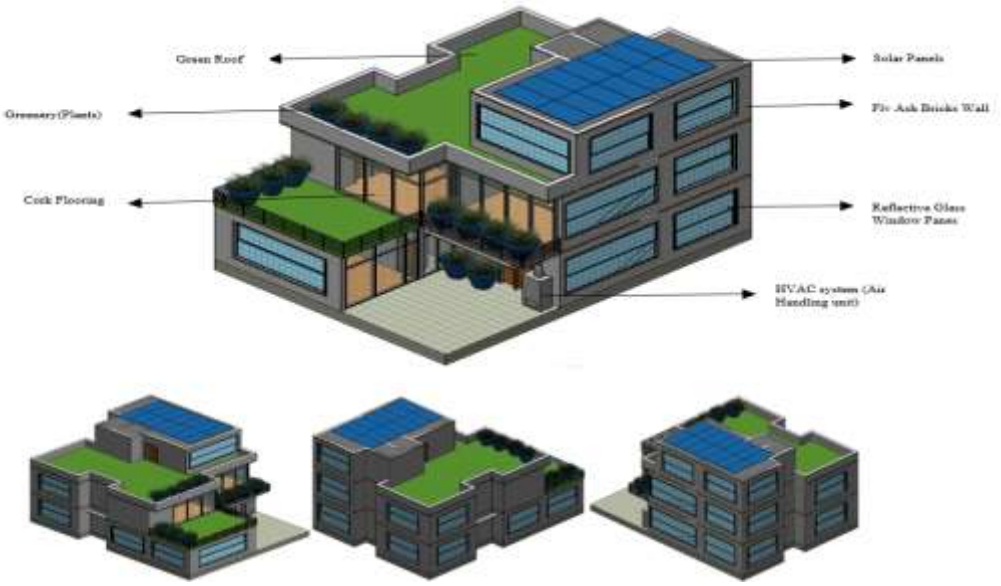

Fig 1: 3D elevations of green building model generated on Autodesk Revit.

Following materials and features were introduced in the model.

- Fly ash bricks are used in walls
- Reflector glass panes window is used in the building,
- Solar panels are placed at the top of building to make it energy efficient,
- HVAC system is installed,

- Cork flooring is used in the covered area,
- Green roof is placed at the top story,
- Water efficiency techniques are applied.

All these materials are energy efficient and eco-friendly.

In this study, a Delphi survey questionnaire as illustrated in table 1 was designed on the basis of past researches and the results interviews. Throughout this study, it has been identified that most of the barriers and strategies that are proposed by the interviewees has also mentioned in the earlier literature. Moreover, all the identified barriers than analyzed as per the importance of each barrier by using Delphi techniques on a Likert scale of five point, with 1 showing not important and 5 signifying extremely important. Sample size can be explained as the number of observations that have taken to obtain the data by statistical means for the purpose of this dissertation, the researcher has selected 50 officers from the financiers of green building technology, public and private institutions, and professionals in government agencies and stakeholders that are involved in the green building technology

Table 1 List of respondents

DISTRIBUTION OF RESPONDENTS	
RESPONDENTS	NO OF RESPONDENTS
ACADMEIA	09
CONSULTANT	07
CONTRACTOR	12
CLIENTS	5
DESIGNERS	10
ADMINISTRATIVE AUTHORITY	07
ALL EXPERTS	50

In data analysis technique it is decided the method to analyze data by qualitative and quantitative means. Method of data analysis depends on the nature of the research topic. For qualitative research, the technique used to analyze data is content analysis. In the content analysis the focus is on information put forward by other scholars in their researches. Chi-square p-value test has also been used to assess the inter-rater agreement. On the other hand, in the quantitative study, mean score analysis technique is used. The adoption of the aforementioned technique would be considered due to the fact that by using this technique the results received from the respondents were competently analyzed which could ultimately meet the aims and objectives of the study.

RESULTS AND DISCUSSIONS

Critical Barriers

Table 2: Mean scores of categories of critical barriers

No	Factors	All Experts		Academia		Consultants		Contractors		Clients		Designers		Administrative Authority	
		Mean	Rank	Mean	Rank	Mean	Rank	Mean	Rank	Mean	Rank	Mean	Rank	Mean	Rank
1	1a	3.42	11	3.56	1	4.43	1	3.58	7	3.40	3	3.10	9	2.71	10
2	1b	3.62	4	3.56	1	4.14	2	4.50	1	3.00	5	3.60	4	3.57	5
3	1c	3.24	14	3.20	3	2.57	8	3.25	11	2.20	8	3.50	5	3.14	8
4	1d	3.20	15	3.20	3	3.86	3	3.33	10	3.20	4	4.00	2	3.57	5
5	2a	3.56	6	3.22	2	3.57	5	3.58	7	2.20	8	3.30	7	3.00	9
6	2b	3.70	3	3.22	2	3.71	4	3.75	5	3.00	5	3.50	5	4.29	2
7	2c	3.80	1	3.22	2	3.86	3	4.00	3	2.80	6	3.70	3	4.43	1
8	2d	3.50	8	3.22	2	3.57	5	3.67	6	2.80	6	3.70	3	3.57	5
9	2e	3.52	7	3.22	2	3.28	7	3.75	5	3.00	5	3.60	4	3.86	4
10	3a	3.76	2	3.22	2	3.43	6	4.25	2	3.00	5	3.70	3	4.14	3
11	3b	3.40	12	3.22	2	3.43	6	3.67	6	3.00	5	3.20	8	3.43	6
12	3c	3.36	13	3.22	2	2.86	8	3.16	12	3.00	5	3.00	10	4.29	2
13	4a	3.46	9	3.22	2	3.57	5	3.33	10	3.00	5	3.60	4	3.14	8
14	4b	3.60	5	3.22	2	3.57	5	3.58	7	3.20	4	3.30	7	4.43	1
15	4c	3.60	5	3.22	2	3.57	5	3.83	4	3.80	1	4.90	1	3.28	7
16	4d	3.44	10	3.22	2	3.57	5	3.42	9	3.00	5	3.40	6	3.28	7
17	4e	2.80	16	3.22	2	2.14	9	3.16	12	2.60	7	2.60	11	3.14	8
18	4f	2.78	17	3.22	2	2.86	7	2.92	13	2.60	7	2.20	12	3.00	9
19	5a	3.50	8	3.22	2	3.57	5	3.53	8	3.60	2	3.10	9	3.57	5
20	5b	3.50	8	3.22	2	3.43	6	3.33	10	3.40	3	3.10	9	4.29	2
Respondents		50		09		07		12		05		10		07	
Chi-Squared test P-value		0.000		0.000		0.000		0.000		0.258		0.008		0.000	

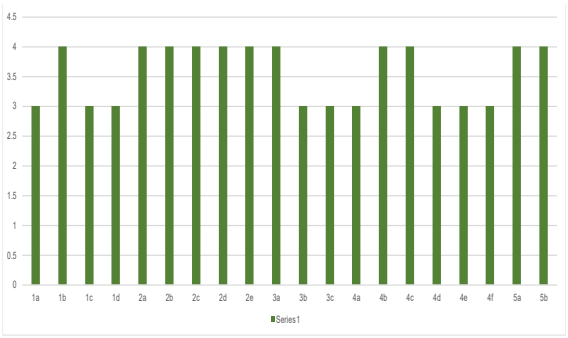

Fig 2: Graph of mean values of different critical barriers.

The critical barriers to the adoption of GBTs have been categorized in five groups including as showed in table 2, governmental, financial, awareness, innovational and market which make it clear that awareness and educational issues are the most critical barriers followed by financial and market issues.

The major critical barrier as showed in figure 2 for GBT adoption in Pakistan is due to lack of awareness and lack of promotion about the green building programs is the major barrier for its adoption. Moreover, high initial cost of GBTs and lack of green building codes is also one of the major barriers for the adoption of GBT in construction industry of Pakistan.

In Fig.2, the bar chart of critical barriers is presented in which each bar shows the level of significance of each factor according to its mean value.

Implementation Strategies

Table 3: Mean scores of categories of implementation strategies

No	Factors	All experts		Academia		Consultants		Contractors		Clients		Designers		Administrative Authority	
		Mean	Rank	Mean	Rank	Mean	Rank	Mean	Rank	Mean	Rank	Mean	Rank	Mean	Rank
1	1a	3.92	1	3.33	6	4.00	4	3.92	1	4.00	1	3.80	4	4.14	4
2	1b	3.64	7	3.33	6	4.14	3	3.83	2	3.60	3	3.40	7	4.43	1
3	1c	3.74	4	3.33	6	4.00	4	3.58	4	3.60	3	4.10	2	4.26	3
4	1d	3.80	2	4.00	2	4.29	2	3.92	1	3.60	3	3.80	4	4.14	4
5	1e	3.64	7	3.67	4	3.29	7	3.92	1	3.60	3	3.70	5	3.57	7
6	1f	3.72	5	4.00	2	3.43	6	3.50	5	3.60	3	3.20	9	3.57	7
7	1g	3.66	6	3.78	3	3.71	5	3.58	4	3.60	3	3.30	8	3.57	7
8	2a	3.54	9	3.78	3	3.00	8	3.83	2	3.20	4	3.30	8	4.43	1
9	2b	3.38	12	3.22	7	3.00	8	3.50	5	2.60	7	2.80	11	4.43	1
10	2c	3.54	9	3.00	8	3.00	8	3.83	2	2.80	6	3.50	6	4.28	2
11	2d	3.72	5	3.33	6	3.43	6	3.92	1	3.20	4	4.00	3	3.86	6
12	3a	3.78	3	3.78	3	4.00	4	3.92	1	3.20	4	4.30	1	3.86	6
13	3b	3.40	11	3.78	3	4.00	4	3.75	3	3.00	5	3.70	5	3.29	8
14	3c	3.58	8	3.56	5	4.43	1	3.92	1	2.60	7	3.50	6	4.00	5
15	3d	3.74	4	4.11	1	4.00	4	3.75	3	2.80	6	3.10	10	4.43	1
16	4a	3.48	10	3.67	4	3.43	6	3.50	5	3.80	2	3.60	6	3.57	7
Respondents		50		09		07		12		05		10		07	
Chi-Squared Test P-value		0.000		0.000		0.000		0.000		0.003		0.000		0.000	

The implementation strategies to the adoption of GBTs have been categorized in four groups including, governmental, financial, awareness, and recognitions which make it clear that creating awareness and educational training are the most effective strategies followed by financial incentives and regulations implementations

- It is concluded that Green Building Technology can be effectively adopted in Pakistan construction industry by creations of public awareness towards green initiatives, promotion of successful green building practices and applying mandatory GB policies, codes and regulations.

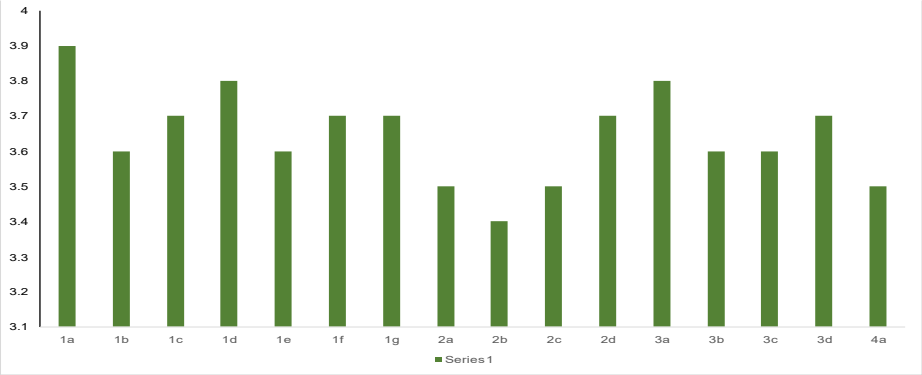

Fig 3: Graph of mean values of different implementation strategies

In Fig.3, the bar chart of implementation strategies is presented in which each bar shows the level of significance of each factor according to its mean value.

Results validation using IRA Analysis

For the analysis of inter-rater agreement, the technique of average deviation (awg) is required. This technique is advantageous because, it minimizes the reliance on the scale of the data. The value of IRA ranging between 0 and 0.3 is an indication of no or lack of agreement, however, if the value ranges from 0.31 to 0.5, the agreement can be deemed as weak. While the values between 0.51 and 0.7 shows moderate agreement and values above 0.7 illustrates strong agreement.

Table 4.: Critical Barriers Agreement Level

Factors	awg	Agreement Level
1a	0.987	Strong
1b	0.618	Moderate
1c	0.602	Moderate
1d	0.520	Moderate
2a	0.741	Strong
2b	0.454	Weak
2c	0.249	No
2d	0.864	Strong
2e	0.823	Strong
3a	0.536	Moderate
3b	0.930	Strong
3c	0.848	Strong
4a	0.946	Strong
4b	0.659	Moderate
4c	0.659	Moderate
4d	0.987	Strong
4e	0.299	No
4f	0.340	Weak
5a	0.864	Strong
5b	0.864	Strong

All the values of agreement levels for critical barriers is mentioned in the table 4, the agreement level is calculated to identify the importance of each factor mentioned in the context, showing that the factors 1a,3b, 4a and 4d having the highest value of agreement level followed by 2d, 2e, 3c, 5a and 5b.

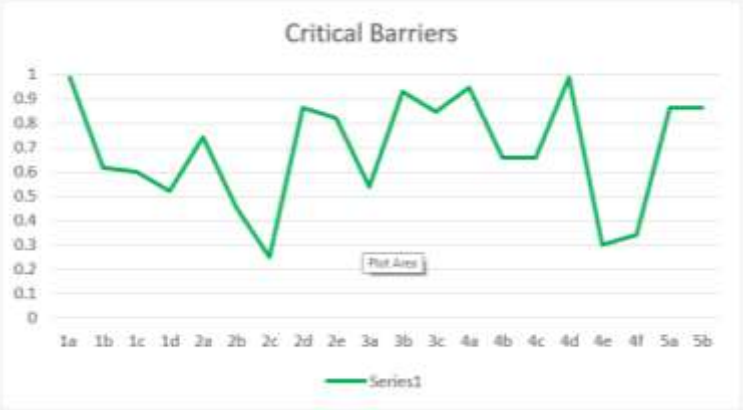

Figure 4: Chart of agreement level of critical barriers.

In Fig.4, the line graph of critical barriers is presented which shows the level of agreement of each factor according to its calculated value. Higher the value of agreement level, more significant will be the factor.

Table 5: Implementation Strategies Agreement Level

Factors	awg	Agreement level
1a	0.807	Strong
1b	0.879	Strong
1c	0.431	Weak
1d	0.901	Strong
1e	0.879	Strong
1f	0.569	Moderate
1g	0.982	Strong
2a	0.719	Moderate
2b	0.910	Strong
2c	0.719	Moderate
2d	0.569	Moderate
3a	0.856	Strong
3b	0.879	Strong
3c	0.466	Weak
3d	0.431	Weak
4a	0.722	Moderate

All the values of agreement levels for implementation strategies is mentioned in the table 5, showing that the factors 1b, 1d, 1e, 1g, 2b, 3a, and 3b having the highest value of agreement level followed by 1a, 2a, 2c, and 4a.
The agreement levels tells the importance and significance of each factor according to its value.

Figure 5: Graph of agreement level of implementation strategies

In Fig.5, the line graph of implementation strategies is given which shows the agreement level of each factor of the portion of implementation strategies according to its calculated value. Higher the agreement level, more significant will be the strategies for the adoption of GBT in Pakistan industry.

CONCLUSIONS AND RECOMMENDATIONS

It has been concluded that the concept of green building refers to the process and developing of structure in a way it ensures the efficient use of resources and mitigates the negative environmental impact that is linked with the construction of the building.

- It is evident that GBTs has now been considered as the most significant way to progress energy efficiencies and the prominent way to realize green building as it plays a central role in achieving sustainability in the construction industry.
- Lack of awareness, greater costs, a lack of standards and regulations, and a lack of technical understanding and proficiency have been listed as some of the major problems with the adoption of GBT.
- The critical barriers to the adoption of GBTs have been categorized in five groups including, governmental, financial, awareness, innovational and market which

make it clear that awareness and educational issues are the most critical barriers followed by financial and market issues.

In order to optimize on GBT and overcome the barriers related to its adoption a set of varied considerations could be made.

- Increasing the awareness along with knowledge and skills regarding the technologies could be considered as one of it.
- The governments should lead to play a significant role in GBT and its implementations, firms must take the initiative to ask for assistance from their respective states through communicating and informing regarding the associated benefits to it.
- The costs associated with GBT also lead to act as a barrier, high research and development may provide the opportunity to bring costs down significantly along with motivating firms to take use of the new technology and proceeding towards attainment of the desired objectives.

REFERENCES

1.AKSHEY B, SWATI B, & DISHA B. (2018). GREEN BUILDINGS - A STEP TOWARDS ENVIRONMENTAL PROTECTION. *I*, *VOL 3*, *NO1*, 1–4. HTTP://WWW.IMEDPUB.COM/RESOURCES-RECYCLING-AND-WASTE-MANAGEMENT/

2. ARCHITECTURE WEEK. (2001). BARRIERS TO BUILDING GREEN. *ARCHITECTURE WEEK*. HTTP://WWW.ARCHITECTUREWEEK.COM/2001/0822/INDEX.HTML

3. ARDITI, D., & PATTANAKITCHAMROON, T. (2006). SELECTING A DELAY ANALYSIS METHOD IN RESOLVING CONSTRUCTION CLAIMS. *INTERNATIONAL JOURNAL OF PROJECT MANAGEMENT*, *24*(2), 145–155. HTTPS://DOI.ORG/10.1016/J.IJPROMAN.2005.08.005

4. CHAN, A. P. C., DARKO, A., AMEYAW, E. E., & OWUSU-MANU, D.-G. (2017). BARRIERS AFFECTING THE ADOPTION OF GREEN BUILDING TECHNOLOGIES. *JOURNAL OF MANAGEMENT IN ENGINEERING*, *33*(3), 04016057. HTTPS://DOI.ORG/10.1061/(ASCE)ME.1943-5479.0000507

5. DARKO, A., CHAN, A. P. C., AMEYAW, E. E., HE, B. J., & OLANIPEKUN, A. O. (2017). EXAMINING ISSUES INFLUENCING GREEN BUILDING TECHNOLOGIES ADOPTION: THE UNITED STATES GREEN

BUILDING EXPERTS' PERSPECTIVES. *ENERGY AND BUILDINGS*, *144*, 320–332. HTTPS://DOI.ORG/10.1016/J.ENBUILD.2017.03.060

6. DJOKOTO, S. D., DADZIE, J., & OHEMENG-ABABIO, E. (2014). BARRIERS TO SUSTAINABLE CONSTRUCTION IN THE GHANAIAN CONSTRUCTION INDUSTRY: CONSULTANTS PERSPECTIVES. *JOURNAL OF SUSTAINABLE DEVELOPMENT*, *7*(1), 134–143. HTTPS://DOI.ORG/10.5539/JSD.V7N1P134

7. HWANG, B. G., & NG, W. J. (2013). PROJECT MANAGEMENT KNOWLEDGE AND SKILLS FOR GREEN CONSTRUCTION: OVERCOMING CHALLENGES. *INTERNATIONAL JOURNAL OF PROJECT MANAGEMENT*, *31*(2), 272–284. HTTPS://DOI.ORG/10.1016/J.IJPROMAN.2012.05.004

8. HWANG, B. G., & TAN, J. S. (2012). GREEN BUILDING PROJECT MANAGEMENT: OBSTACLES AND SOLUTIONS FOR SUSTAINABLE DEVELOPMENT. *SUSTAINABLE DEVELOPMENT*, *20*(5), 335–349. HTTPS://DOI.ORG/10.1002/SD.492

9. JANSSON, J., NILSSON, J., MODIG, F., & HED VALL, G. (2017). COMMITMENT TO SUSTAINABILITY IN SMALL AND MEDIUM-SIZED ENTERPRISES: THE INFLUENCE OF STRATEGIC ORIENTATIONS AND

MANAGEMENT VALUES. *BUSINESS STRATEGY AND THE ENVIRONMENT*, *26*(1), 69–83. HTTPS://DOI.ORG/10.1002/BSE.1901

10. JILONG, W. (2017). DISCUSSION ON APPLICATION OF BUILDING ENERGY EFFICIENCY AND GREEN BUILDING TECHNOLOGY. *JOURNAL OF WORLD ARCHITECTURE*, *1*(3). HTTPS://DOI.ORG/10.26689/JWA.V1I3.180

11. KAUSKALE, L., GEIPELE, I., ZELTINS, N., & LECIS, I. (2017). ENVIRONMENTAL AND ENERGY ASPECTS OF CONSTRUCTION INDUSTRY AND GREEN BUILDINGS. *LATVIAN JOURNAL OF PHYSICS AND TECHNICAL SCIENCES*, *54*(2), 24–33. HTTPS://DOI.ORG/10.1515/LPTS-2017-0010

12. KIBERT, C. J. (2008). *CONSTRUCTION SUSTAINABLE : GREEN BUILDING DESIGN AND DELIVERY*. HTTP://WWW.RESEARCHANDMARKETS.COM/REPORTS/3615691/SUSTAINABLE-CONSTRUCTION-GREEN-BUILDING-DESIGN.PDF

KIBERT, C. J. (2016). SUSTENANCE: GREEN BUILDING DESIGN AND DELIVERY,. *3RD ED.*, *WILEY*, *HOBOKEN*, *NJ*.

13. LI, Y., YANG, L., HE, B., & ZHAO, D. (2014). GREEN BUILDING IN CHINA: NEEDS GREAT PROMOTION. *SUSTAINABLE CITIES AND SOCIETY*, *11*, 1–6. HTTPS://DOI.ORG/10.1016/J.SCS.2013.10.002

14. LITERATURE, R. E. (2008). *REVIEW REVIEWED WORK (S): THE GREEN BUILDING REVOLUTION BY JERRY YUDELSON REVIEW BY : MARCUS T . ALLEN SOURCE : JOURNAL OF REAL ESTATE LITERATURE , 2008 , VOL . 16 , NO . 2 (2008), PP . 253-255 PUBLISHED BY : { AMREALESTATESOC } STABLE URL : HTTPS://W*. *16*(2), 253–255.

15. MERYMAN, H., & SILMAN, R. (2004). SUSTAINABLE ENGINEERING - USING SPECIFICATIONS TO MAKE IT HAPPEN. *STRUCTURAL ENGINEERING INTERNATIONAL: JOURNAL OF THE INTERNATIONAL*

Association for Bridge and Structural Engineering (IABSE), *14*(3), 216–219. https://doi.org/10.2749/101686604777963856

16. O.A., O., P.B., X., & M., S. (2016). Green building incentives: A review. *Renewable and Sustainable Energy Reviews*, *59*, 1611–1621.

17. Papajohn, D., Brinker, C., & El Asmar, M. (2017). MARS: Metaframework for Assessing Ratings of Sustainability for Buildings and Infrastructure. *Journal of Management in Engineering*, *33*(1). https://doi.org/10.1061/(asce)me.1943-5479.0000478

18. Potbhare, V., Syal, M., & Korkmaz, S. (2009). Adoption of green building guidelines in developing countries based on U.S. and India experiences. *Journal of Green Building*, *4*(2), 158–174. https://doi.org/10.3992/jgb.4.2.158

19. Qian, Q. K., & Chan, E. H. W. (2010). Government measures needed to promote building energy efficiency (BEE) in China. *Facilities*, *28*(11), 564–589. https://doi.org/10.1108/02632771011066602

20. Rasolofoson, R. A., Ferraro, P. J., Jenkins, C. N., & Jones, J. P. G. (2015). Effectiveness of Community Forest Management at reducing deforestation in Madagascar. *Biological Conservation*, *184*, 271–277. https://doi.org/10.1016/j.biocon.2015.01.027

21. Rodriguez-Nikl, T., Kelley, J., Xiao, Q., Hammer, K., & Tilt, B. (2015). Structural engineers and sustainability: An opinion survey. *Journal of Professional Issues in*

ENGINEERING EDUCATION AND PRACTICE, *141*(3), 1–9. HTTPS://DOI.ORG/10.1061/(ASCE)EI.1943-5541.0000228

22. SAMER, M. (2013). TOWARDS THE IMPLEMENTATION OF THE GREEN BUILDING CONCEPT IN AGRICULTURAL BUILDINGS: A LITERATURE REVIEW. *AGRICULTURAL ENGINEERING INTERNATIONAL: CIGR JOURNAL*, *15*(2), 25–46.

23. SHAHSAVARI, A., & AKBARI, M. (2018). POTENTIAL OF SOLAR ENERGY IN DEVELOPING COUNTRIES FOR REDUCING ENERGY-RELATED EMISSIONS. *RENEWABLE AND SUSTAINABLE ENERGY REVIEWS*, *90*, 275–291. HTTPS://DOI.ORG/10.1016/J.RSER.2018.03.065

24. SHI, Q., ZUO, J., HUANG, R., HUANG, J., & PULLEN, S. (2013). IDENTIFYING THE CRITICAL FACTORS FOR GREEN CONSTRUCTION - AN EMPIRICAL STUDY IN CHINA. *HABITAT INTERNATIONAL*, *40*, 1–8. HTTPS://DOI.ORG/10.1016/J.HABITATINT.2013.01.003

25. USGBC. (2003). BUILDING MOMENTUM: NATIONAL TRENDS AND PROSPECTS FOR HIGH-PERFORMANCE GREEN BUILDINGS. *U.S. GREEN BUILDING COUNCIL*, *NOVEMBER*, 24.

26. VARONE, F., & AEBISCHER, B. (2001). ENERGY EFFICIENCY: THE CHALLENGES OF POLICY DESIGN. *ENERGY POLICY*, *29*(8), 615–629. HTTPS://DOI.ORG/10.1016/S0301-4215(00)00156-7

27. WILLIAMS, K., & DAIR, C. (2007). WHAT IS STOPPING SUSTAINABLE BUILDING IN ENGLAND? BARRIERS EXPERIENCED BY STAKEHOLDERS IN DELIVERING SUSTAINABLE DEVELOPMENTS. *SUSTAINABLE DEVELOPMENT*, *15*(3), 135–147. HTTPS://DOI.ORG/10.1002/SD.308

28. WILSON, J. L. &, & TAGAZA, E. (2004). GREEN BUILDINGS: DRIVERS AND BARRIERS E LESSONS LEARNED FROM FIVE MELBOURNE DEVELOPMENTS. *REPORT PREPARED FOR BUILDING COMMISSION BY UNIVERSITY OF MELBOURNE AND BUSINESS OUTLOOK AND EVALUATION*.

29. YUDELSON, J., & FEDRIZZI, S. R. (2008). *THE GREEN BUILDING REVOLUTION*. *ISLAND PRESS*. HTTPS://BOOKS.GOOGLE.COM/BOOKS?ID=E2CEAQAAIAAJ

APPENDIX

"Critical Barriers"

Please **encircle** according to your point of view, the following barriers or obstacles to the adoption of Green Building Technology in Pakistan Construction Industry.

1: Not Important **2:** Somewhat Important **3:** Important **4:** Very Important **5:** Extremely Important

Management and government issues:

• Government not providing incentives.	1	2	3	4	5
• Lack of green building codes and regulation.	1	2	3	4	5
• Lack of GBTs promotion by government.	1	2	3	4	5
• Lack of authority and efficiency in enforcing GB laws and regulations.	1	2	3	4	5
• Lack of importance attached by leaders.	1	2	3	4	5

Education and awareness issues:

• Lack of professional knowledge and experts in GBTs.	1	2	3	4	5
• Lack of awareness of GBTs and their benefits.	1	2	3	4	5
• Complex and rigid requirements involved in adopting GBTs.	1	2	3	4	5
• Lack of availability of case studies in this area.	1	2	3	4	5

Financial issues:

• High initial cost of GBTs.	1	2	3	4	5
• Lack of financing schemes.	1	2	3	4	5
• Long payback period from adopting GBTs.	1	2	3	4	5

Innovation issues:

• Resistance to change in conventional methods.	1	2	3	4	5
• Lack of technical training in Green building design and constructions.	1	2	3	4	5
• Lack of adequate design methods.	1	2	3	4	5
• Challenges of innovations in design and construction method.	1	2	3	4	5
• Green building materials aesthetically less pleasing.	1	2	3	4	5
• Poor quality of GB design.	1	2	3	4	5

Market and Materials issues:

• Unavailability of Green building materials in the local market.	1	2	3	4	5
• Lack of interest from client and market demand.	1	2	3	4	5

"Implementation Strategies"

Please **encircle** according to your point of view, the following strategies to the adoption of Green Building Technology in Construction Industry of Pakistan.

1: Not Important **2**: Somewhat Important **3**: Important **4**: Very Important

5: Extremely Important

Government, Regulations and Standard:

• Mandatory GB policies, codes and regulations.	1	2	3	4	5
• Green rating and programs	1	2	3	4	5
• Competent and proactive GBTs promotion teams/authorities.	1	2	3	4	5
• Better enforcement of GB policies after they have been developed	1	2	3	4	5

Incentives:

• Government should provide funding for green building development.	1	2	3	4	5
• Low cost loans from government.	1	2	3	4	5
• Financial incentive and further market-based incentives	1	2	3	4	5
• A strengthened GBTs research and development	1	2	3	4	5

Awareness and training:

• Creation of public awareness towards green initiatives through seminars, workshops and discussions.	1	2	3	4	5
• More publicity through media (e.g., print media, internet and televisions programs.	1	2	3	4	5
• Support from executive management.	1	2	3	4	5
• Promotion of successful green building practices as case examples.	1	2	3	4	5
• GBT-related training programs for developers, contractors and policy makers	1	2	3	4	5
• Availability of institutional framework for effective implementation of green building guidelines.	1	2	3	4	5
• Availability of better information on cost and benefits of GBTs.	1	2	3	4	5

Awards and Recognition:

• Acknowledging and rewarding GBTs adopters publicly	1	2	3	4	5

2nd International Conference on Advances in Civil and Environmental Engineering (ICACEE-2023)

University of Engineering & Technology Taxila, Pakistan

Conference date: 22nd and 23rd February, 2023

Acid hydrolysis of kitchen waste for the production of fermentable sugars

Nayab Zahra[1]

[1]Department of environmental engineering, UET Taxila, Nayab.zahra@uettaxila.edu.pk

ABSTRACT

This work was done to produce reducing sugars using kitchen waste. In this work, KW having high carbohydrates content was physically pretreated (dried and crushed) and then hydrolyzed with diluted acid (H_2SO_4) into reducing sugars. To get maximum reducing sugars acid hydrolysis condition were acid dilutions (1%, 3%, 5%, 7%, and 9%), temperature (81, 91, 101, 111, and 121^oC) and reaction time (20, 40, 60, 80, 100, 120 and140 minutes). Conditions were optimized for acid hydrolysis. Optimized conditions were acid concentration (7%), time (2 hrs.) and temperature (121^oC).

KEYWORDS: Kitchen waste, Reducing sugar, Acid hydrolysis

INTRODUCTION

Natural resources are the great blessings of Allah indeed. Excessive uses of natural resources cause depletion of resources as well as destruction of environment. High raise in price of petroleum and global warming issue has increased the interest of many researchers to use low-cost by-products and waste as raw material for the production of bio-fuel. Bio-fuel, produced from organic waste like kitchen waste, is seen as the alternative renewable energy sources that provide an opportunity to decrease import of oil for transportation and industrial plants and to reduce the burden of municipal solid waste too [1].

Kitchen waste (KW) as a biomass has a great potential to produce biofuel (bioethanol) because KW has a composition of carbohydrates, proteins, lipids, fats. Cellulose, carbohydrates, glycogen, proteins, fats, and starch can be easily hydrolyzed to reducing sugars like glucose which can be converted into biofuel after fermentation of these sugars [2, 3]. For the production of biofuel from biomass many pretreatments have been developed. Pretreatment of biomass makes the hydrolysis of carbohydrates (cellulose, starch, and glycogen) and lipids to its sugars. Particle size reduction increases the surface area of biomass for enzymes or chemicals access to cellulose and glycogen during hydrolysis. Selected pretreatment process must avoid the inhibit by-products formation and degradation of carbohydrate; improve the formation of sugar monomers during hydrolysis. Dilute acid hydrolysis is successful for pretreatment of biomass. High reaction rates can be achieved by the dilute sulfuric acid pretreatment and it significantly improves hydrolysis of cellulose and glycogen [4]. Dilute acid hydrolysis is favourable at high temperature [5]. Two kinds of chemical hydrolysis are usually in practice. (1) Hydrolysis at high temperature (greater than 160°C) for (5-10%) solid loadings [6] and (2) Hydrolysis at low temperature (less than 160°C) with (10-40%) solid loadings [7].

So, researchers are searching for environment friendly and economically feasible technologies to produce bio-fuel from food waste. Dilute acid hydrolysis being a mature technology was successfully established for hydrolysis of biomass. The high reaction rates can be achieved by acid hydrolysis (below 4%) because it would not be expensive at all [8].
Many researchers [9-12] performed experimentation in which saccharification and fermentation took place simultaneously in order to reduce the time and investment cost but little attention has been devoted to thermo-chemical pretreatment of KW before fermentation for the production of biofuel.

MATERIALS AND METHODS

Biomass and Pretreatment

The kitchen waste was collected from house (3 No.), restaurants (2 No.) and cafeterias (3 No.) during January to May 2022. All KW was mixed. Metal pieces and paper glass were separated manually, if present, while the other organic raw material was used. Over 50 % of KW was composed of uncooked fruit and vegetable waste. Cooked and uncooked meat composition was 16% and 15% respectively. While remaining organic waste composition was around 18-19%. Kitchen waste was segregated manually in four categories (Table-1). For chemical composition of sample pH was measured pH meter. Total solids, volatile solids, and moisture content was measured using standard method explained elsewhere [13] while cellulose, hemicellulose, lignin, and protein content was measured according to the following method [14]. KW samples were dries in oven at 103±2°C and then grinded to increase the surface area. A sieve of 200-400 micron is used.

Table 1 Classification of sample

Sr.	Samples	Composition of KW
1.	Sample-1	Mix kitchen waste
2.	Sample-2	Vegetable and salad waste
3.	Sample-3	Fruit waste
4.	Sample-4	Other organic matter (tea, coffee, cooked and uncooked meat, egg shells, bread, dairy and bakery products)

Acid Hydrolysis

The acid hydrolysis was performed in autoclave (SACV-801) at 15*lb* pressure for different acid dilutions (1%, 3%, 5%, 7% and 9%), temperature (81, 91, 101, 111 and 121^{o}C) and reaction time (20, 40, 60, 80, 100, 120 and140 minutes) at a solid to liquid ratio of 1:10 (w/w) (based on total solid) in a 500 mL Erlenmeyer flasks with a working volume of 100 ml. Parameters of hydrolysis were optimized to produce maximum reducing sugars. After the process samples were cooled and

filtered. The filtered samples were used to measure the concentration of reducing sugar by using Miller's method [15].

RESULTS AND DISSCUSION

Feedstock composition

KW was composed of the following: pH 4.61, 20.05 % total solids, 18.78% volatile solids, 80.54% moisture content, 21.34 % cellulose, 17.83 hemicellulose, 7.2 % lignin 21.55% protein and 11.98% fat. This composition of KW is considered as suitable for the production of biofuel. This composition of KW was very similar to other studies that have been reported [16].

Acid hydrolysis

Dilute acid hydrolysis of KW was performed to convert polysaccharides into reducing sugars. Optimization of various parameters for hydrolysis was done to achieve maximum concentration of reducing sugar. For acid hydrolysis only sample-1 (Table-1) was used in optimization of parameters as this sample contains all types of KW and then other sample will be hydrolyzed on these optimized conditions.

Acid Concentration

Five different concentrations of acid i.e., 1%, 3%, 5%, 7% and 9% were used at 121℃ for 2 hours. The concentration of produced reducing sugars was calculated and plotted against concentration of acid (Figure-1). The plot shows that maximum amount of reducing sugars i.e., 1000mg/100g of KW was achieved at 7% acid concentration. After 7% it starts decreasing that shows high concentration of acid cannot convert KW efficiently into reducing sugar.

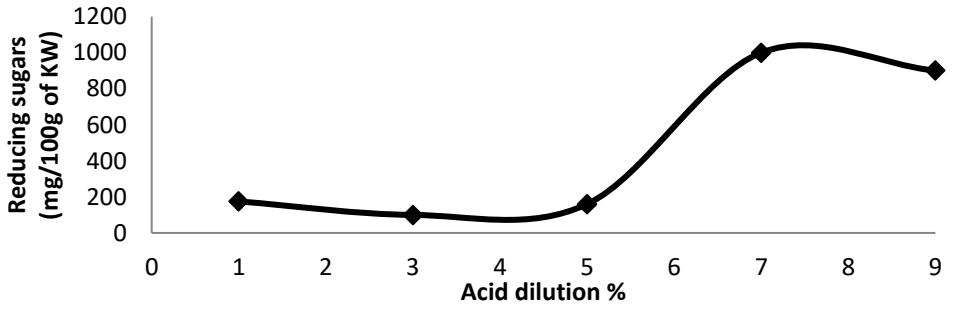

Figure 1 Effect of acid concentration on the production of Reducing Sugars.

Time of Reaction

The sample-1 was hydrolyzed at different times i.e., 20, 40, 60, 80, 100, 120 and 140 minutes at 121℃ and with 7% acid concentration. Figure-3 shows that amount of reducing sugars was increasing gradually as time for acid hydrolysis increasing but after 120 minutes it starts decreasing. As time passes, reducing sugar starts converting into other products that ultimately reduce the overall yield. Therefore at 120 minutes the maximum amount of reducing sugars i.e., 1000mg/100g of KW was achieved.

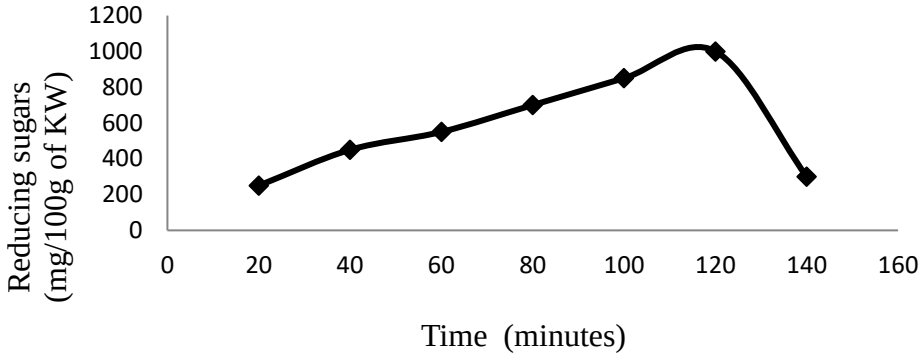

Figure 2 Effect of Reaction Time on the production of Reducing Sugars

Temperature for Hydrolysis

Five different temperatures i.e., 81, 91, 101, 111 and 121℃ were selected to check the effect of temperature on the production of reducing sugars. Figure-3 shows that amount of reducing sugars was increasing gradually as temperature increasing and at 121℃ maximum amounts of reducing sugars i.e., 1000mg/100g of KW was achieved.

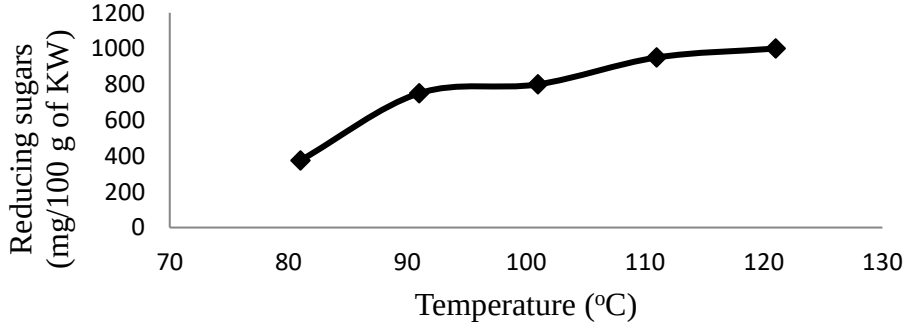

Figure 3 Effect of temperature on the production of Reducing Sugars

Production of Reducing Sugars at Optimum Conditions

After optimizing the conditions i.e., acid concentration, time of reaction and temperature, all four samples were subject for hydrolysis at 7% acid concentration, 121℃ for 2 hours. Figure 4 clearly shows that at optimized condition maximum concentration of reducing sugar was achieved using KW while other samples produced less amount of reducing sugars. The main reason is that KW has all type of waste that gives maximum yield. The samples were collected after hydrolysis, prepared for GC-MS and their concentrations are plotted for comparison (Figure-4).

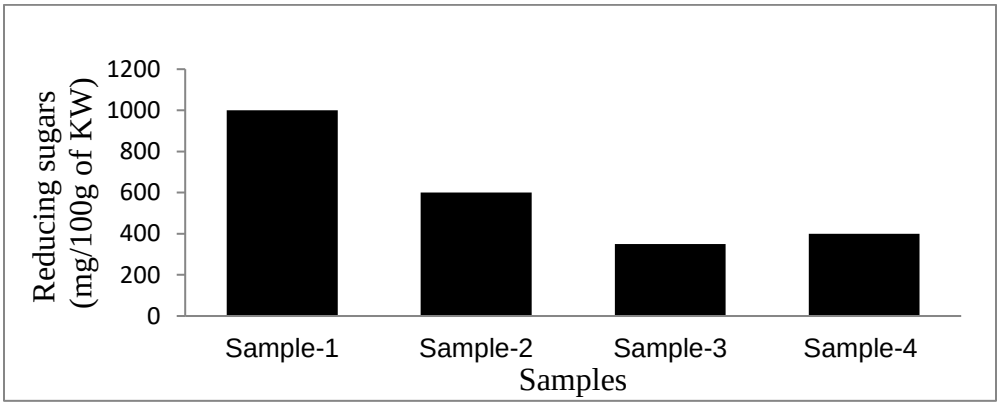

Figure 4 Reducing sugars in samples at optimized conditions.

The Figure-4 shows that production of reducing sugars from sample-1, sample-2, sample-3 and sample-4 was 1000mg/100g, 600mg/100g, 350mg/100g and 400mg/100g respectively. Max amount of reducing sugars was produced by sample-1 because it contains all types of waste like pealing and parts of salad, vegetables and fruits, cooked and uncooked bread, rice, wheat, coffee, tea, eggs shell, dairy beaker products so it is best raw material to produce maximum bio-fuel as compared to other types of waste composition [16, 17].

CONCLUSION

This study shows the potential of KW as substrate to produce fermentable sugars. Moreover, these fermentable sugars can be converted into biofuel after fermentation process. To get the maximum yield of fermentable sugars (reducing sugars) conditions for acid hydrolysis were optimized. However, the maximum yield i.e., 1000mg of reducing sugars/100g of KW was achieved at 7 % acid concentration for 2 hours at 121ºC.

ACKNOWLEDGEMENTS

The support of UET Taxila is highly appreciated.

REFERENCES

1. Goldemberg, J., *Ethanol for a sustainable energy future*. science, 2007. **315**(5813): p. 808-810.
2. Ebrahimian, F., K. Karimi, and R. Kumar, *Sustainable biofuels and bioplastic production from the organic fraction of municipal solid waste.* Waste Management, 2020. **116**: p. 40-48.
3. Mahmoodi, P., K. Karimi, and M.J. Taherzadeh, *Efficient conversion of municipal solid waste to biofuel by simultaneous dilute-acid hydrolysis of starch and pretreatment of lignocelluloses.* Energy conversion and management, 2018. **166**: p. 569-578.
4. Malakar, B., D. Das, and K. Mohanty, *Optimization of glucose yield from potato and sweet lime peel waste through different pre-treatment techniques along with enzyme assisted hydrolysis towards liquid biofuel.* Renewable Energy, 2020. **145**: p. 2723-2732.
5. Rojas-Chamorro, J.A., et al., *Brewer's spent grain as a source of renewable fuel through optimized dilute acid pretreatment.* Renewable Energy, 2020. **148**: p. 81-90.
6. Ramaraj, R. and Y. Unpaprom, *Optimization of pretreatment condition for ethanol production from Cyperus difformis by response surface methodology.* 3 Biotech, 2019. **9**(6): p. 1-9.
7. Zhang, W., et al., *Acetyl-assisted autohydrolysis of sugarcane bagasse for the production of xylo-oligosaccharides without additional chemicals.* Bioresource technology, 2018. **265**: p. 387-393.
8. Shahbazi, A. and B. Zhang, *Dilute and concentrated acid hydrolysis of lignocellulosic biomass.* Bioalcohol production, 2010: p. 143-158.
9. Krishnan, C., et al., *Alkali-based AFEX pretreatment for the conversion of sugarcane bagasse and cane leaf residues to ethanol.* Biotechnol Bioeng, 2010. **107**(3): p. 441-450.
10. Kádár, Z., Z. Szengyel, and K. Réczey, *Simultaneous saccharification and fermentation (SSF) of industrial wastes for the production of ethanol.* Industrial Crops and Products, 2004. **20**(1): p. 103-110.
11. Kim, S. and B.E. Dale, *Global potential bioethanol production from wasted crops and crop residues.* Biomass and Bioenergy, 2004. **26**(4): p. 361-375.
12. Philippidis, G.P., T.K. Smith, and C.E. Wyman, *Study of the enzymatic hydrolysis of cellulose for production of fuel ethanol by the simultaneous saccharification and fermentation process.* Biotechnol Bioeng, 1993. **41**(9): p. 846-853.
13. APHA, A.P.H.A., *Standard Methods for the Examination of Water and Wastewater*. (1992), APHA: Washington, DC, USA.
14. Yang, H., et al., *In-depth investigation of biomass pyrolysis based on three major components: hemicellulose, cellulose and lignin.* Energy & Fuels, 2006. **20**(1): p. 388-393.

15. Miller, G.L., *Use of dinitrosalicylic acid reagent for determination of reducing sugar.* Analytical chemistry, 1959. **31**(3): p. 426-428.
16. Dhiman, S. and G. Mukherjee, *Present scenario and future scope of food waste to biofuel production.* Journal of Food Process Engineering, 2021. **44**(2): p. e13594.
17. Barik, S. and K.K. Paul, *Potential reuse of kitchen food waste.* Journal of environmental chemical engineering, 2017. **5**(1): p. 196-204.

2nd International Conference on Advances in Civil and Environmental Engineering (ICACEE-2023)

University of Engineering & Technology Taxila, Pakistan

Conference date: 22nd and 23rd February, 2023

Evaluation of Water Quality Suitability for Drinking purpose in Pakistan: A Case Study of Taxila City; (II) Bacteriological and Heavy Metal Analysis

Nayab Zahra[1]

[1]Department of environmental engineering, University of engineering and technology, Taxila
Nayab.zahra@uettaxila.edu.pk

ABSTRACT

This research aims to investigate and evaluate the quality of water in Taxila city. Water samples were collected from twenty sampling sites. Two bacteriological parameters (total coliform and fecal coliform) and heavy metals (lead, nickel, chromium, and zinc) were investigated and compared with standards. Results indicate that at some sampling sites, bacteriological parameters such as coliform and fecal coliform were found in the water sample, indicating that to kill coliform and fecal coliform, chlorination of drinking water is required before consumption. Moreover, some heavy metals were also found in water and their concentrations were very high in the water as compared to the guideline values of PEQSDW. Heavy metal contamination may be due to the disposal of untreated industrial wastewater in the sewage system, old pipes, and pipe material used in sanitation.

KEYWORDS: Coliform, Fecal coliform Heavy metals,

INTRODUCTION

In Pakistan, about three million people are affected by water-borne diseases out of which 0.2 million die every year due to the inaccessibility of safe drinking water. There are multiple reasons for this effect which mainly include poor water quality management, lack of implementation and rules, extravagant use of available freshwater. Drinking water quality may become compromised due to a range of processes in between leaving a treatment plant and arriving at the consumer end [1]. In drinking water quality assessment, priority is known to be important to health and portability and known to be generally present in enough quantity to pose health threats [2]. A plethora of researchers reported severe health effects through heavy metals found in drinking water [3-8]. There are various impacts of heavy metals on health, but only significant ones are discussed. Lead may cause reproductive toxicity, carcinogenicity, neurotoxicity, and developmental effects if its intakes are excessive [9]. Similarly, if chromium is consumed continuously it may cause kidney problems and lung cancers [10]. Intake of cadmium can cause hypertension, renal and bone diseases [11]. Excessive intake of calcium may cause the risk of colorectal cancer, osteoporosis, hypertension and stroke, nephrolithiasis (kidney stones), insulin resistance coronary artery disease, and obesity [12]. Nickel can cause derma toxicity and hair loss if it is present in high

concentrations. And even it may cause cancer if present with other heavy metals like copper, zinc, cobalt, and iron [11].
In Pakistan, people more facing many health issues due to poor quality of water. To resolve health issues of society water quality should be monitored regularly in each area. The main purpose of this work is to evaluate the quality of the water by analyzing bacteriological parameters along with notable heavy metals.

EXPERIMENTAL METHODS

Study Area

The Taxila city was chosen as a test case to achieve the objective of this study. The study area lies between latitude 33.74° of North and longitude 72.83° of East. Most of the inhabitants of the study area depend on filtration plants and tube wells for drinking purposes. Localities selected for this study were UET Taxila, HIT gate 5, HMC, Taxila Adda, Aslam market Wah cant and Green Garden as shown in figure 1. Total 60 samples were tested and locations of samples are shown in Table 1. Samples from each location were collected from house connections, tube wells, and filtration plants. Government installed filtration plants for public to provide safe drinking water. WHO Guidelines, 2008 were followed for the collection, transportation, and preservation of all samples. Sampling was done carefully for bacteriological water quality parameter analysis, bottles were rinsed with distilled water and then sterilized according to the Standard method at 121 °C for 15 minutes [13].

Figure 5 Location plan of sampling sites in Taxila

Parameters Tested

Biological parameters were analyzed by using procedures written in standard methods for the examination of water and wastewater [13]. Concentrations of four heavy metals (Lead, Nickel, Chromium, and Zinc) were determined by atomic absorption spectroscopy (Pg, AA500).

RESULTS AND DISCUSSION

Total coliform (T.C) and fecal coliform (F.C)

In Pakistan, microbial pollution has been revealed as one of the serious concerns in rural as well as urban areas. The presence of T.C and F.C in water depicts water contamination with human or

animal feces, plants, soil, etc. The mean values of T.C and F.C are shown at different sampling locations in Figure 2. The standard value according to PEQSDW for T.C and F.C is 0 MPN/100 ml [14]. Fig. 2 shows that water at all tube wells and filters was free from T.C but house connections adjacent to tube wells like T1HC-2, T3HC-1, T3HC-2, and T5HC-2 were contaminated by T.C while the others were free from any contamination. Moreover, water at all tube wells and filters was free from F.C but house connections adjacent to tube wells like T3HC-2 and T5HC-2 were contaminated by F.C while the others were free from any contamination. Overall, it was concluded that the abundance of microbial indicator species (T.C and F.C) were generally low or below detection limits at many points under surveillance in the water distribution network. However, the authors recommend adequate water chlorination so that water quality may be maintained till each house connection as well.

Table 2 Description of sampling points

Sampling Points	**Description**	**Sampling Points**	**Description**
T-1	Tubewell installed at HIT	T3HC-1	House connection no. 1 of T-3
F-1	Filtration plant at HIT	T3HC-2	House connection no. 2 of T-3
T1HC-1	House connection no. 1 of T-1	T-4	Tubewell installed at Wah cant
T1HC-2	House connection no. 2 of T-1	F-4	Filtration plant at Wah cant
T-2	Tubewell installed at UET Taxila	T4HC-1	House connection no. 1 of T-4
F-2	Filtration plant at UET Taxila	T4HC-2	House connection no. 2 of T-4
T2HC-1	House connection no. 1 of T-2	T-5	Tube well installed at Green Gardens
T2HC-2	House connection no. 2 of T-2	F-5	Filtration plant at Green Gardens
T-3	Tubewell installed at HMC	T5HC-1	House connection no. 1 of T-5
F-3	Filtration plant at HMC	T5HC-2	House connection no. 2 of T-5

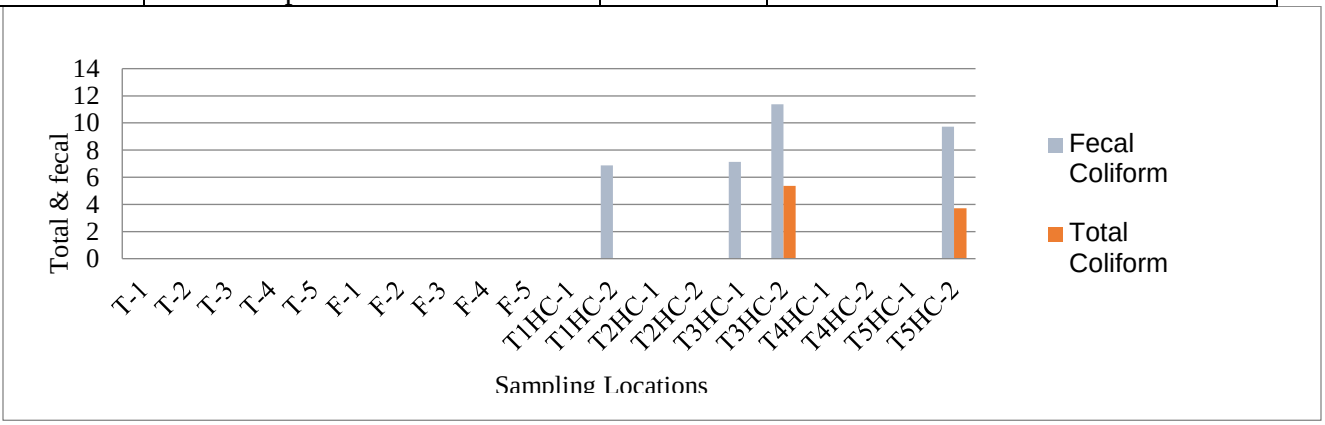

Figure 6 Comparison of total and fecal coliforms at different sampling sites

Heavy metal analysis

Lead: In drinking water, sources of lead can be brass sanitation fitting inside the houses, lead solders, and lead-lined pipes. According to USEPA, pipes and solder joints in household sanitation are a contributor to some amount of lead in tap water [15]. Fig 3 shows that the mean values of lead vary from 0.016 mg/L to 0.423 mg/L. According to the PEQSDW (0.05 mg/L), in 60% of samples mean values of lead were unsatisfactory because these values didn't lie within the prescribed limits of PEQSDW.

Nickel: Nickel is used to manufacture stainless steel and alloys. 1 mg/L concentration of Nickel can be in drinking water due to release from fittings and taps of household sanitation system [16]. Fig 4 clearly shows that values of nickel at all sampling sites were higher than the prescribed limits of PEQSDW (≤0.02 mg/L) except for the only three sampling locations. Mean values of nickel vary from 0.095 mg/L to 0.248 mg/L at T5HC-2 and T1CH-2 respectively. It means that all sources of water except T1 were found unsatisfactory for use of water for drinking purposes.

Chromium: Chromium, if present in drinking water, may cause lung cancer and some kidneys problems [16]. Fig 5 shows that the concentration of chromium varies from 0.845 mg/L to 1.374 mg/L which is higher than the prescribed limits of PEQSDW (≤0.05 mg/L). The highest concentration of chromium was found at T5HC-2 while at F-3, it was the lowest.

Zinc: Figure 6 shows that the concentration of zinc in drinking water varies from 0.926 mg/L to 6.104 mg/L which are under the prescribed limits of PEQSDW (5 mg/L) except T-3 and its adjacent house connections i.e., T3HC-1 and T3HC-2. The highest concentration of zinc was found at T3HC-2 (6.104 mg/L). In this study drinking water is satisfactory concerning zinc at all sources.

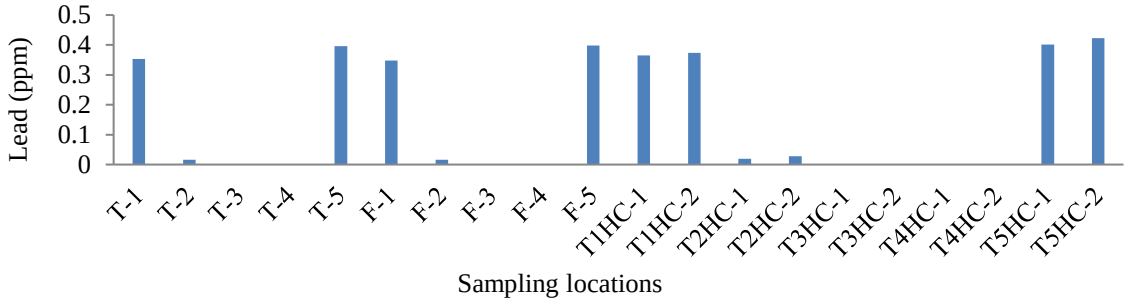

Figure 7 Concentration of lead at different sampling sites

CONCLUSIONS AND RECOMMENDATIONS

Bacteriological parameters at all tube wells and filtration plants were under the prescribed limits of PEQSDW. While at some house connections bacteriological quality of drinking water was unsatisfactory. Heavy metals contamination was also found in most samples which indicates that proper treatment of water is required before consumption as heavy metals cause serious diseases

among humans and this contamination may be due to disposal of untreated industrial wastewater in the sewage system.

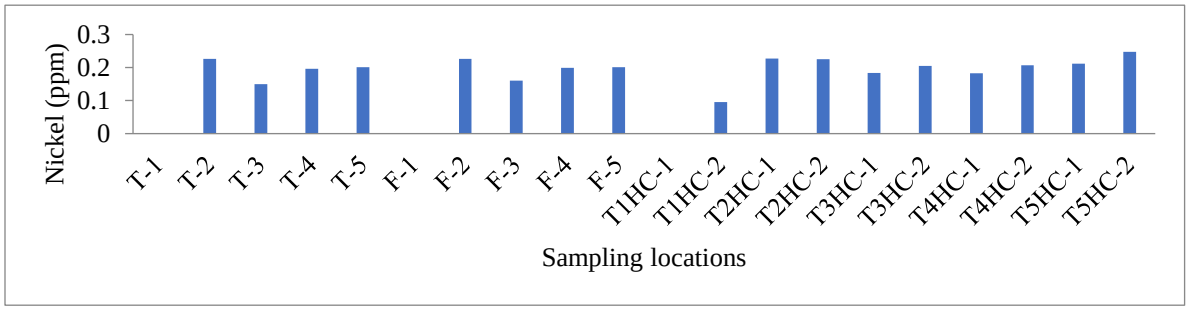

Figure 8 Concentration of nickel at different sampling sites

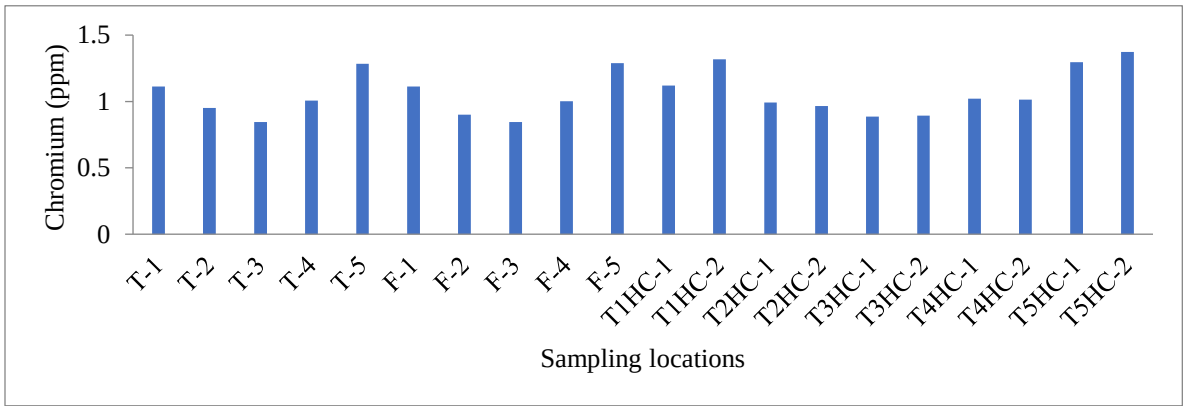

Figure 9 Concentration of Chromium at different sampling sites

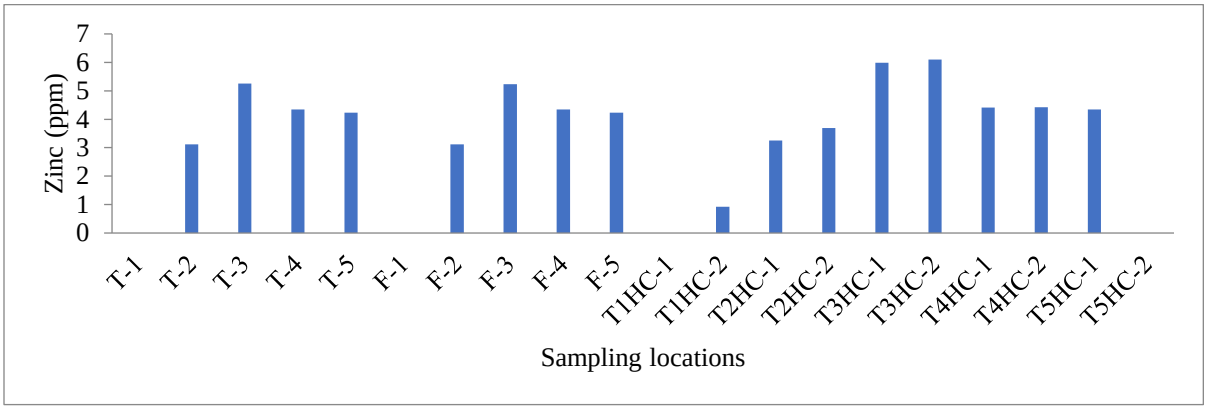

Figure 10 Concentration of zinc at the different sampling sites

ACKNOWLEDGEMENTS

The support of UET Taxila is highly appreciated.

REFERENCES

1. Heibati, M., et al., *Assessment of drinking water quality at the tap using fluorescence spectroscopy.* Water research, 2017. **125**: p. 1-10.
2. Ponsadailakshmi, S., et al., *Evaluation of water quality suitability for drinking using drinking water quality index in Nagapattinam district, Tamil Nadu in Southern India.* Groundwater for Sustainable Development, 2018. **6**: p. 43-49.
3. Szczepanik, M.F., *Filter for removing heavy metals from drinking water*. 1990, Google Patents.
4. Akpor, O. and M. Muchie, *Remediation of heavy metals in drinking water and wastewater treatment systems: Processes and applications.* International Journal of Physical Sciences, 2010. **5**(12): p. 1807-1817.
5. Järup, L., *Hazards of heavy metal contamination.* Br Med Bull, 2003. **68**(1): p. 167-182.
6. Mohan, S.V., P. Nithila, and S.J. Reddy, *Estimation of heavy metals in drinking water and development of heavy metal pollution index.* Journal of Environmental Science & Health Part A, 1996. **31**(2): p. 283-289.
7. Roychowdhury, T., H. Tokunaga, and M. Ando, *Survey of arsenic and other heavy metals in food composites and drinking water and estimation of dietary intake by the villagers from an arsenic-affected area of West Bengal, India.* Science of The Total Environment, 2003. **308**(1): p. 15-35.

8. Tamasi, G. and R. Cini, *Heavy metals in drinking waters from Mount Amiata (Tuscany, Italy). Possible risks from arsenic for public health in the Province of Siena.* Science of The Total Environment, 2004. **327**(1): p. 41-51.
9. Juberg, D.R., *Lead and human health: An update*. 2000: Am Cncl on Science, Health.
10. Organization, W.H., *Guidelines for drinking-water quality: First addendum to volume 1, Recommendations*. Vol. 1. 2006: World Health Organization.
11. Hanaa, M., A. Eweida, and A. Farag. *Heavy metals in drinking water and their environmental impact on human health*. in *International conference on environmental hazards mitigation, Cairo University, Egypt*. 2000.
12. Organization, W.H., *Calcium and magnesium in drinking-water: public health significance*. 2009: World Health Organization.
13. American Public Health Association (APHA), t.A.W.W.A.A.a.t.W.E.F.W., *Standard Methods for the Examination of Water and Wastewater*. 2005, American Public Health Association.
14. Department, E.P., *Punjab Environmental Quality Standards for Drinking Water* 2016, Government of Punjab: Lahore.

2nd International Conference on Advances in Civil and Environmental Engineering (ICACEE-2023)

University of Engineering & Technology Taxila, Pakistan

Conference date: 22nd and 23rd February, 2023

Unravelling the Effect of Chlorination on Degradation of Pharmaceuticals and Elimination from Drinking Water

Asam Shad[1], Shah Bano[2], Asim Yaqub[3], Nimra[4]

[1] Department of Environmental Sciences, COMSATS University Islamabad, Abbottabad Campus, Asamshad@cuiatd.edu.pk

[2] University Institute of Biochemistry and Biotechnology, PMAS Arid Agriculture

[3] Department of Environmental Sciences, COMSATS University Islamabad, Abbottabad Campus

[4] Department of Environmental Sciences, COMSATS University Islamabad, Abbottabad Campus

ABSTRACT

Clean and safe drinking water is essential for maintaining good health and preventing the spread of disease. There are several methods for cleaning drinking water to ensure that it is safe for consumption. Chlorination is one of the widely employed and cost-effective methods for disinfecting drinking water at a centralized level in Pakistan. However, the elimination of organic pollutants, such as pharmaceutical residues, from drinking water remains a challenging task due to factors such as lack of awareness, urbanization, and inadequate sanitation facilities. This research aimed to evaluate the effectiveness of chlorination as a method for the degradation of two selected pharmaceuticals, Aspirin (ASA) and Methylene blue (MB), in drinking water. The study assessed different parameters such as oxidant dose, pH, bicarbonate ion, and chloride ion to evaluate the degradation of ASA and MB in drinking water. The results of the study showed that both ASA and MB degraded as the chlorine dose increased. In the present study the chlorination was found to be highly effective at pH 7. The presence of chloride ions was found to inhibit the degradation of ASA and MB, while the presence of bicarbonate ions accelerated the degradation rate. The findings of this research provide valuable insights into the challenges faced in Pakistan concerning the removal of pharmaceutical residues from drinking water and the application of chlorination as a method for chemical decontamination. The results of this study can be used to inform the development of more efficient and sustainable drinking water treatment strategies in Pakistan. Overall, the study emphasizes the importance of effective and sustainable treatment solutions to address the issue of pharmaceutical residues in drinking water in Pakistan.

KEYWORDS: Chlorination, Pharmaceuticals, Ions, Drinking water

INTRODUCTION

The excretion of pharmaceuticals from human medical care into water effluent necessitates treatment at municipal wastewater treatment facilities [1]. However, studies have demonstrated that conventional water treatment processes are not capable of quantitatively removing pharmaceuticals from the wate [2]. The persistence of pharmaceuticals in secondary effluents and surface waters, which may eventually be used as drinking water sources, poses a potential risk to human health. In response, there is growing concern about these substances and the need to reduce their concentrations in drinking waters by effective treatment techniques, such as chemical oxidation procedures. Using chemical treatments before and after biological treatments may be an effective approach for treating water containing pharmaceuticals, as chemical processes selectively oxidize them into less toxic, readily biodegradable compounds. [3]. Studies have shown that ozonation and advanced oxidation processes, including O_3/H_2O_2, UV/H_2O_2, and Fenton's reagent, exhibit high efficacy in the degradation of pharmaceuticals and X-ray contrast media in both drinking water and wastewater treatment. [4].

Chlorine, both in gas form and as the hypochlorite ion, has also been widely used in water treatments due to its low cost. [5], Chlorine is applied at one or two stages in the water treatment process, serving as a means of peroxidation to initiate primary disinfection at the outset of treatment, and as a post-treatment measure to preserve a disinfectant residual within the distribution system. The hydrolysis of chlorine gas in water results in the following reaction:

$$Cl_2 + H_2O \longrightarrow HOCl + Cl^- + H^+$$

Hypochlorous acid, which is a weak acid, undergoes dissociation in aqueous solutions.:

$$HOCl \longleftrightarrow ClO^- + H^+$$

In Pakistan, the water and sanitation system is inadequate, leading to water contamination caused by fecal matter and pharmaceutical residues. The current study aims to assess the efficacy of chlorination as a method for mitigating the presence of commonly used pharmaceutical products in water.

MATERIAL AND METHODS

The materials used in this research were carefully selected to conduct experiments and analyze the effectiveness of chlorination in degrading the pharmaceuticals in the drinking water.

Chemicals

The research required specific chemicals such as Aspirin (ASA) and Methylene blue (MB), as well as a chlorine solution (8%) which is the oxidant agent used for the chlorination process. The study also used a scavenger, ascorbic acid (1M), to remove the chlorine residuals. Drinking water from a tube well was used as the sample source. To adjust the pH of the water, the researchers used NaOH (0.1) and phosphoric acid (1:15) as the pH adjusters.

Analytical Methods

In addition to the abovementioned chemicals, the study also required a range of glassware such as micropipettes, graduated cylinders, beakers, stirrers, conical flasks, vials, test tubes, a pH meter, and petri dishes. The glassware was used to accurately measure and mix the chemicals, and to conduct experiments and analyze the water samples. For example, micropipettes were used to measure precise volumes of chemicals and graduated cylinders were used to measure larger volumes of water. Beakers and conical flasks were used for mixing and heating the chemicals. A stirrer was used to mix the chemicals and water samples. Vials and test tubes were used to store and test the water samples. A pH meter was used to measure the pH of the water samples and the petri dishes were used to culture the microbial samples. All these materials were essential for conducting experiments and analyzing the effectiveness of chlorination in degrading the pharmaceuticals in the drinking water.

Experimental procedure

In the present study, experiments were conducted utilizing 100 milliliters of water procured from a tube well source. The reaction system consisted of water and two selected

pharmaceutical compounds, ASA and MB. Chlorine solution at a concentration of 1 mM was employed to degrade the selected pharmaceuticals. For ASA, samples were harvested at intervals of 0, 0.5, 1, 2, 3, 5, 7, 8, 9, and 10 minutes. In the case of MB, the degradation time was measured in hours, and samples were harvested at intervals of 0, 1, 3, 6, 9, 12, 15, 18, 21, and 24 hours. The sample volume was 4.5 milliliters, and the reaction was sequenced using ascorbic acid. The samples were analyzed utilizing a spectrophotometer. Furthermore, the effects of pH, oxidant dose, bicarbonate ion, and chloride ions on the degradation process were also investigated. All the experiments were performed in triplicate. The data was analyzed using Microsoft Excel and Origin software for statistical analysis.

RESULTS AND DISCUSSION

Effect of chlorine dose on degradation of ASA

The effect of chlorine dose on the degradation of ASA is shown in **Figure 3.1(a). Figure 3.1(a)** illustrates the results of an experiment in which the degradation of 0.002 mM of ASA was evaluated in the presence of three different doses of chlorine (0.5 mM, 1.0 mM, and 1.5 mM) at a pH of 7.0. The data shows that there was a small difference between the 1.0 mM and 1.5 mM doses, with the highest reaction rate and complete degradation of ASA (100%) observed at the 1.5 mM dose in 20 minutes.

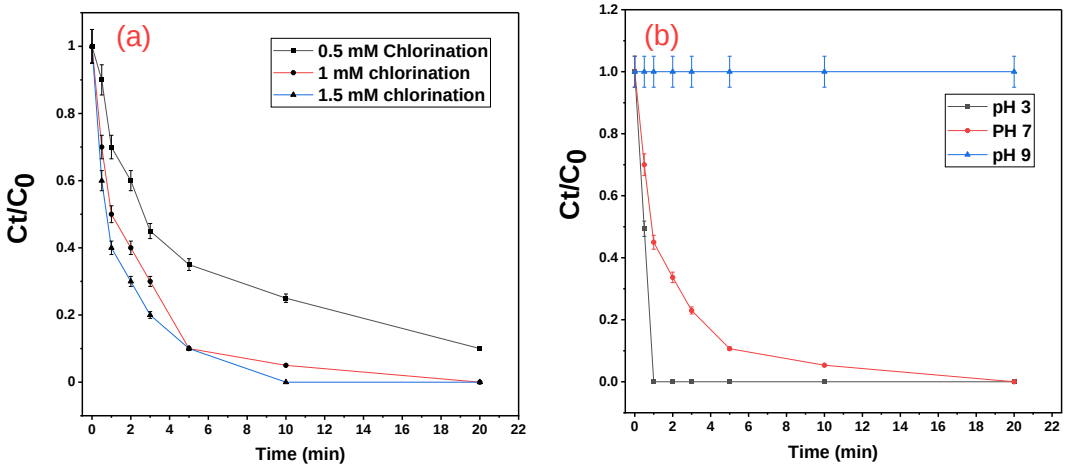

***Figure 3.1**. (a) Effect of chlorination dose on degradation of ASA. Reaction conditions: $[ASA]_0$= 0.002 mM, $[Chlorine\ dose]_0$ = 0.5- 1.5mM, pH=7.0, contact time= 20 min. **(b)** Effect of pH on degradation of ASA. Experimental conditions: [ASA]o = 0.002mM, [Chlorine dose]0 = 1mM, pH range= 3.0, 7.0, 9.0*

Effect of pH on degradation of ASA

The effect of pH on the degradation of ASA is shown in **Figure 3.1(b)**.The results shows that ASA was degraded the fastest at a pH of 3.0 (1 min), followed by pH 7.0 (10 min) and pH 9.0 (20 min). The figure demonstrates that the lowest pH (3.0) resulted in the fastest degradation of ASA. The study evaluated the effect of pH at the minimum, neutral, and maximum levels.

Effect of chlorine dose on MB degradation

The effect of chlorine dose on the degradation of MB is shown in **Figure 3.2(a)**. The results illustrate the effect of different doses of chlorine on the degradation of MB. The data in the figure shows that as the dose of chlorine was increased, the degradation rate of MB also increased. This means that higher doses of chlorine resulted in faster degradation of MB. After considering the results, the study selected a chlorine dose of 1 mM for the reaction mechanism. This decision was made because the study found that 1 mM of chlorine resulted in a suitable balance between the degradation rate and the cost and safety concerns. Overall, this experiment provides insight into the role of chlorine dose in the degradation of MB and highlights the importance of selecting an appropriate chlorine dose for the reaction mechanism.

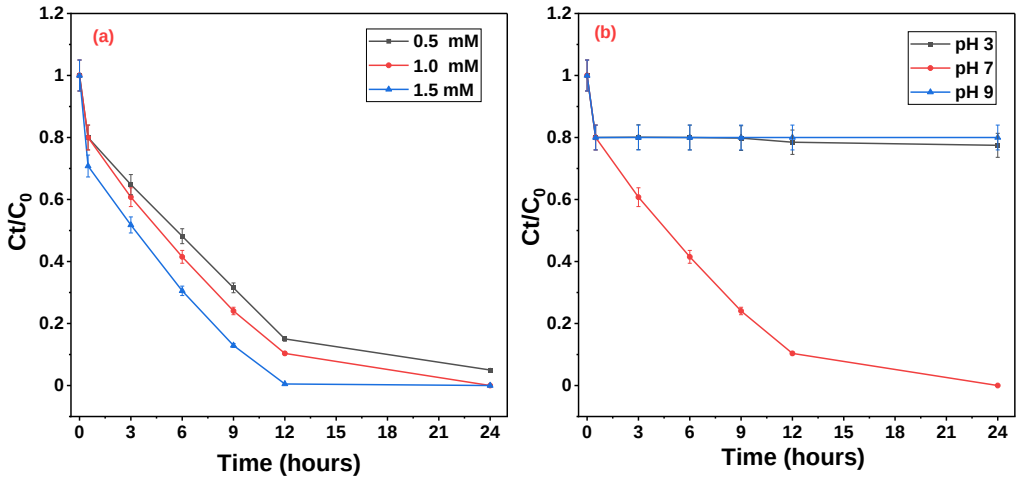

***Figure 3.2(a)** shows the effect of chlorine dose on MB degradation. Experimental conditions: $[MB]_0$ = 0.156 ×10^3mM, $[chlorine\ dose\ ]_0$ = 1.0mM, pH = 7.0. **(b)** Effect of pH on degradation of MB. Experimental conditions: $[MB]_0$ = (0.156x10^3mM), $[chlorine\ dose\ ]_0$ = 1.0mM, pH = (3.0, 7.0, 9.0), contact time 24 hrs*

Effect of pH on degradation of MB

The effect of pH on the degradation of MB is shown in Figure 3.2(b).The data shows that at a pH of 7.0, MB was completely degraded after 24 hours. This degradation rate was faster than at pH 3.0 and 9.0, where only 20% of MB was degraded. This result led to the selection of pH 7.0 for the reaction in this study.

CONCLUSION

In this study, the effectiveness of chlorination as a technique for removing pharmaceuticals from drinking water was evaluated. The results of the study showed that chlorination is an economical and common treatment method that is efficient in the removal of pharmaceuticals. Specifically, it was found that degradation of the selected pharmaceuticals ASA and MB was possible at pH 7.0.

In addition to being an affordable method, the study also highlighted the importance of contact time in achieving complete degradation of pharmaceuticals. ASA was completely degraded within 20 minutes, but it took 24 hours for MB to be 100% degraded. This finding emphasizes the need for a longer contact time for chlorination to effectively remove pharmaceuticals from drinking water.

However, the study also noted that chlorination can lead to the generation of persistent and potentially carcinogenic chlorinated products. This highlights the importance of integrating chlorination with other efficient treatment methods to ensure the safe and effective treatment of drinking water. Overall, the results of this study suggest that chlorination is a viable method for removing pharmaceuticals from drinking water, but it must be used in conjunction with other techniques to achieve optimal results**.**

References

[1] P. Levallois and C. Villanueva Belmonte, *Drinking Water Quality and Human Health*. MDPI, Basel, 2019. doi: 10.3390/BOOKS978-3-03897-727-8.

[2] CDC, “Water Disinfection with Chlorine and Chloramine | Public Water Systems | Drinking Water | Healthy Water | CDC,” *Water Disinfection With Chloirne*, Nov. 2020. https://www.cdc.gov/healthywater/drinking/public/water_disinfection.html (accessed Mar. 22, 2022).

[3] M. Kumari and S. K. Gupta, “Cumulative human health risk analysis of trihalomethanes exposure in drinking water systems,” *J. Environ. Manage.*, vol. 321, p. 115949, Nov. 2022, doi: 10.1016/J.JENVMAN.2022.115949.

[4] W. Li, C. Ding, G. Korshin, J. Li, and H. Cheng, “Effect of chlorination on the characteristics of effluent organic matter and the phototransformation of sulfamethoxazole in secondary wastewater,” *Chemosphere*, vol. 295, May 2022, doi: 10.1016/j.chemosphere.2021.133193.

[5] W. Fu, B. Li, J. Yang, H. Yi, L. Chai, and X. Li, "New insights into the chlorination of sulfonamide: Smiles-type rearrangement, desulfation, and product toxicity," *Chem. Eng. J.*, vol. 331, pp. 785–793, Jan. 2018, doi: 10.1016/j.cej.2017.09.024.

2nd International Conference on Advances in Civil and Environmental Engineering (ICACEE-2023)

University of Engineering & Technology Taxila, Pakistan

Conference date: 22nd and 23rd February, 2023

INFLUENCE OF LIQUID FERTILIZER MADE FROM HUMAN HAIR ON PRODUCTIVITY OF CITRUS PLANT

Sadia Nasreen[1],Emaan Suhail[2],Asma Waseem[3], Samra Israr[4]

[1'2'3'4] Department of Environmental Engineering, University of Engineering and Technology Taxila 47050, Pakistan, sadia.nasreen@uettaxila.edu.pk

ABSTRACT

Human hair is considered as a potential biowaste worldwide, and improper disposal of hair can create multiple environmental problems. Due to unique characteristic features, human waste hair can be efficiently utilized for versatile applications, from agricultural industries to fashion industries. There is a huge business of human hair in many multinational countries and in some rural areas of Pakistan. The continuous demand of such keratinous waste for human need in turn is producing residual waste at an alarming rate that causes environmental degradation. Therefore, our study aims to investigate the possible impacts of waste hair reprocessing activity on environmental health in Pakistan. Due to the presence of total organic carbon and available N-P-K, the soil can sustain the growth and survival of plants; however, the risk of toxic metal accumulation may be persisted. Hence, to enhance the utilization of waste hair in a large scale, a sustainable way to utilize hair waste extremely required that will incorporate environmental and social well-being and provide necessary support towards sustainable development. Chemical fertilizer has been excessively used for high yield of citrus around the world, especially in Pakistan; meanwhile, it deteriorates the citrus orchard soil environment. To resolve the conflict, the use of organic fertilizer provides a promising solution. However, the data about organic fertilizer used in citrus orchard is rarely available. Here, four treatments including CK (no fertilizer), CF (chemical fertilizer),OF(organic fertilizer) OF + CF (chemical fertilizer reduction combined with organic fertilizer; application of N, P2O5, K2O fertilizer and organic fertilizer is 0.564, 0.236, 0.336 and 10 kg/plant), and; application of N, P2O5, K2O fertilizer and bioorganic fertilizer is 0.508, 0.320, 0.310 and 10 kg/plant) were performed in a 'Ponkan' (Citrus reticulata Blanco) orchard to evaluate the effect of organic fertilizer on citrus growth, soil properties etc. when nutrients of fertilizer of each treatment were equal except CK. The data obtained showed that both OF + CF was beneficial to improve soil fertility (soil physicochemical and microbe properties) and citrus growth physiology (growth, nutrient, and photosynthesis), alleviate NO3 -N leaching, and promote yields and growth. Together, organic fertilizer has the potential to substitute partial chemical fertilizer with improvement in soil properties, growth physiology, and yield of citrus.

KEYWORDS: Ponkan; organic fertilizer; soil properties; photosynthesis; growth

INTRODUCTION

As we know that human hair is not considered as such a very important or useful material in our society due to unawareness of the properties which it contains, and which can be useful in various fields and areas [1]. As in almost every metropolitan city and village areas of Pakistan it has been thrown away due to its unusefulness and huge collection which may produce the unhygienic on roads and various streets. This can also produce some allergenic situations in the areas where the various parks and garden areas exist as due to its lower degradation rate it gets decomposed very slowly and remains in the atmosphere for a long time. The cause behind its slower decomposition can be its constituents' elements like carbon, nitrogen, and sulfur etc. On the other hand, human hair contains some useful minerals that if can be recycled can be used in different area for our benefit. Due to these elements some countries like India and China is using these materials to make fertilizers which is an important aspect and material being used in the farms and the fields to protect the crops from various disasters and for better productivity.

In some countries like Japan and USA human hair is being used to make various types of ropes which are being used in various fields like for example-horse riding and in circuses etc. Based on this kind of uses this study has been further explored for the proper utilization of the human hair and it's properties that can be useful in various environmental, social and economic fields and also proves that much worthy the human hair is in these fields whether it's going to produce any harmful effects on the atmosphere and nature or not and what are other fields where it can be used without creating any hardships.

Interestingly, while the hair is dumped as waste in most places, certain kinds of high-quality human hair and its products are also traded internationally at large scales. In 2010, India alone exported ~1 million kg of human hair and its products worth US $238 million, and total global imports were valued at US $1.24 billion [3]. Largely centered on wigs, hair extensions, and so forth, this trade also has been a source of many of the above mentioned environmental and health problems. Due to hair dust and decaying hair, workers of many hair-processing units in India have increased cases of tuberculosis and respiratory tract infections [4, 5]. Improper disposal of hair and other processing waste in many of these units has been a source of pollution and legal conflicts [4, 6]. In one such case of Jalalpur market in New Delhi, India [6], the traders used to put the waste hair to fire. Protests and legal efforts by neighbors in 1998 led to relocation of the processing units to villages in outskirts of New Delhi (personal discussions with Malik, I., 2012), but no systemic improvement was attempted in the processing practices. In Eluru district in Andhra Pradesh (India), dumping of large amount of hair waste from the processing units at the banks of a local river led to pollution, health problems, and conflicts, but the authorities could not resolve the issue because they found no way to deal with the hair waste other than to burn or dump it [4]. These examples show that in spite of a large-scale economy running around human hair, there had been no systemic thinking about environmentally safe management of the human hair waste. Every material uses and technology, however, also has several sociocultural and economic aspects associated with it, which often determine the adaptability of the use or the technology. Developing appropriate utilization for human hair waste in a context therefore requires considering all possible uses and technologies along with their socioeconomic and environmental impacts. While there is

a large body of research literature on the biology of human hair growth [7] and hair care with its sociocultural aspects [8] and there is some research on technologies using human hair (vide infra), there is very little literature on systematic environmentally safe management of human hair waste. Historical and current uses of human hair have been reviewed including the main stream and local/traditional uses as well as technologies that are being developed in various areas of scientific research. This includes the socioeconomic, environmental, and cultural aspects of the trade systems that have developed around some of the large scale uses. Based on this review, problems and gaps in the current human hair utilization are identified and approaches to address. these are discussed. For developing human hair "waste" as a resource, various entrepreneurial
Considerations such as knowledge and skill requirements and potential markets are discussed. Human hair is one of the highest nitrogen-containing (~16%) organic material in nature because it is predominantly made up of (nitrogen-containing) proteins. For comparison, cattle dung contains only ~0.2-0.3% nitrogen. In addition, human hair also contains sulfur, carbon, and 20 other elements essential for plants [12]. In the atmosphere, hair decomposes very slowly, but moisture and keratinolytic fungi present in soil, animal manure, and sewage sludge can degrade hair within a few months [13]. In traditional Chinese agriculture, human hair was mixed with cattle dung to prepare compost that was applied to the fields in the winter season [14, 15]. In some communities in India, hair has been used directly as fertilizer for many fruit and vegetable crops and in making organic manures [16, 17]. Recent experiments on horticulture plants show that direct application of human hair to soil provides the necessary plant nutrients for over two to three cropping seasons [18]. A company named Smart Grow has popularized the fertilizer use of human hair in the USA by selling it in the form of hair mats for potted plants. Small entrepreneurs in the USA are also promoting hair as fertilizer by packaging it in various user-friendly forms such as in tea bags [19]. By mixing human hair with cattle dung and feeding worms on the mixture, it is also possible to make good quality vermicompost within a period of about 2 months [20]. Non composted hair, however, has advantages than composted hair because composting can lead to some loss of nitrogen. While the biological decomposition pathways take a few months, human hair can also be decomposed within a few hours by chemically hydrolyzing it at high temperatures in acid or base solutions. The hydrolyzed solution, which mainly consists of amino acids with some fatty acids and nucleotides, can be used as a liquid fertilizer after neutralization. Experiments using this hydrolysate as foliar spray show enhancement of the chlorophyll content as well as biomass in spinach and wheat plants [21]. Application of the solution to soil also shows improvements in the color and size of Amaranthus dubius [22] and hot pepper plants [23]. Experiments on the hot pepper plants also show increased diversity of soil-intrinsic bacteria, which significantly reduces the spread of a wilt disease in these plants caused by the bacterium Ralstonia solanacearum. Long term impacts of this use, however, need to be assessed. Any kind of hair without toxic contamination can be used for fertilizers. Finely shredded hair, however, is better for faster decomposition. The importance of citrus fruits in world's economy is demonstrated by its wide scale cultivation under tropical and sub-tropical conditions. Citrus has a tremendous socio-economic and cultural impact on the whole society.

The multifold nutritional and medicinal values make this fruit indispensable in several parts of the world. Citrus is primarily valued for the fruit, which is either eaten alone as fresh fruit, processed into juice, or added to dishes and beverages. At the moment, citrus is being grown in Punjab over 52,836 hectares with annual production of 10,49,977 tones. Finally, we will use the liquid fertilizer extracted from human hairs, and we will check the growth of citrus plant.
All these examples indicates then to resolve these kinds of problems there is a need for the utilization of human hair waste so that we can create an environmentally safe management to save the nature and keep the balancing between various factors which generally affects the environment. There are many researchers and scholars who are working on this for creating a sustainable environmental atmosphere which will cause the total reduction in any kind of pollution in the environment and the various factors which are causing this pollution and should be destroyed or being removed off from the nature totally from various techniques. It will help us to understand various methodology via which we can adopt any of these techniques to overcome the problem efficiently and in less time with suitable cost & source.

LITERATURE REVIEW

Literature review is conducted by reviewing different research papers. Chemical fertilizer has been generally overused around the world. Global chemical fertilizer use has been reported to be about 1.9×10^{11} t, with China ranking first in consumption, accounting for 25% of world usage [24]. Due to great importance of chemical fertilizer to crops in China, the use of chemical fertilizer has continuously expanded from 8.8×10^{9} t in 1978 to 6.0×10^{10} t in 2015 [25]. In addition, China's per hectare application of chemical fertilizer, 393.2 kg/hm2, is higher than the international environmentally safe use limit of 225 kg/hm2 and is also about 3.05 times that of the United States and 2.54 times that of the European Union [25,26]. In 2019, China ranked first in citrus production and cultivated area, with about 4.4×10^{8} t and 2.9×10^{7} ha accounting for 27.9% and 29.1% of world production and area [27], respectively. The yields of China's citrus increased further with more fertilizer being applied, especially chemical fertilizer. It is well known that excessive chemical fertilizer application will adversely affect soil physical and chemical properties, resulting in soil hardness and acidification, which eventually lead to a decline in soil organic matter and fertility [28,29]. In addition, chemical fertilizer also negatively impacts crop quality and causes ecological environment damage, such as water pollution, greenhouse gas emission, and N leaching [30]. Moreover, excessive chemical fertilizer application leads to a waste of resources, places a financial burden on farmers, and even reduces the international competitiveness of agricultural products [31]. In contrast, organic fertilizer can improve the physical and chemical properties of soil, such as structure, water retention, nutrients, and cation exchange capacity, and promotes positive biological soil properties, enhancing yield and quality and even alleviating the risks of ecological environment deterioration [32]. However, compared to the quick nutrient release of chemical fertilizers, organic fertilizers have low nutrient concentrations, and nutrient release is too slow to support crops in a short time [33]. A beneficial approach to overcome this problem is reduction of

chemical fertilizers combined with the application of organic fertilizers; this has been shown to better sustain soil fertility compared to applying chemical or organic fertilizers alone [34].

Several studies have reported that chemical fertilizer combined with organic fertilizer application (CFOF) improves soil conditions and promotes plant growth and even yield in comparison with only chemical fertilizer application. For example, combined application of organic and inorganic fertilizers greatly increases soil organic matter and the total nitrogen content of the soil and improves soil microenvironment in wheat/maize fields [21]. Hazarika et al. [22] found similar results. According to Xiao et al. [19], organic fertilizer combined with compound fertilizer improved soil quality, whereas the utilization of compound fertilizer worsened soil quality and made the soil acidize; this result was similar to that of Song et al. [20] and Pachuau et al. [23]. Qiu et al. [15] reported that chemical fertilizer combined with biofertilizer application significantly promoted root growth, improved the rate of nutrient distribution in citrus, and improved the external and internal qualities of tarocco blood orange; this result was similar to those of previous study of citrus [24–26]. According to Pei et al. [7], organic fertilizer is an alternative to chemical fertilizer with no loss in yield and fruit quality for citrus. In addition, apple orchard with organic–inorganic mixed fertilizer promoted soil microbial activity and increased soil organic matter by 16% and crop production by 67% when compared with chemical fertilizer application alone [26] and those results were consistent with research of Lai et al. [27]. Some experiments [28–30] also show that application of CFOF improves plant physiological indexes and yield compared with inorganic fertilizers on their own. These studies indicate that CFOF improves soil microbial activity, enhances physical and chemical soil properties, and promotes the absorption and utilization of nutrients, thus facilitating high crop yields. Chemical fertilizer reduction combined with organic fertilizer application meets the requirements for green ecology and is gradually popular in China [7]. Recently, research on reducing chemical fertilizer use and applying organic fertilizer has focused on the effects of reducing N fertilizer on crop yield and quality while rarely measuring changes to soil properties, orchard environment, and plant physiology, especially in citrus systematically, in response to a reduction in chemical fertilizer combined with increased organic fertilizer when equal nutrients of N, P, and K fertilizers are supplied.

Lemons are one of the most popular citrus fruits in the world, and are widely used for culinary purposes, good source of vitamins and minerals, also lemon is an important export crop for foreign markets and source for cash currency. Citrus requires sixteen essential elements for normal growth, production and quality. Adequate supply of nitrogen, phosphorus and potassium are important for citrus tree growth and productivity (Quaggio et al., 2002). Nitrogen is the key component in mineral fertilizers applied to citrus trees; it has more influence on tree growth, yield, and fruit quality. Potassium is necessary for basic physiological functions such as translocation of sugars, synthesis of proteins and cell division and growth. It is important in fruit growth and enhances its size, flavor and color. Phosphorus is necessary for many life processes such as photosynthesis, synthesis and breakdown of carbohydrates and the transfer of energy within the plant. Today, chemical fertilizers are an indispensible in fruit crop nutrition, but excessive and indiscriminate use of chemical fertilizers have deleterious effects on soil, water, and atmosphere pollution, and reflected on animal and human health, it had also adversely affected the soil fertility, water quality,

yield, and quality of the products (Srivastava, 2012). Biofertilizers of organic manure and biofertilizers has assumed great importance for sustainable production and to improve the soil physical, chemical and biological properties. Also, organic manures and biofertilizers are a good alternative to reduce uses of chemical fertilizers. In this respect, several workers reviewed the significant role of organic manures and biofertilizers in influencing the soil properties and enhancing the growth, yield, and quality of citrus (Dheware and Waghmare, 2009 on sweet orange; Kumar et al., 2011 on lemon; Khehra and Bal, 2014 on lemon; Lal and Dayal, 2014 on acid lime and Khehra and Bal, 2016 on lemon). Soil microbes play an important role in many critical ecosystem processes, including nutrient cycling and homeostasis, decomposition of organic matter, as well as promoting plant health and growth as bio-fertilization (Hayat et al., 2010; El Khayat and Abdel Rehiem, 2013; Khehra, 2014; Babita et al., 2015 and Hadole et al., 2015).
Therefore, the purpose of this research is to explore the effects of CFOF on soil properties, citrus growth physiology, when nutrients of N, P, and K fertilizers are equal and to evaluate the effects of different fertilization treatments on soil environment. This work could provide a theoretical basis for the scientific reduction of chemical fertilizer and identify the amount of organic fertilizer necessary for sustainable development of the citrus industry. As we are using the organic fertilizer made from human hair and method used to extract the protein from human hair is given below

METHOD USED TO EXTRACT THE KERATIN PROTEIN FROM HUMAN HAIR

The most used method is Shindai method for protein extraction from human hair.

Shindai Method

- incubation of the samples at 50°C for 24 h in a buffer.
- Buffer consists of 20 mM Tris-HCl (pH 8.5), 2.6 M thiourea, 5 M urea, and 5% (v/v) 2-mercaptoethanol (2-ME). (shindai solution)

Modified Shindai Method

- addition of various low molecular weight alcohols to the Shindai solution.
- 2-ME or sodium dodecyl sulfate (SDS) will not be used here.

Recovery Rate: 22%-25% of protein extraction

Barthelemy Study

- similar extraction solution as Shindai
- the addition of 0.1% Triton X-100
- incubation at 37°C for 18 h

Recovery Rate: The recovery of proteins was not stated in the report. Instead, nanoscale liquid chromatography coupled to tandem mass spectrometry (NanoLC-MS/MS) was used to analyze the extracted proteins, leading to identification of 56 proteins, including 34 keratins and keratin associated proteins KAPs.

Alkyline lysis Method (Preferred)

Hair will be collected from different barber shops then they will be sterilized with 90% ethanol and cut into 1 cm of length with sterile lab scissors.

1. 5 mg of 1cm long hair will be treated in 300 ul lysis buffer.
2. Lysis buffer consists of NaOH (0.1 M and 0.2 M), sodium dodecylsulfate (SDS; 1% and 2%), beta-mercaptoethanol (β-ME, 2%), ethylenediaminetetraacetic acid (EDTA, 0.01 M)
3. All mixtures were incubated at 90°C for 10 minutes.
4. The whole mixture will be transferred into QIAquick Spin Columns (Qiagen) and centrifuged at 16000 rpm for 5 minutes to separate undissolved hair fractions and supernatant.
5. The protein sample was further purified and precipitated by mixing 1 volume of the supernatant with 4 volumes of pre-cold acetone.
6. The precipitated protein was reconstituted in a sample buffer.
7. Sample buffer contains 7 M urea, 2 M thiourea, 4% 3- [3-Cholamidopropyl) dimethylammonio]-1-propanesulfonate (CHAPS), 2% ampholytes, 5% glycerol.
8. All reconstituted protein samples were later stored at 4°C.
9. The amount of protein recovered from each experiment was measured by Bradford colorimetric method.

Additional Protein Extraction

For additional protein extraction from the human hair, extraction was carried out in two stages.

- At **1st** stage hair sample from an individual was immersed in 300 µl of formulated alkaline-based lysis buffer and incubated based on the optimal time obtained at 90°C.
- At **2nd** stage undissolved hair fractions from the previous extraction were transferred using a pair of sterile forceps into a fresh tube containing 300 µl of lysis buffer with different concentrations of NaOH (0.1, 0.15 and 0.2 M)

- Magnetic stirring was introduced to increase the recovery of protein from the second stage of extraction.
- The solutions were filtered, precipitated, and estimated for protein concentration using the method of Bradford, and recovery was calculated based on the whole fiber weight of hair.

Table 3: Comparison of Protein Extraction Efficiencies from Human Hair

shindai method	23.38 %
Barthelemy study	34 keratins and KAPs (not given in %)
Lee et al Method	45.99 %
Alkyline lysis method	64.76 %

METHODOLOGY

SOIL CHARACTERISTICS

Soil analysis is helpful in formulating and improving a fertilization program because soil testing measures organic matter content, pH, and extractable nutrients. Soil analysis

pH

For pH determination, soil and deionized water mixed solution was made. The pH probe was used to measure the pH of the top layer of the soil mixture in the vile (make sure the glass tip of the probe is submerged in the solution). The top layer of water was gently stirred and waited for the pH reading to stabilize. When the pH reading was stabilized, its pH value was recorded. The pH value of soil sample used for citrus plant came out to be 6.5.

Soil Texture

Soil texture is an estimate of the amount of sand, silt and clay particles present in the soil. It is an inherent property of the soil and cannot be changed by normal agronomic practices. Many physical characteristics of the soil depend on texture, and the clay content is very important. Soil texture affects drainage and structure, which in turn affect how plants will grow in the soil. The clay and organic matter help to bind soil particles together, forming stable aggregates, which are an indicator of good soil structure: good soil drainage, root and seedling penetration, and aeration. Citrus does best in slightly acidic, well-drained loam or sandy loam soils. Very sandy soils require expert management as they have a low water-holding capacity and nutrients are readily leached. Wetter clay soils can cause collar and root rot and the risk of tree death.
Take soil, tap water, and clear container. Remove stones and waste. Take soil in container so that it is three quarters full. Now add water to mix the soil. Let the soil to set for one minute as sand is heavier than silt and clay it settles in less than min. note down the height at the top of sand layer. Then wait for one hour for silt to settle and note down its height. After that wait for one day for clay to settle and note its height. Add three heights to find total portion of soil.

Table 2: Soil texture

Height in ml after	Correspond to the fraction of	Height	Portion expressed in %
One minute	Sand	9ml	9/16 = 56%
One hour	Silt	4ml	4/16 = 25%
One day	Clay	3ml	3/16 = 19%

Nitrogen Content

Nitrogen content in soil samples is found using Kjeldahl method.
Chemical reactions;

Digestion: soil +$KMnO_4$ +NaOH =Ammonia
Distillation: 2NHOH+4H_3BO_3 = 2$(NH_4)2B_4O_7$ +7H_2O
Titration: 2$(NH_4)2B_4O_7$ +5H_2O + H_2SO_4 = $(NH_4)2SO_4$ + 4H_3BO_3

Chemical required;
NaOH, H_3BO_3, $KMnO_4$
Indicator preparation;
Add 0.066g bromocresol green and 0.099g methyl red in distilled water (100ml ethanol)

Procedure;
1. Take 25g of NaOH and distilled water in 1000ml of cylinder. Fill it up to the mark.
2. Take 3.2g of $KMnO_4$ and add distilled water up to the mark in another 1000ml cylinder.
3. Take 20g of boric acid and distilled water in conical flask and heat it on heating plate to mix it properly.
4. Add boric acid solution, 20ml of indicator and distilled water in 1000ml cylinder.
5. Put 5g of soil sample in one cylinder and run the apparatus. After some time, soil, $KMnO_4$, distilled water and NaOH will start getting in cylinder (digestion) and boric acid in flask.
6. After some time, ammonia will go into flask (distillation) and react with boric acid to make ammonium borate.
7. Sample collected in flask will be titrated against 0.02N H_2SO_4 until the color changes from green to pink.
8. Run the blank sample side by side.
   N (%) = (ml of standard acid-ml blank) *0.02N*1.4007/weight of sample in gram
   N (%) = 1.5%

Phosphorous and potassium content

For the determination of P and K in soil samples, di-acid (HNO3–HClO4 = 2:1 ratio v/v) digestion was done on the hot plate at 250C. Spectrophotometer (absorbance at 420 nm) and flame photometer (PFP 7, Jenway, Staffordshire, UK) were used for the final determination of P (ammonium vanadate–ammonium molybdate yellow color method) and K, respectively.
The P and K content was found to be 7.5mg/kg of soil and 103.4mg/kg of soil.

FACTORS EFFECTING THE CITRUS PLANT GROWTH

Growing conditions

Being a tropical and subtropical crop, citrus can be grown in a belt between 40 °N and 40 °S, except at high elevations. Minimum temperature and its duration time are the limiting growth factors sensitivity depends on variety, rootstock, dormancy of the trees and the absolute minimum temperature and its duration.
Intensive citrus cultivation requires the use of fertilizers, close monitoring and control of pests, diseases and weeds, effective irrigation, and control of tree size. The trees begin their productive

life in the third year, and peak productivity takes place when the trees are 10-30 years old, average yields under these conditions are 30-60 t/ha.
Extensive citrus cultivation requires the use of fertilizers, but only moderate monitoring and control of pests, diseases, and weeds. They are generally rain-fed only. Their productive life starts in the fourth year, and peak productivity takes place when the trees are 8-15 years old, average yields under these conditions are 15-25 t/ha.

Soil type

Citrus can be grown on a wide variety of soils, from sand to loam and clay. Both acidic and alkaline soils are acceptable.

Varieties

The genus Citrus is an evergreen tree belonging to the family Rutaceae. It has about 150 genera and 1500 species, all native to the tropical and subtropical regions of Asia and the Malay Archipelago.
The principal citrus scions are:
Orange (C. sinensis Osbeck)
Mandarin (C. reticulata Blanco)
Lemon (C. limon [L.] Burm.)
Lime (C. aurantifolia [Christ.] Swing.
Grapefruit (C. paradisi Macf.)
Pomelo (C. grandis [L.] Osbeck)
The most used rootstocks are:
Rangpur lime (C. limonia Osbeck)
Rough lemon (C. jambhiri Lush.)
Sour orange (C. aurantium L.)
Cleopatra mandarin (C.reshni Hort.)
Trifoliata (P. trifoliata [L.] Raf.)

Climate

Both arid and humid climates are acceptable. As citrus trees are sensitive to low temperatures, the limiting parameter for growing citrus is the minimum temperature prevailing in wintertime.

Irrigation

Irrigation is one of the most important factors in producing a good yield of quality citrus. Irrigation scheduling, knowing how much water to put on and when, has a direct impact on tree health as well as fruit yield, size and quality. Without correct irrigation scheduling, orchards are more susceptible to nutrient deficiencies, physiological disorders, pests and disease.
Correct irrigation scheduling requires an understanding of:

- How much water can be held in the crop root zone.
- How much water the crop uses each day.
- How much water the irrigation system applies.

Citrus has a shallow root system. It is important to aim irrigation at the effective root zone, minimizing the amount of water leaching past. For citrus, the effective root zone is usually in the top 30 to 40 cm, depending on the soil type.

Soil Temperature

Citrus fruits grow best between a temperature range of 13^0C to 37^0C. Temperatures below – 4^0C are harmful for the young plants. Soil temperature around 25^0C seems to be optimum for root growth.

PARAMETERS TO ESTIMATE THE GROWTH OF CITRUS PLANT

There are number of parameters to check or measure the growth of citrus plant.

Height of plant

Measuring the height of plant using any measuring scale before and after the 2 months will show how much the plant have growth by providing the necessary condition and nutrients. Measure the height of the main plant from the border of the container to the top of the main plant stem. Measure the length or height of plant after every 2-3 days.

Weight of plant

Measuring Fresh Weight: While you can technically measure the fresh weight of plants without harming them, the simple act of removing a plant from its growing "medium" can cause trauma and affect the ongoing growth rate and thus your experiment. Measuring the fresh weight of plants is tricky and should probably be saved as a final measure of growth at the end of the experiment. Here is the process for measuring fresh weight:

1. Remove plants from soil and wash off any loose soil.
2. Blot plants gently with soft paper towel to remove any free surface moisture.
3. Weigh immediately (plants have a high composition of water, so waiting to weigh them may lead to some drying and therefore produce inaccurate data).

Measuring dry weight: Since plants have a high composition of water and the level of water in a plant will depend on the amount of water in its environment (which is very difficult to control), using dry weight as a measure of plant growth tends to be more reliable. You can only capture this data once as a final measure at the conclusion of your experiment.

1. Remove the plants from the soil and wash off any loose soil.
2. Blot the plants removing any free surface moisture.
3. Dry the plants in an oven set to low heat (100° F) overnight.

4. Let the plants cool in a dry environment (a Ziploc bag will keep moisture out) - in a humid environment the plant tissue will take up water. Once the plants have cooled weigh them on a scale.
5. Plants contain mostly water, so make sure you have a scale that goes down to milligrams since a dry plant will not weight very much.

New Leaves Grown
Number of leaves (indicates a plant's physiological age)
Counting Leaves:
1. Count and record the number of leaves on each plant.
2. Count every visible leaf on the plant, including the tips of new leaves just beginning to emerge.
3. You may want to place the plant over some graph paper to avoid counting errors.

Frequency of measurement: Every 2-3 days
Leaves length and width
After every 2-3 days measure the leaves length and width using scale.

Number of flowers
It serves as additional indication of plants health.
- 1st Flowering: Record the number of days since initial planting to the first flower. Frequency of measurement: Once
- Number of Flower: Record the number of flowers on each of the plants. Buds should be included in your flower count. Frequency of measurement: Every 2-3 days.

We are taking 4 sets of citrus plant. (3 plants in each set and one plant as blank)
In first set only commercial liquid fertilizer will be used. In second set fertilizer made from human hair will be used, in third set mixture of both will be used and in one plant which is taken as a blank, no fertilizer will be added. At start the height of all the plants were made same.

LIQUID FERTILIZER
Leaf analysis is an essential tool to determine the required plant nutrients. According to leaf analysis results, the fertilization rates and the correct ratio of plant nutrients can help to schedule the fertilization program. Citrus is a heavy feeder, particularly on nitrogen. Fertilizers are generally labeled with numeric ratios such as 3-1-1. Those numbers reflect the ratio of nitrogen (N) to phosphorus (P) to potassium (K), or N-P-K. Because citrus likes a lot of nitrogen, you want to purchase a fertilizer with at least a 2-1-1 ratio, or twice as much nitrogen as phosphorus and potassium. Citrus also requires trace minerals, which may be present in the fertilizer.

RESULTS AND DISCUSSION

PLANT GROWTH

Table presents the effect of CFOF on plant growth index. In comparison with leaf area, thickness of a hundred leaves, all that of CFOF was promoted, In the OF + CF, twig length was longer than that observed in the CK, OF and CF treatments. The plant growth index observed in the OF + CF treatment was higher than that of OF treatment overall.

Table 3: Growth rate of plant

Treatment	Area of Leaf (cm^2)	Thickness of Hundred Leaves (mm)	Length of Twigs (cm)
CK	17.53 ±0.77	26.74 ±0.38	6.98 ±0.54
CF	18.59 ±1.06	27.02 ±0.35	7.60 ±0.86
OF	19.71 ±1.05	27.85 ±0.69	7.96±0.92
OF + CF	20.78 ±1.42	28.88 ±0.74	8.50 ±0.83

CK: no fertilizer; CF: chemical fertilizer; OF: organic fertilizer (extracted from human hair)
OF + CF: chemical fertilizer combined with organic fertilizer; Data are mean standard deviation.

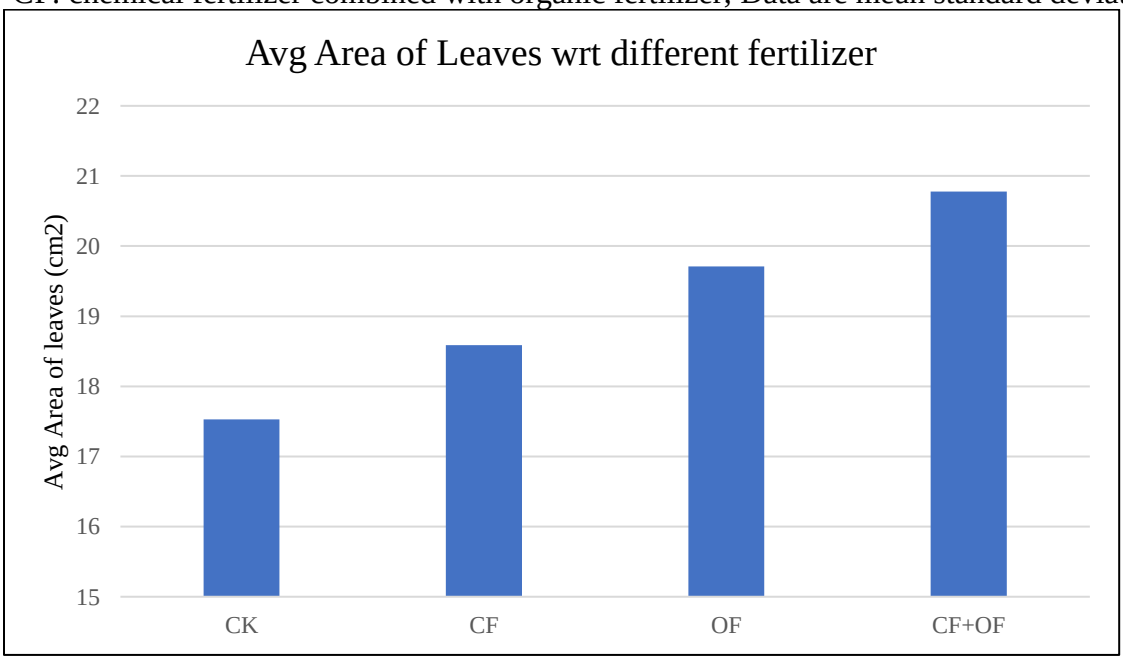

Figure 11: Average area of leaves w.r.t different fertilizer

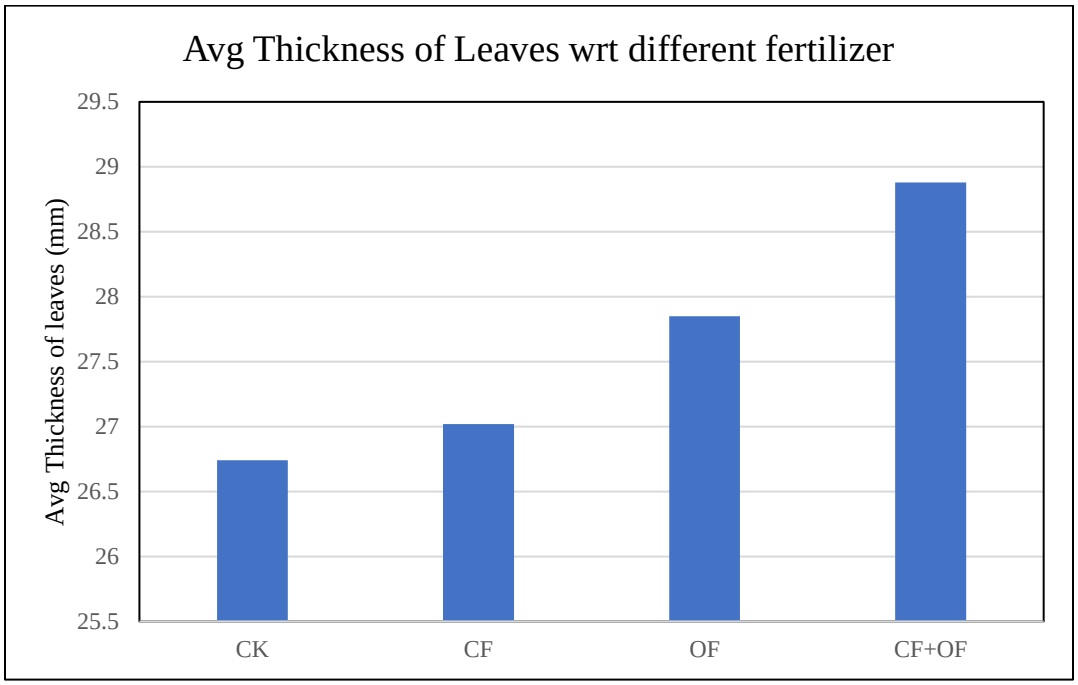

Figure 2: Average thickness of leaves w.r.t different fertilizer

NUTRIENT ELEMENT

Table presents the effect of CFOF on leaf nutrient physiology and twigs. The results showed that N, P, and K contents of leaves and twigs were higher in the OF + CF treatments than that of CK and CF treatments, in general. Moreover, N content of leaves in the OF + CF treatments was significantly higher than that observed in the CK treatment compared with the CK treatment, leaf K content in the OF + CF and treatments was significantly higher by 16.6%, respectively.

Table 4: Nutrient element of plants

Treatment	Leave			Twigs		
	N ($g \cdot kg^{-1}$)	P ($g \cdot kg^{-1}$)	K ($g \cdot kg^{-1}$)	N ($g \cdot kg^{-1}$)	P ($g \cdot kg^{-1}$)	K ($g \cdot kg^{-1}$)
CK	27.95 ± 0.66	1.34 ± 0.16	13.10 ± 0.51	11.17 ± 0.25	0.81 ± 0.06	8.17 ± 0.40
CF	29.15 ± 0.55	1.40 ± 0.05	14.23 ± 0.46	11.70 ± 0.37	0.92 ± 0.07	8.46 ± 0.15
OF	29.30 ± 0.15	1.43 ± 0.04	14.75 ± 0.52	11.85 ± 0.40	0.95 ± 0.08	8.49 ± 0.32
OF + CF	29.47 ± 0.74	1.46 ± 0.02	15.27 ± 0.56	11.97 ± 0.60	0.97 ± 0.04	8.63 ± 0.37

Due to great importance of chemical fertilizer to citrus, chemical fertilizer has been widely used and even overused in order to maintain high citrus yield. This has led to deterioration of soil

properties and ecological environment. However, a combination of chemical and organic fertilizer is not only beneficial in improving the properties and environment of soils, but also promotes crop yield and quality. Here, our work confirmed that CFOF was helpful in increasing citrus yield and improving soil properties. It has previously been reported that the content of soil organic matter, which can strengthen the ability of the soil to maintain and supply fertilizer as well as change the structure of soil aggregates and enhance soil fertility, can effectively be improved by increasing the use of organic fertilizer. Additionally, many studies show that organic fertilizer can improve soil physicochemical properties, such as soil organic matter, total porosity, available N, P, and K of soils. Thus, the combined application of organic fertilizer and chemical fertilizer could greatly enhance soil properties. In this study, the soil physicochemical properties of the OF + CF higher than those of the CK, OF and CF treatments. These results indicate that CFOF raised soil fertility and physicochemical properties and that organic fertilizer could contain several active substances, such as humic acid, amino acid, and microbes, among others, which could promote the formation of soil aggregates, making soil more relaxed and breathable, and strengthening the ability to conserve fertilizer and water to a certain degree.

Soil microbe content, which is often used as an indicator to evaluate soil quality, plays an important role in the soil ecosystem, not only by assuming the responsibility of decomposer but also by promoting nutrient absorption by roots. In addition, as a crucial member of the soil ecosystem, soil enzymes play an important role in mineralization and decomposition of organic materials, because they can react sensitively to changes in soil environment and reflect soil fertility changes. In this study, the soil microbe properties of the OF + CF treatments were higher than those observed in the C, OF and CF treatments. These findings indicate that CFOF improved the soil microbial community structure in a manner that was relative to the organic matter, humic acid, and amino acids and which could increase soil microbial activity

To some extent, different measures of fertilization application can affect the orchard ecological environment. Zhou et al. and Lv et al. report that long-term and short-term application of organic fertilizer combined with synthetic fertilizer can increase. N2O (greenhouse gases) emission. In this study, the CO2 (greenhouse gases) soil carbon flux seen in the OF + CF treatments was higher than that of CK and CF, leading to the possibility that soil biological properties can be improved. The long-term, large amount of chemical fertilizer especially nitrogen fertilizer is a main cause of soil N leaching. Nitrogen fertilizer is decomposed by microbes into NO3-N and NO2-N, and NO3-N is soluble in water and can easily leach, often causing groundwater pollution and endangering human and animal health because of its negative charge and strong mobility in solution. According to Liao et al., chemical fertilizer application decreased the diversity of the diazotrophic community, while chemical fertilizer combined with organic manure improved not only the diversity of the diazotrophic community but also their abundance and nitrogen fixation rate. It has also been reported that chemical fertilizer reduction combined with organic fertilizer application is considered an effective measure to reduce the risk of N leaching in farmland. In this study, NO3-N from the 0–60 cm soil layer of the OF + CF treatments was lower than that of CF, while NO3-N from the 40–60 cm soil layer of the OF + CF treatment was lower than that of the 20–40 cm soil layer. This illustrates that chemical fertilizer combined with organic fertilizer can alleviate the risk

of N leaching and N migration to deep soil, because organic fertilizer contains organic carbon and humic acid and other relative matter, which adsorbs shallow soil NO3-N and inhibits its downward migration.

Nutrition is a key factor affecting quantity and metabolites in plant growth. Citrus is a green plant in all seasons and germinates branches many times a year; consequently, it consumes a several nutrients. Many studies have shown that the use of organic matter like manure, compost, and straw can improve and increase the nutrients of crop Organs. Thus, combined application of organic matter and chemical fertilizer could promote the nutrients of the crop. In this study, N, P and K found in the branches, roots, and fruits of trees treated with OF + CF were higher than that of CK, OF and CF. These findings indicate that CFOF facilitates absorption and distribution of nutrients in citrus. This may be due to organic fertilizer improving soil physicochemical properties and enhancing the ability of absorption and transportation of nutrients by roots, as previously suggested. Ample nutrition plays an indispensable role in plant growth. In this study, the index of plant growth from the OF + CF treatments was better than that of CK, OF and CF, and it was relative to nutrient balance. These results are similar to previous studies. Photosynthesis is a key physiological activity of plants and plays an important role in growth and development. It has been reported that more than 90% of crop biomass is derived from photosynthesis. Chlorophyll fluoresce is an ideal parameter for studying the physiological condition of plant photosynthesis in multiple settings, because it reflects various aspects of photosynthesis, such as light energy absorption, transmission, and photoreaction. In addition, PI of the chlorophyll fluorescence parameter can reflect the optical system performance index of a whole leaf, and PIabs and PItotal comprehensively reflect the light absorption and photosynthetic performance of a leaf. In this study, SPAD, Pn, PIabs, and PItotal measurements in the OF + CF were higher than those of CK, OF and CF. These results indicate that CFOF greatly improved leaf photosynthesis. The promotion of nutrient absorption, leaf growth, and the enzyme activity of leaf-related physiological metabolism could bring about improvement in leaf photosynthesis. These findings are similar to previous studies.

As discussed above, CFOF could increase soil microbial activity, improve soil's physical and chemical properties, enhance nutrient availability in citrus tree organs, and promote citrus growth and photosynthesis. Yield is also an important parameter to measure because of its economic benefits, which are determined by many factors, such as the condition of growth and photosynthesis. Previous studies have shown that yield can be maintained or even significantly increased relative to application of synthetic fertilizer alone. In this study, yield per citrus tree and the contribution rate of fertilizer in the OF + CF treatments were significantly higher than that of CF. This illustrates that CFOF is beneficial for boosting citrus yield. This result might be explained by the fact that chemical fertilizer combined with organic fertilizer could improve soil fertility and enhance the ability of photosynthesis and growth with the above research findings. These results were consistent with previous studies. Consequently, CFOF is beneficial to promoting citrus physiology, improving soil characteristics, and increasing orchard yield, which could meet the requirements of green ecological development.

CONCLUSION

The results of this study show that CFOF is beneficial to improving the physicochemical and microbe properties of soil, promoting nutrient content of citrus plants, enhancing photosynthesis and growth of citrus, and thus promoting orchard yield. In addition, CFOF notably alleviates NO3-N leaching and NO3-N migration to deep soil. In summary, can obtain high yields and ensure good citrus orchard and tree conditions and ecological environment, especially when the OF + CF treatment is used. The application of N, P2O5, K2O fertilizer and bioorganic fertilizer of OF + CF treatment is 0.508, 0.320, 0.310 and 10 kg/plant, respectively.

REFERENCES

1. S. Kumar, J. K. Bhattacharyya, A. N. Vaidya, T. Chakrabarti, S. Devotta, and A. B. Akolkar, "Assessment of the status of municipal solid waste management in metro cities, state capitals, class I cities, and class II towns in India: an insight," Waste Management, vol. 29, no. 2, pp. 883–895, 2022.
2. M. Brebu and I. Spiridon, "Thermal degradation of keratin waste," Journal of Analytical and Applied Pyrolysis, vol. 91, no. 2, pp. 288–295, 2019.
3. UN Comtrade, import values are based on HS2007 codes 050100, 670300, and 670420, 2018.
4. E. Vijayalakshmi, "Hair pollution hits Karnataka. Down to Earth," 2018, http://www.downtoearth.org.in/node/13180.
5. M. Cohen, "India's export of human hair to China is a booming business but it is also entangled in issues of respiratory diseases and child labor. The Standard," 2007, http://www.thestandard.com.hk/news detail.asp?pp cat=31&art id= 50482&sid=14602467&con type=3.
6. I. Malik, "Human hair trade: environmental hazards," Tech. Rep., Vatavaran, New Delhi, India, 1998.
7. C. R. Robbins, Chemical and Physical Behavior of Human Hair, Springer, Heidelberg, Germany, 5th edition, 2012.
8. G. Biddle-Perry and S. Cheang, Eds., Hair: Styling, Culture, and Fashion, Berg, Oxford, UK, 2008. Journal of Waste Management 15
9. M. Muto, T. Isobe, K. Ramu et al., "Contamination of Brominated Flame Retardants (BFRs) in human hair from e-waste recycling site in Vietnam," in Interdisciplinary Studies on Environmental Chemistry—Environmental Pollution and Ecotoxicology, M. Kawaguchi, K. Misaki, H. Sato et al., Eds., pp. 229–237, 2012.
10. J. S. Cox, "The construction of an ancient Egyptian wig (c. 1400 B.C.) in the British Museum," The Journal of Egyptian Archaeology, vol. 63, pp. 67–70, 1977.
11. J. Turner, Brushes: A Handbook for Artists and Artisans, Design Books, 1992.
12. V. D. Zheljazkov, "Assessment of wool waste and hair waste as soil amendment and nutrient source," Journal of Environmental Quality, vol. 34, no. 6, pp. 2310–2317, 2005.
13. M. Sharma, M. Sharma, and V. M. Rao, "In vitro biodegradation of keratin by dermatophytes and some soil keratinophiles," African Journal of Biochemistry Research, vol. 5, no. 1, pp. 1–6, 2011.
14. AAA, "Ropes made of human hair," Ann Arbor Argus, 1898, http://oldnews.aadl.org/node/153517. [15] L. Shiming, "The utilization of human excreta in Chinese agriculture and the challenge faced," EcoSanRes, 2002, http://www.ecosanres.org/pdf files/Nanning PDFs/Eng/Luo%20Shiming%2010 C11rev.pdf.
15. P. Subbiah, "Human hair as fertilizer," Communicator: Sathavu, M. Nam Vazhi Velanmai (Tamil Version of Honeybee), 1998.

16. P. Oudhia, "Revised version of selected Botanical.com articles," Part 2, 2010, http://pankajoudhia.com/.
17. V. D. Zheljazkov, J. L. Silva, M. Patel et al., "Human hair as a nutrient source for horticultural crops," HortTechnology, vol. 18, no. 4, pp. 592–596, 2008.
18. J. Schaffer, "Urbanna Salon offers 'Earth Hair'," Down to Earth NW, 2011, http://www.downtoearthnw.com/stories/2011/ jun/08/urbanna–salon-offers-earth-hair/.
19. A. Bhatta, "No hair-raising experience this," Down to Earth, 2008, http://www.downtoearth.org.in/node/4928.
20. K. R. Yadav, R. K. Sharma, M. P. Yadav, and R. M. Kothari, "Human hair waste: an environmental problem converted into an eco-friendly plant tonic," Fresenius Environmental Bulletin, vol. 4, no. 8, pp. 491–496, 1995.
21. M. M. Rahman, "Fertilizer from hair!!," ChE Thoughts, vol. 1, no. 1, pp. 20–21, 2010
22. Liang, S.S. Studies on NPK Fertilization Status and the Potential of Reducing Application Rate in Major Citrus Planting Regions
23. of China. Master's Thesis, Huazhong Agricultural University, Wuhan, China, 2017. (In Chinese) Pei, Y.; Wu, Y.P.; Zhang, W.; Jiang, Y.B.; Sun, F.L.; Cheng, Y.F.
24. The impacts of substituting organic fertilizers for chemical fertilizer on fruit, leaf, and soil in citrus orchard. Soils Fertil. Sci. China **2021**, 4, 88–95. (In Chinese)
25. Chen, Y.; Hu, S.; Guo, Z.; Cui, T.; Zhang, L.; Lu, C.; Yu, Y.; Luo, Z.; Fu, H.; Jin, Y. Effect of balanced nutrient fertilizer: A case study in Pinggu District, Beijing, China. Sci. Total. Environ. **2021**, 754, 142069. [CrossRef]
26. Gu, B.; Ju, X.; Chang, J.; Ge, Y.; Vitousek, P.M. Integrated reactive nitrogen budgets and future trends in China. Proc. Natl. Acad.Sci. USA **2015**, 112, 8792–8797. [CrossRef]
27. Lv, F.; Song, J.; Giltrap, D.; Feng, Y.; Yang, X.; Zhang, S. Crop yield and N2O emission affected by long-term organic manure.
28. substitution fertilizer under winter wheat-summer maize cropping system. Sci. Total. Environ. **2020**, 732, 139321. [CrossRef]
29. Liu, Z.; Wang, S.; Xue, B.; Li, R.; Geng, Y.; Yang, T.; Li, Y.; Dong, H.; Luo, Z.; Tao, W. Emergy-based indicators of the environmental impacts and driving forces of non-point source pollution from crop production in China. Ecol. Indic. **2021**, 121, 107023. [CrossRef]
30. Yang, G.; Tang, H.; Nie, Y.; Zhang, X. Responses of cotton growth, yield, and biomass to nitrogen split application ratio. Eur. J. Agron. **2011**, 35, 164–170. [CrossRef]
31. Wu, H.; Ge, Y. Excessive application of fertilizer, agricultural non-point source pollution, and farmers' policy choice. Sustainability **2019**, 11, 1165. [CrossRef]
32. Fang, P.; Abler, D.; Lin, G.; Sher, A.; Quan, Q. Substituting organic fertilizer for chemical fertilizer: Evidence from apple growers in China. Land **2021**, 10, 858. [CrossRef]
33. Qiu, F.; Liu, W.; Chen, L.; Wang, Y.; Ma, Y.; Lyu, Q.; Yi, S.; Xie, R.; Zheng, Y. Bacillus subtilis biofertilizer application reduces chemical fertilization and improves fruit quality in fertigated Tarocco blood orange groves. Sci. Hortic. **2021**, 281, 110004.[CrossRef]
34. Chang, K.H.;Wu, R.Y.; Chuang, K.C.; Hsieh, T.F.; Chung, R.S. Effects of chemical and organic fertilizers on the growth, flower quality and nutrient uptake of Anthurium andreanum, cultivated for cut flower production. Sci. Hortic. **2010**, 125, 434–441. [CrossRef]
35. Tejada, M.; Gonzalez, J.L. Effects of the application of a compost originating from crushed cotton gin residues on wheat yield under dryland conditions. Eur. J. Agron. **2003**, 19, 357–368. [CrossRef]

36. Niu, X.S.; Ju, X.T. Organic fertilizer resources and utilization in China. J. Plant Nutr. Fertil. **2017**, 23, 1462–1479. (In Chinese)
37. Xiao, L.; Sun, Q.; Yuan, H.; Lian, B. A practical soil management to improve soil quality by applying mineral organic fertilizer. Acta Geochim. **2017**, 36, 198–204. [CrossRef]
38. Song, H.;Wang, J.; Zhang, K.; Zhang, M.; Hui, R.; Sui, T.; Yang, L.; Du,W.; Dong, Z. A 4-year field measurement of N2O emissions from a maize-wheat rotation system as influenced by partial organic substitution for synthetic fertilizer. J. Environ. Manag. **2020**, 263, 110384. [CrossRef]
39. Yang, Q.; Zheng, F.; Jia, X.; Liu, P.; Dong, S.; Zhang, J.; Zhao, B. The combined application of organic and inorganic fertilizers
40. increases soil organic matter and improves soil microenvironment in wheat-maize field. J. Soils Sediments **2020**, 20, 2395–2404. [CrossRef]
41. paradisi Macf.) to organic and inorganic fertilization in central Sudan. Ann. Agric. Sci. **2011**, 56, 37–41. [CrossRef]
42. Lee, J. Effect of application methods of organic fertilizer on growth, soil chemical properties and microbial densities in organic
43. bulb onion production. Sci. Hortic. **2010**, 124, 299–305.

2nd International Conference on Advances in Civil and Environmental Engineering (ICACEE-2023)

University of Engineering & Technology Taxila, Pakistan

Conference date: 22nd and 23rd February, 2023

Sustainable Energy Production by Co-Pyrolysis of Waste Tire (PET), Waste Oil and Pine Bark to Yield Bio-Fuel

Bilal Asif, Nayab Zahra, Adeen Rehman, Asad Akbar, Muhammad Zaheer Aslam

Department of Environmental Engineering
University of Engineering & Technology Taxila, Pakistan

bilal.asif@uettaxila.edu.pk , Nayab.zahra@uettaxila.edu.pk, 19-ENV-10@students.uettaxila.edu.pk, 19-ENV-29@students.uettaxila.edu.pk ,19-ENV-39@students.uettaxila.edu.pk

ABSTRACT

Biomass "tyres and waste oil are major pollutants that are deteriorating the natural ecosystem, they need to be treated or to be disposed of properly. In this study, pyrolysis was done for the extraction of energy using fixed bed reactor. The thermal decomposition of material was done at elevated temperature (300-800°C) in an oxygen-free environment to decompose solid wastes into char, oil, and gases. The optimum time was 80 to 120 minutes with particle size of 60 -80 mm^2.By using thermal and biological techniques biomass, waste oil and waste tires feedstocks, they were converted into liquid, solid and gaseous fuel. It was fast pyrolysis with heating rate 10-200°C with bio-fuel yield about 50 -60 % by weight, with gas yield of 10-20%, and char production was very low, as temperature increase reduced the yield. Mass ratio for pine bark(P), tyres (T) and waste oil(O) is 50:30:20, for P:T:O respectively. Gas chromatography -mass spectroscopy was used for chemical analysis. The calorific value was estimated to be 45.6 MJ/kg.

KEYWORDS: biomass, bio-fuel, co-pyrolysis, PET polymers, sustainable energy

INTRODUCTION

In recent decades, rapid economic and industrial growth have increased global energy demand for renewable and sustainable energy to mitigate global warming and air pollution [1]. From the point of view of efficient waste management, the chemical treatment of waste is of scientific importance. Waste can be classified into fossil waste and biological waste [2]. One of the biggest fossil wastes is old tires. Around 1.5 billion tires are manufactured worldwide and are typically thrown into the atmosphere each year. Moreover, major renewable energy source, organic waste has great potential to provide an alternative to fossil fuels for the environment [3]. Therefore, from an ecological and economic point of view, the evaluation of used tires and waste biomass is of great importance. Biomass is largely produced every day, its safe disposal is a big issue, which is treated with thermal decomposition. Pyrolysis "is one of the most effective and comprehensive thermochemical conversion processes for both fossil and biological wastes [4].

LITERATURE REVIEW

In the past, the carbon used for heating was called smoke fuel and was produced by the pyrolysis of woody biomass [5]. The main drawbacks of older pyrolysis technology are energy inefficiency, inefficient manufacturing, and air emissions. Therefore, studies are ongoing to absolutely achieve strength harvesting of biomass for technological increase. Oxidation of the fuel, in which the biomass is absolutely oxidized and converted to heat, is function of the combustion stage. But this manner is set 10% much less green and this utilization contributes to excessive levels of environmental pollutants [6]. Pyrolysis is a mixed mechanism of combustion and gasification. Waste tires along with biomass are used to increase the yield and working efficiency of fuel produced. Pyrolysis is consequently part of an impartial conversion era characterized by means of the formation of solid, liquid, and gaseous fuels from the authentic solid biomass without using gasification and combustion and oxidation[7]. Pyrolysis of organic compounds in biomass feedstocks occurs at temperature without air/oxygen at 700-800 °C. To the best of our knowledge this sort of work has not been done yet, we are still working on it to get the best optimum results. Tires were never used before with biomass and waste oil [8].

Table 1: calorific values of ordinary solid fuels used in different industries[9] Yaqoob *et al.*,(*Sustainability (Switzerland)*, vol. 13, no. 6, Mar. 2021)

Fuels	Calorific Value (MJ/kg)
Bituminous coal	32–36.3
Lignite coal	11.7–15.8
Pet coke	32.0–36
Rubber derivative	36–40
Subbituminous coal	29–30.7

MECHANISM OF CO-PYROLYSIS

The mechanisms of co-pyrolysis and normal pyrolysis processes are almost the same. This process essentially takes place without oxygen at low operating temperatures in a closed reactor system. Three basic steps are essential for co-pyrolysis in petroleum processing: sample preparation, co-pyrolysis, and condensation. The figure shows the procedure used for oil production in co-pyrolysis. Samples should be dried and ground prior to co-pyrolysis. The oven system can be used for a 24-hour drying process at a temperature of 105 °C. For industrial applications, internal thermal energy sources can cover the heat demands of raw material drying through process integration. High oxygen content makes it non-volatile, corrosive, immiscible with fossil fuels, thermally unstable, and capable of polymerizing in air. Both tires and oils can transform them into

various products, mostly liquid products. Bio-oil by pyrolysis and co pyrolysis can be used instead of petroleum to be used as fuel.

CO-PYROLYSIS REACTOR

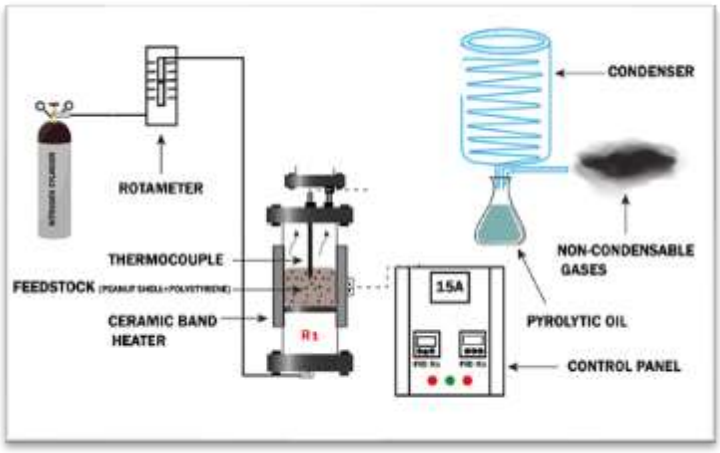

Figure 12 Fixed bed reactor for co-pyrolysis

METHODOLOGY

We collected the waste needed, biomass, tyres, and oil waste. The tire chips and biomass content were washed, dried, and placed in a mild steel fixed bed reactor unit In the reactor, the feedstock was heated without oxygen by oven. The cylindrical reactor is an insulated chamber with an inner diameter of 110 mm, an outer diameter of 115 mm, and a height of 300 mm. The reactor is supplied with 2 kW of power for external heating and the temperature controller is used to regulate the temperature. The reactor retention time was120 minutes maximum. During the process, vapour products moved in the water-cooled condenser and accumulated condensed liquid as fuel. Following was the methodology followed to carry out this research.

In the first chamber of the reactor shown in figure 1, pyrolysis of tire tests occurred in an inactive gas climate (N_2). Therefore, vaporous items were constrained down into the second piece of the reactor where synergist changing occurred within the sight of water fume. The research center scale trial reactor of measurement D = 0.022 m and stature H = 0.16 m was made of hardened steel. The two phases of this reactor were warmed independently by two outer electrical radiators with the choice of controlling the temperature; pyrolysis was done at 500/600 °C and transforming at 800 °C. Parts of co pyrolysis design includes:

Fixed bed reactor

Fixed bed reactor was used and maintained at specific temperature to transform the feedstock into gaseous and then into fuel. Vapor residence time in reactor is an important parameter to achieve maximum yield of liquid. The apparent vapor residence time usually less than second for fast pyrolysis . A cylindrical reactor was designed and fabricated using a stainless-steel pipe. The reactor volume and length were 600 cm it works by heating the feedstock at a temperature more than 700℃ where transformation of feedstock is done with temperature controller attached [10].

Condenser

Due to high temperature the fluid and oil collected is very heated up, by providing cooled water, they were cooled and condensed through pipes [11].

Gas flow (N_2)

Nitrogen is an inert gas, and it was continuously supplied to the reactor to maintain the reactivity and remove the minimum oxygen retain in feedstock [12].

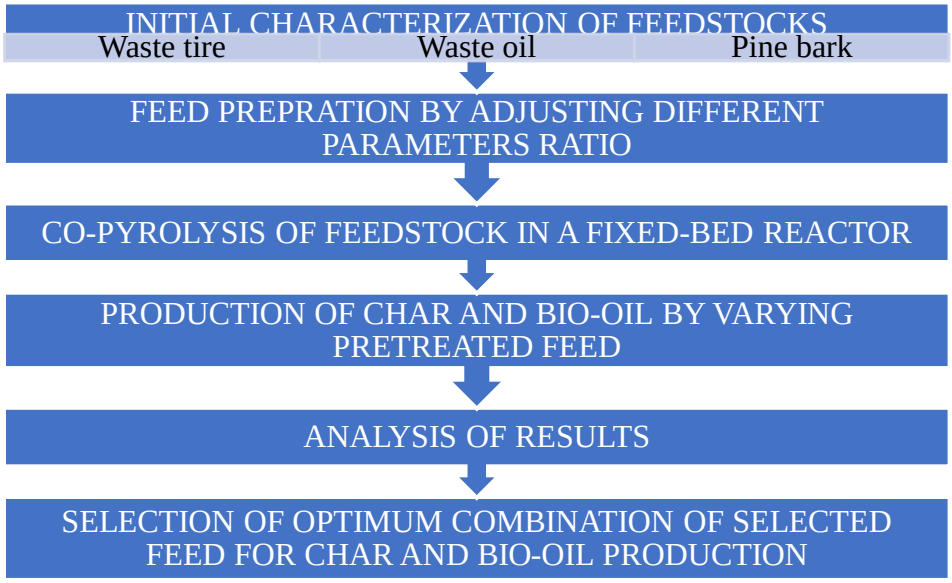

Figure 1 Methodology of co-pyrolysis

BIO-FUEL

Pyrolysis oil is a type of tar and usually contains excessive levels of oxygen considered pure hydrocarbons. This high oxygen content is non-volatile, corrosive, immiscible with fossil fuels, thermally unstable, and can polymerize in air[9]. In this way, it is very different from petroleum products Both tires and oils can transform them into various products, mostly liquid products. H.

Bio-oil by pyrolysis and co-pyrolysis can be used instead of petroleum to be used as fuel. Removal of oxygen from bio-oil or nitrogen from algal bio-oil is called upgrading [13].

FEEDSTOCK

Mass of feedstock used vary with their quantity and yield. For pine bark(P), tyres (T) and waste oil(O) is 50:30:20, for P:T:O respectively.

Figure 2: pine bark

Figure 3: waste oil

Figure 4: Waste tyres

RESULTS AND DISCUSSION

The oil we extracted is not 100 percent efficient, but results obtained shows that its way better than the crude oil, not it can replace diesel but yes, it can be used in many heavy machines and needs a bit refining but still making use of oil from waste is achievement.
Given below is the GM-MS of oil extracted through pyrolysis of our sample.

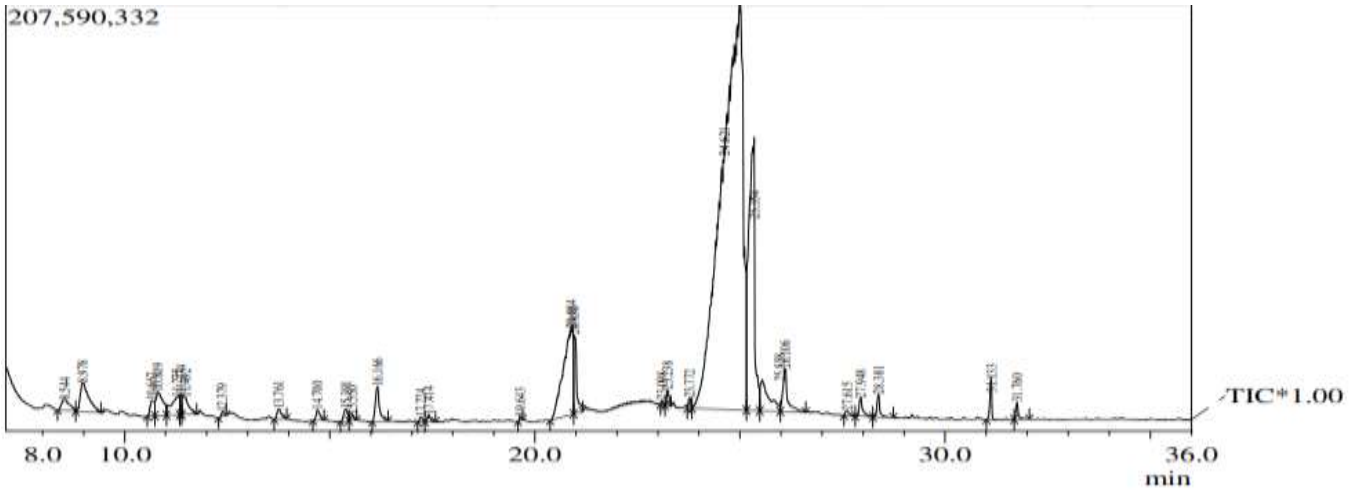

Figure 5 Extracted Oil Sample GC-MS graph.

In evaluation is the fuel chromatograph is offered to recognize how subtle the oil is, in which a capillary”column coated with a stationary (liquid or stable) segment separates the sample into its constituent additives after efficiently vaporizing it into the gasoline phase the retention time of a

chemical is the duration of elution. complex combinations or sample extracts containing loads of different chemical substances can be resolved using GC (fuel chromatography).
An inert provider gasoline, inclusive of helium, hydrogen, or nitrogen, propels the chemical compounds. relying on its boiling factor and polarity, each compound elutes from the column at a special time as additives of the aggregate are separated. Then, expanded molecules and fragments are sent through the mass analyser of the device, which is often a quadrupole or ion trap. right here, ions are divided into groups in line with their various mass-to-fee (m/z) ratios. Ion detection and analysis of fragmented ions can be identified based on their m/z ratios. Conversely, peak regions are related to the amount of the relevant molecule. A complicated sample separated by GC-MS (mass spectroscopy) will result in numerous distinct peaks, each of which generates a distinct mass spectrum utilized for compound "identification.

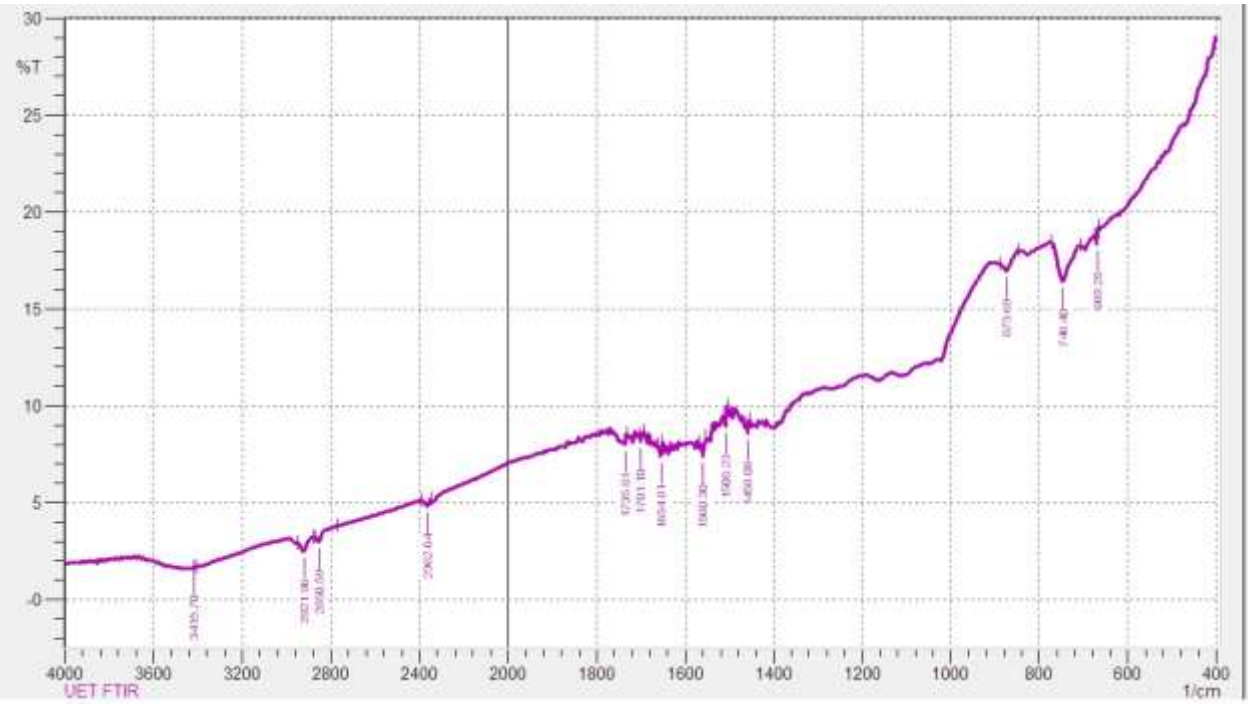

Figure 6:FTIR analysis of BIO-OIL obtained from pyrolysis of waste oil, pine bark and PET

The stretching vibration between 785-540**cm^{-1} is indication of C-Cl functional group. The stretching vibration of 873.69 cm^{-1}** is an indication of C-F functional group. The stretching vibration between 1550-1350cm^{-1} is an indication of N=O or R-NO_2 functional group. The stretching vibration between 1640-1550 cm^{-1} is an indication of N-H functional group. The stretching vibration between 1640-1700 cm^{-1} is an indication of amide or C=O functional group. The stretching vibration between 1725–1700 cm^{-1} is an indication of Carboxylic acid or C=O

functional group. The stretching vibration between 1740–1720cm^{-1} is an indication of aldehyde or C=O functional group. The stretching vibration between 2900-2800 cm^{-1} is an indication of aldehyde or C-H functional group. The stretching vibration between 3000-2850 cm^{-1} is an indication of Alkanes or C-H functional group. The stretching vibration between 3650-3100 cm^{-1} is an indication of N-H or O-H functional group.

REFERNCES

[1] Y. Lu, Y. Wang, J. Zhang, Q. Wang, Y. Zhao, and Y. Zhang, "Investigation on the characteristics of pyrolysates during co-pyrolysis of Zhundong coal and Changji oil shale and its kinetics," *Energy*, vol. 200, p. 117529, Jun. 2020, doi: 10.1016/J.ENERGY.2020.117529.

[2] B. B. Uzoejinwa *et al.*, "Catalytic co-pyrolysis of macroalgal components with lignocellulosic biomass for enhanced biofuels and high-valued chemicals," *Int J Energy Res*, vol. 46, no. 3, pp. 2674–2697, Mar. 2022, doi: 10.1002/ER.7338.

[3] Y. Zhai, Y. Zhu, S. Cui, Y. Tao, X. Kai, and T. Yang, "Study on the co-pyrolysis of oil shale and corn stalk: Pyrolysis characteristics, kinetic and gaseous product analysis," *J Anal Appl Pyrolysis*, vol. 163, p. 105456, May 2022, doi: 10.1016/J.JAAP.2022.105456.

[4] B. Chen *et al.*, "Study of the Co-pyrolysis characteristics of oil shale with wheat straw based on the hierarchical collection," *Energy*, vol. 239, p. 122144, Jan. 2022, doi: 10.1016/J.ENERGY.2021.122144.

[5] A. Shafizadeh *et al.*, "Machine learning predicts and optimizes hydrothermal liquefaction of biomass," *Chemical Engineering Journal*, vol. 445, p. 136579, Oct. 2022, doi: 10.1016/J.CEJ.2022.136579.

[6] P. Otálora, J. L. Guzmán, F. G. Acién, M. Berenguel, and A. Reul, "Microalgae classification based on machine learning techniques," *Algal Res*, vol. 55, p. 102256, May 2021, doi: 10.1016/J.ALGAL.2021.102256.

[7] W. Xu *et al.*, "Identification of paralytic shellfish toxin-producing microalgae using machine learning and deep learning methods," *J Oceanol Limnol*, vol. 40, no. 6, pp. 2202–2217, Nov. 2022, doi: 10.1007/S00343-022-1312-1/METRICS.

[8] W. Xu *et al.*, "Identification of paralytic shellfish toxin-producing microalgae using machine learning and deep learning methods," *J Oceanol Limnol*, vol. 40, no. 6, pp. 2202–2217, Nov. 2022, doi: 10.1007/S00343-022-1312-1/METRICS.

[9] H. Yaqoob *et al.*, "Current status and potential of tire pyrolysis oil production as an alternative fuel in developing countries," *Sustainability (Switzerland)*, vol. 13, no. 6, Mar. 2021, doi: 10.3390/su13063214.

[10] F. Pruvost, S. Cloete, C. Arnaiz del Pozo, and A. Zaabout, "Blue, green, and turquoise pathways for minimizing hydrogen production costs from steam methane reforming with CO2 capture,"

Energy Convers Manag, vol. 274, p. 116458, Dec. 2022, doi: 10.1016/J.ENCONMAN.2022.116458.

[11] M. R. Hamblin, "Shining light on the head: Photobiomodulation for brain disorders," *BBA Clin*, vol. 6, pp. 113–124, Dec. 2016, doi: 10.1016/J.BBACLI.2016.09.002.

[12] F. J. Gutiérrez Ortiz, "Techno-economic assessment of supercritical processes for biofuel production," *J Supercrit Fluids*, vol. 160, p. 104788, Jun. 2020, doi: 10.1016/J.SUPFLU.2020.104788.

[13] N. Dutta, P. Mondal, and A. Gupta, "Optimization of process parameters using response surface methodology for maximum liquid yield during thermal pyrolysis of blend of virgin and waste high-density polyethylene," *J Mater Cycles Waste Manag*, vol. 24, no. 3, pp. 1182–1193, May 2022, doi: 10.1007/S10163-022-01392-Y/TABLES/6.

2nd International Conference on Advances in Civil and Environmental Engineering (ICACEE-2023)

University of Engineering & Technology Taxila, Pakistan

Conference date: 22nd and 23rd February, 2023

Recent Progress in the Use of Capacitive Deionization and Microbial Desalination Cell for Water Treatment - A Critical Review

Abaid Ullah[1], Qurat ul Ain Fatima[2], Muhammad Zafar Iqbal[3], Zoya Mussawar[4]

[1]Department of Environmental Engineering, University of Engineering and Technology Taxila, abaid.ullah@uettaxila.edu.pk

[2]Department of Environmental Engineering, University of Engineering and Technology Taxila, 19-env-9@students.uettaxila.edu.pk

[3]Department of Environmental Engineering, University of Engineering and Technology Taxila, 19-env-32@students.uettaxila.edu.pk

[4]Department of Environmental Engineering, University of Engineering and Technology Taxila, 19-env-5@students.uettaxila.edu.pk

ABSTRACT

The increasing depletion of water resources is a severe obstacle to the sustainable development. Finding new ways to provide clean water is one of the many collaborative activities that will be required to solve this worldwide issue. In this regard, among various methods, electrochemical methods have been used for water treatment. For instance, capacitive deionization (CDI) and microbial desalination cells (MDCs) are capable technologies that can overcome the aforementioned issue. In this regard, current study examines recent advancements in MDC and CDI technologies along with the ongoing research in this field. Moreover, it discusses different configurations of these technologies constructed in the past with different materials and methods to present a better understanding of systems' efficiencies, along with their contribution towards research and development. It further presents the unexplored prospects of MDCs and CDI for future work.

✓ **KEYWORDS:** Capacitive deionization, Energy production, Desalination, Microbial Desalination Cell (MDC), Water treatment.

INTRODUCTION

The world is facing a severe shortage of water. It has been estimated that less than 0.5% of earth's surface is covered with fresh water which is acceptable for human consumption, whereas, 97% of the water is in seas and oceans [1]. Around 25% of the world's population lacks access to drinkable water in a sufficient quantity and quality and more than 80 nations are experiencing a water shortage.

More than 75% of Asia lacks access to clean water, and countries that are home to more than 90% of the region's population are already under a serious water crisis. The gap between water demand and water supply will be 40% by 2030. There is a significant “water stress” issue in Pakistan and this situation is rapidly transitioning to "water shortage" situation and yearly water availability has fallen below 1000m^3 [2]. Thus, there is a need of planning an effective water management approach. Previously, the solutions proposed to manage the water scarcity include construction of massive infrastructure, providing alternative source of water, increasing the supply of water, reducing water usage, revolutionizing water and wastewater treatment [3, 4]. Apart from water saving structures, various methods like multistage flash distillation (MSF), electrodialysis (ED), reverse osmosis (RO) and nanofiltration (NF) have also been used in spite of high-energy consumption to treat saline water sources (e.g., brackish water and seawater). However, these methods are not suitable alternatives for the desalination of saline water due o high energy consumption, brine production and greenhouse gas emissions [5].

Capacitive deionization (CDI) is one of the latest technology for desalination [6]. Compared to conventional processes, its advantages include greater safety, an ability to operate at minimal voltage, no requirement of high-pressure pump and chemical regeneration, quick system cleaning, cost and energy efficiency, and environmentally friendliness [7]. Microbial desalination cell (MDC) is an evolving concept which is a modification of microbial fuel cell (MFC). MDC is used for desalination and treatment of wastewater while generating renewable energy at the same time. It can be integrated with unit operations like electrodialysis and reverse osmosis, and it can also be used as an independent desalination method. Keeping in view the importance of these technologies, this study represents a critical review on the recent researches conducted on both CDI and MDCs.

USE OF CAPACITIVE DESALINATION CELL FOR WATER TREATMENT

CDI has been considered as an innovative, environment friendly, energy efficient and cost-effective technology with a high recovery rate (0.5–1 kWh/m^3) [8]. Electro-sorption and desorption of ion are the two stages for desalination of water by conventional CDI. The two common CDI configurations are flow-by and flow-through CDI (FCDI) [9]. A recent comparison of the long-term stability of these two configurations during desalination indicated that the stability of CDI is enhanced up to 360% by using flow-by configuration which has a lifetime of 18 days as compared to flow-through configuration with a lifetime of 5 days [10]. Due to the existence of a hydrodynamic diffuse boundary layer which inhibits rapid transport of dissolved oxygen to the surface of the cathode, flow-by CDI is a better configuration than flow-through CDI. The reduction of an unequal distribution of potentials in flow-by cells can occur due to the limitation of oxygen reduction on the cathode.

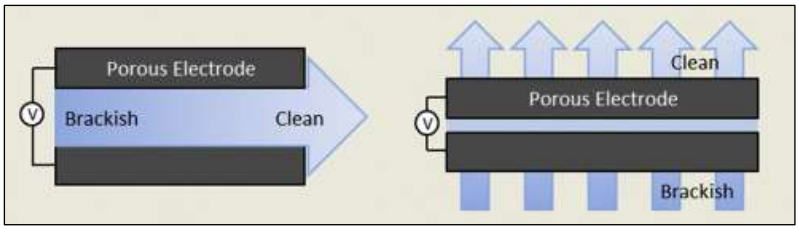

Figure 13: Flow-by vs. flow-through CDI mechanisms.

FCDI is a sustainable saltwater desalination technology with simpler system design and operation, optimized system performance, energy efficient and lower cost with greater ion transport efficiency and adsorption within the electric double layers (EDLs). Unlike other structures, the contact between the adsorbent, dissolved ions and the electrodes is increased by passing the solution in the system directly through macropores of the electrode [11].

Various components are used in the fabrication of lab-scale FCDI cell. These components and their explanation are provided in Table 1.

Table 4: Components of FCDI system.

Components	Details
Current collectors	Graphite, stainless steel, composite current collectors (comprised of graphite paper and acrylic sheets) and titanium plates.

Ion exchange membranes (IEMs)	IEMs can improve the effectiveness of desalination.
Gaskets and spacers	Its job is to not let short circuit happen in the middle of the two current collectors. Some of the gaskets are Silicone, Rubber, Latex [14-16].
Peristaltic pumps	Reducing the feed water flow rate (increasing the residence time of the feed water) improves salt removal efficiency.
End plates	PVC, Polyethylene, Polycarbonates, Stainless steel, Rigid plates of high-density polyethylene (HDPE) and Acrylic.
Power supply	DC power supply is used. FTCDI uses the zero-voltage method, but overtime it decreases the electrode's capacity [17].
Activated carbon (AC) content	5% by weight, 7.5% by weight, 10% by weight, and 12.5% by weight. Desalination performance and charge efficiency improves over time when the AC content is raised (i.e., at 12.5% by weight) [18].
Electrode material	Anode and cathode can be in the form of mesh, graphite plate-based, titanium mesh-membrane, activated carbon and stainless steel.
Faradaic reactions	Influences electrode performance and lifespan, energy efficiency, production of chemical and pH fluctuations of the product water [19].
Hydrodynamic voltammetry	Important for carbon slurries' electro-chemical behavior and to accelerate the speed of transport of mass towards the electrode in a specified way.

USE OF MICROBIAL DESALINATION CELL FOR WATER TREATMENT

Microbial desalination systems come from the root of microbial electrochemical systems in which biological reaction helps to remove salt from saline water and generate electricity, it consists of three chambers i.e., anode chamber, cathode chamber and desalination chamber. The anode chamber facilitates microbes for energy generation and wastewater treatment, while desalination chamber treats saline water [20].

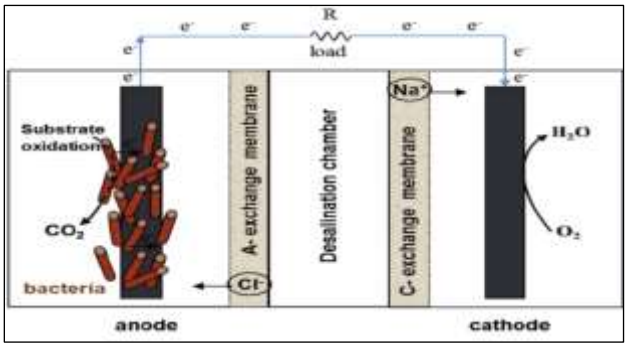

Figure 14: Schematic of microbial desalination cell.

Design Configurations of Microbial Desalination Cell

✓Various design configurations of MDC have been developed by previous researchers including (a) air cathode MDC, (b) bio-cathode MDC, (c) stack structure MDC, (d) recirculation MDC, (e) microbial-electrolysis desalination and chemical-production cell, (f) capacitive MDC, (g) up-flow MDC, (h) osmotic MDC, (i) bipolar membrane MDC, (j) decoupled MDC, (k) separator-coupled stacked-circulation MDC, (l) ion-exchange resin coupled MDC, as explained below.

Air Cathode Microbial Desalination Cell

An air-cathode MDC is made up of three chambers i.e., cathode chamber, anode chamber, and desalination chamber. The cathode chamber contains a cathode that has its external side exposed to the atmosphere for oxygen which serves as terminal acceptor of electron. Platinum and cobalt tetra-methoxy-phenyl-porphyrin has been broadly used as catalyst in air cathode MDC [21].

Bio-cathode MDC

The bio-cathode MDC is made up of a cathode that can utilize microbial biofilm attached onto the cathode that function as a catalyst to aid in the reduction of oxidant. Bio-cathode has been categorized into two domains i.e., aerobic and anaerobic bio-cathodes. In aerobic bio-cathodes, O2 acts as the electron acceptor. Whereas, terminal electron acceptor can be of different catholytes in anaerobic bio-cathode [22].

Stack Structure MDC

It is built with two desalination chambers with anode exchange membranes (AEMs) and cathode exchange membranes (CEMs) between them. Incorporating several ion exchange membranes (IEMs) in arrangement of series results in the enhancement of charge transfer efficiency (CTE) which leads to greater rate of desalination. This configuration permits movement of anions and cations produced within the desalination chamber per number of electron pulse in the external circuit. This mechanism results in improved desalination rate and better CTE [23].

Recirculation MDC

In this type, catholyte and anolyte are recirculated to resolve the problem of pH. For this purpose, both electrolytes are flown via an exterior channel or conduit between the cathode and anode compartments [24].

Microbial-electrolysis desalination and chemical-production cell (MEDCC)

It is a modification of microbial electrolysis desalination cell (MEDC) in which a bipolar membrane (BPM) is placed between AEM/CEMand anode/cathode chamber to produce acid/alkali [25]. In a recent study, alkali and acid production chambers were used for dissolving serpentine and absorbing atmospheric carbon dioxide, respectively [26].

Capacitive MDC (cMDC)

This design uses the combination of CDI and MFC to overcome pH problem of electrolytes. In this configuration, a double layer capacitor is used to stop the migration of anion and cations to cathode and anode chambers though absorption. Later, a novel configuration of cMDC was developed in which the capacitive deionization was used within the MDC. Generally, it consists

of two elements i.e., ion-exchange membrane (IEM) and carbon cloth (as the double capacitive layer) which is inserted between electrode chambers and desalination chamber [27].

Up-Flow MDC (UMDC)

It is a battery-cell like structure that consists of two chambers in co-axial formation. The desalination occurs in the external chamber, and the internal chamber acts as the anode, which are separated by IEMs. Meanwhile, the external layer of UMDC performs the function of cathode, the AEM is wrapped across the anode chamber's external face and the CEM is located outside the desalination chamber [28].

Osmotic MDC (OsMDC)

In this configuration, the AEM of conventional MDC is replaced with a forward osmosis membrane to get more effective water recovery. The intent of this set-up is to make the water from anode section move to desalination section and restrict migration of ions to the anode/cathode compartments from the desalination section. This in turn increases efficiency of the system [29].

Bipolar membrane MDC (BMP-MDC)

The Bipolar membrane in an MDC is made up of CEM and AEM, which are pasted together by a physical operation like pressing which serves as a transitional layer that dissociates the saline water when a voltage is applied. Unlike the conventional MDC, it contains four sections, where the unit which converts salt into base and acid is situated adjacent to the anode compartment [30].

Decoupled MDC

It is made up of anode and cathode units situated between separate containers that are placed in a salt solution. The cathode and anode chambers are constructed in plate configuration with CEMs and AEMs on every side of the chambers. The support structure is a stainless-steel mesh wrapped with a carbon cloth as a current collector. Moreover, a decoupled MDC can also be fabricated with many cathode and anode units connected in series. The catalyst used in decoupled MDC is a combination of three materials i.e. carbon, powder, Nafion layered carbon cloth and platinum [31].

Separator-coupled stacked-circulation MDC (c-SMDC-S)

A total of five chambers are fitted in this configuration including a concentrate chamber, two desalination chambers, an anode chamber and a cathode chamber. The anode chamber has activated carbon particles that enhance the growth of bacteria, and a graphite rod [32]. In this set-up, an air cathode is used which consists of a carbon cloth having one side exposed to air and the other attached with a piece of glass, acting as a separator. It also connects the anode and cathode chamber through a channel for recirculation of electrolyte which is facilitated by an external electrolyte chamber providing buffer free electrolyte [33].

Ion-exchange resin coupled MDC (R-MDC)

In this type, conventional MDC's desalination chamber is filled with cation and anion exchange resins. Generally, the electrodes used in its designing are graphite rods that contain carbon for better electrical conductivity [34].

The power density, chemical oxygen demand (COD) removal capacity, columbic efficiency, and desalination efficiency of above-mentioned configurations are shown in Table 3.

Table 5: Technical efficiencies of different MDC configurations.

Configuration	Power Density	COD Removal	Columbic Efficiency	Desalination Efficiency	Reference
Air-Cathode MDC	480 mW/m^2	-	-	43% to 67%	[21]
Bio-Cathode MDC	-	-	96.2%.	92 %	[35]
Stack Structure MDC	11.8 W/m^3	-	450%	93.4%	[36]
Recirculation MDC	931 mW/m^2	-	-	55 ± 2%	[24]
MEDCC	-	94%	-	22%	[26]
cMDC	-	-	-	88%	[27]
Upflow MDC	38.9W/m^3	-	-	73.8% - 99%	[28]
OsMDC	160W/m^3	-	-	57.8% - 95.9%	[37]
BMP- MDC	-	-	62% - 97%	50% - 63%	[23]
Decoupled MDC	360 mW/m^2	-	78%	95% - 98%	[34]
c-SMDC-S	-	89%	28%	40% - 81%	[38]
R-MDC	650 mW/m^3	78%	58%	93% - 100%	[32]

Table 3 shows that since different configurations of MDCs exhibit variable efficiencies, therefore, it is pertinent to comparatively analyze them. For this purpose, strengths and limitations of these configurations are provided in Table 4.

Table 6: Strengths and limitations of different configurations of MDCs.

Configuration	Strengths	Limitations	Reference
Air-Cathode MDC	High reduction potential and minimal toxic effects of oxygen.	Redox kinetics are slow, high power input and costly.	[25]
Bio-Cathode MDC	Low-cost, no requirement of expensive catalyst, generation of chemicals, concentration of oxygen, and electron received are increased.	-	[25]
Stack Structure MDC	Increase in internal resistance enhances desalination, requires less voltage and produces more energy.	pH imbalance, acidification of anolyte, higher HRT and water loses.	[25]
Recirculation MDC	Balances pH and improves capacity of power density.	Four-fold decrease in the columbic efficiency (CE).	[25, 39]
MEDCC	Better energy recovery, greater CTE, better power density.	High internal resistance and pH imbalance.	[24]
cMDC	pH balance of catholyte and anolyte.	-	[24]
Up-flow MDC	Scaling up is easier, requires no external mixing and makes oxidation more efficient.	-	[25, 40]
OsMDC	High electricity generation, saline water dilution and high treatment capacity.	Membrane biofouling, low columbic efficiency and reduction in separation.	[40, 41]

Configuration	Strengths	Limitations	Reference
Bipolar Membrane MDC	Minimal drop in voltage, efficient membrane selection, low resistance. extended life period, produces chemical, and pH balance.	Requires external energy and is costly.	[29]
Decoupled MDC	Configured electrodes are efficient, varying liquid volume ration is simpler, and easier to control and dismantle, repair, replace and scaling up.	-	[25, 40]
c-SMDC-S	Better CE, avoids pH imbalance, prevents biofouling on the cathode and runs for extended time periods.	-	[38]
Ion-exchange resin coupled MDC	Better charge transfer, less energy consumption and ohmic resistance	Scaling on IEMs, high internal resistance and columbic efficiency drop.	[40]

WAY FORWARD TO FUTURE STUDIES

Future studies on CDI can be conducted on multi-salt composition saline water to understand CDI practicability on real sea water, further studies on characterization of high concentrate wastewater, optimum electrode pore size for effective removal of salts, energy recovery from electrodes, exploring different type of materials for flow-electrodes with high conductivity and greater suspension, selective ion removal from FCDI, removal of negatively charged contaminants (e.g., bacteria), positively charged contaminants (e.g., cationic dyes) and nano-plastics need to be explored. The FCDI is better in large scale applications than CDI and can be explored for more economical full-scale studies. Moreover, in full-scale design, there is a need for pre-treatment and post-treatment of the wastewater. Therefore, full-scale setup of CDI need to be studied to utilize this technology to its full capacity.

Similarly, studies regarding MDCs should be focused on the development of ion-exchange membranes with better resistance to biofouling. Moreover, materials like carbon nanotubes, activated carbon, graphite and other carbonations should be tested for the construction of anode to provide greater surface area and superior bonding of exoelectrogenic bacteria. Various microbial species can also be used in the process of bio-cathode. In addition, finding an effective and sustainable approach for the stabilization of pH in the anode chamber to promote the growth of microbes, and genetic modification of the exoelectrogenic bacteria to enhance their columbic efficiency can be tested in future. Alongside, various types of wastewaters can be explored to assess their treatment and columbic efficiencies. This aspect implies that there is a need of a full-scale set-up design to deeply understand the feasibility and applicability of MDCs.

CONCLUSION

Studies conducted on CDI and MDCs have been reviewed, which are two advanced water desalination technologies that have been the subject of research and development in recent years. Major parameters influencing CDI are capacitance, cell volume, applied voltage, and flow rate. FCDI is the advanced version of CDI, and its most important parameters are conductivity and inter-particle connectivity of the flow electrode material. The literature shows that the MDC is significantly influenced by the exoelectrogens on the biofilm and the electrode material (anode and cathode). In summary, the integration of CDI and MDC has the potential to revolutionize the field of water desalination, thereby providing an efficient and effective solution for producing fresh water. However, further research and developments are needed to fully realize the potential of this technology.

REFERENCES

1. Zou, M.M.a.L., *A study of the capacitive deionisation performance under various operational conditions.* 2012.
2. Parry, J., et al. . *Making Every Drop Count: Pakistan's growing water scarcity challenge*. September 29, 2016 [cited 2022 27 Nov]; Available from: https://www.iisd.org/articles/insight/making-every-drop-count-pakistans-growing-water-scarcity-challenge.
3. Hashim, H.Q. and K.N. Sayl, *Detection of suitable sites for rainwater harvesting planning in an arid region using geographic information system.* Applied Geomatics, 2021. **13**(2): p. 235-248.
4. Zhou, L., et al., *Novel perspective for urban water resource management: 5R generation.* Frontiers of Environmental Science & Engineering, 2021. **15**(1): p. 1-13.
5. Ihsanullah, I., et al., *Desalination and environment: A critical analysis of impacts, mitigation strategies, and greener desalination technologies.* Science of the Total Environment, 2021. **780**: p. 146585.
6. Xing, W., et al., *Versatile applications of capacitive deionization (CDI)-based technologies.* Desalination, 2020. **482**: p. 114390.
7. Choi, J., et al., *Applications of capacitive deionization: Desalination, softening, selective removal, and energy efficiency.* Desalination, 2019. **449**: p. 118-130.
8. He, D., et al., *Faradaic reactions in water desalination by batch-mode capacitive deionization.* Environmental Science & Technology Letters, 2016. **3**(5): p. 222-226.
9. Guyes, E.N., A. Simanovski, and M.E. Suss, *Several orders of magnitude increase in the hydraulic permeability of flow-through capacitive deionization electrodes via laser perforations.* RSC advances, 2017. **7**(34): p. 21308-21313.
10. Cohen, I., et al., *The effect of the flow-regime, reversal of polarization, and oxygen on the long term stability in capacitive de-ionization processes.* Electrochimica Acta, 2015. **153**: p. 106-114.

11. Son, M., et al., *Improving the thermodynamic energy efficiency of battery electrode deionization using flow-through electrodes.* Environmental Science & Technology, 2020. **54**(6): p. 3628-3635.
12. Choo, K.Y., et al., *Study on the electrochemical characteristics of porous ceramic spacers in a capacitive deionization cell using slurry electrodes.* Journal of Electroanalytical Chemistry, 2019. **835**: p. 262-272.
13. Nativ, P., Y. Badash, and Y. Gendel, *New insights into the mechanism of flow-electrode capacitive deionization.* Electrochemistry Communications, 2017. **76**: p. 24-28.
14. Ma, J., et al., *Analysis of capacitive and electrodialytic contributions to water desalination by flow-electrode CDI.* Water research, 2018. **144**: p. 296-303.
15. Ma, J., et al., *Energy recovery from the flow-electrode capacitive deionization.* Journal of Power Sources, 2019. **421**: p. 50-55.
16. Hatzell, K.B. and Y. Gogotsi, *Suspension electrodes for flow-assisted electrochemical systems*, in *Nanomaterials in Advanced Batteries and Supercapacitors*. 2016, Springer. p. 377-416.
17. Zhang, X., et al., *Flow-electrode capacitive deionization utilizing three-dimensional foam current collector for real seawater desalination.* 2022. **220**: p. 118642.
18. Chen, T.-H., et al., *Cation selectivity of activated carbon and nickel hexacyanoferrate electrode materials in capacitive deionization: A comparison study.* 2022. **307**: p. 135613.
19. Zhang, C., et al., *Faradaic reactions in capacitive deionization (CDI)-problems and possibilities: A review.* 2018. **128**: p. 314-330.
20. Liu, Q., B. Xie, and D. Xiao, *High efficient and continuous recovery of iodine in saline wastewater by flow-electrode capacitive deionization.* Separation and Purification Technology, 2022: p. 121419.
21. Mehanna, M., et al., *Microbial electrodialysis cell for simultaneous water desalination and hydrogen gas production.* Environmental science & technology, 2010. **44**(24): p. 9578-9583.
22. Huang, L., J.M. Regan, and X. Quan, *Electron transfer mechanisms, new applications, and performance of biocathode microbial fuel cells.* Bioresource technology, 2011. **102**(1): p. 316-323.
23. Kim, Y. and B.E. Logan, *Microbial desalination cells for energy production and desalination.* Desalination, 2013. **308**: p. 122-130.
24. Qu, Y., et al., *Simultaneous water desalination and electricity generation in a microbial desalination cell with electrolyte recirculation for pH control.* Bioresource technology, 2012. **106**: p. 89-94.
25. Al-Mamun, A., et al., *A review of microbial desalination cell technology: configurations, optimization and applications.* Journal of Cleaner Production, 2018. **183**: p. 458-480.
26. Zhu, X. and B.E. Logan, *Microbial electrolysis desalination and chemical-production cell for CO2 sequestration.* Bioresource technology, 2014. **159**: p. 24-29.
27. Forrestal, C., P. Xu, and Z. Ren, *Sustainable desalination using a microbial capacitive desalination cell.* Energy & Environmental Science, 2012. **5**(5): p. 7161-7167.

28. Jacobson, K.S., D.M. Drew, and Z. He, *Efficient salt removal in a continuously operated upflow microbial desalination cell with an air cathode.* Bioresource technology, 2011. **102**(1): p. 376-380.
29. Chen, X., et al., *Optimization of membrane stack configuration in enlarged microbial desalination cells for efficient water desalination.* Journal of Power Sources, 2016. **324**: p. 79-85.
30. Buck, R., *Ion-selective membranes and electrodes, Access Science*. 2014, McGraw-Hill Education.
31. Ping, Q. and Z. He, *Improving the flexibility of microbial desalination cells through spatially decoupling anode and cathode.* Bioresource technology, 2013. **144**: p. 304-310.
32. Morel, A., et al., *Microbial desalination cells packed with ion-exchange resin to enhance water desalination rate.* Bioresource technology, 2012. **118**: p. 43-48.
33. Chen, S., et al., *Improved performance of the microbial electrolysis desalination and chemical-production cell using the stack structure.* Bioresource technology, 2012. **116**: p. 507-511.
34. Zhang, F., et al., *Microbial desalination cells with ion exchange resin packed to enhance desalination at low salt concentration.* Journal of membrane science, 2012. **417**: p. 28-33.
35. Wen, Q., et al., *Using bacterial catalyst in the cathode of microbial desalination cell to improve wastewater treatment and desalination.* Bioresource Technology, 2012. **125**: p. 108-113.
36. Ge, Z., C.G. Dosoretz, and Z. He, *Effects of number of cell pairs on the performance of microbial desalination cells.* Desalination, 2014. **341**: p. 101-106.
37. Zhang, B. and Z. He, *Improving water desalination by hydraulically coupling an osmotic microbial fuel cell with a microbial desalination cell.* Journal of membrane science, 2013. **441**: p. 18-24.
38. Chen, X., et al., *Sustainable water desalination and electricity generation in a separator coupled stacked microbial desalination cell with buffer free electrolyte circulation.* Bioresource Technology, 2012. **119**: p. 88-93.
39. Shehab, N.A., et al., *Microbial electrodeionization cell stack for sustainable desalination, wastewater treatment and energy recovery.* Proceedings of the Water Environment Federation, 2013. **2013**(19): p. 222-227.
40. Saeed, H.M., et al., *Microbial desalination cell technology: a review and a case study.* Desalination, 2015. **359**: p. 1-13.
41. Tawalbeh, M., et al., *Microbial desalination cells for water purification and power generation: A critical review.* Energy, 2020. **209**: p. 118493.

2nd International Conference on Advances in Civil and Environmental Engineering (ICACEE-2023)

University of Engineering & Technology Taxila, Pakistan

Conference date: 22nd and 23rd February, 2023

TREATMENT OF TEXTILE WASTEWATER BY INTEGRATED ROTATING BIOLOGICAL CONTACTOR AND FENTON PROCESS

Sadia Fida[1], Talha Saleem[1], Ridha Batool[1], Maria Yasmeen[1], Muhammad Zeeshan[1,2,3]

[1] Department of Environmental Engineering, University of Engineering and Technology, Taxila 47080, Pakistan

[2] German Environment Agency, Section II 3.3, Schichauweg 58, 12307, Berlin, Germany

[3] Technische Universität Berlin, Water Treatment, KF4, Str. des 17. Juni 135, 10623, Berlin, Germany

ABSTRACT

Textile wastewater, mainly from dyeing and printing units, needs proper treatment before its disposal into the water bodies. Different physicochemical, biological, and combined treatment processes were applied to remove dyes. However, the efficiency of a rotating biological contactor (RBC) coupled with the Fenton process for textile wastewater has yet to be investigated. Herein, lab-scale three-stage RBC coupled with the Fenton process was used to treat real textile wastewater. The hydraulic retention time (HRT) for RBC unit was 12 h and 30 min for the Fenton process unit. The results revealed that chemical oxygen demand (COD), biological oxygen demand (BOC), and total suspended solids (TSS) were removed above 85 %. In addition, 92 % reduction in color was observed. Overall, the effluent produced from RBC and the Fenton process was safe for disposal and reusable.

KEYWORDS: Textile, Wastewater, Rotating biological contactor, Fenton process

INTRODUCTION

Wastewater of textile units contains many pollutants such as inorganic compounds, dyes, color residues, catalytic chemicals, and cleaning solvents. It has been studied that worldwide, the production of dyes is 700,000 tons each year [1]. Some of these dyes are degraded naturally, but some need special treatment, as they cannot be degraded naturally. In addition, different types of dyes are chemically different from each other [2, 3]. The textile industry consumes large quantities of water and a variety of chemicals. Textile wastewater contains substantial pollution loads in terms of chemical oxygen demand (COD), biological oxygen demand (BOD), total suspended solids (TSS) and heavy metals. Color removal, especially from textile wastewater, has been a big challenge. Thus, effective strategies to remove dyes need to be developed [4]. Textile wastewater needs to be treated as it can cause severe health impacts to aquatic life and human beings [5]. Therefore, it is an utmost need to treat textile wastewater so that problems related to water pollution caused by it can be avoided.

Different treatment techniques such as rotating biological contactor (RBC) and the Fenton process are effectively studies to treat textile wastewater. Previously, RBC was used for the decolorization of wastewater (textile dyes) and colored sugar refinery effluents [6, 7]. Goyal, Sreekrishnan et al.

(2010) reported that RBC removed COD and color above 90 %. Sreeja and Sosamony (2016) reported that the Fenton process removed COD and dye from textile wastewater by 47 % and 82 %, respectively [8]. 95 % decolorization was found using 0.10 g/L of Fe(II), and 2.20 g/L of hydrogen peroxide (H_2O_2) for 90 min at pH 3 for the Fenton process [9]. However, to the best of our knowledge, the performance of RBC integrated with the Fenton process for textile wastewater treatment is not investigated. This study investigated the performance of the RBC coupled with the Fenton process for the real textile wastewater.

MATERIALS AND METHODS

Experimental setup

A lab-scale model of a three-stage RBC followed by the Fenton process was erected (Fig. 1). It consisted of five main parts; (1) primary sedimentation tank (PST), (2) RBC reactor, (3) secondary sedimentation tank (SST), (4) Fenton process unit and (4) clarifier. The primary sedimentation tank has an effective volume of 5 liters and a hydraulic retention time (HRT) of 2 h. The effective volume and HRT of RBC reactor were 15 liters and 12 h, respectively. RBC module consisted of three identical stages connected in series. Initially, each stage comprised of 4 disks (each 6 mm carpet mat with 3 mm acrylic as a support material) and disks were reduced to 3 in the later stages to determine their effect on treatment efficiency. Approximately 40% of disks were submerged into the wastewater in RBC reactor.

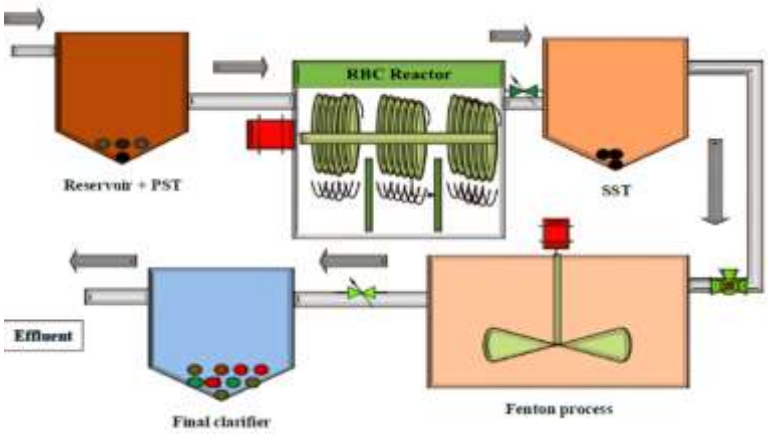

Figure 1: Schematic of experimental setup consisted of a three-stage RBC followed by Fenton process.

Chemical coagulation was conducted using jar test and various dosages of hydrogen peroxide (H_2O_2) and ferrous sulphate ($FeSO_4$) were used.

Wastewater sampling and characterization

Untreated wastewater samples (12 liters) were collected from a textile industry every two months. The collected samples were stored at 4°C. Initial wastewater characterization was performed

within 24 h using the standard methods for the examination of water and wastewater. The parameters tested and the testing procedure used are shown in Table 1.

Table 1: Test parameters and test procedures

Sr. No.	Parameters	Testing procedures
1.	pH	4500-H
2.	Colour	2120-B
3.	TSS (mg/L)	2540-D
4.	BOD_5 (mg/L)	5210
5.	COD (mg/L)	5220
6.	Nitrates (mg/L)	4500-NO_3
7.	Phosphates (mg/L)	4500-P

RESULTS

Wastewater characterization

Results of the initial characterization of untreated textile wastewater indicated that pH was 12.8. Concentrations of TSS, COD, BOD and dissolved oxygen (DO) were 969, 2976, 1095 and 0.2 mg/L, respectively. The temperature of the wastewater was approximately 30 ^oC. The wastewater discharged by the industry contains high level of COD, BOD and TSS and very low level of DO.

Optimum operating conditions for Fenton process

Different doses of H_2O_2 and $FeSO_4$ were used in the Jar test. These doses were decided on the basis of the molar ratio of ferrous to hydrogen peroxide. 1:5, 1:10, 1:15 and 1:20 molar ratios were adopted to reduce the major concerned parameters from the effluent of RBC process (Fig. 2). 1:10 and 1:15 comes out to be the optimum doses with the help of the jar test. This dose was added and results were tested by keeping the speed range from 40 to 110 rpm. 80 rpm was the optimum speed, further used in the Fenton reactor.

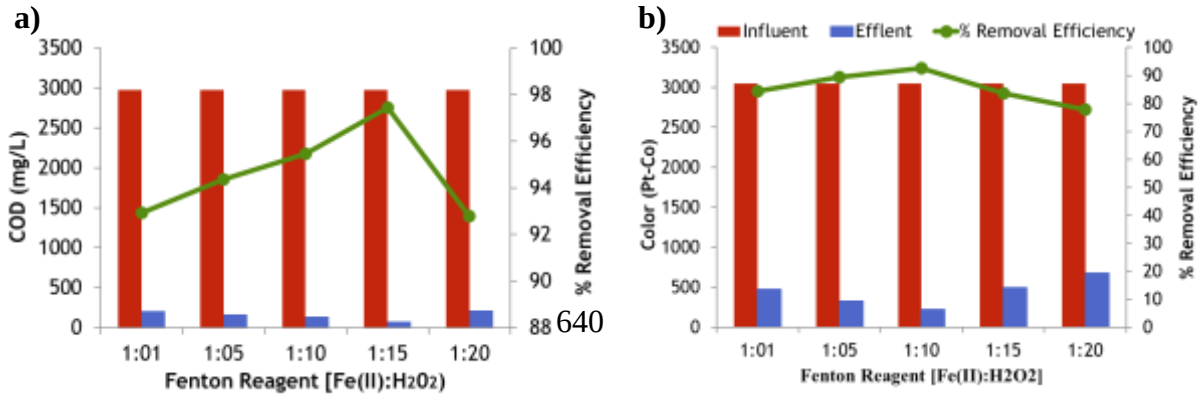

Figure 2: Optimum dosage of hydrogen peroxide (H_2O_2) and ferrous sulphate ($FeSO_4$) for (a) COD and (b) color reduction.

Treatment efficiencies

The results indicated that removals of quality parameters were increased with increased operational time (Fig. 3). Maximum removals using RBC were observed after 15 days of operation. A significant removal (upto to 80%) of TSS was observed. Removals of nitrates and phosphates were less than 20 %, whereas COD and BOD removals were less than 60 %. The poor removals of COD and TSS are attributed to the presence of refractory organic compounds, which were hardly biodegradable. These refractory compounds cannot be readily removed and always remain in the effluent of the biological treatment process [10].

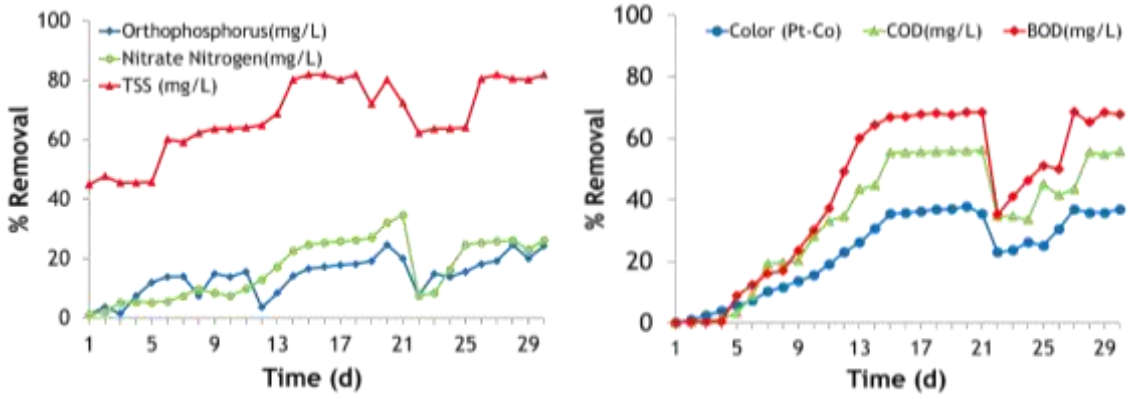

Figure 3: Percentage (%) removal of different quality parameters through RBC.

The overall removals were significantly increased in RBC coupled with Fenton Process (Fig. 4).

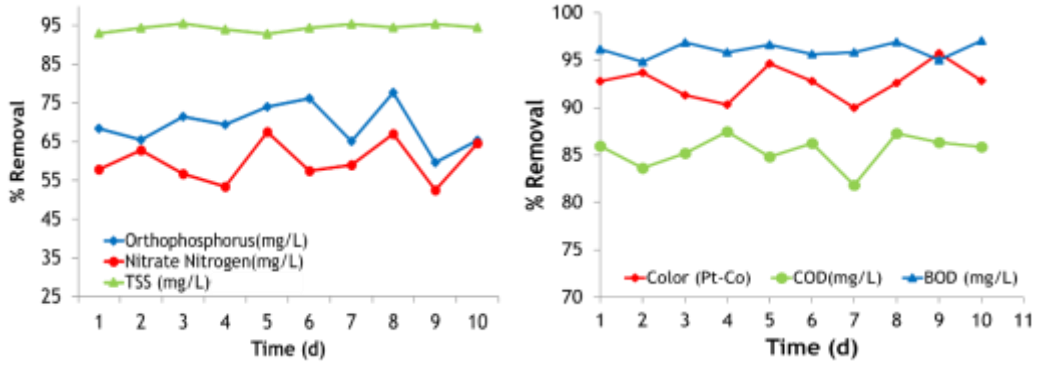

Figure 4: Percentage (%) removal of different quality parameters through RBC coupled with Fenton process.

The removals of TSS, COD and BOD were above 85 %. Higher removals of the quality parameters indicate that RBC coupled with Fenton Process produced effluent of reusable quality and for safe disposal.

CONCLUSION

This study applied the integrated biochemical treatment (RBC coupled with the Fenton process) to treat textile wastewater. The results indicated that COD, BOD and TSS removals were less than 60 % during three-stage RBC. Whereas nitrates and phosphate removals were less than 20 %. In the integrated system, the TSS, BOD and COD removals were above 85 %. Thus, the integrated system increased the effluent quality and produced effluent of reusable quality.

REFERENCES

1. Shanker, U., M. Rani, and V. Jassal, *Degradation of hazardous organic dyes in water by nanomaterials.* Environmental chemistry letters, 2017. **15**: p. 623-642.
2. Puvaneswari, N., J. Muthukrishnan, and P. Gunasekaran, *Toxicity assessment and microbial degradation of azo dyes.* 2006.
3. Babu, B.R., et al., *Cotton textile processing: waste generation and effluent treatment.* Journal of cotton science, 2007.
4. Imtiazuddin, S., M. Mumtaz, and K.A. Mallick, *Pollutants of wastewater characteristics in textile industries.* J Basic App Sci, 2012. **8**: p. 554-556.
5. Khan, S. and A. Malik, *Environmental and health effects of textile industry wastewater.* Environmental deterioration and human health: natural and anthropogenic determinants, 2014: p. 55-71.
6. Axelsson, J., et al., *Decolorization of the textile dyes Reactive Red 2 and Reactive Blue 4 using Bjerkandera sp. Strain BOL 13 in a continuous rotating biological contactor reactor.* Enzyme and Microbial Technology, 2006. **39**(1): p. 32-37.
7. Guimarães, C., et al., *Continuous decolourization of a sugar refinery wastewater in a modified rotating biological contactor with Phanerochaete chrysosporium immobilized on polyurethane foam disks.* Process Biochemistry, 2005. **40**(2): p. 535-540.
8. Sreeja, P. and K. Sosamony, *A comparative study of homogeneous and heterogeneous photo-Fenton process for textile wastewater treatment.* Procedia Technology, 2016. **24**: p. 217-223.
9. Cetinkaya, S.G., et al., *Comparison of classic Fenton with ultrasound Fenton processes on industrial textile wastewater.* Sustainable Environment Research, 2018. **28**(4): p. 165-170.

10. Oller, I., S. Malato, and J. Sánchez-Pérez, *Combination of advanced oxidation processes and biological treatments for wastewater decontamination—a review.* Science of the total environment, 2011. **409**(20): p. 4141-4166.

2nd International Conference on Advances in Civil and Environmental Engineering (ICACEE-2023)

University of Engineering & Technology Taxila, Pakistan

Conference date: 22nd and 23rd February, 2023

Controlling Leachate Infiltration from Dumping Sites By Sustainable Liner From Waste Material

Urwa Zahra1, Saira Shabbir1, Malieka1, Maria Aamir1, Erum Aamir1 * and Babar1

1 Institute Of Environmental Science & Engineering (IESE), National University Of Sciences & Technology, H-12 Islamabad.

Corresponding author erum@iese.nust.edu.pk

Abstract

Leachate is one of the main sources of soil and groundwater contamination. This is an important issue for countries like Pakistan where groundwater is one of the main sources of freshwater. Pakistan requires landfill liners to protect their groundwater resources and citizen health. Because Municipal Solid Waste (MSW) dumping in open sites is one of the most common practices in Pakistan. To address this critical groundwater and soil pollution problem, this research is dedicated to designs liners. The novelty of the study is not only to make simple affordable, cost-effective, efficient sustainable liners with the help of plastic and straw. This research will not only reduce soil and groundwater contamination but will also diminish MSW by using them as raw materials for liner. For liners waste material once collected and crushed laid in layers after mixing with clay is subjected to different tests to check and compare its performance. First, the permeability test, moisture content (MC), cracking, seepage and life span were carried out with different amounts of Plastic Waste (P.W) and Straw Waste (S.W). Both P.C and S.C were mixed with compacted clay at (0.3%, 0.5% and 0.8%). Seepage depth was figured out by measuring the moisture content (MC) at different depths of soil and cracking of both liners was observed by examining the texture of the liners, in order to determine their loading capacity and stabilization. The mechanism supports that the lesser the leachate penetrates, the lower the permeability of the liner and the greater the efficiency of the liner. The liner with a straw content of 0.3%, had minimum permeability (1.05 x 10^(-7)cm/s) and hence optimum straw content was considered as (0.3%) that is (0.23 kg) mixed with (7.8 kg) clay; penetrated to the depth of 10cm and lesser moisture content of (16%) whereas compacted clay of permeability (1.62 x 10^(-6)cm/s) penetrated to a depth of (15cm) with a moisture content of (29.9%). This research. The research improves environment and reduces pollution. Research also addresses two SDG's namely SDG# 3 (good health and well-being), and SDG# 11(sustainable cities and communities).

Keywords: Municipal Solid Waste, leachates, infiltration, straw, groundwater, soil, and pollution.

Introduction

Pakistan is the fifth largest country in the world, which produce about 32.6 million metric tons of MSW per annum with an average waste generation rate of 0.43 kg/capita/day (Mohsin et al. 2020; Ali et. al. 2019 Municipalities manage to collect only 50–60% of generated MSW in Pakistan (Soho et al. 2021). Pakistan is facing serious issues regarding the management of solid waste (Iqbal et al. 2022). Landfill is one of the safest ways to dispose of waste. The major problem with landfill is the production of leachate. The generation of leachate is increased by precipitation over the waste. This waste with water can infiltrate into the underground through a phenomenon called leaching and can pollute well, aquifers and groundwater reservoirs, (Nikbakht et al. 2023). Also, with the passage of time waste can decompose and affect human health by causing pollution. So, there is a dire need to build a properly engineered landfill to avoid this problem that can reduce leachate infiltration and thus avoid groundwater pollution.

So, it is essential to manage increasing solid waste by constructing landfill liners using readily available and relatively cheap material to decrease the permeability of the soil and reduce leachate infiltration and ultimately reduce groundwater pollution which would be environment-friendly practice. The main objective of this research is to design a sustainable layer from waste material that minimizes the infiltration of leachate into underground aquifers to prevent groundwater pollution. Groundwater is a major water source in Pakistan and its contamination can cause severe health and environmental problems (Ishaque et al. 2023). If we can reduce the leachate infiltration to underground water reservoirs, then we will be able to ensure the well-being of people relying on underground water sources for their daily use. This research also targets the use and proper utilization of the potential of wastes like wheat straw and plastic to produce high-efficiency and economical landfill liners. Synthetic liners are extremely expensive $1/m^2 (Kerry L. Hughes, 2018) which equals Rs. 250. /m^2 making these liners, not a feasible option to use, especially be a developing country like Pakistan. To overcome this problem, this research proposed the fabrication of cost-effective and high-efficiency liners using very cheap materials like: Plastic waste & Straw waste.

Methodology

The methodology conceived to achieve the objective of this research is summarized in the figure Lysimeter was built using acrylic material to perform the research using waste material namely plastic and wheat straws. The lysimeters would be filled with an equal depth of 30cm of normal soil. The first practical lysimeter would contain a 15 cm liner above the soil layer. This is the liner that will be constructed using clay and plastic waste. The second practical lysimeter would contain a liner of equal height, but instead of plastic waste wheat straw would be added to the clay to form the liner.

This lysimeter would contain a compacted clay liner of 5.00 cm which is already being used in many research papers to control leachate infiltration. The purpose of making a prototype model in this study is to compare the efficiency of the other 2 liners with this conventional method. Nearly 1-inch gravel layer will be placed below the soil layer to form the base layer of the lysimeter for proper drainage of leachate into the collection system installed at the bottom. Municipal Solid Waste (MSW) will be placed above the liner and the lysimeter will be kept under observation and leachate production would be monitored. The slope given to the base of the lysimeter will help to collect the leachate if it penetrates all the layers below the dumped waste. The efficiency of the liners would depend on the infiltration rate into the soil below the liners. The efficiency of the liners would depend on the infiltration rate into the soil below the liners. The leachate collection system is installed below each lysimeter in case the leachate penetrates the soil thickness in that case the liner efficiency will depend on the volume of leachate collected in the collection system.

The liner would be composed of the following material:

Compacted clay amalgamated with plastic waste.

Compacted clay amalgamated with straw waste.

Initially, it was planned to construct different lysimeters but due to financial constraints, only one lysimeter is used turn by turn to conduct the planned methodology. It is important to monitor permeability, seepage cracking etc. under similar conditions to all the different liner systems so that the only variable i.e is the liner composition. This will help us in an effective comparison of the efficiency of the liners.

Results and analysis

This experiment was to be performed twice, each time replacing only the liner while keeping all the other factors constant. The efficiency of two fabricated liners using plastic waste and wheat straw amalgamated with compacted clay will be studied. The major characteristics of liners were compared and finally the liner with the greater performance efficiency was declared as the most feasible liner to control leachate infiltration in dumping sites.

Optimum straw content

Once the determination of waste composition and average rainfall, the next step was to determine the optimum content of straw that would be used for the fabrication of clay liner mixed with straw. The optimum straw content was calculated by varying the straw content in clay and calculating the permeability using the Falling head method. The amount of straw that resulted in minimum permeability was declared to be the optimum wheat straw content in clay for fabrication of liner.

Straw content (%)	Wt of Straw (g)	Wt of clay (g)	Permeability (cm/sec)

0.0 %0.0 203 1.62 x 10^(-6)

0.3% 0.6 201.74 1.05 x 〖10〗^(-7)

0.5% 1.01 201.33 8.38 x 10^(-7)

0.8% 1.61 200.73 10 x 10^(-7)

It is evident from the above stated results that the optimum content of wheat straw in clay turned out to be 0.3% and the corresponding permeability of 1.05 x 〖10〗^(-7). Hence the liner made using clay mixed with straw waste contained 0.3% straw by weight 3.2. In addition to this same test were carried out for plastic waste and the optimum plastic waste in soil came out to be 0.6%" which is same as reported by Jaya and Sunil, 2011 in their study "Soil stabilization using raw plastic bottles". Such remarkable resemblance with other study gives further validation and weightage to this study and proves that addition of plastic to clay improves its characteristics prominently its permeability is reduced, whereas its strength and load bearing capacity are increased. The addition of plastic to clay also retards its cracking ability and decreases its void ratio. All these facts favor the concept that clay mixed with plastic waste can also prove to be a better barrier against leachate infiltration in dumping sites hence can be used as an effective liner material.

After that comes the most interesting part of the study where performance efficiency comparison of the two-liner fabricated clay mixed with plastic and clay mixed with straw waste after conducting both the experiments and making all the observations.

Comparison based on leachate seepage.

Another factor that helped us compare the performance efficiency of PW mixed clay liner and clay liner mixed with straw waste was the seepage extent at different depths below the liner, at the end of the observation period. The moisture content at different depths was calculated simply by the difference in the weight of soil before and after oven drying at 100 degrees Celsius for 24 hours. The results of moisture content at different depths for the compacted clay liner and clay liner amalgamated with straw waste are summarized in the table 2 below:

Depth of liner + soil 5cm 10cm 15cm

Soil+ plastic waste liner was installed 34.9% 33% 29.9%

Soil+ straw waste liner was installed 26% 16% 12%

It is evident from the table that the clay mixed with straw liner proved to be a much impressive barrier for the leachate infiltration as at depths of 5, 10 and 15cm in the soil below the liner the moisture content was relatively significantly less than the moisture content at same depths for simple compacted clay liner. This fact helps us conclude that clay improved by mixing the optimum content of straw i.e., 0.3% reduces the clay permeability to such an extent where it transforms into a better barrier for leachate infiltration. The graph below again depicts the seepage extent at different depths for compacted clay liner and clay liner mixed with straw waste.

Comparison of cracking

The cracking performance of compacted clay could be assessed by the cracking intensity factor (CIF) which is the ratio of crack area and the total area (Miller et al., 1998; Yesiller et al., 2000). In this study visually inspection of the cracks were done as there was no equipment to do so. The extent for both the liners and compare the properties of cracks to conclude which liner among the two has minimum cracks and can act as a better barrier against leachate infiltration. The figures given below shows the extent of cracking for both the liners. When comparing the cracking of liner fabricated using compacted clay and liner fabricated using straw waste mixed with compacted clay at the end of the observation period. It turned out that the drying and wetting cycle resulted in deep crisscrossed cracks in case of compacted clay liner, while there were only a few shallow cracks for the clay mixed with straw. For compacted clay-fiber mixture, the horizontal tensile strength had been improved by straw fiber as well as friction between soil particles and fibers, which increases the resistance of clay to cracking (Harianto et al., 2008).This fact again gives us a reason to conclude that clay liners improved with straw serves as a better barrier against leachate infiltration, because the deeper and greater the cracks the more easily the leachate penetrates into the soil below.

The cracking results also helped us conclude that in addition to reduction of permeability the straw added to clay also improved its tensile strength due to the greater cohesion of the particles among each other and with wheat straw fiber.Results indicate that the mixed soil with plastic waste is stronger than plain clay therefore plastic waste is a useful consideration in soil improvement and also has less crack. The results were in line with the outcome reported with 1.5% and 3.0% plastic waste study by Soltani-Jigheh, 2016.

Performance efficiency on cracking

Parameters clay liner with straw waste Clay liner with straw waste

Cracking performance Maximum (Deep cracks all over the surface) minimum (no obvious cracks visible)

Seepage depth 15 cm 10 cm

Permeability	1.62 x 10^(-6) cm/sec	1.05 x 10^(-7) cm/sec

The table given summarizes the 3 major parameters and their results in case of using clay liner and in case of using clay liner improved by adding straw. The cracking for compacted clay is much greater than that of clay improved by straw. The seepage depths also show a greater performance efficiency of straw mixed with clay liner and the low permeability of the clay liner improved with straw again favors the fact that it is a much impressive barrier against leachate infiltration as compared to simple compacted clay liner. The extent of cracking, seepage depth and permeability all favor the greater efficiency of clay mixed with straw liner to be used as a landfill barrier to retard the leachate infiltration. Hence these results help us conclude that clay improved with straw is a preferable material to be used as landfill liner as compared to simple compacted clay.

Performance efficiency of Liner of compacted clay improved with plastic waste:

Results shows that the significant improvements in the strength of plastic waste mixed soils due to increased friction between soil and plastic waste and the development of tensile stress in the plastic. It proves the clay resistance to cracking which is important to know as if the landfill liner would contain cracks, it would provide a convenient flow path for rainfall hence increasing the amount of leachate from MSW in landfill. Also, according to another research paper by Benson showed that cracking caused the hydraulic conductivity of clay liner to increase by about three orders of magnitude.

Addition of plastic waste changes the undrained behavior of samples. Undrained behavior can be explained as “If no drainage is possible from a soil, because the permeability is so small that there is no time for outflow of water. This is the undrained behavior of a soil hence it proves that adding the plastic reduces the permeability to that extent that leachate cannot be entered or leave the liner easily” (Arnold, 2017). The consolidation tests show that the initial void ratio of plain soil is higher than that of plastic mixed samples and decreases as the plastic waste content increases. As we all know that the greater the void ratio, the higher the value of the coefficient of permeability so as the void ratio decreases, the permeability also decreases, and seepage will be less using the plastic waste in clay.

The result from experiments, facts and figures extracted from the different research papers gave us the proof that the addition of plastic to clay improves its characteristics prominently its permeability is reduced, whereas its strength and load bearing capacity are increased. The addition of plastic to clay also retards its cracking ability and decreases its void ratio. All these facts favor the concept that clay mixed with plastic can also prove to be a better barrier against leachate infiltration in dumping sites hence can be used as an effective liner material.

Conclusions

The objectives of this study were to, use waste materials for controlling leachate infiltration in, and their comparison in terms of cost, life span, permeability and benefit. By using waste materials that are readily available like wheat straw and plastics and the results led to the conclusion that, the minimum life span is of compacted clay that is 1-2 years whereas compacted clay improved by straw waste lasts in a range 2-10 years depending on the moisture content, the greater the moisture content, the lesser will be the life span of straw liner. Whereas the plastic has the maximum life span of 450 years according to the research paper composite landfill liner design by Haluk Akgun published in April, 2005. All the liners are cost-effective because there are from waste material, but they all need compaction, sieving, land, labor, and installation costs whereas compacted clay is relatively cheaper than straw and plastic liners because the later two liners require additional crushing and cutting cost too.

Time required to construct and install compacted clay liners is lesser than straw and plastic liner due to the additional time needed in the process of crushing and cutting of straw and plastic waste.

Benefits of these liners are all are economical but straw liner is more durable and stronger than compacted clay liner but might be lesser than plastic liner as per research papers as plastic has higher resistance. The straw liner has lower permeability than compacted clay liner, but plastic liner might have even lower permeability than the straw liner.

Conflict of interest: NIL

References

Mohsin, M.; Khan, A.A.; Nasar-u-Minallah, M.; Barkat, T. Assessment of municipal solid waste management practices in Bahawalpur city, Pakistan. Int. J. Econ. Environ. 2020.

Ali, M.; Geng, Y.; Robins, D.; Cooper, D.; Roberts, W.; Vogtländer, J. Improvement of waste management practices in a fast expanding sub-megacity in Pakistan, on the basis of qualitative and quantitative indicators. Waste Manag. 2019, 85, 253–263.

Sohoo, I.; Ritzkowski, M.; Sohu, Z.A.; Cinar, S.Ö.; Chong, Z.K.; Kuchta, K. Estimation of methane production and electrical energy generation from municipal solid waste disposal sites in Pakistan. Energies 2021, 14, 2444

Iqbal A, Abdullah Y, Nizami AS, Sultan IA, Sharif F. Assessment of solid waste management system in Pakistan and sustainable model from environmental and economic perspective. Sustainability. 2022 Oct 5;14(19):12680.

Nikbakht M, Sarand FB, Dabiri R, Hajialilue Bonab M. Investigation of the Leachate Effect on Permeability and Geotechnical Characteristics of Fine-Grained Soil Modified Using Nanoclay–Nanofiber Composites. Water. 2023 Jan;15(2):294

Ishaque, W., Mukhtar, M. and Tanvir, R., 2023. Pakistan's water resource management: Ensuring water security for sustainable development. Frontiers in Environmental Science, 11, p.10.

Haluk Akgun(April, 2005) Composite landfill liner design with Ankara clay, Turkey

W. Chen, Y.-Q. Dong(January, 2014) Feasibility study of clay containing straw fiber as landfill liner material

Uma Shankar, V. Rekha (July, 2017)A comprehensive review of different materials as liners in landfills

Dhanya Jaya, Arya Sunil(December, 2011) soil stabilization using raw plastic bottles

Kerry L. Hughes, Ann D. Christy, and Joe E. Heimlich(2018) Landfill types and liner systems

Minnesota Pollution Control Agency(May, 2006) guidance for soil construction standards and testing frequencies – Landfill Cell Construction

Soltani-Jigheh, H. (2016). Compressibility and Shearing Behaviour of Clayey Soil Reinforced by Plastic Waste, Iran University of Science and Technology 2016

L.Douglas, J. H. S. C., (September 1967). Straw Decomposition, s.l.: Agricultural Extension Service Agricultural Expersiment Station College of Agriculture University of Idaho.

R.P VORONY', E. P. a. D. A., (13 September 1988). Decomposition of wheat straw and stabilization of microbial products, s.l.: Department of Land Resource Science, University of Guelph, Guelph, Ontario.

Verruijt, A., (26 July 2017). Undrained Behaviour of Soils, s.l.: Theory and applications of transport in Porous Media.

Xingwei Ren, Y. Z. Q. D. ,. J. K. D. L. D. W., (31 August 2016). A relation of hydraulic conductivity- void ratio for soils based on Kozeny-Carman equation, s.l.: Faculty of Engineering, China University of Geosciences, Wuhan, China.

Xue Qiang*, L. H.-j. L. Z.-z. L. L., (6 June 2014). Cracking, water permeability and deformation of compacted clay liners improved by straw fiber, s.l.: State key Laboratory of Geomechanics and Geotechnical Engineering, Institute of Rock and soil mechanics, Chinese Acedmy of Sciences, Wuhan 430071, China

2nd International Conference on Advances in Civil and Environmental Engineering (ICACEE-2023)

University of Engineering & Technology Taxila, Pakistan

Conference date: 22nd and 23rd February, 2023

A Review Article: Comparison of Different Rainwater Harvesting Technologies for Improving Sustainability in Water Management Practices

Babar Abbas[1], Waqas Qamar Zaman[2], Fahim Khokhar[2], Waheed Miran[3], Qaiser Uz Zaman[1], Asma Khan[2], Syeda Lubaba[2], Shazry Uba[2] and Zonaira Tariq[2]

1.Department of Environmental Engineering, University of Engineering and Technology, Taxila, 47050

2.Institute of Environmental Sciences and Engineering, National University of Science and Technology (NUST), Islamabad 44000

3. School of chemical and materials engineering, National University of Science and Technology (NUST), Islamabad 44000

ABSTRACT

Formation of an area with smart technique application is emerging topic nowadays. Human civilization can never be obtained without sustainable and prosper water availability. Hence, water is vital in human life. This article describes water conservation along with its smart use in different areas and advances in handling those issues. This article will describe the rainwater harvesting technologies and smart use of harvested water. Thus, using rainwater for different buses will eventually enhance sustainability. Harvested rainwater is natural water used for various purposes if stored efficiently. Rainwater harvesting is a system which is involved in capturing, collects and stores rainwater from rooftops. The typical uses of rainwater include irrigation, ground water recharge, flushing and many more potable and non-potable purposes. With additional filtration and disinfection, harvested rainwater can safely be used for the potable purposes following drinking water quality standards to provide potable water supplies to facilities.

Keywords: Rainwater Harvesting Technologies, Smart Water Usage, Sustainability.

INTRODUCTION

Water shortage and degraded environment has become a biggest challenge of 21st Century. The United Nation's Agenda 2030 involves maintenance of 17 Sustainable Development Goals (SDGs). Water is linked with every SDG. Discussing mainly SDG 11 which is to ''Make cities safe and sustainable''. These researches are important for targeting SDG's also. Sustainable solutions refer to integrated approaches, including technical, financial, and environmental problems (Wong, 2020). Considering all these factors, rainwater harvesting is the well-known technique to cater water shortages and use it for potable or non-potable purposes (Demeke, 2021). Rainwater harvesting is the most reliable and effective technique for the storage and proper usage of rainwater that runs off from rooftops, open grounds, and for many areas from where rain water can be stored. Rainwater Harvesting provides a best way and a good alternative to fulfil he demands of water usage and utilization. It is a good source of water utilization and for storage

purposes. Estimations show that if water naturally be stored and treated will help reduce water shortage. It is effective and will reduce water shortages (Ahammed, 2006).
It is observed that if this concept continues to be adopted in several areas and countries, the use of this rain water will be made efficient for potable purposes also by passing through high quality effective treatments. Pakistan has already crossed the "water scarcity line" in 2007, according to the Pakistan Council of Research in Water Resources (PCRWR). In the areas, where the large amount of rain water can be stored this technique is very beneficial for multiple purposes and for the conservation of energy. The rain water is a natural source of water and it should be preserved for the usage in future in order to sustain the future generation needs for water. It is very beneficial thus an extremely economical way of preservation of rain water for multipurpose. In essence, an increased water storage will eventually be helpful to bear the loss which can be faced in future due to water scarcity. It is estimated that Pakistan is at the deadline of water consumption and if this threat continues to prevail the way it is prevailing and will cause a serious threat for future (Anderson, 2003). Therefore, different rainwater harvesting technologies are required to be aligned for rainwater management and then their comparison in order to choose most suitable technique for the best utilization of rainwater. The factors which are mainly focused while making comparison includes determination of (Ngigi, 2003):

- Intended uses
- Importance of water quality
- Human health risks and treatment for mitigating risks.

RAINWATER HARVESTING: NEED OF HOUR (ARGUMENTS)

1. When rainfall occurs and is not captured, then the runoff interacts with surface flow resulting in pollution (Engr. Babar & Sikandar, 2022).
2. Also, in the areas where marble industry is not functioning properly and the industries are not managing its rainwater properly, so there the rainwater mixes with such wastewater and damages fertile land resulting in pollution (Ahmad, 2012).

- Rain Centers

Rain Centre are established to provide briefing regarding rainwater harvesting. Nowadays, it spreads information related to significance of rain. It describes the influence of collected rainwater from roofs or surfaces (Kalungu, 2015). The rain centers educate people to harvest rainwater during rainy season (Anderson, 2003).

SUSTAINABILITY IN WATER MANAGEMENT PRACTICE

Rainwater harvesting (RWH) ponds are emerging factor promoting sustainability in water management practices. It will help reduce stress on water resources. People are actually lacking the awareness regarding the value and importance of ponds. About 78 to 80% of the ponds were failed to sustain (Boers, (1982)). The objectives sustainability in management of water are diverse.

Practices include control of large flows of water in fields, by using natural stream beds excessive flows of water can be prevented without allowing the water to get wasted, forming proper areas for flood control and water conservations, and storing water for irrigation contributing to water protection in several ways (Ayesha & Fatima, 2022).

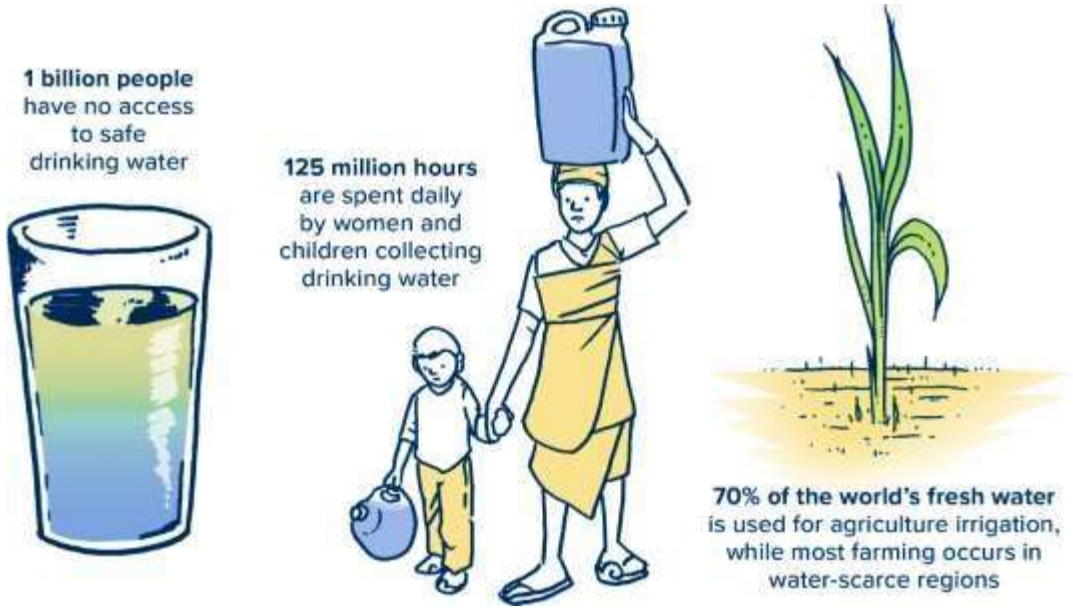

Figure 1. Water Conservation in Irrigation Can Increase Water Use Source: Corral-Verdugo, V., Bechtel, R. B., & Fraijo-Sing, B. (2003)

The collection of rainwater in tanks, containers from different collection points such as roofs has been practiced in Africa and Asia for many years. Discussing the situation of Ethiopia, rainwater harvesting pond are required to provide water for various purposes in agriculture field. The present water shortages are very alarming and the quick management and conservation of this resource is very important (Demeke, 2021). However, this technique was not found to be sustained for many years and was not so stable in water conservation. Various factors which were causing hindrance included (gender, education, and age) and some economic parameters (wealth status, social status, and household perception) (Kalungu, 2015).

1.3 RAINWATER HARVESTING TECHNIQUES

The two main rainwater harvesting techniques include:

- Surface Runoff Harvesting
- Rooftop Rainwater Harvesting.

During the past years, environmental related issues have drastically increased and resulted in the utilization of handsome amount of cost for achieving clean water goal for living beings. The collection and storage of water from the atmosphere has become very rising issue these days and to collect such water will be the demand in near future as the need of water consumption is increasing but the resources to fulfil these needs are depleting (Kalungu, 2015). So, a rainwater harvesting model was required to capture large amount of water wasted as runoff during rain seasons. The microstructure design methods of the water-collection are a new step towards advancements (Meera, 2006).

In addition to this advancement by microstructure design, the better quality and sustainability of the water-harvesting materials is also very important, which is much neglected but is worth to be reported. It is required to have knowledge and study on how to improve the stability and suitability by these structures for overcoming water shortage issues. The variety in water-collecting materials and rainwater harvesting technologies is increasing and more and more advancements are made in this regard with the passage of time depending on the basic intended usage (Abdulla, 2009).

The comparison of rainwater harvesting techniques for improvement of sustainability in water management practices will be discussed in next section of the paper.

COMPARISON OF DIFFERENT RAINWATER HARVESTING TECHNOLOGIES

Rainwater harvesting is a technique for the collection and storage of rainwater from different surfaces, etc. Usually, there are main techniques of rainwater harvesting which includes surface runoff harvesting and rooftop rainwater harvesting. Rainwater is collected by the underground tank which is provided in first technique (Ahammed, 2006). In the second one, rainwater is collected from roof top then it is stored. Rainwater collected from ground is reported to be polluted for potable usage whereas if rainwater is received from the rooftop then the water comparatively suitable for potable purpose (Boers, (1982)).

Rooftop Catchment

The rooftop serves the purpose of a catchment. The quantity of this collected rainwater depends on the different factors including the material of the roof. Other materials such as galvanized iron, concrete, cement, should be preferred over it. The catchments need proper washing from dirt, leaves (Ngigi, 2003). A rainwater harvesting system involves a collection area, a conveyance system, and storage network. The roof of a house or a building is usually set as a collection point. Rainwater that is falling over the roof is transferred to storage via a conveyance system, which typically contains gutter.

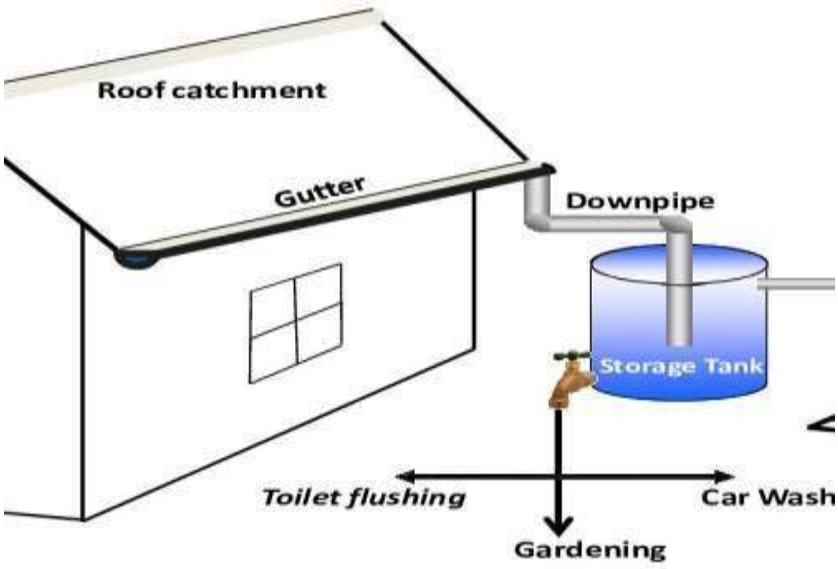

Figure 2. Application of Rainwater Harvesting Technique through Rooftop Catchment (Source: Lye, D. J. (2009))

In order to eliminate the impacts on water quality and roofs, the surfaces should be made chemically inert by using some specified materials. Water is sent to the storage tank in order to get stored. Materials such as steel, fiberglass are commonly used for the construction of tanks. Storage tanks can be created to store water and it is used to typically used to conserve the natural resource and it is located usually at some space away from the structure.

Land Surface Catchment

Runoff will be increased by installation of network of pipes. This technique is effective for irrigation purpose. It is required to enhance the slope by artificial ways. The steeper the slopes, more there are chances of runoff collection and the water will be collected quickly. This technique reduces evaporative losses (Campisano, 2017). The function of collection equipment is to collect rainwater which requires proper setup for the collection of rainwater in chambers. It can be a storage tank. Storage tanks can be installed above or under the ground. Then the conveyance structures which are the structure which is necessary for the primary treatment of rainwater to remove impurities. Then the filtering system which is to make the collected rainwater usable, it must be filtered for removal of all sort of contaminants.

Figure 3. RWH using land surface for catchment area and reservoir for storing rain-off (Source: Mun, J. S., & Han, M. Y. (2012))

There are various filtering systems such as sand filter charcoal filters and PVC filters. Rainwater harvesting in this case is very easy to implement and utilizes less operational and maintenance cost and is less complex for collecting rainwater. In this the runoff capacity is usually enhanced by utilizing various techniques and the land surface is used including collection of runoff and storage of collected water. The ground catchment techniques provide more opportunity than the rooftop catchment for collecting water from greater surface area. By controlling the flows of streams in small storage reservoirs and these are made by using little cost. Examples may include dams, this technology can meet water demands during any period especially during dry season when more water is demanded and required. There is a possibility of water loss during the process of infiltration and, because of the quality of the water collected, this is recommended as a good and beneficial technique for the storage of water for many purposes. Various techniques are there for enhancing the runoff in ground catchment areas which involve: i) clearing vegetation cover, ii) increasing the land slope iii) reducing soil permeability, this can be done by the technique of compaction of soil and usage of different chemicals (Daoud, 2022).

Rock and Surface Catchment System

Catchment areas which uses a bed of rocks for the storage of rain water. A rock catchment is a kind of ground catchment in which rocks are used to make a bed of rock as source of surface runoff stored in either a tank or a dam (Machiwal, 2017).

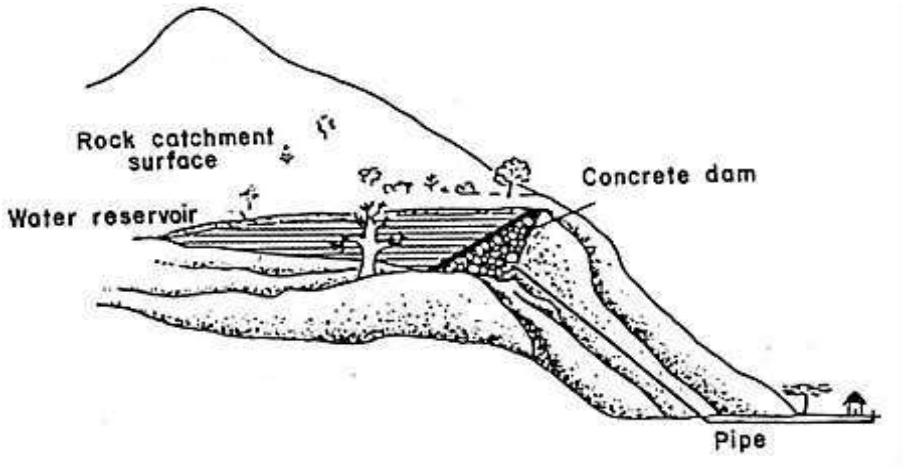

Figure 4. Rock catchment system (Source: Pantelidis, L. (2010))

Rock catchments are, distinguished from roof and surface catchment systems on the basis of various factors such as distinguished gravity flow supplies. Where in suitable sites there exist rock catchment dams are most easy and simple to operate and effective types of rainwater storage system for rock catchments and in various localities where the rock catchments and surface. The water collected from a rock catchment can transfer by gravity to simple storage tanks to the nearby villages and it will enhance sustainability. The runoff moves over the stone and cement made gutters which are constructed on the rock surface in the storage tanks that are contained by using the materials such as concrete or stone dams. These can give a larger quantities of water.

2.1.4 Subsurface Dam and Sand Dam

In sand dams, rainwater is allowed to collect in small containers. These are structures of mud, stone, cement. Another form uses hand-dug wells for water extraction. These are called subsurface dams (GhaffarianHosein, 2016). Much treatment is not required in this case. Such structures are very useful in arid and semiarid locations. The harvesting water can be used for domestic, cattle, and gardening. Sand dams and subsurface dams are made to store the water under the ground. A sand dam is not a big dam and it is used to store water into the riverbed. Sand is collected on the which causes an enlarged groundwater storage capacity.

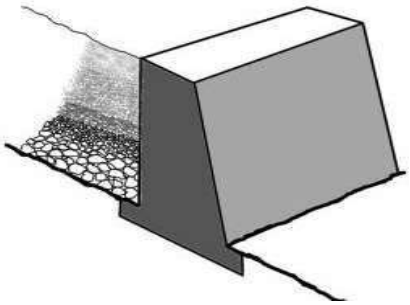

Figure 5. Subsurface Dam and Sand Dam (Source: Lasage, R., Aerts, J. C. J. H., Mutiso, G. C., & De Vries, A. (2008))

Similar to sand dam and a subsurface dam the groundwater flow of a water bath and it is used to store water below the ground surface level. Sand and subsurface dams are in rural areas which are required to store only seasonal available water for livestock, irrigation and for various domestic usage. The high level of investments is required and it is very labor intensive and proper expertise is needed. A sand dam is prominently build over the ground level and there are certain conditions which should be maintained in this. The main aim of it is to capture and store water that accumulates, during the rainwater resulting in additional groundwater storage capacity (Van Ogtrop, 2012). This reservoir is obviously filled the rainy days but the water can be made useful for usage in summer seasons and it should be built in such a way that it should be just out of the reach of the community. But during the dry season water is fully available for the provision. The water quality is most important factor that needs serious considerations as the water can be made clean by using even improved through natural filtration.

Earth Dams Like Ponds and Pans

Earth or mud dams are effective in storage. Such dams are categorized into three types. Hillside dams, charco dams, which are for hilly and flat surfaces. Valley dams are constructed by digging the earth surface. This will eventually increase volume. Before nature was performing the phenomenon of rainwater harvesting (Lopes, 2017). An earth dam is having different layers and they are built in in a layer of 250–400 mm thick, having heavy machinery. The material has 'optimum' value and it is also necessary that need to be flexible.

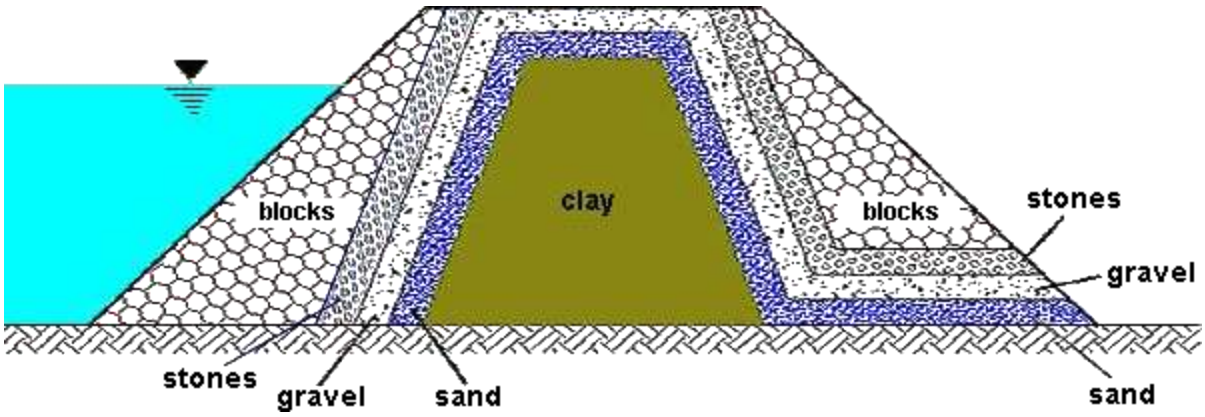

Figure 6. Typical Cross Section of Earth Filled Dams (Source: Lasage, R., Aerts, J. C., Verburg, P. H., & Sileshi, A. S. (2015))

If the soil is too wet, the compaction is not possible. Soil used in the way that it is necessary to achieve this, the water content is necessary to maintain and have a proper moisture content. It is said that if the soil is too dry, effective compaction cannot be done. The water within the soil is affected when it is under the construction process. When the soil is pressed by compaction process the water pressure in the pores will eventually increase. The air in the soil can go in two path it can move out or it can readily move in, increasing the saturation. As the effective strength of the soil is decreased by the less pore size and due to the pressure, the dam can become unstable (Pacey, 1986). Heavily over-loaded clay, such as the Oxford Clay at low stresses can result in the compaction and the pore water pressures are often decreased and this will result in strengthening of the soil.

Recharge Structures

Surface water can recharge the ground water. Rainwater harvesting has proven the best technique for recharging the ground water. It helps in water conservation. The main purpose of this is to restore, reuse, reclaim and recycle the water of underground as water is the most used and utilized resource. Recharge can be by following ways (Sivanappan, 2006);

- Recharging bore wells and dug wells
- Recharge pits
- Shafts Recharging
- Recharge trench

Those areas where conditions are good, groundwater can be recharged to create a pond of water which is used for the recharge. This can be done to overcome the losses due evaporation and results increase water quality.

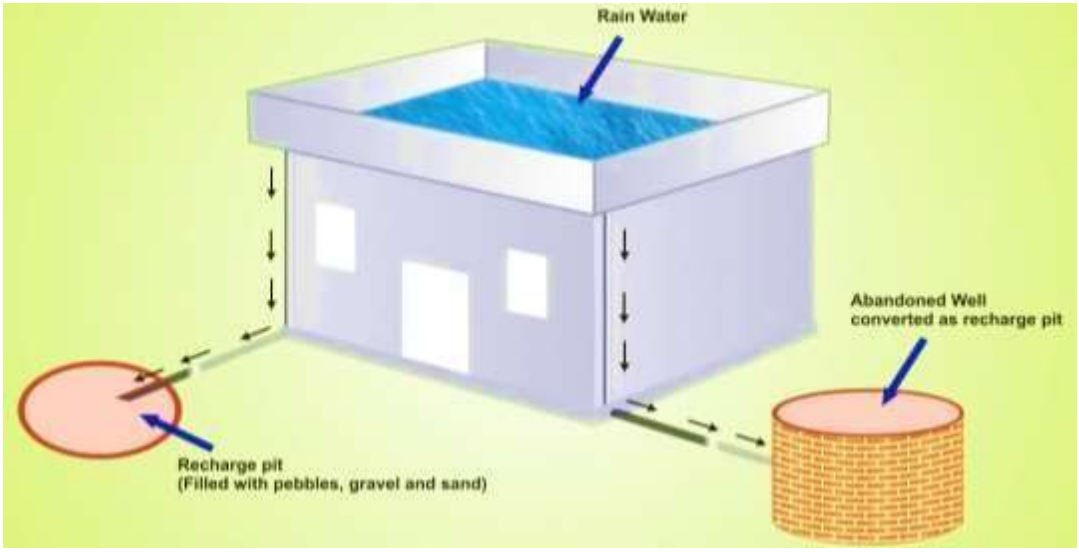

Figure 7. Recharge Structures for Groundwater Recharge (Source: Zeng, C. F., Zheng, G., Xue, X. L., & Mei, G. X. (2019))

Recharge structures can be easily dug in the soil, to a bore well which is converted for recharge solutions. Recharge structures are useful in the areas where the water would not have a time to sink into the ground. The structures are located in smaller areas where water is flowing naturally in to the stream. Another good area is in such a way that it is behind a check dam, at this point water is so that the water is lowered and has enough time for infiltration.

2.1.7 Conservation Tillage

This method produces loosen soil before cultivation. This type of technique is essential in conservation of water by preservation of crop and agriculture. This tillage does not disturb the surface soil structure and it is used for harvesting of crops and farms. (Friedler, 2017).

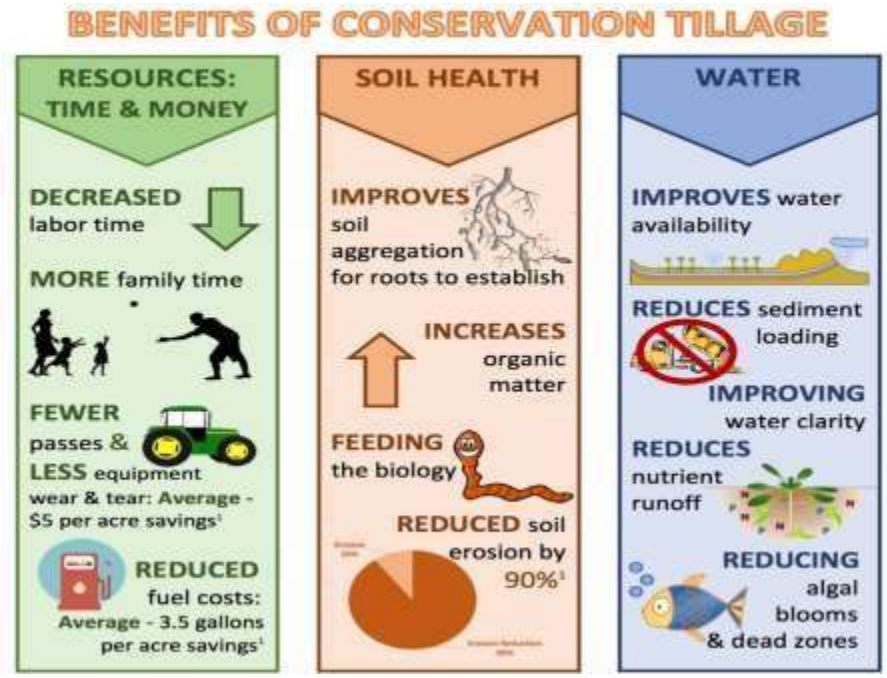

Figure 8. Conservation Tillage (Source: Busari, M. A., Kukal, S. S., Kaur, A., Bhatt, R., & Dulazi, A. A. (2015))

The use of conservation tillage is necessary to require the management on the soil surface. It is necessary that the crop residues, and it play a very important role in conservation tillage. When crop residues are properly set it will result in proper structure and it will; enhance soil quality; restore ecosystems; proper nutrition and increased water conservation and the sustainability to enhance, for example weed suppression; it will decline runoff and leaching of nutrients and also sustain and increase crop productivity resulting in more profit. Conservation tillage can be increase to enhance practices to enhance the soil benefits and provide aa better future from reducing tillage and increase the area. The complementary practices include crop rotations that will increase productivity and planting practices that will adjust the populations, for the proper management of residue; and management of crop nutrient that will eventually increase residue on the soil. Many of these practices are very common and used on agricultural lands in various areas. (Mishra, 2012).

CONCLUSION AND OUTLOOK

ADVANTAGES AND DISADVANTAGES

Table 1 Pros And Cons Of RWH System (Source: Ashanka, P. H., Ruhunuge, R. D. R., Chandrasena, W. K. N., & Dias,

S. V. (2019). Design, Operation and Maintenance Challenges of Roof Based Rain Water Harvesting Systems, Strategies for Improvement to Ensure Domestic Water Sustainability in Anuradhapura Area)

ADVANTAGES	DISADVANTAGES
Simple and easy to install.	System depends on intensity and frequency of rainfall which is uncertain.
Highly qualified labor is not required	Awareness and implementation is less.
Proper training is required.	Cannot be used as the only source of water.
Installation material is easily available.	Structures needs to be well designed.
Provides water at the point of collection, storage and utilization.	Rainfall is unequally distributed during various season in various localities.
Operational cost is almost negligible as compare to bore holes or tube wells. However, energy can be produced by this setup.	---
Not much maintenance cost required.	---
Structures have durability for more than 10 years.	---

COMPARISON OF RAINWATER HARVESTING TECHNIQUES

Table 2. Comparison of rainwater harvesting techniques (Source: Woyessa, Y. E., Pretorius, E., Hensley, M., Van Rensburg, L. D., & Van Heerden, P. S. (2006). Up-scaling of rain-water harvesting for crop production in the communal lands of the Modder River basin in South Africa: Comparing upstream and downstream scenarios.
Sr.
Rooftop Catchment
Land Surface Catchment
Rock and Surface Catchment System
Subsurface Dam and Sand Dam
Earth Dams Like Ponds and Pans
Recharge Structures
Conservation Tillage

1. The roof becomes the catchments, and the rainwater is collected from the roof of the house.

Runoff is used for recharging aquifers by adopting methods from the land surface. A rock catchment is a kind of ground catchment in which rocks are used to make a bed of rock as source of surface runoff which is stored in either a
tank or a dam. These are structures of mud, stone, cement. Another form uses hand-dug wells for water extraction. Earth or mud dams are effective in storage. They are made for the collection of rainwater. Rainwater harvesting has proven the best technique for recharging the ground water. It helps in water conservation. This type of technique is essential in conservation of water by preservation of crop and agriculture.

Rainwater harvesting in Sand dams and Best in those areas where conditions are good, groundwater can be recharged to create a pond of water which is used for the recharge. This can be done to overcome the losses due evaporation and results increase water quality. this case is very easy to subsurface dams are This technique will

2. This method is less expensive and very effective and if implemented properly. implement and utilizes less operational and maintenance cost and is less complex for
collecting rainwater This These are most easy and simple to operate. made to store the water under the ground. A sand dam is not a big dam and
it is used to store They can store quantities of rainwater as runoff which can be treated
to be used. result in enhance soil quality; restore ecosystems; proper nutrition and increased water conservation and technique is effective for water into the the sustainability irrigation purpose riverbed.

4. Rainwater that is falling over the roof is transferred to storage via a conveyance system, which typically contains gutter. It involves the conveyance structures which are the structure which is necessary for the primary treatment of rainwater to remove impurities.

It is effective types of rainwater storage system for rock catchments and in various localities

Sand and subsurface dams are in rural areas which are required to store only seasonal available water for livestock, irrigation. These are categorized into Hillside dams, charco dams, valley dams are constructed by digging the earth surface.

Recharge structures are useful in the areas where the water would not have a time to sink into the ground. Productivity and planting practices that will adjust the populations, for the proper management of residue; and management of crop nutrient

4.Materials such as steel, fiberglass are commonly used for the construction of tanks

There are various filtering systems such as sand filter charcoal filters and PVC filters. The runoff moves over the stone and cement made gutters and are contained by using the materials such as concrete or stone dams. The water can be made clean by using natural filtration. An earth dam is having different layers and they are built in in a layer of 250–400 mm thick, having heavy machinery. Another good area is in such a way that it is behind a check dam, at this point water is so that the water is lowered and has enough time for

infiltration. The use of conservation tillage is necessary to require the management on the soil surface

SCHEMATIC DIAGRAM OF REVIEW ARTICLE

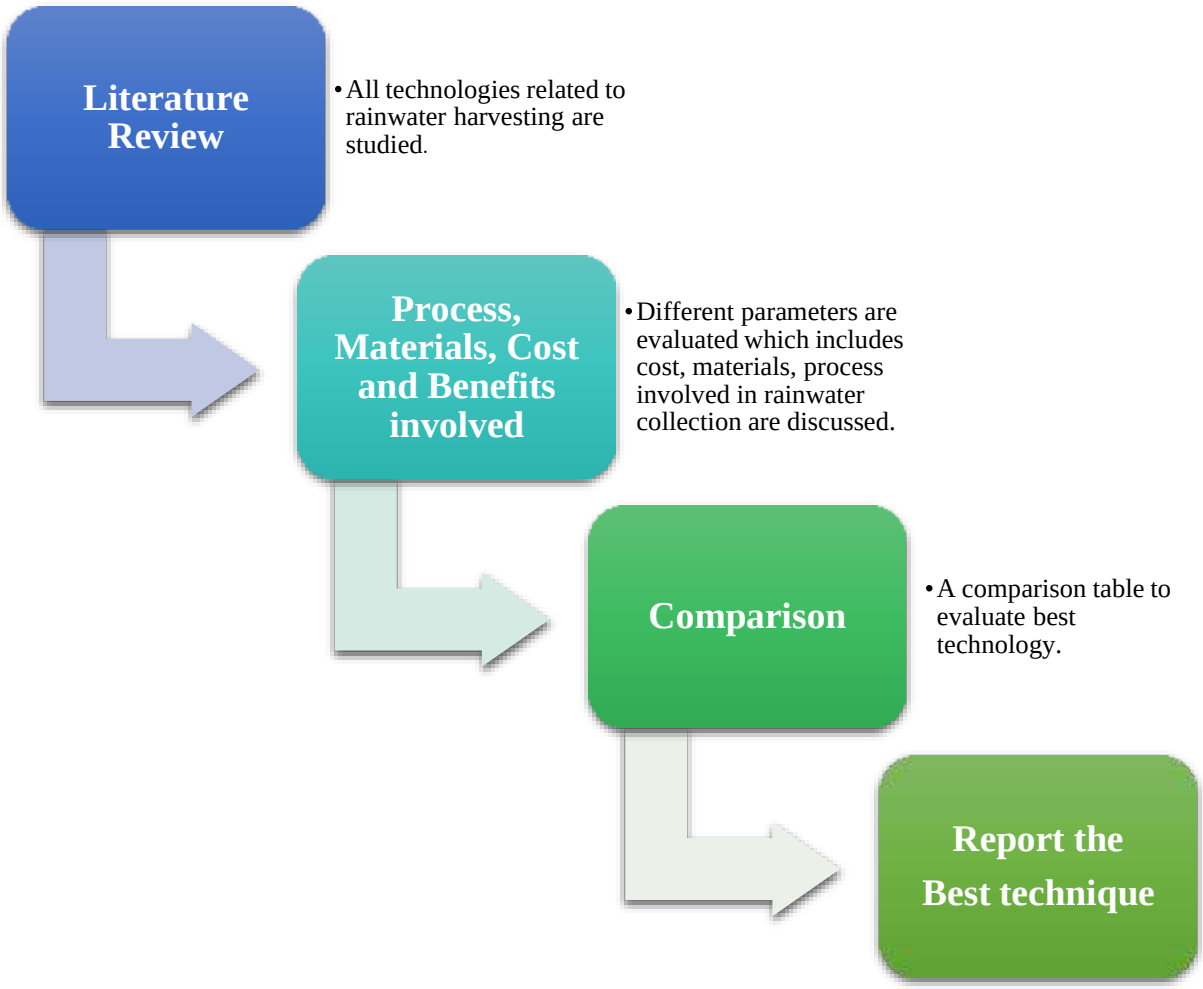

Figure 9. Schematic diagram of review article

SCHEMATIC DIAGRAM OF BEST RAINWATER HARVESTING TECHNIQUE

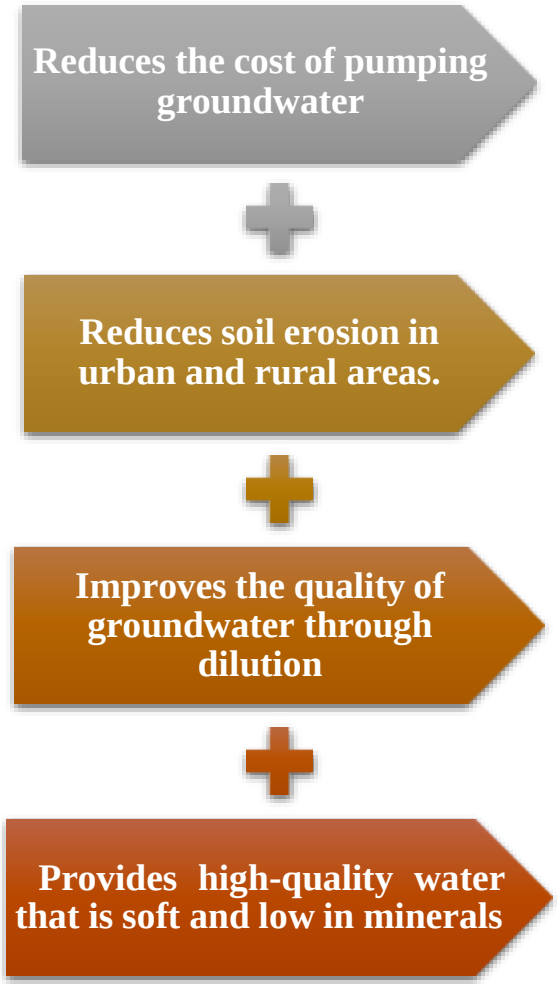

Figure 10. Schematic diagram of best rainwater harvesting technique

MOST FEASIBLE RWH TECHNIQUE

Roof Top Rainwater Harvesting is the most feasible technique compared to others. The chosen technique is best for the accomplishment of SDG's which will help contribute towards sustainability by useful utilization and storage of water. Water is linked with every SDG. Discussing mainly SDG 11 which is to ''Make cities safe and sustainable''.

Considering all these factors, Rooftop Rainwater Harvesting is the well-known technique to cater water shortages and use it for potable or non-potable purposes (Daoud, 2022).

The major advantage of using this is that the water is collected and stored from the top of the roof which serves as catchment. It can be collected, treated and stored for multiple purpose. This technique is not costly and is feasible to implement as its not much expensive, very commonly used, highly recommended and very effective (Demeke, 2021). One of the most important factor is that in this technique treatment as compare to other methods is less required as the rainwater is already collected from rooftop and the first flush is usually diverted resulting in collection of water with relatively less contaminated water which requires less effort and time in treatment thus making it usable for potable and non-potable purposes (Ngigi, 2003).

The quality of RHRW may also vary according to area, location, climatic conditions, organic matter such as the presence of feces, the roof condition, the network of piping and collection and storage systems, proper monitoring and check of system (Kalungu, 2015).

- **RAINWATER USES**

Some potential RHRW include number of uses such as cleaning, washing, flushing, lawn irrigation, gardening, recharge, fire-fighting water demands, making it much pure for consumption, through treatment and monitoring processes. The rainwater harvesting have been widely practiced for potable and non-potable purposes such as irrigation (Aladenola, 2010). Many locations have adopt RHRW as most basic source of water as it is the most used and depleting resource so it must have conserved (Sivanappan, 2006). Roof-harvested rainwater can be useful for drinking in some cases following the parameters, testing criteria, standards after and before treatment although if water standards such as, National Drinking Water Quality Standards (NDWQS), are not obeyed there is need of proper treatment channel before making it usable for potable purpose (Boers, (1982)).

REFERENCES

1. Abdulla, F. A.-S. (2009). Retrieved from Abdulla, F. A., & Al-Shareef, A. W. (2009). Roof rainwater harvesting systems for household water supply in Jordan. Desalination, 243(1-3), 195-207.
2. Ahammed, M. M. (2006). Retrieved from Meera, V., & Ahammed, M. M. (2006). Water quality of rooftop rainwater harvesting systems: a review. Journal of Water Supply: Research and Technology—AQUA, 55(4), 257-268
3. Ahmad, A. &. (2012). Retrieved from Ahmad, Aman & Abbas, Engr. Babar & Habib, Rasikh & Khan, Humayun & Khan, Sher. (2012). PERFORMANCE EVALUATION OF BENCH SCALE MEMBRANE BIOREACTOR (MBR) SYSTEMS. 441.
4. Aladenola, O. O. (2010). Retrieved from Aladenola, O. O., & Adeboye, O. B. (2010). Assessing the potential for rainwater harvesting. Water resources management, 24(10), 2129-2137.
5. Anderson, D. M. (2003). Retrieved from Pandey, D. N., Gupta, A. K., & Anderson, D. M. (2003). Rainwater harvesting as an adaptation to climate change. Current science, 46-59.

6. Ayesha & Fatima, M. (2022). Recycling Paper Waste into Plaster Composite Mixture. .
7. Boers, T. M.-A. ((1982)). Retrieved from A review of rainwater harvesting. Agricultural water management, 5(2), 145-158.: Boers, T. M., & Ben-Asher, J. (1982). A review of rainwater harvesting. Agricultural water management, 5(2), 145-158.
8. Campisano, A. B. (2017). Retrieved from Campisano, A., Butler, D., Ward, S., Burns, M. J., Friedler, E., DeBusk, K., ... & Han, M. (2017). Urban rainwater harvesting systems: Research, implementation and future perspectives. Water research, 115, 195-209.
9. Daoud, M. G. (2022). Retrieved from Daoud, M. G., Lubczynski, M. W., Vekerdy, Z., & Francés, A. P. (2022). Application of a novel cascade-routing and reinfiltration concept with a Voronoi unstructured grid in MODFLOW 6, for an assessment of surface-water/groundwater interactions in a hard-r
10. Demeke, G. G. (2021). Evaluation of the sustainability of existing rainwater harvesting ponds: A case study of Lay Gayint District, South Gondar zone, Ethiopia. Heliyon, 7(7), e07647. Retrieved from Demeke, G. G., Andualem, T. G., & Kassa, M. (2021). Evaluation of the sustainability of existing rainwater harvesting ponds: A case study of Lay Gayint District, South Gondar zone, Ethiopia. Heliyon, 7(7), e07647.
11. Engr. Babar & Sikandar, G. &. (2022). Retrieved from Engr. Babar & Sikandar, Gulshan & Ejaz, Ayesha & Fatima, Minahil. (2022). Recycling Paper Waste into Plaster Composite Mixture.
12. Friedler, E. D. (2017). Retrieved from Campisano, A., Butler, D., Ward, S., Burns, M. J., Friedler, E., DeBusk, K., ... & Han, M. (2017). Urban rainwater harvesting systems: Research, implementation and future perspectives. Water research, 115, 195-209.
13. GhaffarianHosein. (2016). Retrieved from GhaffarianHoseini, A., Tookey, J., GhaffarianHoseini, A., Yusoff,
S. M., & Hassan, N. B. (2016). State of the art of rainwater harvesting systems towards promoting green built environments: a review. Desalination and Water Treatment, 57(1), 95-104.
14. Helmreich, B. &. (2009)). Opportunities in rainwater harvesting. Desalination, 248(1-3), 118-124. Retrieved from Helmreich, B., & Horn, H. (2009). Opportunities in rainwater harvesting. Desalination, 248(1-3), 118- 124.
15. Kalungu, J. W. (2015). Retrieved from Kalungu, J. W., Mbuge, D. O., & Cheruiyot, H. K. (2015). Assessing the impact of rainwater harvesting technology as adaptation strategy for rural communities in Makueni County, Kenya. Springer Berlin Heidelberg.
16. Lopes, V. A. (2017). Retrieved from Lopes, V. A., Marques, G. F., Dornelles, F., & Medellin-Azuara, J. (2017). Performance of rainwater harvesting systems under scenarios of non-potable water demand and roof area typologies using a stochastic approach. Journal of cleaner production, 148, 30
17. Machiwal, D. S. (2017). Retrieved from Machiwal, D., Singh, P. K., & Yadav, K. K. (2017). Estimating aquifer properties and distributed groundwater recharge in a hard-rock catchment of Udaipur, India. Applied Water Science, 7(6), 3157-3172.

18. Meera, V. &. (2006). Retrieved from Meera, V., & Ahammed, M. M. (2006). Water quality of rooftop rainwater harvesting systems: a review. Journal of Water Supply: Research and Technology—AQUA, 55(4), 257-268.
19. Mishra, A. K. (2012). Retrieved from Glendenning, C. J., Van Ogtrop, F. F., Mishra, A. K., & Vervoort, R.
W. (2012). Balancing watershed and local scale impacts of rain water harvesting in India—A review. Agricultural Water Management, 107, 1-13.
20. Nachshon. (2016). Retrieved from Nachshon, U., Netzer, L., & Livshitz, Y. (2016). Land cover properties and rain water harvesting in urban environments. Sustainable Cities and Society, 27, 398-406.
21. Ngigi. (2003). Retrieved from Ngigi, S. N. (2003). Rainwater harvesting for improved food security.
22. Pacey, A. &. (1986). Retrieved from Pacey, A., & Cullis, A. (1986). Rainwater harvesting. The Collection of Rainfall and Runoff in Rural Areas. Intermediate Technology Publ., London.
23. Sivanappan, R. K. (2006). Retrieved from Sivanappan, R. K. (2006, November). Rain water harvesting, conservation and management strategies for urban and rural sectors. In National Seminar on Rainwater Harvesting and Water Management (Vol. 11, No. 12, p. 1). New Delhi, India: Institution of Engin
24. Van Ogtrop, F. F. (2012). Retrieved from Glendenning, C. J., Van Ogtrop, F. F., Mishra, A. K., & Vervoort,
R. W. (2012). Balancing watershed and local scale impacts of rain water harvesting in India—A review. Agricultural Water Management, 107, 1-13.
25. Wong, T. H. (2020). Transforming cities through water-sensitive principles and practices. One Earth, 3(4), 436-447. Retrieved from Wong, T. H., Rogers, B. C., & Brown, R. R. (2020). Transforming cities through water-sensitive principles and practices. One Earth, 3(4), 436-447.